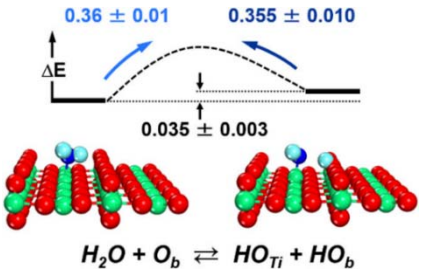

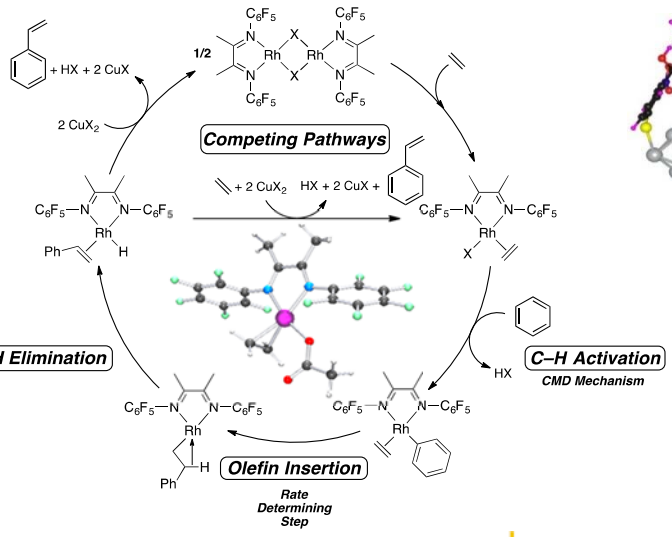

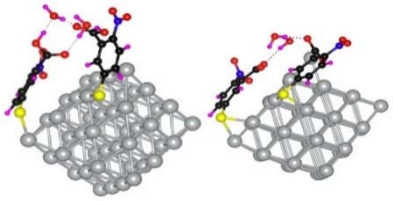

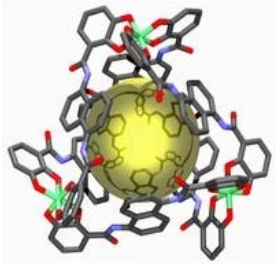

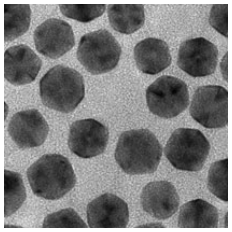

U.S. DEPARTMENT OF ENERGY | Office of Science

2017 Catalysis Science PI Meeting

Catalysis Science for Sustainable Chemistry

Gaithersburg Marriot Washingtonian Center

Gaithersburg, MD

July 26-28, 2017

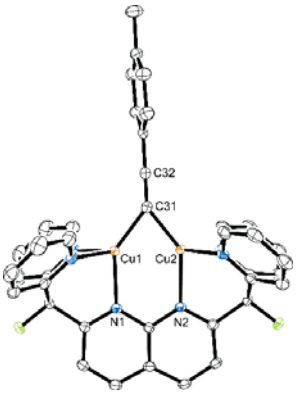

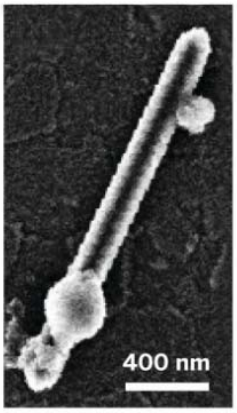

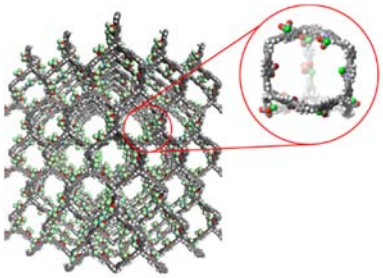

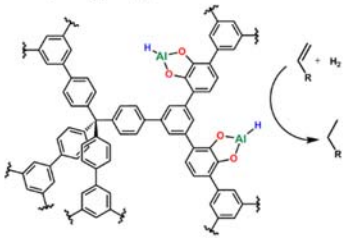

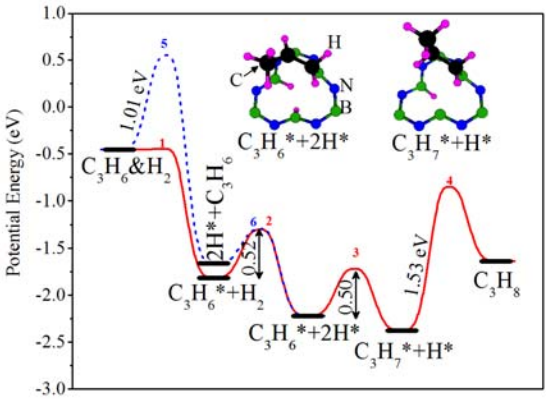

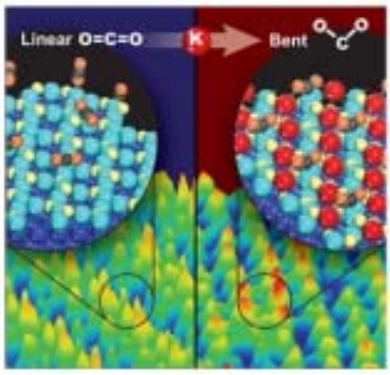

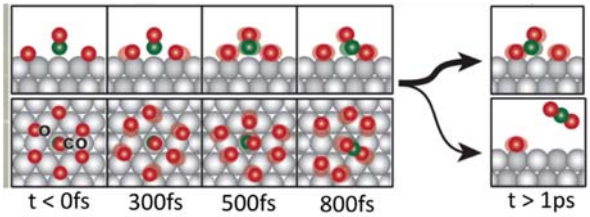

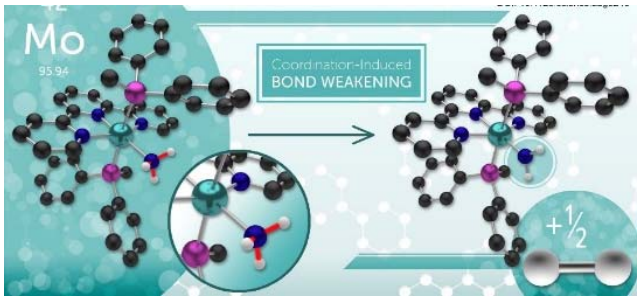

Program and Abstracts for the

2017 BES/Catalysis Science Research PI Meeting: *"Catalysis Science for Sustainable Chemistry"*

Gaithersburg Marriott Washingtonian Center
Gaithersburg, Maryland
July 25-28, 2017

The research grants and contracts described in this document are supported by the U.S. Department of Energy, Office of Science/Basic Energy Sciences, as part of the Catalysis Science Program within the Chemical Sciences, Geosciences and Biosciences Division.

FOREWORD

The 2017 Catalysis Science Research PI Meeting is sponsored by the Division of Chemical Sciences, Geosciences and Biosciences, Office of Basic Energy Sciences (BES), U.S. Department of Energy. It is being held on July 25–28, 2017, at the Marriott Washingtonian Hotel in Gaithersburg, Maryland. The purposes of this meeting are to discuss the recent advances in the chemical, physical, and biological bases of catalysis science, to foster exchange of ideas and cooperation among BES/Catalysis Science Program PIs, and to discuss the new science challenges and opportunities recently emerging in catalytic technologies for energy production and use.

Catalysis research activities within BES emphasize fundamental research aimed at understanding reaction mechanisms and, ultimately, controlling the chemical conversion of natural and artificial feedstocks to useful energy carriers. The long-term goals of this research are to discover fundamental scientific principles, and to produce insightful approaches for the prediction of catalyst structure-reactivity behavior. Such knowledge, integrated with advances in chemical and materials synthesis, *in-situ* and *operando* analytical instrumentation, chemical kinetics and dynamics measurements, and computational chemistry methods, will allow the control of chemical reactions along desired pathways. This new knowledge will impact the efficiency of conversion of natural resources into fuels, chemicals, materials, or other forms of energy, while minimizing the impact to the environment.

This year's meeting pursues the continuing goal of highlighting the potential advances in catalysis science of special relevance to the energy, economic and environmental future of the U.S., with the theme of the "*Catalysis Science for Sustainable Chemistry*". Indeed, catalytic processes continue to account for ~90% of chemical manufacturing, with more than 20% of all industrial products employing catalytic processes in their manufacture. Also significant are the continuing contributions of catalysis for processes leading to cleaner air and water. This year's program includes special sessions on catalysis research in the BES/Energy Frontier Research Centers, and the recently (May, 2017) held "**Basic Research Needs Workshop: Catalysis Science to Transform Energy Technologies**", in addition to 17 oral and 57 poster presentations by BES/Catalysis Science PIs.

Special thanks go to the program investigators and their students, postdocs, and collaborators for their dedication to the continuous success and visibility of the BES/Catalysis Science Program. We also thank Diane Marceau[3], and the Oak Ridge Institute for Science and Education staff (Connie Lansdon!) for the logistical and web support of the meeting. Finally very special thanks go to Raul Miranda[3] for his longstanding and continuing contributions to the BES/Catalysis Science Program, now from his role as Team Lead for Chemical Transformations in the BES/Chemical Sciences, Geosciences and Biosciences Division.

Paul Chirik[1], Ray Gorte[2], Viviane Schwartz[3], Chris Bradley[3] and Chuck Peden[3]

[1]Princeton University
[2]University of Pennsylvania
[3]Catalysis Science Program - Office of Basic Energy Sciences - U.S. Department of Energy

2017 Catalysis Science PI Meeting
Catalysis Science for Sustainable Chemistry

July 25-28, 2017
Marriott Washingtonian, Gaithersburg, MD
Program chairs: Paul Chirik and Ray Gorte

Tuesday Afternoon, July 25

2:00 – 5:00 p.m. **Registration**

Wednesday Morning, July 26

7:00-8:00 a.m. **Breakfast**

OPENING SESSION
Session Chairs: **Paul Chirik and Ray Gorte**

8:00-8:30 am Welcoming remarks
Viviane Schwartz, Chris Bradley and Chuck Peden, DOE/BES/Catalysis Science Program

8:30-8:40 am PI Meeting Theme – "*Catalysis Science for Sustainable Chemistry*"
Paul Chirik, Princeton Univ., **Ray Gorte**, University of Pennsylvania

8:40-9:00 am BES Update
Bruce Garrett, Director, DOE/BES/Chemical Sciences, Geosciences and Biosciences Division

PLENARY SESSION I – CATALYSIS SCIENCE IN THE DOE/BES EFRCS I
Session Chair: **Paul Chirik**, Princeton University

9:00-9:40 am Center for Molecular Electrocatalysis (CME)
Morris Bullock, Pacific Northwest National Laboratory

9:40-10:20 am Inorganometallic Catalysis Design Center (ICDC)
Laura Gagliardi, University of Minnesota

10:20-10:35 am **Coffee Break**

PLENARY SESSION II – CATALYSIS SCIENCE IN THE DOE/BES EFRCS II
Session Chair: **Ray Gorte**, University of Pennsylvania

10:35-11:15 am Center for Direct Catalytic Conversion of Biomass to Biofuels (C3Bio)
Maureen McCann, Purdue University

11:15-11:55 am Catalysis Center for Energy Innovation (CCEI)
Dion Vlachos, University of Delaware

11:55am-12:35pm Integrated Mesoscale Architecture for Sustainable Catalysis (IMASC)
Cynthia Friend, Harvard University

12:35-1:30 pm **Working Lunch**

Wednesday Afternoon, July 26

PI SESSION I – Sustainable Catalysis in Unique Environments
Session Chair: **Raul Lobo, University of Delaware**

1:30-2:10 pm Title: "Cascade Catalysis in Multicompartment Nanoreactors"
Presenter – Marcus Weck, New York University

2:10-2:50 pm Title: "Interfacial Single Site Catalysts in 3-D Environments"
Presenter – Aaron Sadow, Iowa State University and AMES Laboratory

2:50-3:30 pm Title: "Catalysis in Confined Spaces"
Presenter – Dean Toste, UC Berkeley and LBNL

3:30-3:50 pm **Coffee Break**

PI SESSION II – Sustainable Catalysis with Metal Oxides and Extended Structures
Session Chair: **Zdenek Dohnalek, Pacific Northwest National Laboratory**

3:50-4:30 pm Title: "Nanostructured, Targeted Layered Metal Oxides as Active and Selective Heterogeneous Electrocatalysts for Oxygen Evolution"
Presenter – Eranda Nikolla, Wayne State University

4:30-5:10 pm Title: "Catalytic Growth of Molecular-Scale Wiring"
Presenter – Colin Nuckolls, Columbia University

5:10-7:00 pm **Dinner (on your own)**

Wednesday Evening, July 26

7:00-9:00 pm **Posters (Odd numbers)**

Thursday Morning, July 27

7:30-8:30 am **Breakfast**

PI Session III – Sustainable Catalysis at the Nanoscale I
Session Chair: **Lauren Greenlee, University of Arkansas**

8:30-9:10 pm Title: "Understanding and Tuning Catalytic Materials Using Nanocrystal Precursors"
Presenter – Matteo Cargnello, Stanford University and SUNCAT

9:10-9:50 pm Title: "Oxide Engineering at the Nanoscale for Catalyst Supports and Active Sites"
Presenter – Justin Notestein, Northwestern University

9:50-10:10 am **Coffee Break**

PI SESSION IV – Sustainable Catalysis at the Nanoscale II
Session Chair: **Bill Schneider, University of Notre Dame**

10:10-10:50 am Title: "Correlating Structure and Function for Nanoparticle Catalysts"
Presenter – Graeme Henkelman, University of Texas, Austin

10:50-11:30 am Title: "Advances in the Design and Synthesis of Multimetallic Nanocatalysts"
Presenter – Sara Skrabalak, Indiana University

Special Session – Recent Catalysis BRN Workshop
Session Chair: **Chris Bradley, DOE/BES/Catalysis Science**

11:30-12:15 am Basic Research Needs Workshop: Catalysis Science to Transform Energy Technologies
Susanna Scott (UC, Santa Barbara) and/or Johannes Lercher (PNNL)

12:15-1:15 pm **Working Lunch**

Thursday Afternoon, July 27

1:15-3:00 pm **PANEL DISCUSSION – Recent Catalysis BRN Workshop**
Sheng Dai (ORNL), Brent Gunnoe (University of Virginia), Paul Dauenhauer (University of Minnesota), and Aaron Appel (PNNL)
Session Chair: **Viviane Schwartz, DOE/BES/Catalysis Science**

3:00-3:20 pm **Coffee Break**

PI SESSION V – Sustainable Catalysis for Ammonia Synthesis and Use
Session Chair: **Alison Fout, University of Illinois**

3:20-4:00 pm Title: "Ammonia at the Food-Energy-Water Nexus: the Motivation for Alternatives to Haber-Bosch, and Step Catalysis as an Example"
Presenter – Peter Pfromm, Washington State University

4:00-4:40 pm Title: "Ammonia "Splitting" for Renewable Energy Conversion"
Presenter – Mitch Smith, Michigan State University

4:40-5:20 pm Title: "Oxo and Nitrido Chemistry with Metal-Metal Bonds"
Presenter – John Berry, University of Wisconsin, Madison

5:20-7:00 pm **Dinner (on your own)**

Thursday Evening, July 27

7:00-9:00 pm **Posters (Even numbers)**

Friday Morning, July 28

7:00-8:00 am **Breakfast**

PI SESSION VI – Sustainable and Catalysis for Hydrocarbon Chemistry
Session Chair: **John Hartwig, LBNL and UC Berkeley**

8:00-8:40 am Title: "Coordinatively Unsaturated Bis(Phosphinoamide) Ti/Co and Zr/Co Complexes and Their Enhanced Reactivity Towards Small Molecule Substrates"
Presenter – Christine Thomas, Brandeis University

8:40-9:20 pm Title: "Modeling of Late Transition Metal Catalysts for Energy Application"
Presenter – Tom Cundari, University of North Texas

9:20-10:00 pm Title: "Single-Particle/-Molecule Studies of Catalysis"
Presenter – Suzanne Blum, University of California, Irvine

10:00-10:20 am **Coffee Break**

PI SESSION VII - Sustainable Catalysis for Biomass Conversion
Session Chair: **Rob Rioux, Pennsylvania State University**

10:20-11:00 am Title: "Molecular Understanding of Bifunctional Solid Lewis Acid Zeolites for the C-C Coupling of Alpha Keto Acids"
Presenter – Yuriy Román-Leshkov, MIT

11:00-11:40 am Title: "Phosphorous-Silica Catalysts for Renewable Olefin Chemicals"
Presenter – Paul Dauenhauer, University of Minnesota

CLOSING SESSION

Session Chairs: **Paul Chirik and Ray Gorte**

11:40am-12:00pm Closing Remarks
Chirik, Gorte, Schwartz, Bradley, Peden

12:00 pm **Adjourn**

Poster Sessions

Wednesday, July 26, 2017

Aaron Appel, PNNL
Simon Bare, SLAC
Alex Bell, LBNL
Bertrand, Guy
Thomas Bligaard, SLAC
Chen, Jingguang
Chen, Peng
Chirik, Paul
Cox, David
Crooks, Richard
Sheng Dai, ORNL
Max Delferro, ANL
Zdenek Dohnalek, PNNL
Finke, Richard
Fout, Alison
Gates, Bruce
Gorte, Ray
Greenlee, Lauren
Gunnoe, Thomas
Oliver Gutierrez-Tinoco, PNNL
John Hartwig, LBNL
Dave Heldebrant, PNNL
Hicks, Jason
Jackson, Timothy
Jang, Seung Soon
Johannes Lercher, PNNL
Marks, Tobin
Stahl, Shannon – EFRC

Thursday, July 27, 2017

Cong Liu, ANL
Ping Liu, BNL
Lobo, Raul
Mustain, William
Mirica, Liviu
Jens Norskov, SLAC
Oyama, Shigeo
Rahman, Talat
Rioux, Robert
Jose Rodgriguez, BNL
Roger Rousseau, PNNL
Ashi Savara, ORNL
Schneider, Bill
Scott, Susannah
Selloni, Annabella
Sanjaya Senanayake, BNL
Sievers, Carsten
Igor Slowing, AMES
Stahl, Shannon – Core Program
Suib, Steven
Tong, YuYe
Tysoe, Wilfred
Johannes Voss, SLAC
Wachs, Israel
Mike White, BNL
Zili Wu, ORNL
Peidong Yang, LBNL

TABLE OF CONTENTS

Poster Sessions

ABSTRACTS

Plenary Session Abstracts

Morris Bullock

Catalytic H_2 Production and O_2 Reduction: Controlling Proton and Electron Delivery

R. Morris Bullock[a], Shannon S. Stahl[b], James M. Mayer[c], Sharon Hammes-Schiffer[d], Aaron M. Appel [a], Simone Raugei [a], Michael T. Mock [a], Molly O'Hagan [a], Eric S. Wiedner [a]
Center for Molecular Electrocatalysis

[a]Pacific Northwest National Laboratory, Richland, WA 99352
[b]Department of Chemistry, University of Wisconsin-Madison, Madison, WI 53706
[c] Department of Chemistry, Yale University, New Haven, Connecticut 06520
[d]Department of Chemistry, University of Illinois at Urbana-Champaign, Urbana, IL 61801

Presentation Abstract

Electrocatalysts that interconvert between electrical energy and chemical bonds (fuels) are needed for energy storage, particularly because of the increasing availability of solar and wind as sustainable energy sources. Our efforts are focused on "Cheap Metals for Noble Tasks" rather than precious metals. Precise control of the delivery or removal or protons and electrons is required, and we pursue that goal in the context of electrocatalytic multi-electron, multi-proton processes of critical importance to a secure energy future: the production and oxidation of H_2 (2 e^-/2 H^+), the reduction of O_2 (4 e^-/4 H^+), and the interconversion of N_2 and NH_3 (6 e^-/6 H^+). Recent progress includes the design of a nickel complex that is the fastest molecular electrocatalyst for H_2 production *and* an iron complex that is the fastest molecular electrocatalyst for O_2 reduction to water. Understanding relationships between rates (turnover frequencies) and over-potentials helps to elucidate principles that will guide the development of catalysts that deviate from linear scaling relationships. A recent focus in the Center is electron-proton-transfer mediators (EPTMs) as a new catalyst design principle for challenging electrochemical reactions.

Laura Gagliardi

Inorganometallic Catalysis Design Center (ICDC)

Presentation Abstract

The Inorganometallic Catalyst Design Center (ICDC) is an Energy Frontier Research Center funded by the United States Department of Energy. The ICDC is devoted to computationally-guided discovery of a new class of energy-science-relevant catalytic materials and the underlying structure-function relationships that will guide further catalyst discovery. The catalysts determined in the ICDC are intended to be used for natural gas conversion from alkanes to alcohols.

Maureen McCann

Center for Direct Catalytic Conversion of Biomass to Biofuels (C3Bio)

Presentation Abstract

Lignocellulosic biomass has one-third the energy density of crude oil and lacks petroleum's versatility as a feedstock for fuels and chemicals. Chemical catalysis and fast pyrolysis can overcome these limitations by transforming the main components of biomass (cellulose, xylan, and lignin) from grasses and trees directly to liquid hydrocarbons and aromatic co-products. Our data show that, regardless of conversion process, biomass structural complexity at molecular, nanoscale, and mesoscale levels impacts the yields and selectivities of desired reaction products from catalytic and pyrolytic transformations. In stark contrast to oil and petrochemical resources, the structure of renewable carbon resources can be changed in living organisms. By exploiting natural genetic variation, genetic engineering and synthetic biology approaches, we are tailoring the composition and architecture of cell wall components to optimize post-conversion product yields without compromising pre-conversion biomass yields. Our long-term goal is to design liquid hydrocarbon fuels, sourced from plants, with the operational performance of current oil-derived fuels and so increase resilience of the Nation's transportation fuel system.

Supported by C3Bio, an Energy Frontier Research Center funded by the U.S. Department of Energy, Office of Basic Energy Sciences.

Dion Vlachos

Catalysis Center for Energy Innovation (CCEI)

Stavros Caratzoulas[1], Jingguang Chen[2], Paul Dauenhauer[3], Mark Davis[4], Doug Doren[1], Wei Fan[5], Anatoly Frenkel[6], Ray Gorte[7], Marianthi Ierapetritou[8], Friederike Jentoft[5], Chris Jones[9], Raul Lobo[1], Chris Murray[7], Basu Saha[1], Stan Sandler[1], Ilja Siepmann[3], Mark Snyder[10], Klaus Theopold[1], Michael Tsapatsis[3], Dion Vlachos[1], Don Watson[1], Bingjun Xu[1]

[1]*University* of Delaware; [2]*Columbia University;* [3]*University of Minnesota;* [4]*California Institute of Technology;* [5]*University of Massachusetts;* [6]*Brookhaven National Laboratory and Stony Brook University;* [7]*University of Pennsylvania;* [8]*Rutgers University;* [9]*Georgia Institute of Technology;* [10]*Lehigh University*

Presentation Abstract

An overview of the catalysis center for energy innovation will be given focusing on its mission and recent accomplishments. We will discuss biomass degradation to simple derivatives, such as sugars, followed by a number of reactions, such as Lewis and Brønsted acid catalyst driven isomerization and dehydration to convert sugars to valuable intermediate furans. Diels-Alders and dehydration chemistry will be outlined for the production of renewable aromatics, such as para-xylene. Hydrodeoxygenation of biomass will also be discussed as an effective means to remove oxygen and produce certain platform chemicals. Renewable surfactants, dienes, and jet fuel produced for the first time at high yield from lignocellulose will be presented. We will discuss how enabling technologies, such as multiscale modeling and characterization, provide fundamental insights into the mechanisms, the kinetics, and the active sites of catalysts, and how multiscale hierarchical materials with such sites result in unprecedented performance.

Cynthia Friend

Integrated Mesoscale Architecture for Sustainable Catalysis (IMASC)

Presentation Abstract

The core of the IMASC research approach is to integrate fundamental studies of model systems with the design, synthesis and testing of mesoporous catalysts spanning a vast range of pressures, temperatures and materials complexity. Theory and experiment are being combined to establish and test general principles that control reactivity and selectivity. Our team focuses on metallic alloy catalyst materials that have dual functionality. The principal design feature of the catalyst material is to combine a minor amount of active metal that facilitates creation of reactive intermediates with a less active majority phase that transforms these intermediates to desirable products with high selectivity. IMASC research, based on active and inclusive management, is strategically organized into three Focus Areas to tackle some of the most important energy challenges facing the nation.

The IMASC research specifically addresses the grand challenge of "How do we design and perfect atom- and energy efficient synthesis of revolutionary new forms of matter with tailored properties." The "revolutionary" feature here is the design of catalysts that uniquely combine atomic reactive sites and the host properties to achieve behavior controllably different than that of either individual component.

Basic Research Needs Workshop: Catalysis Science to Transform Energy Technologies

Susannah L. Scott,[a,b] and Johannes A. Lercher[c,d]

[a] Department of Chemical Engineering, University of California, Santa Barbara CA
[b] Department of Chemistry & Biochemistry, University of California, Santa Barbara CA
[c] Department of Chemistry and Catalysis Research Center, TU München, Lichtenbergstrasse 4, 85747 Garching, Germany
[d] Institute for Integrated Catalysis, Pacific Northwest National Laboratory, Richland, Washington

Presentation Abstract

The Department of Energy's Office of Basic Energy Sciences hosted a Basic Research Needs workshop May 8-10, 2017, to define future research challenges and opportunities in basic research in the catalysis science that will underpin energy resource conversion and utilization in the next decade. The workshop examined principal technological barriers as well as the underlying scientific principles associated with energy- and atom-efficient processing of energy resources and products derived from them, with the goal of assessing the current status of the field, and identifying bottlenecks and gaps in our fundamental understanding that will enable *a priori* design of catalytic materials and processes for sustainable chemical conversions. The workshop, chaired by Carl Koval (University of Colorado, Boulder) assisted by co-chairs Susannah Scott and Johannes Lercher, consisted of four panels charged with examining (1) Diversified Energy Feedstocks and Carriers; (2) Novel Approaches to Energy Transformations; (3) Advanced Chemical Conversion Approaches; and (4) Crosscutting Capability and Challenges in Synthesis, Theory, and Characterization. Plenary lecturers and panel participants identified priority research directions for advancing energy technologies, for example, through synthesis of catalyst architectures beyond the binding site, control of dynamic catalyst behavior, understanding of complex reaction networks, and the use of machine learning to mine large and heterogeneous datasets.

Wednesday PI
Oral Presentations

Marcus Weck

Cascade Catalysis in Multicompartment Nanoreactors

Marcus Weck (NYU), Christopher W. Jones (GT), Seung Soon Jang (GT), Hung Vu Tran (GT), Li-Chen Lee (GT), Caroline Hoyt (GT), Aaron Cohen (NYU), Michael Küpfert (NYU), Peiyuan Qu (NYU), Connor Callaway (GT)

(NYU) Department of Chemistry and Molecular Design Institute, Department of Chemistry, New York University, New York, NY 10003; (GT) School of Chemical & Biomolecular Engineering and School of Materials Science & Engineering, Georgia Institute of Technology, Atlanta, GA 30332

Presentation Abstract

At any given moment the cell is carrying out a large number of non-orthogonal (and competing) catalytic transformations simultaneously. This is possible by compartmentalizing these transformations and catalysts, thereby shielding them from each other Using such a strategy prevents the different transformations from interfering with one another and enables the system to run a specific reaction in a tailored microenvironment, with a variety of microenvironments existing with differing pH values, salt concentrations, hydrophobic or hydrophilic environments, etc. Additionally, Nature is able to shuttle reactants and products through individual compartments (compartmentalization spatially isolates incompatible or opposing reagents), allowing for cascade or tandem reaction pathways combining (non-orthogonal) transformations for the synthesis of complex molecules. To date, synthetic analogs to such chemical reaction diversity do not exist, though there is significant interest in one-pot, multistep strategies to supersede intermediate work-up procedures. Synthetic multicompartment systems are in their infancy and reports of combining non-orthogonal transformations in one pot have been limited to a few examples, none of them allowing for multiple non-orthogonal and enantioselective transformations. An interdisciplinary research team that can probe all aspects of the design and synthesis of compartmentalizable nanoreactor supports and catalyst synthesis, structure and properties is exploring this topic from both experimental and theoretical points of view. In particular, researchers at GT and NYU are developing design principles for novel multicompartment nanoreactors to support a library of catalysts, both transition metal based and organocatalysts, for tandem catalysis. Using these model systems, the fundamental principles that can be used to understand and design future classes of supported, cooperative catalysts are being elucidated.

DE-FG02-03ER15459: Multi Compartment Nanoreactors as Supports for Incompatible Molecular Catalysts

PIs: Christopher W. Jones, Marcus Weck, Seung Soon Jang
Postdoc(s): Hung Vu Tran, Li-Chen Lee
Student(s): Caroline Hoyt, Aaron Cohen, Michael Küpfert, Peiyuan Qu, Connor Callaway

RECENT PROGRESS

Shell Cross-linked Micelles (SCMs) As Nanoreactors for Tandem Catalysis – Transition Metal Catalysts

The research team has previously utilized shell cross-linked micelles (SCM)s as catalytic support structures to facilitate two step non-orthogonal tandem reactions in one pot.[1,2] This was enabled through site isolation of each catalyst in the corona and the core of the micelle. We are currently increasing the complexity of the system by working on advancing this strategy to a three step tandem reaction sequence by incorporating a third catalyst in a third compartment along the SCM, the cross-linking layer (Figure 1). The reaction sequence that is targeted is the acid catalyzed ketal hydrolysis followed by Rh-TsDPEN catalyzed asymmetric transfer hydrogenation (ATH) and subsequent acylation by DMAP.

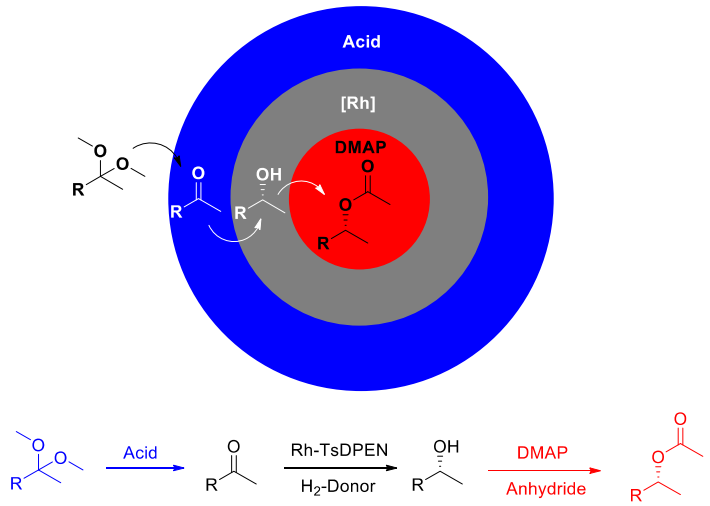

Figure 1. Tri-functional SCM catalyst for the hydrolysis-ATH-acylation tandem reaction.

Our SCM design is based on poly(2-oxazoline)s. Dual functionalized SCMs with a carboxylic acid forming corona and a Rh-TsDPEN confined inside the cross-linked shell were synthesized prior to the three catalytic system (Scheme 1). Self-assembly of the cross-linked triblock copolymer into micelles was confirmed by dynamic light scattering (DLS) in water and methanol with hydrodynamic radii (R_h) of 82 and 40 nm, respectively. Preliminary catalytic tests of the hydrolysis showed 80% conversion within 24 hours and 99% conversion and 80% *ee* within seven days of the ATH. For the first time we enabled function-alization and catalytic activity in the cross-linked shell by Rh-TsDPEN. Optimization of the reaction conditions are currently in progress to improve both the reaction rate and the enantioselectivity.

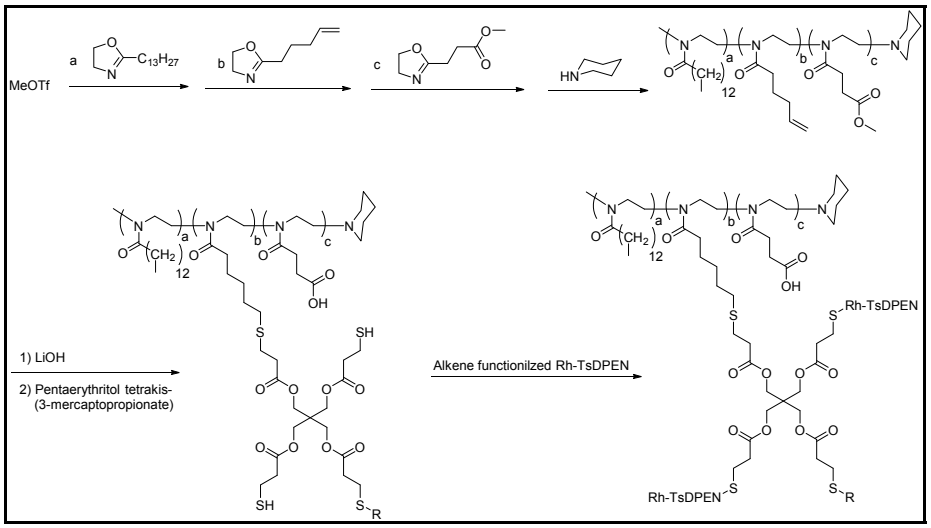

Scheme 1. Synthesis of dual functionalized poly (2-oxazoline) SCM support.

SCMs As Nanoreactors for Tandem Catalysis – Acid/Base Catalysis

The research team has explored the use of a shell cross-linked micelle for the cascade reaction of the acid-catalyzed acetal hydrolysis and subsequent base-catalyzed Henry reaction. The normally incompatible acid and base active species have been isolated in the core and shell of the micelle (Figure 2) to allow for catalysis of the tandem two-step reaction in one pot under mild conditions. A polymer consisting of an ABC-triblock copolymer based on poly(2-oxazoline)s was used to build the complete organocatalytic micelle. To provide thermal stability and ensure site isolation of the acidic, micelle shell from the basic core, the shell was covalently crosslinked through efficient thiol-ene "click" chemistry. The SCM contained a carboxylic acid-functionalized shell and tris(2-aminotheyl)amine (TREN) in the hydrophobic core. In one pot, the carboxylic acid shell catalyzed the acetal deprotection of benzaldehyde dimethyl acetal with 99% conversion in 24 hours at 90 °C under nitrogen with 10 mol % acid. With 0.4 mol % amine in the basic core, the resulting benzaldehyde with nitromethane was converted by the nitroaldol reaction to 86% conversion.[1] This was the first demonstration of this catalyst architecture utilizing two distinct domains containing two opposing organocatalysts for a cascade reaction, leveraging our prior work on incompatible transition metal catalysts.

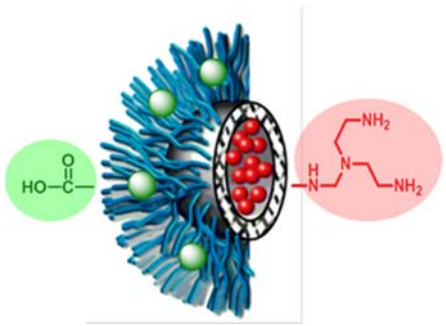

Figure 2. SCM catalyst containing amines in the core and carboxylic acids in the shell for tandem catalysis.

Linear Polymer-supported Cooperative Acid-Base Catalysts for the Aldol Reaction

Cooperative catalysis has been studied extensively by us and others employing mesoporous silica supports with inherent surface acidity and grafted amines. Other design elements that nature has utilized in enzymatic behavior are characteristics such as flexibility, acid-base pairing, and proximity of acid-base pairs. We hypothesized that these features can be modelled on a polymer support with potentially more control than mesoporous silica. A linear poly(styrene) functionalized with different acids and base pairs demonstrated that cooperative catalysis could be achieved with these structures for the aldol condensation. Acid monomers utilized were catechol (diol) to demonstrate a similar acidity to the silanol surface, and a stronger 4-vinyl benzoic acid. The basic monomer (ba) synthesized was a 4-(vinylbenzyl) amine, to include a basic primary amine with a methylene linker to provide an element of flexibility and enhanced basicity. Once deprotected, the polymer catalyst was insoluble, which led to the quantification of exterior accessible sites for catalysis, through titration of acid sites and a coupling reaction with the primary amines to yield

Figure 3. Linear block copolymer catalysts catalyze the aldol reaction via cooperative acid base catalysis fastest when acid and base sites are randomly distributed on the polymer chain.

8.5 mol% of accessible and active sites for catalysis. These random and block copolymer catalysts demonstrated activity higher than mesoporous silica with an initial TOF of 25 h^{-1} (compared to 2.6 h^{-1}).[2] The random copolymer 1:1 diol:ba, with the 1:1 ratio of diol and amine monomer incorporated, showed the highest activity (Figure 3). This first generation of catalyst demonstrated the tunable benefits of polymer synthesis applied to cooperative catalysts through monomer design, controlled polymerization, and overall more degrees of freedom in catalyst design.

Functionalized Multicompartment Micelles As Catalytic Nanoreactors

The research team group is currently developing multicompartment micelles from functionalized block copolymers, to be used a catalytic scaffold for one-pot tandem reactions. As described above, the Weck and Jones groups have shown that the hydrophilic and hydrophobic domains of a core-shell micelle, formed via the self-assembly of a functionalized amphiphilic diblock copolymer, could be functionalized with two, and now three, incompatible catalysts. These systems can be used as nanoreactors to conduct multistep catalytic processes in one pot. The tandem reactions conducted were only successful when the two catalysts were physically isolated from one another in the two domains of a core-shell micelle. We are extending this design principle via the formation of multicompartment micelles from functionalized triphilic block copolymers. Multicompartment micelles feature an additional level of microphase separation within the solvophobic core and thus are an ideal system to covalently bind three incompatible catalysts in isolated domains that are in close proximity to one another. The most common strategy to form multicompartment micelles is through the self-assembly of triphilic block copolymers with hydrophilic, lipophilic, and fluorophilic blocks, where the fluorophilic block microphase separates from both the hydrophilic and lipophilic blocks. To date, all reported block copolymers used to form multicompartment micelles have been comprised of relatively simple monomers that lack functionality. Consequently, the reported applications of such systems remain limited, although several groups have shown that the lipophilic and fluorophilic domains of a multicompartment micelle could be used for the selective uptake of lipophilic and fluorophilic small molecules. We hypothesize that a multicompartment micelle formed via the self-assembly of a functionalized triphilic block copolymer could be used as an advanced nanoreactor, as a natural extension of our expertise in this field.

Linear hydrophilic-lipophilic-fluorophilic ("**ABC**") and lipophilic-hydrophilic-fluorophilic ("**BAC**") triblock copolymers were synthesized using reversible addition-fragmentation chain-transfer (RAFT) polymerization. The final **ABC** and **BAC** triblock copolymers are shown in Figure 4. The carboxylic acid group of the hydrophilic group **A** can be used to form an ester with an alcohol. The aromatic aldehyde of the lipophilic block **B** can form a hydroxylimine via a condensation reaction with a hydroxylamine, while the *para* fluorine of poly(pentafluorostyrene) of the fluorophilic block **C** can undergo a nucleophilic substitution reaction with a thiol.

Following the successful polymerization, the **ABC** and **BAC** triblock copolymers were self-assembled in water and subsequently characterized using dynamic light scattering (DLS), confirming the formation of large nanoscale assemblies. DLS is unable to provide any further insight into the morphology of the self-assembled structures. Therefore, to determine if multicompartment micelles were successfully formed, we used cryo-transmission electron microscopy (cryo-TEM). Cryo-TEM indicated that both the **ABC** and **BAC** triblock copolymers formed corona-shell-core "onion" morphologies (Figure 5), in which the hydrophilic block **A** forms the outer corona (barely visible due to its similar electron density with the aqueous medium), the lipophilic block **B** forms the intermediate shell (medium gray) and the fluorophilic block **C** forms the central core (darkened region). This morphology is in agreement with reported

morphologies of multicompartment micelles formed from triphilic block copolymers.

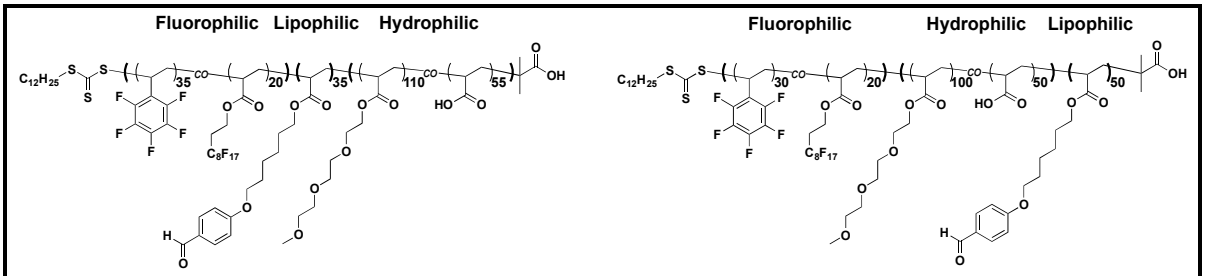

Figure 4. Hydrophilic-lipophilic-fluorophilic "**ABC**" (left) and lipophilic-hydrophilic-fluorophilic "**BAC**" (right) triblock copolymers used to form functionalized multicompartment micelles.

As a control, the hydrophilic-lipophilic **AB** and lipophilic-hydrophilic **BA** diblock copolymers were also self-assembled and investigated using cryo-TEM. In both cases, no evidence of microphase separation within the core was observed, thus confirming that the "onion" morphologies witnessed for the **ABC** and **BAC** triblock copolymers are a result of the incompatibility of the fluorophilic block **C** with both the hydrophilic block **A** and the lipophilic block **B**. From a catalytic standpoint, the existence of a single fluorophilic domain within the core (as opposed to multiple, smaller fluorophilic domains which have also been reported), is highly attractive for one-pot tandem reactions. If three incompatible catalysts are covalently linked to the three blocks, we envision a system where a reactant of choice can diffuse from one domain to another as it reacts in each step of the tandem process.

We have also demonstrated that each block of the **ABC** and **BAC** triblock copolymers can undergo a series of orthogonal post-polymerization reactions, as described above, with simple small molecules. Following the completion of the three post-polymerization reactions, the modified **ABC** and **BAC** triblock copolymers once again can be self-assembled and analyzed using cryo-TEM. We are currently using the same post-polymerization reactions to functionalize the triblock copolymers with modified catalysts, to develop this system as a tripartite nanoreactor. Finally, we are investigating what effect the ratio of the block length of the hydrophilic/hydrophobic blocks has on the overall morphology of the multicompartment micelle. Unlike amphiphilic diblock copolymers, there is little theoretical knowledge to predict the morphology of a multicompartment micelle based on the monomers used, block lengths, block sequence etc. We are hoping that a combination of experimental and computational work can shed light on this area.

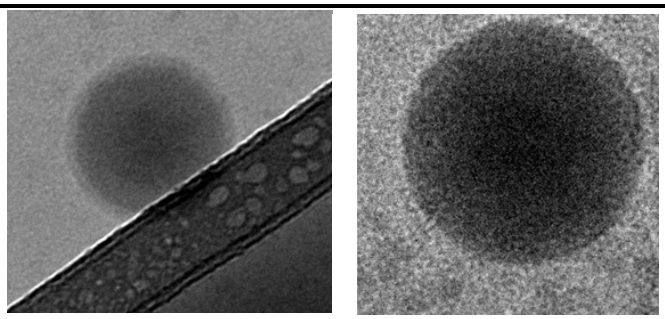

ABC **BAC**

Figure 5: Exemplary cryo-TEM images of multicompartment micelles formed from **ABC** (left) and **BAC** (right) triblock copolymers. Both triblock copolymers form "onions" with a hydrophilic corona, lipophilic shell, and fluorophilic core. Scale bar =100 nm.

Computational Method Development of Miscibility Analysis for Block Copolymer Systems

The multicompartment micelle nanoreactor heavily relies on the ability to tune the miscibility between blocks in block copolymers to tailor reactant and product diffusion through the micelle

layers. Moreover, to achieve the multicompartment nature of the nanoreactor, different micelle layers must be mutually immiscible. With all of this in mind, the ability to determine the miscibility of a given pair of molecules in the multicompartment micelle is clearly an attractive prospect. To this end, the Flory-Huggins interaction parameter χ quantifies the favorability of mixing between two polymers. This interaction parameter depends on many process conditions, not least of which are the temperature and composition of a solution, to properly estimate the intensity of the interaction between a given pair of polymer blocks. Unfortunately, traditional experimental techniques to determine this parameter are fraught with shortcomings.

Previous experimental works that measured the χ-parameter (e.g., by inverse gas chromatography, differential scanning calorimetry, or small-angle neutron scattering) have exposed significant uncertainty, necessitating very precisely known experimental conditions. Even when such precision is possible, the requisite data (Hildebrand or Hansen solubility parameters, cohesive energy densities, etc.) are not always known accurately, if at all.

Due to the many limitations of experimental techniques, we have developed a robust temperature-sensitive model for calculating the χ-parameter for a given pair of molecules via computational simulations. Although this is based in part on existing theories (specifically, density functional theory, molecular dynamics simulation, and Flory-Huggins solution theory), we have established a method of normalizing the interaction energies using the volume enclosed by the Connolly surface, thereby creating an interaction energy density that is analogous to, but distinct from, the cohesive energy density. Our results demonstrate that this method is a viable and systematic way to consistently estimate polymer miscibility from molecular simulations.

We have performed miscibility analyses on a group of molecules proposed by the Weck group. The specific molecules investigated are shown in Figure 6, where both the monomers and small molecules with nearly equal Connolly volumes are shown. Results from these simulations are exhibited in Figure 6. The results in Figure 6 have been confirmed via cryo-TEM. It is worth noting that several trends are evident in all of the studies performed on the miscibility of species A, B, and C. Principally, it is clear that B-C is always the least immiscible pairing, and in fact it is miscible in every study except for the case of monomers with dielectric screening, where the interactions between these species are shielded by the dielectric medium. By contrast, A-B and C-A are extremely immiscible, leading to distinct nanophase separation in these pairings.

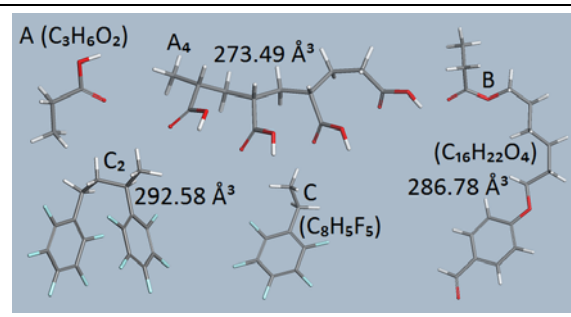

Figure 6. Species A (propionic acid), B (6-(4-formylphenoxy)hexyl propionate), and C (1-ethyl-2,3,4,5,6-pentafluorobenzene), as used in the micelle miscibility study.

Additionally, it should be noted that in both cases, the magnitude of the χ-parameter is significantly higher when dielectric screening is not present, which is to be expected. From this, it should be evident that while it is not necessary to perform time-consuming and computationally intensive explicit solvation modeling to probe miscibility, it is essential to give careful consideration of the implicit solvent effects to correctly replicate the behavior of the polymer system.

Many advantages of our approach over traditional experimental and theoretical methods are apparent from the results presented herein. One of the foremost strengths lies in the reproducibility of the results. In the majority of the cases considered here, the χ-parameter can be determined with remarkable precision, delivering consistent values across several independent simulation runs.

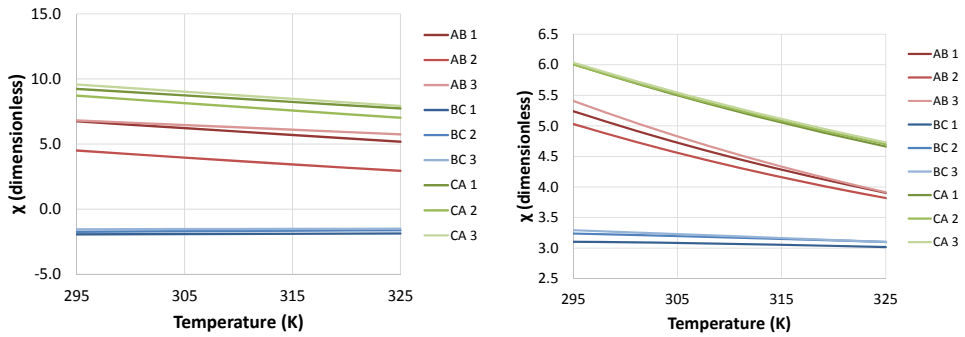

Figure 8. Miscibility data for (a) the monomer pairings and (b) the equal-volume pairings. In both cases, dielectric screening was considered by polar media which is water in this study. Lines which share a color correspond to independent runs of the same calculation to test the consistency of the results (e.g., the blue lines all correspond to B-C calculations).

Moreover, these values have been verified by experimental techniques, which demonstrate the accuracy of this method in comparison to the previous computational methods. Finally, performing miscibility analysis via computational methods offers a straightforward way to enhance the precision of a particular result: by increasing the number of samples and extending the number of repeat units of a molecule in a calculation, the spread in χ-values can be drastically reduced.

Publications Acknowledging this Grant in 2015-2017

Category 1: Sole funding from DOE-BES and this Specific Grant

1. "Co-Salen Complexes as Catalysts for the Asymmetric Henry Reaction - Reversed Enantioselectivity through Simple Ligand Modification." J. Dimroth; M. Weck; *RSC Adv.* **2015**, 5, 29108-29113.

2. "Reaction-Dependent Heteroatom Modification of Acid-Base Catalytic Cooperativity in Aminosilica Materials." E. Moschetta; N.A. Brunelli; C.W. Jones; *Appl. Catal. A. Gen.* **2015**, 504, 429-439.

3. "Post-Grafting Amination of Alkylhalide-Functionalized Silica for Applications in Catalysis, Adsorption and ^{15}N NMR Spectroscopy." E.M. Moschetta; M.A. Sakwa-Novak; J.L. Greenfield; C.W. Jones; *Langmuir* **2015**, 31, 2218-2225.

4. "Co(III) Complexes of Tetradentate X_3L Type Ligands: Synthesis, Electronic Structure, and Reactivity." Y. Feng; L. Burns; L.-C. Lee; C.R. Murdock; C.D. Sherrill; C.W. Jones; *Inorg. Chim. Acta* **2015**, 430, 30-35.

5. "Spatial Arrangement and Acid Strength Effects on Acid-Base Cooperatively." J. Lauwaert; E.M. Moschetta; P. van der Voort; J. Thybaut; C.W. Jones; G. B. Marin; *J. Catal.* **2015**, 325, 19-25.

6. "Molecular Dynamics Simulation Study of Sodium Dodecyl Sulfate Micelle: Water Penetration and Sodium Dodecyl Sulfate Dissociation." B.J. Chun; J.I. Choi; S.S. Jang; *Colloids Surf. A* **2015**, 474, 36-43.

7. "Characterization of Molecular Association of Poly(2-oxazoline)s-based Micelles with Various Epoxides and Diols via the Flory-Huggins Interaction Parameter: A Molecular Dynamics Simulation Approach." B.J. Chun; J. Lu; M. Weck; S. S. Jang; *PhysChemChemPhys* **2015**, 17, 29161-29170.

8. "Compartmentalization of Non-orthogonal Catalytic Transformations for Tandem Catalysis." J. Lu; J. Dimroth; M. Weck; *J. Am. Chem. Soc*. **2015**, 137, 12984-12989.

9. "Characterization of Molecular Association of Poly(2-oxazoline)s-based Micelles with Various Epoxides and Diols via the Flory-Huggins Theory: A Molecular Dynamics Simulation Approach." B. J. Chun; J. Lu; M. Weck; S.S. Jang; *Phys. Chem. Chem. Phys.* **2015**, 17, 29161-29170.

10. "Molecular Dynamics Simulation Study of Sodium Dodecyl Sulfate Micelle: Water Penetration and Sodium Dodecyl Sulfate Dissociation." B. J. Chun; J. I. Choi; S. S. Jang; *Colloids Surf. A*. **2015**, 474, 36-43.

11. "Kinetic and Mechanistic Examination of Acid-Base Bifunctional Aminosilica Catalysts in Aldol and Nitroaldol Condensations." V.E. Collier; N.C. Ellebracht; G. I. Lindy; E.G. Moschetta; C.W. Jones; *ACS Catal*. **2016**, 6, 460-468.

12. "Acid-Base Bifunctional Shell Cross-Linked Micelle Nanoreactor for One-Pot Tandem Reaction." L. -C. Lee; J. Lu; M. Weck; C.W. Jones; *ACS Catal.* **2016**, 6, 784-787.

13. "Dissipative Particle Dynamics Simulation Study of Poly(2-Oxazoline)-based Multicompartment Micelle Nanoreactor." B.J. Chun; C.C. Fisher; S.S. Jang; *PhysChemChemPhys* **2016**, 18, 6284-6290.

14. "Micelle-based Nanoreactors Containing Ru-porphyrin for the Epoxidation of Terminal Olefins in Water." J. Lu; L. Liang; M. Weck; *J. Mol. Catal. A Chem*. **2016**, 417, 122-125.

15. "Dissipative Particle Dynamics Simulation Study of Poly(2-Oxazoline)-based Multicompartment Micelle Nanoreactor." B. J. Chun; C.C. Fisher; S.S. Jang; *Phys. Chem. Chem. Phys.* **2016**, 18, 6284-6290.

16. "Molecular Dynamics Simulations of Aldol Condensation Catalyzed by Alkylamine-Functionalized Crystalline Silica Surfaces." K.C. Kim; E.M. Moschetta; C.W. Jones; S.S. Jang; *J. Am. Chem. Soc*. **2016**, 138, 7664-7672.

17. "Bifunctional Polymer Architectures for Cooperative Catalysis: Tunable Acid-Base Polymers for the Aldol Condensation." C.B. Hoyt; L.-C. Lee; A. E. Cohen; M. Weck; C.W. Jones; *ChemCatChem* **2017**, 9, 137-143.

Aaron D. Sadow

Interfacial Single Site Catalysts in 3D Environments

Aaron D. Sadow, Marek Pruski, Igor Slowing
Ames Laboratory, U.S. DOE, Iowa State University, Ames, IA 50011-3111

Presentation Abstract

The Ames Laboratory collaborative research project brings together the best features of homogeneous and heterogeneous catalysis to understand interfacial effects on structure, mechanism, and efficacy and ultimately enable the design of catalysts with molecular-scale control of conversions. Our approach combines expertise in mesoporous catalyst synthesis, organometallic chemistry, mechanisms of catalytic reactions, and solid-state (SS)NMR spectroscopy. In this presentation, we will discuss synthesis, characterization, and catalytic properties of single-site organometallic catalysts (surface organometallic chemistry) grafted on mesoporous silica nanoparticles, applied in the reduction of oxygenates and in C–N bond formations.[1, 2] To characterize surface catalytic sites, we have prepared new molecular, SiH-containing silazido rare earth compounds and correlated their spectroscopic features, structural properties, and coordination environment. Key data, including one-bond SiH coupling constants ($^1J_{SiH}$) in NMR spectra and SiH stretching frequencies (ν_{SiH}) in IR spectra provide a means for establishing coordination geometry of surface species. Comparison of selectivity in diastereoselective hydroamination reactions between homogeneous and grafted catalytic sites provide an addition handle for identifying the coordination geometry of active sites.[3] We have also found that solvent affects the surface site loading and secondary reactions that may occur during grafting, as assayed by dynamic nuclear polarization (DNP)-enhanced and conventional SSNMR spectroscopy. We also show that despite their oxophilicity, early metal and rare earth single-site catalysts are effective in the reduction of oxygen-containing species through hydroboration and hydrosilylation.

References

1. Eedugurala, N.; Wang, Z.; Chaudhary, U.; Nelson, N.; Kandel, K.; Kobayashi, T.; Slowing, I. I.; Pruski, M.; Sadow, A. D., Mesoporous Silica-Supported Amidozirconium-Catalyzed Carbonyl Hydroboration. *ACS Catal.* **2015**, *5*, 7399-7414. doi: 10.1021/acscatal.5b01671.

2. Eedugurala, N.; Wang, Z.; Yan, K.; Boteju, K. C.; Chaudhary, U.; Kobayashi, T.; Ellern, A.; Slowing, I. I.; Pruski, M.; Sadow, A. D., β-SiH-Containing Tris(silazido) Rare-Earth Complexes as Homogeneous and Grafted Single-Site Catalyst Precursors for Hydroamination. *Organometallics* **2017**, *36*, 1142-1153. doi: 10.1021/acs.organomet.6b00956.

3. Manna, K.; Eedugurala, N.; Sadow, A. D., Zirconium-Catalyzed Desymmetrization of Aminodialkenes and Aminodialkynes through Enantioselective Hydroamination. *J. Am. Chem. Soc.* **2015**, *137*, 425-435. doi: 10.1021/ja511250m.

Catalysis in Confined Spaces

F. Dean Toste
Chemical Sciences Division, Lawrence Berkeley National Laboratory and Department of Chemistry, University of California, Berkeley, CA

Presentation Abstract

For several years, in collaboration with the Raymond and Bergman labs, we have been exploring organic and organometallic reactions that occur in the confined space of self-assembled water-soluble tetrahedral M_4L_6 clusters. For example, cationic phosphinegold(I) complexes encapsulated by an anionic Ga_4L_6 tetrahedral demonstrated higher turnover numbers, rate acceleration and/or produced different products compared to the unencapsulated catalysts. This lecture will focus on our most recent studies of reactions promoted by encapsulation in these supramolecular hosts, induced thermally and/or photochemically, and the mechanisms of these reactions.

Grant or FWP Number: DE-AC02-05CH11231, **FWP** No. CH030201

PI: John Hartwig
Postdoc(s): Trandon Bender
Student(s): Cynthia Hong, Mariko Morimoto, Rebecca Triano, Charles Winslow,

RECENT PROGRESS

The *tris*-bidentate coordination of the catecholate ligands at metal vertices in $[Ga_4L_6^{12-}]$ makes each vertex a stereocenter that is mechanically coupled to the other vertices in the assembly. Therefore, the preparation of the assembly produces a racemic mixture of two homochiral enantiomeric forms (i.e. ΛΛΛΛ-M_4L_6 and ΔΔΔΔ-M_4L_6). While resolution of the racemate had been accomplished, we recently achieved a significant breakthrough in the direct synthesis of enantiopure assamblies by using terephthalamide-based ligand bearing a chiral amide substituent. Compared to the original assemblies, these new amide-substituted assemblies displayed greater stability towards air oxidation and acidic (low pH) solutions. Importantly, the enantiomerically enriched tetrahedral assembly served as an efficient catalyst for asymmetric organic transformations of both cationic (e.g. Aza-Cope rearrangement and the ring-opening of an episulfonium ion by an external nucleophile) and, for the first time, neutral substrates (Prins-type carbonyl-ene cyclization). The Prins cyclization was also employed as a platform to examine the impact of host structure on reactivity and selectivity. To this end, the catecholate-based ligands were modified both at the catechol (ortho-amide substitution) and at the naphthalene spacer (pyrene substitution). Changes in the chelating catecholate portion produced large and tunable variations in the reaction rates (rate acceleration 10^4-10^5), but not in the product selectivity. In contrast, replacing the naphthalene with the larger pyrene-based spacer engendered substrate-dependent variations on diastereo- and enantioselectivity. These observations provide an initial

demonstration of the impact of size and shape of confined catalytic active sites on reactivity and selectivity.

Several new transformations and modes of reactivity catalyzed by the [$Ga_4L_6^{12-}$] assembly were discovered during the past three years. Transformations within the confined space of the assembly occurred with selectivities and outcomes that have not been achieved in bulk solution. For example, we reported that substitution reactions catalyzed by the tetrahedral assembly proceeded with overall retention of configuration. This retention contrasts sharply with the inversion of configuration observed when the same solvolytic displacement reaction was performed in solution. Similarly, the aza-Prins cyclization catalyzed by the supramolecular assembly of 5-aminoalkenes and formaldehyde proceeded through a mechanism terminated by a 1,5-hydride shift instead of the direct trapping by water that occurs in bulk solution. The divergent selectivity was posited to arise from constrictive binding of the substrate (transition state) in the confined space within the supramolecular catalyst.

In addition, we discovered that the tetrahedral cages absorb light and use this energy to induce reactions of encapsulated guests. Mechanistic studies suggest that the photoexcited bridging group of the supramolecular assembly donates electrons to bound guests via photoinduced electron transfer (PET). The hypothesis that PET occurs was supported by transient absorption spectroscopy and electrochemical measurements. Using this platform, cinnamyl ammonium substrates underwent a 1,3-rearrangement to form the thermodynamically unfavored product. This reactivity is available only through supramolecular photochemistry in which confinement prevents separation of the amine and allyl cation intermediates, allowing them to recombine to afford the overall rearranged product.

We have previously demonstrated that cationic transition-metal complexes are readily encapsulated by the anionic, supramolecular , tetrahedral Ga_4L_6 host in water. In addition, we showed that the encapsulated complexes are more efficient catalysts in some cases than those in bulk solution. For example, the rate of gold-catalyzed intramolecular hydroalkoxylation of allenes increased 8.7 fold when the encapsulated cationic phosphinegold(I) complex was used as the catalyst. Based on these initial findings, we studied encapsulated phosphineAu(I) complexes as catalysts for a variety of one-pot tandem reactions in which one step is catalyzed by esterases and lipases. In the past year, we demonstrated that supramolecular catalysis can be leveraged to enable new processes mediated by transition metals, through catalysis of individual events in a catalytic cycle. It was discovered that the Ga_4L_6 supramolecular tetrahedra catalyzed alkyl-alkyl reductive elimination from gold(III) and platinum(II) complexes. Moreover, the observed rate acceleration of 1.9×10^7 fold relative to background for reductive elimination from dimethylgold(III) complexes was the largest observed for a synthetic microenvironment catalyst. Subsequently, this property was leveraged to create a cross coupling reaction employing both a platinum catalyst and a nanovessel-based catalyst, in which both the cluster and a platinum precatalyst were necessary for efficient turnover.

Redox-Based Reagents for Chemoselective Methionine Bioconjugation

The LBNL catalysis group also has sought methods to create new structures in which a catalyst component can be embedded in a biological milieu. To this end, Chang and Toste have sought methods for the bioconjugation of chemicals to cells and individual enzymes. Often, such bioconjugation is conducted with a cysteine owing to its nucleophilicity, but tethering chemicals through these thiols can inhibit the function of the protein. In contrast to the substantial body of literature on cysteine bioconjugation, analogous methods for methionine labeling under physiological conditions remain largely underdeveloped. A major chemical challenge in

developing a selective methionine modification reaction under pH-neutral physiological conditions is its relatively weak nucleophilicity, which precludes identifying an appropriate methionine-specific electrophilic partner in the presence of competing, more nucleophilic amino acids. As such, twe developed a strategy for bioconjugation to methionine that explits the redox reactivity and reported a method, termed Redox Activated Chemical Tagging (ReACT) that enables chemoselective methionine bioconjugation in proteins and proteomes.

Metal Nanoparticles Catalyzed Selective Carbon-Carbon Bond Formation Activation in the Liquid Phase

Encapsulated heterogeneous catalysts are unusual, and a collaboration between Toste and Somojai has led to system in which encapsulation of heterogeneous catalysts in organic polymers allows reactions of nanoparticles on soluble substrates in solution. As an example, ring-opening reactions of cyclopropane derivatives were conducted under hydrogen catalyzed by metal nanoparticles (NPs) in the liquid phase catalyzed by 40-atom rhodium (Rh) NPs, encapsulated by dendrimer molecules and supported in mesoporous silica under hydrogen. The turnover frequency (TOF) was higher than that of other metals or the Rh homogeneous catalyst counterparts. The generation of the dendrimer and surface group also affected the reaction rate and activation energy.

Mapping Catalytic Reaction Sites with High Spatial Resolution using AFM-IR.

In collaboration with Prof. Elad Gross (Hebrew University). we mapped the site-dependent reactivity of Pt atoms using synchrotron-sourced IR nanomicroscopy (Figure 5). Chemically-active self-assembled molecules (N-heterocyclic carbenes), with a functional hydroxyl group were anchored to the nanoparticle's surface. The oxidation of the functional -OH group from alcohol into acid and its reversible reduction back alcohol on different surface sites were monitored under oxidizing and reducing conditions, respectively. This method provided nanometer (20-25nm) resolution catalyst sites and allowed for observation that low coordinated Pt atoms located along the nanoparticle's perimeter are more catalytically-active than Pt atoms found on the flat surface of the nanoparticle. The technique was also applied to study nitro-reduction on the surface of gold nanoparticle catalysts.

Publications Acknowledging this Grant in 2014-2017

(I) Exclusively funded by this grant;

- Hong, C. M.; Kaphan, D. M.; Bergman, R. G. Raymond, K. N.; Toste, F. D.; *J. Am. Chem. Soc.* **2017**, *139,* 8013.
- Ye, R.; Zhao, J.; Yuan, B.; Liu, W.-C.; De Araujo, J. R.; Fuacher, F. F.; Chang, M.; Toste, F. D.; Somorjai, G. A.; *Nano. Lett.* **2017**, *17*, 584.
- Wu, C.-Y.; Wolf, W. J.; Levratovsky, Y.; Bechtel, H. A.; Martin, M. C.; Toste, F. D.; Gross, E.; *Nature*, **2017**, *541*, 511.
- Levin, M. D.; Kaphan, D. M.; Hong, C. M.; Bergman, R. G.; Raymond, K. N.; *J. Am. Chem. Soc.,* **2016**, *138*, 9775.
- Ye, R.; Yuan, B.; Zhao, J.; Ralston, W. T.; Wu, C.-Y.; Barin, E.-U.; Toste, F. D.; Somorjai, G. A. *J. Am. Chem. Soc*. **2016**, *138*, 8533.
- Hart-Cooper, W. M.; Sgarlata, C.; Perrin, C. L.; Toste, F. D.; Raymond, K. N.; Bergman, R. G. *Proc. Natl. Acad. Sci.,* **2015**, *112*, 15303.
- Kaphan, D. M.; Levin, M. D.; Bergman, R. G.; Raymond, K. N.; Toste, F. D; *Science* **2015**, *350*, 1235.

- Dalton, D. M.; Ellis, S. R.; Nichols, E. M.; Mathies, R. A.; Toste, F. D.; Raymond, K. N.; Bergman R. G.; *J. Am. Chem. Soc.* **2015**, *137*, 10128.
- Kaphan, D. M.; Toste, F. D.; Bergman, R. G.; Raymond, K. N.; *J. Am. Chem. Soc.,* **2015**, *137*, 9202.
- Shu, X-Z.; Nguyen, S. C.; He, Y.; Oba, F.; Zhang, Q.; Canlas, C.; Somorjai, G. A.; Alivisatos, A. P.; Toste, F. D.; *J. Am. Chem. Soc.* **2015**, *115*, 7083.
- Brown, C.; Toste, F. D.; Bergman, R. G.; Raymond, K. N. *Chem. Rev*. **2015**, *115*, 3012.
- Hart-Cooper, W. M.; Zhao, C.; Triano, R. M.; Yaghoubi, P.; Haxel, L.; Buford, K. N.; Toste, F. D.; Bergman, R. G.; Raymond, K. N. *Chem. Sci.* **2015**, *6*, 1383.
- Gross, E.; Toste, F. D.; Somorjai, G. A. *Catal. Lett.* **2015**, *145*, 126.
- Zhao, C.; Toste, F. D.; Raymond, K. N; Bergman, R. G. *J. Am. Chem. Soc*. **2014**, *136*, 14409.
- Shu, X.-Z.; Zhang, M; He, Y.; Frei, H.; Toste, F. D. *J. Am. Chem. Soc.*, **2014**, *136*, 5844.
- Zhao, C.; Crimmin, M. R.; Toste, F. D.; Bergman, R. G. *Acc. Chem. Res*., **2014**, *47*, 517.
- Gross, E.; Shu, X.-Z.; Alayoglu, S.; Bechtel, H. A.; Martin, M. C.; Toste, F. D.; Somorjai, G. A. *J. Am. Chem. Soc.* **2014**, *136*, 3624.
- Zhang, Q.; Shu, X.-Z.; Lucas, J. M.; Toste, F. D.; Somorjai, G. A.; Alivisatos, A. P. *Nano Lett.* **2014**, *14*, 379.

(II) Jointly funded by this grant and other grants with leading intellectual contribution from this grant;

- Zhao, J.; Nguyen, S. C.; Ye, R.; Ye, B.; Weller, H.; Somorjai, G. A.; Alivisatos, A. P.; Toste, F. D. *ACS Central. Sci.* **2017**, *3*, 482-488.
- Lin, S.; Yang, X.; Jia, S.; Weeks, A. M.; Hornsby, M.; Lee, P. S.; Nichiporuk, R. V.; Iavarone, A. T.; Wells, J. A.; Toste, F. D.; Chang, C. J. *Science* **2017**, *355*, 597-602.

(III) Jointly funded by this grant and other grants with relatively minor intellectual contribution from this grant;

- K. A. Goulas, S. Sreekumar, Y. Song, P. Kharidehal, G. Gunbas, P. J. Dietrich, G. R. Johnson, Y. C. Wang, A. M. Grippo, L. C. Grabow, A. A. Gokhale, F. D. Toste, *J. Am. Chem. Soc.* **2016**, *138*, 6805.
- Balakrishnan, M.; Sacia, E. R.; Sreekumar, S.; Gunbas, G.; Gokhale, A. A.; Scown, C. D.; Toste, F. D.; Bell, A. T. *Proc. Natl. Acad. Sci*. **2015**, *112*, 7645.

Tuning the Electrochemical Activity of Layered, Nonstoichiometric Metal Oxides for Oxygen Reduction/Evolution: Effect of Surface Termination and Composition

XiangKui Gu, Juliana Carnerio, Anirban Das and Eranda Nikolla
Department of Chemical Engineering and Materials Sciences, Wayne State University, Detroit, Michigan-48202 (USA)

Nonstoichiometric, mixed ionic-electronic conducting oxides, such as the first Ruddlesden-Popper (R-P) series of layered oxides (A_2BO_4), have attracted increasing interest because of their high oxygen exchange ability that makes them suitable for many electrocatalytic energy conversion and storage applications involving oxygen evolution and reduction. Surface oxygen exchange is the process that governs oxygen reduction and evolution on these oxides. We have recently shown through a combination of quantum chemical density functional theory (DFT) calculations, controlled synthesis of well-defined nanostructures, state-of-the-art characterization techniques (atomic level imaging and electron energy loss spectroscopy), and isotopic labeling kinetic studies that the surface structure of these oxides plays a critical role in their surface oxygen exchange activity. Using a reverse micro-emulsion method, we have demonstrated an approach for synthesizing nanostructured R-P oxide electrocatalysts with controlled surface structure. These nanostructures are thoroughly characterized using atomic-resolution high angle annular dark field (HAADF) imaging along with electron energy-loss spectroscopy (EELS) performed using an aberration corrected scanning transmission electron microscope (STEM). Controlled kinetic isotopic and electrochemical studies are used to develop structure/performance relationships to identify R-P oxides with optimal electrocatalytic activity. These findings pave the way for utilization of nanostructured, layered, nonstoichiometric metal oxides as non-precious metal-based electrocatalysts for oxygen reduction and evolution.

DE-SC0014347: Nanostructured, Targeted Layered Metal Oxides as Active and Selective Heterogeneous Electrocatalysts for Oxygen Evolution

PI: Eranda Nikolla
Postdoc(s): XiangKui Gu and Anirban Das
Institution: Wayne State University, Detroit, MI

RECENT PROGRESS

First Principles studies of the facts that govern oxygen reduction/evolution on R-P oxides

We have employed density functional theory (DFT) calculations to investigate the underlying factors that control the activity of first-series R-P oxides toward surface oxygen exchange (Figure 1). We have focused on the effects of the A- and B-site composition and surface termination on

the energetics of the elementary steps associated with this process. A microkinetic modeling analysis is used to develop activity trends. A "volcano"-type relationship between the calculated rates and the binding energies of O_2 on a surface oxygen vacancy for the different R-P oxides is found, suggesting that this O_2 binding energy is a good activity descriptor for these materials. We show that among the terminations and compositions considered, Co-oxide terminated La_2CoO_4 exhibits an optimal O_2 binding strength on a surface oxygen vacancy that allows for the best compromise between the energetics associated with oxygen vacancy formation and O_2 dissociation, thus resulting in the highest rates. In general, we find that A-site doping of R-P oxides leads to low oxygen exchange rates.

Synthesis and catalytic activity of controlled nanostructured R-P oxide electrocatalysts

Undoped $La_2NiO_{4+\delta}$ (LNO) and Fe, Co, and Cu-doped nanostructured lanthanum nickelate oxides ($La_2Ni_{0.88}Fe_{0.12}O_{4+\delta}$ (Fe-LNO), $La_2Ni_{0.88}Co_{0.12}O_{4+\delta}$ (Co-LNO), and $La_2Ni_{0.80}Cu_{0.20}O_{4+\delta}$ (Cu-LNO), respectively) have been synthesized using a facile reverse micro-emulsion method. The crystal structures of the synthesized oxides (Co-LNO, Cu-LNO, Fe-LNO and LNO) are analyzed using powder X ray diffraction (XRD) and the spectra are compared with that of the standard bulk LNO, which has a K_2NiF_4 structure within the I4/mm space group. The morphology of the LNO and B-site doped LNO nanostructures is analyzed using scanning electron microscopy showing predominantly nanorod-shaped geometry for all the synthesized oxides. Surface structure characterization of these synthesized nanostructures is imperative for proper development of structure-function relations. Characterization of the surface is conducted using HR-STEM-HAADF, LEIS and EDS elemental mapping. These studies confirm the termination of the nanostructures by (001) transition metal oxide surfaces. The activity toward surface oxygen exchange was determined using $^{18}O_2$ labeled isotopic experiments on these nanostructured R-P oxides. Among all the catalysts tested, Co-LNO displayed the best performance for the surface oxygen exchange process in terms of the lowest apparent activation energy and highest normalized rates (TOFs) at a particular temperature as compared to the other catalysts. The experimental results indicate that the activity trend for thermochemical surface oxygen exchange follows: Co-LNO> Fe-LNO > LNO > Cu-LNO; consistent with the DFT predictions. To evaluate the potential of the Ni-site doping on improving the electrochemical activity of the R-P oxides toward electrochemical oxygen reduction, the most catalytically active nanostructured Co-doped LNO is tested, and compared to LNO nanorods using button cell geometry SOFCs. In these experiments, we have used an anode-supported SOFCs (Ni – YSZ (anode)|YSZ (electrolyte)|YSZ – R-P oxides (cathode)), where the anode is exposed to pure hydrogen (50 ml min^{-1}) and the cathode to atmospheric air. In these cells, the O_2 molecules are reduced ($1/2\ O_2 + 2e^- \Rightarrow O^{2-}$) on the R-P oxide at the cathode generating oxygen ions (O^{2-}), which are transported through the YSZ electrolyte to the anode, where H_2 electro-oxidation ($H_2 + O^{2-} \Rightarrow H_2O + 2e^-$) takes place. The electrochemical performance results suggest that doping the Ni-site of nanostructured LNO with Co leads to significant improvement in the overall cell performance at both temperatures. The power densities of the cells containing Co-doped LNO are ~ 50% higher than the ones with LNO nanorods. No significant changes are observed in the crystal structure of the Co-doped LNO nanorods after electrochemical studies, suggesting that doping the B-site of LNO with small concentration of Co enhances the oxygen reduction activity of the lanthanum nickelate oxide without compromising stability.

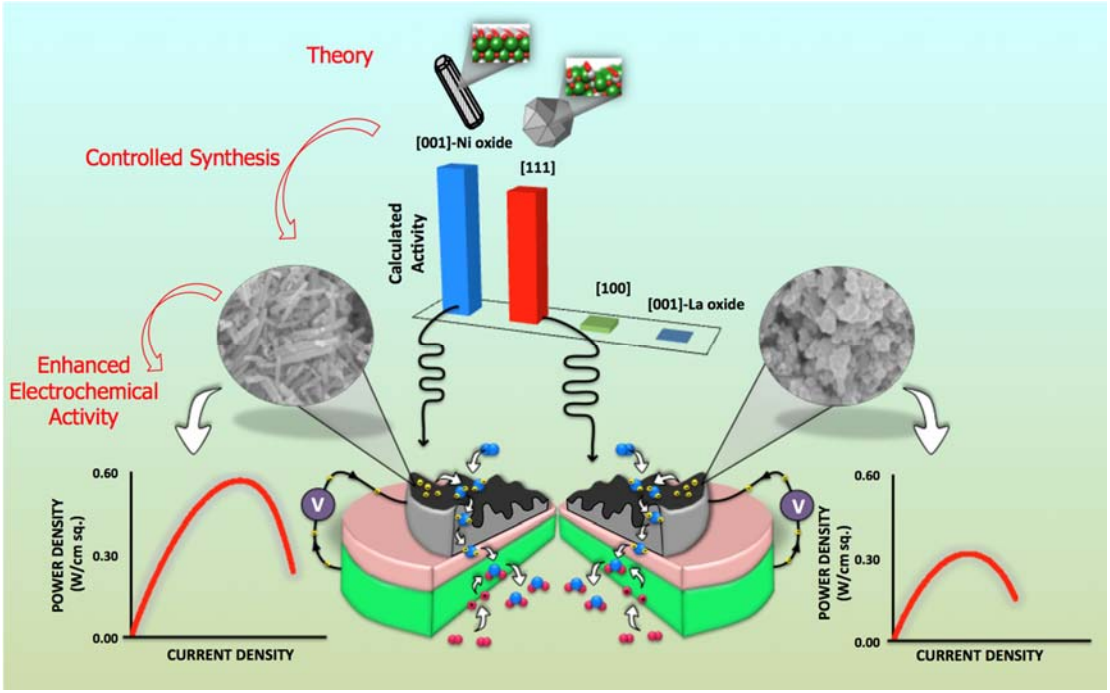

Figure 1: Schematic of the combined experimental/theoretical approach used to engineer R-P oxide electrocatalysts for oxygen reduction/evolution.

Publications Acknowledging this Grant in 2014-2017

(IV) Exclusively funded by this grant;

1. Gu X.; Carneiro, J. S. A.; Das, A.; Ariyasingha, N.; Nikolla E.; "Design Principles for Tuning the Activity of Mixed Metal Oxides for High Temperature Electrochemical Oxygen Reduction", under review (2017).
2. Gu X.; Nikolla E.; "Design of Ruddlesden-Popper Oxides with Optimal Surface Oxygen Exchange Properties for Oxygen Reduction and Evolution from First Principles", ***ACS Catalysi***s, under review (2017).
3. Das A.; Xhafa E.; Nikolla E. "Electro- and thermal-catalysis by layered, first series Ruddlesden-Popper oxides", ***Catal. Today - Special Issue on "Catalysis by Mixed Oxides"***, 277 (2016) 214.

Catalytic Growth of Molecular Scale Wiring

Colin Nuckolls
Columbia University, Department of Chemistry

This DOE funding has been essential in developing an important class of new materials—nanostructured carbon. While carbon nanostructures (e.g. fullerenes, carbon nanotubes, and graphene) gather an enormous amount of scientific attention, they are currently limited by the chemistry that is used to synthesize, functionalize, position, and pattern them. The underpinning of this grant is development of new catalytic methods to synthesize nanostructured forms or carbon, methods to use them in highly efficacious electronic and optoelectronic devices, and the plans to use these nanostructured forms of carbon as catalysts themselves.

There are three primary goals of this project: (1) To develop the catalytic the methods to create nanostructured forms of carbon such as graphene ribbons and macrocycles; (2) To study nanostructured forms of carbon as electronic and electronic devices of interest to the DOE; (3) To utilize these nanostructured forms of carbon's ability to accept, donate, and transfer electrons as a means to create new catalytic systems.

The two broad areas of accomplishment that will be presented are: (A) in developing the chemistry to create long graphene ribbons that have utility as electron acceptors in photodetector and photovoltaic devices; (B) in developing the chemistry to create cyclic, conjugated forms of nanocarbon and studying their utility in photodetector and photovoltaic devices. These two areas are highlighted below.

DE-FG02-01ER15264: Catalytic Growth of Molecular Scale Wiring

Postdoc(s): Thomas Sisto
Student(s): Melissa Ball, Grisha Etkin, Nathaniel Schuster, Boyuan Zhang

RECENT PROGRESS

Long graphene ribbons as electron acceptors

Two recent publications in *The Journal of the American Chemical Society*[9,10] describe a new molecular design for the efficient synthesis of donor-acceptor, cove-edge graphene nanoribbons and their properties in solar cells. These nanoribbons are long (~5 nm), atomically precise, and soluble. Their structure is shown in Figure 1. The design is based on the fusion of electron deficient perylene diimide oligomers with an electron rich alkoxy pyrene subunit (Figure 1A). This strategy of alternating electron rich and electron poor units facilitates a visible light fusion reaction in >95% yield, while the cove-edge nature of these nanoribbons results in a high degree of twisting along the long axis. Studying this visible light cyclization will be a priority in the coming funding period. The rigidity of the backbone yields a sharp longest wavelength

absorption edge. These nanoribbons are exceptional electron acceptors, and organic photovoltaics fabricated with the ribbons show efficiencies of ~8% without optimization.

We built off of the studies described above and its molecular design to yield ultra-narrowband organic photodetectors. The design is based on the series of helically-twisted molecular ribbons we have developed in our DOE project. We fabricate charge collection narrowing photodetectors based on four different helical ribbons that differ in the wavelength of their response. The photodetectors made from these materials have narrow spectral response with full-width at half maxima of < 20 nm. The devices reported here are superior by approximately a factor of 5 to those from traditional organic materials due to the narrowness of their response. Moreover, the active layers for the helical ribbon-based photodetectors are solution cast but have performance that is comparable to the state-of-the-art narrowband photodetectors made from methylammonium lead trihalide perovskite single crystals. The ultra-narrow bandwidth for detection results from the helical ribbons' high absorption coefficient, good electron mobility, and sharp absorption edges that are defined by the twisted molecular conformation.

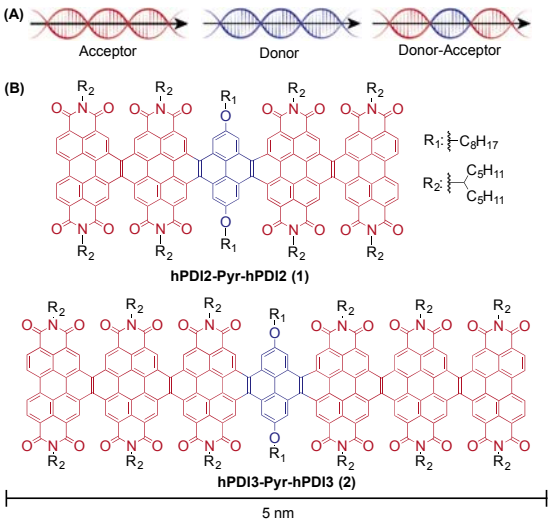

Figure 1. (A) Electron poor, electron rich, and donor-acceptor ribbons. (B) Two ribbons designed and synthesized here are hPDI2-Pyr-hPDI2 (1) and hPDI3-Pyr-hPDI3 (2).

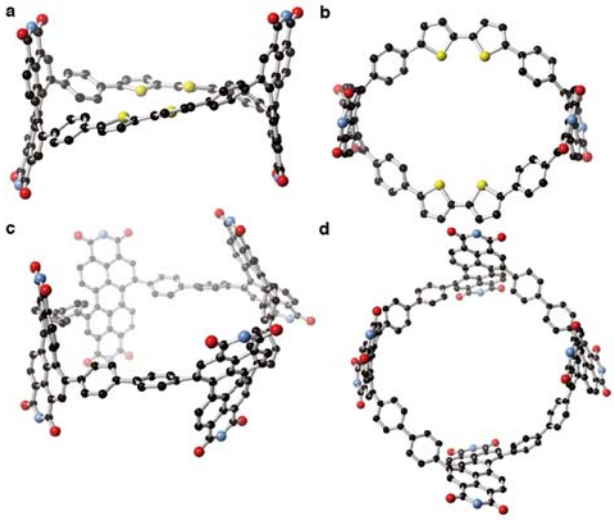

Figure 2. Macrocycles used to study the importance of conjugation and macrocyclizaton in organic devices. (a) Energy minimized structures from DFT for **cPBPB**. The (*S,S*)-stereoisomer is shown. (b) Cavity view of **cPBPB**. (c) Energy minimized structures from DFT for **cP$_4$**. The (*S,S,S,S*)-stereoisomer is shown. (d) Cavity view for **cP$_4$**. Carbon = gray, nitrogen = blue, oxygen = red, sulfur = yellow. Hydrogen atoms have been removed to clarify the view. A methyl group substitutes the sidechains in the calculations. The methyl group, too, has been removed to clarify the view in the structures presented here.

Cyclic, conjugated nanocarbon

In parallel with our studies on ribbons we have also been studying macrocycles that are conjugated. The methods to make these macrocycles are unique and provide an interesting avenue to study how to synthesize them through new catalytic methods. Moreover, we have had an important finding that will have vast implications: macrocyclization can be a strategy to produce new materials. These studies were detailed in two manuscripts in *The Journal of the American Chemical Society*.[3,8]

Under our DOE funding we have compared analogous cyclic (Figure 2) and acyclic π-conjugated molecules as n-type

electronic materials and find that the cyclic molecules have numerous benefits in organic photovoltaics (OPVs). This is the first report of such a direct comparison. We designed two conjugated cycles for this study. Each comprises four subunits; one combines four electron-accepting, redox-active, diphenyl-perylenediimide subunits, and the other alternates two electron-donating bithiophene units with two diphenyl-perylenediimide units. We compare the macrocycles to acyclic versions of these molecules and find that, relative to the acyclic analogs, the conjugated macrocycles have bathochromically shifted UV-vis absorbances and are more easily reduced. In blended films, macrocycle-based devices show higher electron mobility and good morphology. All of these factors contribute to the more than doubling of the power conversion efficiency observed in organic photovoltaic devices with these macrocycles as the n-type, electron transporting material. These results the importance of geometric design in creating new molecular semiconductors and will be of lasting importance. The ease with which we can design and tune the electronic properties of these cyclic structures charts a clear path to creating a new family of cyclic, conjugated molecules as electron transporting materials in optoelectronic and electronic devices.

Publications Acknowledging this Grant in 2014-2017

Please classify your publications into three categories according to the source of support for the work published:

(I) Exclusively funded by this grant

1. Ball, M.; Zhong, Y.; Wu, Y.; Schenck, C.; Ng, F.; Steigerwald, M.; Xiao, S.; Nuckolls, C. Contorted Polycyclic Aromatics. *Acc. Chem. Res.* **2014**, 141219065025003.
2. Ball, M.; Fowler, B.; Li, P.; Joyce, L. A.; Li, F.; Liu, T.; Paley, D.; Zhong, Y.; Li, H.; Xiao, S.; et al. Chiral Conjugated Corrals. *J. Am. Chem. Soc.* **2015**, *137*, 9982–9987.
3. Ball, M.; Zhong, Y.; Fowler, B.; Zhang, B.; Li, P.; Etkin, G.; Paley, D. W.; Decatur, J.; Dalsania, A. K.; Li, H.; et al. Macrocyclization in the Design of Organic N-Type Electronic Materials. *J. Am. Chem. Soc.* **2016**, *138*, 12861–12867.

(II) Jointly funded by this grant and other grants with leading intellectual contribution from this grant

4. Zhong, Y.; Trinh, M. T.; Chen, R.; Wang, W.; Khlyabich, P. P.; Kumar, B.; Xu, Q.; Nam, C.-Y.; Sfeir, M. Y.; Black, C.; et al. Efficient Organic Solar Cells with Helical Perylene Diimide Electron Acceptors. *J. Am. Chem. Soc.* **2014**, *136*, 15215–15221.
5. Chen, Q.; Trinh, M. T.; Paley, D. W.; Preefer, M. B.; Zhu, H.; Fowler, B. S.; Zhu, X.-Y.; Steigerwald, M. L.; Nuckolls, C. Strain-Induced Stereoselective Formation of Blue-Emitting Cyclostilbenes. *J. Am. Chem. Soc.* **2015**, *137*, 12282–12288.
6. Zhong, Y.; Trinh, M. T.; Chen, R.; Purdum, G. E.; Khlyabich, P. P.; Sezen, M.; Oh, S.; Zhu, H.; Fowler, B.; Zhang, B.; et al. Molecular Helices as Electron Acceptors in High-Performance Bulk Heterojunction Solar Cells. *Nat Commun* **2015**, *6*.

7. Choi, B.; Capozzi, B.; Ahn, S.; Turkiewicz, A.; Lovat, G.; Nuckolls, C.; Steigerwald, M. L.; Venkataraman, L.; Roy, X. Solvent-Dependent Conductance Decay Constants in Single Cluster Junctions. *Chem. Sci.* **2016**, *7*, 2701–2705.
8. Zhang, B.; Trinh, M. T.; Fowler, B.; Ball, M.; Xu, Q.; Ng, F.; Steigerwald, M. L.; Zhu, X.-Y.; Nuckolls, C.; Zhong, Y. Rigid, Conjugated Macrocycles for High Performance Organic Photodetectors. *J. Am. Chem. Soc.* **2016**, *138*, 16426–16431.
9. Sisto, T. J.; Zhong, Y.; Zhang, B.; Trinh, M. T.; Miyata, K.; Zhong, X.; Zhu, X.-Y.; Steigerwald, M. L.; Ng, F.; Nuckolls, C. Long, Atomically Precise Donor–Acceptor Cove-Edge Nanoribbons as Electron Acceptors. *J. Am. Chem. Soc.* **2017**, *139*, 5648–5651. (II)
10. Zhong, Y.; Sisto, T. J.; Zhang, B.; Miyata, K.; Zhu, X.-Y.; Steigerwald, M. L.; Ng, F.; Nuckolls, C. Helical Nanoribbons for Ultra-Narrowband Photodetectors. *J. Am. Chem. Soc.* **2017**, *139*, 5644–5647.

(III) Jointly funded by this grant and other grants with relatively minor intellectual contribution from this grant

11. Chen, Z.; Paley, D. W.; Wei, L.; Weisman, A. L.; Friesner, R. A.; Nuckolls, C.; Min, W. Multicolor Live-Cell Chemical Imaging by Isotopically Edited Alkyne Vibrational Palette. *J. Am. Chem. Soc.* **2014**, *136*, 8027–8033.
12. Hiszpanski, A. M.; Woll, A. R.; Kim, B.; Nuckolls, C.; Loo, Y.-L. Altering the Polymorphic Accessibility of Polycyclic Aromatic Hydrocarbons with Fluorination. *Chem. Mater.* **2017**, *29*, 4311–4316.
13. Gao, J.; Sengar, N.; Wu, Y.; Jockusch, S.; Nuckolls, C.; Clancy, P.; Loo, Y.-L. Contorted Octabenzocircumbiphenyl Sorts Semiconducting Single-Walled Carbon Nanotubes with Structural Specificity. *Chem. Mater.* **2017**, *29*, 595–604.

Thursday PI
Oral Presentations

Matteo Cargnello

Understanding and Tuning Catalytic Materials Using Nanocrystal Precursors

Matteo Cargnello, Joshua Willis, Emmett Goodman
Department of Chemical Engineering and SUNCAT Center for Interface Science and Catalysis, Stanford University, Stanford, CA

Presentation Abstract

Catalytic processes are central to the goal of a sustainable future. A promising approach in developing catalytic materials is represented by the design of catalytic sites based on the knowledge of reaction mechanisms and structure-property relationships and aided by computation, and in the precise synthesis of these sites at the atomic and molecular level. The materials-pressure gap, however, still hinder the full realization of this strategy. Nanocrystal precursors, with tunable active sites and compositions, can help bridge this gap. The goal of this talk is to show how this approach can provide not only fundamental understanding of catalytic reactions, but also represent a way to precisely engineer catalytic sites to produce efficient catalysts that are active, stable and selective for several important catalytic transformations. More in detail, I will briefly show our efforts in better understanding the mechanism of colloidal nanocrystal formation, to control their structure and composition at the nanometer level. I will then show the use of uniform monometallic Pd and bimetallic Pd/Pt catalysts to understand trends in methane combustion, and Ru catalysts for low-temperature methane conversion to syngas. In all these works, a strong connection to efforts in theory and structural characterization within SUNCAT has been crucial to obtain precious structure-property relationships. This knowledge is used to prepare more efficient catalysts for hydrocarbon activation and other processes for sustainable production of fuels and chemicals.

Grant or FWP Number: SUNCAT FWP

PI: Jens Nørskov
Student: Joshua J. Willis

Justin M. Notestein

Support Engineering: Quantifying and Controlling Nanostructured Oxide Surfaces

Zhenyu Bo[1], M. Alexander Ardagh[2], Scott L. Nauert[2], Nicholas E. Thornburg[2], Todd R. Eaton[2], Justin M. Notestein[2]
Northwestern University, Center for Catalysis and Surface Science and [1]Department of Materials Science Engineering or [2]Department of Chemical and Biological Engineering

Presentation Abstract

Mixed oxides are ubiquitous catalysts and catalyst supports. Oxide identity and physical structure are common handles for catalyst optimization, and with additional options from precursor identity (e.g. alkoxide or chloride, mononuclear or multinuclear) and synthesis strategy (e.g. atomic layer deposition, ALD), there are many opportunities for the synthesis of new or better-controlled catalytic structures. However, with this comes the explicit need to better understand their chemical identity at catalytically-relevant scales. This talk will discuss two research themes supported in our group as a part of the Institute for Catalysis in Energy Processes (ICEP) at Northwestern University. In the first part, we use phosphonic acids and a dihydroxyanthraquinone dye to quantify the number and strength of Lewis acid sites in MOx-SiO_2 catalysts for H_2O_2 activation and in CuO-MOx catalysts for oxidative dehydrogenation. In the second part, we build off this understanding of mixed oxide catalysts, and describe our group's approach to create thin layers of one oxide that can be tuned to fully or partially coat a primary oxide particle by templated sol-gel or ALD. In various contexts, these materials can exhibit unusual reactant shape selectivity, have strong Brønsted acidity, help isolate embedded Lewis sites, or provide a support for highly disperse metal nanoparticles, and several of these examples will be highlighted.

DE-FG02-03ER15457: Institute for Catalysis in Energy Processes (ICEP)

PI: Peter C. Stair[3] (lead)

Additional PIs: M. Bedzyk[1], L. Broadbelt[2], O. Farha[3], F. Geiger[3], J. Hupp[3], H. Kung[2], M. Kung[2], T. Lohr[3], L. Marks[1], T. Marks[3], S. Nguyen[3], J. Notestein[2], K. Poeppelmeier[3], G. Schatz[3], N. Schweitzer[2], R. Snurr[2], R. Van Duyne[3], E. Weitz[3]

Affiliations(s): Northwestern University, Center for Catalysis and Surface Science and [1]Department of Materials Science and Engineering or [2]Department of Chemical and Biological Engineering or [3]Department of Chemistry

RECENT PROGRESS

The overarching ICEP goal is to address the inhomogeneity challenge in heterogeneous catalysis, thereby leading to the creation of catalysts with unique types of active sites in an atom-precise

fashion. To achieve this advance we exploit novel catalytic structures and synthetic possibilities together with atomic-scale structural information and electronic properties with accuracies unattainable a decade ago. These are coupled to chemical and catalytic reaction experiments that are sensitive and instructive as to these properties. The ICEP team is organized into three complementary and interacting thrusts, each of which focuses on different classes of catalytic materials within this overall goal. Each thrust incorporates materials design, synthesis, characterization, modeling, and catalytic reaction experiments. Two to three recent achievements of each of three thrusts are briefly described below, focusing on new results or significant project expansions since the prior year.

Thrust I: ***Understanding and Control of Metal-Oxide Interfaces***

Here, catalysts are designed to better understand, control, and tune the catalytic properties of late transition metal nanoparticles, clusters and atoms. Epitaxial stabilization and overcoating and artificial SMSI via atomic layer deposition are used to obtain both high reactivity and stability.

A significant aspect of the ICEP effort is development of oxide supports with controlled shapes, surfaces, and compositions to test hypotheses about metal nanoparticle/support interactions. In the past year, **Poeppelmeier** and **L. Marks** have made available quantities of Ti-rich $SrTiO_3$ (001) and (110) faceted nanoparticles for experimentation as catalyst supports, enabling a move beyond proof-of-concept studies. Likewise, these investigators have synthesized high surface area $LnScO_3$ (Ln = lanthanide) particles, which appear to be dominated by pseudo-perovskite Sc-rich (001) faces, and are progressing towards faceted nanoparticles of $LnGaO_3$ as well as a route to probe the role of support lattice spacing in creating epitaxial stabilization of supported metal nanoparticles. This work includes modelling the thermodynamics and kinetics of the growth and correlating this with the atomic surface structure as well as the synthesis conditions. As an example of the use of these particles, **Bedzyk**, **L. Marks**, **Poeppelmeier** and **Stair** have explored support-induced metal nanoparticle shape control of Pd on TiO_2-rich surfaces of $SrTiO_3$ nanocuboids with (001) faces and nanodecahedra with (110) faces. Understanding these materials and their application in CO oxidation involved a combination of analytical approaches, aberration-corrected microscopy, and density functional methods.

In a second project area, **L. Marks**, **T. Marks**, and **Stair** explored organometallic grafting and oxide overcoating to prepare well-defined metal sites on high surface area supports. Single-atom Pt sites were prepared using deposition of the pincer complex (^{Ph}PCP)Pt-OH on Al_2O_3 (**Figure 1**), while highly dispersed, low-coordinate Pd clusters were synthesized by grafting the related Pd^{II} PCP-pincer complex (^{tBu}PCP)Pd-OH on SiO_2. The metals in these materials were stabilized by atomic layer deposition (ALD) of an oxide overcoat before calcination of the ancillary ligands and reduction, with TiO_2 and ZnO overlayers found to be more

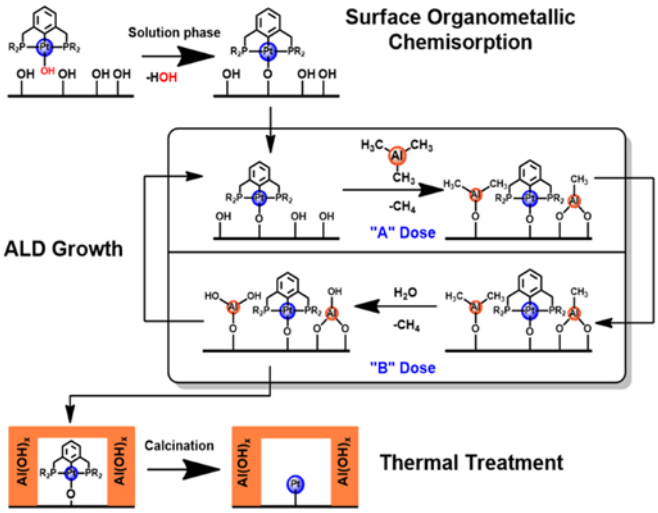

Figure 1. Overall schematic for proposed single Pt atom synthetic methodology combining surface organometallic chemisorption and ALD.

effective in stabilizing sites than were Al_2O_3 overcoats. In the case of the Pd catalysts, for example, CO DRIFTS showed a high fraction of linear CO adsorption sites, indicating low-coordinate Pd. The superior catalytic performance of these catalyst centers in aerobic alcohol oxidation versus a control catalyst indicates that these low-coordinate sites are catalytically relevant. In parallel, **Van Duyne, Schatz** and **Stair** have extended their work using SERS and density functional theory to understand the mechanisms of trimethylaluminum deposition during alumina ALD on a metal surface. A bottom-up picture is being developed for the aluminum oxide clusters that result after 2-3 cycles, and this model is being extended to ALD of other oxides with the goal of generating cluster structures relevant to a number of catalytic reactions.

Thrust II: ***Atom-Scale Control of Critical Oxide-Oxide Interfaces.***

Here, we seek to control the nature and activity of active oxygens on oxide catalyst surfaces consisting of isolated metal cations, well-defined oxide clusters, and single acid sites at oxide-support interfaces. This is enabled by lattice and electronic tuning of nanocrystalline supports, precursor design and novel deposition strategies, and oxide nanocavity structures.

Using conventional and non-conventional precursors for supported CuO_X over a wide range of supports, **Notestein** has developed an understanding of how the CuO_X structure, reducibility, and activity in cyclohexane oxidative dehydrogenation (ODH) evolves with loading, precursor, and support. (**Figure 2**) In some of the first reports of alkane ODH over supported CuO_X, both activity and selectivity were seen to increase with increasing Lewis acidity of the support. This finding includes both conventional oxide supports as well as highly Lewis acidic supports like Ta_2O_5 or Nb_2O_5, and is due in part to a perturbation of the CuO_X electronic structure, as understood from UV-visible spectroscopy. Support Lewis acidity was probed using a chemisorbed dye method.

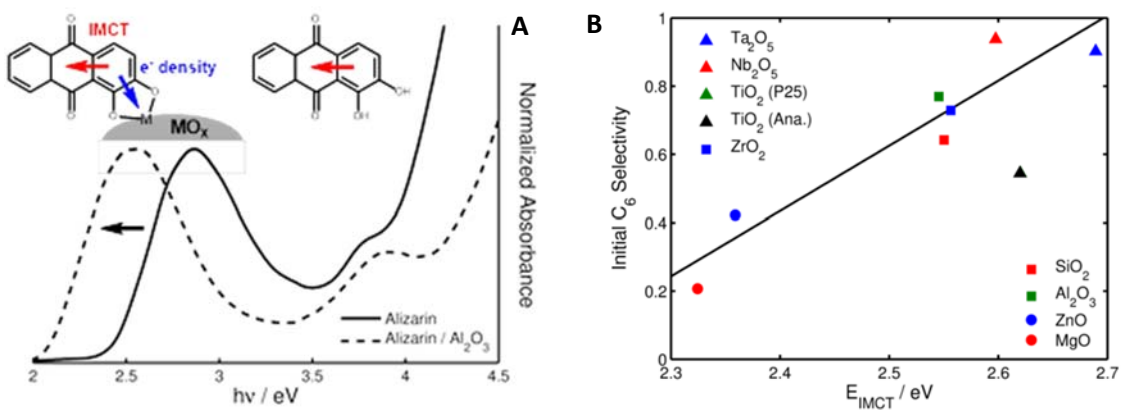

Figure 2. Diffuse reflectance UV-visible spectroscopy, with and without added alizarin dye as a reporter of surface Lewis acidity (A), is used to correlate trends in CuOx-catalyzed cyclohexane oxidative dehydrogenation activity and selectivity (B).

In parallel, **Weitz** has developed new IR tools to interrogate complex and reducible oxide surfaces, while **Bedzyk** installed a high-energy XPS unit to be applied to a UHV surface chamber / diffractometer housed at sector 5 of the Advanced Photon Source for the first-ever combination of X-ray standing wave and XPS studies. Working closely with quantum chemical modeling provided by **Schatz**, supported oxide surfaces will be interrogated with unprecedented spatial and chemical resolution over the next year.

In a second set of collaborative projects, precision ALD syntheses are used to interrogate heterobimetallic oxide interfaces present in supported oxides. In this manner, **Schweitzer**, **Schatz**,

Snurr, T. Marks and **Stair** have synthesized $VO_X/TiO_X/Al_2O_3$ catalysts for ODH, finding preferential deposition of VO_X on TiO_X domains, a finding supported by Raman, catalytic rates, and DFT calculations. The same team has also synthesized MoO_X/SiO_2 materials to understand the structural origin for the very low fractions of active sites for metathesis catalysis. Finally, **Schweitzer**, **T. Marks**, **Stair**, and **Notestein** have created SiO_X/Al_2O_3 materials by both ALD and controlled sol-gel deposition as new classes of Brønsted acid catalysts for reactions including dehydration and cracking of alkyl benzenes. In a collaboration with DOE Ames Laboratory, Dynamic Nuclear Polarization (DNP)-enhanced ^{29}Si-^{29}Si double-quantum/single-quantum (DQ/SQ) correlation NMR spectroscopy provided a detailed picture of these acidic catalysts (Figure 3).

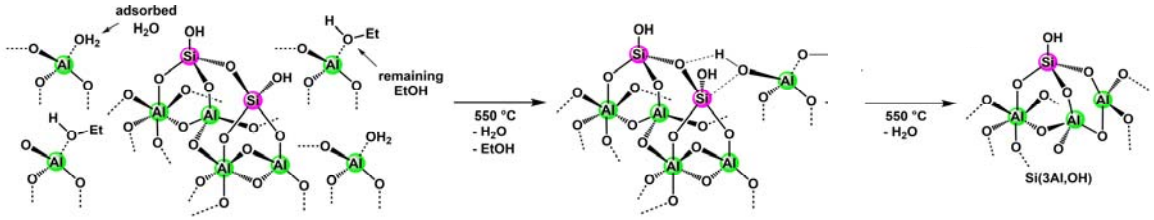

Figure 3. Schematic of surface SiOx species as created by atomic layer deposition and their evolution during calcination to isolated SiOH groups, as demonstrated by DNP- enhanced ^{29}Si-^{29}Si double-quantum/single-quantum (DQ/SQ) correlation NMR spectroscopy.

Finally, **Stair** and **Notestein** have furthered the concept of oxide nanobowls, and specifically their use as supports for metal nanoparticles, in a project that is cross cutting with Thrust I. It was found that deposition of Pt by either incipient wetness impregnation or strong electrostatic adsorption into $SiO_2@TiO_2$ or $SiO_2@Al_2O_3$ nanocavities gives high dispersion, thermal stability, and in the latter case, statistically less than 1 Pt per nanocavity as a facile route towards single-atom catalysts.

Thrust III: ***Understanding-Based Manipulation of Catalytic Environments*****.**

Here, we tune the environment near catalytic sites to make them more active, selective, and robust by combining ICEP's capabilities in molecularly-oriented catalyst design and synthesis with the hard matter synthetic and analytical toolboxes available in Thrusts I and II, with a collaborative focus on novel catalytic structures and environments.

One set of projects focuses on utilizing metal organic frameworks (MOFs) to understand and control the catalyst active site environment (**Figure 4**). **Hupp** and **Farha** developed sulfated MOF-808-SO_4, which was shown to maintain supported Pd as the divalent cation, in contrast to partial reduction for the unsulfated parent MOF-808. Structural analysis and catalytic investigations are ongoing for this material. In parallel, **Nguyen** performed tandem olefin epoxidation with H_2, O_2, and cyclooctene using a bifunctional material consisting of Pd nanoparticles encapsulated in a MOF which was subsequently functionalized with a Mo salen complex.

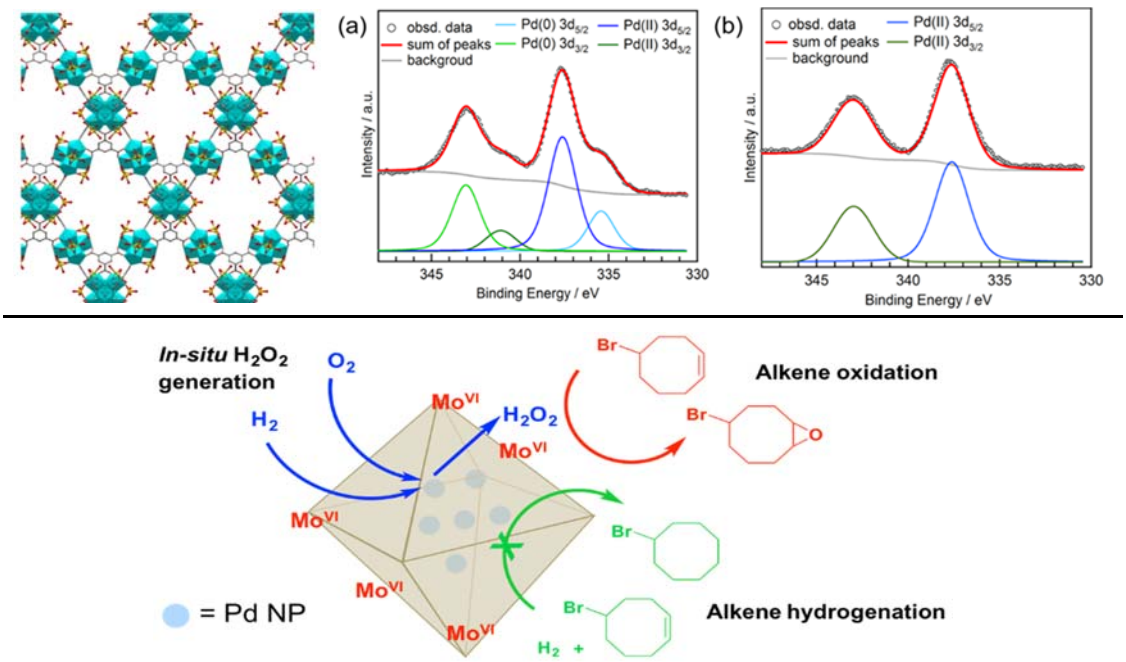

Figure 4. Two routes to utilizing metal organic frameworks to understand and probe the environment around active sites. (top) Sulfonated MOF-808 (crystal structure, left) is a crystallographically-regular mimic for important, but irregular sulfated oxides. XPS shows that this support maintains divalent Pd in (b), unlike the parent MOF in (a). (bottom) A MOF structure can also scaffold tandem catalysis. Here, embedded Pd nanoparticles catalyze H_2O_2 formation from H_2 and O_2, while exterior Mo salen sites utilize the H_2O_2 for epoxidation. The MOF pores prevent competitive hydrogenation of cyclooctene by the buried Pd nanoparticles.

In a different route to marry homogeneous and heterogeneous catalysis, **Lohr**, **T. Marks** and **Stair** prepared a single-site hexavalent molybdenum di-oxo species by grafting MoO_2Cl_2(dme) onto activated carbon (Mo@C, **Figure 5**). Extensive characterization including *in situ* X-ray absorption spectroscopy is consistent with a highly reactive, mononuclear Mo^{VI} center initially possessing 2 Mo=O, and two Mo-O at different bond lengths. Approximately 40-50% of these Mo centers reduce at the lowest temperature TPR-H_2 peak reported to date (218 °C) to give a structure consistent with Mo^{VI}(=O)(OH)(H). Among other reactions, Mo@C catalyzes transesterification of esters and triglycerides and dehydrogenation of aqueous MeOH and EtOH to the corresponding aldehyde. This new catalytic system is base- and oxidant-free and not deactivated by water, hence is compatible with biomass-derived alcohol feedstocks.

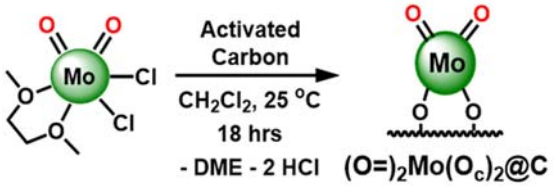

Figure 5. XAS and TPR-confirmed structure of the Mo dioxo active site derived from a molecular precursor. This carbon-supported catalyst is active for alcohol dehydrogenation, transesterification, and carbonyl coupling under mild conditions.

Finally, **Kung** explored new hydrocarbon oxidation chemistry using molecular O_2 with small Au clusters formed from Au pre-catalysts Au/SiO_2 or AuCl. Supported, nm-size Au particles are poorly active for selective epoxidation of cyclooctene, while the active species are solubilized atomic Au clusters that are present in ng mL^{-1} concentrations and stabilized by ligands derived

from the oxidized hydrocarbon products. These Au clusters generate initiators and propagators to trigger cyclooctene auto-oxidation. Spectroscopic characterization suggests that 7-8 atom clusters are effective initiators. These Au clusters are also effective in selective oxidation of cyclohexene, and solubilized Pt clusters, formed in a similar manner, also generate initiators for cyclooctene epoxidation. **Broadbelt** has developed a general microkinetic model for cyclic alkene oxidation, (**Figure 6**) that rationalizes the selectivities to different products and determines the relative contribution of homogeneous chemistry to the observed oxidation.

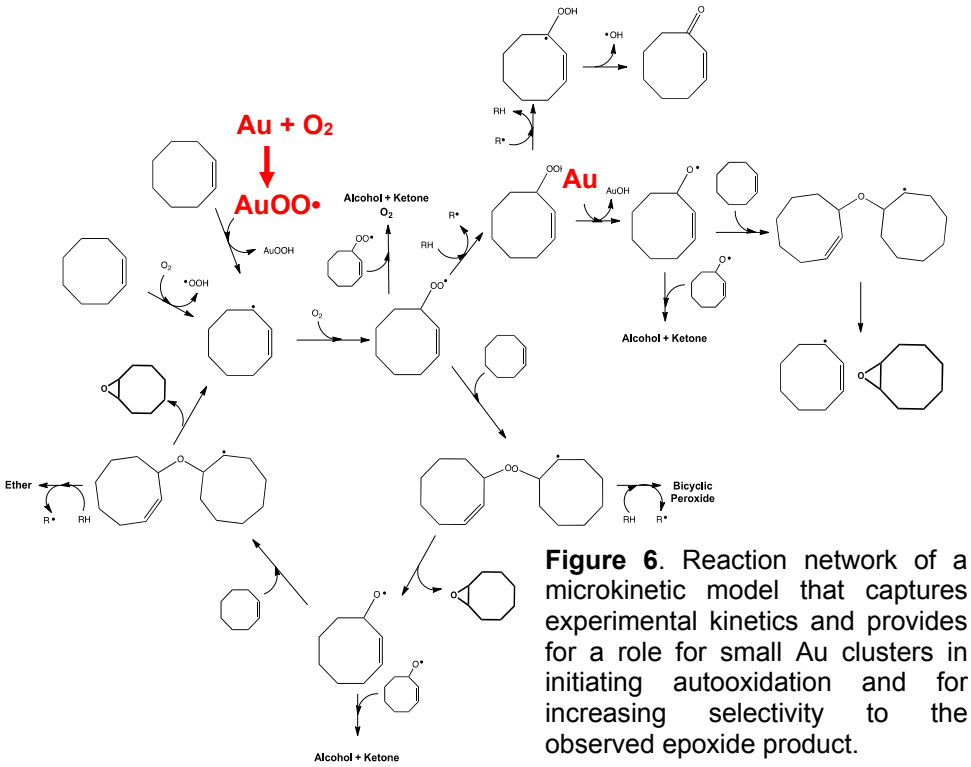

Figure 6. Reaction network of a microkinetic model that captures experimental kinetics and provides for a role for small Au clusters in initiating autooxidation and for increasing selectivity to the observed epoxide product.

Publications Acknowledging this Grant in 2014-2017

Thrust 1 – Metal-Oxide Interactions, Laurence D. Marks

1. Bachrach, M.; Marks, T. J.; Notestein, J. M., Understanding the Hydrodenitrogenation of Heteroaromatics on a Molecular Level. *ACS Catalysis* **2016,** *6* (3), 1455-1476.
2. Bachrach, M.; Morlanes-Sanchez, N.; Canlas, C. P.; Miller, J. T.; Marks, T. J.; Notestein, J. M., Increasing the Aromatic Selectivity of Quinoline Hydrogenolysis Using Pd/MOx-Al_2O_3. *Catalysis Letters* **2014,** *144* (11), 1832-1838.
3. Bachrach, M.; Marks, T. J.; Notestein, J. M., C-N bond hydrogenolysis of aniline and cyclohexylamine over TaOx-Al_2O_3. *New Journal of Chemistry* **2016**, *7*, 6001-6004.
4. Chen, B. R.; George, C.; Lin, Y. Y.; Hu, L. H.; Crosby, L.; Hu, X. Y.; Stair, P. C.; Marks, L. D.; Poeppelmeier, K. R.; Van Duyne, R. P.; Bedzyk, M. J., Morphology and oxidation state of ALD-grown Pd nanoparticles on TiO_2- and SrO-terminated $SrTiO_3$ nanocuboids. *Surface Science* **2016,** *648*, 291-298.

5. Ding, K.; Gulec, A.; Johnson, A. M.; Schweitzer, N. M.; Stucky, G. D.; Marks, L. D.; Stair, P. C., Identification of active sites in CO oxidation and water-gas shift over supported Pt catalysts. *Science* **2015,** *350* (6257), 189-192.
6. Hackler, R. A.; McAnally, M. O.; Schatz, G. C.; Stair, P. C.; Van Duyne, R. P., Identification of Dimeric Methylalumina Surface Species during Atomic Layer Deposition Using Operando Surface-Enhanced Raman Spectroscopy. *Journal of the American Chemical Society* **2017,** *139* (6), 2456-2463.
7. Lin, Y. Y.; Wu, Z. L.; Wen, J. G.; Ding, K. L.; Yang, X. Y.; Poeppelmeier, K. R.; Marks, L. D., Adhesion and Atomic Structures of Gold on Ceria Nanostructures: The Role of Surface Structure and Oxidation State of Ceria Supports. *Nano Letters* **2015,** *15* (8), 5375-5381.
8. Liu, S.; Tan, J. M.; Gulec, A.; Crosby, L. A.; Drake, T. L.; Schweitzer, N. M.; Delferro, M.; Marks, L. D.; Marks, T. J.; Stair, P. C., Stabilizing Single-Atom and Small-Domain Platinum via Combining Organometallic Chemisorption and Atomic Layer Deposition. *Organometallics* **2017,** *36* (4), 818-828.
9. Liu, S.; Tan, J. M.; Gulec, A.; Schweitzer, N. M.; Delferro, M.; Marks, L. D.; Stair, P. C.; Marks, T. J., Direct Synthesis of Low-Coordinate Pd Catalysts Supported on SiO_2 via Surface Organometallic Chemistry. *ACS Catalysis* **2016,** *6* (12), 8380-8388.
10. Liu, B. H.; McBriarty, M. E.; Bedzyk, M. J.; Shaikhutdinov, S.; Freund, H. J., Structural Transformations of Zinc Oxide Layers on Pt(111). *Journal of Physical Chemistry C* **2014,** *118* (49), 28725-28729.
11. Masango, S. S.; Peng, L. X.; Marks, L. D.; Van Duyne, R. P.; Stair, P. C., Nucleation and Growth of Silver Nanoparticles by AB and ABC-Type Atomic Layer Deposition. *Journal of Physical Chemistry C* **2014,** *118* (31), 17655-17661.
12. Masango, S. S.; Hackler, R. A.; Henry, A. I.; McAnally, M. O.; Schatz, G. C.; Stair, P. C.; Van Duyne, R. P., Probing the Chemistry of Alumina Atomic Layer Deposition Using Operando Surface-Enhanced Raman Spectroscopy. *Journal of Physical Chemistry C* **2016**, *120* (7), 3822-3833.
13. Masango, S. S.; Hackler, R. A.; Large, N.; Henry, A. I.; McAnally, M. O.; Schatz, G. C.; Stair, P. C.; Van Duyne, R. P., High-Resolution Distance Dependence Study of Surface-Enhanced Raman Scattering Enabled by Atomic Layer Deposition. *Nano Letters* **2016** *16* (7) 4251-4259.
14. Mashayekhi, N. A.; Kung, M. C.; Kung, H. H., Selective oxidation of hydrocarbons on supported Au catalysts. *Catalysis Today* **2014,** *238*, 74-79.
15. Pan, Q.; Liu, B. H.; McBriarty, M. E.; Martynova, Y.; Groot, I. M. N.; Wang, S.; Bedzyk, M. J.; Shaikhutdinov, S.; Freund, H. J., Reactivity of Ultra-Thin ZnO Films Supported by Ag(111) and Cu(111): A Comparison to ZnO/Pt(111). *Catalysis Letters* **2014,** *144* (4), 648-655.
16. Stoltz, S. E.; Ellis, D. E.; Bedzyk, M. J., Structure and reactivity of zero-, two- and three-dimensional Pd supported on $SrTiO_3$(001). *Surface Science* **2014,** *630*, 46-63.
17. Stoltz, S. E.; Ellis, D. E.; Bedzyk, M. J., Interface of Pt with $SrTiO_3$(001); A combined theoretical and experimental study. *Surface Science* **2015,** *633*, 8-16.

Thrust 2 – Oxide-Oxide Interactions, Justin M. Notestein

1. Ardagh, M. A.; Bo, Z. Y.; Nauert, S. L.; Notestein, J. M., Depositing SiO_2 on Al_2O_3: a Route to Tunable Brønsted Acid Catalysts. *ACS Catalysis* **2016,** *6* (9), 6156-6164.
2. Beletskiy, E. V.; Hou, X. L.; Shen, Z. L.; Gallagher, J. R.; Miller, J. T.; Wu, Y. Y.; Li, T. H.; Kung, M. C.; Kung, H. H., Supported Tetrahedral Oxo-Sn Catalyst: Single Site, Two Modes of Catalysis. *Journal of the American Chemical Society* **2016**, *138* (13), 4294-4297.
3. Beletskiy, E. V.; Shen, Z. L.; Riofski, M. V.; Hou, X. L.; Gallagher, J. R.; Miller, J. T.; Wu, Y.; Kung, H. H.; Kung, M. C., Tetrahedral Sn-silsesquioxane: synthesis, characterization and catalysis. *Chemical Communications* **2014**, *50* (99), 15699-15701.

4. Beletskiy, E. V.; Wu, Y. Y.; Kung, M. C.; Kung, H. H., Addition of Sn-O'Pr across a C=C Bond: Unusual Insertion of an Alkene into a Main-Group-Metal-Alkoxide Bond. *Organometallics* **2016**, *35* (3), 301-302.
5. Bhattacharyya, K.; Wu, W. Q.; Weitz, E.; Vijayan, B. K.; Gray, K. A., Probing Water and CO_2 Interactions at the Surface of Collapsed Titania Nanotubes Using IR Spectroscopy. *Molecules* **2015**, *20* (9), 15469-15487.
6. Bo, Z. Y.; Eaton, T. R.; Gallagher, J. R.; Canlas, C. P.; Miller, J. T.; Notestein, J. M., Size-Selective Synthesis and Stabilization of Small Silver Nanoparticles on TiO_2 Partially Masked by SiO_2. *Chemistry of Materials* **2015**, *27* (4), 1269-1277.
7. Drake, T. L.; Stair, P. C., Vapor deposition of molybdenum oxide using bis(ethylbenzene) molybdenum and water. *Journal of Vacuum Science & Technology A* **2016,** *34* (5), 7.
8. Eaton, T. R.; Boston, A. M.; Thompson, A. B.; Gray, K. A.; Notestein, J. M., Counting Active Sites on Titanium Oxide-Silica Catalysts for Hydrogen Peroxide Activation through *In Situ* Poisoning with Phenylphosphonic Acid. *Chemcatchem* **2014,** *6* (11), 3215-3222.
9. Eaton, T. R.; Campos, M. P.; Gray, K. A.; Notestein, J. M., Quantifying accessible sites and reactivity on titania-silica (photo) catalysts: Refining TOF calculations. *Journal of Catalysis* **2014,** *309*, 156-165.
10. Feng, Z.; Ma, Q.; Lu, J.; Feng, H.; Elam, J. W.; Stair, P. C.; Bedzyk, M. J., Atomic-scale cation dynamics in a monolayer VOX/α-Fe2O3 catalyst. *RSC Advances* **2015**, *5* (126), 103834-103840.
11. Feng, Z.; McBriarty, M. E.; Mane, A. U.; Lu, J.; Stair, P. C.; Elam, J. W.; Bedzyk, M. J., Redox-driven atomic-scale changes in mixed catalysts: VOX/WOX/α-TiO_2 (110). *RSC Advances* **2014**, *4* (110), 64608-64616.
12. Johnson, A. M.; Quezada, B. R.; Marks, L. D.; Stair, P. C., Influence of the Metal Oxide Substrate Structure on Vanadium Oxide Monomer Formation. *Topics in Catalysis* **2014**, *57* (1-4), 177-187.
13. Jurca, T.; Peters, A. W.; Mouat, A. R.; Farha, O. K.; Hupp, J. T.; Lohr, T. L.; Delferro, M.; Marks, T. J., Second-generation hexavalent molybdenum oxo-amidinate precursors for atomic layer deposition. *Dalton Transactions* **2017,** *46* (4), 1172-1178.
14. Kwon, S.; Schweitzer, N. M.; Park, S.; Stair, P. C.; Snurr, R. Q., A kinetic study of vapor-phase cyclohexene epoxidation by H_2O_2 over mesoporous TS-1. *Journal of Catalysis* **2015**, *326*, 107-115.
15. Kwon, S.; Liao, P. L.; Stair, P. C.; Snurr, R. Q., Alkaline-earth metal-oxide overlayers on TiO_2: application toward CO_2 photoreduction. *Catalysis Science & Technology* **2016,** *6* (21), 7885-7895.
16. McBriarty, M. E.; Ellis, D. E., Cation synergies affect ammonia adsorption over VO_X and $(V,W)O_X$ dispersed on α-Al_2O_3 (0001) and α-Fe_2O_3 (0001). *Surface Science* **2016**, *651*, 41-50.
17. McBriarty, M. E.; Campbell, G. P.; Drake, T. L.; Elam, J. W.; Stair, P. C.; Ellis, D. E.; Bedzyk, M. J., Atomic-Scale View of VOx-WOx Co-reduction on the alpha-Al_2O_3 (0001) Surface. *Journal of Physical Chemistry C* **2015,** *119* (28), 16179-16187.
18. Mouat, A. R.; Kobayashi, T.; Pruski, M.; Marks, T. J.; Stair, P. C., Direct Spectroscopic Evidence for Isolated Silanols in SiOx/Al_2O_3 and Their Formation Mechanism. *J. Phys. Chem. C* **2017,** *121* (11), 6060-6064.
19. Mouat, A. R.; George, C.; Kobayashi, T.; Pruski, M.; van Duyne, R. P.; Marks, T. J.; Stair, P. C., Highly Dispersed SiOx/Al_2O_3 Catalysts Illuminate the Reactivity of Isolated Silanol Sites. *Angewandte Chemie-International Edition* **2015**, *54* (45), 13346-13351.
20. Mouat, A. R.; Mane, A. U.; Elam, J. W.; Delferro, M.; Marks, T. J.; Stair, P. C., Volatile Hexavalent Oxo-amidinate Complexes: Molybdenum and Tungsten Precursors for Atomic Layer Deposition. *Chemistry of Materials* **2016**, *28* (6), 1907-1919.
21. Nauert, S. L.; Schax, F.; Limberg, C.; Notestein, J. M., Cyclohexane oxidative dehydrogenation over copper oxide catalysts. *Journal of Catalysis* **2016,** *341*, 180-190.
22. Savara, A.; Weitz, E., Elucidation of Intermediates and Mechanisms in Heterogeneous Catalysis Using Infrared Spectroscopy. *Annual Review of Physical Chemistry* **2014**, *65*, 249-273.

Cross-Cutting Thrusts 1 and 2

1. Crosby, L.; Enterkin, J.; Rabuffetti, F.; Poeppelmeier, K.; Marks, L., Wulff shape of strontium titanate nanocuboids. *Surface Science* **2015,** *632*, L22-L25.
2. Crosby, L. A.; Kennedy, R. M.; Chen, B. R.; Wen, J. G.; Poeppelmeier, K. R.; Bedzyk, M. J.; Marks, L. D., Complex surface structure of (110) terminated strontium titanate nanododecahedra. *Nanoscale* **2016,** *8* (37), 16606-16611.
3. Hu, L. H.; Wang, C. D.; Kennedy, R. M.; Marks, L. D.; Poeppelmeier, K. R., The Role of Oleic Acid: From Synthesis to Assembly of Perovskite Nanocuboid Two-Dimensional Arrays. *Inorganic Chemistry* **2015,** *54* (3), 740-745.
4. Lin, Y. Y.; Wen, J. G.; Hu, L. H.; McCarthy, J. A.; Wang, S. C.; Poeppelmeier, K. R.; Marks, L. D., Electron-induced Ti-rich surface segregation on $SrTiO_3$ nanoparticles. *Micron* **2015,** *68*, 152-157.
5. Lin, Y. Y.; Wu, Z. L.; Wen, J. G.; Poeppelmeier, K. R.; Marks, L. D., Imaging the Atomic Surface Structures of CeO_2 Nanoparticles. *Nano Letters* **2014,** *14* (1), 191-196.
6. Marks, L. D.; Chiaramonti, A. N.; Rahman, S. U.; Castell, M. R., Transition from Order to Configurational Disorder for Surface Reconstructions on $SrTiO_3$(111). *Physical Review Letters* **2015,** *114* (22), 6.
7. Wang, S. C.; Xie, H.; Lin, Y. Y.; Poeppelmeier, K. R.; Li, T.; Winans, R. E.; Cui, Y. R.; Ribeiro, F. H.; Canlas, C. P.; Elam, J. W.; Zhang, H. B.; Marshall, C. L., High Thermal Stability of La_2O_3- and CeO_2-Stabilized Tetragonal ZrO_2. *Inorganic Chemistry* **2016,** *55* (5), 2413-2420.
8. Wang, Z.; Loon, A.; Subramanian, A.; Gerhold, S.; McDermott, E.; Enterkin, J. A.; Hieckel, M.; Russell, B. C.; Green, R. J.; Moewes, A.; Guo, J.; Blaha, P.; Castell, M. R.; Diebold, U.; Marks, L. D., Transition from Reconstruction toward Thin Film on the (110) Surface of Strontium Titanate. *Nano Letters* **2016,** *16* (4), 2407-2412.
9. Wen, J. G.; Lin, Y. Y.; Sheng, H.; Wang, L.; Miller, D. J.; Wu, Z.; Poeppelmeier, K. R.; Marks, L. D., Atomic Surface Structures of Oxide Nanoparticles with Well-defined Shapes. *Microsc. Microanal.* **2016,** *22 (Suppl 3)* 360-361.

Thrust 3 – Molecule-Metal-Environment Interactions, Harold H. Kung

1. Adhikari, D.; Miller, A. W.; Baik, M. H.; Nguyen, S. T., Intramolecular ring-opening from a CO_2-derived nucleophile as the origin of selectivity for 5-substituted oxazolidinone from the (salen)Cr-catalyzed aziridine + CO_2 coupling. *Chemical Science* **2015**, *6* (2), 1293-1300.
2. Bae, Y. S.; Liu, J.; Wilmer, C. E.; Sun, H.; Dickey, A. N.; Kim, M. B.; Benin, A. I.; Willis, R. R.; Barpaga, D.; LeVan, M. D.; Snurr, R. Q., The effect of pyridine modification of Ni-DOBDC on CO_2 capture under humid conditions. *Chemical Communications* **2014**, *50* (25), 3296-3298.
3. Brydon, R. R. O.; Broadbelt, L. J., Mechanistic modeling of the partial oxidation of 1,3-propanediol: Comparison of free-radical and concerted mechanisms. *Industrial & Engineering Chemistry Research* **2017**, *56* (23) 6599-6607.
4. Brydon, R. R. O.; Broadbelt, L. J., Mechanistic modeling of the partial oxidation of propanediols: Comparison of free-radical and concerted mechanisms. *Industrial Engineering and Chemistry Research* **2017**, in revision.
5. Galloway, J. M.; Kung, M.; Kung, H. H., Synthesis and characterization of bifunctional surfaces with tunable functional group pairs. *Surface Science* **2016**, *648*, 284-290.
6. Grosso-Giordano, N. A.; Eaton, T. R.; Bo, Z.; Yacob, S.; Yang, C.-C.; Notestein, J. M., Silica support modifications to enhance Pd-catalyzed deoxygenation of stearic acid. *Applied Catalysis B: Environmental* **2016**, *192*, 93-100.
7. Haag, D.; Kung, H. H., Metal Free Graphene Based Catalysts: A Review. *Topics in Catalysis* **2014,** *57* (6-9), 762-773.
8. Howarth, A. J.; Liu, Y. Y.; Li, P.; Li, Z. Y.; Wang, T. C.; Hupp, J.; Farha, O. K., Chemical, thermal

and mechanical stabilities of metal-organic frameworks. *Nature Review of Materials* **2016,** *1* (3).
9. Karagiaridi, O.; Vermeulen, N. A.; Klet, R. C.; Wang, T. C.; Moghadam, P. Z.; Al-Juaid, S. S.; Stoddart, J. F.; Hupp, J. T.; Farha, O. K., Functionalized Defects through Solvent-Assisted Linker Exchange: Synthesis, Characterization, and Partial Postsynthesis Elaboration of a Metal-Organic Framework Containing Free Carboxylic Acid Moieties. *Inorganic Chemistry* **2015**, *54* (4), 1785-1790.
10. Klet, R. C.; Tussupbayev, S.; Borycz, J.; Gallagher, J. R.; Stalzer, M. M.; Miller, J. T.; Gagliardi, L.; Hupp, J. T.; Marks, T. J.; Cramer, C. J.; Delferro, M.; Farha, O. K., Single-Site Organozirconium Catalyst Embedded in a Metal-Organic Framework. *Journal of the American Chemical Society* **2015**, *137* (50), 15680-15683.
11. Kung, H. H.; Kung, M. C., Inspiration from Nature for Heterogeneous Catalysis. *Catalysis Letters* **2014**, *144* (10), 1643-1652.
12. Kung, M. C.; Riofski, M. V.; Missaghi, M. N.; Kung, H. H., Organosilicon platforms: bridging homogeneous, heterogeneous, and bioinspired catalysis. *Chemical Communications* **2014**, *50* (25), 3262-3276.
13. Liu, S.; Li, J.; Jurca, T.; Stair, P. C.; Lohr, T. L.; Marks, T. J., Efficient carbon-supported heterogeneous molybdenum-dioxo catalyst for chemoselective reductive carbonyl coupling. *Catalysis Science and Technology* **2017**, *7*, 2165-2169.
14. Lohr, T. L.; Mouat, A. R.; Schweitzer, N. M.; Stair, P. C.; Delferro, M.; Marks, T. J., Efficient catalytic greenhouse gas-free hydrogen and aldehyde formation from aqueous alcohol solutions. *Energy Environ. Sci.* **2017**, advance article.
15. Mouat, A. R.; Lohr, T. L.; Wegener, E. C.; Miller, J. T.; Delferro, M.; Stair, P. C.; Marks, T. J., Reactivity of a Carbon-Supported Single-Site Molybdenum Dioxo Catalyst for Biodiesel Synthesis. *ACS Catalysis* **2016,** *6* (10), 6762-6769.
16. Nguyen, H. G. T.; Mao, L.; Peters, A. W.; Audu, C. O.; Brown, Z. J.; Farha, O. K.; Hupp, J. T.; Nguyen, S. T., Comparative study of titanium-functionalized UiO-66: support effect on the oxidation of cyclohexene using hydrogen peroxide. *Catalysis Science & Technology* **2015**, *5* (9), 4444-4451.
17. Nguyen, H. G. T.; Schweitzer, N. M.; Chang, C. Y.; Drake, T. L.; So, M. C.; Stair, P. C.; Farha, O. K.; Hupp, J. T.; Nguyen, S. T., Vanadium-Node-Functionalized UiO-66: A Thermally Stable MOF-Supported Catalyst for the Gas-Phase Oxidative Dehydrogenation of Cyclohexene. *ACS Catalysis* **2014**, *4* (8), 2496-2500.
18. Paddock, R. L.; Adhikari, D.; Lord, R. L.; Baik, M. H.; Nguyen, S. T., [(Salcen)Cr^{III} + Lewis base]-catalyzed synthesis of N-aryl-substituted oxazolidinones from epoxides and aryl isocyanates. *Chemical Communications* **2014**, *50* (96), 15187-15190.
19. Planas, N.; Mondloch, J. E.; Tussupbayev, S.; Borycz, J.; Gagliardi, L.; Hupp, J. T.; Farha, O. K.; Cramer, C. J., Defining the Proton Topology of the Zr-6-Based Metal-Organic Framework NU-1000. *Journal of Physical Chemistry Letters* **2014**, *5* (21), 3716-3723.

Other DOE Catalysis Acknowledgements

1. Childers, D. J.; Schweitzer, N. M.; Shahari, S. M. K.; Rioux, R. M.; Miller, J. T.; Meyer, R. J., Modifying structure-sensitive reactions by addition of Zn to Pd. *Journal of Catalysis* **2014,** *318*, 75-84.
2. Childers, D. J.; Schweitzer, N. M.; Shahri, S. M. K.; Rioux, R. M.; Miller, J. T.; Meyer, R. J., Evidence for geometric effects in neopentane conversion on PdAu catalysts. *Catalysis Science & Technology* **2014,** *4* (12), 4366-4377.
3. Gu, W. X.; Stalzer, M. M.; Nicholas, C. P.; Bhattacharyya, A.; Motta, A.; Gallagher, J. R.; Zhang, G. H.; Miller, J. T.; Kobayashi, T.; Pruski, M.; Delferro, M.; Marks, T. J., Benzene Selectivity in Competitive Arene Hydrogenation: Effects of Single-Site Catalyst - Acidic Oxide Surface Binding Geometry. *Journal of the American Chemical Society* **2015,** *137* (21), 6770-6780.

4. Jiang, X. F.; Huang, H.; Chai, Y. F.; Lohr, T. L.; Yu, S. Y.; Lai, W. Z.; Pan, Y. J.; Delferro, M.; Marks, T. J., Hydrolytic cleavage of both CS_2 carbon-sulfur bonds by multinuclear Pd(II) complexes at room temperature. *Nature Chemistry* **2017,** *9* (2), 188-193.
5. Liu, S.; Motta, A.; Mouat, A. R.; Delferro, M.; Marks, T. J., Very Large Cooperative E□ects in Heterobimetallic Titanium-Chromium Catalysts for Ethylene Polymerization/Copolymerization. *Journal of the American Chemical Society* **2014,** *136*, 10460-10469.
6. McInnis, J. P.; Delferro, M.; Marks, T. J., Multinuclear Group 4 Catalysis: Olefin Polymerization Pathways Modified by Strong Metal-Metal Cooperative Effects. *Accounts of Chemical Research* **2014,** *47* (8), 2545-2557.
7. Peroff, A. G.; Weitz, E.; Van Duyne, R. P., Mechanistic studies of pyridinium electrochemistry: alternative chemical pathways in the presence of CO_2. *Physical Chemistry Chemical Physics* **2016**, 18 (3), 1578-1586.
8. Stalzer, M. M.; Delferro, M.; Marks, T. J., Supported Single-Site Organometallic Catalysts for the Synthesis of Valuable Polyolefins. *Catalysis Letters* **2014,** *145*, 3-14.
9. Stalzer, M. M.; Nicholas, C. P.; Bhattacharyya, A.; Motta, A.; Delferro, M.; Marks, T. J., Single-Face/All-cis Arene Hydrogenation by Supported Single-Site d^0 Organozirconium Catalyst. *Angew.Chem. Int.Ed* **2016,** *55*, 5263-5267.
10. Wu, W. Q.; Weitz, E., Modification of acid sites in ZSM-5 by ion-exchange: An in-situ FTIR study. *Applied Surface Science* **2014**, *316*, 405-415.
11. Yacob, S.; Park, S.; Kilos, B. A.; Barton, D. G.; Notestein, J. M., Vapor-phase ethanol carbonylation with heteropolyacid-supported Rh. *Journal of Catalysis* **2015,** *325*, 1-8.
12. Yacob, S.; Kilos, B. A.; Barton, D. G.; Notestein, J. M., Vapor phase ethanol carbonylation over Rh supported on zeolite 13X. *Applied Catalysis A-General* **2016,** *520*, 122-131.

Graeme Henkelman

Alloy nanoparticle catalysts: Tunable or not?

Graeme Henkelman
The University of Texas at Austin, Department of Chemistry

Presentation Abstract

Metal nanoparticles of only 100-200 atoms are synthesized using a dendrimer encapsulation technique to facilitate a direct comparison with density functional theory (DFT) calculations in terms of both structure and catalytic function. Structural characterization is done using electron microscopy, x-ray scattering, and electrochemical methods. Combining these tools with DFT calculations is found to improve the quality of the structural models. DFT is also successfully used to predict trends between structure and composition of the nanoparticles and their catalytic function for reactions including the reduction of oxygen and selective hydrogenation. This investigation demonstrates some remarkable properties of the nanoparticles, including facile structural rearrangements and nanoscale tuning parameters which can be used to optimize catalytic rates. In this presentation I will focus on a pair of random alloy bimetallic nanoparticles which have complete different trends in hydrogenation activity as a function of composition. Pd/Au is found to be tunable as a function of composition whereas Pt/Au is not. The reason behind these different behaviors will be discussed.

DE-FG02-13ER16428: Testing the Predictive Power of Theory for Determining the Structure and Activity of Nanoparticle Electrocatalysts

PI: Richard Crooks (PI) and Graeme Henkelman (co-PI)
Postdoc(s): Zhiyao Duan
Student(s): Nevena Ostojic and Hao Li

RECENT PROGRESS

Development of the ALD oxide/Pt DEN model interface

We showed that fully passivating, 2.5 nm thick, Al_2O_3 layers could be deposited onto carbon electrodes via atomic layer deposition (ALD). More importantly, subsequent adsorption of Pt dendrimer encapsulated nanoparticles (DENs) onto the oxide surface leads to an electrocatalytically active interface (Scheme 1). These results are important, because they provide a general approach for studying electrocatalytic reactions on nonconductive oxide surfaces. The dendrimer host provides important functions: stabilizing the DENs against aggregation and immobilizing them on the electrode surface via specific interactions with the oxide. Although structurally not as well defined as DENs, metal oxides deposited via ALD are the best option available for our electrocatalysis studies. Because it is electrically insulating and has a low dielectric constant, we have used Al_2O_3 for the purposes of hindering charge transfer between an electrode and redox

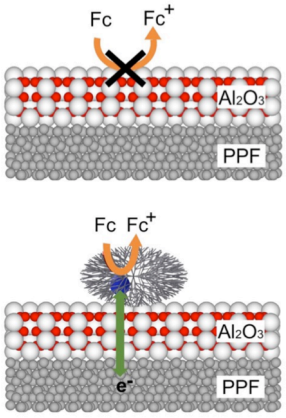

Scheme 1

molecules in solution. We reported that Al_2O_3 films thicker than 3.5 nm fully passivate electron transfer (eT) between underlying pyrolyzed polymer film (PPF) electrodes and solution phase ferrocenedimethanol (Fc in Scheme 1). Our main interest in this type of model system is in understanding how reactions electrocatalyzed by metal nanoparticle (NPs) are affected by the presence of oxide surfaces. Our principle findings are as follows. First, pinhole free, electrochemically passivating Al_2O_3 films can be deposited onto PPF electrodes. Second, when DENs containing an average of only 55 atoms each are deposited onto the Al_2O_3 surface, eT between the underlying PPF electrode and solution phase Fc is recovered. This facilitated eT is insensitive to the thickness of the ALD oxide layers up to 3.5 nm, but partial current recovery is still observed for films up to 5.7 nm thick. Third, the supported DENs are electrocatalytically active for the ORR. Fourth, the supported DENS are robust, surviving up to 40 consecutive voltammetric scans and 10 min of sonication in 0.5 M H_2SO_4 without significant change in electrochemical activity.

Electrocatalytic reduction of oxygen on Pt DENs in the presence and absence of interactions between the nanoparticles and an electrode surface

We show that it is possible to remove the dendrimer shell from the encapsulated NPs without significantly changing their size. Removal of the dendrimer is critical for studying metal NP/support interactions, because the dendrimer prevents intimate contact between the NP and the support. The key result is our finding that UV/O_3 can be used to remove the dendrimers from surface confined Pt DENs without changing their size, shape, or electrocatalytic properties. This is important because it means that results obtained using DENs reliably extrapolate to the electrocatalytic properties of other types of naked NPs. As mentioned earlier, the other major finding is that because the dendrimer can be cleanly removed without significantly changing the DENs, it possible to study electrocatalytic reactions in the presence and absence of support interactions. This means that DENs are a near perfect system for studying support effects, because the exact same electrode can be examined with support effects turned on or off simply by removing the dendrimer by UV/O_3 (Scheme 2). These results are important for three reasons. First, they lead to a general means for preparing highly monodisperse, stabilizer free mono and bimetallic nanoparticles (NP) in the 0.5-3.0 nm size range. Second, we are now in a position to begin answering fundamental questions about how the presence of a dendrimer affects the catalytic properties of DENs. Third, and most importantly, we are ready to begin including the additional complexity of support interactions into our research.

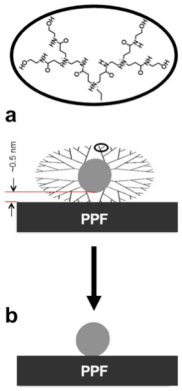

Scheme 2

Interfacial site of Au/SnO2 for the oxygen reduction reaction

Now that we have shown that DENs can be immobilized on thin ALD oxide supports with or without their dendrimer shell, we are ready to begin examining the effect of the oxide on the catalytic properties of the metal electrocatalyst. The Henkelman group has identified the Au NP/SnO_2 system as a good target for the ORR. Accordingly, this will be the first system we test experimentally using our DEN/ALD approach. It is known that O_2 adsorption is the first elementary step for the ORR. However, neither Au nor a

stoichiometric SnO_2 surface can adsorb O_2 by itself alone, and therefore the ORR cannot proceed on Au or SnO_2. By combining Au and a stoichiometric SnO_2 surface (Fig. 1), we find that O_2 can adsorb at the interfacial and perimeter sites with adsorption energies close to the Pt(111) surface (the best catalyst known for the ORR). The adsorption is made possible in the hybrid system as a result of eT from Au to SnO_2. The theoretical value of the overpotential of ORR at the interfacial site is 0.52 V. The value is only 0.07 V higher than that on Pt(111) surface, which makes Au/SnO_2 promising as an ORR catalyst. Following our approach of allowing theory to lead experiment, these predictions will be tested experimentally by the Crooks group during the coming year.

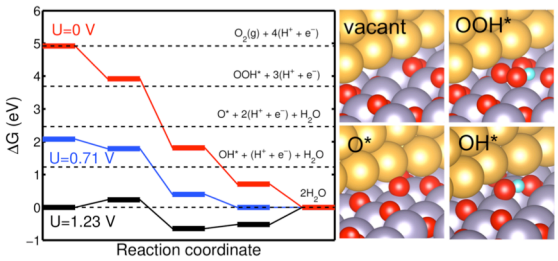

Figure 1. *Free energy landscape along the reaction coordinate of ORR at various electric potentials. The figures on the right show adsorption structures of intermediates at Au/SnO_2 interfacial sites.*

Publications Acknowledging this Grant in 2014-2017

Category I Publications*

Ostojic, N.; Thorpe, J. H.; Crooks, R. M. Electron Transfer Facilitated by Dendrimer Encapsulated Pt Nanoparticles Across Ultrathin, Insulating Oxide Films. *J. Am. Chem. Soc.* **2016**, 138, 6829.

Duan Z.; Henkelman G. O_2 activation at the Au/MgO(001) interface boundary facilitates CO oxidation" *Phys. Chem. Chem. Phys.* **2016**, 18, 5486.

Ostojic N.; Crooks R. M. Electrocatalytic Reduction of Oxygen on Platinum Nanoparticles in the Presence and Absence of Interactions with the Electrode Surface. *Langmuir* **2016**, 32, 9727.

Anderson R. M.; Yancey D. F.; Loussaert J. A.; Crooks R. M. Multistep Galvanic Exchange Synthesis Yielding Fully Reduced Pt Dendrimer Encapsulated Nanoparticles. *Langmuir* **2015**, 30, 15009.

Zhang L.; Anderson R. M.; Crooks R. M.; Henkelman G. Correlating Structure and Function of Metal Nanoparticles for Catalysis. *Surf. Sci.* **2015**, 640, 65-72.

Luo L.; Zhang L.; Henkelman G.; Crooks R. M. Unusual Activity Trend for CO Oxidation on PdxAu140-x@Pt Core@Shell Nanoparticle Electrocatalysts. *J. Phys. Chem. Lett.* **2015**, 6, 2562−2568.

Anderson R. M.; Yancey D. F.; Zhang, L.; Chill, S. T.; Henkelman, G.; Crooks, R. M. A Theoretical and Experimental Approach for Correlating Nanoparticle Structure and Electrocatalytic Activity. *Acc. Chem. Res.* **2015**, 48, 1351-1357.

Chill, S. T.; Anderson, R. M.; Yancey, D. F.; Frenkel, A. I.; Crooks, R. M.; Henkelman, G. Probing the Limits of Conventional Extended X-Ray Absorption Fine Structure Analysis Using Thiolated Au Nanoparticles. *ACS Nano* **2015**, 9, 4036-4042.

Duan, Z.; Henkelman, G. CO Oxidation at the Au/TiO2 Boundary: The Role of the Au/Ti5c Site. *ACS Catal.* **2015**, 5, 1589-1595.

H. Fu, Z. Duan, and G. Henkelman, "Computational Study of Structure and Reactivity of Oligomeric Vanadia Clusters Supported on Anatase and Rutile TiO_2 Surfaces" *J. Phys. Chem. C* **119**, 15160−15167 (2015).

Zhang, L.; Henkelman, G. Computational Design of Alloy-Core@Shell Metal Nanoparticle Catalysts. *ACS Catal.* **2015**, 5, 655-660.

Loussaert, J. A.; Fosdick, S. E.; Crooks, R. M. Electrochemical Properties of Metal Oxide Coated Electrodes Prepared by Atomic Layer Deposition. *Langmuir* **2014**, 30, 13707.

Duan, Z.; Henkelman, G. CO oxidation on the Pd(111) surface. *ACS Catal.* **2014**, 4, 3435-3443.

L. Luo, Z. Duan, H. Li, J. Kim, G. Henkelman, and R. M. Crooks, "Tunability of Adsorbate Binding on Bimetallic Alloy Nanoparticles for Optimization of Catalytic Hydrogenation" *J. Am. Chem. Soc.* **139**, 5538-5546 (2017).

** These publications may include acknowledgements to our sustaining endowment from the Robert A. Welch Foundation and instrumentation grants.*

Category II Publications

Yu, W.-Y.; Zhang, L.; Mullen, G.; Henkelman, G.; Mullins C. B. Oxygen Activation and Reaction on Pd−Au Bimetallic Surfaces. *J. Phys. Chem. C* **2015**, 119, 11754−11762.

Yu, W.-Y.; Zhang, L.; Mullen, G. M.; Henkelman, G.; Mullins, C. B. Effect of Annealing in Oxygen on Alloy Structures of Pd-Au Bimetallic Model Catalysts. *Phys. Chem. Chem. Phys.* **2015**, 17, 20588−20596.

Anderson, R. M.; Zhang, L.; Wu, D.; Brankovic, S. R.; Henkelman, G.; Crooks, R. M. A Theoretical and Experimental In-Situ Electrochemical Infrared Spectroscopy Study of Adsorbed CO on Pt Dendrimer-Encapsulated Nanoparticles. *J. Electrochem. Soc.* **2015**, 163, H3061-H3065.

Mullen, G. M.; Zhang, L.; Evans Jr., E. J.; Yan, T.; Henkelman, G.; Mullins, C. B. Control of Selectivity in Allylic Alcohol Oxidation on Gold Surfaces: The Role of Oxygen Adatoms and Hydroxyl Species. *Phys. Chem. Chem. Phys.* **2015**, 17, 4730-4738.

Liu, H.; An, W.; Li, Y.; Frenkel, A. I.; Sasaki, K.; Koenigsmann, C.; Su, D.; Anderson, R. M.; Crooks, R. M.; Adzic, R. R.; Liu, P.; Wong, S. S. In Situ Probing of the Active Site Geometry of Ultrathin Nanowires for the Oxygen Reduction Reaction. *J. Am. Chem. Soc.* **2015**, 137, 12597.

Mullen, G. M.; Zhang, L.; Evans Jr., E. J.; Yan, T.; Henkelman, G.; Mullins, C. B. Oxygen and hydroxyl species induce multiple reaction pathways for the partial oxidation of allyl alcohol over Au(111). *J. Am. Chem. Soc.* **2014**, 136, 6489-6498.

Anderson, R. M.; Crooks, R. M. High Efficiency Generation Collection Microelectrochemical Platform for Interrogating Electroactive Thin Films. *Anal. Chem.* **2014**, 86, 9962.

García, S.; Zhang, L.; Piburn, G. W.; Henkelman, G.; Humphrey, S. M. Microwave synthesis of classically immiscible rhodium-silver and rhodium-gold alloy nanoparticles: Highly active hydrogenation catalysts. *ACS Nano* **2014**, 8, 11512-11521.

Category III Publications: None

Advances in the Design & Synthesis of Multimetallic Nanocatalysts

Sara E. Skrabalak,[1]* Chenyu Wang,[1] Moitree Laskar,[1] Kallum Koczkur,[1] Josie Legere,[1] Hamed Ataee-Esfahani,[1] Ethan Harak,[1] Xiahan Sang,[2] Raymond Unocic,[2] Paul Patton,[1] and Dale Harak[3]
[1]Indiana University – Bloomington, Department of Chemistry
[2]Oak Ridge National Laboratory, Center for Nanophase Materials Sciences
[3]Rockhurst University, Department of Chemistry

Presentation Abstract

Central to many industrial processes and the realization of sustainable energy platforms are heterogeneous catalysts. The performances of these catalysts are governed by interplay between electronic and geometric factors, and controlling these parameters to achieve efficient catalysis remains a grand challenge. As will be shown, the performance of bimetallic nanocatalysts can be precisely controlled through the selection of suitable nanocrystal shapes (*i.e.,* faceting) and core@shell architectures (*i.e.,* shell thickness). This work was conducted in model Au@Pd and Rh@Pt systems on account of the synthetic accessibility of these nanostructures through seeded methods. The structural features of these nanocatalysts can be manipulated to tune the strength of symmetry-matched surface-adsorbate interactions through the engineered surface strain. Recently, we expanded the classes of core@shell nanocatalysts that are possible by using seed-mediated co-reduction to synthesize multimetallic NPs composed of intermetallic cores and either monometallic or random alloy shells. For example, face-centered cubic Pt-Cu random alloy shells were deposited on PdCu B2 intermetallic seeds, giving rise to faceted core@shell nanoparticles with highly strained surfaces. High resolution transmission electron microscopy revealed orientation-dependent surface strains, and these core@shell nanoparticles provide higher specific and mass activities for the oxygen reduction reaction when compared to conventional catalysts. Moreover, these intermetallic@random alloy nanoparticles displayed high endurance, undergoing 10,000 cycles with only a slight decay in activity and no apparent structural changes. With this advancement in seeded methods, novel architecturally controlled multimetallic nanocrystals can be designed, synthesized, and then applied as catalysts to diverse chemical transformations. Validation of new catalysts designs can bring unprecedented efficiency to many chemical processes and conserve both natural resources and economic capital, which are requisite for a sustainable future.

DE-SC0010489: Decoupling the Electronic and Geometric Parameters of Metal Nanocatalysts

Postdoc(s): Chenyu Wang, Kallum Koczkur, Hamed Ataee-Esfahani
Student(s): Moitree Laskar, Josie Legere, Ethan Harak

RECENT PROGRESS

Decoupling the Geometric Parameters of Shape-Controlled Monometallic Nanocatalysts

The structural features of metal nanoparticles such as crystallite size and shape are important to catalytic activity and selectivity. Thus, correlating the performance of metal nanocatalysts to these structural features is important to understanding and designing better catalysts. We undertook a systematic study in which the size and shape effects of Pd nanocrystals are examined as they were applied as semihydrogenation catalysts. Seed-mediated growth methods were used to achieve samples composed of different-sized {100}-terminated Pd nanocubes and {111}-terminated Pd nanoctahedra, which served as model systems to evaluate the role of surface structure to activity and selectivity. As we found, the intrinsic catalytic activity of both Pd nanocubes and octahedra toward selective hydrogenation of 2-hexyne increased with increasing nanocrystal size. Moreover, octahedra were more efficient catalysts compared to nanocubes when normalized to the total number of surface atoms. These results indicated that the geometric size effect can be decoupled from the geometric shape effect by keeping the nanocrystal shape constant and vice versa (Figure 1 left).

Manipulating Reactivity of Shape-Controlled Metal Nanocatalysts through Bimetallic Architecture

Manipulating the electronic structure of metal nanocrystals is one way of altering their catalytic activities. This ability has been demonstrated in two model core@shell systems – Au@Pd and Rh@Pt – where nanoparticle size, shape, and shell thickness were precisely controlled. In this way, particles with variable bimetallic architecture but identical geometric features were compared for the first time to provide insight into how electronic regulation of a catalytic process can be achieved in core@shell systems. In both systems, an optimal shell thickness was identified for maximum reaction rate, with decreased performances observed when shells were too thin or too thick. These results support the concept of a "volcano" plot between the reaction rate and adsorption energies. That is, weakly adsorbing molecular substrates may not bind sufficiently on the catalyst surface to

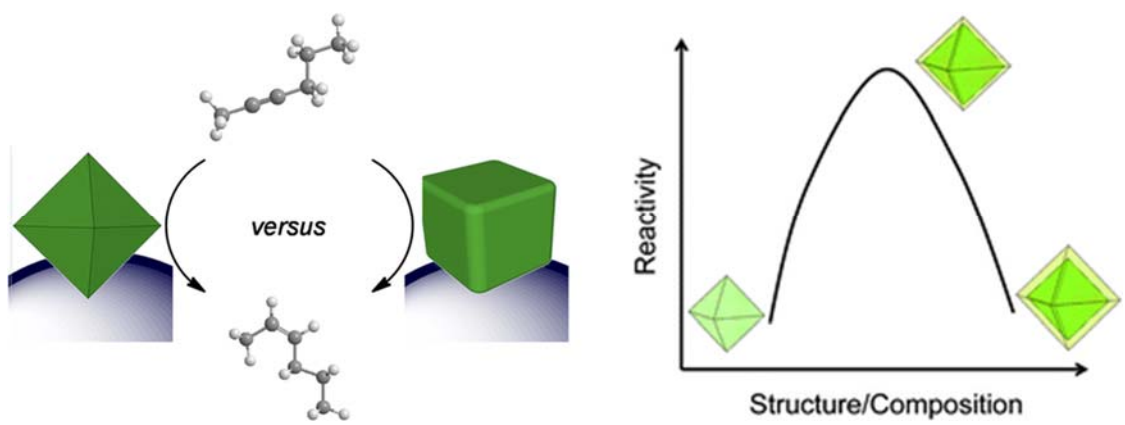

Figure 1. Schemes illustrating that the geometric parameters of particle size and shape can be precisely tuned for optimal catalysis (left) and the electronic parameters of a nanocatalyst can be manipulated through bimetallic architecture for optimal catalysis (right).

facilitate the necessary bond breaking and making steps. Whereas, strongly adsorbing molecular substrates may poison the catalyst surface. Our results indicate that these interactions can be manipulated through the core@shell architecture (Figure 1 right).

Size-Dependent Disorder-Order Transformation in the Synthesis of Intermetallic Nanocatalysts

Conventionally, intermetallic particles are obtained through annealing of nanoparticles of a random alloy distribution. However, this method inevitably leads to sintering of the nanoparticles and generates polydisperse samples. We demonstrated in a model PdCu system that monodisperse intermetallic (B2 phase) PdCu nanoparticles can be achieved at mild conditions by seed-mediated co-reduction using PdCu nanoparticle seeds with a random alloy distribution (A1 phase). The approach is outlined in Figure 2. A time-evolution study suggests that the particles overcome an activation barrier that depends on particle size or surface energy for the ordering process to occur. This synthetic advance should enable other intermetallic compositions to be achieved as monodisperse samples. Moreover, our results suggest that the high-temperature annealing procedures typically used to convert random alloy nanoparticles to intermetallic nanoparticles may not be required to achieve the desired phase; rather, the annealing procedures may be necessary for *inter*particle diffusion and sintering to reach the critical particle size.

Deposition of Highly Strained Alloyed Shells on Intermetallic Nanoparticles for Enhanced

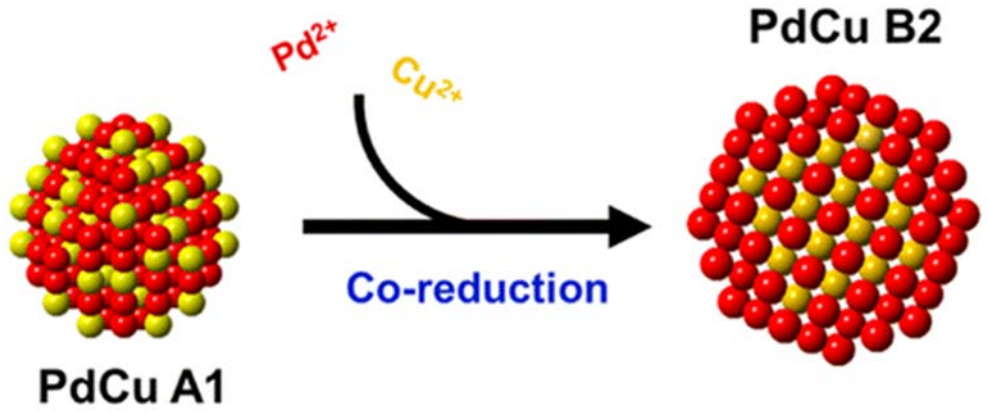

Figure 2. Scheme showing how seed-mediated co-reduction can be used to grow alloyed particles to larger dimensions and facilitate the phase transition to the intermetallic phase.

Electrocatalysis

Bimetallic core@shell nanoparticles are widely studied nanocatalysts but often have limited lattice mismatch and surface compositions. We have initiated investigations into core@shell nanoparticles with greater compositional complexity and lattice misfit. In particular, we have demonstrated that random alloyed shells can be deposited on intermetallic seeds by seed-mediated co-reduction. This deposition is facet-dependent, giving rise to highly strained surfaces that are orientation dependent. This work was initiated through the use of PdCu B2 intermetallic nanoparticles as seeds, with deposition of Pt-M shells. In one example, Pt-Cu shells were deposited, where compressive strains were greater on Pt-Cu {200} than {111} facets. These core@shell nanoparticles provide higher specific area and mass activities for the oxygen reduction

reaction when compared to conventional Pt-Cu nanoparticles (Figure 3). Moreover, these intermetallic@random alloy nanoparticles displayed high endurance, undergoing 10,000 cycles with only a slight decay in activity and no apparent structural changes.

Manipulating Bimetallic Architecture through Metal-selective Capping Agent Interactions

As the previous studies highlight, bimetallic architecture is important to the performance of

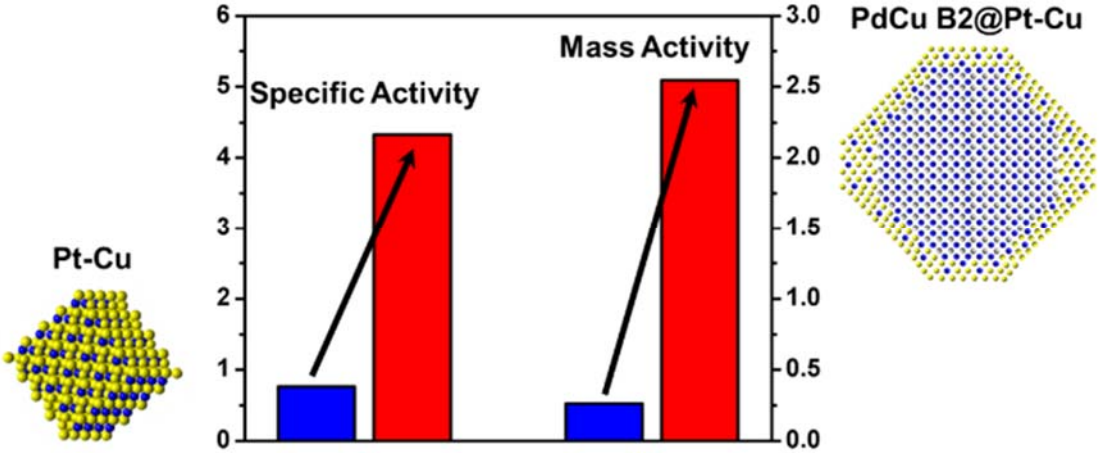

Figure 3. Seed-mediated co-reduction can be used to deposit highly strained alloyed shells on intermetallic seeds for enhanced electrocatalysis, shown here for PdCu B2@Pt-Cu nanoparticles (red bars) used as catalysts for the oxygen reduction reaction compared to PtCu nanoparticles (blue bars).

nanocatalysts. Thus, development of synthetic tools toward multicomponent nanomaterials is a necessity. The selection of capping agents is central to achieving high quality nanostructures. In the case of monometallic nanostructure synthesis, this selection is guided largely by empirical trends. However, for bimetallic nanostructures, this selection is complicated by the diversity of surface-capping agent interactions possible during growth. Yet, we have shown that independent manipulation of the different metals during bimetallic nanostructure formation can be achieved by using two capping agents with interactions selective for one metal each. We demonstrated this concept with Pluronic F127 and NaBr during the co-reduction of Pd and Pt precursors in water with L-ascorbic acid. Notably, Pd2+ binds to Br- more strongly than Cl- and Br- selectively promotes the expression of {100} facets. Pluronic F127 is a well-known stabilizer in the synthesis of branched Pt nanostructures. These tendencies were exploited to achieve octopodal and dendritic Pd@Pt nanoparticles selectively (Figure 4). Our findings demonstrate that two capping agents can be used to independently manipulate the growth regimes of metals in the synthesis of bimetallic nanostructures.

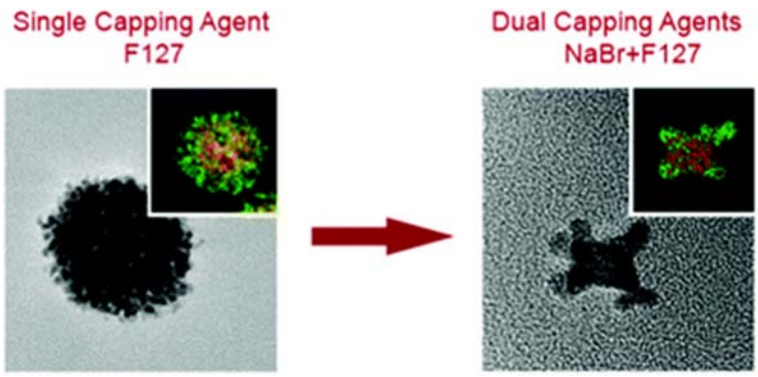

Figure 4. Electron microscopy and elemental mapping (insets, red = Pd and green = Pt) of core@shell Pd@Pt nanodendrites (left) and octopods (right), where the bimetallic architecture is controlled through the selection of specific metal-capping agent interactions.

Publications Acknowledging this Grant in 2014-2017

(I) Exclusively funded by this grant

Harak, E. W.; Koczkur, K. M.; Harak, D. W.; Patton, P.; Skrabalak, S. E.* "Designing Efficient Catalysts through Bimetallic Architecture: Rh@Pt Nanocubes as a Case Study" Submitted.

Ataee-Esfahani, H.; Skrabalak, S. E.* "Overgrowth *versus* Galvanic Replacement: Mechanistic Roles of Pd Seeds during the Deposition of Pd-Pt" Submitted.

Wang, C.; Sang, X.; Chen, D. P.; Unocic, R.; Skrabalak, S. E.* "Facet-Dependent Deposition of Highly Strained Alloyed Shells on Intermetallic Nanoparticles for Enhanced Electrocatalysis" *Nano Letters,* **2017,** in revisions.

Ataee-Esfahani, H.; Skrabalak, S. E.* "Manipulating the Architecture of Pd@Pt Nanostructures through Metal-Selective Capping Agent Interactions" *Chemical Communications,* **2016,** *52,* 10783-10786. DOI: 10.1039/c6cc04849h.

Wang, C.; Chen, D. P., Sang, X.; Unocic, R.; Skrabalak, S. E.* "Size-Dependent Disorder-Order Transformation in the Synthesis of Monodisperse Intermetallic PdCu Nanocatalysts" *ACS Nano,* **2016,** *10,* 6345 – 6353. DOI: 10.1021/acsnano.6b02669.

Laskar, M.; Skrabalak, S. E.* "A Balancing Act: Manipulating Reactivity of Shape-Controlled Metal Nanocatalysts through Bimetallic Architecture" *Journal of Materials Chemistry A* (invited manuscript – Emerging Investigator Issue), **2016,** *4,* 6911-6918. **DOI:** 10.1039/C5TA09368F.

Laskar, M.; Skrabalak, S. E.* "Decoupling the Geometric Parameters of Pd Nanocatalysts" *ACS Catalysis,* **2014,** *4,* 1120-1128. DOI: dx.doi.org/10.1021/cs401064d.

Ammonia at the food-energy-water nexus: the motivation for alternatives to Haber-Bosch, and step catalysis as an example

Peter H. Pfromm*, Bin Liu**, Viktor Chikan**
*Voiland School of Chemical Engineering and Bioengineering, Washington State University; ** Department of Chemical Engineering and ***Department of Chemistry, Kansas State University

Presentation Abstract

A brief overview of the technical and economical boundary conditions of existing industrial scale ammonia synthesis will lead to the motivation to investigate ammonia synthesis approaches other than the classical Haber-Bosch process. The current status of step catalysis using nitrides as the dinitrogen activation vehicle will be shown. This will be followed by an outlook towards potential other uses of activated nitrogen from nitrides, and avenues to continuous ammonia synthesis using nitride membranes

Grant or FWP Number: DE-SC0016453 Step Catalysis to Synthesize Fossil-Free Ammonia at Atmospheric Pressure

Post Doc: Hongfu Luo
Students: Michael Heidlage, Nannan Shan, Nathan Flesher

RECENT PROGRESS

Overview, Goals
Affordable fossil free ammonia synthesis will enable high yield sustainable crop production for a growing world population while preserving the planet and making the best use of water and land. Simple technology amenable to intermittent operation using renewable energy will be made available through step catalysis activating dinitrogen at atmospheric pressure by nitride formation, followed by ammonia harvest when contacting nitrides with gaseous hydrogen.

Approach
Metal alloys will be produced in form of nanoparticles to take advantage of the opportunities to balance the nitride formation vs. ammonia synthesis tasks. The properties of nanoparticles are expected to offer further options to maximize nitrogen uptake, ammonia yield, and reaction kinetics.

Progress

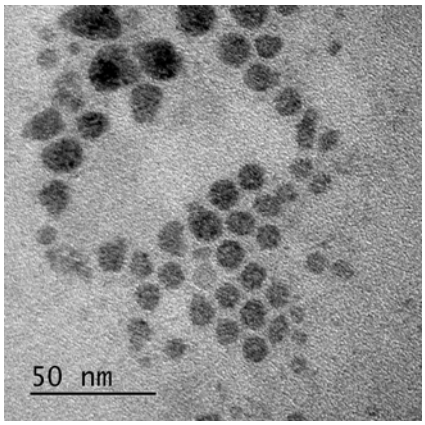

Figure 1: TEM image of Mn nanoparticles obtained with colloidal synthesis.

Nanoparticle Synthesis

Colloidal synthesis of Mn nanoparticles is replicated using a method described in the literature. Mn alloy nanoparticles are obtained by replacing $MnCl_2$ with 50% molar ratio of $MnCl_2$ and MCl_2 (M=Fe, Cr, Ni). In a typical synthesis, a total of 50 mg metal chlorides with appropriate molar ratio and 260 µL oleic acid are added to 10 mL of diphenyl ether in the glovebox. In another vessel 5 mL of diphenyl ether were mixed with 3.0 mL of 1.6 M n-BuLi in hexane in the glovebox. The former solution is then heated to 200 °C followed by injection of the latter solution. The mixture is heated for 20 min before being cooled to room temperature. It is then transferred into the glovebox and quenched with an equal volume of methanol, and centrifuged for 30 min at 8000 rpm. The supernatant is decanted and the product is washed three times with methanol, followed by three times with n-hexane. The particles are dispersed in toluene and drop coated onto a carbon coated copper grid for TEM imaging.

Figure 1 shows a TEM image of Mn nanoparticles with uniform size and spherical shape, indicating successful replication of the method. Mn/Fe nanoparticles obtained with same method are spherical in shape and have an average diameter of about 30 nm.

Modeling

Current theoretical modeling carried out by Liu's group, based on density functional theory (DFT), has been focusing on NH3 formation via the reduction of pure manganese nitride (i.e., Mn4N) and Fe-doped Mn4N model systems at 700°C and 1 atm. All DFT calculations were performed using the Vienna Ab initio Simulation Package (VASP).

The reaction scheme describing the reduction of a stoichiometric N-terminated Mn4N surface, and the first NH3 molecule formation can be expressed by (R1-R5) below, where the asterisk represents the open surface site, and 'g', and 'v' in the parentheses represent gas phase, and the site missing a lattice N, respectively.

$$3/2H_2(g) + * \rightarrow 3H* \quad \text{(R1)}$$

$$Mn_4N* + H* \rightarrow NH* + Mn_4N(v) \quad \text{(R2)}$$

$$NH* + H* \rightarrow NH_2* + * \quad \text{(R3)}$$

$$NH_2* + H* \rightarrow NH_3* + * \quad \text{(R4)}$$

$$NH_3* \rightarrow NH_3(g) + * \quad \text{(R5)}$$

R1 represents H2 dissociative adsorption. R2-R4 represent stepwise NHx (x = 1-3) formation, and R5 represents NH3 desorption.

According to the proposed mechanism (R1-R5), we are able to identify two potential rate-limiting factors that could govern NH3 formation activity: (1) binding strength of H/NH2/NH3, and (2) diffusion energy barrier of lattice N (ΔE_{diff}). The first factor can influence the overall free energy ($\Delta G_{NH_3^*}$) for NH3 formation, while the second factor determines the kinetics of nitrogen-supply to the surface. Hence, based on the pure Mn4N model, we further propose that both $\Delta G_{NH_3^*}$ and ΔE_{diff} need to be lowered to facilitate the thermodynamics and kinetics.

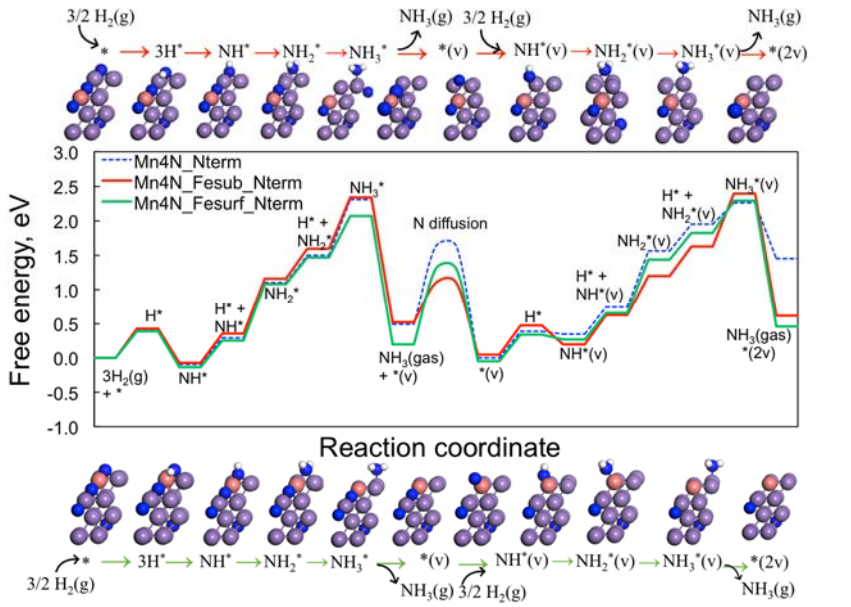

Figure 2: Free energy diagram for NH_3 production (2 NH_3 molecules) on pure Mn_4N (dashed blue as the reference), and Fe-doped Mn_4N (red corresponds to sublayer substituted by one Fe atom, and green corresponds to the top layer substituted by one

As the hypothesis for the overall project, we have proposed that higher conversion of lattice N to NH3 can be achieved with gaseous H2 at elevated temperature compared to pure Mn nitride. Fe-doped Mn4N has been applied to the reduction/NH3 formation cycle. One Mn atom in the sublayer and on the surface is substituted with an Fe atom, denoted by Mn4N_Fesub_Nterm (red) and Mn4N_Fesurf_Nterm (blue), respectively. The resulting free energies diagrams are shown in Figure 2.

The modeling has presented a very intriguing phenomenon, i.e., Fe at different locations of the Mn4N crystal play different roles in the reduction/NH3 formation cycle. As shown above, in both models, the doping is able to improve the NH3 formation activity (either by lowering the lattice N diffusion barrier or lowering the reaction endothermicity), thus, provide encouraging evidence in support of our hypothesis. Furthermore, in both cases, the Fe dopant is able to stabilize the reduced nitride.

Ammonia synthesis by step catalysis: Mn and alloys

In Year 1, the goals of the engineering team are to (1) characterize bulk alloys produced via x-ray diffraction (XRD), and (2) Fine-tune the nitrogen-fixation and NH_3 synthesis reaction procedures using unalloyed Mn as a reference.

Mn-Fe and Mn-Ni samples were prepared in an induction furnace. XRD was used for the bulk of the phase identification and semi-quantitative analysis. Preliminary semi-quantitative results showed several alloy phases including MnNi, $MnNi_3$, and $Fe_{0.8}Mn_{0.2}$.

Nitrogen was fixed to Mn at 1 atm. N2 pressure and at varying times and temperatures to determine the optimum conditions for maximum N content in Mn. According to **Error! Reference source not found.**, the optimum condition for Mn nitridation at 1 atm. is 800 °C for 120 min where 8.7 ± 0.9 wt.% of the solid is nitrogen. Fixation of nitrogen as nitride requires nitrogen dissociation at the gas-solid interface, diffusion of nitrogen into the bulk Mn matrix initially, and later through a growing "shell" of Mn nitride product towards bulk unreacted Mn at the particle core. Another

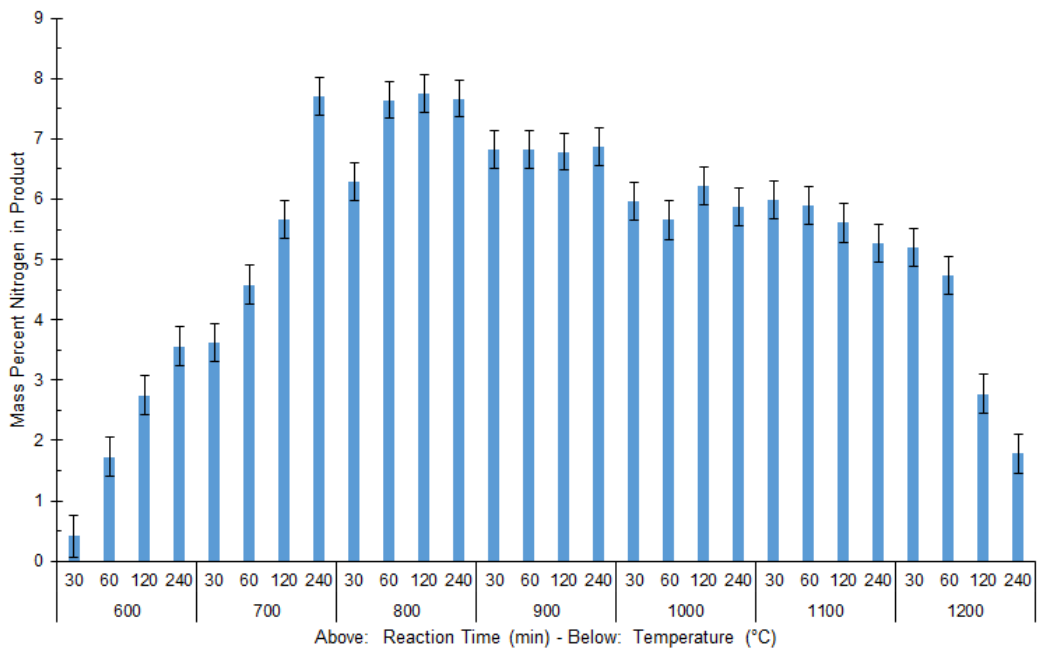

Figure 3: Nitrogen content of solid products from nitridation reactions performed at 1 atm. N_2. Error bars are from error propagation.

complexity is that initially formed Mn4N further reacts to Mn6N2.58 with time.

This behavior is similar to that of other interstitial nitride behavior such as Cr2N to CrN. Mn6N2.58, with the higher N/Mn ratio, becomes the major product after 2 hours at 800 °C corresponding to the maximum in fixed nitrogen at this temperature. Above 800 °C fixed nitrogen yields decrease even as residence times increase. The maximum of 8.7 ± 0.9 wt.% N is fixed at 800 °C and 120 minutes, almost all as Mn6N2.58. Unfortunately, Mn6N2.58 is not detected at any temperature without at least some Mn4N. Particle size reduction can likely shorten the required time significantly due to the strong dependence of diffusion on particles size.

Publications Acknowledging this Grant in 2014-2017

Jointly funded by this grant and other grants with relatively minor intellectual contribution from this grant

1. Conference Paper: Heidlage, M., Pfromm, P. H. Manganese as a Redox Reactant for Sustainable Thermochemical Ammonia Synthesis, American Institute of Chemical Engineers Annual Meeting, San Francisco, CA, November 13, 2016

Electrocatalytic ammonia splitting at ambient temperatures

Reza Ghazfar, Thomas Hamann, Daniel Little, Faezeh Zadeh, and Milton R. Smith, III
Michigan State University, Department of Chemistry

Presentation Abstract

The combined biological and abiological production of ammonia from N_2 is one of the largest scale chemical syntheses on Earth. The reaction of N_2 and H_2 to make NH_3 is thermoneutral. Thus, very little of the energy in H_2 is lost in NH_3 synthesis. Thus, the regeneration of H_2 and N_2 from NH_3 can potentially generate H_2 efficiently. Since ammonia liquefies at low pressure, has an energy density similar to methanol, has been transported across the U.S. by pipeline for decades, and N_2 is atmosphere abundant, ammonia is an attractive liquid fuel for storing and distributing H_2.

Compared to NH_3 synthesis, its conversion to N_2 and H_2 has received far less attention. Most reactions require high temperatures, which can exceed those of the Haber-Bosh process. Electrolysis offers the possibility of 'on demand' H_2 generation, but the most efficient examples are run in aqueous media using catalysts that are alloys of precious metals.

The conversion of liquid NH_3 to H_2 and N_2 at ambient temperatures has never been described with a molecular catalyst. Our initial results towards this goal will be presented.

Grant or FWP Number: Grant Title
Grant Title Second Line if Necessary

Postdoc(s):
Student(s): Reza Ghazfar, Daniel Little, and Faezeh Zadeh,

RECENT PROGRESS

NH_3(l) oxidation at Fe electrodes.
Platinum group metals (PGMs) are common electrodes for electrolysis. We examined oxidation at Fe electrodes to determine how the most Earth abundant metal would perform as an anode. We found that even though Fe anodes were much more sensitive to trace moisture than Pt electrodes, their performance rivals that of Pt anodes when NH_3(l) is distilled from Na(s). Trace H_2O also affected the performance of NH_3(l) electrolysis at Pt anodes, and electrolysis of rigorously dry NH_3(l) occurs at somewhat lower overpotentials relative to our initial report ($\eta \sim$ 1100 mV @ 10 mA·cm^{-2}). Compared to Fe, ca. 10x higher [H_2O] was required to achieve the same level of poisoning for Pt anodes.

At short reaction times Fe dissolution as $Fe(NH_3)_6^{2/3+}$ from the anode was competitive with $NH_3(l)$ oxidation. This is was offset by relatively rapid formation of FeN_x at the anode surface, which substantially curbed the rate of Fe dissolution relative to the rate for $NH_3(l)$ oxidation. Even though FeN_x anodes have essentially identical overpotentials to their Pt counterparts under these conditions, the finding that FeN_x is a suitable alternative to Pt as an anodic material is significant.

Designing transition metal complexes for catalyzing NH_3 oxidation

We have expanded on preliminary results as outlined in our proposal. For example, trisamine complex **1** (Scheme 1) had previously been prepared as part of an MSU-seeded, internal collaboration. Cyclic voltammetry of **1** in THF gave a complex series of waves in the anodic scan, and the cathodic return indicated that several of the oxidations were irreversible. Attempts to deprotonate **1**, yielded the dimer **2**, and some of the complexity in the cyclic voltammograms (CVs) may result from chemical processes, like dimerization, after oxidation.

We had proposed to synthesize monoamine complexes (**3**) by reacting bipyridine ligands with **1** to both simplify the CVs and provide a handle for changing redox behavior by varying the 4,4´-substituents on the bipyridine ligand (Scheme 2). Somewhat surprisingly, neither

Scheme 1

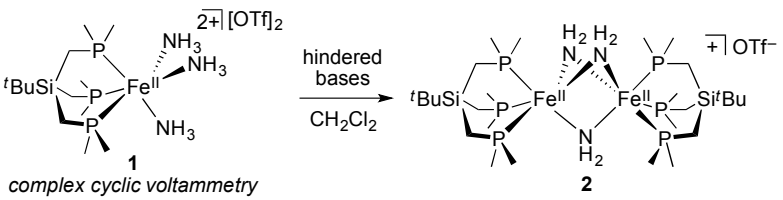

complex cyclic voltammetry

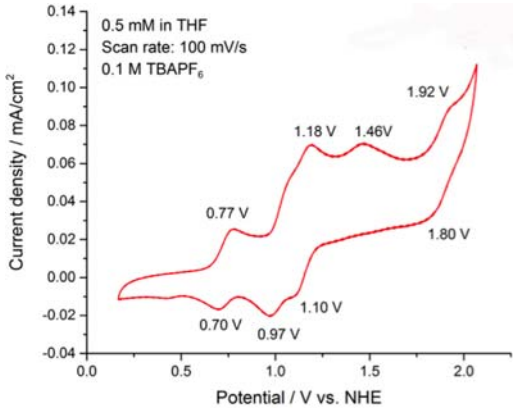

Scheme 2

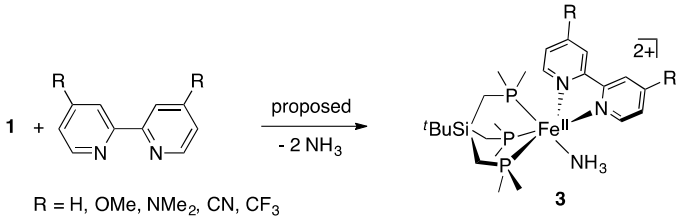

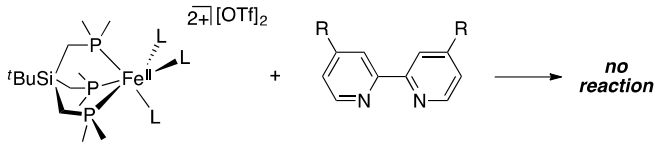

Scheme 3

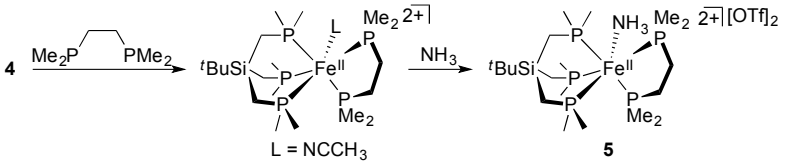

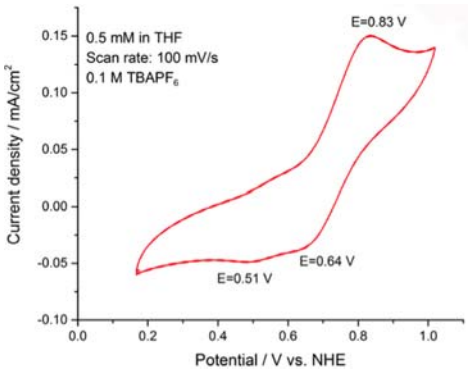

compound **1** nor trisacetonitrile complex **4** reacted with bipyridine ligands under any conditions. Nevertheless, 1,2-bis(dimethyl) phosphino ethane reacted with **4** yielding a pentaphosphine acetonitrile complex en route to monoamine compound **5** (Scheme 3). CVs for compound **5** are much simpler than those for compound **1**, and preliminary studies indicate a shift in the onset potential for oxidations of NH_3 in the presence of catalytic quantities of compound **5**.

We also proposed to examine the oxidations of Ru^{II} monoamine complexes in anhydrous media since Meyer and co-workers have shown that NH_3 ligand in compound **6** can be oxidized by six electrons to form nitro compound **7**. As shown in Scheme 4, it was proposed that the first N–O bond forms via nucleophilic attack of water at the electrophilic imido N in undetected Ru^{IV} intermediate **8**, which is generated by a two-electron oxidation of compound **6**. Hydroxylamine intermediate **9** then undergoes a sequence of oxidations, attack of a second equivalent of water and loss of five protons to yield nitro compound **7**.

Scheme 4

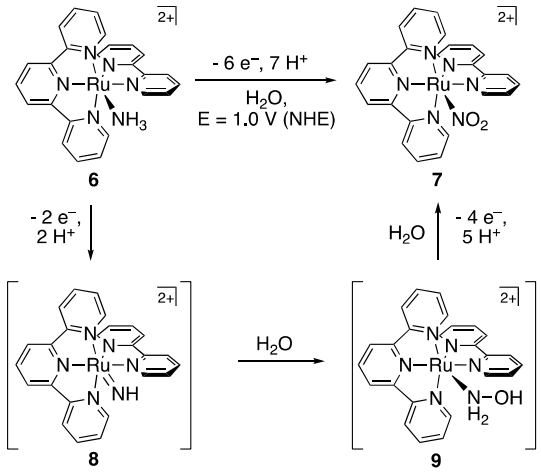

Thompson and Meyer *JACS* **1981**, *103*, 5577-5579

Our premise in this part of the project is that N–N bond formation should be favored if oxidations are carried out under anhydrous conditions in the presence of NH_3. Our first step toward this aim was to synthesize compound **10** and assess its electrochemical behavior in anhydrous THF. As shown in Scheme 5, **10** can be reversibly oxidized at ~ 1.3 V vs. NHE. At this potential, NH_3 oxidation at the Pt anode will compete based on our previous work.

Scheme 5

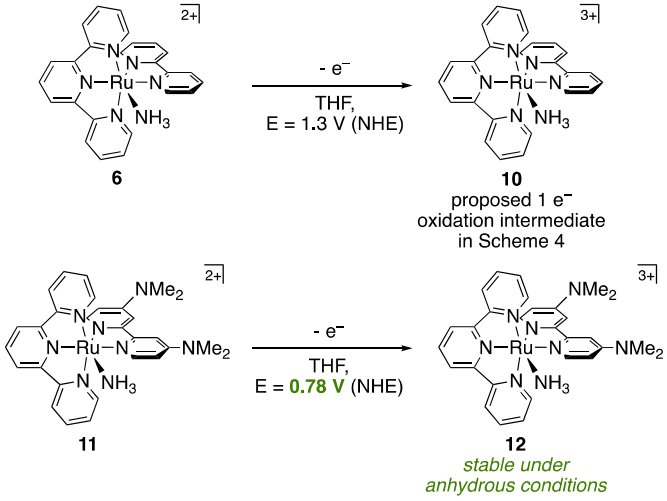

To lower the oxidation potential, we prepared the 4,4′-dimethylaminobipyridine analog (**12**) of compound **10**. As shown in Scheme 5, the $Ru^{2+/3+}$ is lowered by ~ 500 mV. Recent results indicate Ru^{III} amine complex **13** can be isolated. This is significant because Thompson and Meyer had previously proposed that the bpy analog, Ru^{III} intermediate **11**, undergoes redox disproportionation to generate Ru^{II} amine complex **6** and Ru^{IV} imido intermediate **8** in the synthesis of compound **7** through the six-electron oxidation of compound **6** (Scheme 4).

The isolation of compound **12** is fortuitous, but can be understood when one considers that the proposed redox disproportion of intermediate **10** to compound **6** and intermediate **8** would require a base. Since H_3O^+(aq) is more stable than protonated THF, the fact that **12** can be isolated under anhydrous conditions is a result of THF's weak basicity.

Elucidating the reaction mechanisms for catalytic NH_3 oxidation

When green THF solutions of paramagnetic compound **12** are treated with NH_3, the color rapidly changes to maroon, and ^{1}H NMR spectra indicate that compound **11** is generated along with another diamagnetic Ru compound. We have very recently seen that solutions on **11** in THF with excess NH_3 generate significant currents at potentials where background oxidation at the Pt anode is negligible. We are currently working to identify the products of the catalytic process.

Publications Acknowledging this Grant in 2016-2017

(II) Jointly funded by this grant and other grants with leading intellectual contribution from this grant;

1. Little, D. J.; Edwards, D. O.; Smith, M. R., III; Hamann, T. W. As Precious as Platinum: Iron Nitride for Electrocatalytic Oxidation of Liquid Ammonia. *ACS Appl. Mater. Interfaces* **2017**, *9*, 16228-16235.

John F. Berry

Oxo and Nitride Chemistry with Metal-Metal Bonds

University of Wisconsin - Madison

Presentation Abstract

Non-classical coordination compounds are those that contain metal-metal or metal-ligand multiple bonds. Our research group's approach to combining metal-metal and metal-ligand multiple bonds in novel polyfunctional structures will be presented. The chemistry of metal-metal-oxo and -nitrido compounds will be discussed in comparison to their monometallic analogs. The relationship between electronic structure and reactivity in this class of compounds will be emphasized, highlighting the important role of three-center/four-electron bonding, which engenders these compounds with exceptional electrophilic reactivity.

DE-SC0016442: Novel Homogeneous Electrocatalysts for the Nitrogen Reduction Reaction

PI: John F. Berry
Postdoc(s): Christian Wallen
Student(s): Tristan Brown, Michael Roy, Sungho Park
Affiliations(s): University of Wisconsin - Madison

RECENT PROGRESS

New Oxypyridinate Paddlewheel Ligands for Alkane-Soluble, Sterically Protected Ru_2(II,III) and Ru_2(II,II) Complexes

In order to prepare Ru_2 complexes capable of small molecule activation, we have designed new sterically-demanding ligands that support Ru_2(II,II) and Ru_2(II,III) complexes having a vacant coordination site. Using these ligands, we have explored the ability of Ru_2 complexes to coordinate weak σ-donor ligands, including dichloromethane and decane.

Unusual Magnetic Anisotropy and One-Electron Reduction of Pd(II) Acetate and Chelate-Stabilized Analogues

Using the chelating dicarboxylate ligand esp^{2-}, the properties of triangular Pd_3 compounds are studied in the solid state and in solution. Variable-temperature NMR and DFT studies reveal unusual chemical shifts for protons directly above or below the plane of the Pd atoms. The compounds also show a surprising quasi-reversible reduction wave between –880 and –1200 mV

vs. Fc/Fc^+. EPR spectra of reduced samples indicate a localized Pd(II)-Pd(II)-Pd(I) electronic structure.

Synthesis, characterization and solution behavior of a systematic series of pentapyridyl-supported Ru^{II} complexes: Comparison to bimetallic analogs

A series of Ru^{II} complexes stabilized with the pentapyridyl ligand Py_5Me_2 (Py_5Me_2 = 2,6-bis(1,1-bis(2-pyridyl)ethyl)pyridine) and with an axial X ligand (X = Cl^-, H_2O, N_3^-, MeCN) were prepared and characterized in the solid state and in non-aqueous solution. The cyclic voltammograms of these complexes in MeCN reflect a reversible substitution of the axial X ligand with MeCN. Irreversible ligand substitution of $[(Py_5Me_2)RuN_3]^+$ is also observed in propylene carbonate, but only at oxidizing potentials that decompose the azide ligand. The monometallic chloride and azide species are compared with analogous Ru_2 metal–metal bonded complexes, which have been reported to undergo irreversible chloride dissociation upon reduction.

Anilinopyridinate-Supported Ru_2^{x+} (x = 5 or 6) Paddlewheel Complexes with Labile Axial Ligands

Five new metal–metal bonded Ru_2 compounds are presented and discussed: $Ru_2(ap)_4ONO_2$ (**2**), $[Ru_2(ap)_4NCMe][BF_4]$ (**3**), $Ru_2(ap)_4FBF_3$ (**4**), $Ru_2(ap)_4OTf$ (**5**), and $[Ru_2(ap)_4OTf][Ag(OTf)_2]$ (**6**) (ap = 2-anilinopyridinate). All compounds have a (4,0) arrangement of the ap ligands about the Ru–Ru bond and contain one sterically blocked axial site and one site containing a labile ligand. These compounds display some of the shortest Ru–Ru distances known for this class of compounds. We demonstrate a reversible interconversion between compounds **3** and **4** as the MeCN and BF_4^- ligands are readily displaced. Despite the presence of labile axial ligands, compounds **2** – **5** remain high spin with an $S = 3/2$ ground state as determined by EPR spectroscopy.

A Synthetic Oxygen Atom Transfer Photocycle from a Diruthenium Oxyanion Complex

Three new diruthenium oxyanion complexes have been prepared, crystallographically characterized, and screened for their potential to photochemically unmask a reactive Ru–Ru≡O intermediate. The most promising candidate, $Ru_2(chp)_4ONO_2$ (**4**, chp = 6-chloro-2-hydroxypyridinate), displays a set of signals centered around m/z = 733 amu in its MALDI-TOF mass spectrum, consistent with the formation of the $[Ru_2(chp)_4O]^+$ ($[\mathbf{6}]^+$) ion. These signals shift to 735 amu in **4***, which contains an ^{18}O-labeled nitrate. EPR spectroscopy and headspace GCMS analysis indicate that NO_2• is released upon photolysis of **4**, also consistent with the formation of **6**. Photolysis of **4** in CH_2Cl_2 at room temperature in the presence of excess PPh_3 yields $OPPh_3$ in 173% yield; control experiments implicate **6**, NO_2•, and free NO_3^- as the active oxidants. Notably, $Ru_2(chp)_4Cl$ (**3**) is recovered after photolysis. Since **3** is the direct precursor to **4**, the results described herein constitute the first example of a synthetic cycle for oxygen atom transfer that makes use of light to generate a putative metal oxo intermediate.

Publications Acknowledging this Grant in 2014-2017

(I) Exclusively funded by this grant:

1. Park, S.; Berry, J. F. *Dalton Trans*. ASAP. Synthesis, characterization and solution behavior of a systematic series of pentapyridyl-supported Ru^{II} complexes: Comparison to bimetallic analogs
2. Corcos, A. R.; Berry, J. F. *Dalton Trans.* **2017**, *46*, 5532-5539. Anilinopyridinate-Supported Ru_2^{x+} (x = 5 or 6) Paddlewheel Complexes with Labile Axial Ligands
3. Corcos, A. R.; Pap, J. S.; Yang, T; Berry, J. F. *J. Am. Chem. Soc.* **2016**, *138*, 10032-10040. A Synthetic Oxygen Atom Transfer Photocycle from a Diruthenium Oxyanion Complex

Friday PI
Oral Presentations

Christine M. Thomas

Coordinatively Unsaturated Bis(Phosphinoamide) Ti/Co and Zr/Co Complexes and Their Enhanced Reactivity Towards Small Molecule Substrates

Christine M. Thomas,* Kathryn M. Gramigna, Bing Wu, Diane A. Dickie, Mark W. Bezpalko, and Bruce M. Foxman
Brandeis University, Department of Chemistry

Presentation Abstract

The combination of early and late transition metals into a single heterobimetallic scaffold has been demonstrated as a successful strategy for tuning redox potentials and facilitating small molecule activation processes. Using a tris(phosphinoamide) ligand framework, our group has assembled a diverse family of early/late heterobimetallic complexes with varying degrees of, in some cases unprecedented, metal-metal multiple bonding. The most promising reactivity has been observed using the reduced Zr^{IV}/Co^{-I} complex (THF)Zr(MesNP^{i}Pr$_2$)$_3$CoN$_2$ (Mes = 2,4,6-trimethylphenyl), which has been shown to undergo one-, two-, and four-electron transfer processes, activating a variety of σ (e.g. O-H, N-H, C-X) and π (e.g. C=O) bonds. In many of these cases, one of the three phosphinoamide ligands dissociates from Co and anchors itself in an η^2 fashion to the Zr center to allow substrates to simultaneously access the two metals. While this ligand hemilability may be perceived as advantageous, it may also add unnecessary steps to productive reaction profiles. In many cases, we have also observed that reductants such as H_2 or HBR_2 cleave one of the phosphinoamide P-N bonds in an undesired pathway that hinders catalytic activity. We have, thus, extended our family of heterobimetallic complexes to bis(phosphino)amide-linked bimetallic frameworks that are more open, leaving the metal-metal bond more accessible to substrates. A series of bis(phosphinoamide)-linked Ti/Co and Zr/Co complexes have been synthesized, revealing that equally strong metal-metal interactions can form with just three supporting ligands. In particular, the reduced Zr/Co bis(phosphinoamide) complex (THF)(I)Zr(XylNP^{i}Pr$_2$)$_2$Co(PR$_3$) (Xyl = 3,5-dimethylphenyl, PR$_3$ = PMe$_3$, PMePh$_2$) readily oxidatively adds H_2 to afford stable bimetallic dihydride species, (THF)(I)Zr(XylNP^{i}Pr$_2$)$_2$(μ-H)Co(H)(PR$_3$). (THF)(I)Zr(XylNP^{i}Pr$_2$)$_2$Co(PR$_3$) also undergoes facile C-H activation when treated with phenylacetylene. The ability of Zr/Co bis(phosphinoamide) complexes to catalyze the hydrogenation of alkenes and alkynes at room temperature and 1 atm of H_2, will be discussed, along with spectroscopic studies to investigate the resting state of the catalyst and the mechanism of the reaction.

DE-SC0014151: Metal-Metal Interactions in Heterobimetallic Complexes as a Strategy to Promote Multielectron Redox and Small Molecule Activation Processes

PI: Christine M. Thomas
Postdoc(s): Bing Wu, Jeremy P. Krogman, Kathleen Taylor
Student(s): Kathryn M. Gramigna, Gursu Culcu, Hongtu Zhang

RECENT PROGRESS

Heterobimetallic complexes with two bridging ligands

Since we have previously discovered that (1) bis(phosphinoamide) Ti/Co complexes are more reactive than their tris(phosphinoamide) counterparts and (2) that Zr/Co complexes are more reactive than Ti/Co complexes, it seemed logical to target Zr/Co bis(phosphinoamide) complexes. Although their synthesis was not as straightforward as the Ti analogues, a Zr^{IV}/Co^{I} complex has been synthesized and can be reduced to generate Zr^{IV}/Co^{-I} complexes. The reduced complex

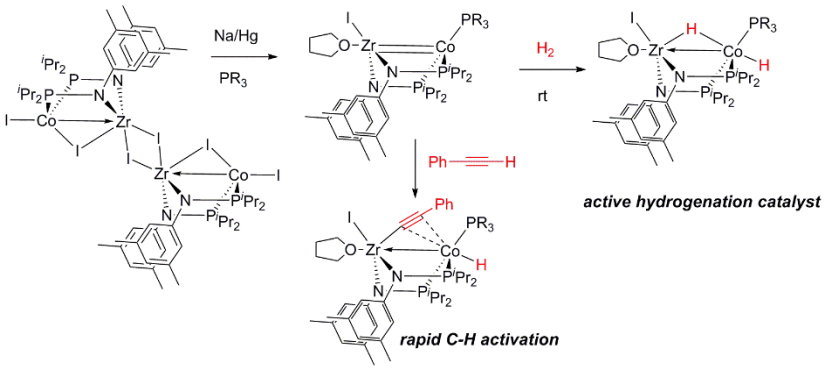

(THF)(I)Zr(XylNP^{i}Pr$_2$)$_2$Co(PR$_3$) can be isolated and is very reactive towards small molecule substrates. For example, addition of H_2 to (THF)(I)Zr(XylNP^{i}Pr$_2$)$_2$Co(PR$_3$) rapidly generates a bimetallic dihydride complex, (THF)(I)Zr(XylNP^{i}Pr$_2$)$_2$(μ-H)Co(H)(PR$_3$). Preliminary results also show that (THF)(I)Zr(XylNP^{i}Pr$_2$)$_2$Co(PR$_3$) is an active catalyst for the hydrogenation of alkenes and alkynes under mild conditions (rt; 1 atm H_2). (THF)(I)Zr(XylNP^{i}Pr$_2$)$_2$Co(PR$_3$) also readily oxidatively adds the C-H bond of phenylacetylene through a cooperative bimetallic pathway.

Heterobimetallic Nb/M complexes.

Owing to our success with Zr/Co complexes, we sought to synthesize isoelectronic Nb/Fe complexes, hypothesizing that the enhanced redox properties of Nb might aid further in facilitating multielectron redox pathways. A Nb^{IV}/Fe^{I} complex ClNb(^{i}PrNPPh$_2$)$_3$FeBr and its two-electron reduction product Nb(^{i}PrNPPh$_2$)$_3$FePMe$_3$ were synthesized and characterized structurally and spectroscopically. These compounds are directly analogous to the Zr/Co complexes that we

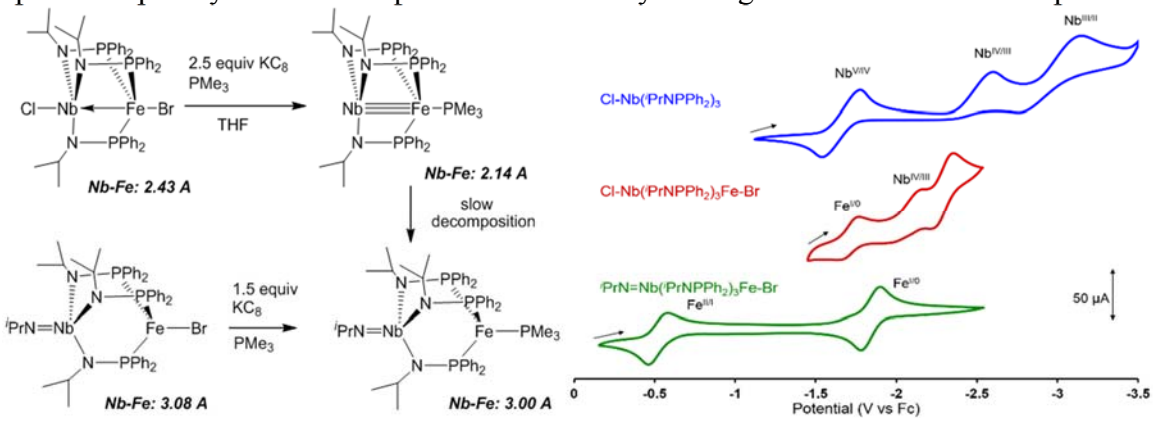

previously reported, and feature the first examples of Nb-M single and triple bonds (M ≠ Nb), respectively. Nb(^{i}PrNPPh$_2$)$_3$FePMe$_3$, which features a coordinatively unsaturated trigonal

monopyramidal geometry at the Nb center, is quite reactive and undergoes intramolecular decomposition over time to afford the bimetallic imido-Nb^V/Fe complex $^iPrN{=}Nb(^iPrNPPh_2)_3FePMe_3$.The latter imido complex can be synthesized independently from the Fe^I precursor $^iPrN{=}Nb(^iPrNPPh_2)_3FeBr$, and neither Nb^V imido complex contains a Nb-M bond, they serve as an important "control" compounds for studies of the effect of through-ligand communication on the redox behavior of the Fe centers. It was found that while direct Fe→Nb dative interactions lead to large anodic shifts of the $Fe^{I/0}$ redox couple, in line with previous studies of the Zr/Co system, these interactions also cause the $Nb^{IV/III}$ potential to shift ca. 400 mV in the positive direction, suggesting that metal-metal interactions diminish electron density at both metal centers even in the presence of a dative interaction. Further, the Fe center in imido-protected complex $^iPrN{=}Nb(^iPrNPPh_2)_3FeBr$ is still substantially easier to reduce than a monometallic Fe^I complex, indicating that the early metal can affect redox potentials even in the absence of direct metal-metal interactions.

Unlike the Zr/M system, where M is limited to Co, a series of analogous Nb/M complexes (M = Fe, Co, Ni, Cu) can be synthesized, allowing for a systematic exploration of metal-metal bonding, redox properties, reduction products, and reactivity as a function of metal-metal combination.

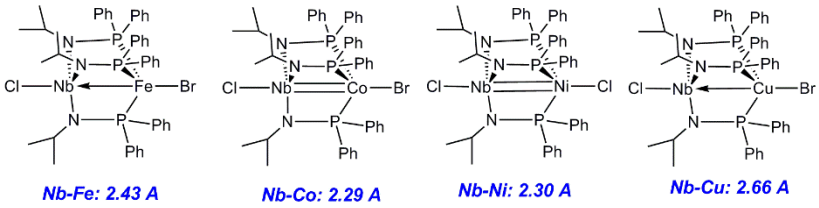

Mechanistic studies of C=O bond cleavage reactions

Our group has also continued to study the mechanism of C=O bond cleavage by the heterobimetallic Zr/Co complex $(THF)Zr(MesNP^iPr_2)_3CoN_2$. Previously, we had found that the *para*-substituents of diaryl ketones greatly affected whether an $S = 0$ ketone adduct or $S = 1$ ketyl radical complex formed upon addition to $(THF)Zr(MesNP^iPr_2)_3CoN$. In the case of *para*-OMe substituents, the difference in energy between the S = 0 and $S = 1$ products is sufficiently small that both species are observed. When the bound N_2 is removed under vacuum, the ketyl/ketone adduct mixture converts to the μ-oxo carbene complex $(MesNP^iPr_2)Zr(MesNP^iPr_2)_2(\mu\text{-}O)CoCO$ via C=O bond oxidative addition. A diamagnetic intermediate, identified as a side-bound ketone adduct, was observed during this reaction.

The reactivity of $(THF)Zr(MesNP^iPr_2)_3CoN_2$ towards aldehydes and alkyl-substituted ketones was also explored in an effort to determine (1) whether electron transfer also occurred upon substrate coordination and (2) if C=O bond cleavage pathways from these products also afforded cobalt carbenes. $(THF)Zr(MesNP^iPr_2)_3CoN_2$ does react with anisaldehyde and acetophenone via electron transfer pathways to form C-C radical coupling products, respectively. Removal of N_2 and thermolysis of the acetophenone-derived product does not afford a carbene product, but C=O bond cleavage does occur to form an oxo-bridged species.

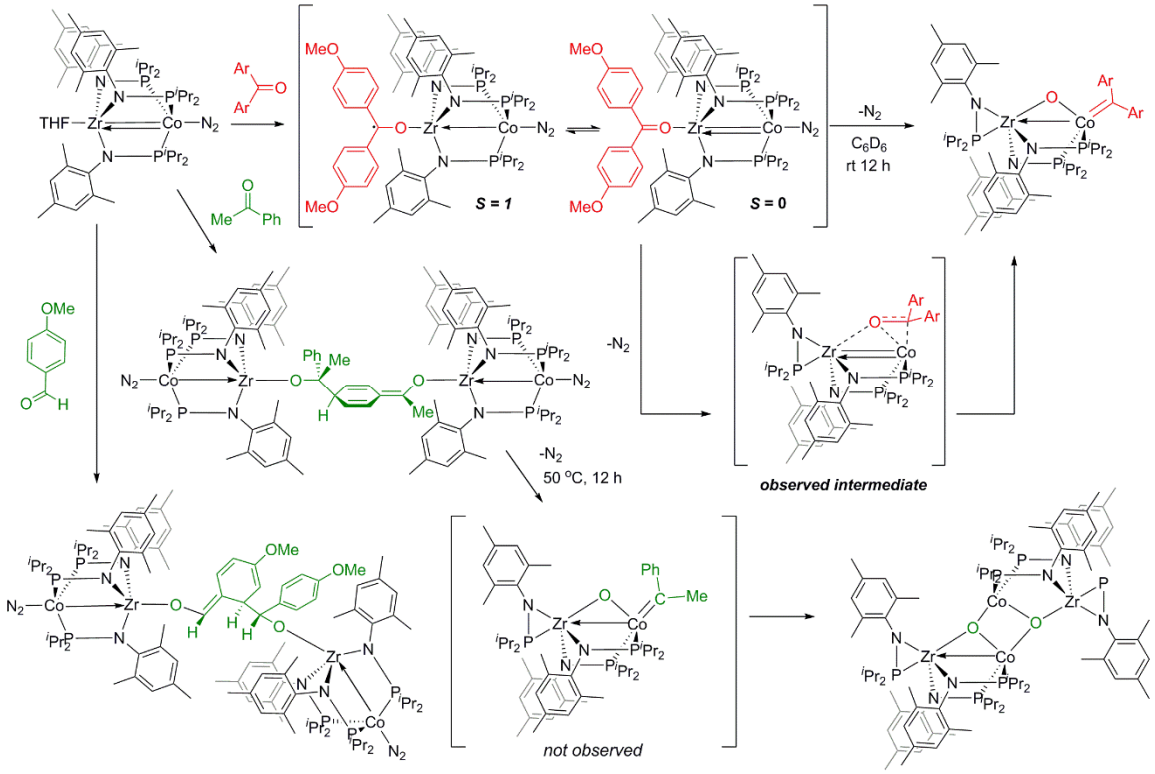

Publications Acknowledging this Grant in 2014-2017

(I) *Exclusively funded by this grant*

(1) Culcu, G.; Iovan, D. A.; Krogman, J. P.; Wilding, M. J. T.; Bezpalko, M. W.; Foxman, B. M.; Thomas, C. M. *J. Am. Chem. Soc.* **2017**, *accepted*, DOI: 10.1021/jacs.7b04151

(2) Wu, B.; Wilding, M. J. T.; Kuppuswamy, S.; Bezpalko, M. W.; Foxman, B. M.; Thomas, C. M. *Inorg. Chem.* **2016**, *55*, 12137-12148.

(3) Krogman, J. P.; Bezpalko, M. W.; Foxman, B. M.; Thomas, C. M. *Dalton Trans.* **2016**, *45*, 11182-11190.

(II) *Jointly funded by this grant and other grants with leading intellectual contribution from this grant*

(1) Zhang, H.; Wu, B.; Marquard, S. L.; Dickie, D. A.; Bezpalko, M. W.; Foxman, B. M.; Thomas, C. M. *Organometallics* **2017**, submitted.

Small Ligands Behaving Badly: Redox Non-innocence in Earth-Abundant 3d Metal Catalysts

Thomas R. Cundari
University or North Texas

Presentation Abstract

"Green" replacements for platinum group metals (PGMs) have been of considerable interest in the catalysis community. Within the larger field of sustainable catalysis, the use of potentially redox non-innocent (RNI) ligands in conjunction with Earth-abundant 3d metals (which are, of course, more prone to 1-e^- or radical chemistry vis-à-vis their 4d and 5d congeners) to mimic the even-e^- chemistry of PGM catalytic cycles has been the intensely studied by experimentalists. Our group has sought to develop computational modeling tools and the intellectual advances necessary to understand (and eventually design) catalyst systems whereby a RNI ligand and a 3d metal may be synergized to deliver 2 e^- to a metal-ligand active site for the purposes of productive catalytic reactions such as the activation and functionalization of strong chemical bonds such as aliphatic C—H or olefinic C=C bonds. In addition to elaborately constructed (typically conjugated) organic supporting ligand scaffolds, our most recent research, in concert with experimental efforts, shows evidence of RNI behavior – not only in terms of formal oxidation states that do not correspond to those expected by simple bonding principles but that change in redox poise during the course of a reaction – in unexpected chemical moieties including multiply bonded ligands (*e.g.*, imide/imidyl and oxide/oxyl) and even saturated, ring-strained hydrocarbyls (such as 1-norbornyl). This talk will provide an overview of our past and current work in this area with some thoughts on future directions.

DE-FG02-03ER15387: Modeling of Late Transition Metal Catalysts for Energy Applications

UNT Postdoc(s):
Dr. Sarina M. Bellows – SiGNa Chemistry
Dr. J. Brannon Gary – Stephen F. Austin U.
UNT Graduate Student(s):
Ms. (now Dr.) Hengameh Fallah – Columbia U.
Ms. Sarah K. Khani (MS Student) – MPI
Mr. (now Dr.) Glenn R. Morello – Center for Theoretical and Computational Chemistry (Tromso)
Mr. Catherine Moulder – UNT
Mr. (now Dr.) Dale R. Pahls – Argonne Nat. Lab.
Ms. Riffat Parveen – UNT
Vitor H. M. da Silva – U. de São Paulo

UNT Undergraduate Student(s):
Mr. Eduardo Monotya – UNT
Ms. Catherine Moulder – UNT

RECENT PROGRESS

Significant recent progress has been made in both key research thrusts – catalytic arene functionalization (including direct styrene production), and catalytic hydrocarbon functionalization reactions by Earth-abundant metal complexes (primarily late 3d metals) with redox non-innocent ligands. Twelve (12) refereed publications acknowledging DOE-BES support via **DE-FG02-03ER15387** were published in just the past year. DOE-supported research has also been acknowledged in invited seminars by the PI, and by his undergraduate, graduate, postdoctoral and faculty research collaborators.

Our recent DOE-BES supported research has described the work of 6 Ph.D. research students (including one visiting Ph.D. student from Brazil); 1 M.S. student (now pursuing her Ph.D. in Germany); 2 postdoctoral associates (who have or will soon move on to full-time jobs); 2 undergraduate research assistants (one of whom is pursuing here Ph.D. in Chemistry, while the other is finishing up his senior year in the upcoming academic year) in the Cundari group. Additionally, many other early-career scientists in the laboratories of our faculty collaborators – Gunnoe (U. Va.), Wolczanski (Cornell U.), *etc.* – have participated in leading edge research at the interface of theory and experiment (see below for participants, publications, presentations).

Redox Non-Innocent Supporting Ligation

A major theme in our DOE-BES supported research has been to develop the essential intellectual underpinning by which redox non-innocent supporting ligands may be used in conjunction with Earth-abundant (primarily 3d) transition metals to effect catalytic transformations that are relevant to energy applications. Of particular interest is being able to identify systems whereby <u>both</u> the metal and supporting ligand may deliver electrons to an active site for the purposes of carrying out productive catalysis, with emphasis on the activation of strong aliphatic C—H bonds.

In conjunction with the Wolczanski group, an interesting intramolecular C—C activation/ coupling reaction was evaluated for Co and for Li complexes. Quantum mechanical calculations in our lab led to the surprising prediction that for the two-step mechanism (C—H bond activation followed by C—C bond coupling), it was the latter transition state that defined the highest point on the reaction coordinate, **Figure 1**. Our computational proposal sparked further kinetic isotope effects (KIE) experiments, which produced a modest KIE of 1.16(9), consistent with our predictions. Furthermore, comparing Co and Li (the latter being an

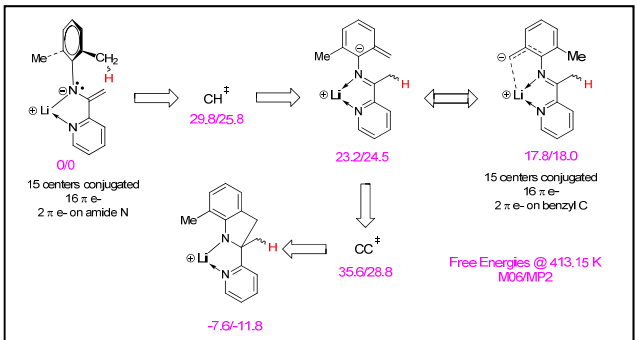

Figure 1. Relative free energies (in kcal/mol) of a C—C bond coupling reaction pathway determined with DFT (M06) and correlated wavefunction (MP2) techniques.

obviously redox innocent metal) results implies that it is the ligand that plays the major role in mediating the redox bond coupling.

Earth-abundant olefin metathesis catalysts have garnered considerable experimental attention. Our group investigated purported high-valent 3d metal alkylidenes with potentially redox non-innocent supporting ligands. Electronic structure calculations on [*mer*-{κ-C,N,C-(2-C_6H_4)CH=N(1,2-C_6H_4)C(^{i}Pr)=}Fe(PMe_3)$_3$]$^+$, whose synthesis was reported by Wolczanski *et al.*, suggest that it is best viewed as an Fe(II) ion bound to a carbenium ion, rather than a true Fe(IV)-alkylidene, **Figure 2**. Consistent with this proposal, experimental attempts to identify olefin metathesis or carbene transfer chemistry displayed alternative reactivity. Two additional L_nFe=CHR compounds were thus structurally characterized by Wolczanski *et al.* from these efforts; metrical parameters of the latter (from experiment and computation), in addition to electronic structure calculations by our group, suggest that these too are not Fe(IV)-alkylidenes, but rather Fe(II) centers coordinated by a conjugated vinyl ligand with extensive delocalization in their π-systems.

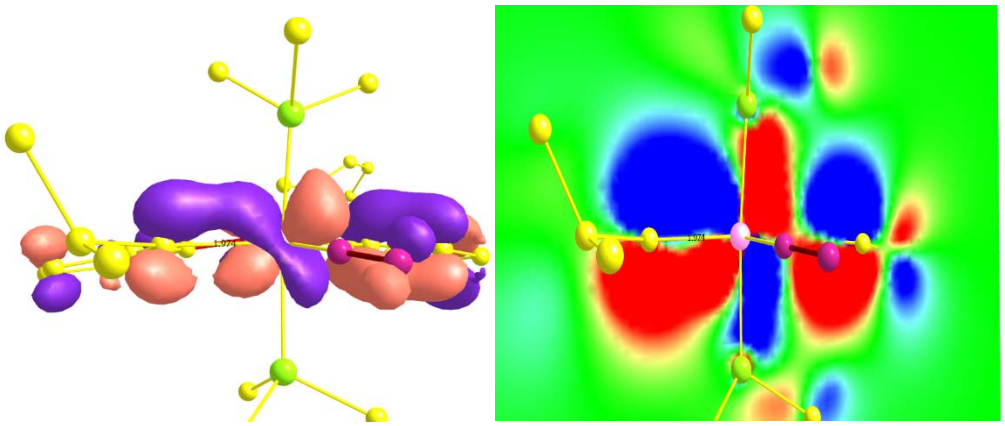

Figure 2. Plot of Fe-C "π bond" (left) and contour plot of same orbital (right, in a plane containing the FeC bond of interest) for a novel complex synthesized by Wolczanski *et al.* As can be seen in the plots the orbital is very polarized and more closely resembles an Fe(II)-carbenium rather than a Fe(IV)-alkylidene.

More recent research in collaboration with Wolczanski's group has extended this work to NHC-supported "Fe(IV)" imides. Two potentially interesting observations from the preliminary calculations indicate the potential for (a) small multiply bonded ligands and (b) strained hydrocarbyl groups to act in a redox non-innocent fashion. Moreover, this research has started to clarify the essential electronic features needed for effective redox non-innocence in terms of both orbital energy matching and LCAO-MO orbital delocalization, as well as the computational advances needed to model these challenging chemical and catalytic systems.

Catalytic Olefin Hydroarylation and Direct Styrene Synthesis

With our long-time experimental collaborators (and fellow DOE-BES grantees) in the Gunnoe group, we contributed an invited manuscript summarizing our many papers on utilizing scorpionate complexes for catalysis, most notably olefin hydroarylation laying out our mechanistic studies of this important catalytic process (including side reactions) via the close integration of theory (Cundari group) and experiment (Gunnoe group).

Styrene is currently produced from benzene and ethylene through the intermediacy of ethylbenzene, which must be dehydrogenated in a separate step. For this reason, we have invested significant effort in understanding the factors that control the formation of alkyl-arenes via hydroarylation catalysis with our experimental collaborators in the Gunnoe group. However, a direct oxidative conversion of benzene and ethylene to styrene could provide a more efficient route, but achieving high selectivity and yield for this reaction has been challenging. In 2015, we reported with Gunnoe's group a Rh catalyst (^{Fl}DAB)Rh(TFA)(η^2–C_2H_4) [^{Fl}DAB = N,N′-bis(C_6F_5)-2,3-dimethyl-1,4-diaza-1,3-butadiene; TFA = trifluoroacetate] that converts benzene, ethylene, and Cu(II) acetate to styrene, Cu(I) acetate, and acetic acid with 100% selectivity, yields ≥ 95%, and turnover numbers > 800. More recently, we reported a more thorough mechanistic study of this system in collaboration with Gunnoe. Examining reaction rates, their dependence on catalyst concentration, ethylene pressure and Cu(II) oxidant, as well as isotope effects, indicates competing pathways involve mono- and bi-metallic Rh intermediates.

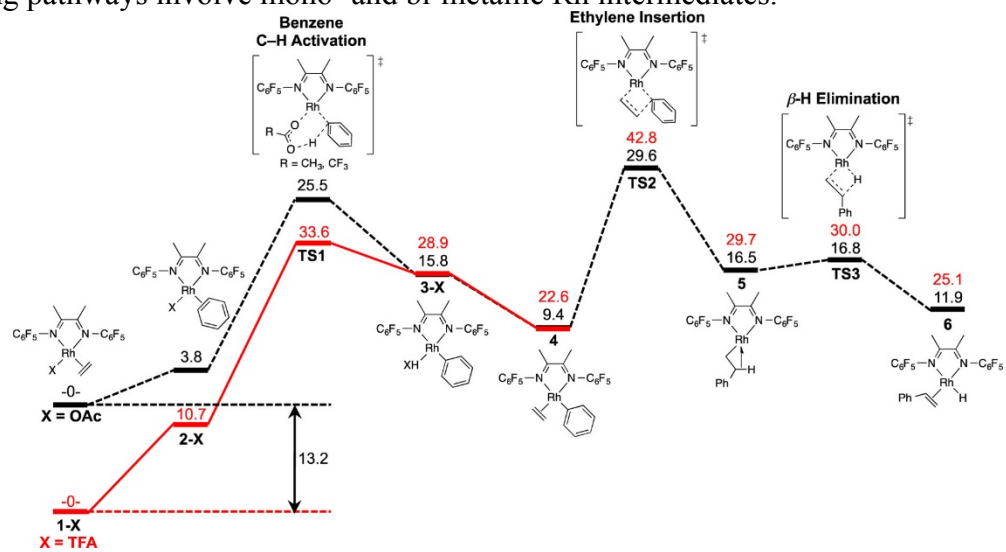

Figure 3. Calculated Gibbs Free Energies [B3LYP/LANL2DZ+6-311++G(d,p), kcal/mol] Including Solvent (SMD-benzene) and Dispersion Corrections for Lowest Energy Calculated Pathway for Styrene Production Using (^{Fl}DAB)Rh(OAc)(η^2–C_2H_4) (Black) and (^{Fl}DAB)Rh(TFA)(η^2–C_2H_4) (Red) at 423 K.

The computations suggest an interesting change in the highest point on the reaction coordinate for Rh (ethylene insertion) versus the Pt(II) catalysts (C-H activation) studied in an earlier grant period, **Figure 3**. This change appears to be due to the reduced electrophilicity of these neutral Rh(I) versus the earlier cationic Pt(II) catalysts. Perhaps more importantly from a catalyst design scenario, our computations indicate that modulation of the free energy surface can be effected via the choice of the 4th ligand, either trifluoroacetate (TFA) or acetate (OAc), **Figure 3**, potentially even more so than seen for the Pt(II) catalysts. We hypothesize that this is due to the switch in C-H activation mechanism from oxidative addition/reductive elimination to a concerted metalation-deprotonation (CMD) pathway. Moving forward, strategies for reducing the olefin insertion barrier for these neutral Rh(I) catalysts would seem to be a profitable initiative for theory. Proactive studies of Pd(II)(^{Fl}DAB) for styrene synthesis have been conducted in our laboratory, and reveal interesting differences in relation to the known Rh(I) catalysts.

Publications Acknowledging this Grant in 2014-2017

All grants are Type II Jointly funded by this grant and other grants with leading intellectual contribution from grant **DE-FG02-03ER15387** *as they utilize the UNT CASCaM high performance computing facilities, which have been funded by several NSF MRI grants such as CHE-1531468.*

281 - Joslin, E. E.; Quillian, B.; Gunnoe, T. B.; Cundari, T. R., Sabat, M.; Myers, W. H. C–H Activation of Pyrazolyl Ligands by Ru(II). *Inorg. Chem.* **2014**, *53*, 6270 - 6278.

283 - Pt^{II} Catalyzed Hydrophenylation of α-Olefins: Variation of Linear: Branched Products as a Function of Ligand Donor Ability. McKeown, B. A.; Prince, B. M.; Ramiro, Z.; Gunnoe, T. B; Cundari, T. R. *ACS Catalysis* **2014**, *4*, 1607 - 1615.

287 - Freitag, C. R.; Birk, F. J.; Ou, W. C.; Cundari, T. R. Modeling of Late 3d Transition Metal Metathesis of tert-Butoxide Complexes with Amines *Polyhedron* **2014**, *80*, 112 - 116.

292 - Hydrophenylation of Ethylene using a Cationic Ru(II) Catalyst: Comparison to a Neutral Ru(II) Catalyst Burgess, S. A.; Joslin, E. E.; Gunnoe, T. B.; Cundari, T. R.; Sabat, M.; Myers, W. H. *Chem. Sci.* **2014**, *5*, 4355 – 4366.

294 - The Curious Case of Mesityl Azide and Its Reactivity with $bpyNiEt_2$. Otten, B. M.; Figg, T. M.; Cundari, T. R. *Inorg. Chem.* **2014**, *53*, 11633 – 11639.

301 - Experimental and Computational Studies of the Ruthenium-Catalyzed Hydrosilylation of Alkynes: Mechanistic Insights to Regio- and Stereoselective Formation of Vinylsilanes Yi, C.; Gao, R.; Pahls, D. R., T. R. *Organometallics* **2014**, *33*, 6937 – 6944.

302 - Mindiola, D. J.; Waterman, R.; Iluc, V. M.; Cundari, T. R.; Hillhouse, G. L. Reactivity Studies of a Three-Coordinate Nickel Complex Featuring a Terminal Imido Ligand. Carbon-Hydrogen Activation, C-N Bond Formation, and Cycloaddition Chemistry. *Inorg. Chem.* 2014, *33*, 13227 - 13238.

304 - Vaughan, B. A.; Webster-Gardiner, M. S.; Cundari, T. R.; Gunnoe, T. B. A Rhodium Catalyst for Single-Step Styrene Production. *Science* **2015**, *348*, 421 – 424.

306 - Fallah, H.; Cundari, T. R. Reductive Functionalization of Methyl Ligands by 3d Metal Catalysis. *Comp. Theor. Chem.* **2015**, *1069*, 86 - 957/15.

308 - Lindley, B. M.; Wolczanski, P. T.; Cundari, T. R.; Lobkovsk, E. B. 1st Row Transition Metal and Lithium Pyridine-ene-amide Complexes Exhibiting N- and C-Isomers and Ligand-based Activation of Benzylic C-H Bonds *Organometallics* **2015**, *34*, 4656 – 4668. Hillhouse Memorial Issue.

309 - S. L. Teaw; B. W. Thornton; F. Jia; J. Qian; D. R. Pahls; T. R. Cundari DFT Study Reductive Functionalization in Cis and Trans Cobalt-Methyl-Bipyridine Complexes *Comp. Theor. Chem.* **2015**, *1072*, 102 – 105.

314 - Transition Metal Mediated C−H Activation and Functionalization: The Role of Poly(pyrazolyl)borate and Poly(pyrazolyl)alkane Ligands. McKeown, B. A.; Lee, J. P.; Mei, J.; Cundari, T. R.; Gunnoe, T. B. *Euro. J. Inorg. Chem.* **2016**, *15 - 16*, 2296 – 2311 (invited).

321 - Fe(IV) Alkylidenes Are Actually Fe(II), and a Related Octahedral Fe(II) Alkylidene Is a Conjugated Vinyl Complex. Jacobs, B. P.; Agarwal, R. G.; Wolczanski, P. T.; Cundari, T. R.; MacMillan, S. N. *Polyhedron* **2016**, *116*, 47 – 56. (invited, M. L. Green issue).

322 – The Mechanism of N-N Double Bond Cleavage by an Iron(II)-Hydride Complex. *J. Am. Chem. Soc.* **2016**, *138*, 12112 – 12123.

323 – N-Heterocyclic Carbene-Based Nickel and Palladium Complexes: A DFT Comparison of the Mizoroki-Heck Catalytic Cycles. da Silva, V. H. M.; Braga, A.; Cundari, T. R. *Organometallics* 2016, 35, 3170 - 3181.

324 – Density Functional Study of Oxygen-Insertion into Niobium-Phosphorus Bonds: Novel Mechanism for Liberating P_3^- Synthons. Morello, G. R.; Cundari, T. R. *Organometallics* 2016, 35, 3624 - 3634.

328 – Mechanistic Studies of Single-Step Styrene Production Using a Rhodium(I) Catalyst. Vaughan, B. A.; Khani, S. K.; Gary, J. B.; Kammert, J. D.; Webster-Gardiner, M. S.; McKeown, B. A.; Davis, R. J.; Cundari, T. R.; Gunnoe, T. B. *J. Am. Chem. Soc.* **2017**, *139*, 1486 - 1498.

332 – Redox non-innocence permits catalytic nitrene carbonylation by (dadi)Ti=NAd (Ad = adamantyl). Heins, S. P.; Morris, W. D.; Wolczanski, P. T.; Lobkovsky, E. B.; Cundari, T. R. *Chem. Sci.* **2017**, *8*, 3410 - 3418.

333 – Methane Manifesto: A Theorist's Perspective on Catalytic Light Alkane Functionalization. Cundari, T. R. Comm. Inorg. Chem.– in press. (invited)

334 - Elusive Terminal Copper Arylnitrene Intermediates. Bakhoda, A. G.; Jiang, Q.; Bertke, J. A.; Cundari, T. R.; Warren, T. H. *Angew. Chem. Int. Ed.* **2017**, *56*, 6426 – 6430 (communication).

335 - Studies of the Decomposition of the Ethylene Hydrophenylation Catalyst TpRu(CO)(NCMe)Ph. Joslin, E. E.; McKeown, B. A.; Cundari, T. R.; Gunnoe, T. B. *J. Organomet. Chem.* – in press. Invited.

336 - Three Coordinate Copper(II) Aryls: Key Intermediates in C-O Bond Formation. Kundu, S.; Greene, C.; Williams, K. D.; Salvador, T. K.; Bertke, J. A.; Cundari, T. R.; Warren, T. H. *J. Am. Chem. Soc.* – in press.

338 - Comparison of Pd^{II} vs Rh^{I}-catalyzed Catalytic Cycle for Single Step Styrene Production. Ceylan, Y. S.; Cundari, T. R. *Comp. Theor. Chem.* – submitted.

341 - Effect of Ancillary Ligands on Oxidative Addition of CH_4 to Re(III) Complexes: A = B, Al, CH, SiH, N, P Using MP2, CCSD(T) and MCSCF Methods. Parveen, R.; Cundari, T. R. *J. Phys. Chem. A* – submitted.

Single Turnover at Molecular Catalysts
DE-SC0016467

Suzanne A. Blum
University of California, Irvine

Presentation Abstract

Catalyst improvement often relies on predictive models built on an understanding of the location of catalytic reactivity. Yet determining the location of reactivity is a long-standing analytical challenge in catalysis because minor components that are difficult to detect by ensemble analytical techniques can be responsible for all of the catalytic reactivity observed on the bulk scale. We herein achieve the first single-turnover fluorescence microscopy imaging at molecular catalysts: the detection of individual monomer insertion events at an industrially important, unmodified molecular ruthenium ring-opening metathesis polymerization (ROMP) catalyst. Imaging data showed that monomers were inserted into polynorbornene after precipitation (heterogeneous catalysis), but monomers were not inserted into polydicyclopentadiene after precipitation at a sufficient rate for detection. Ruthenium was present, however, at a level detectable by energy dispersive X-ray spectroscopy (EDS) in the precipitated polydicyclopentadiene but not in the highly catalytically active precipitated polynorbornene. This contrast shows that the presence of ruthenium alone is insufficient to predict the degree or location of its catalytic reactivity. These results establish the key fundamentals of this technique for imaging the reactivity of individual molecular catalysts under synthetically relevant conditions: in organic solvent, at ambient pressure and temperature, and at ~10 mM in substrate—even when they are the minor components.

DE-SC0016467: Single-Molecule Fluorescence Tools at the Interface of Homogeneous and Heterogeneous Catalysis

Postdoc(s): Dr. Nozomi Saito
Student(s): Quinn T. Easter

RECENT PROGRESS

Single Turnover at Molecular Polymerization Catalysts

Catalysis is a multibillion-dollar world-wide industry, yet the determination of the phase and thus local environment of active catalysts is a long-standing analytical challenge. The primary challenge is that many active catalysts do not build up to sufficient concentrations relative to

inactive components for detection and most analytical instruments are best suited to measuring only the major components in a mixture. This is especially true in reactions at the homogenous/heterogeneous interface where the (unknown) location of the active catalyst can have a profound effect on its local environment and thus reactivity and selectivity. This lack of precise information about the nature of active catalysts inhibits the development of predictive models for improvement. Herein we employ fluorescence microscopy with sensitivity for single-monomer insertions under catalytic conditions at individual molecular catalysts. Resultant imaging data determines the phase and location of active molecular ruthenium polymerization catalysts with the industrially important monomer norbornene, and enabled comparison of polymerization activity in precipitated polynorbornene with that of polydicyclopentadiene.

While well-known in biological systems, zeolite, and nanoparticle catalysis, this is the first example of achieving the single-turnover detection limit with a molecular catalyst by single-molecule fluorescence microscopy. The added challenge with molecular catalysts is that, in contrast to zeolites and nanoparticles, their small molecular size means that they diffuse rapidly in solution; thus, several reported single-molecule fluorescence microscopy studies of stoichiometric reactions of molecular species have employed chemical modification to tether the species to glass in order to reduce their motion and make them sufficiently stationary for imaging. In contrast, the current experiments employ unmodified ruthenium catalyst **1** (Figure 1). Catalyst **1** is widely employed in the industrial syntheses of polymers, pharmaceutical candidates, and complex molecules. No tethering of the catalyst to an artificial surface, which may alter its reactivity, is necessary. Instead, the experiments herein harness the changing solubility and large size of growing polymers in a precipitation polymerization reaction to aid in imaging the active catalyst. Active catalysts derived from **1** within precipitated polymers were sufficiently stationary for imaging of single ROMP reactions.

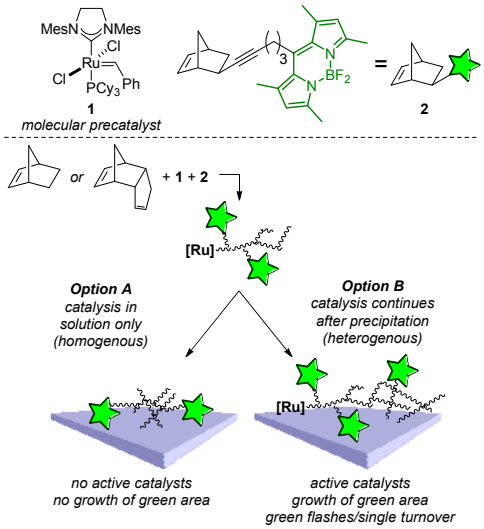

Figure 1. Experiment schematic to locate the active catalysts. Squiggly lines represent polymers. **Option A.** Monomer insertion occurs only in solution (homogeneous catalysis only). After precipitation, the polymer does not contain active catalysts. **Option B.** Precipitated aggregated polymers contain active catalyst and monomers continue to insert after precipitation (homogeneous and heterogeneous catalysis). Mes = 2,4,6-trimethylphenyl.

Progress in imaging the reactions of molecular transition metal complexes has been reported: Our group previously measured the kinetics of stoichiometric ligand exchange reactions at single molecular platinum complexes by tethering a ligand to a glass surface. We also showed that solid insoluble catalyst **1** was surface-inactive towards dicyclopentadiene polymerization, but studies did not examine if catalysis continued in the precipitated polymer. Recently, detection of individual ligand dissociation events at glass-immobilized molecular palladium complexes was achieved, which is a key catalyst initiation step but not a turnover step.

Achieving the ultimate single-turnover limit at a molecular catalyst herein enabled differentiation between ring-opening metathesis polymerization (ROMP) reaction pathways. After initiation of the reaction in solution, the reaction could proceed through two mechanistic options as detailed in Figure 1: Option A, terminate in solution with the catalysts no longer active towards polymerization after precipitation of the aggregated polymer (only homogeneous catalysis), or Option B, continue after precipitation of the polymer, wherein active catalysts contained on the aggregated precipitated polymer strands continue insertion of monomers (i.e., homogeneous and heterogeneous catalysis).

This study was enabled by probe **2**, which contained a norbornene/alkyne reactive group capable of participating in metathesis tethered via an aliphatic chain to a green BODIPY fluorophore. The fluorophore was designed as a spectator in that it was intentionally separated from the norbornene unit by the aliphatic tether; thus, incorporation of probe **2** into the growing polymer via reaction of the norbornene unit would not affect the fluorescence.

The key imaging concept was that the majority of monomer **2** remained in solution diffusing rapidly and was therefore not detected in total internal reflectance fluorescence (TIRF) mode. Only when probe **2** reacted with active catalyst within a precipitated polymer did its diffusion become slowed, resulting in its imaging as a bright green point source of light. If precipitated polymers contained active catalysts, incorporation of probe **2** by ROMP would therefore create a single bright green flash at a polymer-containing location on the surface that was previously dark (corresponding to Option B in Figure 1). If, in contrast, the precipitated polymer did not contain active catalysts, no incorporation of tagged monomer occurred and no flashes would be observed (corresponding to Option A in Figure 1). Importantly, this strategy would image only the behavior from *active* ruthenium catalysts, because *inactive* ruthenium would not incorporate monomer and would not produce a fluorescence signal.

The strategy to resolve the signals of individual chemical reactions was to dope a small amount of probe **2** into a sample of mostly untagged monomer. In this way, the fluorescence signal from insertion of individual probe molecules could be resolved due to the low background from the untagged monomers that composed the majority of the sample. Specifically, probe **2** was added to the reaction at 2×10^{-13} M with 2.6×10^{-2} M untagged monomer in heptane, leading to an ultimate ratio of tagged-to-untagged monomer of $1{:}1.3 \times 10^{11}$, or 1 in 130 billion monomers was labeled with a tag. Thus, the polymer formed under these conditions maintained similar physical and chemical properties to the untagged polymer, and the addition of the probe was not expected to produce physical or chemical artifacts that significantly affected the study of the native catalytic polymerization.

Probe **2** was doped into separate polymerization reactions with two different ROMP monomers: norbornene and dicyclopentadiene (Figure 2). First, the norbornene system was examined. Examination of this sample from t = 2–25 min showed an incredibly dynamic image, with multiple flashes occurring across the image. Each frame showed only a few green signals, however, a composite image provided a straightforward way to assess the locations of all signals in the sample. Figure 2a shows a composite image of this activity from t = 7–11 min. The locations of the precipitated polynorbornene polymers on the coverslip surface are easily determined due to their green fluorescence, which results from summing multiple resolvable individual events in this composite polymerization image. Conditions were chosen for initial experiments wherein photobleaching of tagged monomer was faster than its incorporation, leading to disappearance of the signal shortly after incorporation. Individual bright flashes were resolvable in these areas by eye (example expansion, Figure 1a). Notably, some polymers showed high activity (many regions of flashing, or multiple sequential flashing in the same region), whereas others showed more limited activity. Thus, a spatial distribution of activity was also resolved.

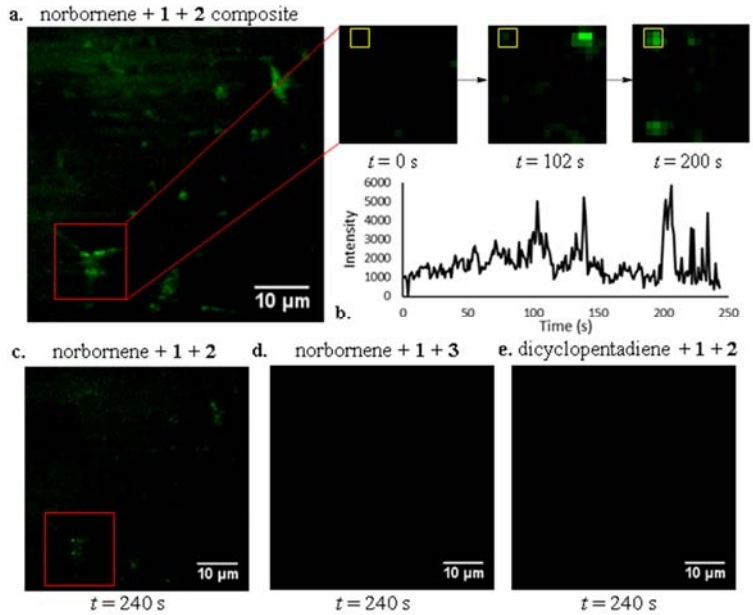

Figure 2. a. Composite image made from the sum of all signal over time of reaction of norbornene, with catalyst **1** and probe **2**. Precipitated polynorbornene is visible as bright green features on the surface of glass. These polymers exhibited catalytic activity, as evidenced by bright green quantized flashes at specific time points that corresponded to reaction with single monomers of **2** shown in expansions. **b.** Intensity vs. time trace of region within yellow box. Reactions with individual molecules of **2** are observable as peaks. **c.** –**e**. Comparison of identical time points with catalyst **1** and: **c.** norbornene with **2** with green signals, **d.** norbornene with control probe **3** which was dark, and **e**. dicyclopentadiene with **2** which is dark and did not exhibit incorporation of monomer **2**.

Publications Acknowledging this Grant in 2014-2017

This is a new grant, starting in August 2016

(I) Exclusively funded by this grant

1. Kazuhiro, K.; Blum, S. A. "Structure–Reactivity Studies of Intermediates for Mechanistic Information by Subensemble Fluorescence Microscopy." *ACS Catal.* **2017**, *7*, 3786–3791.

2. Easter, Q. T.; Blum, S. A. "Single Turnover at Molecular Polymerization Catalysts." *Submitted* May 26, 2017.

Molecular Understanding of Bifunctional Solid Lewis Acid Zeolites for the C-C Coupling of Alpha Keto Acids

Yuriy Román-Leshkov and Jennifer Lewis
Department of Chemical Engineering, Massachusetts Institute of Technology

Presentation Abstract

There is growing interest to develop biobased routes for the renewable production of direct and functional replacements for petroleum-based chemicals. Dicarboxylic acids and esters are key building blocks in many polymerization reactions. These important molecules play a central role in the biobased chemicals portfolio, yet only a few diacids are produced commercially from biobased sources. In this presentation, an alternative route to generate diacids or diesters at scale via the C-C coupling of keto acids or esters using Lewis acid zeolites will be demonstrated. Coupled reactivity and NMR-based characterization studies were used to develop a fundamental understanding of the mechanism and kinetics of the C-C coupling reaction and to identify structural fingerprints related to catalyst activity. Specifically, using trimethyl phosphine oxide (TMPO) adsorption and ^{31}P MAS NMR spectroscopy, we revealed various chemical environments within the pores of Sn-Beta. The ^{31}P resonances were assigned to sites in the Sn-Beta zeolites by correlating the variation of ^{31}P NMR spectra from selective titration experiments using increasing TMPO contents with the corresponding changes in the ^{119}Sn NMR spectra. Next, the quantitative assignments for each site obtained from the ^{31}P NMR were correlated to catalytic activity for the glucose isomerization and aldol condensation reactions. Overall, the method developed in this work can be used to identify and quantify distinct active sites of within the framework of low-defect Lewis acidic zeolites regardless of heteroatom identity

Grant or FWP Number: DE-SC0016214
Grant Title: Molecular Understanding of Bifunctional Solid Lewis Acid Zeolites for the C-C Coupling of Alpha Keto Acids

PI: Yuriy Roman-Leshkov
Postdoc(s): N/A
Student(s): Jennifer D. Lewis

RECENT PROGRESS

The main activities for this reporting period centered around developing methods for pinpointing active site speciation and reactivity in Lewis acid zeolites using ^{31}P MAS NMR of adsorbed TMPO. We resolved several distinct ^{31}P resonances between δ = 50 and 65 ppm that represent

several chemical environments related to the Lewis acidic heteroatoms in the Beta framework. The ^{31}P resonances were assigned to sites in the Sn-Beta zeolites by correlating the variation of ^{31}P NMR spectra from selective titration experiments using increasing TMPO contents with the corresponding changes in the ^{119}Sn NMR spectra. Next, the quantitative assignments for each site obtained from the ^{31}P NMR were correlated to catalytic activity for the glucose isomerization and aldol condensation reactions. The rate of glucose isomerization could only be associated with the ^{31}P MAS NMR resonance at δ = 55.0 ppm, which amounted to 12–32% of total Sn sites. In contrast, multiple Sn species were shown to contribute to aldol condensation activity.

Phosphorous-31 MAS NMR spectra were taken after dosing a representative Sn-Beta sample (Si/Sn molar ratio of 300, Sn-Beta-300b) with different loadings of TMPO as shown in Figure 1. The TMPO occupancy at each chemical shift was calculated from the relative peak area normalized by the total P and Sn contents, as given in Table 1. The narrow signals observed when TMPO is bound to Lewis acidic sites in Sn-Beta is a result of the low-defect zeolite pore structure that confines the TMPO to specific geometries, providing a uniform and ordered chemical environment with a narrow range of chemical shifts associated with each site. These confinement effects and the high sensitivity of ^{31}P nuclei to their chemical environment afford superb resolution to distinguish several distinct chemical environments.

Table 1 Percent TMPO occupancy normalized by Sn content from deconvolution of ^{31}P MAS NMR spectra for TMPO adsorbed on Sn-Beta-300b at different loadings.

TMPO/Sn ratio[a]	TMPO occupancy (%) at each ^{31}P MAS NMR resonance (ppm)[b]					
	63.1	59.9	58.6	57.1	55.0	51.5
0.12	–	–	9	–	3	–
0.48	1	14	24	–	8	–
1.09	7	21	21	27	26	8
1.14	4	38	18	25	28	2

[a] from ICP-MS. [b] % TMPO occupancy at X ppm = (mol P/g-cat)(mol Sn/g-cat)$^{-1}$(area % at δ = X ppm).

At low TMPO loading (TMPO/Sn molar ratio = 0.12), two resonances appear at δ = 55.0 and 58.6 ppm at approximately a 1:3 ratio. When the TMPO dosing is increased to TMPO/Sn = 0.48, the TMPO occupancy at these main resonances increase at the same ratio, and new environments are observed as a shoulder at δ = 59.9 ppm and a small resonance (< 1%) at δ = 63.1 ppm. At TMPO loadings above unity (TMPO/Sn = 1.09 and 1.14), all of the signals increase except for the resonance at δ = 58.6 ppm, which appears to have saturated at a TMPO occupancy around 20%. At these higher TMPO concentrations, new signals appear at δ = 57.1 and 51.5 ppm, although the total occupancy of TMPO at the latter resonance is low at < 8%. Importantly, samples with TMPO/Sn > 1 contain an excess of TMPO, so at least one of the observed signals must be generated by TMPO that is not associated with Sn and/or a second TMPO bound to a Sn site that is already titrated. A second TMPO could occupy an outer coordination sphere or potentially interact with a silanol adjacent to the Sn site.

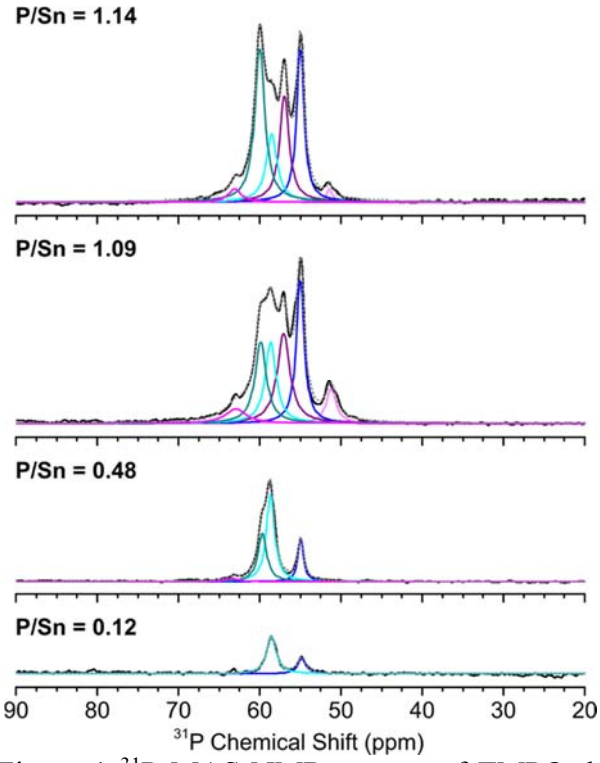

Figure 1 ^{31}P MAS NMR spectra of TMPO dosed on Sn-Beta-300b at different loading levels. Spinning sidebands appear outside the field of view. Spectra are shown in black, while the Lorentzian peak curves are shown in light pink (δ = 51.5 ppm), blue (δ = 55.0 ppm), purple (δ = 57.1 ppm), cyan (δ = 58.6 ppm), dark cyan (δ = 59.9 ppm), and magenta (δ = 63.1 ppm). The overall fit is shown as a light gray dotted curve.

Peak assignments were further validated with ^{119}Sn MAS NMR spectra of ^{119}Sn-enriched Sn-Beta samples with a Si/Sn ratio ~300 (^{119}Sn-Beta-300m) dosed with TMPO. Note that these measurements have a low signal to noise ratio even with 97.4% isotope enrichment due to the low Sn content of the materials, resulting in a higher error for quantification. As expected, the pristine, dehydrated ^{119}Sn-Beta-300m exhibits ^{119}Sn resonances corresponding to two different tetrahedral Sn environments in the zeolite framework at δ = –434 and –443 ppm with approximately a 30:70 ratio. However, when TMPO is adsorbed onto Sn-Beta at low loadings, ^{119}Sn MAS NMR spectra of ^{119}Sn-Beta-300m dosed with TMPO/Sn = 0.52 shows tetrahedral tin at δ = –450 ppm and two signals assigned to penta-coordinated tin at δ = –580 and –600 ppm, which display the expected chemical shift anisotropy (CSA). The resonances at δ = –580 and –600 ppm appear at a 17:83 ratio and can be clearly assigned to ^{31}P MAS NMR resonances at δ = 55.0 and 58.6 ppm, respectively, which appear in approximately the same ratio (12:88_Indeed, we expect to see ^{119}Sn resonances corresponding to penta-coordinated Sn-TMPO adducts to lower frequency from those of the tetrahedral signals by ca. –200 to –300 ppm units. These resonances should display prominent spinning sidebands due to the CSA of the five-coordinate Sn. At higher TMPO loadings, it is possible that two molecules will coordinate to the Sn center, resulting in hexa-coordinated Sn that will appear at even lower frequencies. Indeed, phosphine oxides are known to form 1:2 Sn to P adducts with organotin chlorides in the presence of excess phosphine oxide. It should be noted that for this particular ^{31}P MAS NMR spectrum, the resonances at 58.6 and 59.9 ppm are indistinguishable and are treated as one environment.

Increasing the TMPO loading to TMPO/Sn = 1.17 resulted in the appearance of a resonance at δ = –735 ppm corresponding to hexa-coordinated Sn. As expected, no four-coordinate tin remains at this excess titration level. The ^{31}P and ^{119}Sn spectra provide TMPO occupancies and relative Sn speciation that are consistent with our preliminary peak assignments. The introduction of a second TMPO molecule (δ = 57.1 ppm) to an existing TMPO-Sn adduct at δ = 55.0 ppm would results in a decrease in the penta-coordinated resonance at δ = –580 ppm and the appearance of the hexa-coordinated resonance at δ = –733 ppm. According to the TMPO occupancy, these signals should appear in a 1:2 ratio. The signals at δ = 58.6 and 59.9 ppm, which we consider to be similar environments, account for over half of the TMPO occupancy and can still be compared to the ^{119}Sn MAS NMR resonance at δ = –600 ppm. The low signal to noise of the ^{119}Sn MAS NMR spectra makes it difficult to assign the minor resonances at δ = 51.5 and 63.1 ppm. However, the ^{119}Sn MAS NMR results give us confidence that the ^{31}P MAS NMR resonances at δ = 55.0 and 58.6 ppm are due to single TMPO molecules interacting with two different Sn site configurations. The resonance at δ = 59.9 ppm is likely similar to the δ = 58.6 ppm site, and δ = 57.1 ppm can be assigned to a second TMPO bound to the δ = 55.0 ppm site.

Publications Acknowledging this Grant in 2014-2017

1. Garg, A., Milina, M., Ball, M., Hunt, S. T., Dumesic, J. A., & **Román-Leshkov, Y.*** Transition Metal Nitride Core-Noble Metal Shell Nanoparticles as Highly CO Tolerant Catalysts. Angew. Chem. Int. Ed. DOI: 10.1002/anie.201704632 (2017); Status: Published; Acknowledgement of federal support **YES.**
2. Hendon, C. H., Hunt, S. T., Milina, M., Butler, K. T., Walsh, A., & **Román-Leshkov, Y.*** Realistic Surface Descriptions of Heterometallic Interfaces: The Case of TiWC Coated in Noble Metals. J. Phys. Chem. Lett. 7:4475-4482 (2016); Status: Published; Acknowledgement of federal support **YES.**
3. Gunther, W. R., Michaelis, V. K., Griffin, R. G., & **Román-Leshkov, Y.*** Interrogating the Lewis acidity of metal sites in Beta zeolites with 15N pyridine adsorption coupled with MAS NMR spectroscopy J. Phys. Chem. C. 120:28533–28544 (2016); Status: Published; Acknowledgement of federal support **YES.**
4. Hunt, S. T., Milina, M., Wang, Z., & **Román-Leshkov, Y.*** Activating Earth-Abundant Electrocatalysts for Efficient, Low-Cost Hydrogen Evolution/Oxidation: Sub-Monolayer Platinum Coatings on Titanium Tungsten Carbide Nanoparticles. Energy Environ. Sci. 9:3290-3301 (2016); Status: Published; Acknowledgement of federal support **YES.**

Activation of Cellulose with Alkaline Earth Metals

Paul J. Dauenhauer, Matthew Neurock
University of Minnesota, Chemical Engineering and Materials Science
421 Washington Ave. SE, Minneapolis, MN 55455 USA

Presentation Abstract

Heterolytic cleavage of cellulose glycosidic bonds enables the depolymerization and deconstruction of long-chain glucan biopolymers to small molecules. The homogeneity of cellulose ether linkages (β, 1-4) allows for a common activating mechanism leading to rapid chain scission. As originally proposed by Shafizadeh and co-workers[1], the activating mechanism of cellulose dominates the overall chemistry at 500 °C. In this work, we reveal the existence of two kinetic regimes of intra-chain cellulose activation transitioning at 467 °C[2]. The high temperature activation mechanism associated with energy technologies (e.g. gasification, pyrolysis) exhibits high activation energy (~53 kcal/mol) and pre-exponential (10^{16} s^{-1}) consistent with the mechanism of concerted transglycosylation[3]. The insertion of alkaline earth metals including calcium substantially enhance the rate of high temperature activation, by lowering the transition temperature at which this mechanism dominates[4,5]. Measured apparent activation energy, pre-exponential, and rate expressions are reported for calcium catalysis.

[1] Bradbury, A. G. W.; Sakai, Y.; Shafizadeh, F. A kinetic model for pyrolysis of cellulose. J. Appl. Polym. Sci. **1979**, 23, 3271−3280.
[2] Krumm, C.; Pfaendtner, J.; Dauenhauer, P.J.; **Millisecond Pulsed Films Unify the Mechanisms of Cellulose Fragmentation,** *Chem. Materials* **2016**, 28(9), 3108-3114.
[3] Zhu, C.; Krumm, C.; Facas, G.; Neurock, M.; Dauenhauer, P.J.; **Energetics of Cellulose and Cyclodextrin Glycosidic Bond Cleavage** *Reaction Chem. and Eng.* **2017,** 2, 201-214...
[4] Facas, G.; Maliekkal, V.; Neurock, M.; Dauenhauer, P.J.; Activation of Cellulose with Alkaline Earth Metals. In preparation.
[5] Zhu, C.; Maduskar, S.; Paulsen, A.D.; Dauenhauer, P.J.; Alkaline earth metal catalyzed thin-film pyrolysis of cellulose. *ChemCatChem* **2016**, 8(4), 818-829.

DE-SC0016346: Promoted Cellulosic Pathways and Mechanisms via Impregnated Natural Metal Catalysts (2016-2019)

PI: Paul J. Dauenhauer **Co-PI:** Matthew Neurock
Student(s): Greg Facas, Vineet Maliekkal

Poster Presentations

Aaron M. Appel

Designing Catalysts Using an Energy-Based Approach: Molecular Catalysis for CO_2 Reduction

Aaron Appel, John Linehan, Eric Wiedner
Institute for Integrated Catalysis, Pacific Northwest National Laboratory

Presentation Abstract

The utilization of energy from intermittent and distributed sources, such as from solar and wind, would be facilitated by efficient energy storage with a high capacity. Storage in the form of chemical fuels can satisfy this requirement, but results in the need for the design of efficient catalysts for the relevant chemical transformations. The reduction of CO_2 can be advantageous over the use of H_2, as liquid fuels can be produced from CO_2 and thereafter used in transportation. The aim for our work is to develop knowledge of the parameters required for designing catalysts with unprecedented performance. In working towards this aim, we study each of the reduction steps in the overall transformation of CO_2 to liquid fuels.

Understanding the role of solvent upon catalysis is a route to controlling the activity of catalysts through modulation of the individual reaction steps. Towards this goal, catalysts for the hydrogenation of CO_2 to formate have been studied in both organic solvents and aqueous solution. For the relevant catalytic intermediates and overall reaction, the solvent has a substantial role in impacting the reaction thermodynamics. Studies of two series of bis(diphosphine) complexes will be presented: nickel hydrides and cobalt hydrides. For each series, the reactivity will be compared between organic solvents and aqueous solution.

FWP-47319: Low-Temperature Catalytic Routes for Energy Carriers via Spatial and Chemical Organization

PI: Johannes Lercher

Development of in-situ/operando Synchrotron Methods: Syngas Conversion to Higher Oxygenates

Simon R. Bare[1], Adam S. Hoffman[1], Joseph Singh[2], Arun Asundi[2], Stacey F. Bent[2]
[1]SSRL, SLAC National Accelerator Laboratory
[2]Department of Chemical Engineering, Stanford University

Presentation Abstract

A thrust area for the expanded experimental catalyst characterization effort at SUNCAT is the development of an integrated collaboration with Stanford Synchrotron Radiation Lightsource (SSRL) at SLAC National Accelerator Laboratory. As such, the facile and relevant application of synchrotron-based x-ray methods to elucidate the structure of working catalysts is essential to the success of the initiative. We report on our progress in this area and use the thermal heterogeneous catalyzed conversion of syngas ($CO + H_2$) to higher oxygenates as a prototypical example of the work that has been achieved. Following leads from DFT calculations, where it was determined that blocking step sites would lead to higher selectivity, a zinc promoted cobalt oxide catalyst, prepared using ALD techniques, was tested for this reaction and selectivity to higher oxygenates was observed. Using a combination of *in-situ* and *in-operando* XAFS and XRD we have elucidated the structure of the active cobalt phase in this catalyst. For the synchrotron XRD data we first had to design, construct and test a plug-flow *in-situ* XRD cell capable of operation up to 30 bar and 400°C together with the ability to deliver and control the flow of gases at high pressure. Using this cell, we have studied the Co-only and the Zn-promoted Co catalyst, during initial activation (reduction), reaction, carburization, and the decomposition as a function of process conditions in pure CO and CO/H_2. Similarly, we have used the complementary method of in-situ XAFS to monitor the chemical state of the cobalt and the zinc. We will also highlight plans for the future development of *in-situ* synchrotron characterization techniques to be applied across the SUNCAT research portfolio.

SUNCAT FWP
SLAC National Accelerator Laboratory

PI: Jens Norskov
Co-PIs: Stacey F. Bent, Simon R Bare
Postdoc(s): Adam S. Hoffman
Student(s): Joseph Singh, Arun Asundi

Alexis T. Bell

Studies of Heterogeneous Catalysts for Strategic Formation of C-C, C-O, and C-N Bonds

Chemical Sciences Division, Lawrence Berkeley National Laboratory, Berkeley, CA 94720

Presentation Abstract

The objectives of this program are to establish detailed relationships between the composition and structure of active sites and their catalytic activity for the targeted formation of C-C, C-O, and C-N bonds involved in the formation of fuels and chemicals. The experimental and theoretical work undertaken provides informs the design of highly active and selective catalysts for producing desired products. Recent efforts have focused on the formation of C-N bonds during ammoxidation of propene to acrylonitrile and the formation of C-C bonds during the condensation of ethanol to butanol, the condensation of acetone to MIBK, the disproportionation of propene to butene and ethene, and the Fischer-Tropsch synthesis of linear alkenes.

FWP Number: CH030201
Grant Title: Catalysis Program*

Postdoc(s): Sankaranaryanapillai Shylesh
Student(s): Lance Bettison, Christopher Ho, John Howell

RECENT PROGRESS

Propene ammoxidation

Propene ammoxidation over $Bi_2Mo_3O_{12}$ produces nitrogen-containing products - acrylonitrile, acetonitrile, HCN, and N_2, - together with acrolein and a small amount of CO_x. Experimental and theoretical studies were conducted in order to elucidate the pathways by which N atoms are incorporated into products. Propene consumption rate is first order in propene and zero order in ammonia (for NH_3/C_3H_6 = 0-2) and oxygen (for $O_2/C_3H_6 \geq 1.5$) partial pressures, and has an activation energy (E_a = 22 kcal/mol). The kinetics for propene oxidation are also first order in propene partial pressure and zero order in oxygen and the activation barrier is identical to that for propene ammoxidation, suggesting the same rate-limiting step for both reactions. Two N-containing species are found to be relevant for ammoxidation: NH_3 adsorbed via a dative bond to Bi^{3+} ions that reacts with propene-

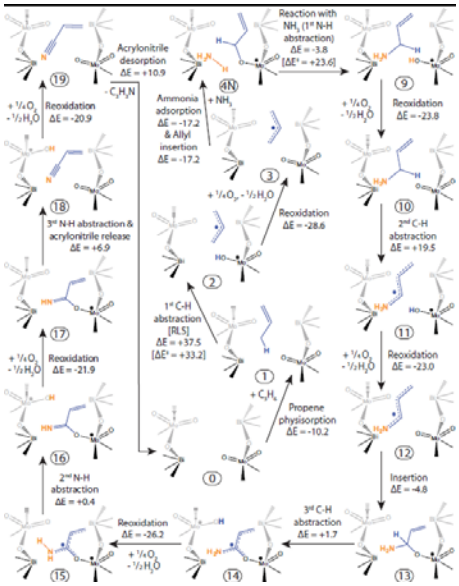

Fig. 1 Proposed mechanism for propene ammoxidation over $Bi_2Mo_3O_{12}$.

derived allyl species to form products with C-N bonds, and metastable M-NH (M = Mo, Bi) groups that are responsible for NH_3 oxidation to N_2. A reaction mechanism (Fig. 1) has been proposed that captures all of the experimentally observed trends in product distribution as a function of partial pressures and temperature. Theoretical analysis of the proposed reaction pathway reveals that oxidation and ammoxidation of propene involve a common, rate-limiting step, the dissociative adsorption of propene to form and allyl alkoxide and Mo-OH species. The first of these species can then undergo hydrogen abstraction to form acrolein or reaction with NH_3 adsorbed on Bi^{3+} sites to form allylamine. Sequential dehydrogenation of allylamine produces acrylonitrile (see Fig. 1), a finding supported by experimental evidence. The calculated activation barrier for allyalkoxide dehydrogenation to acrolein in 35.9 kcal/mol, but that to form acrylonitrile is 23.6 kcal/mol. Therefore, in the presence of adsorbed NH_3, the pathway to acrylonitrile is strongly favored. The formation of acetonitrile and HCN occurs via Markovnikov addition of NH_3 across the C=C bond of adsorbed allylamine and subsequent of the much weakened C-C in the resulting species. Water produced as a byproduct of propene ammoxidation does not affect the product distribution but inhibits the formation of N_2 by hydrolysis of Mo=NH species, thereby reducing the consumption of NH_3 due to oxidation.

Multi-step, multi-catalytic reactions

The conversion of ethanol to butanol offers a means for valorizing ethanol produced by fermentation of biomass-derived sugars. Previous studies have shown that hydroxyapatite (HAP: $Ca_5(PO_4)_3OH$) is active for ethanol coupling to butanol, but much controversy remains regarding the mechanism of this reactions and the nature of the active sites. The mechanism and kinetics for ethanol coupling to *n*-butanol over hydroxyapatite (HAP) were investigated at 573 – 613 K. *In-situ* titration experiments revealed that the active sites for acetaldehyde and butanol formation are different. In combination with FTIR studies, it was found that ethanol dehydrogenation is catalyzed by Ca-O sites, whereas condensation of acetaldehyde is catalyzed by CaO/PO_4^{3-} pairs (see Fig. 2). Measurements of the reaction kinetics at various ethanol (3.5 – 9.4 kPa) and acetaldehyde (0.055 – 0.12 kPa) partial pressures reveal that direct condensation involving two ethanol molecules does not play a significant role in butanol formation; instead, *n*-butanol is formed via a Guerbet pathway. At a constant acetaldehyde pressure, enolate formation is rate-limiting and ethanol inhibits acetaldehyde condensation rates by competitive adsorption. A model of the reaction kinetics based on the mechanism shown in Fig. 2 was developed and found to be consistent with all experimental observations.

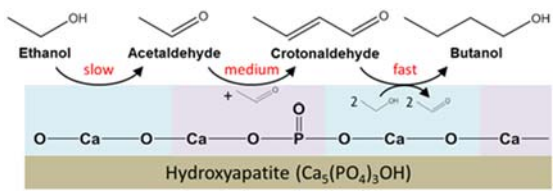

Fig. 2 Schematic of reaction mechanism for ethanol condensation to butanol over HAP.

HAP is also an effective catalyst for aldol condensation of ketones, a process that can be used to form oligomers of biomass-derived ketone. To understand the mechanism and kinetics of aldol condensation, we have investigated the aldol condensation of acetone to mesityl oxide (MO) over HAP. Since the condensation reaction is reversible, we used a physical mixture of HAP and Pd/SiO_2 and added H_2 to the feed in order to shift the reaction equilibrium towards the hydrogenated product, MIBK. Isotopic scrambling experiments with H_6/D_6-acetone give a binomial distribution of deuterated reactants, showing that enolate formation from the ketone is rapid. An inverse isotope effect (k_H/k_D = 0.5) was observed consistent with DFT calculations

suggesting that acetone and diacetone alcohol (DAA) are in pseudo-equilibrium, as was confirmed by feeding DAA into the reactor and observing 87% yield of acetone and 13% yield of methyl isobutyl ketone (MIBK). These results indicate that dehydration of DAA to MO is the rate-limiting step in the reaction pathway.

To explore the effects of cation composition on the activity of HAP, Ca^{2+} was systematically replaced with different cations. A cation-exchange method at a controlled pH of 7.0 was used to minimize surface restructuring. XRD, BET, ICP-OES and XPS characterization show that the bulk structure and surface area of the exchanged samples are unaffected by preferential ion substitution at the surface. For cation-exchanged samples, aldol condensation rates pass through a maximum with decreasing Sanderson electronegativity of the substituted cation, indicating that basic sites are needed to catalyze the reaction (see Fig. 3). This was verified by *in-situ* CO_2 and pyridine titration. However, too strong of a base leads (i.e., too low a Sanderson electronegativity) leads to irreversible adsorption of water and decreased activity as demonstrated by the barium-substituted HAP. More accurate quantification of Lewis basicity based on the partial charge of surface oxygen atoms, which are responsible for the proton abstraction steps in the condensation pathway, have been obtained from DFT calculations.

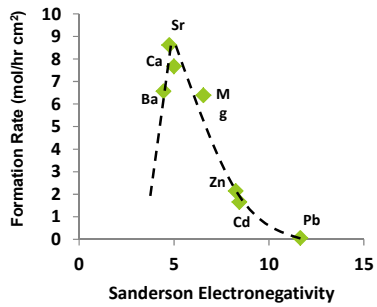

Fig. 3 Comparison of acetone condensation rates for cation-exchanged HAP catalysts. $P_{acetone}$ = 5 kPa, P_{H2} = 5 kPa, T = 373 K, HAP = 10 mg, 3%Pd/SiO_2 = 40 mg.

Propene metathesis catalyzed by isolated tungstate sites

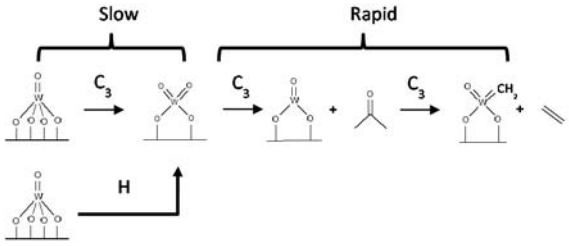

Fig. 4 Illustration of the activation of isolated tungstate species during pretreatment in He and O_2 followed by exposure to propene.

Isolated tungstate species have been reported to be effective catalysts for the methathesis of alkene. A detailed investigation of the properties of silica-supported tungsten oxide catalysts for propene metathesis was conducted with the goal of identifying the processes involved in the formation of catalytically active site. To probe the influence of dispersion, samples were prepared across a range of W-loadings by incipient wetness impregnation of amorphous silica and ion exchange of mesoporous SBA-15. The samples were characterized by nitrogen adsorption, UV-vis, Raman, and X-ray absorption spectroscopy (XAS). Catalytic activity per W atom was observed to increase with W surface concentration up to the point where WO_3 nanoparticles are formed. The catalytic performance of all samples was enhanced two-fold by pretreatment in He relative to pretreatment in air. In situ characterization of He-pretreated samples by Raman and XAS showed an increase in the relative concentration of isolated dioxo W(6+) species relative to mono-oxo W(6+) species, and in situ XAS data collected during propene metathesis indicated that a similar conversion occurs for air-pretreated samples in the presence of propene. For both air- and He-pretreated catalysts an activation period was observed, during which activity increased and then reached a steady-state. This period was significantly longer for air-pretreated catalysts and

was accompanied by the transient formation of acetone. While acetone was not observed during the much shorter transient for He-pretreated samples, *in situ* XAS showed that reduction of these samples occurred upon contact with propene. It is also notable that independent of the manner of catalyst preparation or pretreatment, the rate of propene metathesis is first order in propene and has an activation energy of 200 kJ/mol. A model is proposed (see Fig. 4) to explain why only a fraction of the isolated tungstate species are active for propene metathesis (~5%) and why this fraction increases with increasing concentration of W dispersed on silica.

Effects of metal oxide promoters on the activity and selectivity of Co/SiO_2 for FTS

Co/SiO_2 is an active Fischer-Tropsch synthesis (FTS) catalyst but requires promotion to minimize the formation of CH_4 and maximize the formation of C_{5+} products. MnO_x is one of the most effective promoters for this purpose. A detailed study of the effects of MnOx on FTS over Co/SiO_2 was conducted with the aim of identifying how MnOx interacts with Co nanoparticles and affects the mechanism of CO hydrogenation. MnO_x was found to increase both the apparent rate constant for CO consumption and the equilibrium constant for CO adsorption, as well as the rate of CO dissociation. Quantitative analysis of STEM-EDS elemental maps (see Fig. 5) revealed that the promoter accumulates preferentially on the surface of Co nanoparticles at low Mn loadings, resulting in a sharp increase in the product selectivity with increased Mn loadings. For catalysts prepared with loadings of Mn/Co > 0.1, additional Mn accumulates as nanometer-scale MnO particles on the support. *In situ* IR spectra of adsorbed CO show that MnO_x increases the abundance of adsorbed CO and weakens the C–O bonds. Cleavage of the C–O bond is promoted by Lewis acid-base interactions between the Mn^{2+} cations located at the edges of MnO islands covering the Co nanoparticles and the O atom of CO adsorbates adjacent to the MnO islands. Similar studies were conducted with Co on SiO_2 promoted by oxides of Ce, Gd, La and Zr. The extent to which these promoters decrease the formation of CH_4 and increase the formation of C_{5+} hydrocarbons depends on both the oxide loading and the composition. STEM-EDS maps demonstrate that the propensity for a given metal oxide to associate with Co affects the sensitivity of the product distribution to changes in the loading of the promoter (see for example the right side of Fig. 6). For all promoters, the maximum effect of promoter on product distribution occurred for a Co surface coverage of 0.5. The oxidation state of the promoter under reaction conditions, determined by in situ XANES, was used to calculate relative Lewis acidity of the promoter. A strong positive correlation was found between the selectivity for C_{5+} products and the Lewis acidity of the promoter (Fig. 7), suggesting that the promotional effects are a consequence

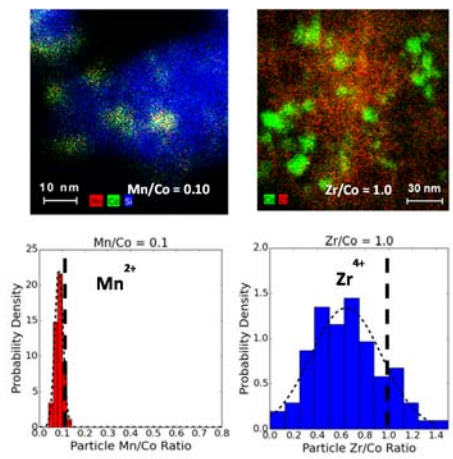

Fig. 5 High-resolution STEM-EDS maps and particle Mn/Co and Zr/Co ratios for MnO and ZrO_2 promoters dispersed on Co/SiO_2. In both cases, the coverage of Co NPs by MO_x is about 0.5.

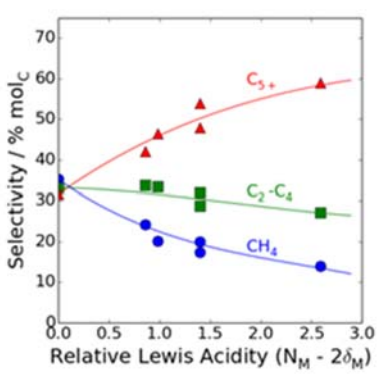

Fig. 6 Effects of relative Lewis acidity of the metal in a metal oxide promoter on the CH_4, C_2-C_3, and C_{5+} selectivities of hydrocarbons formed over oxide-promoted Co/SiO_2.

of Lewis acid-base interactions between the reaction intermediates and the promoters, which are metal cations. This conclusion was supported by DFT calculations.

Publications Acknowledging this Grant in 2014-2017

1. Nell, A.: Getsoian, A. B.; Werner, S.; Kiwi-Minsker, L.; Bell, A. T. Preparation and Characterization of High-Surface-Area $Bi_{(1-x)/3}V_{1-x}Mo_xO_4$ Catalysts. *Langmuir*, **2014**, *30*, 873-880.
2. Getsoian, A. B.; Zhai, Z.; Bell, A. T. Band-Gap Energy as a Descriptor of Catalytic Activity for Propene Oxidation over Mixed Metal Oxide Catalysts. *J. Am. Chem. Soc.*, **2014**, *136*, 13684-13697.
3. Johnson, G. R.; Werner, S.; Bell, A. T. An Investigation into the Effects of Mn Promotion on the Activity and Selectivity of Co/SiO_2 for Fischer-Tropsch Synthesis: Evidence for Enhanced CO Adsorption and Dissociation. *ACS Catal.*, **2015**, *5*, 5888-5903.
4. Johnson, G. R.; Bell, A. T. Role of ZrO_2 in Promoting the Activity and Selectivity of Co-Based Fischer–Tropsch. *ACS Catal.*, **2015**, *6*, 100-114.
5. Zhai, S.; Wütschert, M.; Licht, R. B.; Bell, A. T. Effects of Catalyst Structure on the Oxidation of Propene to Acrolein. *Catal. Today*, **2016**, *261*, 146-153.
6. Ho, C.; Shylesh, S.; Bell, A. T.; Mechanism and Kinetics of Ethanol Coupling to Butanol over Hydroxyapatite. *ACS Catal.*, **2016**, *6*, 938-949.
7. Johnson, G. R.; Bell, A. T. Effects of Lewis Acidity of Metal-Oxide Promoters on the Activity and Selectivity of Co-Based Fischer-Tropsch Catalysts. *J. Catal.*, **2016**, *338*, 250-264.
8. Licht, R. B.; Vogt, D.; Bell, A. T. The Mechanism and Kinetics of Propene Ammoxidation over α-Bismuth Molybdate. *J. Catal.*, **2016**, *339*, 228-241.
9. Dombrowski, J.: Bell, A. T.: Tilley, T. D. $Ga[OSi(O(t)Bu)_3]_3 \cdot THF$, a Thermolytic Molecular Precursor for High Surface Area Gallium-Containing Silica Materials of Controlled Dispersion and Stoichiometry. *Dalton Trans.*, **2016**, *45*, 11025-11034.
10. Howell, J.: Li, Y.-P.: Bell, A. T. Propene Metathesis over Supported Tungsten Oxide Catalysts: A Study of Active Site Formation. *ACS Catal.*, **2016**, *6*, 7728−7738.
11. Licht, R. B.; Getsoian, A. B.; Bell, A. T. The Role of Local Site Geometry on the Hydrogen Abstraction Ability of Scheelite Mixed Metal Molybdates. *J. Phys Chem.*, **2016**, *120*, 29233–29247.
12. Licht, R. B.; Bell, A. T.; A DFT Investigation of the Mechanisms of Propene Ammoxidation over α-Bismuth Molybdate. *ACS Catal.*, **2017**, *7*, 161-176.

Stable carbenes and related species as powerful tools in organometallic chemistry

Guy Bertrand
UCSD-CNRS Joint Research Chemistry Laboratory (UMI 3555), Department of Chemistry and Biochemistry, University of California San Diego, La Jolla, CA 92093-0358 (USA)

Presentation Abstract

Over the years, the success of homogeneous catalysis can be attributed largely to the development of a diverse range of ligand frameworks that have been used to tune the behavior of the various systems. Spectacular results in this area have been achieved using cyclic diaminocarbenes, the so-called N-heterocyclic carbenes (NHCs), mainly because of their strong σ-donor properties. Although it is possible to cursorily tune the structure of NHCs, any diversity is still far from matching their phosphorus-based counterparts, which is one of the great strengths of the latter. We have discovered new types of stable cyclic carbenes, as well as related carbon-based and boron-based ligands, which feature even stronger σ-donor properties than NHCs. The synthesis, electronic properties, and catalytic activity of complexes bearing our ligands will be presented, and comparisons with their NHC cousins will be discussed.
We also found that our novel ligands allow for the isolation of catalytically active complexes, which were supposed to be only transient intermediates. Among them, bis(copper) complexes involved in the very popular CuAAC reaction (Click Chemistry) will be discussed. We will show that this discovery allows for developing novel catalytic transformations.

DE-SC0009376: Transition-metal-catalyzed functionalization of ammonia, hydrazine, and basic anilines

Postdoc(s): Max Hansmann, Eder Tomás-Mendivil
Student(s): Cory M. Weinstein, Erik A. Romero, Daniel R. Tolentino, Jesse L. Peltier

RECENT PROGRESS

Bicyclic (alkyl)(amino)carbenes (BICAACs): Stable carbenes more ambiphilic than CAACs[#23]

In 2005, our group reported the synthesis of stable cyclic (alkyl)(amino)carbenes (CAACs) which result from the replacement of one of the two amino substituents of classical NHCs by a quaternary carbon atom. This modification increases both the nucleophilicity and electrophilicity of the carbene center, thereby allowing CAACs to outperform NHCs for the stabilization of paramagnetic species, and the activation of small molecules and enthalpically strong bonds. Additionally, CAAC-metal bonds are stronger than in NHC complexes, which allowed for promoting difficult transition metal catalyzed reactions under very demanding conditions. This

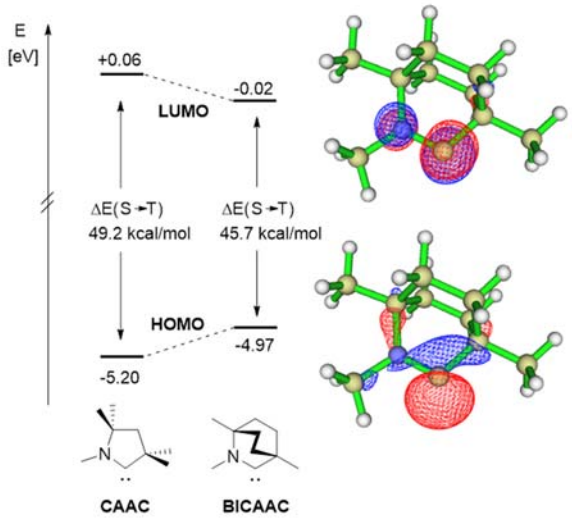

year, we have prepared stable bicyclic (alkyl)(amino)carbenes (BICAACs) and showed that this modification of the CAAC skeleton leads to a geometry similar to that of NHCs (fan-like geometry) but different to that of CAACs. Moreover, this novel family of carbenes displays enhanced σ-donating and π-accepting properties compared to those of CAACs, and thus NHCs. Of particular importance, BICAACs are readily accessible from abundant and cheap trivertal, and can be stored in the solid state at room temperature over a year.

Synthesis of hemilabile cyclic (alkyl)(amino)carbenes (HemiCAACs) and applications in catalysis[#30]

The possibility of tailoring NHCs for specific tasks by attachment of ancillary functional groups has been pivotal for the success of these ligands in organometallic chemistry. Chelating NHC ligands provide remarkable chemical stability to high-valent metal centers, and have found widespread application in oxidation catalysis. In addition, they allow for bifunctional cooperativity, including the generation of hemilabile coordination sites, and some of their complexes feature luminescent and phosphorescent properties. We have found simple and scalable synthetic procedures allowing for the preparation of a variety of hitherto unknown hemilabile bidentate CAACs. As proof of principle for the potential of this novel type of carbenes in organometallic chemistry, we have first shown that their gold metal complexes can promote the difficult oxidative addition of biphenylene. These results demonstrate that the pendant donor group strongly stabilizes the gold(III) center, and suggest that such hemilabile bidentate ligands should be suitable for catalysis involving high oxidation states. Additionally, we found that copper and gold complexes bearing HemiCAACs promote the hydroarylation of alkenes and the *anti*-Markovnikov hydrohydrazination of alkynes. It is` important to note that under the same experimental conditions, the monodentate (CAAC)CuO^{t}Bu complex is much less selective, demonstrating the prominent role played by the imine functionality.

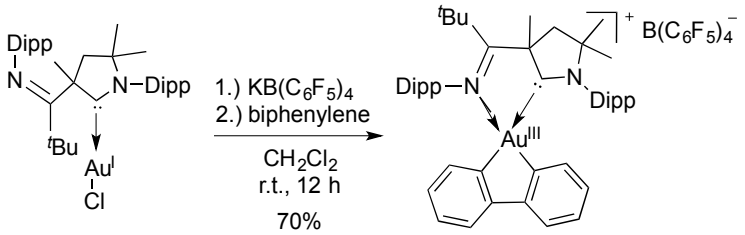

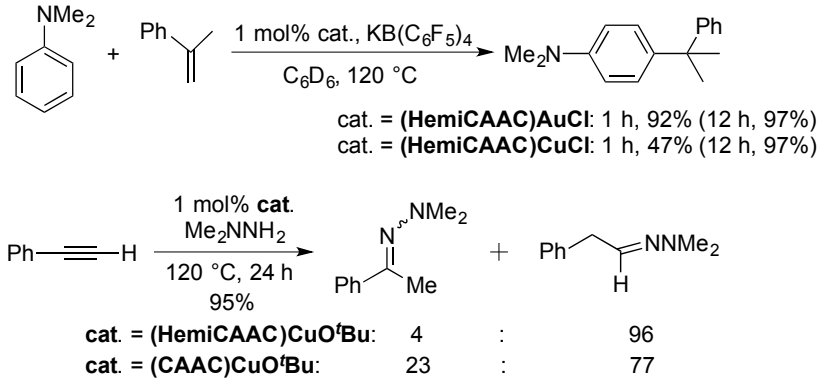

Nucleophilic T-shaped (LXL)metal-pincer complexes based on mesoionic carbenes[#1#,19,#28]

In 2014 we reported the synthesis of a monoanionic LXL-pincer ligand featuring two 1,2,3-triazol-5-ylidenes flanking a carbazolide scaffold. This ligand was shown to stabilize reactive late transition metal complexes as a result of the donating ability of both the mesoionic carbenes (MICs) and the central coordinating amido moiety. We recently show that this ligand allows for the preparation of (LXL)Au(I) complexes, which in contrast to the well studied Au(III)-pincer complexes were unknown. The strong electron-donating properties of the ligand, coupled with its peculiar geometry, makes the Au(I) center reactive towards electrophiles. Importantly, protonation leads to the first cationic Au(III) hydride complex, which shows protic and not hydridic behavior.

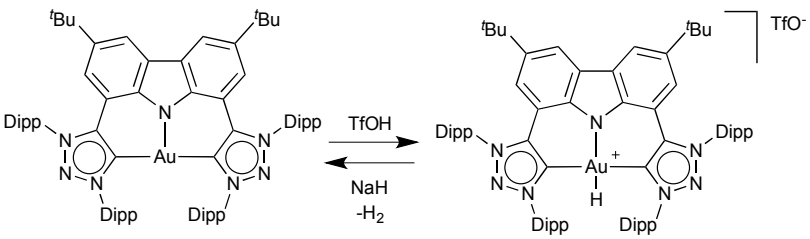

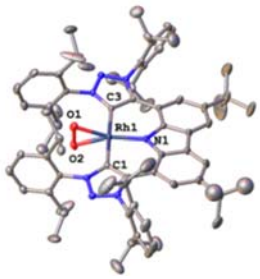

With the same ligand, we also prepared an air-stable rhodium(I)-oxygen adduct which catalyzes the homo-dimerization and hydrothiolation of alkynes, affording the *gem*-enyne and α-vinyl sulfide isomers, respectively, with excellent selectivity. A one-pot stepwise strategy allows the selective catalytic preparation of non-symmetric bis-vinyl sulfides, as well as the alkyne dimerization-hydrothiolation tandem reaction**.**

Spectroscopic Evidence for a Monomeric Copper(I) Hydride, and Crystallographic Characterization of a Monomeric Silver(I) Hydride[#22]

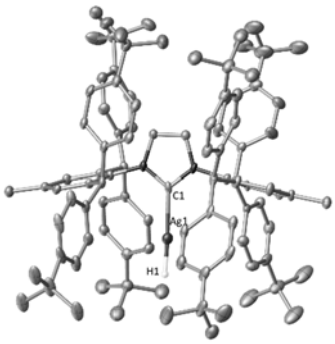

Copper hydride complexes have been postulated as the active catalysts in a myriad of reaction. However, although Wurtz discovered a polymeric copper hydride as early as 1844, low nuclearity coinage metal hydrides have challenged the skills of synthetic chemists for decades. This year we reported the unprecedented spectroscopic characterization of a monomeric LCuH complex, which is in equilibrium in solution with its dimer $[LCuH]_2$, as well as the isolation and crystallographic characterization of the first monomeric LAgH complex. This has been possible thanks to the use of a very bulky NHC ligand, bearing 2,6-bis[di(4-tert-butylphenyl)methyl]-4-methylphenyl substituent (Ar**).

Ancillary Ligand-Free Copper Catalyzed Hydrohydrazination of Terminal Alkynes with NH_2NH_2.[#16]

We and others have already shown that the hydrohydrazination of unactivated alkynes and allenes is efficiently promoted by cationic (L)Au(I) complexes (L: CAAC, *Pyr*NHC, MIC, BAC, saNHC). Based on these results, we questioned if copper complexes could also promote the hydrohydrazination of alkynes. It is interesting to note that so far, even for the hydroamination reaction, there are only a few reports dealing with the Cu-catalyzed intermolecular version. Optimization of the reaction was performed using a stoichiometric mixture of parent hydrazine and phenylacetylene, as a model substrate, at 100 ºC for 12h with 5 mol% of copper complex. In the presence of 5 mol% KBArF, the bulky (IPr*)CuCl afforded complete conversion. At this stage,

control experiments were performed to confirm our initial observations. To our surprise, while no reaction was observed using either KBarF, (IPr*)CuCl or CuCl alone, quantitative formation of hydrazone occurred in the presence of a stoichiometric mixture of CuCl/KBArF (5 mol%). Replacing CuCl by $CuCl_2$ also led to full conversion albeit in lower yield (86%).
The methodology tolerates a broad range of functional groups, allows for the synthesis of symmetrical and unsymmetrical azines, and can be extended to hydrazine derivatives and amines. In contrast to other metal catalyzed reactions allowing the functionalization of parent hydrazine, this process being ancillary ligand-free is economically viable.

Publications Acknowledging this Grant in 2014-2017

(I) Exclusively funded by this DOE grant

#1 Bezuidenhout, D. I.; Kleinhans, G.; Guisado-Barrios, G.; Liles, D. C.; Ung, G.; Bertrand, G. Isolation of a potassium bis(1,2,3-triazol-5-ylidene)carbazolide: A stabilizing pincer ligand for reactive late transition metal complexes. *Chem. Commun* **2014,** *50*, 2431-2433.

#2 Dielmann, F.; Andrada, D. M.; Frenking, G.; Bertrand, G. Isolation of Bridging and Terminal Coinage Metal−Nitrene Complexes. *J. Am. Chem. Soc.* **2014***, 136,* 3800-3802.

#3 Weinberger, D. S.; Amin SK, N.; Mondal, K. C.; Melaimi, M.; Bertrand, G.; Stückl, A. C.; Roesky, H. W.; Dittrich, B.; Demeshko, S.; Schwederski, B.; Kaim, W.; Jerabek, P.; Frenking, G. Isolation of neutral mononuclear copper complexes stabilized by two cyclic (alkyl)(amino)carbenes. *J. Am. Chem. Soc.* **2014***, 136,* 6235–6238.

#4 Ung, G.; Soleilhavoup, M.; Bertrand, G.; Peters, J. C. Isolable 2-coordinate Fe(0) and Co(0) complexes supported by cyclic (alkyl)(amino)carbenes. *Angew. Chem. Int. Ed.* **2014**, *53*, 8427–8431.

#5 Jin, L.; Weinberger, D. S.; Melaimi, M.; Moore, C. E.; Rheingold, A. L.; Bertrand, G. Trinuclear gold clusters supported by CAAC ligands: Mimics for gold heterogeneous catalysts. *Angew. Chem. Int. Ed.* **2014**, *53*, 9059–9063.

#6 Hu, X.; Martin, D.; Melaimi, M.; Bertrand, G. Gold-Catalyzed Hydroarylation of Alkenes with Dialkylanilines. *J. Am. Chem. Soc.* **2014***, 136,* 13594-13597.

#7 Jerabek, P.; Roesky, H. W.; Bertrand, G.; Frenking, G. Coinage Metals Binding as Main Group Elements. Structure and Bonding of the Carbene Complexes $[TM(cAAC)_2]$ and $[TM(cAAC)_2]+$ (TM = Cu, Ag, Au). *J. Am. Chem. Soc.* **2014***, 136,* 17123-17135.

#8 Dielmann, F.; Bertrand, G. Reactivity of a Stable Phosphinonitrene towards Small Molecules. *Chem. Eur. J.* **2015**, *21*, 191-198.

#9 Tolentino, D. R.; Jin, L.; Melaimi, M.; Bertrand, G. Mesoionic Carbene-Gold(I) Catalyzed Bis-Hydrohydrazination of Alkynes with Parent Hydrazine. *Chem. Asian J.* **2015**, DOI: 10.1002/asia.201403408.

#10 Bidal, Y. D.; Lesieur, M.; Melaimi, M.; Cordes, D. B.; Slawin, A. M. Z.; Bertrand, G.; Cazin, C. S. J. A simple access to transition metal cyclopropenylidene complexes. *Chem. Commun.* **2015**, *51*, 4778-4781.

#11 Hu, X.; Soleilhavoup, M.; Melaimi, M.; Chu, J.; Bertrand, G. Air Stable Cyclic (Alkyl)(amino)carbene Copper Complexes as Catalysts for the Hydrolytic Dehydrogenation of BH_3NH_3. *Angew. Chem. Int. Ed.* **2015**, *54*, 6008-6011.

#12 Jin, L.; Tolentino, D. R.; Melaimi, M.; Bertrand, G. Isolation of Bis(copper) Key Intermediates in Cu-Catalyzed Azide–Alkyne "Click Reaction". *Science Adv.* **2015**, *1*, e1500304.

#13 Bidal, Y. D.; Lesieur, M.; Melaimi, M.; Nahra, F.; Cordes, D. B.; Athukorala Arachchige, K. S.; Slawin, A. M. Z.; Bertrand, G.; Cazin, C. S. J. Copper(I) complexes bearing carbenes beyond classical NHCs: Synthesis and catalytic activity in "Click Chemistry". *Adv. Synth. Catal.* **2015**, *357*, 3155-3161.

#14 Rao, B.; Tang, H.; Zeng, X.; Liu, L.; Melaimi, M.; Bertrand, G. Cyclic (Amino)(aryl)carbenes (CAArCs) as Strong σ-Donating and π-Accepting Ligands for Transition Metals. *Angew. Chem. Int. Ed.* **2015**, *54*, 14915-14919.

#15 Jin, L.; Romero, E. A.; Melaimi, M.; Bertrand, G. The Janus Face of the X Ligand in the Copper Catalyzed Azide Alkyne Cycloaddition. *J. Am. Chem. Soc.* **2015**, *137*, 15696-15698.

#16 Peltier, J. L.; Jazzar, R.; Melaimi, M.; Bertrand, G. Ancillary Ligand-Free Copper Catalyzed Hydrohydrazination of Terminal Alkynes with NH_2NH_2. *Chem. Commun.* **2016**, *52*, 2733 – 2735.

#17 Hu, X.; Martin, D.; Bertrand, G. Room temperature hydroamination of alkynes with anilines catalyzed by anti-Bredt di(amino)carbene gold(I) complexes. *New J. Chem.* **2016**, *40*, 5993-5996.

#18 Romero, E. A.; Peltier, J. L.; Jazzar, R.; Bertrand, G. Catalyst-Free Dehydrocoupling of Amines, Alcohols, and Thiols with Pinacol Borane and 9-Borabicyclononane (9-BBN). *Chem. Commun.* **2016**, *52*, 10563-10565.

#19 Kleinhans, G.; Hansmann, M. M.; Guisado-Barrios, G.; Liles, D. C.; Bertrand, G.; Bezuidenhout, D. I. Nucleophilic T-shaped (LXL)Au(I)-Pincer Complexes: Protonation and Alkylation. *J. Am. Chem. Soc.* **2016**, *138*, 15873-15876.

#20 Romero, E. A.; Jazzar, R.; Bertrand, G. (CAAC)CuX-catalyzed hydroboration of terminal alkynes with pinacolborane directed by the X-ligand. *J. Organomet. Chem.* **2017**, *829*, 11-13.

#21 Romero, E. A.; Peltier, J. L.; Jazzar, R.; Bertrand, G. Copper-Catalyzed Dehydrogenative Borylation of Terminal Alkynes with Pinacolborane. *Chem. Sci.* **2017**, *8*, 165-168.

#22 Romero, E. A.; Olsen, P. M.; Jazzar, R.; Soleilhavoup, M.; Gembicky, M.; Bertrand, G. Spectroscopic Evidence for a Monomeric Copper(I) Hydride, and Crystallographic Characterization of a Monomeric Silver(I) Hydride. *Angew. Chem. Int. Ed.* **2017**, *56*, 4024-4027.

#23 Tomás-Mendivil, E.; Hansmann, M. M.; Weinstein, C. M.; Jazzar, R.; Melaimi, M.; Bertrand, G. Bicyclic (Alkyl)(amino)carbenes (BICAACs): Stable Carbenes more Ambiphilic than CAACs. *J. Am. Chem. Soc.* **2017**, *139*,. doi.org/10.1021/jacs.7b04640

(II) Jointly funded by this grant and other grants with leading intellectual contribution from this grant

#24 Ruiz, D. A.; Melaimi, M.; Bertrand, G. An efficient synthetic route to stable bis(carbene)borylenes [$(L_1)(L_2)$BH]. *Chem. Commun* **2014,** *50,* 7837-7839.

#25 Dahcheh, F.; Martin, D.; Stephan, D. W.; Bertrand, G. Synthesis and Reactivity of a CAAC-Aminoborylene Adduct: A Hetero-Allene or an Organoboron Isoelectronic with Singlet Carbenes? *Angew. Chem. Int. Ed.* **2014**, *53*, 13159-13163.

#26 Marx, V. M.; Sullivan, A. H.; Melaimi, M.; Virgil, S. C.; Keitz, B. K.; Weinberger, D. S.; Bertrand, G.; Grubbs, R. H. Cyclic Alkyl Amino Carbene (CAAC) Ruthenium Complexes as Remarkably Active Catalysts for Ethenolysis. *Angew. Chem. Int. Ed.* **2015**, *54*, 1919-1923.

#27 Martin, D.; Marx, V. M.; Grubbs, R. H.; Bertrand, G. A Ruthenium Catalyst for Olefin Metathesis Featuring an Anti-Bredt N-Heterocyclic Carbene Ligand. *Adv. Synth. Catal.* **2016**, *358*, 965-969**.**

#28 Kleinhans, G.; Guisado-Barrios, G.; Liles, D. C.; Bertrand, G.; Bezuidenhout, D. I. A Rhodium(I) Oxygen Adduct as a Selective Catalyst for One-Pot Sequential Alkyne Dimerization-HydrothiolationTandem Reactions. *Chem. Commun.* **2016**, *52*, 3504-3507.

#29 Bidal, Y. D.; Santoro, O.; Melaimi, M.; Cordes, D. B.; Slawin, A. M. Z.; Bertrand, G.; Cazin, C. S. J. Generalization of the Copper to Late Transition Metal Transmetallation to Carbenes beyond N-Heterocyclic Carbenes, *Chem. Eur. J.* **2016**, *22*, 9404-9409.

#30 Chu, J.; Munz, D.; Jazzar, R.; Melaimi, M.; Bertrand, G. Synthesis of Hemilabile Cyclic (Alkyl)(amino)carbenes (CAACs) and Applications in Organometallic Chemistry, *J. Am. Chem. Soc.* **2016**, *138*, 7884-7887.

(III) Jointly funded by this grant and other grants with relatively minor intellectual contribution from this grant;

#31 Soleilhavoup, M.; Bertrand, G. Cyclic (Alkyl)(Amino)Carbenes (CAACs): Stable Carbenes on the Rise. *Acc. Chem. Res.* **2015**, *48*, 256-266.

#32 Jin, L.; Melaimi, M.; Kostenko, A.; Karni, M.; Apeloig, Y.; Moore, C. E.; Rheingold, A. L.; Bertrand, G. Isolation of cationic and neutral (allenylidene)(carbene) and bis(allenylidene)gold Complexes. *Chem. Sci.* **2016**, *7*, 150-154.

#33 Pranckevicius, C.; Liu, L.; Bertrand, G.; Stephan, D. Synthesis of a Carbodicyclopropenylidene: A Carbodicarbene based Solely on Carbon. *Angew. Chem. Int. Ed.* **2016**, *55*, 5536-5540.

#34 Melaimi, M.; Jazzar, R.; Soleilhavoup, M.; Bertrand, G. Cyclic (Alkyl)(Amino)Carbenes (CAACs): Recent developments. *Angew. Chem. Int. Ed.* **2017**, *56*, DOI: 10.1002/anie.201702148

Thomas Bligaard

Using on-the-fly surrogate machine learning models to accelerate catalysis studies

Paul C. Jennings[1], Steen Lysgaard[2], Zachary W. Ulissi[1], Andrew J. Medford[3], Tejs Vegge[2], Jens S. Hummelshøj[4], Jens K Nørskov[1], and Thomas Bligaard[5]

1. SUNCAT, Department of Chemical Engineering, Stanford University
2. Department of Energy Conversion and Storage, Technical University of Denmark
3. School of Chem. and Biochem. Engineering, Giorgia Institute of Technology
4. Toyota Research Institute, Los Altos
5. SUNCAT, SLAC National Accelerator Laboratory

Presentation Abstract

Analyzing catalytic processes and computationally searching for catalyst materials often involve analyzing a large number of elementary reaction steps, surface facets, and catalyst compositions. This leads to a need for performing a very large number of atomic-scale simulations, even for relatively simple catalytic reactions. Performing this large number of simulations with accurate density functional theory leads to intractably large computer resource demands. Progress is instead often attained through the use of "intuition" to simplify reaction networks, materials complexity, and the studied morphologies. We propose, as an alternative, to use machine learning models trained on-the-fly to automate the modeling process and reduce the overall computational complexity. We illustrate a couple of studies in which we attain some orders of magnitude speed-ups.

Metal Carbides and Bimetallic Alloys as Low-cost Electrocatalysts

Jingguang G. Chen
Department of Chemical Engineering, Columbia University

Presentation Abstract

It is well known that the electronic and catalytic properties of transition metals can be modified by alloying either with carbon or with another metal. The resulting metal carbides or bimetallic alloys often demonstrate properties that are distinctively different from those of the parent metals. The goal of our research program is to identify carbide and bimetallic catalysts to either substantially reduce or completely replace Pt-group metals in electrocatalysis. Many electrochemical devices, such as electrolyzers, fuel cells and photoelectrochemical cells, currently require Pt-group metals (Pt, Pd, Ir, Rh, Ru) as electrocatalysts. The high costs and limited supplies of these precious metals create potentially prohibitive barriers to market penetration and scale-up production of devices requiring large catalyst loadings.

Our research efforts involve three parallel approaches: (1) UHV experiments and DFT calculations on single crystal surfaces to predict general trends, (2) synthesis and characterization of the corresponding polycrystalline films and powder catalysts, and (3) electrocatalytic evaluation of these materials as low-cost alternatives to replace Pt-group metal catalysts. In the past year we utilized these approaches to investigate the hydrogen evolution reaction (HER) and the CO_2 reduction reaction (CO_2RR).

DE-FG02-13ER16381: Metal Carbides and Bimetallic Alloys as Low-cost Electrocatalysts

PI: Jingguang Chen
Student(s): Brian Tackett; Tyra Zhang

RECENT PROGRESS

A. Metal-Modified Carbides as HER Electrocatalysts in Alkaline Electrolyte

During the past year we have performed experimental and theoretical studies to determine the feasibility of using metal-modified carbides as HER catalysts in both acid and alkaline electrolytes. Although results from our previous studies have confirmed the feasibility of using low-coverage of Pt-group metals supported on metal carbides for HER in acid electrolyte, the stability of these catalysts in alkaline environment is not explored. We selected molybdenum carbide (Mo_2C) thin films and high surface area nanocrystalline particles to determine the effect of metal modification on the activity and stability in alkaline environment. The molybdenum carbide (Mo_2C) films and powders with modified Pt and Pd, as well as non-Pt group metals such

as Ag, Cu and Ni. We used DFT-calculated hydrogen binding energy (HBE) value as a descriptor of HER activity. Values were calculated for metal overlayers on both Mo-terminated and C-terminated Mo_2C. The C-terminated surface was previously reported as the most stable and most probable surface, but Mo-terminated surfaces were also likely to be present as a result of the nanocrystalline structure of the synthesized catalysts. Compared with the HBE of -0.46 eV on Pt(111), Pt- and Pd- on C-terminated Mo_2C and Cu- and Ni- on Mo-terminated Mo_2C were most similar. It was therefore expected that those materials would have high HER activity. In parallel, electrochemical performance of each metal-modified Mo_2C sample was evaluated. The HER activity trends observed in both acid and alkaline are consistent with the calculated HBE values for C-terminated Mo_2C. X-ray photoelectron spectroscopy (XPS) revealed that metal particles remained on the carbide substrates before and after HER testing. These results confirmed the feasibility of using Pt-group and non-Pt group metals to modify carbides for HER in alkaline electrolyte.

B. Investigation of CO_2 Electrochemical Reduction to Synthesis Gas ($CO + H_2$)

During the past year we have also explored the electrochemical CO_2RR to simultaneously produce carbon monoxide (CO) and hydrogen (H_2) on carbon supported palladium (Pd/C) nanoparticles in an aqueous electrolyte. The synthesis gas product has a CO to H_2 ratio between 0.5 and 1, which is in the desirable range for thermochemical synthesis of methanol and Fischer-Tropsch reactions using existing industrial processes. *In situ* X-ray absorption spectroscopy in both near-edge (XANES) and extended regions (EXAFS) and *in situ* X-ray diffraction show that Pd has transformed into β-phase palladium hydride (β-PdH) during the CO_2RR. DFT calculations demonstrate that the binding energies of both adsorbed CO and H, as well as a key reaction intermediate, HOCO, are significantly weakened on PdH than on Pd surfaces, and that these energies are potential descriptors to facilitate the search for more efficient electrocatalysts for syngas production through the CO_2RR.

Electrochemical CO_2RR can utilize off-peak electricity or intermittent renewable energy sources to convert CO_2 to value-added liquid fuels and chemical feedstocks, representing a green approach for energy storage and carbon recycling. CO_2RR is extremely challenging as CO_2 is among the most chemically stable carbon-based molecules. Large overpotential is required to activate CO_2 to form the $CO_2^{-}\cdot$ intermediate and to produce further reduced chemicals. Meanwhile, simultaneous HER is almost inevitable during the CO_2RR in aqueous electrolytes, making the Faradaic efficiency and selectivity for the CO_2RR to be very low. At present, Cu is found to be the only element that can produce a broad mix of as many as 16 C1-C3 molecules, but with low yield and selectivity. Reducing CO_2 to carbon monoxide (CO) appears to be more achievable as it involves the transfer of only two protons and two electrons. Because of the simultaneous HER during the CO_2RR in aqueous electrolytes, materials with low HER activities are typically targeted in order to obtain high Faradaic efficiency towards CO. Among them, Au and Ag are the most studied elements for CO production as they show very low HER activities and preferentially reduce CO_2 to CO, and efforts are being pursued to make the CO_2RR more efficient by creating various nanostructures of Au and Ag.

In our opinion, however, electrochemical co-production of CO and H_2 with tunable CO/H_2 ratios is very beneficial as they can be directly used as synthesis gas (syngas) for methanol synthesis and Fischer-Tropsch reactions. This is particularly appealing because the direct electrochemical CO_2RR to methanol or other liquid fuels currently has a very low Faradaic efficiency and selectivity, and the subsequent product separation is also highly energy-demanding.

As an alternative, a two-step synthetic route involving electrochemical syngas production with controlled CO/H_2 ratios, followed by the thermochemical methanol synthesis or Fischer-Tropsch reactions using existing industrial processes should be more economically viable. Moreover, targeting the formation of syngas opens up more opportunities for electrocatalyst development. Material search is no longer limited to Au or Ag, which has extremely low HER activities. Efforts may be switched from suppressing the HER activity of the catalysts to controlling the relative activities of the CO_2RR and HER by tuning the material properties. Thus catalysts with moderate HER activities can be potentially good options for the electrochemical syngas production. For example, Pd, usually considered as a good HER catalyst, can generate CO at a very similar Faradaic efficiency as for H_2 (1:1), and thus can be an excellent candidate for electrochemical syngas production. From a scientific perspective, however, the fact that Pd can continuously reduce CO_2 to CO seems to be counterintuitive because Pd is well known for its being subjected to CO poisoning due to its strong binding to adsorbed CO. A thorough understanding of the CO_2RR mechanism on Pd is missing in the previous studies, which is essential for bridging material properties to its electrochemical performance, and for further providing guidance for designing electrocatalysts for converting CO_2 to syngas. In our study we identified the electronic and compositional properties of Pd under the CO_2RR conditions using *in situ* XANES, EXAFS and XRD. The *in situ* characterization results, combined with DFT calculations, reveal the origin of the CO selectivity on Pd to be the greatly reduced CO binding energy due to the *in situ* formation of β-phase Pd hydride (PdH).

The electrochemical activity of Pd towards the CO_2RR was evaluated on ~4 nm Pd nanoparticles supported on Vulcan carbon (40wt% Pd/C, Fig.1a) using the chronoamperometry method in CO_2-saturated high purity 0.5 M sodium bicarbonate ($NaHCO_3$) electrolyte. The two halves of the H-shape electrolysis cell was separated and connected by a Nafion® 117 membrane in between. The one half with the working electrode (Pd/C deposited on a rectangular glassy carbon) and the reference electrode (saturated calomel electrode) was filled with 45 mL electrolyte, leaving a 10 mL headspace and kept airtight during the reaction. The gas phase products were quantified using gas chromatography (GC) after the CO_2RR between 10 and 60 minutes, and the liquid phase products were analyzed using NMR.

Fig.1b shows representative chronoamperometry CO_2 reduction current densities at given potentials. The major gas phase products are CO and H_2 from the CO_2RR on Pd/C. Fig.1c shows that the total Faradaic efficiency of CO and H_2 has reached 80% during the reaction Formic acid (data not shown) is the only liquid product that is generated at all investigated potentials. The concentrations are on the order of 10^{-5} M in the electrolyte, which accounts for roughly 5% of the total charge. With increasing overpotentials, the CO and H_2 current densities both increase (Fig.1d), with H_2 at a faster rate, resulting in a decreased CO to H_2 ratio at more negative potentials. This is caused by the mass transfer limitation of CO_2 molecules to the electrode surface due to its limited solubility, while the HER is not influenced by the transport of the proton donor, i.e. H_2O. Thus, the focus of the current study is placed on the data at lower current density region, as they do not interfere with the mass transport and more reflect the intrinsic kinetics of CO and H_2 generation during the CO_2RR and HER. The CO/H_2 ratio at higher potentials such as −0.5 V ~ −0.6 V is found to be between 0.5:1 and 1:1, which is similar to the range of syngas compositions for methanol synthesis.

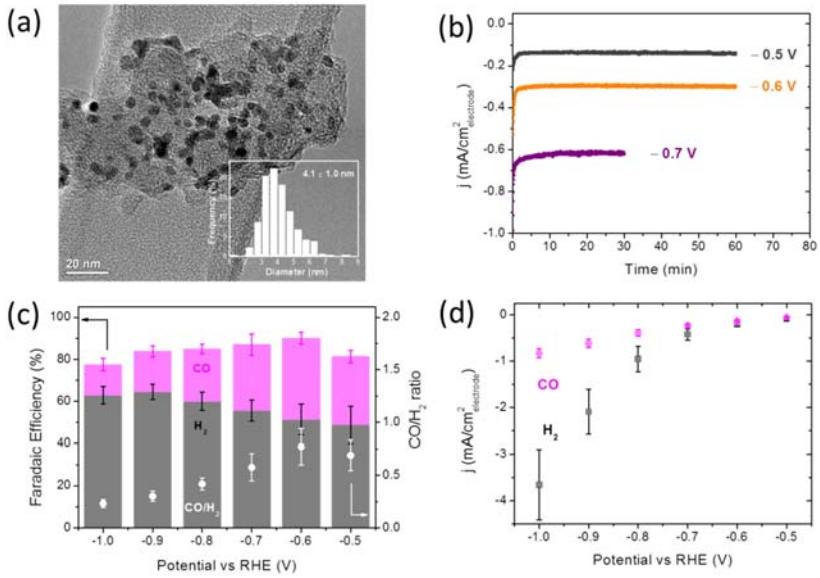

Figure 1. CO_2RR on Pd/C in CO_2-saturated 0.5 M $NaHCO_3$. (a): High resolution transmission electron microscopy image and particle size distribution of Pd/C; (b): current-time transients of the CO_2RR on Pd/C at given potentials; (c): Faradaic efficiencies of CO and H_2, and CO to H_2 ratio at different potentials; and (d): CO and H_2 current densities during the CO_2RR on Pd/C. The error bar in (a) is the standard deviation of the particle size constructed on at least 300 particle counts. The error bars in (c) and (d) are standard deviations obtained from 5 experimental repeats. From Sheng et al. *Energy & Environmental Science*, 10 (2017) 1180.

In summary, our electrochemical study, combined with *in situ* XANES, EXAFS, and XRD measurements and DFT calculations unravel the origin of CO selectivity on Pd to be the *in situ* formation of β-PdH under the CO_2RR conditions. The formation of PdH significantly lowers the binding energies of both adsorbed *CO and *H, and in turn tunes the selectivity towards simultaneous produced CO and H_2 during the CO_2RR. The current study indicates that the binding strengths of CO, H and HOCO can be used as the reaction descriptors, and tuning the relative adsorption strength of CO, H and HOCO should offer the opportunity to control the relative reaction rates of the CO_2RR and HER, and in turn tune the syngas composition. We are currently applying this design strategy to search for two classes of catalysts with reduced Pd loading: (1) low coverage Pd supported on transition metal carbides and (2) Pd-M alloys with M being non-Pt group metals. Our DFT results have identified several promising catalyst formulations. Synthesis and electrochemical evaluations are underway to identify the feasibility of using these materials as efficient and low-cost electrocatalysts for syngas production through the CO_2RR.

Publications Acknowledging this Grant in 2014-2017

(I) Exclusively funded by this grant;

1. W. Sheng, S. Kattel, S. Yao, B. Yan, C.J. Hawxhurst, Q. Wu and J.G. Chen*, "Electrochemical Reduction of CO_2 to Synthesis Gas with Controlled CO/H_2 Ratios", *Energy & Environmental Science*, 10 (2017) 1180-1185.
2. W. Wan, B.M. Tackett and J.G. Chen*, "Reactions of water and C1 molecules on carbide and metal-modified carbide surfaces", *Chemical Society Reviews*, 46 (2017) 1807-1823.
3. L. Lin, W. Sheng, S. Yao, D. Ma* and J.G. Chen*, "Pt/Mo_2C/C-cp as a Highly Active and Stable Catalyst for Ethanol Electrooxidation", *Journal of Power Sources*, 345 (2017) 182-189.
4. E.G. Mahoney, W, Sheng, M. Cheng, K.X. Lee, Y. Yan and J.G. Chen, "Analyzing the electrooxidation of ethylene glycol and glucose over platinum-modified gold electrocatalysts in alkaline electrolyte using in-situ infrared spectroscopy", *Journal of Power Sources*, 305 (2016) 89-96
5. Q. Zhang, B.M. Tackett, Q. Wu and J.G. Chen*, "Trends in Hydrogen Evolution Activity of Metal-Modified Molybdenum Carbides in Alkaline and Acid Electrolytes", *ChemElectroChem*, 3 (2016) 1686-1693
6. B.M. Tackett, Y.C. Kimmel and J.G. Chen*, "Metal-Modified Niobium Carbides as Low-Cost and Impurity-Resistant Electrocatalysts for Hydrogen Evolution in Acidic and Alkaline Electrolytes", *International Journal of Hydrogen Energy*, 41 (2016) 5948-5954
7. M.D. Porosoff, B. Yan and J.G. Chen*, "Catalytic reduction of CO_2 by H_2 for synthesis of CO, methanol and hydrocarbons: Challenges and opportunities", *Energy & Environmental Science*, 9 (2016) 62-73
8. L. Wang, E.G. Mahoney, S. Zhao, B. Yang and J.G. Chen, "Low Loading of Platinum on Transition Metal Carbides for Hydrogen Oxidation and Evolution Reactions in Alkaline Electrolyte", *Chemical Communications*, 52 (2016) 3697-3700
9. Q. Lu, G.S. Hutchings, W. Yu, Y. Zhou, R.V. Forest, R. Tao, J. Rosen, B.T. Yonemoto, Z. Cao, H. Zheng, J.Q. Xiao, F. Jiao* and J.G. Chen*, "Highly Porous Non-precious Bimetallic Electrocatalysts for Efficient Hydrogen Evolution", *Nature Communications*, 6 (2015) 6567
10. L. Yang, Y.C. Kimmel, Q. Lu and J.G. Chen*, "Effect of pretreatment on the particle size and oxygen reduction activities of low-loading platinum on titanium carbide powder electrocatalysts", *Journal of Power Sources*, 287 (2015) 196-202
11. M. Myint, Y. Yan and J.G. Chen*, "Reaction Pathways of Propanal and 1-Propanol on Fe/Ni(111) and Cu/Ni(111) Bimetallic Surfaces", *Journal of Physical Chemistry C*, 118 (2014) 11340-11349
12. W. Sheng, Z. Zhuang, M. Gao, J. Zheng, J.G. Chen* and Y. Yan*, "Correlating hydrogen oxidation/evolution reaction activity on platinum at different pH with measured hydrogen binding energy", *Nature Communications*, 6 (2015) 5848
13. Y.C. Kimmel, L. Yang; T.G. Kelly, S.A. Rykov and J.G. Chen*, "Theoretical Prediction and Experimental Verification of Low Loading of Platinum on Titanium Carbide as Low-Cost and Stable Electrocatalysts", *Journal of Catalysis*, 312 (2014) 216-220

14. Y.C. Kimmel, X. Xu, W. Yu, X. Yang and J.G. Chen*, "Trends in Electrochemical Stability of Transition Metal Carbides and Their Potential Use as Supports for Low-Cost Electrocatalysts", *ACS Catalysis*, 4 (2014) 1558-1562
15. T.G. Kelly, K.X. Lee and J.G. Chen*, "Pt-modified Molybdenum Carbide for the Hydrogen Evolution Reaction: From Model Surfaces to Powder Electrocatalysts", *Journal of Power Sources*, 271 (2014) 76-81
16. T.G. Kelly and J.G. Chen*, "Controlling C-O, C-C and C-H Bond Scission for Deoxygenation, Reforming, and Dehydrogenation of Ethanol using Metal-modified Molybdenum Carbide Surfaces", *Green Chemistry*, 16 (2014) 777-784
17. T.G. Kelly, A.L. Stottlemyer, X. Yang and J.G. Chen*, "Theoretical and experimental studies of ethanol decomposition and electrooxidation over Pt-modified tungsten carbide", *Journal of Electrochemical Society*, 161 (2014) E3165-3170
18. E.G. Mahoney, W. Sheng, Y. Yan, and J.G. Chen*, "Platinum-Modified Gold Electrocatalysts for the Hydrogen Oxidation Reaction in Alkaline Electrolytes", *ChemElectroChem*, 1 (2014) 2058-2063

(II) Jointly funded by this grant and other grants with leading intellectual contribution from this grant;

19. J. Wang, W. Wang, Z. Wang, J.G. Chen* and C.-J. Liu*, "Porous MS_2/MO_2 (M=W, Mo) Nanorods as Efficient Hydrogen Evolution Reaction Catalysts", *ACS Catalysis*, 6 (2016) 6585-6590
20. Y. Zhou, Q. Lu, Z. Zhuang, G.S. Hutchings, S. Kattel, Y. Yan, J.G. Chen*, J.Q. Xiao* and F. Jiao*, "Oxygen Reduction at Very Low Overpotential on Nanoporous Ag Catalysts", *Advanced Energy Materials*, 5 (2015) 1500149
21. Q. Lu, J. Rosen, Y. Zhou, G.S. Hutchings, Y.C. Kimmel, J.G. Chen and Feng Jiao, "A Highly Selective and Efficient Electrocatalyst for Carbon Dioxide Reduction", *Nature Communications*, 5 (2014) 3242
22. W. Sheng, A.P. Bivens, M. Myint, Z. Zhuang, R.V. Forest, Q. Fang, J.G. Chen* and Y. Yan*, " Non-precious Metal Electrocatalyst with High Activity for Hydrogen Oxidation Reaction in Alkaline Electrolytes", *Energy & Environmental Science*, 7 (2014) 1719-1724

(III) Jointly funded by this grant and other grants with relatively minor intellectual contribution from this grant;

23. M. Dunwell, Q. Lu, J.M. Heyes, J. Rosen, J.G. Chen, Y. Yan, F. Jiao, and B. Xu, "The Central Role of Bicarbonate in the Electrochemical Reduction of CO_2 on Gold", *Journal of the American Chemical Society*, 139 (2017) 3774-3783
24. K.A. Kuttiyiel, K. Sasaki, G-G. Park, M.B. Vukmirovic, L. Wu, Y. Zhu, J.G. Chen and R.R. Adzic, "Janus Structured Pt-FeNC Nanoparticles as Catalyst for the Oxygen Reduction Reaction", *Chemical Communications*, 53 (2017) 1660-1663

Chemical Imaging of Single-Particle Photoelectrocatalysis

Xianwen Mao, Mahdi Hesari, Peng Chen
Department of Chemistry and Chemical Biology, Cornell University

Presentation Abstract

Single-molecule super-resolution fluorescence microscopy was used to selectively map hole- and electron-induced surface reactions on single semiconductor nanoparticles performed as photoanodes for photoelectrochemical water oxidation. The high-resolution activity maps of surface charge carrier reactions are coupled with local photoelectrochemical current measurements at the sub-particle level. Oxygen evolution catalysts could then be deposited onto the semiconductors site-selectively using controlled photoelectrodeposition. These techniques are employed to study different facets and different locations within a single facet of single $BiVO_4$ nanocrystals, as well as along the length of TiO_2 nanorods.

DE-FG02-10ER16199 / DE-SC0004911: Chemical Imaging of Single□Particle Photoelectrocatalysis

Postdoc(s): Xianwen Mao (25%), Mahdi Hesari (50%)

RECENT PROGRESS

Establish the design principles of catalyst-modified $BiVO_4$ semiconducting crystals with facet-dependent electron/hole activities. We synthesized monoclinic $BiVO_4$ with truncated bipyramid morphology (Figure 1a inset) by a facial hydrothermal process. SEM imaging (Figure 1a, b) shows that the majority of the as-synthesized $BiVO_4$ crystals exhibit the desired truncated bipyramid morphology with well-defined (010) and (110) facets. The photocurrent-potential characteristic (Figure 1c) of a bulk $BiVO_4$ film integrated onto an indium-doped tin oxide (ITO) electrode tested under 405 nm illumination in a 0.5 M phosphate buffer solution with 0.5 M Na_2SO_4 (pH = 7.4) shows an onset potential at 0.1 V versus Ag/AgCl, consistent with the value reported in literature for undoped monoclinic $BiVO_4$. Selective catalyst deposition onto different facets of a single $BiVO_4$ particle will be performed by a photochemical deposition method, which relies on the photogenerated electrons or holes to induce reductive or oxidative deposition of the catalyst. This photochemical method permits a localized catalyst deposition site where a focused laser illuminates, as we previously demonstrated. Figure 1d (upper panel) shows the transmission image of a single $BiVO_4$ particle observed using optical microscope; the (010) and (110) facets of $BiVO_4$ are easily identifiable, allowing us to steer a focused laser beam towards different facets. Figure

1d (lower panel) shows the transmission image of the same $BiVO_4$ particle with a focused 405 nm laser beam directed onto the (010) facet.

To verify that $BiVO_4$ exhibits facet-dependent electron/hole activities, we employed single-molecule fluorescence microscopy to map the surface reactions of photogenerated electrons/holes, as schematically illustrated in Figure 1e. In a typical experiment, the potential of the ITO electrode (E, versus Ag/AgCl) was fixed while a N_2-purged electrolyte solution containing nanomolar nonfluorescent probe molecules flowed through the microfluidic cell. Continuous 405 nm illumination generated charge carriers within $BiVO_4$ particles; these photogenerated holes or electrons convert nonfluorescent probe molecules oxidatively or reductively to fluorescent product molecules. The 532 nm laser was used to excite the product molecules, the fluorescence of which was captured by the camera, generating a sequence of fluorescence images (i.e., catalytic movies). Notably, $BiVO_4$ exhibits intrinsic fluorescent emission under 405 and 532 nm illuminations in the absence of probe molecules (Figure 1f). To capture the fluorescence of the product molecule alone, we developed a procedure to correct for the $BiVO_4$ intrinsic emission by subtracting averaged $BiVO_4$ fluorescence signal without the probe molecules from the catalytic movies collected with the probe molecules. The $BiVO_4$ intrinsic emission-corrected movies were analyzed by a home-written MATLAB program, as we described previously. Briefly, the fluorescence of each product molecule was fitted with by a 2D Gaussian point spread function (PSF), permitting determination of the centroid position of this molecule with nanometer precision. The standard deviation (σ_x or σ_y) of the fitted 2D PSF was used to select single-molecule events in order to construct super-resolution reaction images. Figure 1g shows an example of the σ_x distribution for a $BiVO_4$ intrinsic

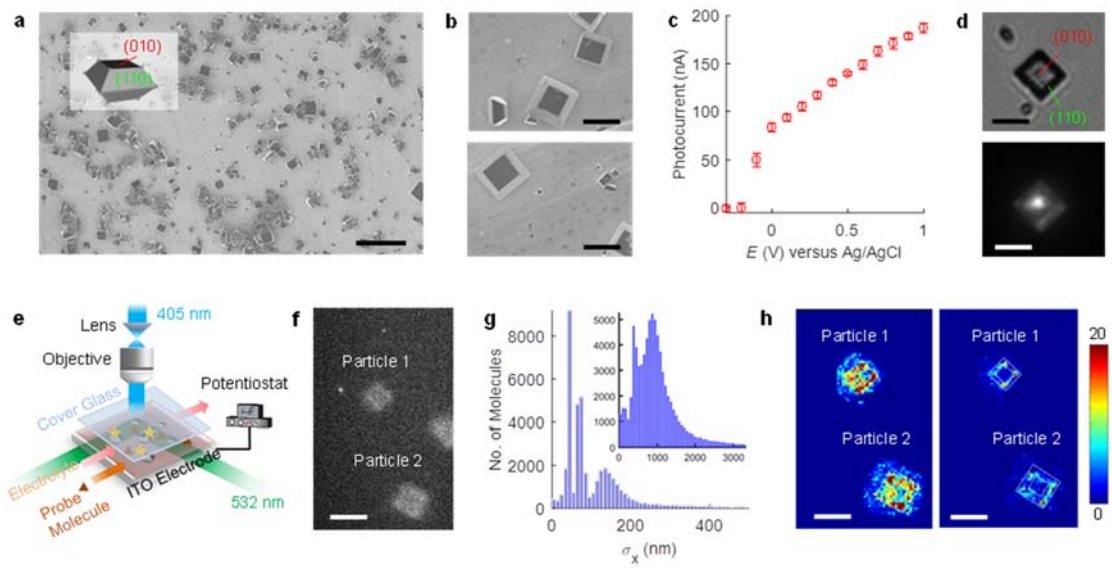

Figure 1. (a) SEM image of $BiVO_4$ particles. Inset: cartoon illustration of a single $BiVO_4$ crystal possessing a truncated bipyramid morphology with (010) and (110) facets identified. Scale bar: 20 μm. (b) Representative large-magnification SEM images of single $BiVO_4$ particles. Scale bar: 3 μm. (c) Photocurrent versus potential for a bulk $BiVO_4$ film. (d) Transmission images of a single $BiVO_4$ crystal (upper panel: without laser illumination; lower panel: with a focused laser beam on the (010) facet. Scale bar: 5 μm. (e) Experimental setup for single-molecule fluorescence imaging of photoelectrocatalysis via 532 nm total internal reflection excitation and 405 nm epi-fluorescence excitation, in a microfluidic photoelectrochemical flow cell. (f) Fluorescence image of two $BiVO_4$ particles with 405 and 532 nm illumination and E = 0.1 V without the probe molecules, showing the intrinsic emission of $BiVO_4$. Scale bar: 5 μm. (g) σ_x distribution for a $BiVO_4$ intrinsic emission-corrected catalytic movie. Inset shows the results obtained without intrinsic emission correction. (h) Super-resolution hole surface reaction mapping of two $BiVO_4$ particles (E = 0.1 V) (left panel: illuminated by 405 and 532 nm; right panel: illuminated by 532 nm). Scale bar: 5 μm.

emission-corrected movie; we observed a population centered at ~150 nm, consistent with the diffraction-limited width of a single-molecule PSF of the fluorescent molecule used in our study (126 nm). σ_y had a similar distribution. As a control, Figure 1g inset shows the σ_x distribution for the same catalytic movie without $BiVO_4$ intrinsic emission correction; a much broader distribution was obtained, indicating an inability to obtain information on single-molecule events. Figure 1h shows the super-resolution hole surface reaction mapping of two $BiVO_4$ particles (left panel: illuminated by 405 and 532 nm; right panel: illuminated by 532 nm). 532 nm also generated charge carriers with $BiVO_4$ through mid-gap excitation. These super-resolution images show that holes were preferentially accumulated on the (110) facet, consistent with the observation reported previously[1].

Probe intra-facet variation of electronic properties of $BiVO_4$ using sub-particle photocurrent measurements. To probe intra-facet electronic structure variation, we carried out sub-particle photocurrent measurements, as in our previously studies, whereby a focused 405 nm laser beam was directed to the $BiVO_4$ (010) facet, and moved from the facet center towards to the edge. Notably, the illumination region always resides on the (010) facet. The diameter of a tightly focused 405 nm laser beam was determined to be 380 nm via 2D Gaussian fitting of the laser reflection image, significantly smaller than the lateral dimension of the $BiVO_4$ particles with a typical (010) facet side length of ~ 2 to 6 μm. Hence our experimental setup allows for measuring photocurrents locally at different spots on the same facet. We found that the photocurrent difference increased with an increasing distance away from the particle centroid, suggesting position-dependent photocatalytic activity on a single $BiVO_4$ (010) facet.

Investigate transversal vs. longitudinal charge transfer in single TiO_2 nanorod photoanodes. Rutile TiO_2 nanorods were synthesized following previously published protocol. The average diameter and length of nanorods are 181 ± 7 and 1865 ± 182 nm, respectively. The TiO_2 nanorods were spin-coated and annealed on an Interdigitated Array ITO (IDA-ITO) electrode (10 μm width with 5 μm interval, and thickness of 100 ± 2 nm). The IDA-ITO electrode was then assembled in a microfluidic photoelectrochemical cell and served as a working electrode (WE). To perform in-*situ* photoelectrochemical study, Ag/AgCl and Pt wire were used as reference and counter electrodes. Then, the photoelectrochemical/microfluidic cell assembled on our inverted microscope. Single molecule super-resolution microscopy performed using a wide-filed illumination of 375 nm and 532 nm lasers. The 375 nm laser was used to excite TiO_2 nanorods (photogenerate electron (e^-) and hole (h^+)) and 532 nm laser probes the product of a fluorogenic probe molecules (resorufin, λ_{em}=585 nm) on the surface of nanorods (Figure 2C) under total internal reflection fluorescence (TIRF) microscopy condition.

Among the dispersed nanorods on the IDA-ITO electrode, those individual (with relatively *long* length*)* nanorods that *randomly* laid on both ITO and glass parts of the IDA-ITO electrode were chosen to study their *transversal and longitudinal charge transfer* properties. In-*situ* electrochemical photocurrent measurement was performed using chronoamprometry technique to collect photogenerated charge carriers. The *focused* 375 nm laser was parked at different positions along a nanorod by moving microscope stage to locally excite nanorods (Figure 2A). As a control, the photocurrent of ITO or glass was also collected and then subtracted from the nanorod photocurrent to obtain <u>*net*</u> photocurrent. There appears to be an inverse correlation between photocurrent and distance to the electrode edge, as the larger distances have lower photocurrents (Figure 2B). The photocurrent decay follows an exponential decay with distance that could have

two origins; (1) difference between nominal applied potential and actual local potential, (2) loss of photogenerated charge carrier (e^-) while transporting along the nanorod.

We used single-molecule super-resolution reaction imaging to map charge carrier (h^+ and e^-) reactivity, as we developed previously. Our primarily single molecule super-resolution imaging data (Figure 2D) show that there is a spatial correlation between hole and electron reactivity on a nanorod surface. We will examine how the reactivity rate may depend on the distance to the electrode edge. This could support the photocurrent decay as it is mentioned above.

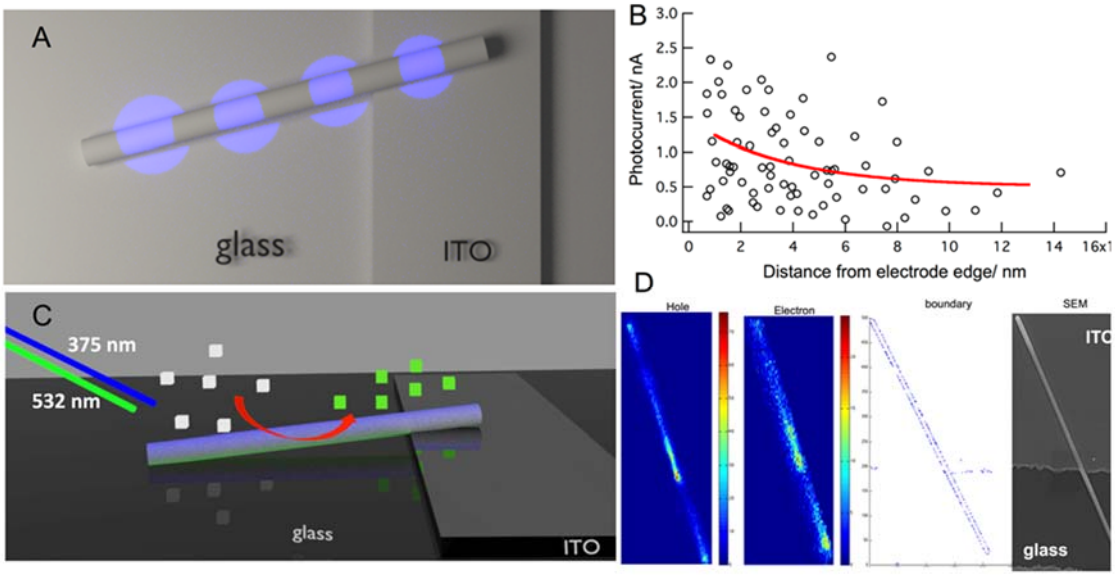

Figure 2. (A) Schematic illustrations of local laser illumination at different locations on a single TiO_2 nanorod. The blue circles represent different laser spots on a TiO_2 nanorod. (B) A scatter plot of photocurrent *vs*. distance from electrode edge obtained during chronoamperometry experiment at 200 mV using a *focused* 375 nm laser. The red line represents a exponential fit. (C) Schematic of wide-filed single molecule TIRF experiment of a nanorod. The white and green cubes represent nonfluorescent probe molecules and fluorescent product molecules, respectively. (D) Two-dimensional (2D) histograms of hole and electron induced reactions on a TiO_2 nanorod along with corresponding nanorod structural boundary obtained from its SEM image.

Publications Acknowledging this Grant in 2014-2017

(I) Exclusively funded by this grant;

None.

(II) Jointly funded by this grant and other grants with leading intellectual contribution from this grant;

1. Sambur, J. B.; Chen, P., Distinguishing Direct and Indirect Photoelectrocatalytic Oxidation Mechanisms Using Quantitative Single-Molecule Reaction Imaging and Photocurrent Measurements. *J. Phys. Chem. C.* **2016,** 120, 20668-20676.
2. Sambur, J. B.; Chen, T.-Y.; Choudhary, E.; Chen, G.; Nissen, E. J.; Thomas, E. M.; Zou, N.; Chen, P., Sub-particle reaction and photocurrent mapping to optimize catalyst-modified photoanodes. *Nature* **2016,** *530*, 77-80.

3. Shen, H.; Zhou, X.; Zou, N.; Chen, P., Single-Molecule Kinetics Reveals a Hidden Surface Reaction Intermediate in Single-Nanoparticle Catalysis. *J. Phys. Chem. C* **2014**, *118*, 26902-26911.
4. Sambur, J. B.; Chen, P., Approaches to Single-Nanoparticle Catalysis. *Annu. Rev. Phys. Chem.* **2014,** *65*, 395-422.
5. Chen, P.; Zhou, X.; Andoy, N. M.; Han, K.-S.; Choudhary, E.; Zou, N.; Chen, G.; Shen, H., Spatiotemporal Catalytic Dynamics within Single Nanocatalysts Revealed by Single-Molecule Microscopy. *Chem. Soc. Rev.* **2014,** *43*, 1107-1117.

(III) Jointly funded by this grant and other grants with relatively minor intellectual contribution from this grant;

None.

Understanding Nitrogen Fixation

Mate J. Bezdek, Sangmin Kim, Paul Chirik
Department of Chemistry, Princeton University, Princeton, NJ 08544

Presentation Abstract

The interconversion of elemental nitrogen with its elements – nitrogen hydrogenation in the forward; ammonia oxidation to N_2 and H_2 in reverse – is a fundamental challenge in basic energy sciences. Discovery of batch processes compatible with renewable rather than fossil fuel derived hydrogen is an attractive for development of ammonia as a zero-carbon fuel. Our program has focused on understanding and applying proton coupled electron transfer (PCET) to form and break nitrogen-hydrogen bonds in coordination complexes. Key to this effort has been developing the fundamental thermodynamic parameters associated with nitrogen-containing ligands in a variety of coordination complexes. This understanding has enabled the synthesis of ammonia via PCET from metal amides using H_2 as the stoichiometric reductant. In addition, molybdenum complexes in unusual oxidation states have been synthesized that render the N-H bonds in ammonia below the thermodynamic potential for spontaneous H_2 evolution and provides a blueprint for envisioning long-standing ammine complexes as sources of molecular hydrogen.

Grant or FWP Number: DE-SC0006498

Student(s): Mate J. Bezdek, Sangmin Kim

RECENT PROGRESS

Recent efforts have focused on understanding the mechanism of hydrogen evolution from terpyridine molybdenum ammine complexes. To better understand the thermodynamics, kinetics and molecularity of the key H-H bond forming step, the molybdenum amido and imido complexes supported by a mixed terpyridine and bis(phosphine) ligand environment, $[(^{Ph}Tpy)(PPh_2Me)_2Mo(NHtBuAr)][BArF^{24}]$ [^{Ph}Tpy = 4'-Ph-2,2',6',2"-terpyridine; tBuAr = 4-*tert*-butyl-C_6H_4; ArF^{24} = $(C_6H_3\text{-}3,5\text{-}(CF_3)_2)_4$)] and $[(^{Ph}Tpy)(PPh_2Me)_2Mo(NtBuAr)][BArF^{24}]$ have been synthesized and structurally characterized. The stoichiometric interconversion of the complexes was achieved by oxidative and reductive proton coupled electron transfer (PCET) using 2,4,6-tri-*tert*-butylphenoxyl radical and $[(^{Ph}Tpy)(PPh_2Me)_2Mo(NH_3)][BArF^{24}]$, respectively, and the free energy change for the transformation was experimentally bracketed between 45.8 and 52.3 kcal/mol (in close agreement with a DFT-computed value of 48.0 kcal/mol). These studies provide a thermochemical foundation for achieving a key step in the interconversion of ammonia with its elements using well-defined complexes of molybdenum. In addition, phosphine and N-heterocyclic carbenes derivatives of the parent ammine complexes, $[(^{Ph}Tpy)(L)_2Mo(NH_3)][BArF^{24}]$ have also been synthesized and thermochemical measurements have determined "non-classical" behavior, meaning the N-H bonds are below the value for hydrogen evolution.

These findings as well as strategies for the synthesis of new metal nitrides that ideally will form N-N bonds will be presented.

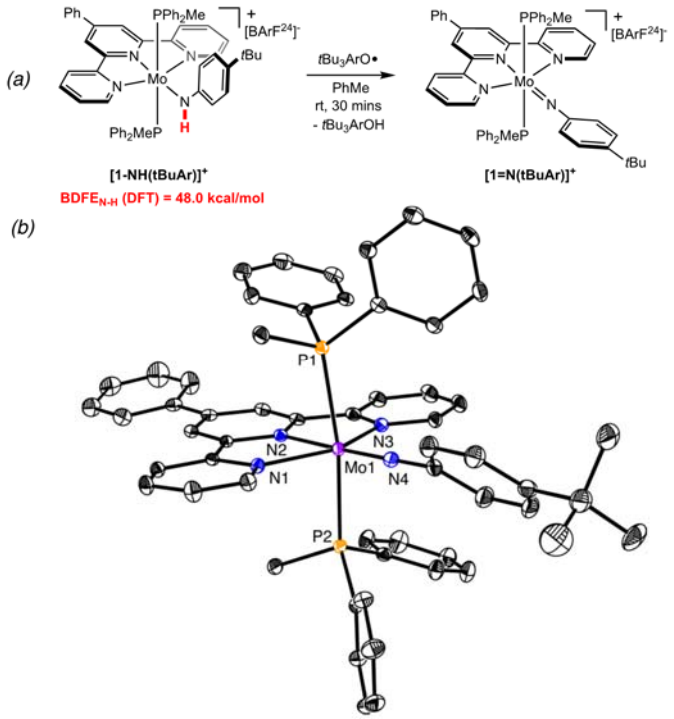

Publications Acknowledging this Grant in 2014-2017

(I) Exclusively funded by this grant;

1. Margulieux, G. W.; Bezdek, M. J.; Turner, Z. R.; Chirik, P. J. "Ammonia activation, H_2 evolution, and nitride formation from a molybdenum complex." *J. Am. Chem. Soc.* **2017**, *139*, 6110-6113.
2. Bezdek, M. J.; Pappas, I.; Chirik, P. J. "Determining and understanding N-H bond strengths in synthetic nitrogen fixation cycles." *Topics in Organometallic Chemistry* **2017**, DOI: 10.1007/3418_2016_8.
3. Bezdek, M.; Guo, S.; Chirik, P. J. "Coordination induced bond weakening of ammonia, water, hydrazine with a molybdenum complex." *Science* **2016**, *354*, 730-733.
4. Bezdek, M. J.; Guo, S.; Chirik, P. J. "Terpyridine molybdenum dinitrogen chemistry: Synthesis of dinitrogen complexes that vary by five oxidation states." *Inorg. Chem.* **2016**, *55*, 3117-3127.
5. Pappas, I.; Chirik, P. J. "Ammonia synthesis by hydrogenolysis of titanium-nitrogen bonds using proton coupled electron transfer." *J. Am. Chem. Soc.* **2015**, *137*, 3498-3501. (Selected for *JACS Spotlight*).
6. Milsmann, C.; Semproni, S. P.; Chirik, P. J. "N-N bond cleavage of 1,2-diarylhydrazines and N-H bond formation via H-atom transfer in vanadium complexes supported by a redox-active ligand." *J. Am. Chem. Soc.* **2014**, *136*, 12099-12107.
7. Margulieux, G. W.; Semproni, S. P.; Chirik, P. J. "Photochemically-induced reductive elimination as a route to a zirconocene complex with a strongly activated N_2 ligand." *Angew. Chem. Int. Ed.* **2014**, *53*, 9189-9192.

MnO(100): Initial Experimental Benchmarks for Adsorption and Co-Adsorption on the Ordered Surface and Oxidation to Mn^{3+} Surface Compounds

Han Chen, Xu Feng and David F. Cox
Department of Chemical Engineering, Virginia Polytechnic Institute and State University, Blacksburg, VA 24060

Presentation Abstract

Work has been undertaken to establish experimental benchmarks for adsorption and reaction on surfaces of transition metal oxides with highly correlated electronic structures which pose difficulties for modeling with DFT. CO adsorption and CO_2 and H_2O coadsorption on MnO(100) have been examined. For all adsorbates examined, DFT (as opposed to DFT+U) gives unrealistic adsorption geometries with long-range surface reconstructions or dramatic local bonding rearrangements even for very weakly adsorbed molecules. DFT+U gives more realistic geometries. DFT+U-D3 does an excellent job of reproducing the experimental value of adsorption energy for CO on a MnO(100) flat terrace (agreement within 0.4 kJ/mol). Agreement is reasonable for water, with DFT+U-D3 under-binding H_2O by about 12 kJ/mol compared to experiment, and but problematic for CO2 adsorption where an over-binding by more than 40 kJ/mol is predicted. For H_2O and CO_2 coadsorption, DFT+U-D3 predicts that bicarbonate formation is preferred at defect sites but not on flat terraces, in agreement with experiment.

The preparation of a surface oxide with Mn^{3+} cations from MnO(100) has also been examined to allow a future investigation of the chemistry of Mn^{3+} ($3d^4$) for comparison to previous work showing differences in selectivity for hydrocarbon conversion on Cr^{3+} ($3d^3$) and Fe^{3+} ($3d^5$) which vary from dehydrogenation and C-C coupling reactions over Cr_2O_3 to nonselective oxidation over Fe_2O_3 single crystal surfaces. Oxidation of clean and Na-precovered MnO(100) was investigated by X-ray photoelectron spectroscopy (XPS), temperature programmed desorption (TPD) and low energy electron diffraction (LEED). XPS results indicate that a Mn_3O_4-like and a Mn_2O_3-like surfaces can be formed by various oxidation treatments of clean and nearly-stoichiometric MnO(100), while a $NaMnO_2$-like surface was produced by oxidation of the MnO(100) pre-covered with a high coverage of metallic Na. Water TPD results suggest that water adsorption is sensitive to the surface Mn oxidation states on these different material surfaces.

DE-FG02-97ER14751: Hydrocarbon Oxidation, Dehydrogenation and Coupling over Model Transition Metal Oxide Surfaces

Student(s): Han Chen, Xu Feng (graduated)

RECENT PROGRESS

Adsorption Benchmarks on MnO(100)

Experimental work has been completed for CO, CO_2 and H_2O adsorption on MnO(100) using temperature programmed desorption (TPD). The primary desorption features for CO, CO_2 and H_2O are all first order and attributed to adsorbates on flat terraces. Experimental values of the adsorption energy are extracted from the activation energy for desorption typically measured in TPD. CO adsorbs molecularly, and desorbs with a primary feature at 130 K attributed to desorption from terraces, with additional contributions in a broad tail that extend to over 300K and is attributed to desorption from defects. CO_2 adsorbs molecularly, and desorbs from 200 - 500 K from surface defect sites and at 150 K from terraces. Water adsorbs molecularly on terraces and desorbs with a peak maximum at 260 K at low coverages. Water also dissociates on surfaces defects with desorption temperatures ranging between 300 and 600 K. For water and CO_2 coadsorption, TPD shows that when water is adsorbed prior to CO_2, water blocks uptake of CO_2 on both terrace and defect sites. When CO_2 is adsorbed prior to water, water displaces pre-adsorbed CO_2 on terrace sites, but stabilizes CO_2 adsorption around defect sites through the formation of bicarbonate.

Our computational work on MnO(100) has examined DFT (PBE-GGA), DFT+U (PBE-GGA+U) and as many as four different methods for accounting for van der Waals (vdW) interactions. We find that for MnO(100) the DFT (PBE-GGA) functionals give poor representations of the surface structure in the presence of all the adsorbates we have considered so far. Even adsorbates that interact very weakly give rise to nonphysical long-range reconstructions or dramatic local modifications of the Mn-O bonding in the surface layer. DFT+U gives a more believable surface structure devoid of long-range reconstructions for all adsorbates, so DFT+U has been our primary tool for examining the MnO(100) surface chemistry. A representative comparison of our experimental results with DFT+U-D3 is given in Table 1 for adsorption on MnO(100) *terraces*.

For adsorption at defects, steps and isolated oxygen vacancies have been examined for the three adsorbates. While neither of these defects are a good match for the experimental data, they all predict more strongly bound adsorbates as seen experimentally. DFT also accurately predicts that bicarbonate formation is stable at surface defects and not on terraces, in agreement with experiment.

Table 1. Comparison of Experimental and DFT Adsorption Energies on MnO(100) Terraces

Adsorbate on MnO(100) terrace sites	Experimental Adsorption Energy (kJ/mol)	PBE+U-D3 Adsorption Energy (kJ/mol)	ΔE (exp-DFT) (kJ/mol)
CO	-36.8	-37.138	0.34
CO_2	-41.8	-84.600	42.8
H_2O	-75.0	-63.492	-11.51

MnO(100) Oxidation and Compound Formation

Oxidation of clean and Na-precovered MnO(100) was investigated by X-ray photoelectron spectroscopy (XPS), temperature programmed desorption (TPD) and low energy electron diffraction (LEED). XPS results indicate that Mn_3O_4-like and a Mn_2O_3-like surfaces can be formed by various oxidation treatments of clean and nearly-stoichiometric MnO(100), while a $NaMnO_2$-like surface can be produced by oxidation of the MnO(100) pre-covered with a high coverage of metallic Na. LEED shows no long range order for these modifications of the MnO(100) surface. TPD indicates that water can be used as a probe molecule to distinguish between surface Mn^{2+} and Mn^{3+} surface cations. These surface preparations will be used in the next phase of our work to investigate the reactions of hydrocarbon fragments on surface Mn cations with different oxidation states.

Publications Acknowledging this Grant in 2014-2017

(I) Exclusively funded by this grant;

1. X. Feng, X.; Cox, D. F. Na Deposition on MnO(100). *Surface Science* **2016**, *645*, 23-29.
2. Dong, Y.; Brooks, J. D.; Chen, T. L.; Mullins, D. R.; Cox, D. F. Reactions of methyl groups on a non-reducible metal oxide: the reaction of iodomethane on stoichiometric α-Cr_2O_3(0001). *Surface Science* **2015**, *641*, 148-153.
3. Dong, Y.; Brooks, J. D.; Chen, T. L.; Mullins, D. R.; Cox, D. F. Methylene migration and coupling on a non-reducible metal oxide: the reaction of dichloromethane on stoichiometric α-Cr_2O_3(0001). *Surface Science* **2015**, *632*, 28-38.

(II) Jointly funded by this grant and other grants with leading intellectual contribution from this grant;

4. Gibbs, G. V.; Ross, N. L.; Cox, D. F. Sulfide Bonded Atomic Radii. *Physics and Chemistry of Minerals,* **in press**.
5. Gibbs, G. V.; Ross, N. L.; Cox, D. F. Bond length estimates for oxide crystals with a molecular power law expression. *Physics and Chemistry of Minerals* **2015**, *42*, 587-593.
6. Gibbs, G. V.; Ross, N. L.; Cox, D. F.; Rosso, K. M. Insights into the crystal chemistry of earth materials rendered by electron density distributions: Pauling's rules revisited. *American Mineralogist* **2014**, *99*, 1071-1084.
7. Gibbs, G. V.; Ross, N. L.; Cox, D. F.; Rosso, K. M.; Iversen, B. B.; Spackman, M. A. Pauling Bond Strength, Bond Length and Electron Density Distributions. *Physics and Chemistry of Minerals* **2014**, *41*, 17-25.

Electron Transfer Facilitated by Dendrimer-Encapsulated Pt Nanoparticles Across Ultra-Thin, Insulating Oxide Films

Nevena Ostojic, Graeme Henkelman, and Richard M. Crooks
The University of Texas at Austin, Department of Chemistry

Presentation Abstract

Electrocatalytic oxygen reduction at carbon electrodes fully passivated by Al_2O_3 is reported. Specifically, pyrolyzed polymer film (PPF) electrodes were prepared and then coated with pinhole-free Al_2O_3 layers ranging in thickness from 2.5 to 5.7 nm. All of these ultrathin oxide film thicknesses completely passivated the PPF electrodes, resulting in no faradaic current for either inner-sphere or outer-sphere electrochemical reactions. The electrodes could, however, be reactivated by immobilizing Pt dendrimer-encapsulated nanoparticles (DENs), containing an average of 55 atoms each, on the oxide surface. These PPF/Al_2O_3/Pt DEN electrodes were completely stable under a variety of electrochemical and solution conditions, and they are active for simple electron-transfer reactions and for more complex electrocatalytic processes. We also show that ultraviolet/ozone (UV/O_3) treatment can be used to remove sixth-generation, hydroxyl-terminated poly(amidoamine) (PAMAM) dendrimers from dendrimer-encapsulated Pt nanoparticles (Pt DENs) previously immobilized onto a pyrolyzed photoresist film (PPF) electrode. Results from X-ray photoelectron spectroscopy, scanning transmission electron microscopy, and electrochemical experiments indicate that removal of the dendrimer proceeds without changes to the size, shape, or electrocatalytic properties of the encapsulated nanoparticles. The UV/O_3 treatment did not damage the PPF electrode. The electrocatalytic properties of the DENs before and after removal of the dendrimer were nearly identical. This approach for preparing well-defined oxide electrodes opens the door to a better understanding of the effect of oxide supports on reactions electrocatalyzed by metal nanoparticles.

Sheng Dai

Synthesizing Cooperative Metal-Support Interfaces for Catalysis

Cheng-Cheng Tian, Huiyuan Zhu, and Sheng Dai
Chemical Sciences Division, Oak Ridge National Laboratory, Oak Ridge, TN 37831

Presentation Abstract

Understanding the cooperative interactions of metals with active supports is essential to tailoring their catalytic activities and/or control of reaction pathways. These interfacial interactions can be achieved through two mechanisms: (1) interfacial charge redistribution (electronic interaction) and (2) interfacial atom transport (chemical interaction). In the last two years, a number of new advances have been made by our BES team toward tuning the metal-support interactions . The success of our approach capitalizes on nanoconfined spaces (e.g., confined interface restructuring),[1,2] complex oxide supports (e.g., perovskite oxides),[3-5] and 2D material edge sites (e.g., boron nitride),[6,7] demonstrating that uniquely strong interfacial interactions and cooperativities between nanoparticles and supports can emerge through judicious structural choices of metals and supports. Our poster presentation will focus on the following three synergistically linked research activities: (1) sacrificial strong metal-support interactions, (2) "intelligent" metal-support interactions, and (3) charge-flow metal-support interactions. The interconnections among the above three metal-support interactions will be also discussed.

1. Zhan, W. C.; He, Q.; Liu, X. F.; Guo, Y. L.; Wang, Y. Q.; Wang, L.; Guo, Y.; Borisevich, A. Y.; Zhang, J. S.; Lu, G. Z.; Dai, S. A Sacrificial Coating Strategy Toward Enhancement of Metal-Support Interaction for Ultrastable Au Nanocatalysts. *J. Am. Chem.Soc.* **2016**, *138*, 16130-16139.
2. Zhan, W. C.; Shu, Y.; Sheng, Y. J.; Zhu, H. Y.; Guo, Y. L.; Wang, L.; Guo, Y.; Zhang, J. S.; Lu, G. Z.; Dai, S. Surfactant-Assisted Stabilization of Au Colloids on Solids for Heterogeneous Catalysis. *Angew. Chem.-Int. Edit.* **2017**, *56*, 4494-4498.
3. Lu, H.; Zhang, P.; Qiao, Z.-A.; Zhang, J.; Zhu, H.; Chen, J.; Chen, Y.; Dai, S. Ionic liquid-mediated synthesis of meso-scale porous lanthanum-transition-metal perovskites with high CO oxidation performance. *Chem. Commun.* **2015**, *51*, 5910-5913.
4. Zhu, H. Y.; Zhang, P. F.; Dai, S. Recent Advances of Lanthanum-Based Perovskite Oxides for Catalysis. *ACS Catal.* **2015**, *5*, 6370-6385.
5. Tian, C. C.; Zhu, X.; Abney, C. W.; Liu, X. F.; Foo, G. S.; Wu, Z. L.; Li, M. J.; Meyer, H. M.; Brown, S.; Mahurin, S. M.; Wu, S. J.; Yang, S. Z.; Liu, J. Y.; Dai, S. Toward the Design of a Hierarchical Perovskite Support: Ultra-Sintering-Resistant Gold Nanocatalysts for CO Oxidation. *ACS Catal.* **2017**, *7*, 3388-3393.
6. Zhu, W. S.; Gao, X.; Li, Q.; Li, H. P.; Chao, Y. H.; Li, M. J.; Mahurin, S. M.; Li, H. M.; Zhu, H. Y.; Dai, S. Controlled Gas Exfoliation of Boron Nitride into Few-Layered Nanosheets. *Angew. Chem.-Int. Edit.* **2016**, *55*, 10766-10770.
7. Zhu, W. S.; Wu, Z. L.; Foo, G. S.; Gao, X.; Zhou, M. X.; Liu, B.; Veith, G. M.; Wu, P. W.; Browning, K. L.; Lee, H. N.; Li, H. M.; Dai, S.; Zhu, H. Y. Taming interfacial electronic properties of platinum nanoparticles on vacancy-abundant boron nitride nanosheets for enhanced catalysis. *Nat. Commun.* **2017**, *8* 15291. DOI: 10.1038

Isolated, Well-Defined Organovanadium(III) on Silica: Single-Site Catalyst for Hydrogenation of Alkenes and Alkynes

Hyuntae Sohn,[1] Jeffrey Camacho-Bunquin,[1] Ryan. R. Langeslay,[1] Patricia. A. Ignacio-de Leon,[2] Jens Niklas,[1] Oleg Poluektov,[1] Cong Liu,[1] Justin G. Connel,[3] H. Kim,[1] Peter C. Stair,[1,4] Magali Ferrandon,[1] and Massimiliano Delferro[1]

[1]Chemical Sciences and Engineering Division, [2]Energy Systems Division, [3]Material Science Division, Argonne National Laboratory. [4]Department of Chemistry, Northwestern University
delferro@anl.gov

Presentation Abstract

Hydrogenation of unsaturated hydrocarbons using noble metals such as Ru, Rh, Pd and Pt has been extensively investigated over the past few decades in both homogeneous and heterogeneous systems. Recently, the utilization of late first-row transition metals (Fe, Co, Ni and Cu) have garnered much attention due to their lower cost and abundance. The hydrogenation activity of early- and mid-first row transition metals (Sc, Ti, V, Cr, Mn), however, have not been rigorously studied other than for their role as metal ion dopants to hydrogenation catalysts. Our group recently developed a series of well-defined, site-isolated first-row organo-transition metal catalysts (V^{III}, Cr^{III}, Mn^{II}, Co^{II} and Ni^{II}) supported on a catechol-containing porous organic polymer (CatPOP) which are active for alkyne semi-hydrogenation. Among the catalysts tested, superior hydrogenation activity was observed using the [(CatPOP)V^{III}(Mes)(THF)], with turnover frequency (TOF) 40 times higher than others. As a follow-up study, we incorporated same organovanadium (III) species on the redox-innocent silica support (SiO_2) via surface organometallic synthesis. Through a combination of characterization techniques (ICP, ^{1}H NMR, TGA-MS, DRIFTS), the presence of one mesityl and one THF donor groups bound to the vanadium center was confirmed. Results of EPR, XPS, DR-UV/Vis and XAS experiments verified isolated V(III) sites. The catalytic performance of the [(SiO_2)V^{III}(Mes)(THF)] catalyst was examined for hydrogenation of diphenylacetylene and 1-octene in the liquid-phase, and hydrogenation of ethylene in the gas-phase. In both cases, the catalyst showed unprecedented high hydrogenation reactivity. Kinetic poisoning experiments were conducted using 2,2'-bipyridine and confirmed that all V sites are active. All of these results show that the redox properties of the support is not a prerequisite to obtain high hydrogenation activity over the [(SiO_2)V^{III}(Mes)(THF)] catalyst.

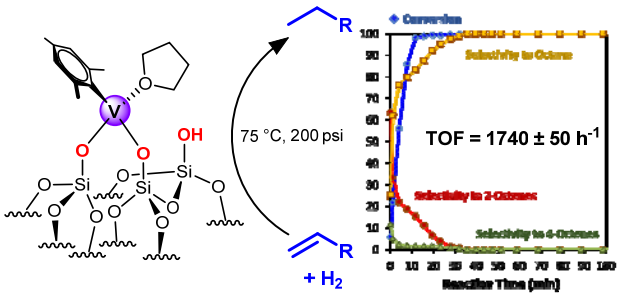

FWP50966: Tunable Single-Site Catalysts for Selective Functionalization of Alkanes

Principal Investigators: Massimiliano Delferro (Lead PI),[1] Larry A. Curtiss,[1] Adam S. Hock,[1,2] Peter C. Stair.[1,3]
ANL Staff members: Cong Liu (theory), Jeffrey Camacho-Bunquin (synthesis), Jeremy Kropf (X-ray).
Postdocs: Rachel C. Klet, David Kaphan, Hyuntae Sohn, Ryan R. Langeslay
Graduate student: Yiqing Zhao[2]
Contractor: HackSung Kim[3]
Affiliations: [1]Chemical Sciences and Engineering Division, Argonne National Laboratory, [2]Department of Chemistry, Illinois Institute of Technology, [3]Department of Chemistry, Northwestern University

RECENT PROGRESS

Goals

The long-term goal of our current efforts are to understand and manipulate isolated, "homogeneous-in-function" supported single-site catalysts for kinetically-limited transformations (e.g., alkane C–H activation and functionalization) and elucidation of the operant mechanisms. The energy input required to drive such reactions using traditional heterogeneous catalysts could compromise the product selectivity and stability, resulting in a distribution of reaction products and deactivation, respectively. The use of single-site catalysts overcomes these problems. Our group recently developed synthetic control of isolated, single-site catalysts on metal oxide supports (i.e. SiO_2) employing the tools of surface organometallic chemistry (SOMC) and atomic layer deposition (ALD). The nature of these active site support platforms provides efficient and general routes to isolated, single-site surface species that exhibit catalytic activity, selectivity and stability, notably under reaction conditions where their molecular analogs are largely unstable and/or unreactive.

Description of the Results

Our group achieved successes in two major project thrusts in FY16-17. The first project thrust has been focused on control of the reactivity and stability of sensitive single-atom catalysts supported on *tailored metallo-ligand environments/surfaces* (Thrust 1). By employing stepwise synthesis of multicomponent catalyst scaffolds, we successfully developed site-isolated organometallic catalysts on surfaces equipped with metal anchoring sites/promoter ions. The effectiveness of this design strategy was demonstrated in the well-differentiated chemoselectivity of organoplatinum sites for hydrogenation and dehydrogenation reactions as influenced by the nature of the promoter ions/anchoring sites (e.g., Zn^{2+}, B^{3+}). The generality of this design approach was also demonstrated in the enhancement of alkane dehydrogenation activity of Co^{2+} sites on Zr^{4+}-modified silica surfaces. In parallel, we have developed *rational design via well-defined, single-site catalysts* on support platforms for controlled hydrocarbon transformations such as non-oxidative dehydrogenation of alkanes to alkenes and its microscopic reverse, alkene hydrogenation (Thrust 2). Our recent achievements cover advances in the (1) synthesis of well-defined, supported organometallic sites using state-of-the-art synthetic techniques (e.g., ALD, surface organometallic

synthesis), (2) development of spectroscopic strategies to elucidate operant reaction mechanisms and (3) computationally guided development of supported single-atom catalytic sites.

Thrust 1: Promoter and Anchoring Site Effects in Single-Site Catalysts

During the past grant period, we reported the synthesis of isolated, low-coordinate Zn^{2+} sites on silica via strong electrostatic adsorption. This catalyst is active for propylene hydrogenation (200 ˚C) and propane dehydrogenation (550 ˚C). Computational studies coupled with *in situ* XAS experiments, suggested the involvement of tri-coordinate Zn^{2+} sites and an alkyl-zinc intermediate in the catalytic cycle. Full characterization of this intermediate is difficult due to its intrinsic instability and sensitivity to reaction conditions. To address these challenges, our group has employed an integrated atomic-layer deposition-catalysis (I-ALD-Cat) testing tool that allows for *in-situ* synthesis of site-isolated Zn^{2+} catalytic centers by ALD, and immediate reactivity evaluation under plug-flow reactor conditions. Alkyl-zinc and zinc oxide-type sites are synthesized via ALD of diethylzinc on high-surface-area silica. A series of ALD experiments afforded Zn/SiO_2 platform systems that provided key insights into the reactivity and stability of the proposed Zn^{2+} intermediates at the sub-monolayer level as shown in Figure 1. Open-shell 16-electron, tri-coordinate ethylzinc(II)-silica sites exhibit higher activity for propylene hydrogenation-propane dehydrogenation reactions compared to precatalyst 18-electron, tetra-coordinate zinc oxide-type centers. We demonstrated that the Zn^{2+} dispersity is a critical factor that influences catalyst reactivity and stability. Surface saturation with Zn^{2+} sites (~75% of a monolayer) results in zinc agglomeration and catalyst deactivation, rendering the materials unreactive.

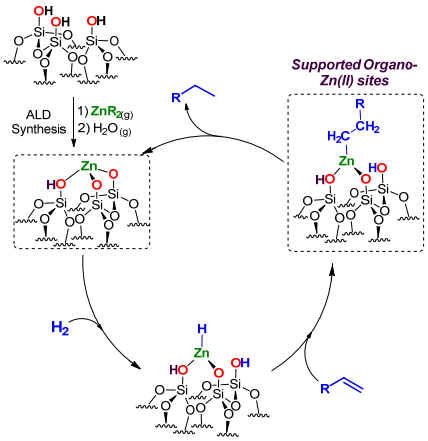

Figure 1. ALD synthesis of reactive Zn sites on SiO_2.

We have built upon our atomically precise modification of oxide surfaces by using the Zn^{2+} as anchoring sites. This approach allowed us to develop a strategy to stabilize well-defined, site-isolated organoplatinum sites on oxide supports. Single-atom catalysts based on highly reducible noble metals (e.g., Pt) remains challenging due to their susceptibility to sintering.

Air-stable, well-defined, isolated organoplatinum(IV) precatalysts were deposited on Zn^{2+}(submonolayer)/SiO_2 surfaces (*vide supra*), employing mild ALD and solution-phase synthesis conditions under which SiO_2 is largely unreactive (Figure 2). The straightforward deposition of the trimethyl(methylcyclopentadienyl)platinum(IV) precursor is attributed to the increased acidity of surface silanols associated to Zn^{2+} cations. DFT modeling of the platination reaction suggests that the metalation of Zn^{2+}-bound silanols is thermodynamically more favorable (ΔG = -12.4 kcal/mol) than with silanols of non-modified SiO_2. The results of a combination of spectroscopic (e.g., XAS, SS ^1H and ^{13}C MAS NMR, DRIFTS, DR-UV-Vis) and surface characterization (e.g., TPR) techniques are consistent with the presence of site-isolated Pt^{4+} sites, with the ligand environment influenced by the synthesis methods and conditions. The Pt^{4+} centers

deposited by ALD ($Pt/Zn/SiO_2$-$_{ALD}$) are stabilized by the methylcyclopentadienyl ligand and three anionic siloxy groups. On the other hand, the Pt^{4+} sites deposited via solution-phase synthesis ($Pt/Zn/SiO_2$-$_{soln}$) are stabilized by a methylcyclopentadienyl ligand, two unreacted methyl groups, and an anionic siloxy group. In order to determine the differences between single-atom $Pt/Zn/SiO_2$ and $Pt(NP)/SiO_2$, chemoselective hydrogenation of nitroaryl substrates as a probe reaction has been employed. Solution-phase, chemoselective hydrogenation of a series of functionalized nitroaryls to the corresponding anilines was achieved under mild conditions employing $Pt/Zn/SiO_2$ with excellent tolerance of other hydrogenation-sensitive functionalities (e.g., vinyl, aldehyde, ketone, esters, nitriles and halides). On the other hand, $Pt(NP)/SiO_2$ fully hydrogenated the $–NH_2$ group and other unsaturated functionality (i.e., alkene and carbonyl groups). TPR and variable-temperature DRIFTS experiments under H_2 provided important insights into the precatalyst activation mechanism. In particular for $Pt/Zn/SiO_2$-$_{soln}$, at the reaction temperature of 135 °C, the $Pt–CH_3$ groups are hydrogenolyzed while the CpMe ligand is not cleaved. This suggests that the ancillary ligand is necessary for the observed chemoselectivity.

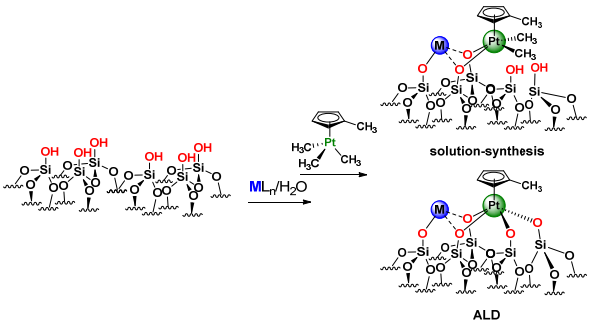

Figure 2. Supported bimetallic $Pt|Zn|SiO_2$ prepared via organometallic grafting and ALD

In parallel, our current understanding of single-site dehydrogenation catalysts has evolved from the view that Lewis acidity was the most important catalyst descriptor to the view that metal-oxygen bond strength is more important for many catalytic applications. In catalysts with filled d-shells, the barrier to β-hydride elimination is the rate-determining step (e.g., Zn^{2+} and Ga^{3+}). However, for mid-transition metal catalysts (e.g., Co^{2+}) with partially filled d-orbitals the heterolytic cleavage of the R-H bond to form a metal-alkyl appears to be rate-determining. Thus, we have prepared a silica support for the single-site Co^{2+} catalyst with approximately one monolayer of catalytically inactive zirconium oxide; the resulting $Co/Zr/SiO_2$ catalysts exhibit propane dehydrogenation rates over ~2 times higher per cobalt center while retaining the very high selectivity (> 98 %) and stability of the original Co/SiO_2 catalyst. These results suggest that the electrophilic zirconium in the Co-O-Zr facilitates the heterolytic cleavage of the R-H bond, which in turn, produces a more active catalyst than the Co-O-Si system. In essence, this work enables the tuning of the electronic nature of isolated heterogeneous catalytic sites with a level of precision only previously realized with homogeneous ligands.

Thrust 2: Rational Design of Supported Single-Site Catalysts

The accessibility of spectroscopic techniques to probe the transformations of supported catalytic sites under reaction conditions remains a grand challenge in fundamental catalysis research. For example, Ga catalysts on solid supports such as zeolites and oxides are employed for a range of industrial alkane activation and functionalization processes. Despite the diverse and rigorous attempts to understand the mechanism of these alkane transformations, the nature of the active Ga

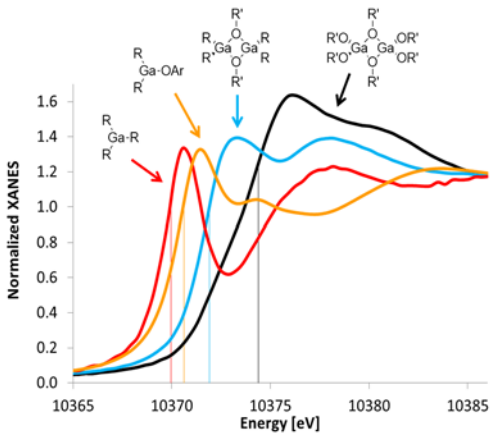

Figure 3. Normalized XANES spectra of $Ga(CH_2SiMe_3)_3$ (red), $Ga(^tBu)_2(OAr)$ (orange), $[Ga(CH_2SiMe_3)_2(OSiPh_3)]_2$ (light blue), and $[Ga(OSiPh_3)_3]_2$ (black).

species has not been definitively elucidated. Hence, our group postulated that well-defined, homogeneous molecular organometallic complexes that mimic the changes in the Ga^{3+} coordination environment can elucidate the oxidation state of the active Ga species. A series of Ga^{3+} organometallic model compounds have been prepared, and their XANES spectra compared to those of the heterogeneous Ga-SiO_2 catalyst acquired under reducing conditions (Figure 3). The resulting spectra clearly demonstrate that shifts in XANES edge energy cannot be assumed to arise from the change in oxidation state from Ga^{3+} to Ga^{+}. This range overlaps with the edge energy range of known Ga^{+} compounds. Consequently, XANES edge energy cannot definitively distinguish Ga^{3+} alkyls or hydrides from Ga^{+}, thus the formation of Ga^{3+} alkyl or hydride intermediates cannot be ruled out. Comparison of the XANES spectrum of Ga-SiO_2 exposed to hydrogen at high temperature with the XANES spectra of molecular reference compounds further suggests that these catalysts may contain three-coordinate Ga^{3+} dihydride species rather than Ga^{+}. Grafting of molecular models to silica support confirms the similarity between spectra of three-coordinate Ga alkyls and *in-situ* spectra of supported Ga-SiO_2 catalysts under reducing conditions. These findings agree with the observation in the literature of the formation of Ga–H species under catalytic conditions, suggesting that Ga^{3+} hydrides are mechanistically relevant. Finally, catalytic activity of Ga-SiO_2 catalysts for olefin hydrogenation – the microscopic reverse of alkane dehydrogenation –is observed at temperatures as low as 110°C, and it is chemically unlikely that Ga^{3+} can be reduced under such mild conditions. Therefore, we believe that Ga^{3+} does not undergo reduction to Ga^{+} during alkane dehydrogenation, and that C–H bond activation on Ga^{3+} catalysts instead proceeds via a non-redox, heterolytic cleavage mechanism involving Ga^{3+} alkyl and hydride intermediates.

Having demonstrated that Ga catalysts proceed via a non-redox mechanism, we hypothesized that more Lewis acid ions, such as Group 3 transition metals, could be more active dehydrogenation catalysts. Surprisingly, we found that Lewis acidic Sc and Y alkyls are inactive for alkane dehydrogenation. Both site-isolated Sc-alkyl and Y-alkyl sites are catalytically active for olefin hydrogenation at room temperature; however, these catalysts undergo thermal decomposition, likely due to an alkyl transfer from the metal center to the silica, at temperatures well below those required for alkane dehydrogenation to become thermodynamically feasible. From these results, we conclude that (1) silica-supported single-site Sc- and Y-containing metal-alkyl or metal-hydride groups catalyze olefin hydrogenation, but (2) unlike supported Cr, Fe, Co, Zn, and Ga catalysts, the Sc and Y analogs cannot generate a metal alkyl or hydride species in-situ. Heterolytic dissociation under dehydrogenation conditions is prevented from occurring due to the relatively higher strength of the Sc–O and Y–O bonds.

Publications Acknowledging Exclusively this Grant in 2014-2017

1) Sohn, H.; Camacho-Bunquin, J.; Langeslay, R. R.; Ignacio-de Leon, P. A.; Niklas, J.; Poluektov, O. G.; Liu, C.; Connell, J. G.; Yang, D.; Kropf, J.; Kim, H.; Stair, P. C.; Ferrandon, M.; Delferro, M. Supported Single-Site Organo-Vanadium(III) Catalyst on Silica for Hydrogenation of Alkenes and Alkynes. *Chem. Commun.* **2017**, DOI: 10.1039/c7cc01876b (Special issue: ChemComm Emerging Investigators Issue 2017).
2) Camacho-Bunquin, J.; Ferrandon, M.; Das, U.; Dogan, F.; Liu, C.; Larsen, C.; Curtiss, L. A.; Hock, A. S.; Miller, J. T.; Nguyen, S. T.; Marshall, C. L.; Delferro, M.; Stair, P. C. Supported Aluminum Catalysts for Olefin Hydrogenation. *ACS Catal*. **2017**, *7*, 689-694.
3) Camacho-Bunquin, J.; Aich, P.; Ferrandon, M.; Getsoian, A.; Das, U.; Dogan, F.; Curtiss, L.; Miller, J. T.; Marshall, C. L.; Hock, A. S.; Stair, P. C. Single-Site Zinc on Silica Catalysts for Propylene Hydrogenation and Propane Dehydrogenation. Synthesis and Reactivity Evaluation through Integrated Atomic Layer Deposition-Catalysis Experimentation. *J. Catal.* **2017**, *345*, 170-182. (Editor's Choice)
4) Getsoian A; Hu B; Miller J.T.; Hock A.S. Supported single site Sc and Y alkyl catalysts for Olefin Hydrogenation. *Organometallics,* **2017**, *accepted*.
5) Getsoian, A.; Das, U.; Camacho-Bunquin, J,; Zhang, G; Gallagher, J. Hu, B; Schaidle, J.; Ruddy, D. A.; Kraft, S. J.; Henley, J.; Curtiss, L. A. Miller, J. T.; Hock, A.S. Oxidation State and Ligand Field Effects in Ga K-edge XANES: Mechanistic Implications for Alkane Dehydrogenation by Ga-Zeolite Catalysts. *Catal. Sci. Technol.* **2016**, *6*, 6339-6353.
6) Das, U.; Zhang, G.; Hu, B.; Hock, A. S.; Redfern, P. C.; Miller, J. T.; Curtiss, L. A. Effect of Siloxane Ring Strain and Cation Charge Density on the Formation of Coordinately Unsaturated Metal Sites on Silica: Insights from Density Functional Theory (DFT) Studies. *ACS Catal.* **2015**, *5*, 7177-7185.
7) Camacho-Bunquin, J.; Shou, H.; Aich, P.; Beaulieu, D. R.; Klotzsch, H.; Bachman, S.; Marshall, C. L.; Hock, A. S.; Stair, P. C. Catalyst Synthesis and Evaluation Using A High-Throughput Atomic Layer Deposition–Catalysis Testing Tool *Rev. Sci. Instrum.* **2015**, *86*, 084103/084101-084103/084107.
8) Hu, B.; Schweitzer, N. M.; Zhange, G.; Kraft, S. J.; Childers, D. J; Lanci, M. P.; Miller, J. T.; Hock, A. S. Isolated Fe^{II} on Silica As a Selective Propane Dehydrogenation Catalyst. *ACS Catal.* **2015**, *5*, 3494-3503.
9) Camacho-Bunquin, J.; Siladke, N. A.; Zhang, G.; Niklas, J.; Poluektov, O. G.; Nguyen, S. T.; Miller, J. T.; Hock, A. S. Synthesis and Catalytic Hydrogenation Reactivity of a Chromium Catecholate Porous Organic Polymer. *Organometallics* **2015**, *34*, 947-952.
10) Hu, B.; Schweitzer, N. M.; Das, U.; Kim, H. K.; Stair, P. C.; Curtiss, L. A.; Hock, A. S.; Miller, J. T. Selective Propane Dehydrogenation with Single Site Co^{II} on SiO_2 by a Non-redox Mechanism. *J. Catal.* **2015**, *322*, 24-37.
11) Tanabe, K. K.; Ferrandon, M.; Siladke, N. A.; Kraft, S. J.; Zhang, G.; Niklas, J.; Poluektov, O. G.; Lopykinski, S. J.; Bunel, E. E.; Krause, T. R.; Miller, J. T.; Hock, A. S.; Nguyen, S. T. Discovery of highly selective alkyne semi-hydrogenation catalysts based on 1st-row transition metallated porous organic polymers. *Angew. Chem. Int. Ed.* **2014**, *53*, 12055-12058.
12) Kraft, S. J.; Zhang, G.; Childers, D.; Dogan, F.; Miller, J. T.; Nguyen, S. T.; Hock, A. S., Rhodium Catechol Containing Porous Organic Polymers: Defined Catalysis for Single-Site and Supported Nanoparticulate Materials. *Organometallics* **2014**, *33*, 2517-2522.

13) Schweitzer, N. M.; Hu, B.; Das, U.; Kim, H.; Greeley, J.; Curtiss, L. A.; Stair, P. C.; Miller, J. T.; Hock, A. S. Propylene Hydrogenation and Propane Dehydrogenation by a Single-Site Zn^{2+} on Silica Catalyst. *ACS Catal.* **2014**, *4*, 1091-1098.

In preparation

14) Langeslay, R. R.; Hu, B.; Getsoian, A.; Zhang, G.; Delferro, M.; Miller, J. T.; Hock, A. S. Olefin and Arene Hydrogenation by a Silica Supported Well-Defined Fe^{2+} Catalyst.
15) Liu, C; Camacho-Bunquin, J.; Ferrandon, M.; Kaphan, D.; Sohn, H.; Yang, D.; Das, U.; Yang, B.; Stair, P. C.; Hock, A. S.; Curtiss, L. A.; Delferro, M. First-principle Calculation Guided Design of Silica-supported, Single-atom Heterogeneous Catalysts for Alkene Hydrogenation.
16) Camacho-Bunquin, J.; Sohn, H.; Ferrandon, M.; Kaphan, D.; Ignacio-de Leon, P.; Pruski, M.; Hock, A. S.; Stair, P. C.; Delferro, M. On the Mechanism of Platinum Deposition: Effects of Synthesis Techniques on Active Site Nuclearities and Catalytic Nitroaryl Hydrogenation Selectivity.
17) Sohn, H.; Camacho-Bunquin, J.; Liu, C; Ferrandon, M.; Marshall, C. L.; Stair, P. C.; Hock, A. S.; Delferro, M. Platinum-Promoted Zinc on Silica as Highly Active and Selective Catalysts for the Non-Oxidative Dehydrogenation of Propane.
18) Camacho-Bunquin, J.; Sohn, H.; Ferrandon, M.; Ignacio-de Leon, P.; Stair, P. C.; Delferro, M. Platinum Nanoalloys for Selective *n*-Butane Dehydrogenation to 1,3-Butadiene.
19) Zhao, Y.; Sohn, H.; Hock, A. S. The Effects of Zr Promotion on Supported Co Dehydrogenation Catalysts.
20) Camacho-Bunquin, J.; Sohn, H.; Ferrandon, M.; Ignacio-de Leon, P.; Delferro, M. Promoted Platinum Catalysts for Selective C_4 Diene and Alkyne Hydrogenation in the Presence of Excess Butenes.

Patents

21) Multimetallic catalysts for selective hydrogenation of dienes. Camacho-Bunquin, J.; Ferrandon, M.; Delferro, M. 15/484,928.
22) Multimetallic catalysts. Camacho-Bunquin, J.; Ferrandon, M.; Delferro, M.; Stair, P. C. U.S. Patent Application Number: 62/402,218.
23) Multimetallic catalysts for alkane dehydrogenation and synthesis thereof. Stair, P. C.; Camacho-Bunquin, J.; Marshall, C. L.; Hock A. S. U.S. Patent Application Number: 15/157,109.

Publications Acknowledging Jointly Funded by this Grant and Other Grants with Leading Intellectual Contribution from this Grant in 2014-2017

24) Huang, Z.; Liu, D.; Camacho-Bunquin, J.; Zhang, G.; Yang, D.; López-Encarnación, J. M.; Jellinek, J.; Xu, Y.; Ferrandon, M.; Lei, A.; Bunel, E. E.; Delferro, M. Supported Single-Site Ti(IV) on a Metal–Organic Framework for the Hydroboration of Carbonyl Compounds. *Organometallics*, submitted.
25) Ignacio-de Leon, P.; Klet, R.; Ferrandon, M.; Nauert, S.; Savereide, L.; Delferro, M.; Camacho-Bunquin, J.; Notestein, J. M.; Nguyen, S. T Promoter Effects on Catalyst Selectivity and Stability for Propylene Partial Oxidation to Acrolein. *ACS Catal.*, submitted.

26) Cybulskis, V. J.; Pradhan, S. U.; Lovón-Quintana, J. J.; Hock, A. S.; Hu, B.; Zhang, G.; Delgass, W. N.; Ribeiro, F. H.; Miller J. T. The Nature of the Isolated Gallium Active Center for Propane Dehydrogenation on Ga/SiO_2. *Catal. Lett.* **2017**, *147*, 1252-1262.
27) Martynowycz, M. W.; Hu, B.; Kuzmenko, I.; Bu, W.; Hock, A.; Gidalevitz, D. Monomolecular Siloxane Film as a Model of Single Site Catalysts *J. Am. Chem. Soc.* **2016**, *138*, 12432-12439.
28) Krogman, J. P.; Gallagher, J. R.; Zhang, G.; Hock, A. S.; Miller, J. T.; Thomas C. Definitive Assignment of the Oxidation States of Zr and Co in a Highly Reactive Heterobimetallic Zr/Co Complex Using X-ray Absorption Spectroscopy (XANES). *Dalton Trans.* **2014**, 13852-13857.
29) Maria, S.; Poli, R.; Gallagher, K. J.; Hock, A. S.; Johnson, M. J. A. Ether Complexes Of Molybdenum(III) And (IV) Chloride. *Inorg. Synth.* **2014**, *36*, 15-19.
30) Broderick, E. M.; Browne, S. C.; Johnson, M. J. A.; Hitt, T. A.; Girolami, G. S. Dimolybdenum and Ditungsten Hexa(Alkoxides). *Inorg. Synth.* **2014**, *36*, 96-102.

Publications Acknowledging Jointly Funded by this Grant and Other Grants with Relatively Minor Intellectual Contribution from this Grant in 2014-2017.

31) Jung, D.; Saleh, L. M. A.; Berkson, Z.; Hwang, J. Y.; El-Kady, M. F.; Titarenko, E.; Shao, Y.; McCarthy, K.; Wixtrom, A. I.; Guo, J.; Martini, I. B.; Kraemer, S.; Wegener, E. C.; Saint-Cricq, P.; Langeslay, R. R.; Delferro, M.; Brosmer, J. L.; Chapman, K. W.; Miller, J. T.; Duan, X.; Kaner, R. B.; Zink, J. I.; Chmelka, B. F.; Spokoyny A. M. Molecular Doping Approach for Hybrid Metal Oxide Materials. *Nat. Mater.* **2017**, submitted.
32) Canossa, S.; Bellè, E.; Delferro, M.; Predieri, G.; Graiff, C. Structural motifs in heteroleptic copper and cadmium selenites *Inorg. Chim. Acta* **2017**, doi: 10.1016/j.ica.2017.05.043
33) B. Yang, B.; C. Liu, C.; Halder, A.; Tyo, E.; Martinson, A. B. F.; Seifert, S.; Zapol, P.; Curtiss, L. A.; Vajda, S. Copper Cluster Size Effect in Methanol Synthesis from CO_2. *J. Phys. Chem. C.* **2017**, *121*, 10406–10412.
34) Tan, G.; Xu, R.; Xing, Z.; Yuan, Y.; Lu, J.; Wen, J.; Liu, C.; Ma, L.; Zhan, C.; Liu, Q.; Wu, T.; Jian, Z.; Shahbazian-Yassar, R.; Ren, Y.; Miller, D. J.; Curtiss, L. A.; Ji, X.; Amine, L. A. Burning Lithium in CS_2 for High-performing Compact Li_2S-graphane Nanocapsules for Li-S Batteries. *Nat. Ener.* **2017**, accepted.
35) Tan, G.; Chong, L.; Amine, R.; Lu, J.; Liu, C.; Yuan, Y.; Wen, J.; He, K.; Bi, X.; Guo, Y.; Wang, H.-H.; Shahbazian-Yassar, R.; Hallaj, S. A.; Miller, D. J.; Liu, D.; Amine, K. Toward Highly Efficient Electrocatalyst for Li–O_2 Batteries Using Biphasic N-Doping Cobalt@Graphene Multiple-Capsule Heterostructures. *Nano Lett.* **2017**, *17*, 2959–2966.

Zdenek Dohnálek

Formation of Gas Phase Radicals in Surface Reactions: Deoxygenation of Phenylmethanol on Rutile TiO_2(110)

Long Chen[a] R. Scott Smith[a] Bruce D. Kay[a] and Zdenek Dohnálek[a,b]

[a]Pacific Northwest National Laboratory, Physical and Computational Sciences Directorate and Institute for Integrated Catalysis, Richland, WA 99354, USA

[b]Voiland School of Chemical Engineering and Bioengineering, Washington State University, Pullman, Washington 99163, USA

Presentation Abstract

Understanding the reaction pathways of lignin-derived molecules on catalyst surfaces is of great importance for the sustainable production of energy carriers. In this regard, the role of radicals in the reaction mechanisms leading to functionalized aromatics has been extensively argued. The involvement of radical species has been firmly established for a small number of simple reactions on high surface area oxide catalysts, such as oxidative coupling of methane and selective oxidation of propylene. In this work, the reaction pathways of simple lignin-derived aromatic alcohols, i.e. phenol, phenylmethanol, and 2-phenylethanol, on a prototypical model oxide surface, rutile TiO_2(110), are studied using a combination of molecular beam dosing and temperature programmed desorption (TPD). For phenylmethanol, the coverage dependent TPD data show that about 40% of molecules adsorbed on the surface at a saturation coverage are converted to reaction products indicating that the reactions proceed on regular five-fold coordinated Ti sites. This is in contrast to aliphatic alcohols where the reactions are shown to proceed exclusively on bridging oxygen vacancy defect sites. The studies of OD-labelled phenylmethanol demonstrate that a fraction of OD hydrogen is transferred to the benzyl group to form toluene that desorbs between 300 K and 480 K. In the competing reaction, the OD hydrogen is converted to water at ~350 K. Once the OD hydrogen is depleted above 480 K, the remaining plenylmethoxy surface species dissociate yielding benzyl radicals in the gas phase. Combined, these results show that the conversion of phenylmethanol on TiO_2(110) proceeds via a unique chemistry. In contrast, both phenol and 2-phenylethanol exhibit expected surface chemistry analogous to that of aliphatic alcohols. These findings reveal for the first time the formation of free radical species from the interaction of phenylmethanol with TiO_2(110) and demonstrate a new direct mechanism for deoxygenation of lignin-derived benzylic alcohols to aromatics on TiO_2.

FWP 47319: Low Temperature Catalytic Routes for Energy Carriers via Spatial and Chemical Organization

PI: Johannes Lercher

Termolecular Nucleation of Nanoparticle Catalyst Formation Hides Under Second-Order Kinetics and Is Room-Dust-Dependent

Richard G. Finke[1], Saim Özkar[2]
[1] Department of Chemistry, Colorado State University, Fort Collins, CO 80523 USA,
[2] Department of Chemistry, Middle East Technical University, 06800 Ankara, Turkey.

Presentation Abstract

The nucleation step underlying the synthesis of a prototype $Ir(0)_{\sim 300}$ nanoparticle catalyst, formed from 300 equivalents of a $[(1,5\text{-COD})Ir{\bullet}P_2W_{15}Nb_3O_{62}]^{8-}$ precursor (hereafter = $(COD)Ir{\bullet}POM^{8-}$), was studied. The kinetic and mechanistic results include establishing: the Kinetically Effective Nucleus (KEN), the role of dust in the nucleation process, and discovery of the remarkable 2.4-fold narrowing of the nanoparticle size-dispersion post simple microfiltration to remove room dust from the solution and reaction flasks. The results provide the first evidence for the KEN being (just) termolecular in Ir and involving H_2 and dust, KEN = $\{Ir_3H_{2x}POM{\bullet}dust\}^6$. The results also reveal that all of the size-narrowing effect of removing dust removal comes in the nucleation step and its associated rate constant, which is lowered by ≥5 fold by microfiltration removal of the dust.

DE-FG02-03ER15453: Nanoparticle Catalysts: Nucleation Mechanistic Studies Plus Mechanism-Enabled Population Balance Modeling En Route to Nanoparticle Size and Size-Distribution Understanding and Control

PI: Professor Richard G. Finke
Postdoc(s): Dr. Saim Özkar

RECENT PROGRESS

Overview of Publications
Fourteen publications to date have been produced under our DOE support since 2014; a list of their titles follows[i,ii,iii,iv,v,vi,vii,viii,ix,x,xi,xii xiii,xiv] and provides a concise description of the contents of those publications. All but the last two publications listed have been funded exclusively by our DOE grant. Three of these 14 publications are related to the title topic of "*Termolecular Nucleation of Nanoparticle Catalyst Formation Hides Under Second-Order Kinetics and Is Room-Dust-Dependent",* and it is those 3 publications that are highlighted below.

Fundamental Studies of Nanoparticle Nucleation
Nanoparticle catalyst formation begins with *nucleation*, that crucial, presently ill-understood,

first process that underlies the resultant size and size distribution of nanoparticle catalysts. Nanoparticle catalyst size and size-distributions are, in turn, crucial factors underlying especially particle-size ("structure"-) sensitive catalytic reactions as well as optimum catalytic selectivity. *Yet even just the molecularity of nucleation for nanoparticle catalyst formation was unknown until our recent publications.*[i,xiii,xiv] Classical Nucleation Theory (CNT) predicts a high-reaction-order due to a reversible, Ir = A process, nA □ A_n, where A_n is the putative "Critical Nucleus" of CNT.

The composition of the Kinetically Effective Nucleus (KEN)[i] was established recently for the first time for an $Ir(0)_{\sim 300}$ nanoparticle catalyst from 300 equivalents of a $[(1,5\text{-COD})Ir{\bullet}P_2W_{15}Nb_3O_{62}]^{8-}$ precursor (hereafter = $(COD)Ir{\bullet}POM^{8-}$) under hydrogen, the overall stoichiometry demonstrated[i] to be that in the scheme below:

$$300\ [(1,5\text{-COD})Ir{\bullet}P_2W_{15}Nb_3O_{62}]^{8-} + 750\ H_2 \longrightarrow$$

$$1\ Ir(0)_{\sim 300} + 300\ [P_2W_{15}Nb_3O_{62}]^{9-} + 300$$  $$+ 300\ H^+$$

The kinetics of nucleation were found to be overall just *second-order*[i] in the [**A**] = $[(COD)Ir{\bullet}POM^{8-}]$, not a higher order as CNT predicts. Intriguingly, further kinetic studies revealed that nucleation is actually *termolecular in [Ir]*, corresponding to a KEN of Ir_3, due the involvement of the dissociative equilibrium, K_{Diss}, shown in the overall mechanism uncovered, mechanism #III of three considered, mechanisms I and II provided elsewhere having been disproved:[xi]

(III) Alternative Termolecular Nucleation

$$2\left[(COD)Ir{\cdot}POM^{8-} + 2\ solv \underset{}{\overset{K_{Diss}}{\rightleftharpoons}} (COD)Ir(solv)_2^+ + POM^{9-}\right]$$

$$2\ (COD)Ir(solv)_2^+ + (COD)Ir{\cdot}POM^{8-} \xrightarrow[+\ 7.5\ H_2]{k_{1(alt.termol)}} 3\ Ir(0) = Ir(0)_3 + POM^{9-} + 3\ H^+ + 3\ \text{cyclooctane} + 4\ solv$$

$$\text{Net:}\quad 3\ (COD)Ir{\cdot}POM^{8-} \xrightarrow{+\ 7.5\ H_2} 3\ Ir(0) = Ir(0)_3 + 3\ POM^{9-} + 3\ H^+ + 3\ \text{cyclooctane}$$

The key nucleation step was shown to also involve H_2, establishing the Kinetically Effective Nucleus for a nanoparticle catalyst formation for the first time as shown below, KEN = $\{Ir_3H_{2x}POM\}^{6-}$:[xi]

$$3\ Ir(I)^+ + POM^{9-} + xH_2 \square \{Ir_3H_{2x}POM\}^{6-} \rightarrow \rightarrow 3\ Ir(0) + POM^{9-} + 2xH^+$$

In a subsequent publication,[xii] the KEN was found to also involve room dust, KEN = $\{Ir_3H_{2x}POM{\bullet}\mathbf{dust}\}^{6-}$, the removal of the dust by 0.2 μm microfiltration having the large, previously little precedented effect of slowing the nucleation rate constant by a factor of ~5 to ~7.6 (depending on the precise experiment and its conditions). Remarkably, the simple-to-apply microfiltration step also narrowed the size-distribution of the resulting $Ir(0)_n$ nanoparticles *by a factor of 2.4 from ±19% to ±8%!*[xii]

Over 33 conclusions, insights, and relevant caveats are listed in the Summary and Conclusions sections of the 3 papers,[i,xi,xii] five of the most important being: (i) that the KEN is small, Ir_3, and involves Ir-H bonds and one equivalent of POM and dust, $\{Ir_3H_{2x}POM\bullet dust\}^{6-}$; (ii) that Classical Nucleation Theory (CNT) and its higher order, reversible association of nA A_n (i.e., for A = Ir and where A_n is the elusive, never actually detected, "Critical Nucleus" concept of CNT), are disproven for the example of an $Ir(0)_{\sim 300}$ nanoparticle catalyst formation; (iii) that low, bi- to ter-molecular nuclearity in monomer, A (i.e., a KEN of $A_{2\text{-}3}$) looks to be much more general than preciously realized for a broader range of nucleation and growth systems throughout nature[i,xi]; (iv) that dust is involved and that the nucleation is, therefore, heterogeneous;[xii] and (v) that removal of the dust is a synthetically simple-to-apply, yet highly effective, way to reduce the resultant nanoparticle size dispersion by a factor of 2.4, to a near-record narrow dispersion for a self-assembly reaction of only ±8%.[xii] The other conclusions and insights are listed in our publications.[i,xi,xii]

Publications Acknowledging this Grant in 2014-2017

(I) Publications Exclusively funded by this grant

[i] Laxson, W. W.; Finke, R. G. Nucleation is Second Order: An Apparent Kinetically Effective Nucleus of Two for $Ir(0)_n$ Nanoparticle Formation From $[(1,5\text{-COD})Ir^{I}\bullet P_2W_{15}Nb_3O_{62}]^{8-}$ Plus Hydrogen. *J. Am. Chem. Soc,* **2014**, *136,* 17601-17615.

[ii] Kent, P. D.; Mondloch, J. E.; Finke, R. G. A Four-Step Mechanism for the Formation of Supported-Nanoparticle Heterogeneous Catalysts in Contact with Solution: The Conversion of Ir(1,5-COD)Cl/γ -Al_2O_3 to $Ir(0)_{\sim 170}$/γ-Al_2O_3". *J. Am. Chem. Soc.* **2014**, *136*, 1930-1941.

[iii] Bayram, E.; Lu, J.; Aydin, C.; Browning, N. D.; Özkar, S.; Gates, B. C.; Finke, R. G. Agglomerative Sintering of an Atomically Dispersed Ir_1/Zeolite Y Catalyst: Compelling Evidence Against Ostwald Ripening But for Bimolecular and Autocatalytic Agglomeration Catalyst Sintering Steps. *ACS Catalysis*, **2015**, *5*, 3514-3527.

[iv] Kent, P. D.; Mondloch, J. E.; Finke, R. G. Syntheses of Heterogeneous $Ir(0)_{\sim 600\text{-}900}$/γ -$Al_2O_3$ From One-Pot vs Isolated Preparations of the Precatalyst Ir(1,5-COD)Cl/γ-Al_2O_3: Discovery of Two, Competing, Trace "Ethyl Acetate Effects on the Key, Nucleation Step and Resultant Product. *ACS Catalysis*, **2016**, *6*, 5449-5461.

[v] Bayram, E.; Linehan, J. C.; Fulton, J. L.; Szymczak, N. K.; Finke, R. G., Determining the True Catalyst Derived from the $[RhCp^*Cl_2]_2$ Precatalyst System: Is it Single-Metal RhCp*-Based, or a Sub-nanometer Rh_4 Cluster-Based, Cyclohexene Hydrogenation Catalysis at Room Temperature and Mild Pressures?. *ACS Catalysis* **2015**, *5*, 3876-3886.

[vi] Laxson, W. W.; Özkar, S.; Finke, R. G., The Tri-Niobium, Wells-Dawson Type Polyoxoanion, $[(n\text{-}C_4H_9)_4N]_9P_2W_{15}Nb_3O_{62}$: Improvements in the Synthesis, Its Reliability, the Purity of the Product and the Detailed Synthetic Procedure. *Inorg. Chem*. **2014**, *53*, 2666-2676.

[vii] Laxson, W. W.; Özkar, S.; Folkman, S.; Finke, R. G. The Story of a Mechanism-Based Solution to an Irreproducible Synthesis Resulting in an Unexpected Closed-System Requirement for the $LiBEt_3H$-Based Reduction: the Case of the Novel Subnanometer

Cluster, $[Ir(1,5\text{-}COD)(\mu\text{-}H)]_4$, and the Resulting Improved, Independently Repeatable, Reliable Synthesis. *Inorg. Chim Acta.*, **2015**, *432*, 250-257.

[viii] Özkar, S.; Finke, R. Palladium(0) Nanoparticle Formation, Stabilization, and Mechanistic Studies: $Pd(acac)_2$ as a Preferred Precursor, $[Bu_4N]_2HPO_4$ Stabilizer, Plus the Stoichiometry, Kinetics, and Minimal, 4-Step Mechanism of the Palladium Nanoparticle Formation and Subsequent Agglomeration Reactions. *Langmuir*, **2016**, *32*, 3699-3716.

[ix] Crooks,A.; Yih, K.-H.; Li, L.; Yang, J. C.; Özkar, S.; Finke, R. G. Unintuitive Inverse Dependence of the Apparent Turnover Frequency, TOF_{app}, on Precatalyst Concentration: A Quantitative Explanation in the Case of Ziegler-type Nanoparticle Catalysts Made from $[(1,5\text{-}COD)Ir(\mu\text{-}O_2C_8H_{15})]_2$ and $AlEt_3$. *ACS Catalysis* **2015**, *5*, 3342-3353.

[x] Bentea, L.; Watzky, M. A.; Finke, R. G. Sigmoidal Nucleation and Growth Curves Across Nature Fit by the Finke-Watzky Model of Slow Continuous Nucleation and Autocatalytic Growth: Explicit Formulas for the Lag and Growth Times Plus Other Key Insights. *J. Phys. Chem. C.*, **2017**, *121*, 5302-5312.

[xi] Özkar, S.; Finke, R. Nanoparticle Nucleation is Termolecular and Involves Hydrogen: Evidence for a Kinetically Effective Nucleus of Three, $\{Ir_3H_{2x}\bullet P_2W_{15}Nb_3O_{62}\}^{6-}$, in $Ir(0)_n$ Nanoparticle Formation From $[(1,5\text{-}COD)Ir^{I}\bullet P_2W_{15}Nb_3O_{62}]^{8-}$ Plus Hydrogen. *J. Am. Chem. Soc.* **2017**, 139, 5444-5452.

[xii] Özkar, S.; Finke, R. Dust Effects On Nucleation Kinetics and Nanoparticle Product Size-Distributions: The Illustrative Case Study of a Prototype $Ir(0)_n$ Transition-Metal Nanoparticle Formation System. *Langmuir*, **2017**, in press, ASAP, **DOI:** 10.1021/acs.langmuir.7b01219.

<u>(II) Jointly funded by this grant and other grants with leading intellectual contribution from this grant</u>

(No publications under this category (II))

<u>(III) Jointly funded by this grant and other grants with relatively minor intellectual contribution from this grant;</u>

[xiii] Stracke, J. J.; Finke, R. G. Water Oxidation Catalysis Beginning with $Co_4(H_2O)_2(PW_9O_{34})^{10-}$ when Driven by the Chemical Oxidant Ruthenium(III)tris(2,2'-bipyridine): Stoichiometry, Kinetic, and Mechanistic Studies En Route to Identifying the True Catalyst. *ACS Catalysis* **2014**, *4*, 79-89.

[xiv] Stracke, J. J.; Finke, R. G. Distinguishing Homogeneous from Heterogeneous Water Oxidation Catalysis When Beginning with Polyoxometalates. *ACS Catalysis* **2014**, *4*, 909-933.

Bio-Inspired Oxyanion Reduction

Alison R. Fout, Courtney L. Ford, Zachary Gordon, Michael Drummond and Yun Ji Park
University of Illinois at Urbana-Champaign

Presentation Abstract

Multi-electron transformations featuring base metals are both particularly challenging and interesting. A series of multi-dentate ligand frameworks containing both hydrogen bond donating and accepting moieties in the secondary coordination sphere have been synthesized and reactivity will be described. These transformations feature the reduction of inorganic oxyanions which are generally considered to be non-complexing anions, poor nucleophiles and kinetically inert to oxidation and reduction. The catalytic reduction of nitrite, nitrate and chlorine oxyanions will be presented as well as mechanistic studies. The hydrogen bonding in the secondary coordination sphere of the ligand plays an important role in oxyanion reduction.

DE-SC0016026: Bio-inspired Catalysts Featuring Earth Abundant Metals and Secondary Coordination Sphere Interactions for the Reduction of Oxyanions

RECENT PROGRESS

The Reduction of Selenate and Selenite

Currently we are trying to increase the scope of substrates/oxyanions and, through further mechanistic studies and ligand modifications, to develop these into better catalytic processes. Other oxyanions include selenate (SeO_4^{2-}) and selenite (SeO_3^{2-}) which are common groundwater contaminants due to their high solubility and bioavailability. Microorganism have uniquely demonstrated the ability to reduce these anions to benign and insoluble elemental selenium. Bacterial reduction leads to the formation of red selenium nanoparticles (nanoSe^0) which has distinctive spectral and optical properties. NanoSe^0 is gaining interest in nanotechnology (due to its photoconductivity), medicine (due to antimicrobial and anticancer activities), and in environmental biotechnologies. Thus far, selenate and selenite reduction is limited to bioorganisms: no synthetic complex has yet been able to reduce the oxyanions to elemental selenium. The addition of selenite to the [N(afa^{Cy})$_3$Fe(OTf)](OTf) species resulted in an immediate reaction to form the iron(III)-oxo, [N(afa^{Cy})$_3$FeO][OTf], and subsequent precipitation of a red solid (Figure 2). Refluxing the red solid in the presence of PPh_3 confirmed

Figure 2. Precipitated Se^0.

the formation of $Se{=}PPh_3$. This result is very exciting and we are currently comparing the elemental selenium formed in our reaction to the highly desired nanoSe^0 and quantifying yields and turnovers.

Publications Acknowledging this Grant in 2014-2017

(I) Exclusively funded by this grant;

1. Gordon, Z.; Drummond, M. J.; Bogart, J. A.; Schelter, E. J.; Lord, R. L.; Fout, A. R. "Tuning the Fe(II/III) Redox Potential in Non-heme Fe(II)-Hydroxo Complexes through Primary and Secondary Coordination Sphere Modifications." *Inorg. Chem.*, **2017**, *56*, 4852-4863.
2. Ford, C. L.;* Park, Y.;* Matson, E. M.; Gordon, Z.; Fout, A. R. "A bio-inspired iron catalyst for nitrate and perchlorate reduction." *Science*, **2016**, *354*, 741-743. *authors contributed equally.
   Highlighted in Halford, B. (2016, November). Iron complex reduces oxyanion pollutants. *C&EN*, 10, 94(45), p.10, and Brennan, M. (2017, January). Nitrate NO more. *Nature Chemistry* 9, p.8.

Precisely Synthesized/Structurally Uniform Single- and Pair-Site Noble Metal Catalysts on Crystalline Porous Supports

Bruce C. Gates
University of California Davis

Presentation Abstract

We report a family of supported molecular catalysts consisting of single, isolated metal complexes and metal pair sites on zeolite MgO supports, having characterized them by IR, EXAFS, NMR spectroscopies and by density functional theory. The data determine structures, including the metal–support interface structures and identification of the ligands on the metals. A few examples are mentioned in the following section.

FG02-04ER15513: Precisely Synthesized/Structurally Uniform Single- and Pair-Site Noble Metal Catalysts on Crystalline Porous Supports

Student(s): Louise Debefve, C. Y. Fang, Erjia Guan, Adam S. Hoffman, Andrew Palermo

RECENT PROGRESS

***HERFD characterizing supported atomically dispersed catalysts* (with S. R. Bare).** We report high-energy-resolution X-ray absorption spectroscopy detection of ethylene and CO ligands adsorbed on catalytically active iridium centers isolated on zeolite HY and on MgO supports. The data are supported by density functional theory and FEFF X-ray absorption near-edge modelling, together with IR spectra. The results demonstrate that high-energy-resolution X-ray absorption spectra near the iridium L_{III} ($2p_{3/2}$) edge provide clearly ascribable, distinctive signatures of the ethylene and CO ligands and illustrate effects of supports and other ligands. This X-ray absorption technique is markedly more sensitive than conventional IR spectroscopy for characterizing surface intermediates, and it is applicable to samples having low metal loadings and in reactive atmospheres and is expected to have an increasing role in catalysis research by facilitating the determination of mechanisms of solid-catalyzed reactions through identification of reaction intermediates in working catalysts.

Atomically dispersed iridium catalyst supported on a platform of three Ir atoms (with A. Katz). A saturated Ir_4 carbonyl cluster comprising a tetrahedral metal frame and three *tert*-butyl-calix[4]arene$(OPr)_3(OCH_2PPh_2)$ ligands (Ph = phenyl; Pr = propyl) was characterized with variable-temperature ^{13}C NMR spectroscopy, with the data showing the absence of scrambling of the CO ligands at temperatures up to 313 K. This demonstration of distinct sites for

the CO ligands extends to the reactivity and catalytic properties when the cluster is supported on dehydroxylated silica, as shown by the occurrence of selective decarbonylation in a reaction with trimethylamine N-oxide (TMAO) as an oxidant, which, reacting in the presence of ethylene, leads to the selective bonding of an ethyl ligand at the apical Ir site, where calixarenes are not located. By using TMAO in an atmosphere of ethylene we were able to dial in the number of catalytically active sites for ethylene hydrogenation. Reaction orders in the catalytic ethylene hydrogenation reaction of approximately ½ and 0 for H_2 and C_2H_4, respectively, nearly match those for conventional noble-metal catalysts and are representative of a two-site catalytic model according to which one site bonds only to hydrogen, whereas the other bonds both hydrogen and olefin.

Single-site osmium catalysts exhibiting novel reactivities and catalytic activity for oxidation (with D. A. Dixon). MgO-supported osmium dioxo species, described as $Os(CO)_2\{O_{support}\}_{1^{or^2}}$ (the brackets denote O atoms of the MgO surface), formed from $Os_3(CO)_{12}$ via supported $Os(CO)_2$, and characterized by IR and EXAFS spectroscopies, STEM, and density functional theory, react with ethylene at 298 K to form osmium glycol species or with CO to give osmium mono- and di-carbonyls. The latter is the precursor of a CO oxidation catalyst characterized by a turnover frequency of 4.0×10^{-3} (molecules of CO)/(Os atom×s) at 473 K; the active species are inferred to be osmium monocarbonyls. The structures and frequencies calculated at the level of density functional theory with the B3LYP functional bolster the experimental results and facilitate structural assignments. The lowest-energy structures have various osmium oxidation and spin states. The results demonstrate not only new chemistry of the supported single-site catalysts but also their complexity and the value of complementary techniques used in concert to unravel the chemistry.

Iridium pair sites on supports (with N. D. Browning). Binuclear metal species are the simplest metal clusters, and metal pair-sites on supports may be considered the first steps from atomically dispersed to metal cluster catalysts. In our earlier work, we investigated supported rhodium dimers made from various precursors, which were found to exhibit higher activities than comparable single-atom species. Now we have synthesized a novel catalyst with paired-iridium sites on MgO powder by using the precursor $Ir(\mu\text{-}OMe)(1,5\text{-cod})]_2$. The metal pairs are site-isolated as shown by STEM images and EXAFS spectroscopy and they exhibit markedly greater activity than their single-atom counterparts and undergo slower deactivation in ethylene hydrogenation catalysis.

Publications Acknowledging this Grant in 2014-2017

I. Serna, P.; Yardimci, D.; Kistler, J. D.; Gates, B. C. Formation of supported rhodium clusters from mononuclear rhodium complexes controlled by the support and ligands on rhodium, *PhysChemChemPhys*, **2014**, *16*, 1262.

III. Okrut, A.; Runnebaum, R. C.; Ouyang, X.; Lu, J.; Aydin, C.; Hwang, S.-J.; Zhang, S.; Olantunji-Ojo, O. A.; Durkin, K. A.; Dixon, D. A.; Gates, B. C.; Katz, A., Selective molecular recognition by nanoscale environments in a supported iridium cluster catalyst, *Nat. Nanotechnol.*, **2014**, *9*, 459.

I. Martinez-Macias, C.; Xu, P.; S.-J. Hwang, Lu, J.; Chen, C.-Y.; Browning, N. D.; Gates, B. C. Iridium complexes and Clusters in Dealuminated Zeolite HY: Distribution between Crystalline and Impurity Amorphous Regions, *ACS Catal*, **2014**, *4*, 2662.

I. Kistler, J. D.; Chotigkrai, N.; Xu, P.; Enderle, B.; Praserthdam, P.; Chen, C.-Y.; Browning, N. D.; Gates, B. C. A Single-Site Platinum CO Oxidation Catalyst in Zeolite KLTL: Microscopic and Spectroscopic Determination of the Locations of the Platinum Atoms, *Angew. Chem. Int. Ed.*, **2014**, *53*, 8904.

I. Serna, P.; Gates, B. C. Molecular Metal Catalysts on Supports: Organometallic Chemistry Meets Surface Science, *Acc. Chem. Res.*, **2014**, *47*, 2612.

II. Dixon, D. A.; Katz, A.; Arslan, I.; Gates, B. C. Beyond Relationships between Homogeneous and Heterogeneous Catalysis, *Catal. Lett.*, **2014,** *144*, 1785.

II. Yang, D.; Chen, M.; Martinez-Macias, C.; Dixon, D. A.; Gates, B. C. Mononuclear iridium dinitrogen complexes bonded to zeolite HY, *Chem. Eur. J.,* **2015**, *21*, 631.

III. Bayram, E.; Lu, J.; Aydin, C.; Browning, N. D.; Ozkar, S.; Finney, E.; Gates, B. C.; Finke, R. Agglomerative Sintering of an Atomically Dispersed Ir_1/Zeolite Y Catalyst: Compelling Evidence Against Ostwald Ripening but for Bimolecular and Autocatalytic Agglomeration Catalyst Sintering Steps, *ACS Catal.* **2015***, 5*, 3514.

I. Xu, P.; Lu, J.; Aydin, C.; Debefve, L.; Browning, N. D.; Chen, C. Y.; Gates, B. C. Imaging Individual Lanthanum Atoms in Zeolite Y by Scanning Transmission Electron Microscopy: Evidence of Lanthanum Pair Sites, *Micropor. Mesopor. Matl*, **2015**, *213*, 95.

I. Gates, B. C. From Catalyst Preparation toward Catalyst Synthesis, *J. Catal.,* **2015**, *328*, 72.

III. Arslan, I.; Roehling, J. D.; Ogino, I.; Batenburg, K. J.; Zones, S. I.; Gates, B. C.; Katz, A. Genesis of Delaminated-Zeolite Morphology: 3-D Characterization of Changes by STEM Tomography, *J. Phys. Chem. Lett.*, **2015**, *6*, 2598.

III. Zhang, S.; Katz, A.; Gates, B. C.; Dixon, D. A. Structures, Relative Energies, and Ligand Dissociation Energies of Iridium Carbonyl Phosphine Clusters, *Comp. Theo. Chem.*, **2015**, *1069,* 18.

I. Martinez Macias, C.; Chen, M.; Dixon, D. A.; Gates, B. C. Single-Site Zeolite-Anchored Organoiridium Carbonyl Complexes: Characterization of Structure and Reactivity by Spectroscopy and Computational Chemistry, *Chem. Eur. J.*, **2015**, *21*, 11825.

I. Martinez-Macias, C.; Serna, P.; Gates, B. C. Isostructural Zeolite-Supported Rhodium and Iridium Complexes: Tuning Catalytic Activity and Selectivity by Ligand Modification, *ACS Catal.*, **2015**, *5*, 5647.

III. Chen, M.; Serna, P.; Lu, J.; Gates, B. C.; Dixon, D. A. Molecular Models of Site-Isolated Cobalt, Rhodium, and Iridium Catalysts Supported on Zeolites: Ligand Bond Dissociation Energies, *Comp. Theo. Chem.*, **2015**, *1074*, 58.

III. Han, C. W.; Iddir, H.; Uzun, A.; Curtiss, L. A.; Browning, N. D.; Gates, B. C.; Ortalan, V. Migration of Single Iridium Atoms and Tri-iridium Clusters on MgO Surfaces: Aberration-Corrected STEM Imaging and Ab Initio Calculations, *J. Phys. Chem. Lett.*, **2015**, *6*, 4675.

III. Maity, N.; Barman, S.; Callens, E.; Samantaray, M. K.; Abou-Hamad, E.; Minenkov, Y.; D'Elia, V.; Hoffman, A. S.; Widdifield, C. M.; Cavallo, L.; Gates, B. C.; Basset, J.-M.

Controlling the Hydrogenolysis of Silica-Supported Tungsten Pentamethyl Leads to a Class of Highly Electron Deficient Partially Alkylated Metal Hydrides, *Chem. Sci.*, **2016**, *7*, 1558.

I. Kistler, J. D.; Serna, P.; Asakura, K.; Gates, B. C. Surface Metal Complexes and their Applications," in "X-Ray Absorption and X-Ray Emission Spectroscopy: Theory and Applications, J. van Bokhoven and C. Lamberti, editors, Wiley, Chichester, **2016**, pp. 773-808.

I. Yang, D.; Xu, P.; Guan, E.; Browning, N. D.; Gates, B. C. Rhodium pair-sites on magnesium oxide: Synthesis, characterization, and catalysis of ethylene hydrogenation *J. Catal.*, **2016**, *338*, 12.

I. Gates, B. C. Concluding remarks: Progress toward design of solid catalysts, *Faraday Disc.*, **2016**, *188*, 591.

II. Hoffman, A. S.; Debefve, L. M.; Bendjerious-Sedjerari, A.; Ould Chikh, S.; Bare, S. R.; Basset, J.-M.; Gates, B. C. Transmission and Fluorescence X-ray Absorption Spectroscopy Cell/Flow Reactor for Powder Samples under Vacuum or in Reactive Atmospheres, *Rev. Sci. Instrum.*, **2016**, *87*, 073108.

I. Yang, D.; Xu, P.; Browning, N. D.; Gates, B. C. Tracking Rh Atoms in Zeolite HY: First Steps of Metal Cluster Formation and Influence of Metal Nuclearity on Catalysis of Ethylene Hydrogenation and Ethylene Dimerization, *J. Phys. Chem. Lett.*, **2016**, *7*, 2537.

I. Hoffman, A. S.; Fang, C. Y.; Gates, B. C. Homogeneity of Surface Sites in Supported Single-Site Metal Catalysts: Assessment with Band Widths of Metal Carbonyl Infrared Spectra, *J. Phys. Chem. Lett.*, **2016**, *7*, 3854.

I. Yang, D.; Zhang, S.; Xu, P.; Browning, N. D.; Dixon, D. A.; Gates, B. C. Single-site osmium catalysts on MgO: reactivity and catalysis of CO oxidation *Chem. Eur. J.*, **2017**, *23*, 2532.

II. Hoffman, A. S.; Sokaras, D.; Zhang, S.; Debefve, L. M.; Fang, C.-Y.; Gallo, A.; Kroll, T.; Dixon, D. A.; Bare, S. R.; Gates, B. C. High-Energy Resolution X-Ray Absorption Spectroscopy for Identification of Reactive Surface Species on Supported Single-Site Catalysts *Chem. Eur. J.*, in press, **2017**.

I. Ogino, I.; Serna, P.; Gates, B. C. Supported Catalysts, in R. Dronskowski, S. Kikkawa, and A. Stein, editors, "Handbook of Solid State Chemistry," Wiley, New York, in press, **2017**.

Raymond J. Gorte

Fabrication of Nano-Structured Catalyst Supports by ALD

R. J. Gorte and T. M. Onn
Chemical & Biomolecular Engineering
University of Pennsylvania
Philadelphia, PA 19104

Presentation Abstract

Interactions between a transition-metal catalyst and its support can strongly alter the stability and activity of the catalyst. Important examples include support effects with ceria and the so-called "Intelligent Catalysts" in which the metal can be redispersed by reversible ex-solution from a perovskite lattice. However, the surface areas of these functional supports are often too low or unstable; and, in the case of perovskites, the length scales for ingress and egress may be too long to take advantage of the effect. We are addressing these issues by depositing very thin films of various functional oxides, ~1 to 2 nm thick, onto high-surface-area supports, including Al_2O_3 and $MgAl_2O_4$, by Atomic Layer Deposition. We have demonstrated that a wide range of oxides can be deposited as dense, uniform, conformal films on various supports. The films exhibit surprisingly good thermal stability and provide catalytic properties similar to observed with bulk oxides, but with higher surface areas.

DE-FG02-13ER16380: Nano-Structured Catalysts for Improved Oxide-Metal Interactions

Student(s): Tzia Ming Onn, Chao Lin

RECENT PROGRESS

High-Surface-Area Ceria Prepared By ALD on Al_2O_3 Support

Al_2O_3 powders were modified by Atomic Layer Deposition (ALD) of CeO_2 to produce composite catalyst supports for Pd. The weight of the support was found to increase linearly with the number of ALD cycles. This, together with TEM images, indicated that the CeO_2 grows as a dense, conformal film, with a growth rate of 0.02 nm per cycle. The films showed good thermal stability under oxidizing conditions. XRD measurements on a sample with 28-wt% CeO_2 showed no evidence for crystalline CeO_2 until calcination above 1073 K. Water-gas-shift rates on 1-wt% Pd catalysts supported on the CeO_2 ALD-modified Al_2O_3 were essentially identical to rates on conventional Pd-CeO_2 catalysts and much higher than rates on a catalyst in which Pd was supported on Al_2O_3 with CeO_2 added by infiltration. The WGS rates, together with results from FTIR and CO-O_2 pulse studies, suggest that all of the Pd is in contact with CeO_2 on the ALD-

prepared supports and that it should be possible to prepare high-surface-area, functional supports using ALD.

High-Surface-Area, Iron-Oxide Films Prepared by Atomic Layer Deposition on γ-Al_2O_3

High-surface-area iron oxides were prepared by Atomic Layer Deposition (ALD) on 130-m^2/g γ-Al_2O_3 for use as a catalyst support. Measurements of the sample mass, surface area, and pore-size distribution as a function of the number of ferrocene-O_2 ALD cycles at 623 K suggested that the iron oxide grew as a dense, conformal film with a growth rate similar to 0.016-nm per cycle. While films with 20 ALD cycles (20Fe_2O_3-Al_2O_3, 0.25 g Fe_2O_3/g Al_2O_3) were difficult to distinguish by HAADF STEM, EDS mapping indicated the Al_2O_3 was uniformly coated. Raman Spectroscopy showed the films were in the form of Fe_2O_3; but XRD measurements on samples with as many as 100 ALD cycles (100Fe_2O_3-Al_2O_3, 0.84 g Fe_2O_3/g Al_2O_3) showed no evidence for crystalline iron-oxide phases, even after calcination at 1073 K. Specific rates for the water-gas-shift (WGS) reaction on the ALD-coated samples were significantly lower than those on bulk Fe_2O_3. However, addition of 1 wt.% Pd to Fe_2O_3/Al_2O_3 supports prepared by ALD exhibited specific rates that were much higher than that observed when 1 wt.% Pd was added to Fe_2O_3/Al_2O_3 prepared by conventional impregnation of Fe salts, suggesting more uniform contact between the Pd and FeO_x phases on samples prepared by ALD.

High-surface area Ceria-Zirconia Films Prepared by Atomic Layer Deposition:

Ceria-zirconia, solid solutions were prepared as thin, dense films on a 130-m^2/g γ-Al_2O_3 by Atomic Layer Deposition (ALD) for use as catalyst supports. $Ce_{0.5}Zr_{0.5}O_2$ solid solutions were grown by alternating between $Ce(TMHD)_4$ and $Zr(TMHD)_4$ precursors during ALD cycles. 50 precursor-oxidation cycles resulted in a material with 0.77 g $Ce_{0.5}Zr_{0.5}O_2$ per g γ-Al_2O_3, corresponding to an average film thickness of 1.0 nm. The lattice parameter obtained from XRD was consistent with formation of a solid solution and scanning transmission electron microscopy (STEM) showed the mixed oxide was uniformly deposited. When impregnated with 1-wt% Pd, the ALD-prepared $Ce_{0.5}Zr_{0.5}O_2$-γ-Al_2O_3 catalyst showed CO-oxidation activity similar to Pd on bulk $Ce_{0.5}Zr_{0.5}O_2$; however, the ALD-prepared sample maintained much of its surface area and catalytic activity when heated to temperatures up to 1273 K.

Preparation of high-surface-area $LaFeO_3$ supports on $MgAl_2O_4$:

Films of $LaFeO_3$ were grown on γ-Al_2O_3 and $MgAl_2O_4$ by alternating deposition of La_2O_3 and Fe_2O_3 using ALD. For films thicker than 1 nm, XRD showed formation of the perovskite structure by 600 °C. The perovskite reacted with γ-Al_2O_3 to form $LaAlO_3$ above 800 °C but the films were stable on $MgAl_2O_4$. TEM showed the films form dense, uniform overlayers on $MgAl_2O_4$. When used as a support for Pd, evidence is found for rapid egress/ingress of the Pd particles at 800 °C, which is more than 100 degrees lower than what is found for bulk perovskites.

Publications Acknowledging this Grant in 2013-2016

Exclusively funded by this grant

1. "High-surface area Ceria-Zirconia Films Prepared by Atomic Layer Deposition", T. M. Onn, S. Dai, J. Chen, X. Pan, G. W. Graham, and R. J. Gorte, Catalysis Letters, DOI 10.1007/s10562-017-2053-1.
2. "High-Surface-Area, Iron-Oxide Films Prepared by Atomic Layer Deposition on γ-Al_2O_3", T. M. Onn, M. Monai, S. Dai, L. Arroyo-Ramirez, S. Zhang, X. Ye, X. Pan, G. W. Graham, P. Fornasiero, R. J. Gorte, Applied Catalysis A 534 (2017) 70-77.
3. "High-Surface-Area Ceria Prepared By ALD on Al_2O_3 Support", T.M. Onn, S. Zhang, L. Arroyo-Ramirez, X. Ye, C. Wang, X. Pan, G.W. Graham, and R. J. Gorte, Applied Catalysis B, 201 (2017) 430-437.
4. "Phosphorus poisoning during wet oxidation of methane over Pd@CeO_2/Graphite model catalysts", M. Monai, T. Montini, M. Melchionna, T. Duchoň, P. Kúš, N. Tsud, K. Prince, V. Matolin, R. J. Gorte, P. Fornasiero, Applied Catalysis B, 197 (2016) 271-79.
5. "Improved Thermal Stability and Methane-Oxidation Activity of Pd/Al_2O_3 Catalysts by Atomic Layer Deposition of ZrO_2", T. M. Onn, S. Zhang, L. Arroyo-Ramirez, Y.-C. Chung, G. W. Graham, X. Pan, R. J. Gorte, *ACS Catalysis*, **2015**, *5*, 5696-5701.
6. "A Comparison of Hierarchical Pt@CeO_2/Si-Al_2O_3 and Pd@CeO_2/Si-Al_2O_3", L. Arroyo-Ramírez, C. Chen, M. Cargnello, C. B. Murray, and R. J. Gorte, *Catalysis Today*, **2015**, *253*, 137-141.
7. "Efficient Removal of Organic Ligands From Supported Nanocrystals by Fast Thermal Annealing Enables Catalytic Studies on Well Defined Active Phases", M. Cargnello, C. Chen, B. Diroll, V. Doan-Nguyen, R. J. Gorte, and C. B. Murray, *Journal of the American Chemical Society*, **2015**, *137*, 6906-11.
8. "Structure, morphology and catalytic properties of pure and alloyed Au-ZnO hierarchical nanostructures", M. Cargnello, D. Sala, C. Chen, M. D'Arienzo, R. J. Gorte, and C. B. Murray, *RSC Advances*, **2015**, *5*, 41920-33.
9. "Supported Platinum-Zinc Oxide Core-Shell Nanoparticle Catalysts for Methanol Steam Reforming", L. Arroyo-Ramírez, Chen Chen, M. Cargnello, C. B. Murray, P. Fornasiero, and R. J. Gorte, *Journal of Materials Chemistry* A, **2014**, *2*, 19509-14.
10. "Methane catalytic combustion over hierarchical Pd@CeO_2/Si-Al_2O_3: Effect of the presence of water", M. Monai, T. Montini, Chen Chen, E. Fonda, R. J. Gorte, P. Fornasiero, *ChemCatChem*, **2015**, *7*, 2038-46.
11. "Thermodynamic and catalytic properties of Pd@ZrO_2/Si-Al_2O_3 core-shell catalysts", Chen Chen, Yu-Hao Yeh, Matteo Cargnello, Christopher B. Murray, Paolo Fornasiero, Raymond. J. Gorte, *ACS Catalysis*, **2014**, *4*, 3902-09.
12. "Au@TiO_2 core-shell nanostructures with high thermal stability", Chen Chen, Mengxue Shi, Matteo Cargnello, Paolo Fornasiero, Christopher B. Murray, and Raymond. J. Gorte, *Catalysis Letters*, **2014**, *144*, 1939-45.

Peptide Control of Electrocatalyst Surface Environment and Catalyst Structure: Initial Experiments and Theory Development

Lauren F. Greenlee,[a] Sergio I.P. Bakovic,[a] Julie N. Renner,[b] Charles Loney,[b] Michael J. Janik,[c] Sharad Maheshwari[c]
[a]Ralph E. Martin Department of Chemical Engineering, University of Arkansas
[b]Department of Chemical Engineering, Case Western Reserve University
[c]Department of Chemical Engineering, The Pennsylvania State University

Presentation Abstract

Low-temperature electrochemical ammonia synthesis from di-nitrogen (N_2) with heterogeneous catalysts continues to suffer from extremely low Faradaic efficiencies (< 1%). The hydrogen evolution reaction (HER) is predicted and experimentally demonstrated to outcompete the nitrogen reduction reaction (N_2RR). Meanwhile, the nitrogenase enzymes found in nature enable selective N_2RR at Fe/Mo metal centers. Both theoretical efforts to identify optimal metal catalyst surfaces and synthetic efforts to develop metal-based heterogeneous catalysts strongly suggest that traditional approaches to catalyst design, such as creating bimetallic compositions or core-shell/alloy morphologies are not sufficient to shift reaction selectivity away from HER and toward N_2RR. As a result, novel approaches are needed that can alter the local surface chemistry of heterogeneous catalysts and thus allow experimental deviation from linear scaling relationships that theoretically predict HER over N_2RR. Our approach is to use a tunable peptide platform, based on key sequence motifs of the nitrogenase enzyme catalyst center, to modulate the local surface environment of key heterogeneous catalyst surfaces. We have started this project by designing a suite of peptides that are tuned for hydrophobicity and pKa and conducting an initial evaluation of peptide attachment to gold electrodes, along with high-resolution quartz crystal microbalance measurement of water adsorption. In addition, the synthesis method for bimetallic (Fe/Ni) thin film electrodes has been established via electrochemical deposition, and development of the theoretical framework for our catalyst surface and peptide surface chemistry, with thermodynamic calculations for N_2 and atomic hydrogen (H^*) binding to a Fe(100) surface, has been developed. In initial calculations for transition state activation energies, results suggest a Heyrovsky-type mechanism, where the proton comes from a water molecule, rather than a Tafel-type mechanism, where the proton comes from the catalyst surface.

DE-SC0016529: Peptide Control of Electrocatalyst Surface Environment and Catalyst Structure: A Design Platform to Enable Mechanistic Understanding and Synthesis of Active and Selective N_2 Reduction Catalysts

RECENT PROGRESS

Aim 1: Peptide Sequence Design and Attachment to Gold Electrodes

Tripeptides were designed to 1) bind to gold surfaces[1] 2) have a range of hydrophobicity (8.5-11.4 Kcal/mol) and 3) have a range of isoelectric points (3.1-9.5). The C-terminal amino acid in the design is cysteine, and serves as the gold anchor through well-known thiol chemistry. The other two peptides in the design vary such that the same hydrophobicity is achieved with a range of isoelectric points, and vice versa. Binding of one of these tripeptides, VRC, was assessed using a quartz crystal microbalance with dissipation (QCM-D) with a gold sensor (Fig. 1). The QCM-D resonates at a known frequency, and as material sticks to the sensor that frequency changes and mass can be calculated. In this experiment, the frequency decreases as the gold sensor is exposed to solution of peptide in deionized (DI), indicating that the tripeptide is binding to the gold sensor, and plateaus after about 25 minutes. When water is added, only a slight increase (<10%) in frequency is observed, indicating that some non-specifically bound peptides are being removed from the sensor. The majority of the layer is stable, as no further frequency shifts are observed. Using the Sauerbrey model, mass can be calculated and it is estimated that approximately 70 ng/cm^2 is left on the sensor after the rinse step. QCM-D also allows monitoring of changes in frequency dissipation. These changes can give information about the mechanical properties of the layers adsorbed to the sensor. The data show that dissipation does not change significantly in the experiment, indicating that the film is relatively ridgid. Using the Voigt viscoelastic module, thickness can be estimated from frequency and dissipation changes. The model indicates that the film is approximately 0.7 nm thick. Assuming 3.5 Å per amino acid (0.35 nm), the peptide film is likely one mono layer thick. In summary: 1) tripeptides have been designed to span a range of hydrophobicity and isoelectric points and 2) tripeptides form a stable monolayer on gold.

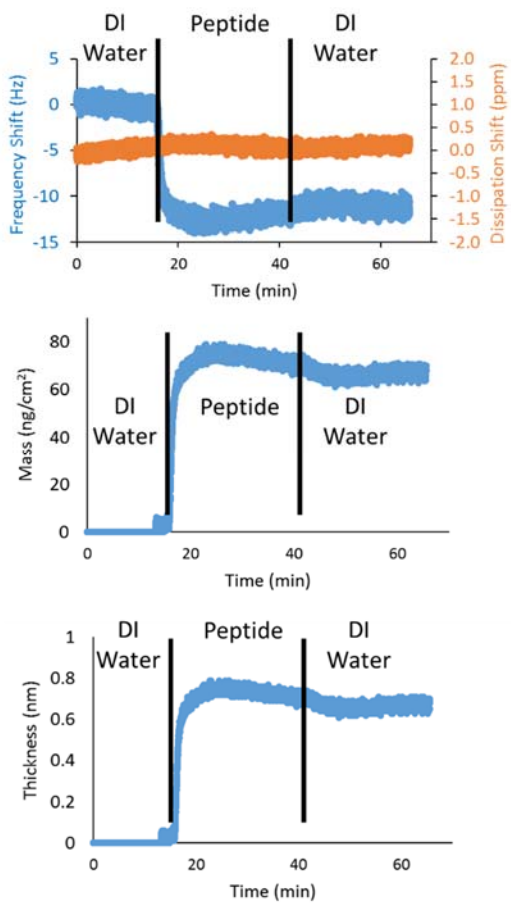

Figure 1: QCM-D monitoring shows tripeptides adhere to gold in a stable monolayer.

Aim 2: Electrocatalyst Film Synthesis

The first objective of Aim 2 was to synthesize bimetallic thin films via an atomic layer deposition (ALD) approach. Our initial approach was to use commercially-available iron and nickel ALD precursors, along with ozone, to produce iron-nickel oxide thin films. While this method, in theory, can provide well-controlled thin films of specific compositions (i.e., molar ratios of Fe:Ni in a bimetallic film), our experimental efforts demonstrated that the reaction was

inefficient within the ALD chamber, resulting in high usage of both metal precursors and ozone. In addition, obtaining films with thicknesses greater than several nanometers is also prohibitive in terms of the amount of precursor used. As a result, we have moved to synthesizing thin films with an electrochemical deposition approach, which has been established for iron-nickel oxides/hydroxides by the Boettcher group.[2] With this approach, we have successfully synthesized bimetallic thin films of controlled composition and thickness. The films are synthesized using an in situ electrochemical chamber and our high-resolution quartz crystal microbalance (QCM), where a solution of aqueous metal precursors is flowed through the chamber, chronopotentiometry (i.e., constant current) is used to deposit a bimetallic oxide film onto the QCM crystal electrode (Au), and the QCM measures film thickness in real time via the change in resonant frequency. With this synthesis approach (Fig. 2a), we have successfully synthesized films for a wide range of bimetallic iron-nickel compositions, from 5:95 Fe:Ni to 95:5 Fe:Ni (mol:mol). Initial characterization of these films includes QCM quantification of film thickness and XRD characterization of phase (Fig. 2b, c).

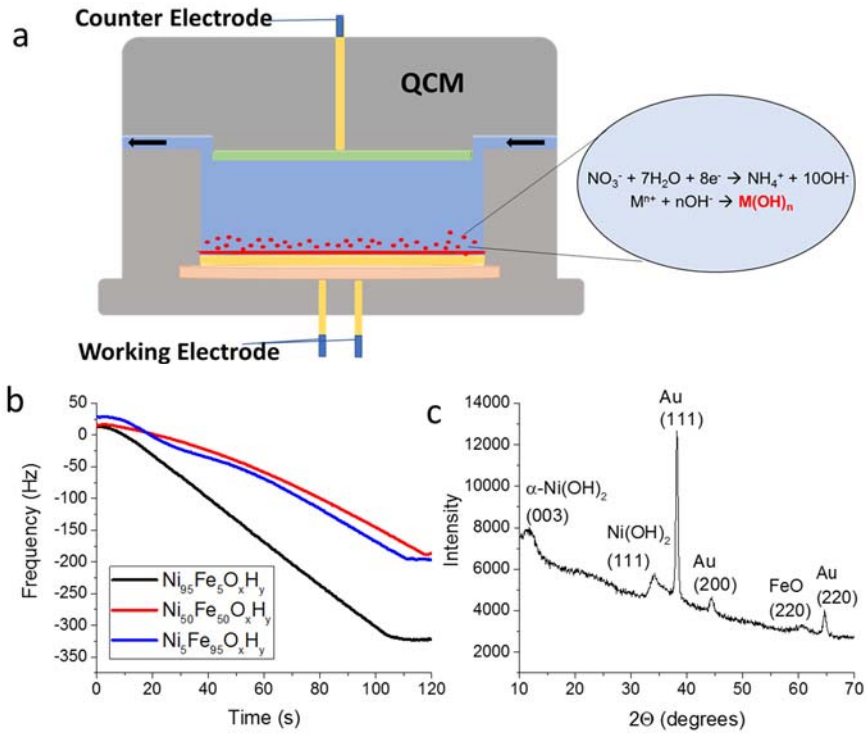

Figure 2. (a) Schematic of film synthesis, (b) measurement of film deposition via change in resonant frequency of the QCM crystal substrate, and (c) XRD characterization of film phase for a 50:50 Fe:Ni film.

Aim 3: Theoretical Framework

The overall goals of this aim is to determine, using density functional theory (DFT), the impact of electrolyte environment on activation barriers for coupled proton/electron transport to surface N_xH_y intermediates. We will examine how proton transport is impacted by key amino acids identified from Aim 1 and catalyst surfaces developed in Aim 2.

To date, we have investigated the reduction of surface-bound N_2* and N* species. DFT calculations have examined the Tafel (direct surface hydrogenation, Fig. 3a) and Heyrovsky (water-mediated, Fig. 3b) transfer of protons to dinitrogen on Fe(100) and other late transition metal surfaces. We have determined that the water-mediated transfer is more rapid, suggesting that a reaction environment that alters the structure and dynamics of water adjacent to the surface may alter the rate of important elementary reduction steps. We have used an approach developed in the Janik group to calculate these barriers as a function of electrode potential. The water-assisted barrier for N_2* reduction to N_2H* is 0.93 eV at 0 V-RHE (relative to a reversible hydrogen electrode). We are now examining how this barrier changes when the multiple water molecules are included in proton transfer path, as well as the extent to which different proton-donating functionalities (alcohols, carboxylic acids, amines) alter this reduction barrier. We also examine the Tafel and Heyrovsky barriers associated with the hydrogen evolution reaction to examine how these non-selective reactions are impacted by the same functional groups.

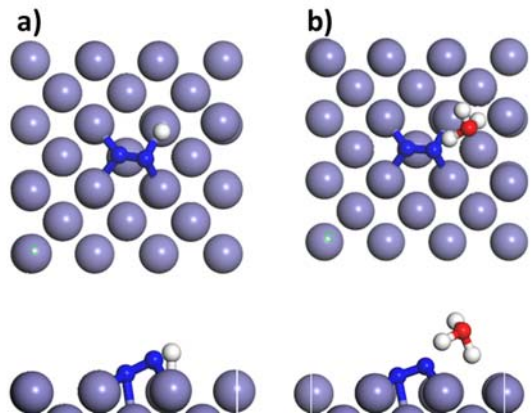

Figure 3. Transition states for N_2* reduction to N_2H* through the a) Tafel mechanism (E_{act} = 1.07 eV at 0 V-RHE) and the b) Heyrovsky mechanism (E_{act} = 0.93 eV at 0 V-RHE).

A second effort of our DFT work is to examine the structure of short peptides on metal surfaces, such that functional groups that accelerate N_2 reduction can be tethered to the surface region. We have located the optimal structures on Au(111) for cysteine and short cysteine-peptide chains using DFT. These models are needed to examine the impact of peptides on reduction processes, and will continue to be integrated with experimental efforts examining peptide impacts on gas adsorption and N_2 reduction.

Publications Acknowledging this Grant in 2014-2017. None to report.

References

(1) Li, T.; He, X. X.; Wang, Z. X., The Application of Peptide Functionalized Gold Nanoparticles. In *Functional Nanoparticles for Bioanalysis, Nanomedicine, and Bioelectronic Devices, Vol 2*, Hepel, M.; Zhong, C. J., Eds. American Chemical Society: Washington, D.C., **2012**, pp 55-68.

(2) Stevens, M. B.; Enman, L. J.; Batchellor, A. S.; Cosby, M. R.; Vise, A. E.; Trang, C. D. M.; Boettcher, S. W., Measurement Techniques for the Study of Thin Film Heterogeneous Water Oxidation Electrocatalysts. *Chem. Mater.* **2017,** *29* (1), 120-140.

Development of Transition Metal Catalysts for the Functionalization of Carbon-Hydrogen Bonds: Fundamental Studies of Catalytic Hydroarylation of Olefins

T. Brent Gunnoe[a], Junqi Chen[a], Michael S. Webster-Gardiner[a], Benjamin A. Vaughan[a], Weihao Zhu[a], Bradley A. McKeown[a] Thomas R. Cundari[b]

[a]Department of Chemistry, University of Virginia, Charlottesville, VA 22904

[b]Center for Advanced Scientific Computing and Modeling (CASCaM), Department of Chemistry, University of North Texas, Denton, TX 76203

Presentation Abstract

The selective catalytic functionalization of C–H bonds of hydrocarbons remains one of the foremost challenges facing synthetic chemists. The ability to selectively manipulate C–H bonds of arenes, alkanes and more complex organic molecules would open the door to a wide range of useful synthetic transformations. For example, the addition of aromatic C–H bonds across olefin C=C bonds, olefin hydroarylation, provides an atom economical reaction with broad potential including applications in both commodity scale processes as well as fine chemical synthesis. We have been studying olefin hydroarylation (to produce alkyl aromatics) and oxidative olefin hydroarylation (to produce alkenyl aromatics) catalyzed by well-defined Fe, Ni, Ru, Rh and Pt catalysts. For Pt(II) catalysts of the type $[(^{x}bpy)Pt(Ph)(THF)]^{+}$ (^{x}bpy = 4,4'-disubstituted-2,2'-dipyridyl ligands), kinetic studies suggest that catalyst deactivation occurs through a bimolecular pathway with the formation of Pt(s). Recently, we reported that $(^{Fl}DAB)Rh(TFA)(\eta^2–C_2H_4)$ [^{Fl}DAB = *N,N'*-bis(pentafluorophenyl)-2,3-dimethyl-1,4-diaza-1,3-butadiene; TFA = trifluoroacetate] converts benzene, ethylene and Cu(II) salts to styrene, Cu(I) salt, and acid with high selectivity and yields ≥ 95%. We have extended these studies to new Rh(I) catalysts and demonstrated the ability to produce straight-chain alkenyl arenes when α-olefins are used. Also, regioselectivity for substituted benzenes is not directed by the electronic properties of the substituent but rather is catalyst directed for meta and para positions.

Grant Number: DE-SC0000776

Grant Title: Development of Transition Metal Catalysts for the Functionalization of Carbon-Hydrogen Bonds: Fundamental Studies of Catalytic Hydroarylation of Olefins

PI: T. Brent Gunnoe

Postdocs: N/A

Students: Michael Webster-Gardiner (G), Junqi Chen (G), Benjamin Vaughan (G), Weihao Zhu (G), Abigail Cole (U), John Gordon (U)

Collaborators: Thomas R. Cundari (University of North Texas), Daniel H. Ess (Brigham Young University), William Goddard III (California Institute of Technology), Robert Davis (University of Virginia)

RECENT PROGRESS

Objective 1. *Study catalytic olefin hydroarylation using Ru^{II} catalysts supported by poly(pyrazolyl) ligands with similar or reduced electron density relative to TpRu(CO)(NCMe)Ph.* Previous studies have indicated that Ru(II) catalysts with trispyrazolylborate (Tp) or trispyrazolylmethane ligands are selective for ethylbenzene production. In those studies, using cyclic voltammetry data we demonstrated that complexes with more electron-deficient Ru centers gave improved catalyst longevity. To further decrease the electron density the cationic Ru(II) complex

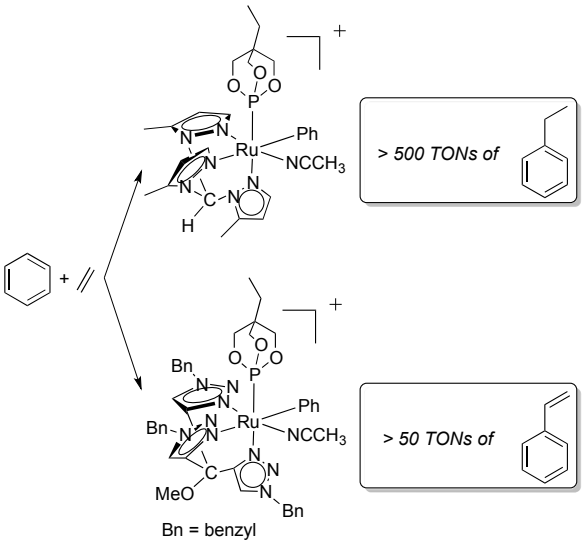

Scheme 1. Comparison of previously reported cationic trispyrazolylalkane Ru catalyst and new cationic tristriazolylmethanol Ru catalyst.

$[(CH_3OTTM)Ru[P(OCH_2)_3CEt](NCMe)Ph][BAr'_4]$ (CH_3OTMM = 4,4',4''-(methoxymethanetriyl)-tris(1-benzyl-1H-1,2,3-triazole), BAr'_4 = tetrakis[3,5-bis(trifluoromethyl)phenyl]borate) was synthesized. In contrast to several related Ru(II) catalysts, both neutral and cationic, the new cationic Ru(II) catalyst with the CH_3OTMM ligand selectively produces styrene (> 50 TONs in 4 h; Scheme 1). We have demonstrated that ethylene serves as the oxidation to produce ethane.

Objective 2. *Continue to study the influence of ancillary ligands on Pt^{II} catalyzed olefin hydroarylation using chelating N,N- and related chelating ligands.* No new results to report.

Objective 3. *Extend chemistry of (^{x}bpy)Pt^{II} to Rh^I catalysts.* Previously, we reported the direct and single-step conversion of benzene, ethylene, and a Cu(II) oxidant to styrene using the Rh(I) catalyst (^{Fl}DAB)Rh(TFA)(η^2-C_2H_4) [^{Fl}DAB = *N,N'*-bis(pentafluorophenyl)-2,3-dimethyl-1,4-diaza-1,3-butadiene; TFA = trifluoroacetate] to give quantitative yields (with Cu(II) as the limiting reagent) and selectivity combined. Recent studies examining catalysis with the complex (^{Fl}DAB)Rh(OAc)(η^2-C_2H_4) shows that the reaction rate has a dependence on catalyst concentration between first- and half-order, which varies with both temperature and ethylene concentration, a first-order dependence on ethylene concentration with saturation at higher concentrations of ethylene, and a near zero-order dependence on the concentration of Cu(II) oxidant. The kinetic isotope effect (C_6H_6 vs. C_6D_6) was found to vary linearly with the order in (^{Fl}DAB)Rh(OAc)(η^2-C_2H_4), exhibiting no KIE when [Rh] was in the half-order regime, and a k_H/k_D value of 6.7(6) when [Rh] was in the first-order regime. Based on these results, the following conclusions were drawn:

(1) Combined experimental and computational studies are consistent with catalysis that proceeds through benzene C–H activation, displacement of coordinated acetic acid by ethylene, rate-limiting insertion of ethylene into the Rh–Ph bond, and β-hydride elimination followed by liberation of styrene and reaction with Cu(II).

(2) The apparent induction period observed for catalysis with (^{Fl}DAB)Rh(TFA)(η^2-C_2H_4) (TFA = trifluoroacetate) is not likely the result of *in situ* formation of insoluble Rh nanoparticles as the active catalyst. Rather, (^{Fl}DAB)Rh(TFA)(η^2-C_2H_4) converts to (^{Fl}DAB)Rh(OAc)(η^2-C_2H_4) (OAc = acetate) *in situ*, which catalyzes styrene production at a faster rate than the TFA analog. The difference in rate of catalysis for Rh-OAc vs. Rh-TFA is likely a result of the difference in ground state energies rather than OAc/TFA influence on transition states, since the proposed rate determining step occurs once the carboxylate ligands are completely dissociated.

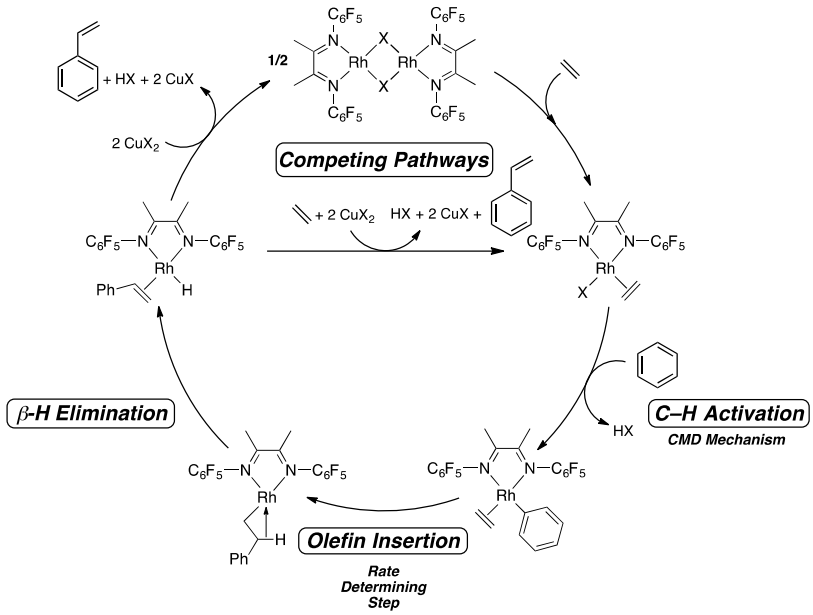

Scheme 2. Proposed pathway for Rh catalyzed alkenylation of arenes.

(3) A mechanism for catalysis with (^{Fl}DAB)Rh(X)(η^2-C_2H_4) (X = OAc or TFA) likely involves two pathways whose contributions vary with [C_2H_4] and temperature (Scheme 2). Accordingly, the derived rate law predicts different behavior at low and high [C_2H_4]. At low [C_2H_4], the limiting form predicts half-order in [Rh], first-order in ethylene, zero-order in Cu, and an inverse dependence on acid concentration. At high [C_2H_4], the limiting form predicts first-order in [Rh], and zero-order dependence on all others. Saturation behavior has been observed for ethylene, and the rate of reaction is suppressed in the presence of added acid at low [C_2H_4] but not at high [C_2H_4]. The kinetics are also consistent with computational modeling, which predicts rate-limiting ethylene insertion into the Rh–Ph bond. However, alternative explanations of the kinetic data are possible, such as inhibition of catalysis upon reaction of the catalyst with acid (to remove Rh from the catalytic cycle) that is influenced by concentration of ethylene. Despite other possible explanations for this complex catalytic process, our mechanistic proposal is consistent with both experimental and computational data and, we believe, is the mechanistic model that is most consistent with the data.

Linear alkyl benzenes are global chemicals that are produced by acid-catalyzed reactions that involve the formation of carbocationic intermediates. One outcome of the acid-based catalysis is that 1-phenylalkanes cannot be produced (despite the moniker linear alkyl benzenes, these compounds are primarily mono-branched alkyl arenes). We demonstrated that [Rh(μ-OAc)(η^2-

$C_2H_4)_2]_2$ catalyzes production of 1-phenyl substituted alkene products via oxidative arene vinylation (Scheme 3). Since C=C bonds can be used for many chemical transformations, the formation of unsaturated products provides a potential advantage over current processes that produce saturated alkyl arenes. Conditions that provide up to 10:1 linear:branched ratio were achieved, and catalytic turnovers > 1470 were demonstrated. In addition, electron-deficient and electron-rich substituted benzenes were successfully alkylated. The Rh catalysis provides *ortho:meta:para* selectivity that is opposite to traditional acid-based catalysis.

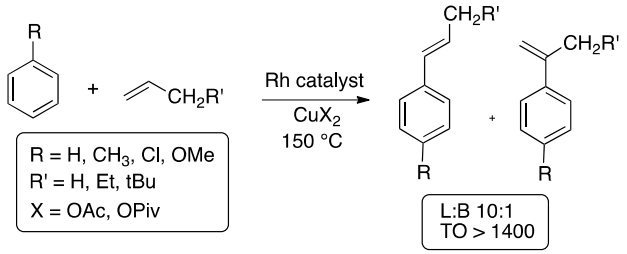

Scheme 3. Rh catalyzed conversion of arenes and olefins to "straight-chain" alkenyl arenes.

In an effort to develop air stable Rh catalysts, we recently prepared a series of "capping arene" supported Rh^I complexes, (5-fp)Rh(TFA), (H-fp)Rh(TFA)(η^2-C_2H_4), (F-fp)Rh(TFA)(η^2-C_2H_4), (OMe-fp)Rh(TFA)(η^2-C_2H_4) were synthesized and tested for oxidative olefin hydroarylation reactions (Scheme 4). This series of ligands positions an arene ring near the Rh center, thus blocking a coordination site. We expected that this would inhibit oxidation from the Rh^I to Rh^{III}, which might render reaction with dioxygen less favorable. In preliminary experiments we have demonstrated proof of concept. In one case, catalytic activity *for a period greater than one month with no apparent loss of activity* has been demonstrated. This reaction involves multiple air recycle steps of Cu(I) to Cu(II).

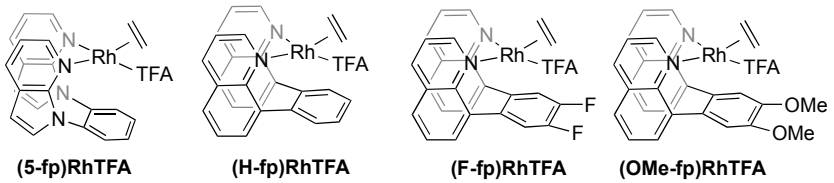

Scheme 4. Examples of new Rh(I) complexes isolated and tested as catalysts for oxidation olefin hydroarylation to produce alkenyl arenes. These complexes are air stable and demonstrate extended catalyst lifetime compared to previously reported Rh catalysts.

Publications Acknowledging this Grant in 2014-2017

I. Exclusively funded by this grant

12. "Catalytic synthesis of "super" linear alkenyl arenes using an easily prepared Rh(I) catalyst" Webster-Gardiner, M. S., Chen, J., Vaughan, B. A., McKeown, B. A., Schinski, W., Gunnoe, T. B.* *J. Am. Chem. Soc.* **2017** *139*, 5474-5480. DOI: 10.1021/jacs.7b01165. This manuscript was highlighted in *Chemical and Engineering News* **2017**, *95*(*17*), 8.

II. Jointly funded by this grant and other grants with leading intellectual contribution from this grant

11. "Studies of the Decomposition of the Ethylene Hydrophenylation Catalyst TpRu(CO)(NCMe)Ph" Joslin, E. E., McKeown, B. A., Cundari, T. R., Gunnoe, T. B.* Invited manuscript accepted *J. Organomet. Chem.* **2017** ASAP (special issue dedicated to Professor John Gladysz "Organometallic

Chemistry: from Stereochemistry to Catalysis to Nanochemistry"). DOI: 10.1016/j.jorganchem.2017.03.051 (other acknowledged grant is DOE BES grant for computational collaborator)

10. "Mechanistic Studies of Single-Step Styrene Production Using a Rhodium(I) Catalyst" Vaughan, B. A., Khani, S. K., Gary, J. B., Kammert, J. D., Webster-Gardiner, M. S., McKeown, B. A., Davis. R. J., Cundari, T. R.*, Gunnoe, T. B.* *J. Am. Chem. Soc.* **2017**, *139*, 1485-1498. DOI: 10.1021/jacs.6b10658 (other acknowledged grant is DOE BES grant for computational collaborator)
9. "Combined Furan C–H Activation and Furyl Ring-Opening by an Iron(II) Complex" Taylor, K. H., Kalman, S. E., Gunnoe, T. B.*, Sabat, M. *Organometallics* **2016**, *35*, 1978–1985. DOI: 10.1021/acs.organomet.6b00276 (other acknowledged grant is for purchase of instrumentation).
8. "Transition Metal Mediated C–H Activation and Functionalization: The Role of Poly(pyrazolyl)borate and Poly(pyrazolyl)alkane Ligands" McKeown, B. A., Lee, J. P., Mei, J. J., Cundari, T. R., Gunnoe, T. B.* *Eur. J. Inorg. Chem.* **2016**, 2296-2311 (special issue "The Significance of Scorpionate Ligands 50 Years on"). DOI: 10.1002/ejic.201501470
7. "Phosphine and *N*-Heterocyclic Carbene Ligands on Pt(II) Shift Selectivity from Ethylene Hydrophenylation toward Benzene Vinylation" Brosnahan, A. M., Talbot, A., McKeown, B. A., Kalman, S. E., Gunnoe, T. B.*, Ess, D. H.*, Sabat, M. *J. Organomet. Chem.* **2015** *793*, 248-255 (invited contribution for special issue in memoriam of Alexander E. Shilov). DOI: 10.1016/j.jorganchem.2015.03.019 (other acknowledged grant is DOE BES grant for computational collaborator)
6. "A Rhodium Catalyst for Single-Step Styrene Production" Vaughan, B. A., Webster-Gardiner, M. S., Cundari, T. R.*, Gunnoe, T. B.* *Science* **2015**, *348*, 421-424. This manuscript was highlighted in *Chemical and Engineering News* **2015**, *93 (17)*, 26. DOI: 10.1126/science.aaa2260
5. "Formation of Hydroxyindenyl and Vinylidene Ligands by Reaction of Internal Alkynes with Cp*Fe(CO)(NCMe)Ph" Kalman, S. E., Gunnoe, T. B.*, Sabat, M. *Organometallics* **2014**, *33*, 5457-5463. DOI: 10.1021/om500748v (other acknowledged grant is for purchase of instrumentation)
4. "Hydrophenylation of Ethylene using a Cationic Ru(II) Catalyst: Comparison to a Neutral Ru(II) Catalyst" Burgess, S. A., Joslin, E. E., Gunnoe, T. B.*, Cundari, T. R.*, Sabat, M., Myers, W. H. *Chem. Sci.* **2014**, *5*, 4355-4366. DOI: 10.1039/C4SC01665C (other acknowledged grants are DOE BES grant for computational collaborator and grant for purchase of instrumentation)
3. "C–H Activation of Pyrazolyl Ligands by Ru(II)" Joslin, E. E., Quillian, B., Gunnoe, T. B.*, Cundari, T. R.*, Sabat, M., Myers, W. H. *Inorg. Chem.* **2014**, *53*, 6270-6279. DOI: 10.1021/ic500811n (other acknowledged grant is DOE BES grant for computational collaborator)
2. "Pt(II) Catalyzed Hydrophenylation of □-Olefins: Variation of Linear:Branched Products as a Function of Ligand Donor Ability" McKeown, B. A., Prince, B. M., Ramiro, Z., Gunnoe, T. B.*, Cundari, T. R.* *ACS Catalysis* **2014**, *4*, 1607-1615. DOI: 10.1021/cs400988w (other acknowledged grant is DOE BES grant for computational collaborator)

III. Jointly funded by this grant and other grants with relatively minor intellectual contribution from this grant

1. "Aerobic Epoxidation of Olefin by Platinum Catalysts Supported on Mesoporous Silica Nanoparticles" Munz, D., Wang, D., Moyer, M. M., Webster-Gardiner, M. S., Kunal, P., Watts, D., Trewyn, B. G.*, Vedernikov, A. N.*, Gunnoe, T. B.* *ACS Catalysis* **2016**, *6*, 4584–4593. DOI: 10.1021/acscatal.6b01532

Oliver Y. Gutiérrez

Catalytic and Electrocatalytic Conversion of Bio-Oil in Aqueous Phase at Mild Conditions

Oliver Y. Gutiérrez, Udishnu Sanyal, Nirala Singh, John Fulton, Charles Campbell, Nigel Browning, Layla Mehdi, Manh Thuong Nguyen, Vassiliki-Alexandra Glezakou, Roger Rousseau, Donald Camaioni, Johannes A. Lercher
Pacific Northwest National Laboratory, Physical and Computational Sciences Directorate and Institute for Integrated Catalysis, Richland, WA 99354, USA

Presentation Abstract

Understanding of catalytic reductions is critically needed to accelerate low temperature conversion processes that stabilize bio oils and thereby render them useful for synthesis of fuels and chemicals. Thus, this project aims to understand the conversion of oxygenated organic compounds under mild conditions utilizing external H_2 (catalytic hydrogenation) or cathodic potential (electrocatalytic hydrogenation) as sources of reduction equivalents.
Hydrogenation of model compounds, including phenols, aryl ethers and benzaldehyde, on carbon-supported noble metals were performed to elucidate mechanisms of the catalysis. The effects of temperature, hydrogen chemical potential (tuned either by H_2 pressure or cathodic potential), and nature of the metal on rates, coverages and state of the metal have been assessed by detailed kinetic investigations and physicochemical methods to characterize the state of the catalyst and of the reacting molecules, including X-ray adsorption spectroscopy and high-resolution scanning tunneling electron microscopy.

The work has shown high specificity of molecular structure and nature of the metal. For instance, aromatic rings in phenolic compounds undergo hydrogenation to cyclic aliphatic ketones, which are hydrogenated to the corresponding alcohols. In stark contrast, the carbonyl group in benzaldehyde is hydrogenated without hydrogenating the aromatic ring. The results suggest that hydrogenation of aromatic rings occurs via stepwise hydrogen addition to adsorbed species regardless of the origin of the hydrogen (proton reduction or H_2 dissociation). Interestingly, the electrocatalytic hydrogenation of carbonyl groups appears to involve a true electrochemical step, with lower reaction barriers than thermal catalysis. DFT-MD simulations are used to understand metal-reactant interactions and the observed reaction pathways.

Overall, electrocatalysis can provide higher conversion rates than thermal catalysis at mild reaction conditions. However, H_2 evolution is a prevalent side reaction that competes with the reduction of organic compounds limiting the efficiency of electrocatalytic reduction. The relative rates of hydrogenation and H_2 evolution are controlled by surface coverages of H and organic substrates, as well as the intrinsic rates of hydrogenation and H combination on the particular metals.

John Hartwig

Catalysis Program at Lawrence Berkeley National Laboratory: Harnessing Complexity for Catalytic Efficiency

Overview and Scope of the Program:

The overarching goal of the Catalysis Program at Lawrence Berkeley National Laboratory is to reveal new concepts that enable the design and synthesis of new catalysts, the understanding and design of new catalytic mechanisms, and the realization of new catalytic transformations. New concepts are needed to move the field of catalysis from empiricism to design and to advance the current design of catalysts to structures that enable new classes of reactions and make existing reactions more practical. The types of catalysts and the types of catalytic reactions studied by the Berkeley Catalysis Program, and the classes of mechanisms by which the catalysts react, are broad in scope but converge on several themes, which have been the focal point of investigations over the past several years. The three themes focus on the discovery and development new catalysts and catalytic processes involving multifunctional active sites, conducting catalysis in confined environments that alter the interactions of the substrate and catalyst, and integrated catalysis that combines two or more of homogeneous catalysis, heterogeneous catalysis, biocatalysis, and even informatics. Over the past three years, nine papers from this group appeared in or have been accepted to *Science*, *Nature* and *PNAS*.

The theme on multidimensional catalysis focuses on processes like the selective reactions at typically unreactive bonds (such as C-H bonds, C-C bonds, C=C bonds of unactivated alkenes, and the C=O bonds of carbon dioxide) and the selective conversion of alcohols derived from biomass. A majority of the transformations are being addressed by using multiple catalysts in multi-step processes, multiple catalytic sites in a single solid catalyst, multiple metals held by ligands designed to juxtapose two metals, and allosteric triggering of one metal by coordination of another to a distal atom of a ligand. Studies on single metal sites provide the foundation for this work on more complex catalytic systems. The theme on catalysis in confined environment was initiated by work focusing on catalysis within a supramolecular nanovessel, and success in this program has motivated research on a broader range of confined spaces, such as alternative supramolecular cages, zeolites, the pores of metal-organic frameworks (MOFs), the active sites of artificial enzymes, and whole cells. The third theme, termed “Integrated Catalysis” builds upon successes with catalysis in confined spaces, a growing capability of this Catalysis Program in biocatalysis, and a long-standing strength of LBNL in combining materials science with catalysis. Research on this topic encompasses the creation of artificial metalloenzymes and cyborgian cells that integrate materials with chemical biology to create artificial biosynthetic pathways.

Highlights from specific projects within these topics are described below.

Recent Results on Subtask 1: Multifunctional Catalytic Active Sites: New Systems, New Reactions, and New *Operando* Methods for Monitoring the Reactivity of Such Catalysts

Palladium-Catalyzed, Site-Selective Direct Allylation of Aryl C–H Bonds by Silver-Mediated C–H Activation: The functionalization of C-H bonds inevitably involves one step that cleaves the C-H bond and a second step that creates a functional group within the intermediate formed by C-H bond cleavage. One challenge facing the development of such processes is the need for the same catalyst to undergo both of these steps. An alternative approach is to create catalysts or catalytic systems in which these functions are separated into two sites. Although such separation of steps can occur in heterogeneous catalysts containing multiple metals and active sites, such catalytic functionalization by two homogeneous sites is rare. During the past few years, Hartwig discovered a system involving palladium and silver for the coupling of unactivated arenes with allylic esters (Figure 1). His mechanistic studies showed that the silver, not the palladium, cleaves the C-H bond, while the palladium leads to formation of the carbon-carbon bond in the product after transmetallation of an aryl group, formed by C-H bond cleavage at silver, to an allylpalladium intermediate.

Figure 1.

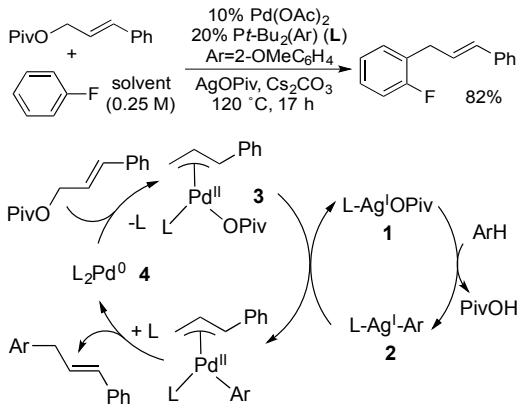

Mechanistic Investigation of Water Oxidation by a Molecular Cobalt Oxide Analogue and Manganese-Cobalt Oxido Cubanes: Oxide catalysts for the oxygen-evolution reaction (OER) are the essential water-splitting component in artificial photosynthesis. Investigations into the activity of these catalysts show that they are often more active after doping with a metal impurity or additive, suggesting that there are cooperative effects that influence OER mechanisms in heterometallic systems. However, the origins of such effects are not well understood. Tilley has sought well-defined complexes that can elucidate the origins of these effects.

Figure 2.

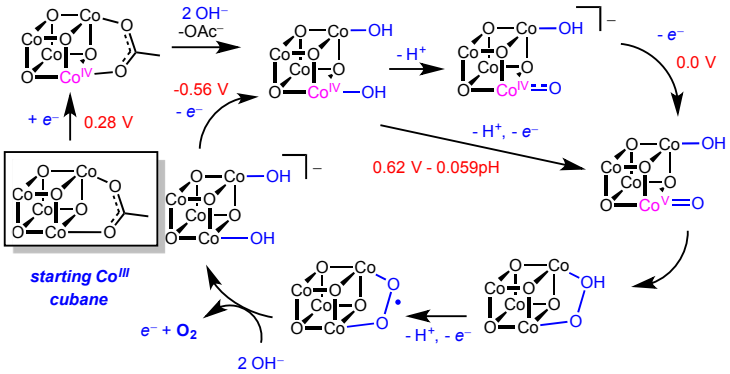

Recently, his group modeled the catalytic edge site of the layered oxide-hydroxide CoOOH with the molecular tetracobalt oxido cubane $Co_4(\square_3\text{–}O)_4(OAc)_4py_4$, which providee a rare, comprehensive, experimental elucidation of the mechanism of O–O bond formation by a well-defined model of the Mn-based site in photosystem II and heterogeneous Co systems (Figure 2).[1] Detailed kinetic studies and isotopic labeling implicated a formal Co^V oxidation state in the intermediate forming the O-O bond and the involvement of only terminal oxygen ligands (oxo,

hydroxyl, aquo) in the formation of O_2. The $[Co_4(\mu\text{-}O)_4(pyr)_4(OAc)_3]^+$ fragment remains intact and binds hydroxide (or water) to its surface, promoting proton-coupled electron transfers, and mediating O–O bond formation. The study of *hetero*metallic model oxido clusters would elucidate the mechanisms of reactions of more complex OER systems, but this endeavor is severely limited by the lack of rational synthetic routes to suitable mixed-metal species. An advance toward the goal of controlled preparation of *hetero*metallic model oxido clusters is the first syntheses of mixed manganese-cobalt oxido cubanes using a rational approach. These $[MnCo_3O_4]$ cubanes may be regarded as Mn-doped versions of the $[Co_4O_4]$ cubane OER catalyst, and serve as useful models for Mn-doped CoO_x. The new $[MnCo_3O_4]$-based clusters, e.g. $MnCo_3O_4(OAc)_5py_3$, are ligated by simple air- and water-stable carboxylate and pyridine ligands, and ligand exchange reactions allow systematic modifications of the Mn coordination sphere. Structural and spectroscopic studies of the clusters suggest an $[Mn(IV)Co(III)_3]$ electronic structure.[1-3]

Second-Sphere Functionalized Iron Porphyrins for Electrocatalytic Reduction of Carbon Dioxide: The development of catalysts based on earth-abundant metals that are capable of electrochemically converting carbon dioxide (CO_2) selectively into value added compounds remains one of the central challenges in the solar fuel community. Chris Chang has conducted a series of systematic studies that reveal with molecular structures the high degree of tunability of molecular electrocatalysts for this demanding reaction. Synthetic incorporation of protic functional groups in the secondary coordination sphere of iron polypyridine and porphyrin complexes enabled the development of non-heme and heme iron-based CO_2 electroreduction catalysts. They showed that small variations of the ligand backbone in two separate families of molecules resulted in drastically altered catalytic performances. This suite of molecular catalysts was generated using the base metal iron and the systems react with significant selectivities for the reduction of CO_2, even in the presence of large amounts of water.

Electrochemical Activation of CO_2 through Atomic Ordering Transformations of AuCu Nanoparticles: The structure and properties of multimetallic nanoparticles are highly tunable because their compositions can be controlled. For this reason, they have been studied for various catalytic applications in which their properties overcome the drawbacks of single component systems. In contrast to the simple combination of elements, in which they are randomly distributed, precise positioning of atoms in a crystal lattice becomes possible when a thermodynamically accessible phase exists. This positioning of atoms creates a distinction between a disordered alloy and an ordered intermetallic structure, and the transition between the two different phases is the, so called, order-disorder transformation.

Peidong Yang has focused on developing synthetic strategies to promote ordering transformations from the initial alloy and investigating the structure and properties of these ordered structures for applications in magnetism and catalysis (Figure 3). It has been shown that Au-Cu bimetallic systems exhibit electrocatalytic properties for CO_2 reduction controlled by their composition. Precise control of elemental configurations within

Figure 3

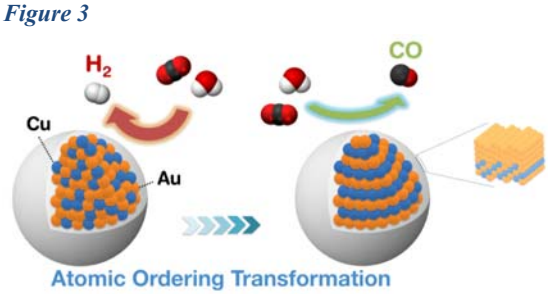

multimetallic nanoparticles could enable access to functional nanomaterials with significant performance benefits. This can be achieved down to the atomic level by the disorder-to-order transformation of individual nanoparticles. By systematically controlling the ordering degree, Yang showed that the atomic ordering transformation applied to AuCu nanoparticles activates them to act as selective electrocatalysts for CO_2 reduction. In contrast to the disordered alloy nanoparticle, which catalyzes hydrogen evolution, ordered AuCu nanoparticles selectively convert CO_2 to CO at a faradaic efficiency reaching 80%. CO formation was achieved with a reduction in overpotential of ~200 mV, and catalytic turnover was enhanced by 3.2-fold. In comparison to a pure gold catalyst, mass activities with respect to the use of elemental gold were also improved. Atomic level structural investigations revealed three atomic gold layers over the intermetallic core to be the origin of enhanced catalytic behavior. Furthermore, thermochemical DFT calculations suggest that the enhanced CO_2 reduction activities observed for ordered intermetallic AuCu nanoparticles arise from the compressively strained Au overlayers formed.

New Methods for Operando Studies of Catalytic Processes: Time-Resolved (2 s) Study of the Initial Steps of the Catalytic Hydrogenation of CO: From Branched Isomers to Unsaturated Molecules: Methods to obtain spectral data on catalytic reactions while they are occurring have been a recent focal point of heterogeneous catalysis, and the LBNL Catalysis Program has sought new methods for observation of such reactions. For example, Salmeron has been studying the structures of ruthenium catalysts supported on TiO_2 for methanation of CO_2. He has recently used ambient-pressure X-ray photoelectron spectroscopy to determine the chemical state of this catalyst under reaction conditions (Figure 4). The active state of ruthenium was found to be metallic, and monitoring of surface adsorbates in the steady state showed that CHx species, the growth units of C_nH_m hydrocarbon chains, were favored over adsorbed carbon monoxide at increasing temperatures.[4]

Figure 4.

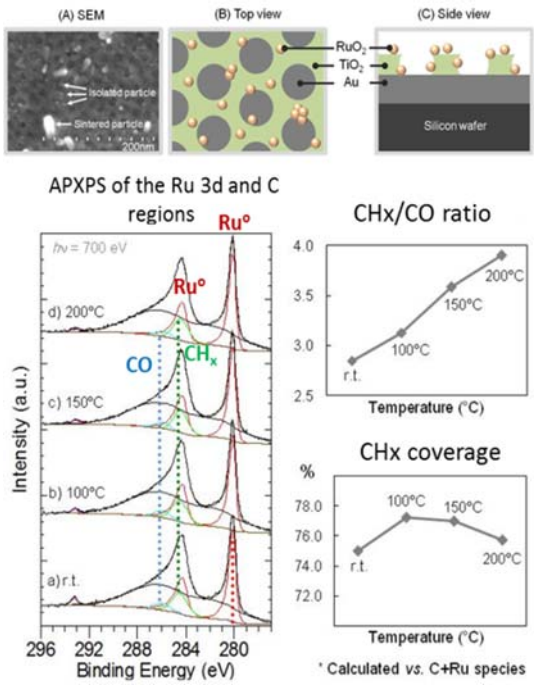

The catalytic hydrogenation of carbon monoxide, known as the Fischer−Tropsch process, is a technologically important, complex multipath reaction which produces long-chain hydrocarbons. To access the initial kinetics and the mechanism, Somojai developed a reactor that provides information under nonsteady state conditions. He tested a CoMgO catalyst for this process and monitored the initial product formation within 2 s of exposure to CO as well as the time dependence of high molecular weight products (in a 60 s window). He found a drastic change in the product selectivity over this time. The process formed branched isomers (C4 and C5) in the first 25 s without forming unsaturated products. A subsequent decline (at ~35 to 40 s) of branched isomers coincides with the detection of olefins (from C2 to C5), and these changes in product composition indicate a change in the reaction path.

Mapping Catalytic Reaction Sites with High Spatial Resolution using AFM-IR: In collaboration with Prof. Elad Gross (Hebrew University). Toste mapped the site-dependent reactivity of Pt atoms using synchrotron-sourced IR nanomicroscopy (Figure 5). Chemically-active self-assembled molecules (N-heterocyclic carbenes), with a functional hydroxyl group were anchored to the nanoparticle's surface. The oxidation of the functional -OH group from alcohol into acid and its reversible reduction back to alcohol on different surface sites were monitored under oxidizing and reducing conditions, respectively. This method provided nanometer (20-25nm) resolution catalyst sites and allowed for observation that low coordinated Pt atoms located along the nanoparticle's perimeter are more catalytically-active than Pt atoms found on the flat surface of the nanoparticle. The technique was also applied to study nitro-reduction on the surface of gold nanoparticle catalysts.

***Figure 5**. The combination of synchrotron infrared radiation with scattering, scanning near-field optical enables infrared spectroscopic investigations with nanometer spatial resolution.*

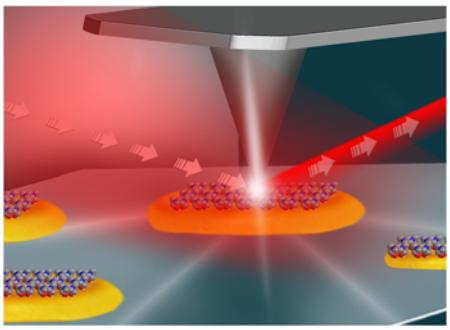

Subtask 2: Catalysis in Confined Spaces

Light-Driven Rearrangement of Confined Molecules Promoted by Photoinduced Electron Transfer from Supramolecular Host: By encapsulating a catalyst active site in a confined space, the interactions of the substrate with the catalyst, equilibria for generating reactive intermediates, and the selectivity of reaction intermediates can be altered. The Toste, Bergman and Raymond team showed that tetrahedral cages can absorb light and use this energy to induce reactions of encapsulated guests (Figure 6). Mechanistic studies suggest that the photoexcited bridging group of the supramolecular assembly donates electrons to bound guests via photoinduced electron transfer (PET), as evidenced by transient absorption spectroscopy and electrochemical measurements, which allowed estimation of a negative Gibbs energy for electron transfer. Using this platform, cinnamyl ammonium substrates underwent a 1,3-rearrangement to form the thermodynamically unfavored product. This reactivity was only observed by supramolecular photochemistry, in which confinement prevents separation of the amine and allyl cation intermediates, allowing them to recombine to afford the overall rearranged product.

***Figure 6**. M4L6-mediated photochemical 1,3-rearrangement of cinnamyl ammonium cations.*

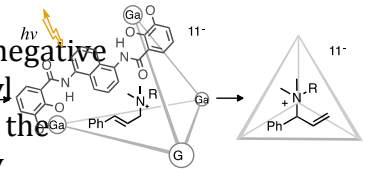

Supramolecular Assembly Catalyzes Carbon-Carbon Bond Formation from Organometallic Complexes up to 1 Million Times Faster: Enables Catalytic Process Previously Prohibited by Slow Reductive Elimination: Raymond, Bergman, and Toste have previously demonstrated that cationic transition metal complexes are readily encapsulated by the anionic Ga_4L_6 tetrahedral supramolecular host in water. In the past year, they demonstrated that supramolecular catalysis can be leveraged to enable new processes mediated by transition metals, through catalysis of individual events in a catalytic cycle. Initially, supramolecular catalysis of an elementary organometallic process that might be incorporated into a catalytic cycle was examined. It was discovered that the Ga_4L_6 supramolecular tetrahedra catalyzed alkyl-alkyl reductive elimination from gold(III) and platinum(II) complexes (Figure

7A). Moreover, the observed rate acceleration of 1.9 x 10^7 fold relative to background for reductive elimination from dimethylgold(III) complexes was the largest observed for a synthetic microenvironment catalyst. Subsequently, this property was leveraged to create a cross coupling reaction employing both a platinum catalyst and a nanovessel-based catalyst, in which both the cluster and a platinum precatalyst were necessary for efficient turnover. The full mechanistic details of this synergistic process were delineated through kinetic and structural analysis (Figure 7B).

***Figure** 7. Supramolecular catalysis of reductive elimination (B) Synergistic supramolecular and platinum catalysis of carbon-carbon bond formation.*

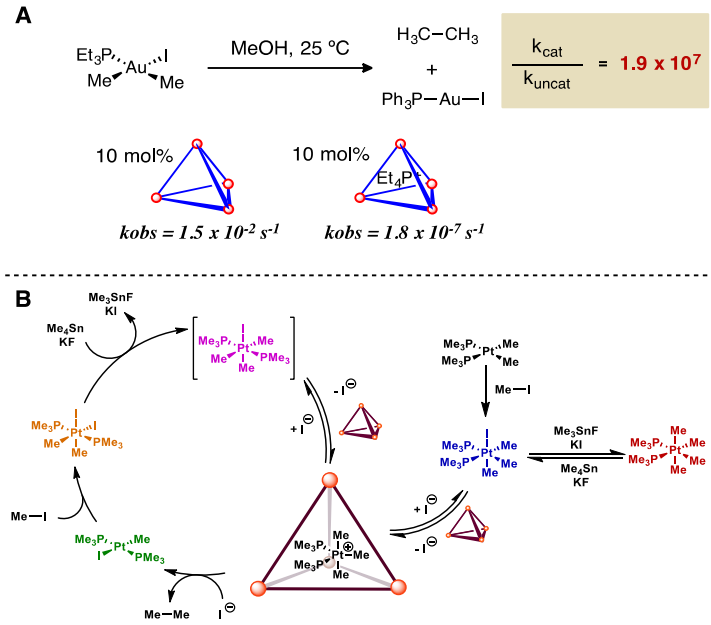

Redox-Based Reagents for Chemoselective Methionine Bioconjugation: The LBNL catalysis group also has sought methods to create new structures in which a catalyst component can be embedded in a biological milieu. To this end, Chang and Toste have sought methods for the bioconjugation of chemicals to cells and individual enzymes. Often, such bioconjugation is conducted with a cysteine owing to its nucleophilicity, but tethering chemicals through these thiols can inhibit the function of the protein. In contrast to the substantial body of literature on cysteine bioconjugation, analogous methods for methionine labeling under physiological conditions remain largely underdeveloped. A major chemical challenge in developing a selective methionine modification reaction under pH-neutral physiological conditions is its relatively weak nucleophilicity, which precludes identifying an appropriate methionine-specific electrophilic partner in the presence of competing, more nucleophilic amino acids. As such, they developed a strategy for bioconjugation to methionine that explits the redox reactivity and reported a method, termed Redox Activated Chemical Tagging (ReACT) that enables chemoselective methionine bioconjugation in proteins and proteomes.[5]

Metal Nanoparticles Catalyzed Selective Carbon-Carbon Bond Activation in the Liquid Phase: Encapsulated heterogeneous catalysts are unusual, and a collaboration between Toste and Somojai has led to system in which encapsulation of heterogeneous catalysts in organic polymers allows reactions of nanoparticles on soluble substrates in solution. Ring-opening reactions of cyclopropane derivatives were conducted under hydrogen catalyzed by metal nanoparticles (NPs) in the liquid phase catalyzed by 40-atom rhodium (Rh) NPs, encapsulated by dendrimer molecules and supported in mesoporous silica under hydrogen. The turnover frequency (TOF) was higher than that of other metals or the Rh homogeneous catalyst counterparts. Rh(0) acted as the active site in the NP, and the capping agent played facilitated the ring-opening reaction kinetics. Larger particle sizes tended to react with higher TOF for Rh NPs encapsulated in

either dendrimer or poly(vinylpyrrolidone). The generation of the dendrimer and surface group also affected the reaction rate and activation energy.

Synthetic Biology Approaches to Production of Value-Added Chemicals from Carbon Dioxide: The biological cell is an intricate confined space in which catalysis occurs, and such systems are being studied and exploited in the LBNL Catalysis Program. Michelle Chang has been working on synthetic biology approaches to utilize CO_2 as a building block for production of value-added chemicals. Although photosynthetic CO_2 fixation has been the major focus in the use of living systems for CO2 conversion, there are a large number of organisms that are capable of fixing CO_2 without light input and using electrons either in the form of direct current or H_2 as an energy source (Figure 8). Chang has been developing methods to engineer these hosts for new biosynthetic capa–city and to transplant the CO_2-fixation pathways into more routine industrial microbes, such as *Escherichia coli*. Chang has used RNA sequencing to uncover differential gene regulation under CO_2 - compared to sugar-fed growth conditions and observed upregulation of all known genes involved in the Wood-Ljungdahl pathway for CO_2 fixation. Methanogens also use the Wood-Ljungdahl pathway to produce the key acetyl coenzyme A (CoA) building blocks, but their physiology provides better support for developing downstream pathways that use acetyl-CoA to make complex small molecule targets. She have developed methods to express multiple genes at levels similar to *E. coli*, which is a key advance for pathway engineering and has shown that redox cofactor availability is the key limitation and that cellular NAD(P)H can be increased by manipulating the biosynthetic pathway to produce nicotinamide cofactors.

Figure 8. *CO_2 metabolism in cells. (A) Autotrophs fix CO_2 as a carbon source and utilize either light or hydrogen to produce reducing equivalents to power biosynthesis. (B) Engineering of acetogens to take advantage of the acetyl-CoA pool to provide a key building block for biosynthesis.*

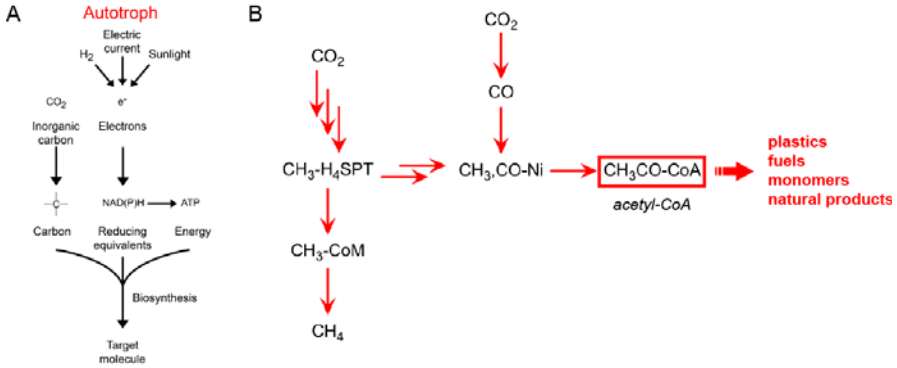

Subtask 3. Integration of Catalytic Processes

Abiological Catalysis Artificial Haem Proteins Containing Noble Metals in Place of Iron Having the Kinetics of Natural Enzymes: During the past three years, Hartwig and Clark have built a productive[6-8] collaborative program on the creation of artificial metalloenzymes. Catalysis by enzymes and transition metals enables modern strategies in organic synthesis.[9] However, natural metalloenzymes are rarely used in synthetic chemistry, in part due to the limited scope of reactions that they catalyze. To expand the utility of metalloenzymes, two approaches have been followed in the past. One approach exploits the promiscuity of enzymes and enhances this reactivity by directed evolution.[10] The second creates artificial metalloenzymes by affixing abiological metal complexes within proteins.[11-12]

At the intersection of these approaches lies a third strategy that Hartwig and Clark have followed: the substitution of just the native metal of a natural metalloenzyme with an abiological metal.[13-17] This strategy introduces a new metal and its accompanying reactivity into the system while retaining the natural, evolvable substrate-binding site of the protein scaffold. Following this approach, they have created and then evolved in the laboratory artificial metalloenzymes formed by replacing the iron in the porphyrin (PIX) cofactor of heme proteins with metals ([M]) not found in nature. To evaluate rapidly the activity of artificial [M]-PIX enzymes carrying diverse metals, they created an array of catalysts by combining various mutants of apo myoglobin and various [M]-PIX cofactors in a combinatorial fashion. By this method, they obtained Fe(Cl)-, Co(Cl)-, Cu-, Mn(Cl)-, Rh-, Ir(Cl)-, Ir(Me)-, Ru(CO)- and Ag variants of myoglobin mutants carrying various coordinating and non-coordinating amino acids at the position of the axial ligand (Figure 9). This catalyst array was assayed for activity in the model reaction to convert diazoesters to chiral benzofurans. Myoglobins (myo) containing non-native metals formed active catalysts, instead of those containing iron. The artificial metalloenzymes containing an Ir(Me)-PIX cofactor were the most active. To demonstrate that these artificial enzymes could be evolved to select for selective systems, they sought to evolve the catalysts for enantioselective C-H bond functionalization. Indeed, mutants of Ir(Me)-PIX-Myo were identified that form either enantiomer of seven benzofuran congeners with up to 92:8 er, 7,200 TON, and 97% yield.

Figure 9. Artificial metalloenzyme bearing an Ir porphyrin core in place of nature Fe heme.

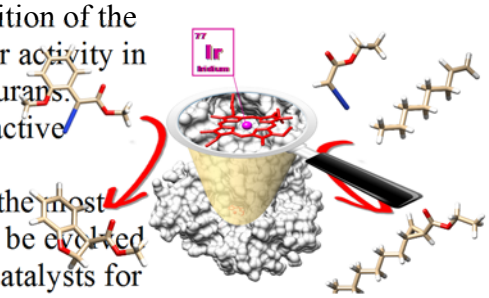

To create Ir(Me)-PIX enzymes with stronger similarity to the activity and selectivity of natural enzymes, the myoglobin scaffold was replaced with that of CYP119, a thermally stable P450 designed by nature to bind and react with organic substrates. Indeed, variants of Ir(Me)-CYP119 created by laboratory evolution catalyzed the same intramolecular C-H insertion reactions as those catalyzed by myoglobin, but with up to 98% ee. Moreover, substrates with sterically hindered or unactivated C-H bonds also reacted in the presence of Ir(Me)-PIX CYP119 variants. Intermolecular insertion reactions of carbenes into C-H bonds were catalyzed efficiently by Ir(Me)-PIX CYP119 variants. Upon applying directed evolution to improve the activity of Ir(Me)-PIX enzymes, Hartwig and Clark identified a mutant that forms benzofuran products with 2250 turnovers per hour, 35000 total turnovers and enzyme efficiency (k_{cat}/K_M) that is more than 1000 times greater than that of any artificial metalloenzyme created previously. Moreover, this variant is the first selective artificial metalloenzyme to react with kinetic parameters comparable to those of natural enzymes. Subsequent studies revealed that Ir(Me)-PIX enzymes catalyze cyclopropanation[8] and amination[18] reactions. They catalyze the cyclopropanation of both activated and unactivated, as well as terminal and internal, alkenes, which is a much broader scope of substrates than those that react with Fe-P450s. Ir(Me)-PIX CYP119 variants catalyze cyclopropanation reactions with up to 99% ee, 99.5% de, and 76% yield. Ir(Me)-PIX CYP119s also are highly chemoselective catalysts for the insertion of nitrenes into C-H bonds. In sharp contrast to Fe-P450s that produce equal or greater amounts of sulfonamide byproducts, Ir(Me)-PIX CYP119s catalyze the same transformation with > 25:1 selectivity for desired product sultam over the sulfonamide. Together, these results demonstrate that the replacement of the

metal in porphyrin-binding enzymes is an effective strategy to create artificial metalloenzymes that are suitable for evolution to generate enzymes that catalyze abiological reactions with levels of activity and selectivity that can reach those of natural enzymes. Considering the rich chemistry of metalloporphyrins, this methodology should seed the creation of many artificial metalloenzymes with diverse reactivity.

Snap Deconvolution – Combining Chemical Design and Informatics for High Throughput Discovery of Catalytic Reactions: Despite efforts to develop high-throughput discovery of new reactions, most existing methods are restricted to specific classes of reactions, require expensive technology, or require extensive pre-functionalization of starting materials or laborious workup of reaction mixtures. Herein we present a new approach to conduct multidimensional high throughput experiments for catalyst discovery that combines chemical methods with information technology to automate the analysis and interpretation of mass spectral data. By this approach, chemically inert and electronically innocent substituents enable identification of the reactants that form an unknown product by comparing the molecular masses of the products formed from multiple sets of reactants containing the same functional groups but different substituents. With this novel HT method, we discovered a previously unknown reaction between two components in the mixture, the hydroallylation of alkynes, and an unknown nickel-catalyzed variant of a reaction between three-components in the mixture, the diarylation of an alkyne (Figure 10).

Figure 10*. The principle of Snap Deconvolution: differences in masses of the products of a reaction occurring in α, β, and γ sets of substrates are distinct and allow to the reactants that form a product to be identified. Thus, a computer program is able to identify chemical reactions by pairwise comparison of peaks in the GC/MS spectra of reaction mixtures.*

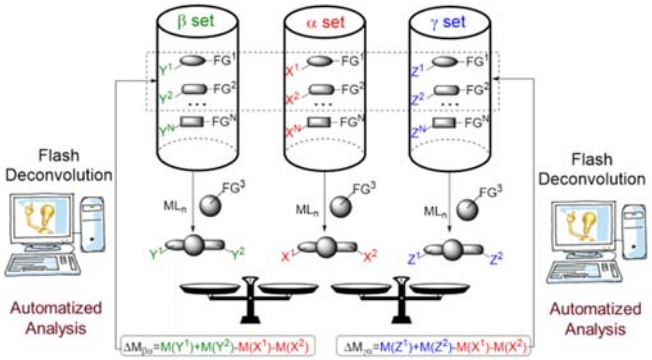

Citations

1. Nguyen, A. I.; Ziegler, M. S.; Oña-Burgos, P.; Sturzbecher-Hohne, M.; Kim, W.; Bellone, D. E.; Tilley, T. D., Mechanistic Investigations of Water Oxidation by a Molecular Cobalt Oxide Analogue: Evidence for a Highly Oxidized Intermediate and Exclusive Terminal Oxo Participation. *J. Am. Chem. Soc.* **2015,** *137*, 12865-12872. **DOI**: 10.1021/jacs.5b08396

2. Nguyen, A. I.; Wang, J.; Levine, D. S.; Ziegler, M. S.; Tilley, T. D., Control and Empirical Prediction of Redox Potentials for Co_4O_4 Cubanes over a 1400 mV Range: Implications for the Feasibility of a Co(V)-Oxo Species. *Chem. Sci.* **2017,** *in press*. **DOI**: 10.1039/C7SC00627F

3. Nguyen, A. I.; Suess, D. L. M.; Darago, L. E.; Oyala, P. H.; Levine, D. S.; Ziegler, M. S.; Britt, R. D.; Tilley, T. D., Manganese-Cobalt Oxido Cubanes Relevant to Manganese-Doped Water Oxidation Catalysts. *J. Am. Chem. Soc.* **2017,** *139*, 5579–5587. **DOI**: 10.1021/jacs.7b01792

4. Carenco, S.; Sassoye, C.; Faustini, M.; Eloy, P.; Debecker, D. P.; Bluhm, H.; Salmeron., M., The Active State of Supported Ruthenium Oxide Nanoparticles during Carbon Dioxide Methanation. *J. Phys. Chem. C* **2016,** *120*, 15354–15361.
5. Lin, S.; Yang, X.; Jia, S.; Weeks, A. M.; Hornsby, M.; Lee, P. S.; Nichiporuk, R. V.; Iavarone, A. T.; Wells, J. A.; Toste, F. D.; Chang, C. J., Redox-Based Reagents For Chemoselective Methionine Bioconjugation. *Science* **2017,** *355*, 597-602.
6. Key, H. M.; Dydio, P.; Clark, D. S.; Hartwig, J. F., Abiological Catalysis by Artificial Haem Proteins containing Noble Metals in Place of Iron. *Nature* **2016,** *534* (7608), 534-537. **DOI**: 10.1038/nature17968
7. Dydio, P.; Key, H. M.; Nazarenko, A.; Rha, J. Y.-E.; Seyedkazemi, V.; Clark, D. S.; Hartwig, J. F., An Artificial Metalloenzyme with the Kinetics of Native Enzymes. *Science* **2016**, in press.
8. Key, H. M.; Dydio, P.; Liu, Z.; Rha, J. Y. E.; Nazarenko, A.; Seyedkazemi, V.; Clark, D. S.; Hartwig, J. F., Beyond Iron: Iridium-Containing P450 Enzymes for Selective Cyclopropanations of Structurally Diverse Alkenes. *ACS Central Science* **2017,** *in press*.
9. Hartwig, J. F., *Organotransition Metal Chemistry*. Univ Science Books: 2010.
10. Hyster, T. K.; Arnold, F. H., P450BM3-Axial Mutations: A Gateway to Non-Natural Reactivity. *Isr. J. Chem* **2015,** *55* (1), 14.
11. Lewis, J. C., Artificial Metalloenzymes and Metallopeptide Catalysts for Organic Synthesis. *ACS Catal.* **2013,** *3* (12), 2954.
12. Ringenberg, M. R.; Ward, T. R., Merging the Best of Two Worlds: Artificial Metalloenzymes for Enantioselective catalysis. *Chem. Comm.* **2011,** *47* (30), 8470.
13. Abe, S.; Hirata, K.; Ueno, T.; Morino, K.; Shimizu, N.; Yamamoto, M.; Takata, M.; Yashima, E.; Watanabe, Y., Polymerization of Phenylacetylene by Rhodium Complexes within a Discrete Space of apo-Ferritin. *J. Am. Chem. Soc.* **2009,** *131* (20), 6958.
14. Bordeaux, M.; Singh, R.; Fasan, R., Intramolecular C(*sp3*)-H Amination of Arylsulfonyl Azides with Engineered and Artificial Myoglobin-based Catalysts. *Bioorg. Med. Chem.* **2014,** *22* (20), 5697.
15. Jing, Q.; Kazlauskas, R. J., Regioselective Hydroformylation of Styrene Using Rhodium-Substituted Carbonic Anhydrase. *Chem. Cat. Chem.* **2010,** *2* (8), 953.
16. Jing, Q.; Okrasa, K.; Kazlauskas, R. J., Stereoselective Hydrogenation of Olefins Using Rhodium-Substituted Carbonic Anhydrase—A New Reductase. *Chem. Eur. J.* **2009,** *15* (6), 1370.
17. Oohora, K.; Kihira, Y.; Mizohata, E.; Inoue, T.; Hayashi, T., C(*sp3*)−H Bond Hydroxylation Catalyzed by Myoglobin Reconstituted with Manganese Porphycene. *J. Am. Chem. Soc.* **2013,** *135* (46), 17282.
18. Dydio, P.; Key, H. M.; Hayashi, H.; Clark, D. S.; Hartwig, J. F., Chemoselective, Enzymatic C–H Bond Amination Catalyzed by a Cytochrome P450 Containing an Ir(Me)-PIX Cofactor. *J. Am. Chem. Soc.* **2017,** *139* (5), 1750-1753.

Catalysis Program Publications 2015–2017

2015

1. Ahn, H.S.; Yano, J.; Tilley, T. D., Water Oxidation by Cobalt Centers on Various Oxide Surfaces: The Effects of Oxide Surface Acidity and Oxygen Atom Affinity on Catalysis. *ACS Catal.,* **2015**, *5*, 2573–2576. DOI: 10.1021/cs502120f.

2. Alayoglu, S.; Somorjai, G.A., Ambient Pressure X-ray Spectroscopy for Probing Monometallic, Bimetallic, and Oxide-Metal Catalysts under Reactive Atmosphere and Catalytic Reaction Conditions. *Topics in Catalysis,* **2015***, 59* (5), 420–438. DOI: 10.1007/s11244-015-0534-2.

3. Balakrishnan, M.; Sacia, E R.; Sreekumar, S.; Gunbas, G.; Gokhale, A.A.; Scown, C.D.; Toste, F.D.; Bell, A.T., Novel Pathways for Fuels and Lubricants from Biomass Optimized using Life Cycle Greenhouse Gas Assessment. *Proc. Natl. Acad. Sci*., **2015,** *112*, 7645. DOI: 10.1073/pnas.1508274112

4. Beaumont, S.; Somorjai, G.A., Conquering Catalyst Complexity: Nanoparticle Synthesis and Instrument Development for Molecular and Atomistic Characterization under *In situ* Conditions. *Topics in Catalysis,* **2015***, 58,* 560–572. DOI: 10.1007/s11244-015-0398-5.

5. Brown, C.; Toste, F.D.; Bergman, R.G.; Raymond, K.N., Supramolecular Catalysis in Metal-Ligand Cluster Hosts. *Chem. Rev.,* **2015**, *115*, 3012. DOI: 10.1021/cr4001226.

6. Brown, C.J.; Bergman, R.G.; Toste, F.D.; Raymond, K.N., Supramolecular Catalysis in Metal-Ligand Cluster Hosts. *Chem. Rev.*, **2015**, 115, 3012–3035. DOI: 10.1002/chin.201529299.

7. Carenco, S.; Wu, C.-H.; Shavorskiy, A.; Alayoglu, S.; Somorjai, G.A.; Bluhm, H.; Salmeron, M., Chemical and Structural Evolution of Nickel-Cobalt Nanoparticles for Oxygenate Selectivity in CO_2-based Fischer-Tropsch Synthesis. *Small,* **2015**, *11* (25), 3045–3053. DOI: 10.1002/smll.201402795.

8. Chantarojsiri, T.; Sun, Y.; Long, J.R.; Chang, C.J., Water-Soluble Iron(IV)-Oxo Complexes Supported by Pentapyridine Ligands: Axial Ligand Effects on Hydrogen Atom and Oxygen Atom Transfer Reactivity. *Inorg. Chem.,* **2015**, *54*, 5879–5887. DOI: 10.1021/acs.inorgchem.5b00658.

9. Dalton, D.M.; Ellis, S.R.; Nichols, E.M.; Mathies, R.A.; Toste, F.D.; Raymond, K.N.; Bergman, R.G., Supramolecular $Ga_4L_6^{12-}$ Cage Photosensitizes 1,3-Rearrangement of Encapsulated Guest via Photoinduced Electron Transfer. *J. Am. Chem. Soc.,* **2015**, *137*, 10128. DOI: 10.1021/jacs.5b06317.

10. Davenport, T.C.; Tilley, T.D., Dinuclear First-Row Transition Metal Complexes with a Naphthyridine-Based Dinucleating Ligand. *Dalton Trans.,* **2015**, *44*, 12244–12255. DOI: 10.1039/c4dt02727b.

11. Gross, E.; Somorjai, G.A., Molecular Catalysis Science: Nanoparticle Synthesis and Instrument Development for Studies under Reaction Conditions. *J. Catalysis.,* **2015***, 328*, 91–101. DOI: 10.1016/j.jcat.2014.12.031.

12. Gross, E.; Toste, F.D.; Somorjai, G.A., Polymer-encapsulated Metallic Nanoparticles as a Bridge between Homogeneous and Heterogeneous Catalysis. *Cat. Lett.,* **2015**, *145,* 126–138. DOI: 10.1007/s10562-014-1436-9.

13. Hart-Cooper, W.M.; Zhao, C.; R. Triano, M.; Yaghoubi, P.; Haxel, L.; Buford, K.N.; Toste, F.D.; Bergman, R.G.; Raymond, K.N., The Effect of Host Structure of the Selectivity and Mechanism of Catalytic Intramolecular Prins Cyclizations. *Chem. Sci.,* **2015**, *6*, 1383. DOI: 10.1039/c4sc02735c.

14. Hart-Cooper, W.; Carmelo, S.; Perrin, C.L.; Toste, F.D.; Bergman, R.G.; Raymond, K.N., Protein-like Proton Exchange in a Synthetic Host Cavity. *PNAS*, **2015**, *112*, 15303–15307. DOI: 10.1073/pnas.1515639112.

15. Johnson, G.R.; Bell, A.T., Role of ZrO_2 in Promoting the Activity and Selectivity of Co-Based Fischer–Tropsch. *ACS Catal*., **2015**, *6*, 100–114. DOI: 10.1021/acscatal.5b02205.

16. Johnson, G.R.; Werner, S.; Bell, A.T., An Investigation into the Effects of Mn Promotion on the Activity and Selectivity of Co/SiO_2 for Fischer-Tropsch Synthesis: Evidence for Enhanced CO Adsorption and Dissociation. *ACS Catal.*, **2015**, *5*, 5888–5903. DOI: 10.1021/acscatal.5b01578.

17. Jurss, J. W.; Khnayzer, R.S.; Panetier, J.A.; El Roz, K.A.; Nichols, E.M.; Head-Gordon, M.; Long, J.R.; Castellano, F.N.; Chang, C.J., Bioinspired Design of Redox-Active Ligands for Multielectron Catalysis: Effects of Positioning Pyrazine Reservoirs on Cobalt for Electro- and Photocatalytic Generation of Hydrogen from Water. *Chem. Sci.,* **2015**, *6*, 4954–4972. DOI: 10.1039/C5SC01414J.

18. Kaphan, D.M.; Levin, M.D.; Bergman, R.G.; Raymond, K.N.; Toste, F.D., A Supramolecular Microenvironment Strategy for Transition Metal Catalysis. *Science*, **2015**, *350,* 1235–1238. DOI: 10.1126/science.aad3087.

19. Key, H.M.; Clark, D.S.; Hartwig, J.F., Generation, Characterization, and Tunable Reactivity of Organometallic Fragments Bound to a Protein Ligand. *J. Am. Chem. Soc.*, **2015**, *137*, 8261–8268. DOI: 10.1021/jacs.5b04431.

20. Levine, D.S.; Tilley, T.D.; Andersen, R.A., Intermolecular C–H Bond Activations by Monoanionic, PNP-Supported Scandium Dialkyl Complexes. *Organometallics,* **2015**, *34*, 4647–4655. DOI: 10.1021/acs.organomet.5b00213.

21. Li, C.S.; Melaet, G.; Ralston, W.T.; An, K.; Brooks, C.; Ye, Y.; Liu, Y. S.; Zhu, J.; Guo, J.; Alayoglu, S.; Somorjai, G.A., High Performance Hybrid Oxide Catalyst of Manganese and Cobalt for Low Pressure Methanol Synthesis. *Nature Comm.,* **2015***, 6,* 6538. DOI: 10.1038/ncomms7538.

22. Liberman-Martin, A.L.; Bergman, R.G.; Tilley, T.D., Lewis Acidity of Bis(perfluoro–catecholato)silane: Aldehyde Hydrosilylation Catalyzed by a Neutral Silicon Compound. *J. Am. Chem. Soc.,* **2015**, *137*, 5328–5331. DOI: 10.1021/jacs.5b02807.

23. Lin, S.; Diercks, C.S.; Zhang, Y.; Kornienko, N.; Nichols, E.M.; Zhao, Y.; Paris, A.R.; Kim, D.; Yang, P.; Yaghi, O.M.; Chang, C.J., Covalent Organic Frameworks Comprising Cobalt Porphyrins for Catalytic Co_2 Reduction in Water. *Science,* **2015**, *346*, 1208–1213 DOI: 10.1126/science.aac8343.

24. Liu, C.; Gallagher, J.J.; Sakimoto, K.K.; Nichols, E.M.; Chang, C. J.; Chang, M.C.Y.; Yang, P., Nanowire–bacteria Hybrids for Unassisted Solar Carbon Dioxide Fixation to Value-Added Chemicals, *Nano Lett.* **2015**, *15*, 3634–3639. DOI: 10.1021/acs.nanolett.5b01254.

25. Musselwhite, N.; Na, K.; Sabyrov, K.; Alayoglu, S.; Somorjai, G.A., Mesoporous Aluminosilicate Catalysts for the Selective Isomerization of n-Hexane: The Role of Surface Acidity and Platinum Metal. *J. Am. Chem. Soc.,* **2015**, *137* (32), 10231–10237. DOI: 10.1021/jacs.5b04808.

26. Musselwhite, N.; Somorjai, G.A., Atomic Scale Foundation of Covalent and Acid-base Catalysis in Reaction Selectivity and Turnover Rate. *Topics in Catalysis,* **2015***, 58,* 184–189. DOI: 10.1007/s11244-014-0356-6.

27. Na, K.; Somorjai, G.A., Hierarchically Nanoporous Zeolites and Their Heterogeneous Catalysis Current Status and Future Perspective. *Cat. Lett.,* **2015**, *145,* 193–213. DOI: 10.1007/s10562-014-1411-5.

28. Nguyen, A.I.; Ziegler, M.S.; Oña-Burgos, P.; Sturzbecher-Hohne, M.; Kim, W.; Bellone, D.E.; Tilley, T.D., Mechanistic Investigation of Water Oxidation by a Molecular Cobalt Oxide Analogue: Evidence for a Highly Oxidized Intermediate and Exclusive Terminal Oxo Participation. *J. Am. Chem. Soc.,* **2015**, *137*, 12865–12872. DOI: 10.1021/jacs.5b08396.

29. Nichols, E.M.; Gallagher, J.J.; Liu, C.; Su, Y.; Resasco, J.; Yi, Y.; Sun, Y.; Yang, P.; Chang; M.C.Y.; Chang, C.J., Hybrid Bioinorganic Approach to Solar-to-Chemical Conversion, *Proc. Natl. Acad. Sci. U.S.A.* **2015**, *112*, 11461–11466.

30. Park, J.Y.; Baker, L.R.; Somorjai, G.A., The Role of Hot Electrons in Surface Chemistry and Catalytic Reactions. *Chem. Rev.,* **2015***, 115* (8), 2781–2817. DOI: 10.1021/cr400311p.

31. Schramm, Y.; Takeuchi, M.; Semba, K.; Nakao, Y.; Hartwig, J.F., Anti-Markovnikov Hydroheteroarylation of Unactivated Alkenes with Indoles, Pyrroles, Benzofurans, and Furans Catalyzed by a Nickel–*N*-Heterocyclic Carbene System. *J. Am. Chem. Soc.*, **2015**, *137*, 12215–12218. DOI: 10.1021/jacs.5b08039.

32. Shu, X-Z.; Nguyen, S. C.; He, Y.; Oba, F.; Zhang, Q.; Canlas, C.; Somorjai, G. A.; Alivisatos, A.P.; Toste, F.D. Silica-Supported Cationic Gold(I) Complexes as Heterogeneous Catalysts for Regio- and Enantioselective Lactonization Reactions. *J. Am. Chem. Soc*., **2015**, *115*, 708. DOI: 10.1021/jacs.5b04294.

33. Zee, D. Z.; Chantarojsiri, T.; Long, J.R.; Chang, C.J., Metal-Polypyridyl Catalysts for Electro- and Photochemical Reduction of Water to Hydrogen. *Acc. Chem. Res.,* **2015**, *48*, 2027–2036 DOI: 10.1021/acs.accounts.5b00082.

34. Chen, S.; Mercado, B.Q.; Bergman, R.G.; Ellman, J.A., Regio- and Diastereoselective Synthesis of Highly Substituted, Oxygenated Piperidines from Tetrahydropyridines. *J. Org. Chem.,* **2015**, *80*, 6660–6668. DOI: 10.1021/acs.joc.5b00816.

35. Cheng, Lei; Wu, Cheng Hao; Jarry, Angelique; Chen, Wei; Ye, Yifan; Zhu, Junfa; Kostecki, Robert; Persson, Kristin; Guo, Jinghua; Salmeron, Miquel; Chen, Guoying; Doeff, Marca. Interrelationships among Grain Size, Surface Composition, Air Stability and Interfacial Resistance of Al-substituted $Li_7La_3Zr_2O_{12}$ Solid Electrolytes. *ACS Applied Materials & Interfaces,* **2015**, *7*, 17649−17655. DOI: 10.1021/acsami.5b02528.*Collaboration with Marca Doeff project in the Energy Efficiency and Renewable Energy, Office of Vehicle Technologies, U.S. Department of Energy under contract no. DE-AC02-05CH11231*.

36. Choi, K.M.; Na, K.; Somorjai, G.A.; Yaghi, O., Chemical Environment Control and Enhanced Catalytic Performance of Platinum Nanoparticles Embedded in Nanocrystalline Metal-Organic Frameworks. *J. Am. Chem. Soc.,* **2015**, *137* (24), 7810–7816. DOI: 10.1021/jacs.5b03540. *The study of the enhanced catalytic performance of metal-organic framework in the presence of platinum was carried out by this FWP.*

37. Kaphan, D.M.; Toste, F.D.; Bergman, R.G.; Raymond, K.N., Enabling New Modes of Reactivity via Constrictive Binding in a Supramolecular-Assembly-Catalyzed Aza-Prins Cyclization. *J. Am. Chem. Soc.*, **2015**, *137*, 9202–9205. DOI: 10.1021/jacs.5b01261. *Fellowship support from NIH Basic Medical Sciences.*

38. Kornienko, N.; Zhao, Y.; Kley, C.S.; Zhu, C.; Kim, D.; Lin, S.; Chang, C.J.; Yaghi, O.M.; Yang, P., Metal–Organic Frameworks for Electrocatalytic Reduction of Carbon Dioxide. *J. Am. Chem. Soc.,* **2015**, *137*, 14129–14135 DOI: 10.1021/jacs.5b08212. *Efforts by C.J.C. laboratory involve data acquisition and analysis on the electrocatalytic CO_2 reduction results.*

39. Lee, H.; Nedrygailov, L.; Lee, C.; Somorjai, G.A.; Park, J.Y., Chemical Reaction-induced Hot Electron Flows on Pt Colloid Nanoparticles under Hydrogen Oxidation: Impact of Nanoparticle Size. *Angewandte Chemie Int. Ed.,* **2015**, *15*, 2340–2344. DOI: 10.1002/anie.201410951. *Size dependent Pt nanoparticle activity stidoes of hydrogen oxidation was carried out by this FWP.*

40. Liu, C.; Gallagher, J.J.; Sakimoto, K.K.; Nichols, E.M.; Chang, C.J.; Chang, M.C.Y.; Yang, P., Nanowire–Bacteria Hybrids for Unassisted Solar Carbon Dioxide Fixation to Value-Added Chemicals. *Nano Lett.,* **2015**, *15*, 3634–3639. DOI: 10.1021/acs.nanolett.5b01254. *Efforts by C.J.C. laboratory involve data acquisition and analysis of the CO_2 reduction products from hybrid systems.*

2016

1. Brown, C. J.; Kokai, A.; Miller, G. M.; Bergman, R. G.; Raymond, K. N., Improved Scope and Diastereoselectivity of C-H Activation in an Expanded Supramolecular Host. *Supramol. Chem.*, **2016**, 28*,* 188–191. DOI: 10.1080/10610278.2015.1122196.

2. Cao, Z.; Kim, D.; Yu, Y.; Xu, J.; Lin, S.; Wen, X.; Nichols, E. M.; Jeong, K.; Reimer, J. A.; Yang, P.; Chang, C. J. , A Molecular Surface Functionalization Approach to Tuning Nanoparticle Electrocatalysts for Carbon Dioxide Reduction, *J. Am. Chem. Soc.,* **2016**, *138*, 8120–8125. DOI: 10.1021/jacs.6b02878.

3. Carenco, S.; Capucine Sassoye; Marco Faustini; Pierre Eloy; Damien P. Debecker; Hendrik Bluhm; Miquel Salmeron., The Active State of Supported Ruthenium Oxide Nanoparticles during Carbon Dioxide Methanation. *J. Phys. Chem. C*, **2016,** *120* (28), 15354–15361. DOI**:** 10.1021/acs.jpcc.6b06313.

4. Dombrowski, J. P.; Johnson, G. R.; Bell, A. T.; Tilley, T. D., $Ga[OSi(O^tBu)_3]_3$•THF, A Thermolytic Molecular Precursor for High Surface Area Gallium-Containing Silica Materials of Controlled Dispersion and Stoichiometry. *Dalton Trans.,* **2016**, *45*, 11025–11034. DOI: 10.1039/C6DT01676F.

5. Dong, Y.; Lipschutz, M. I.; Tilley, T. D. Regioselective, Transition Metal-Free C–O Coupling Reactions involving Aryne Intermediates. *Org. Lett.,* **2016**, *18*, 1530–1533. DOI: 10.1021/acs.orglett.6b00183.

6. Goulas, K. A.; Sreekumar, S.; Song, Y.; Kharidehal, P.; Gunbas, G.; Dietrich, P. J.; Johnson, G. R.; Wang, Y. C.; Grippo, A. M.; Grabow, L. C.; Gokhale, A. A.; Toste, F. D., Synergistic Effects in Bimetallic Palladium-Copper Catalysts Improve Selectivity in Oxygenate Coupling Reactions. *J. Am. Chem. Soc*., **2016**, *138*, 6805. DOI: 10.1021/jacs.6b02247.

7. Ho, C.; Shylesh, S.; Bell, A. T., Mechanism and Kinetics of Ethanol Coupling to Butanol over Hydroxyapatite. *ACS Catal*., **2016**, *6*, 938–949. DOI: *10.1021/acscatal.5b02672*.

8. Howell, J.; Li, Y.-P.; Bell, A. T., Propene Metathesis over Supported Tungsten Oxide Catalysts: A Study of Active Site Formation. *ACS Catal*., **2016**, DOI: 10.1021/acscatal.6b01842.

9. Johnson, G. R.; Bell, A. T., Effects of Lewis Acidity of Metal-Oxide Promoters on the Activity and Selectivity of Co-Based Fischer-Tropsch Catalysts. *J. Catal*., **2016**, *338*, 250–264. DOI**:** 10.1016/j.jcat.2016.03.022.

10. Landry, A.M.; Iglesia, E., Synthesis of Bimetallic AuPt Clusters with Clean Surfaces via Sequential Displacement-Reduction Processes. *Chem. Mater.*, **2016**, *28*, 2872–5886. DOI: 10.1021/acs.chemmater.6b02346.

11. Landry, A.M.; Iglesia, E., Displacement-reduction Routes to PtPd Clusters and Mechanistic Inferences for the Synthesis of other Bimetallic Compositions. *J. Cat.*, **2016**, *344*, 389–400. DOI: 10.1016/j.jcat.2016.10.007.

12. Liberman-Martin, A.L.; Levine, D.S.; Liu, W.; Bergman, R G.; Tilley, T.D., Biaryl Reductive Elimination is Dramatically Accelerated by a Remote Lewis Acid Chemical Switch: Evidence for an Unusual Bidentate Ligand Dissociation Mechanism. *Organometallics,* **2016**, *35*, 1064–1069. DOI: 10.1021/acs.organomet.5b01003.

13. Liberman-Martin, A.L.; Levine, D.S.; Ziegler, M.S.; Bergman, R.G.; Tilley, T.D., Lewis Acid-Base Interactions between Platinum(II) Diaryl Complexes and Bis(perfluorophenyl)zinc: Strongly Accelerated Reductive Elimination Induced by a Z-type Ligand. *Chem. Comm.,* **2016**, *52*, 7039–7042. DOI**:** 10.1039/c6cc02433e

14. Liberman-Martin, A.L.; Ziegler, M.S.; DiPasquale, A.G.; Bergman, R.G.; Tilley, T.D., Functionalization of an Iridium–Diamidocarbene Complex by Ligand-Based Reactions with Titanocene and Zirconocene Sources. *Polyhedron,* **2016**, *116*, 111–115. DOI: 10.1016/j.poly.2016.03.044.

15. Licht, R.B.; Vogt, D.; Bell, A.T., The Mechanism and Kinetics of Propene Ammoxidation over α-Bismuth Molybdate. *J. Catal*., **2016**, *339*, 228–241. DOI: 10.1016/j.jcat.2016.04.012.

16. Licht, R.B.; Getsoian, A.B.; Bell, A.T. Identifying the Unique Properties of α-$Bi_2Mo_3O_{12}$ for the Activation of Propene. *J. Phys. Chem. C*, **2016**, *120*, 29233–29247. DOI: 10.1021/acs.jpcc.6b09949.

17. Melaet, G.; Ralston, W.; Liu, W.C.; Somorjai, G., Product Distribution Change in the Early Stages of Carbon Monoxide Hydrogenation over Cobalt Magnesium Fischer-Tropsch Catalyst. *Catalysis Today*, **2016**, *272*, 69–73. DOI: 10.1016/j.cattod.2016.03.027.

18. Na, K.; Yoon, Y.; Somorjai, G.A., Control of Model Catalytic Conversion Reaction over Pt Nanoparticle Supported Mesoporous BEA Zeolite Catalysts. *Catalysis Today*, **2016,** *265,* 225–230. DOI: 10.1016/j.cattod.2015.08.058.

19. Park, J.Y.; Somorjai, G.A., Hot Electron Surface Chemistry at Oxide-Metal Interfaces: Foundation of Acid-Base Catalysis. *Cat. Lett.,* **2016,** *146,* 1–11. DOI: 10.1007/s10562-015-1657-6.

20. Su, J.; Xie, C.; Chen, C.; Yu, Y.; Kennedy, G.; Somorjai, G.A.; Yang, P., Insights into the Mechanism of Tandem Alkene Hydroformylation over Nanocrystalline Catalyst with Multiple Interfaces. *J. Am. Chem. Soc.,* **2016**, *138*, 11568–11574.

21. Niu, Z.; Becknell, N.; Yu, Y.; Kim, D.; Chen, C.; Kornienko, N.; Somorjai, G.A.. Yang, P., Anisotropic Phase Segregation and Migration of Pt in Nanocrystals en route to Nanoframe Catalysts. *Nature Materials,* **2016,** 15, 1188–1194.

22. Palla, K.S.; Hurlburt, T.J.; Buyanin ,A.M.; Somorjai, G.A.; Francis, M.B., Site-selective Oxidative Coupling Reactions for the Attachment Enzymes to Glas Surfaces through DNA Directed Immobilization. *J. Am. Chem. Soc.* **2016**, *139*, 1967–1974.

23. Kennedy, G.; Melaet, G.; Han, H.-L.; Ralston, W.T.; Somorjai, G.A., *In situ* Spectroscopic Investigation into the Active Sites for Crotonaldehyde Hydrogenation at the Pt Nanoparticle-Co_3O_4 Interface. *ACS Catal.,* **2016,** *6*, 7140–7147. DOI: 10.1021/acscatal.6b01640.

24. Sgarlata, C.; Raymond, K.N., Untangling the Diverse Interior and Multiple Exterior Guest Interactions of a Supramolecular Host by the Simultaneous Analysis of Complementary Observables. *Anal. Chem*., **2016**, 88, 6923–6929. DOI: 10.1021/acs.analchem.6b01684.

25. Xi, Y.; Butcher, T.W.; Zhang, J.; Hartwig, J.F., Regioselective, Asymmetric Formal Hydroamination of Unactivated Internal Alkenes. *Angew. Chem. Int. Ed.*, **2016**, *55*, 776–780. DOI: 10.1002/anie.201509235.

26. Xi, Y.; Hartwig, J.F., Diverse Asymmetric Hydrofunctionalization of Aliphatic Internal Alkenes through Catalytic Regioselective Hydroboration. *J. Am. Chem. Soc*., **2016**, *138*, 6703–6706. DOI: 10.1021/jacs.6b02478.

27. Ye, R.; Hurlburt, T.; Sabyrov, K.; Alayoglu, S.; Somorjai, G. A., Molecular Catalysis Science: Perspective on Unifying the Fields of Catalysis. *PNAS,* **2016,** *113,* 5159–5166. DOI: 10.1073/pnas.1601766113.

28. Ye, R.; Yuan, B.; Zhao, J.; Ralston, W.; Wu, C.Y.; Barin, E.U.; Toste, D.F.; Somorjai, G.A., Metal Nanoparticles Catalyzed Selective Carbon-Carbon Bond Activation in the Liquid Phase. *J. Am. Chem. Soc.,* **2016***, 138*, 8533–8537. DOI: 10.1021/jacs.6b03977.

29. Zhai, S.; Wütschert, M.; Licht, R. B.; Bell, A. T., Effects of Catalyst Structure on the Oxidation of Propene to Acrolein. *Catal. Today*, **2016**, *261*, 146–153. DOI: 10.1016/j.cattod.2015.06.011.

30. Dydio, P; Key, H.M.; Nazarenko, A.; Rha, J.Y.-E.; Seyedkazemi, V.; Clark, D.S.; Hartwig, J.F., An Artificial Metalloenzyme with the Kinetics of Native Enzymes. *Science*, **2016**, *6308*, 102–106. DOI: 10.1126/science.aah4427.

31. Key, H.M.; Dydio, P.; Clark, D.S.; Hartwig, J.F., Abiological Catalysis by Artificial Haem Proteins Containing Noble Metals in Place of Iron. *Nature*, **2016**, *354*, 534–537. DOI: 10.1038/nature17968.

32. Axelson, J.C.; Gonzalez, M.I.; Meihaus, K.R.; Chang, C. J.; Long, J.R., Synthesis and Characterization of a Tetrapodal NO_4^{4-} Ligand and Its Transition Metal Complexes. *Inorg. Chem.* **2016**, *55*, 7527–7534. DOI: 10.1021/acs.inorgchem.6b00908. *Efforts by C.J.C. laboratory involve direction the synthesis and structural characterization of first-row transition metal complexes with pentadentate ligands*.

33. Levin, M.; Kaphan, D.; Hong, C.; Bergman, R.G.; Raymond, K.; Toste, F.D., Scope and Mechanism of Cooperativity at the Intersection of Organometallic and Supramolecular Catalysis. *J. Am. Chem. Soc.*, **2016**, *138*, 9682–9693. DOI: 10.1021/jacs.6b05442. *Fellowship support from NIH General Medical Sciences*.

34. Liu, H.-J.; Cai, I.C.; Fedorov, A.; Ziegler, M.S.; Copéret, C.; Tilley, T.D., Tricoordinate Organochromium(III) Complexes Supported by Bulky Silylamido Ligands Produce Ultra-High-Molecular Weight Polyethylene in the Absence of Activators. *Helv. Chim. Acta*, **2016**, *99*, 859–867. DOI: 10.1002/hlca.201600199. *This DOE program supported the synthesis, characterization and reactivity studies of the 3-coordinate Cr alkyl complexes. The polymerization studies were carried out at the ETH.*

35. Ziegler, M.S.; Lakshmi, K.V.; Tilley, T.D., Aryl Group Transfer from Tetraarylborato Anions to an Electrophilic Dicopper(I) Center and a Mixed-Valence *m*-Aryl Dicopper(I,II) Complex. *J. Am. Chem. Soc.,* **2016**, *138*, 6484–6491. DOI: 10.1021/jacs.6b00802. *This work is almost entirely supported by this DOE program; our collaborator Lakshmi obtained the EPR spectra.*

36. Kashif, M.K.; Milhuisen, R.A.; Nippe, M.; Hellerstedt, J.; Zee, D.Z.; Duffy, N.W.; Halstead, B.; De Angelis, F.; Fantacci, S.; Fuhrer, M. S.; Chang, C. J.; Cheng, Y.-B.; Long, J. R.; Spiccia, L.; Bach, U., Cobalt Polypyridyl Complexes as Transparent Solution-Processable Solid-State Charge Transport Materials. *Adv. Energy Mater*. **2016**, 1600874. DOI: 10.1002/aenm.201600874.

37. Zhang, J.; Shrestha, R.; Hartwig, J.F.; Zhao, P. A Decarboxylative Approach for Regioselective Hydroarylation of Alkynes. *Nature Chem.* **2016**, *8,* 1444. DOI: 10.1038/NCHEM.2602. *The high-throughput catalyst discovery and development was conducted at UC Berkeley and was supported by this DOE program. Work at NDSU was supported by NSF.*

38. Lee, S.Y.; Hartwig, J.F. Palladium-Catalyzed, Site-Selective Direct Allylation of Aryl C-H Bonds by Silver-Mediated C-H Activation: A Synthetic and Mechanistic Investigation. *J. Am. Chem. Soc.* **2016**, *138*, 15278–15284. DOI: 10.1021/jacs.6b10220. *SYL is supported by an NIH postdoctoral fellowship; her supplies and operating expenses were supported by this DOE program.*

2017

1. Carenco, S.; Liu, Z.; Salmeron, M., The Birth of Nickel Phosphides Catalysts: Monitoring Phosphorus Insertion into Nickel. *ChemCatChem*., **2017**, DOI: 10.1002/cctc.201601526R1.

2. Choi, K.-M.; Kim, D.; Rungtaweevoranit, B.; Trickett, C.A.; Barmanbek, J.T.D.; Alshammari, A.S.; Yang, P.; Yaghi, O.M., Plasmon-Enhanced Photocatalytic CO_2 Conversion within Metal-Organic Frameworks Under Visible Light, *J. Am. Chem. Soc*., **2017**, *139*, 356–362. DOI: 10.1021/jacs.6b11027.

3. Deraedt, C.; Melaet, G.; Ralston, W.; Ye, R.; Somorjai, G.A., Platinum and Other Transition Metal Nanoclusters (Pd, Rh) Stabilized by PAMAM Dendrimer as Excellent Heterogeneous Catalysts: Application to the MethylCycloPentane (MCP) Hydrogenative Isomerization. *Nano Letters.,* **2017**, *17*, 1853–1862. DOI: 10.1021/acs.nanolett.6b05156.

4. Dydio, P.; Key, H.M.; Hayashi, H.; Clark, D.S.; Hartwig, J.F., Chemoselective, Enzymatic C-H Bond Amination Catalyzed by a Cytochrome P450 Containing an Ir(Me)-PIX Cofactor. *J. Am. Chem. Soc.,* **2017**, *139*, 1750–1753. DOI: 10.1021/jacs.6b11410.

5. Guillo, P.; Lipschutz, M. I.; Fasulo, M. E.; Tilley, T. D., Tantalum-Polyhedral Oligosilsesquioxane (POSS) Complexes as Structural Models and Functional Catalysts for Epoxidation. *ACS Catal.,* **2017**, *7*, 2303–2312. DOI: 10.1021/acscatal.7b00020.

6. Hong, C.M.; Kaphan, D.M.; Bergman, R.G. Raymond, K.N.; Toste, F.D., Conformation Selection as the Mechanism of Guest Binding in a Flexible Supramolecular Host. *J. Am. Chem. Soc.,* **2017**, *139*, in press.

7. Key, H.M; Dydio, P.; Liu, Z.; Rha, J.Y-E.; Nazarenko, A.; Seyedkazemi, V.; Clark, D.S.; Hartwig, J.F.; Beyond Fe: Iridium-Containing P450 Enzymes for Selective Cyclopropanations of Structurally Diverse Alkenes. *ACS Cent. Sci.* **2017**, *3*, 302–308. DOI:10.1021/acscentsci.6b00391.

8. Kim, D.; Becknell, N.; Yu, Y.; Yang, P., Room-Temperature Dynamics of Vanishing Copper Nanoparticles Supported on Silica, *Nano Letters*, **2017**, in press.

9. Levine, D.S.; Tilley. T.D.; Andersen, R.A., Evidence for the Existence of Group 3 Terminal Methylidene Complexes. *Organometallics,* **2017**, *36*, 80–88. DOI: 10.1021/acs.organomet.6b00394.

10. Li, Y.; Cui, F.; Ross, M.B.; Kim, D.; Sun, Y.; Yang, P., Structure-sensitive CO_2 Electroreduction to Hydrocarbons on Ultrathin Five-Fold Twinned Copper Nanowires, *Nano Letters*, **2017**, *17*, 1312–17. DOI: 10.1021/acs.nanolett.6b05287.

11. Licht, R.B.; Bell, A.T., A DFT Investigation of the Mechanism of Propene Ammoxidation over □-Bismuth Molybdate. *ACS Catalysis*, **2017**, *7*, 161–176. DOI: 10.1021/acscatal.6b02523.
Lin, S.; Yang, X.; Jia, S.; Weeks, A.M.; Hornsby, M.; Lee, P.S.; Nichiporuk, R.V.; Iavarone, A.T.; Wells, J.A.; Toste, F.D.; Chang, C.J., Redox-Based Reagents for Chemoselective Methionine Bioconjugation. *Science,* **2017**, *355*, 597–602. DOI: 10.1126/science.aal3316.

12. Lipke, M.C.; Liberman-Martin, A.; Tilley, T.D., Electrophilic Activation of Silicon-Hydrogen Bonds in Catalytic Hydrosilations. (review article) *Angew. Chem. Int. Ed.,* **2017**, *56*, 2260–2294. DOI: 10.1002/anie.201605198.

13. Nguyen, A. I.; Suess, D. L. M.; Darago, L. E.; Oyala, P. H.; Levine, D. S.; Ziegler, M. S.; Britt, R. D.; Tilley, T. D., Manganese-Cobalt Oxido Cubanes Relevant to Manganese-Doped Water Oxidation Catalysts. *J. Am. Chem. Soc.,* **2017**, *139*, 5579–5587. DOI: 10.1021/jacs.7b01792.

14. Nguyen, A. I.; Wang, J.; Levine, D. S.; Ziegler, M. S.; Tilley, T. D., Control and Empirical Prediction of Redox Potentials for Co_4O_4 Cubanes over a 1400 mV Range: Implications for the Feasibility of a Co(V)-Oxo Species. *Chem. Sci.,* **2017**, Advance Article. DOI: 10.1039/C7SC00627F.

15. Ralston, W.T.; Melaet, G.; Saephan, T.; Somorjai, G.A.; Evidence of Structure Sensitivity in the Fischer-Tropsch Research on Model Cobalt Nanoparticles by Time-Resolved Chemical Transient Kinetics. *Angewandte Chemie*, **2017**, accepted.

16. Sabyrov, K.; Musselwhite, N.; Melaet, G.; Somorjai, G.A., Hydroisomerization of *n*-Hexadecane: Remarkable Selectivity of Platinum Nanoparticles Supported on Mesoporous Silica Post-

Synthetically Modified with Aluminum. *Catal. Sci. Technol.*, **2017**, *7*, 1756–1765. DOI: 10.1039/C7CY00203C.

17. Sakimoto, K.K.; Kornienko, N.; Yang, P.D., Cyborgian Material Design for Solar Fuel Production: The Emerging Photosynthetic Biohybrid Systems, *Acc. Chem. Res.*, **2017**, *50*, 476–481. DOI: 10.1021/acs.accounts.6b00483.

18. Suslick, B.A.; Liberman-Martin, A.L.; Wambach, T.C.; Tilley, T.D., Olefin Hydroarylation Catalyzed by (Pyridyl-Indolate)Pt(II) Complexes: Catalytic Efficiencies and Mechanistic Aspects. *ACS Catal.,* accepted. DOI: 10.1021/acscatal.7b01560.

19. Tatsumi, H.; Liu, F.; Han, H.-L.; Carl, L.M.; Sapi, A.; Somorjai, G.A., Alcohol Oxidation at Platinum-Gas and Platinum-Liquid Interfaces: The Effect of Platinum Nanoparticle Size, Water Coadsorption, and Alcohol Concentration. *J. Phys. Chem. C*, **2017**, *121*, 7365–7371. DOI: 10.1021/acs.jpcc.7b01432.

20. Troshin, K.; Hartwig, J.F., Snap Deconvolution: an Informatics Approach to High Throughput Discovery of Catalytic Reactions. *Science*, **2017**, accepted.

21. Wu, C.-H.; Eren, B.; Bluhm, H.; Salmeron, M.B., An Ambient-Pressure X-ray Photoelectron Spectroscopy Study of Cobalt Foil Model Catalyst under CO, H2, and their Mixtures. *ACS Catal.*, **2017**, *7*, 1150–1157. DOI: 10.1021/acscatal.6b02835.

22. Wu, C.-Y.; Wolf, W.J.; Levratovsky, Y.; Bechtel, H.A.; Martin, M.C.; Toste, F.D.; Gross, E., High Spatial Resolution Mapping of Catalytic Reactivity on Pt Nanoparticles. *Nature*, **2017**, *541*, 511–515. DOI: 10.1038/nature20795.

23. Ye, Q.; Ziegler, M. S.; Lakshmi K. V.; Tilley,T. D., Titanium Imido Complexes by Displacement of $–SiMe_3$ and C–H Bond Activation in a Ti^{III} Amido Complex, Promoted by a Cyclic (Alkyl)(Amino) Carbene (cAAC) *Eur. J. Inorg. Chem.,* **2017**, 2484–2487. DOI: 10.1002/ejic.201700295.

24. Ye, R.; Zhao, J.; Yuan, B.; Liu, W.-C.; De Araujo, J. R.; Fuacher, F. F.; Chang, M.; Toste, F.D.; Somorjai, G.A., New Insights into Aldol Reactions Catalyzed by Heterogenized Homogeneous Catalysts. *Nano. Lett.,* **2017**, *17*, 584–589. DOI: 10.1021/acs.nanolett.6b04827.

25. Yun, Y.; Araujo, J.R.; Melaet, G.; Baek, J.; Archanjo, B.S.; Oh, M.-H.; Alivisatos, A.P.; Somorjai, G.A., Activation of Tungsten Oxide for Propane Dehydrogenation and Its High Catalytic Activity and Selectivity. *Catal. Lett.,* **2017***,* 147, 622. DOI: 10.1007/s10562-016-1915-2.

26. Zhao, J.; Nguyen, S.C.; Ye, R.; Ye, B.; Weller, H.; Somorjai, G.A.; Alivisatos, A.P.; Toste, F.D., A Comparison of Photocatalytic Activities and of Gold Nanoparticles Following Plasmonic and Interband Excitation and a Strategy for Harnessing Interband Hot Carriers for Solution Phase Oxidative Photo-catalysis. *ACS Central. Sci.,* **2017**, *3*, in press.

27. Ziegler, M.S.; Lakshmi, K.V.; Tilley, T.D., Dicopper Cu(I)Cu(I) and Cu(I)Cu(II) Complexes in Copper-Catalyzed Azide-Alkyne Cycloaddition, *J. Am. Chem. Soc.* **2017**, *139*, 5378–5386. DOI: 10.1021/jacs.6b13261.

Chemical Synergies of Capturing and Converting CO_2

David J. Heldebrant
Pacific Northwest National Laboratory

Presentation Abstract

Global CO_2 demand (80Mtpa) is met via extraction from natural geological reservoirs, while anthropogenic waste sources exceed 18,000 Mtpa. CO_2 may be a waste gas, but the energy cost of collecting, concentrating and purifying it is not free. Current costs of collecting CO_2 from natural sources are cheap, on the order of $20/ton, while projections for capture from coal exhaust are $60/ton and projections for direct air capture have been projected to be as high as $1,000/ton. The high costs are due to the energy costs associated with intensive steps of regenerating a capture solvent (85 kJ/mol) and compression (12 kJ/mol) that are often neglected by proponents of CO_2 utilization. Performing catalysis on CO_2 captured in solution avoids some of the energy associated with capture and compression by combining them into a single step, but more importantly, the reduction of CO_2 can be catalytic with respect to capture solvent. There are other advantages of converting CO_2 in a capture solvent, notable that catalysis can be performed at lower CO_2 pressures due to the 5 wt% of CO_2 in solution at 1 atm, where the high concentration allows for faster kinetics. There are potentially other lower free-energy pathways available as the CO_2 is concentrated in a highly polar ionic medium which stabilizes charged intermediates inherent to reactive pathways in conversions of CO_2. It is not by coincidence that the same chemicals used to promote chemical conversions are the same chemicals that are used to capture CO_2 from dilute gas streams. In capture, the CO_2 is attacked by a nucleophile and is re-hybridized, producing an acid/base salt. This is similar to when CO_2 is hydrogenated and captured with a base to produce a formate salt. We present the chemical synergies of capture and conversion of CO_2, demonstrating that anionic carboxylates (captured CO_2), are more reactive than previously thought. We present evidence of the catalytic reduction of anionic carboxylates using molecular catalysts, demonstrating the first observations of an inner sphere mechanism. A combination of *operando* spectroscopy and mechanistic studies were used to observe the insertion of alkylcarbonates and carbamates into metal hydride bonds at ambient conditions. The new finding opens new doors for catalytic conversions of CO_2. The symbiosis of capture and conversion allows for the tuning the hydride acceptor strength of CO_2 by controlling the properties of the capture solvent, enabling the thermodynamic pairing of both the hydride donor (catalyst) and acceptor (captured CO_2).

Jason C. Hicks

Advancing Sustainable Ammonia Synthesis through Plasma-Assisted Catalysis

Patrick Barboun[a], Francisco Herrera[b], Jongsik Kim[a], Prateek Mehta[a], Paul Rumbach[b], David B. Go[a,b], Jason C. Hicks[a], and William F. Schneider[a]

University of Notre Dame, [a]Department of Chemical & Biomolecular Engineering, [b]Department of Aerospace & Mechanical Engineering

Presentation Abstract

The industrial Haber-Bosch process for ammonia synthesis from nitrogen and hydrogen is carried out at high pressures (100-200 bar) and temperatures (400-500 °C). N_2 dissociation is the fundamental barrier for this reaction, and there has been a longstanding desire to develop ways to activate this N-N triple bond under less extreme conditions. We have demonstrated that is possible to produce ammonia at atmospheric pressure and temperatures between 100 - 200 °C by coupling the catalyst with a non-thermal plasma. It is speculated that the plasma assists in activating the source gas by generating reactive species, such as vibrationally or electronically excited N_2*, ions, and radicals, which interact on the catalyst surface to produce ammonia. Recently, we have varied the gas composition and space velocity to determine if and how catalyst-plasma interactions affect ammonia production using a variety of catalysts (Fe/MgO, Ru/MgO, Pt/MgO, Ni/MgO, and Co/MgO). We determined that the yield of ammonia increases and that plasma-catalyst interactions are more apparent at lower H_2 concentrations. Our initial computational efforts have been focused on developing an understanding of the maximum rate enhancements that may be possible by vibrational excitation of the N_2 molecules, using the well-established thermal catalysis reaction pathways as a baseline. Our model suggests that the optimal catalysts under thermal conditions may not be the most active in the influence of the plasma. We have also coupled these results with detailed plasma characterization experiments using optical emission spectroscopy to further characterize the vibrational temperature of N_2 under reaction conditions in order to relate the plasma properties to the calculations and reaction measurements. We observe the N_2 vibrational temperature has a clear trend that is strongly dependent on the gas composition, decaying linearly as the N_2 partial pressure increases. We are currently exploring the relationship between the vibrational temperature and the population of vibrationally-excited species at different energy levels to correlate this population distribution with catalytic reaction rates.

DE-SC0016543: Advancing Sustainable Ammonia Synthesis through Plasma-Assisted Catalysis

PIs: Jason C. Hicks, David B. Go, William F. Schneider
Postdoc(s): Jongsik Kim, Paul Rumbach
Student(s): Patrick Barboun, Francisco Herrera, Prateek Mehta

RECENT PROGRESS

The objectives of this project are to perform systematic plasma catalysis experiments supported by computational models that capture the molecular-scale physics and chemistry to use plasma-assisted catalysis as an alternative, scalable means to achieve the sustainable synthesis of ammonia. We hypothesize that careful control of the plasma properties coupled with appropriate catalyst selection will generate non-thermal intermediates and open surface kinetic pathways at low temperature (< 200°C) and ambient pressure to facilitate high NH_3 production rates.

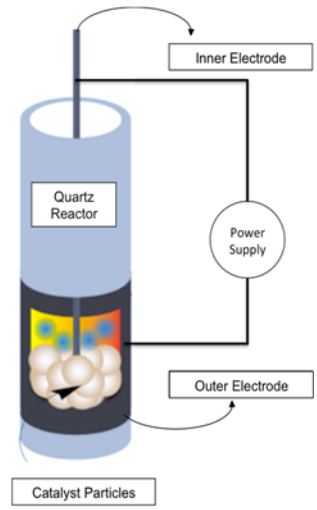

Figure 1. Schematic diagram of the plasma reactor used in performance testing for catalysts.

Experiments were performed to determine if, and under what conditions, plasma-catalyst interactions enhance ammonia yields. These experiments were conducted in a custom-built plasma reactor shown in Figure 1. The reactor consists of a quartz tube with a tungsten rod in the center as the inner electrode and a steel mesh wrapped around the tube for the outer electrode. The electrodes are connected to a high voltage power source to generate a non-thermal, non-equilibrium atmospheric-pressure plasma called a dielectric barrier discharge (DBD). An oscilloscope was used to monitor the electrical power deposited into the DBD.

Due to our familiarity with nickel-based catalysts, we began our experiments by synthesizing a Ni/MgO catalyst via typical wet impregnation followed by a calcination in air and reducing in hydrogen with a metal loading of 5 wt. %. Experiments were then performed on this material in a DBD at 10 W, and the ammonia yield was monitored when different ratios of nitrogen and hydrogen were fed. To measure background contributions by the plasma and the support (sans catalyst), NH_3 yields were measured under identical conditions for an empty (DBD-only) reactor and in the DBD reactor packed with MgO. No external heating was provided in any of the above experiments, and the measured gas temperature due to heating by the DBD was around 115°C. The results of these three sets of experiments are plotted in Figure 2. Yields of ammonia were observed in all experiments, increasing at higher N_2:H_2 ratios. Moreover, the plasma-Ni/MgO combination consistently yielded more NH_3 than the plasma-MgO and plasma-only systems. Thermal catalytic measurements at 115°C were also performed in the absence of the plasma---no ammonia yields were observed under these conditions. The above experiments thus demonstrate that plasma-generated

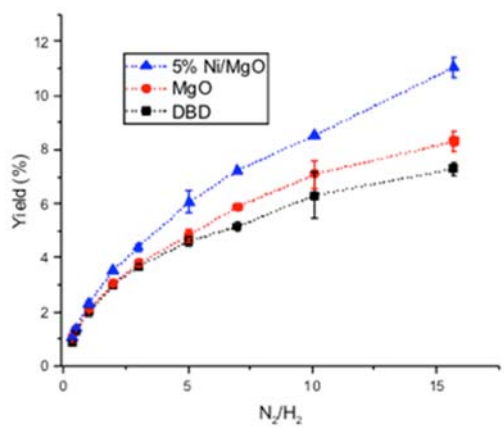

Figure 2. Yield of ammonia as a function of the composition of the feed stream in the plasma reactor with DBD/Ni/MgO (blue), DBD/MgO (red), and DBD in the absence of a catalyst (black).

intermediates interact to form ammonia in the plasma phase, and that the catalysts present in the reactor can influence the ammonia yield.

The increase in NH_3 yield over plasma or catalyst alone suggests mechanistic departures from conventional thermal catalysis. In thermal NH_3 synthesis, the rate-determining step is typically the activation of the robust N-N triple bond. We hypothesize that the plasma assists in ammonia production by exciting the nitrogen species, which are further activated on the surface of the catalyst. In non-thermal plasmas, most of the discharge power is localized within vibrational excitations of the gas molecules, which are significantly easier to generate than electronic excitation or ionization. Consequently, our initial computational efforts have been focused on developing an understanding of the maximum rate enhancements that may be possible by vibrational excitation of the N_2 molecules, using the well-established thermal catalysis reaction pathways as a baseline. We propose that vibrational excitation lowers the barrier for N_2 dissociation, i.e., we write the corresponding rate constant as $k(E_v, T_g) = A\exp(-\frac{E_a - E_v}{k_b T_g})$, where E_v is the energy of the vibrational level. We assume the other reaction steps---hydrogen dissociative adsorption and hydrogenation of surface adsorbed NH_x species, proceed as they would in thermal catalysis.

We used density functional theory (DFT) calculated reaction and activation energies from the CatApp database to compute ammonia synthesis rates for a series of metal catalysts. Using Bronsted-Evans-Polyani relations and adsorption energy scaling relations, the DFT results were used to construct volcano plots of reaction rates at 1 atm and 473 K, as a function of the nitrogen binding energy. These plots are shown in Fig. 3(a) for metal step sites, which are conventionally known to be the active sites in thermal catalysis. The TOFs plotted in this figure correspond to the Sabatier rate, i.e., the maximum possible rate in the limit of zero conversion and assuming ideal coverages. The different color lines show the NH_3 synthesis rates with N_2 molecules assumed to be in different vibrational states (up to 4 vibrational levels are shown). Metals on the right leg of the volcano are rate limited by N_2 activation, while those on the left leg are limited by a hydrogenation step. In the absence of vibrational excitation, our model recovers the best-known thermal catalysts, Ru and Fe, near the top of the volcano. However, under vibrational excitation, the rates of ammonia synthesis

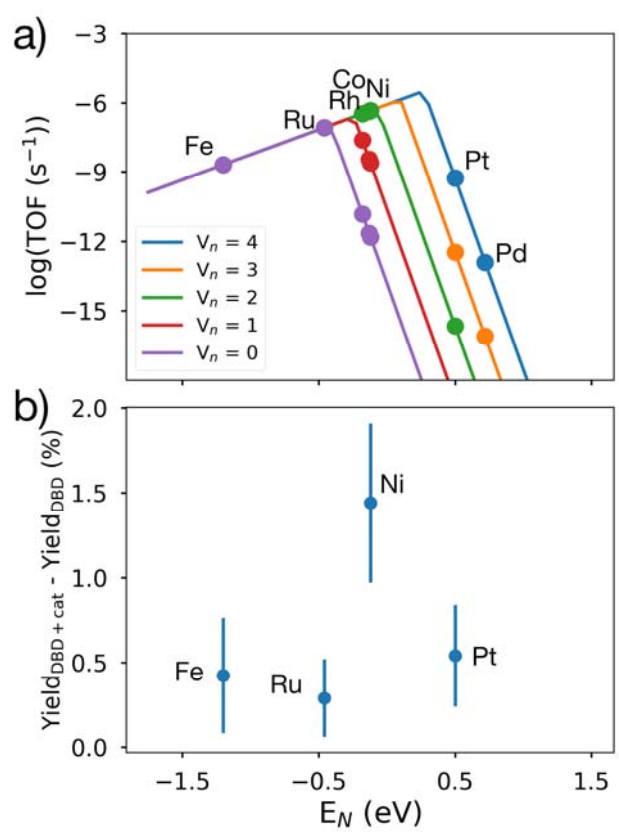

Figure 3. (a) Sabatier rates of NH_3 synthesis with the N_2 feeds in different levels of vibrational excitation. Reaction conditions: 1:3 N_2:H_2 ratio, 1 atm total pressure, 473 K. (b) Measured plasma-corrected ammonia yields for different metal catalysts supported on MgO.

may increase by several orders of magnitude for metals on the right leg of the volcano, until a hydrogenation step becomes rate limiting. Our model thus suggests that the optimal catalysts under thermal conditions may not be the most active when under the influence of the plasma. Despite the rate enhancements by vibrational species, the maximum rates on step sites are several orders of magnitude lower than those obtained under Haber-Bosch conditions (10^{-2} s^{-1} at 100 bar and 673 K). However, since hydrogenation steps may become rate limiting under plasma conditions, the optimal active site motifs may be different from thermal catalysis. We predict that sites on metal terraces, which have lower hydrogenation barriers than step sites, exhibit higher rates (not shown) if the plasma can activate nitrogen molecules to an extent that N_2 dissociation is not rate limiting.

Initial experimental measurements (performed similarly to the Ni/MgO results described above) of ammonia yields for Fe, Ru, Ni, and Pt, are qualitatively consistent with the model predictions (See Fig. 3(b)). Fe and Ru, which bind N too strongly show very small NH_3 yields in the plasma. Ni catalysts show the highest ammonia yields. Pt which binds N weaker than Ni shows yields comparable to those of Fe and Ru, suggesting that the effective vibrational excitation is insufficient to activate the nitrogen molecules on the Pt surface. We are in the process of synthesizing catalysts with different amounts of terrace and step sites to compare with the predictions.

In order to understand these results from the perspective of the plasma properties, we aimed to characterize various plasma properties, most notably the vibrational temperature, which reflects the distribution of vibrational states in the gas, but the also the electron temperature and electron density, which correspond to the electron kinetics and thus reactions that excite nitrogen and hydrogen molecules. The purpose is to correlate these findings to the plasma catalysis measurements and understand how these parameters affect the production of ammonia and the mechanisms behind plasma-assisted catalysis.

Our strategy was to use optical emission spectroscopy (OES) and to correlate the measured nitrogen transitions to properties in the DBD. To conduct these measurements, we built a DBD reactor nearly identical to the one used in the plasma-assisted catalysis measurements, with a small modification to allow for better optical access. As shown in Fig. 4a, the spectrometer is integrated "in-line" with the DBD plasma, such that is acquires all the light emitted by the plasma down the length of the tube. This configuration was used to mitigate the impact of external discharges (outside the reactor tube) and other light sources on the OES measurements.

Building upon the plasma catalysis measurements in Fig. 2, we have performed several OES measurements at various ratios of N_2/H_2. We extracted the N_2 vibrational and rotational temperatures of the DBD by comparing our spectroscopic measurements with a modeled optical emission spectrum using the software Specair™. Figure 4b shows that the N_2 vibrational temperature has a clear trend that is strongly dependent on the gas composition, decaying linearly as the N_2 partial pressure increases. Currently, we believe that these results may indicate that the population of vibrationally-excited N_2 species directly impacts the plasma-catalyst interaction, as the different vibrational states can shift the volcano curve (Fig. 3a), although we have yet to fully resolve the interaction.

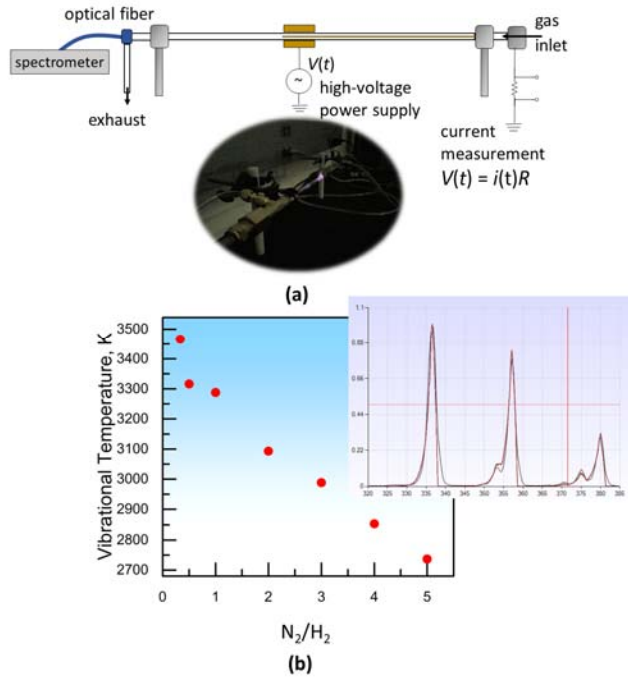

Figure 4. (a) Experimental set-up consisting of a tube DBD plasma reactor and an optical fiber coupled to a spectrometer. (b) Vibrational temperature (T_v) as a function of the gas composition (N_2/H_2) with inset showing an example of an emission spectrum used to obtain T_v.

Timothy A. Jackson

Ligand Perturbations Influence C-H Bond Oxidation Reactions by Mn^{IV}-oxo Complexes

Timothy A. Jackson, Allyssa E. Massie, and Melissa C. Denler
Department of Chemistry and Center for Environmentally Beneficial Catalysis, University of Kansas

Presentation Abstract

In recent years, hydrogen-peroxide-activating manganese catalysts have been shown to be capable of selective and efficient C-H bond oxidation reactions. The proposed mechanisms for these catalysts often feature manganese(IV)-oxo complexes as hydrogen-atom or oxygen-atom transfer agents. However, isolated manganese(IV)-oxo species show a remarkable range of reactivity, with some species capable of attacking only highly activated C-H bonds and others being able to oxidize the strong C-H bonds of cyclohexane. In this presentation, we describe out recent efforts aimed at understanding the basis of the varied reactivity of manganese(IV)-oxo complexes. Using the pentadentate N4py ligand, and derivatives with perturbations in ligand donor strength, we assembled a series of manganese(IV)-oxo adducts showing systematic changes in both spectroscopic properties and chemical reactivity. From detailed kinetic studies of hydrocarbon oxidation by these manganese(IV)-oxo species, we have shown that decreased equatorial ligand donor strength correlates with enhanced hydrogen-atom transfer rates. The basis of this correlation is discussed within the context of a two-state reactivity model, as well as a thermodynamic model for reactivity.

DE-SC0016359: Mechanistic Studies to Enable Aerobic Oxidation of C-H Bonds by Manganese Catalysts

Students: Allyssa E. Massie, Melissa C. Denler, Joshua Parham, Eleanor Stewart-Jones

RECENT PROGRESS

Motivation and Project Goals

The long-term goal of this project is to develop mechanistic knowledge to enable the design of manganese catalysts for the aerobic oxidation of C-H bonds. At present, this goal is being addressed through detailed studies of the elementary steps critical to manganese oxidation catalysts. These include developing an understanding of hydrogen-atom and oxygen-atom transfer reactions by high-valent manganese-oxo species, which are the initiating steps in C-H bond oxidation and functionalization.

Electronic Structure Contributions to Manganese(IV)-oxo Reactivity

In 2013, our lab reported a Mn^{IV}-oxo adduct supported by the pentadentate, aminopyridyl ligand N4py (Figure 1A). Kinetic studies showed that $[Mn^{IV}(O)(N4py)]^{2+}$ carried out the oxidation of dihydroanthracene (a hydrocarbon commonly used for comparing hydrogen-atom transfer reactivities) with a second-order rate constant larger than that of most Mn^{IV}-oxo species (Leto *et al. Chem. Commun.* **2013**, *49*, 5378). At the time we had attributed the enhanced reactivity of $[Mn^{IV}(O)(N4py)]^{2+}$ to its high $Mn^{III/IV}$ reduction potential (800 mV versus SCE). However, Nam and Shaik, who had independently reported the $[Mn^{IV}(O)(N4py)]^{2+}$ complex, ascribed the high reactivity to a two-state reactivity model, where a low-lying ^4E excited state offers a lower barrier for hydrogen-atom transfer than the $^4B_1$ ground state (Figure 1B). This prediction was based on density functional theory (DFT) computations (see Cho, *et al. J. Phys. Chem. Lett.* **2012**, *3*, 2851).

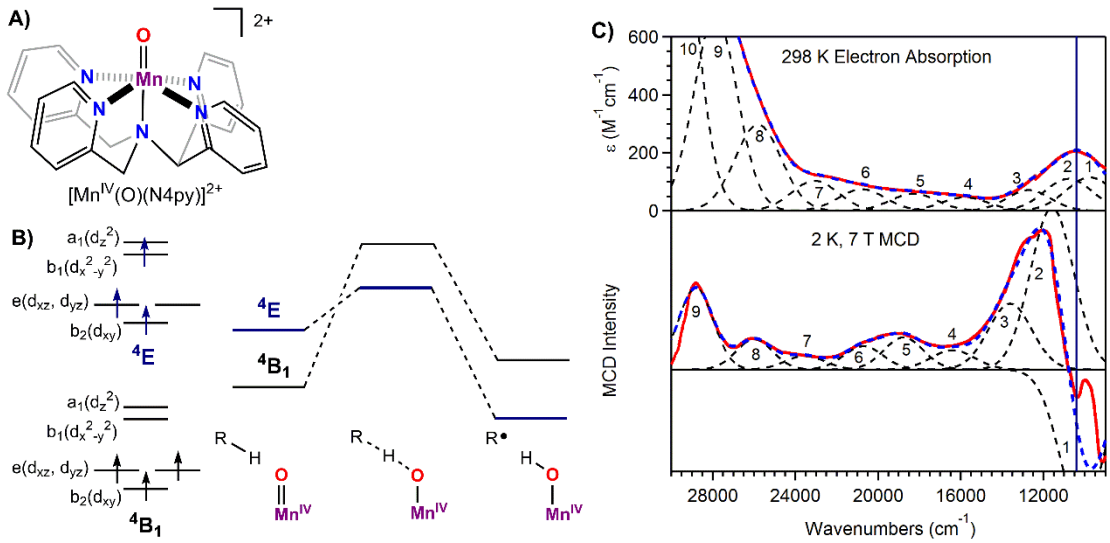

Figure 1. *A) Molecular structure of $[Mn^{IV}(O)(N4py)]^{2+}$. B) Reaction coordinate diagram from hydrogen-atom transfer by $[Mn^{IV}(O)(N4py)]^{2+}$ based on DFT computations (from Cho, et al. J. Phys. Chem. Lett.* ***2012****, 3, 2851). Electronic configurations for $^4B_1$ and ^4E states are shown. C) Electronic absorption and MCD spectra of $[Mn^{IV}(O)(N4py)]^{2+}$. Individual electronic transitions, obtained from a Gaussian deconvolution, are included. The vertical line marks the electronic transitions contributing to the ^4E state.*

To evaluate this two-state reactivity model, we first used a combination of electronic absorption and magnetic circular dichroism (MCD) spectroscopy to experimentally identify the ^4E excited state of $[Mn^{IV}(O)(N4py)]^{2+}$. A state with true, or near, orbital degeneracy, such this ^4E state, should appear as a derivative-shaped feature in the MCD spectrum (so-called pseudo-*A* term). Such a feature is observed in the MCD spectrum of near 10 500 cm^{-1} (950 nm), which corresponds to the maximum of a band in the electronic absorption spectrum (Figure 1C). Using a graphical analysis of the sign of the MCD pseudo-*A* term, as well as high-level CASSCF/NEVPT2 computations, we confirmed that the electronic transitions at 10 500 cm^{-1} arise from the ^4E state predicted to be involved in hydrogen-atom transfer reactivity. However, the experimental energy of this state is ~5 000 cm^{-1} (~14 kcal/mol) higher in energy than that predicted by previous DFT computations. Thus, stabilization of this state (*i.e.*, through

interactions with a substrate C-H bond) would be required in order for this state to be energetically-relevant for hydrocarbon oxidation.

To determine if this state could be stabilized by Mn^{IV}=O bond elongation (which is the major distortion of the Mn^{IV}-oxo unit along the hydrogen-atom transfer reaction coordinate), we performed CASSCF/NEVPT2 approach to determine the energy of the $^4B_1$ and ^4E ground state as a function of the Mn=O distance. Unlike DFT methods, the wavefunction-based CASSCF/NEVPT2 computations can treat states with orbital degeneracy and properly incorporate multiplet effects important in determining the energies of ligand-field states. This computational analysis showed no stabilization of the ^4E state upon Mn=O bond elongation; however, the ^4E state did develop significant Mn^{III}-oxyl character. Thus, if the ^4E state were thermally accessible, or stabilized by interactions with substrate, the high Mn^{III}-oxyl character could render this state a potent oxidant. Current work is aimed at extending our CASSCF/NEVPT2 computations to include structures with relevant substrate molecules.

Ligand-Field Perturbations Influence Manganese(IV)-oxo Reactivity

As an additional means of determining contributions to reactivity in Mn^{IV}-oxo complexes, we generated derivatives of the N4py ligand with perturbed electronic and steric properties. The ^{DMM}N4py derivative contains electron-rich pyridines, whereas the 2pyN2Q ligand contains quinoline donors that, because of steric clash between the bulk of the quinolines and the Mn center, reduce ligand-to-manganese charge donation (Figure 2A). The differences in equatorial ligand field strength caused by these ligands can be appreciated by their electronic absorption spectra (Figure 2B). The near-IR absorption band arises from the ^4E (Mn^{IV} $3d_{xz/yz} \rightarrow 3d_{x^2-y^2}$) excited state. Changes in donor strength of the equatorial ligand influence the energy of the Mn^{IV} $3d_{x^2-y^2}$ acceptor orbital, causing blue- and red-shifts for stronger and weaker donation, respectively. Additional characterization of the Mn^{IV}-oxo complexes was achieved by X-band electron paramagnetic resonance (EPR) and Mn K-edge X-ray absorption spectroscopies.

In addition to tuning the electronic properties of the Mn^{IV}-oxo units, the ^{DMM}N4py and 2pyN2Q ligand derivatives also greatly influence the rates at which these complexes attack the C-H bonds of hydrocarbon substrates. Figure 2C shows plots of log(k_2) (where k_2 is the second-order rate constant for oxidation of a particular hydrocarbon) versus substrate C-H bond dissociation energy for the oxidation of a variety of hydrocarbons by $[Mn^{IV}(O)(N4py)]^{2+}$, $[Mn^{IV}(O)(^{DMM}N4py)]^{2+}$, and $[Mn^{IV}(O)(2pyN2Q)]^{2+}$. For each substrate, $[Mn^{IV}(O)(^{DMM}N4py)]^{2+}$ carries out oxidation 10-fold slower than that of $[Mn^{IV}(O)(N4py)]^{2+}$, whereas $[Mn^{IV}(O)(2pyN2Q)]^{2+}$ performs substrate oxidation 10-fold faster than $[Mn^{IV}(O)(N4py)]^{2+}$. Because the ^4E excited-state energies of these Mn^{IV}-oxo complexes decrease in the order $[Mn^{IV}(O)(^{DMM}N4py)]^{2+} > [Mn^{IV}(O)(N4py)]^{2+} > [Mn^{IV}(O)(2pyN2Q)]^{2+}$, the observed variation in rates is consistent with the previously proposed two-state reactivity model. However, the rate data also correlate with the $Mn^{III/IV}$ reduction potentials of these complexes, suggesting that the faster oxidation rates of $[Mn^{IV}(O)(2pyN2Q)]^{2+}$ are because of a larger thermodynamic driving force for these reactions. Future experiments will probe these observed correlations using a more diverse set of Mn^{IV}-oxo complexes.

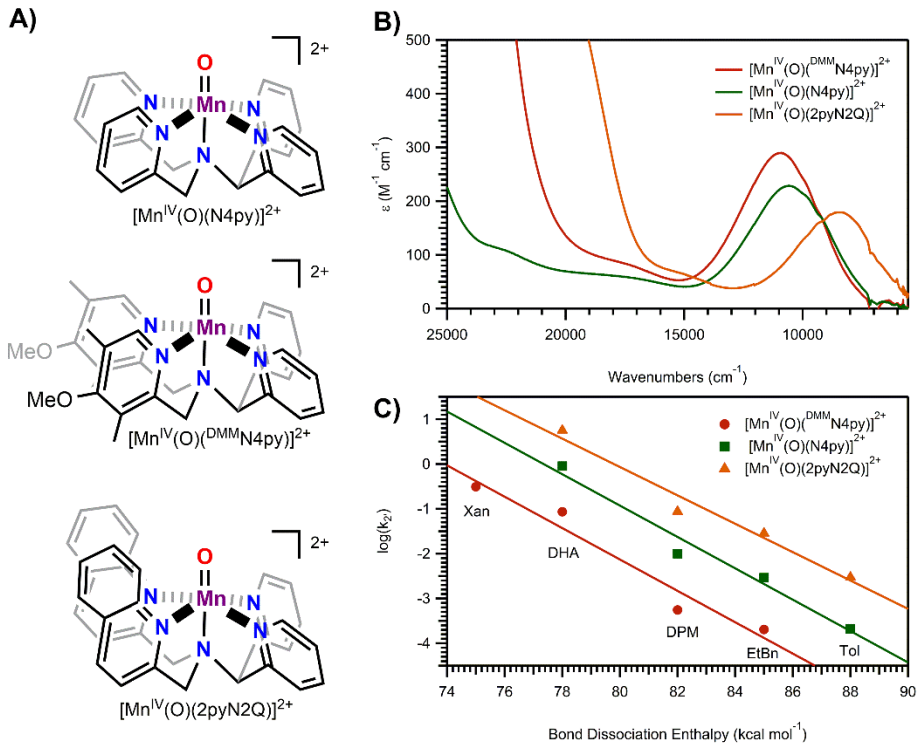

Figure 2. *A) Molecular structures of Mn^{IV}-oxo complexes with N4py, ^{DMM}N4py, and 2pyN2Q ligands. B) Electronic absorption spectra of Mn^{IV}-oxo complexes. C) Plots of log(k_2) versus substrate bond dissociation energy. Substrate abbreviations are as follows: Xan = xanthene, DHA = 9,10-dihydroanthracene, DPM = diphenylmethane, EtBn = ethylbenzene, Tol = toluene.*

Publications Acknowledging this Grant in 2014-2017

(I) Jointly funded by this grant and other grants with leading intellectual contribution from this grant;

1. Leto, D. F.; Massie, A. A.; Rice, D. B.; Jackson, T. A. *J. Am. Chem. Soc.* **2016**, *138*, 15413-15424.
2. Massie, A. A.; Denler, M. C.; Cardoso, L. T.; Walker, A. N.; Hossain, M. K.; Day, V. W.; Nordlander, E.; Jackson, T. A. *Angew. Chem. Int. Ed.* **2017**, *56*, 4178-4182.

(II) Jointly funded by this grant and other grants with relatively minor intellectual contribution from this grant;

3. Jensen, S. C.; Davis, K. M.; Sullivan, B.; Hartzler, D. A.; Seidler, G. T.; Casa, D. M.; Kasman, E.; Colmer, H. E.; Massie, A. A.; Jackson, T. A.; Pushkar, Y. *J. Phys. Chem. Lett.* **2017**, 2584-2589.

Johannes Lercher

Understanding Catalysis of Lignin to Fuels on a Molecular Level

Johannes Lercher,[a,b] Don Camaioni,[a] Donghai Mei,[a] Nigel Browning,[a] Mirek Derewinski,[a] Yong Wang,[a] John Fulton,[a] Jian Zhi Hu,[a] Andreas Jentys[b]

[a]Pacific Northwest National Laboratory, Physical and Computational Sciences Directorate and Institute for Integrated Catalysis

[b]Technical University Munich, Department of Chemistry

Presentation Abstract

The catalyzed-conversion of lignin to alkane energy carriers requires a cascade of reactions for deconstructing and reducing the polymeric, highly oxofunctionalized material. While lignin is the most intractable component of lignocellulose, its conversion to useful products is particularly important, because the carbon in lignin is the most reduced fraction of lignocellulose. Our recent work has been structured to investigate the catalysis of steps important for the deconstruction of lignin, for hydrogenation and hydrodefunctionalization of oxygenated intermediates, and for C–C bond coupling reactions to adjust the size of the product molecules. This has been complemented by focusing on understanding the state and stability of catalysts in the reaction media. We emphasize understanding of the principal chemistry, and we are gradually deepening that by studying more complex representatives of the principal monomers, as well lignin itself, in the envisioned chemistries and to synthesize new generations of catalysts, basing the directions on the physicochemical insight realized by these studies. Key insights highlighted in the poster include demonstrations that confinement in pores significantly enhances rates for acid-catalyzed dehydration and alkylation reactions that the presence of hydronium ion also enhances rates of metal-catalyzed reactions involving H_2, and that solvents critically control the activity of catalysts.

FWP 47319: Low Temperature Catalytic Routes for Energy Carriers via Spatial and Chemical Organization

PI: Johannes Lercher
Co-PI's: Aaron Appel, Tom Autrey, David Baker (U Washington), Garry Buchko, Morris Bullock, Don Camaioni, Mirek Derewinski, David Dixon (U Alabama), Zdenek Dohnálek, Bojana Ginovska, Vassiliki-Alexandra Glezakou, Oliver Gutierrez Tinoco, David Heldebrant, Enrique Iglesia (UC Berkeley), Abhi Karkamkar, Bruce Kay, Gregory Kimmel, John Linehan, Donghai Mei, Roger Rousseau, Greg Schenter, Wendy Shaw, Janos Szanyi, Yong Wang (Washington State U), Eric Wiedner.

RECENT PROGRESS

The program has been restructured and focuses on the elementary reactions of the reduction of oxygenates to hydrocarbon energy carriers. The two thrusts focus on the elementary steps of hydrogenation reactions of CO_2 and more complex (unsaturated) oxygenates, i.e., alcohols, ethers catalyzed by metals (hydrogen addition, hydrogenolysis) and acid catalyzed reactions such as elimination of water, hydrolysis of ether bonds and alkylation of aromatic compounds. Our strategy is to explore and understand the molecular and atomistic pathways of selected reactions on catalysts spanning from single-crystal surfaces via dispersed, supported catalysts to molecular complexes. The fundamental understanding of the elemental steps of reaction sequences enables the emerging knowledge-based design of novel catalysts that operate at lower temperatures and with higher rates than practiced today. We believe we can make rapid progress on our research objectives using an integrated approach enabled by the synergy within our multidisciplinary team focusing on three crosscutting research themes that are common to many of the research activities: (1) multifunctional catalytic sites or catalytic sites acting in concert, (2) spatially constrained, chemospecific environments of active centers, and (3) use of condensed phase to stabilize reactants, intermediates, and products for particular catalytic pathways.

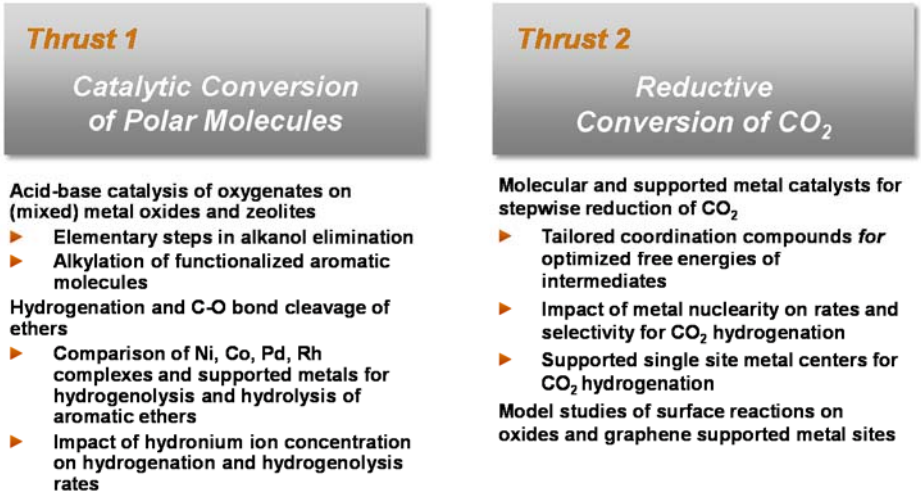

Examples of Recent Results

Understanding the impact of reaction media for alkylation of aromatic compounds. Alkylation of aromatic molecules with alkanols or alkenes is the key reaction to adjust the size of fuel molecules as well as to include small molecules typically formed by deconstruction of lignocellulose into the pool of liquid fuels. The steric constraints of the zeolite pores are indispensable to achieve acceptable rates of alkylation under mild conditions. Depending on the solvent, the active site is either a Brønsted acid site (BAS) of the zeolite or a hydrated hydronium ion. In decalin, phenol alkylation with cyclohexanol is catalyzed by the BAS of the zeolite. The initially low rate of phenol-cyclohexanol alkylation is caused by the presence of cyclohexanol dimers in H-BEA pores. Detailed kinetic analysis and isotope labeling experiments show that alcohol dimers do not generate stable carbenium ions, which act as sole alkylating agent. At the same time, these cyclohexanol dimers hinder also the adsorption and protonation of the olefin produced, blocking other pathway to carbenium ions. With decreasing concentration of cyclohexanol, the abundance of adsorbed alcohol monomers enhances the rate of reaction, enabling both the generation of carbenium ions in the dehydration pathway and the re-adsorption of cyclohexene. The re-adsorption of the olefin and its protonation at the BAS enable this reaction pathway, requiring a relatively low activation energy to form the carbenium ion. Though the formation of alcohol dimers is greatly reduced in water, the stabilization of the adsorbed state of

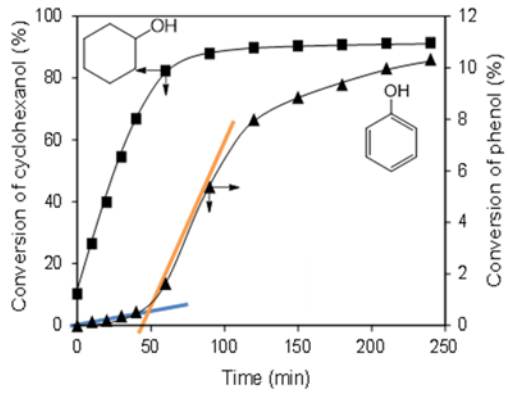

Figure 1. *Variation of rates (slope in conversion graph) at different times during the alkylation of phenol with cyclohexanol catalyzed by HBEA zeolite in decalin.*

the alcohol by water, leads to a higher activation barrier than monomers have in an apolar solvent. Similarly, the olefin protonation by the hydronium ion has a significantly higher barrier than protonation by a framework-bound proton. Surprisingly, the rate of alkylation is also very low as long as the alcohol is present, demonstrating that the time-averaged presence of carbenium ions in the dehydration pathway in water is by far lower than in presence of cyclohexene and that the association of cyclohexene with the hydronium ion is hindered by the presence of cyclohexanol.

Single Facet Anatase TiO_2 (101) and (001) nanomaterials as Model Catalysts for Alcohol Dehydration. We synthesized and applied two anatase titania model catalysts, with preferential exposure of (101) and (001) facets for isopropanol dehydration. A series of microscopic and spectroscopic techniques, including XRD, SEM/TEM, NH_3-TPD, and pyridine-IR, were employed to correlate the structure properties of the model catalysts to their catalytic performance. The Lewis site was found to be the active site, based on 2,6-di-tert-butyl pyridine titration. The higher activity for TiO_2 (101) catalyst was ascribed to its higher acid strength and density as compared to TiO_2 (001). Reaction rate profiles as a function of partial pressure showed a Langmuir-Hinshelwood mechanism for both model catalysts, where the surface dehydration was the rate-limiting step. The kinetic isotope effect measurement indicated that the β C-H bond cleavage governed the reaction rate and the dehydration appeared to follow a concerted E2 elimination pathway, fully supported by theoretical calculations. This work clearly revealed the nature of active sites, mechanisms, and faceting effects for model anatase catalysts in alcohol dehydration. The results shed lights on designing highly efficient metal oxide catalysts for dehydration process during the conversion of biomass-derived molecules.

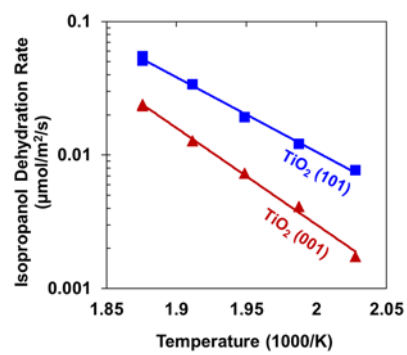

Figure 2. Arrhenius plots of isopropanol dehydration on (■) TiO_2 (101) and (▲) TiO_2 (001) catalysts. 1 bar, 2 kPa isopropanol, 220-260 °C, and GHSV = 2 $L \cdot min^{-1} \cdot g^{-1}_{cat}$.

1,2-Ethanediol and 1,3-Propanediol Conversions over $(MO_3)_3$ (M=Mo, W) Nanoclusters. The dehydration and dehydrogenation reactions of 1,2-ethanediol and 1,3-propanediol molecules on $(MO_3)_3$ (M=Mo, W) nanoclusters were studied using density functional and coupled cluster (CCSD(T)) theory. The reactions are initiated by formation of a Lewis acid-base complex with an additional hydrogen bond. Dehydration is the dominant reaction proceeding via a metal bis-diolate. Acetaldehyde, the major product for 1,2-ethanediol, is produced by α-hydrogen transfer from one CH_2 group to the other. For 1,3-propanediol, the C-C bond breaking pathways to produce C_2H_4 and HCH=O simultaneously and proton transfer to generate propylene oxide have comparable barrier energies. The barrier to produce propanal from the propylene oxide complex is less than that for epoxide release from the cluster. On the Mo_3O_9 cluster, a redox reaction channel for 1,2-ethanediol to break the C-C bond to form two formaldehyde molecules and then to produce C_2H_4 is slightly more favorable than the formation of acetaldehyde. For W^{VI}, the energy barrier for the reduction pathway is larger due to the lower reducibility of W_3O_9. Similar reduction on Mo^{VI} for 1,3-propanediol to form propene is not a

favorable pathway compared to the other pathways as additional C-H bond breaking is required in addition to breaking a C-C bond. The dehydrogenation and dehydration activation energies for the selected glycols are larger than the reactions of ethanol and 1-propanol on the same clusters. The CCSD(T) method is required as DFT with the M06 and B3LYP functionals does not predict quantitative energies on the potential energy surface.

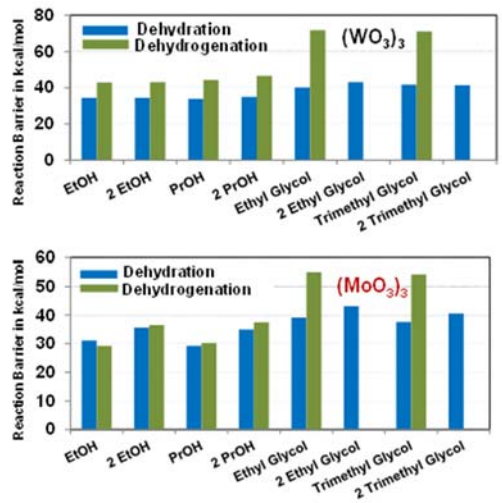

Figure 3. Lowest maximum CCSD(T) barriers in kcal/mol for the conversion of ethanol, 1-propanol, ethylene glycol and trimethylene glycol on M_3O_9 (M = Mo, W) clusters at 298 K.

Site specific measurement of acid/base properties on TiO_2(110). The relative stability of molecularly and dissociatively bound water has been debated for decades on many oxide surfaces, but it has never been successfully measured. We have constructed a new combined supersonic molecular beam, scanning tunneling microscopy (STM) instrument and carried out novel measurements that in combination with ab initio molecular dynamics yield a detailed kinetic and dynamic description of water deprotonation equilibrium on TiO_2(110) (Figure 4). We measured the deprotonation/protonation barriers of 0.36 eV and find that molecularly bound water is preferred over the surface-bound hydroxyls by only 0.035 eV. We demonstrate that long-range electrostatic fields emanating from the oxide lead to steering and reorientation of the molecules approaching the surface, activating the O-H bonds and inducing deprotonation. The developed methodology for studying metastable reaction intermediates prepared with a high-energy molecular beam in the STM can be readily extended to other systems to clarify a wide range of important bond activation processes.

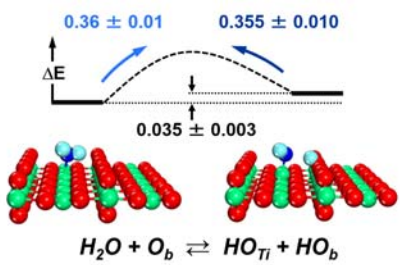

Figure 4. Potential energy surface for water deprotonation on TiO_2(110) determined in this study.

Larger scale molecular simulations accessing operando morphology and reactivity of catalytic systems. Modern electron structure theory coupled with molecular dynamics allows one to examine the structure and dynamics of complex reactive systems at elevated temperature. These simulations can both rationalize the way catalysts work, but also allow for unique discoveries which may arise spontaneously out of the simulations. Using advances simulations consisting of hundreds of atoms for millions of configurations several new transient phenomena have been discovered. For instance, simulations have that Au_{20} on a rutile TiO_2, exhibits liquid-like morphology upon CO adsorption, due to charge transfer from the support during catalytic conversion of CO to CO_2.

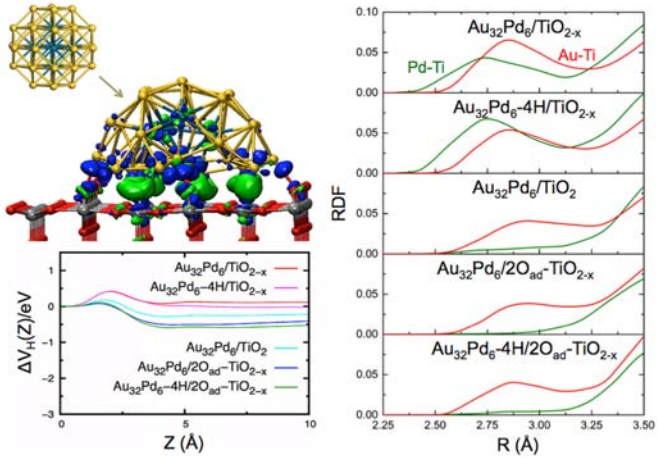

Figure 5. *Redox effects on the structure and morphology of supported AuPd nanoalloys.*

Likewise the reactivity and dynamics of Au nanoparticles on both titania and ceria reveal the dynamic formation of single Au atoms forming Au-CO^+ intermediates before CO_2 is formed. The Au atom is re-integrated with the Au nanoparticle to fully complete the catalytic cycle. Similar studies have shown that modulations of the redox state of both the support and nanoparticles can have a dramatic impact on the accessibility of Pd atoms in mixed AuPd nanoalloys (Figure 5).

Controlling product selectivity through mechanistic understanding. Our recent work on CO_2 reduction over Pd/Al_2O_3 bifunctional catalysts has focused on SSITKA/*operando* FTIR studies. Product selectivity was determined by the balance between the rate of formate decomposition to CO and the rate of strongly-held CO hydrogenation to CH_4. When the pool of decomposing formates provides enough CO to completely fill the pool of strongly adsorbed CO but do not populate the pool of weakly held CO, CH_4 forms with high selectivity. However, when CO hydrogenation is slow the decomposing formate pool is able to fill both the weakly and strongly adsorbed pools of CO. In this case large amount of the weakly held CO can desorb into the gas phase, and we observe CO production with high selectivity. This hypothesis was tested on Pd/Al_2O_3 catalysts with different metal loadings, but very similar metal particle size distribution in CO_2 hydrogenation. We found that at similar CO_2 conversion levels the three catalysts exhibited very different selectivities to CO and CH_4 formation: the catalyst with the lowest Pd loading showed the highest CO selectivity, while the catalyst with the highest Pd loading exhibited the highest CH_4 selectivity (Fig. 1). These results show that by understanding the mechanism of CO_2 reduction tailor-made catalysts with desired selectivities can be designed.

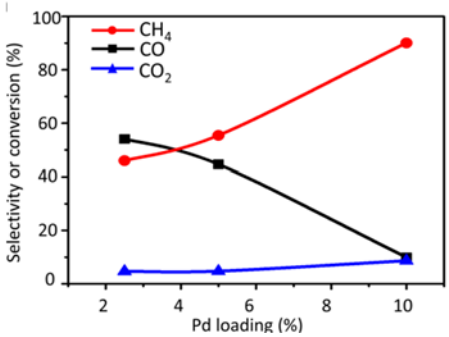

Figure 6. Controlling selectivities in CO_2 reduction on Pd/Al_2O_3 catalysts through mechanistic understanding.

The Role of Solvent in Catalysis: Molecular Catalysis for CO_2 Reduction in Water. For the hydrogenation of CO_2 to formate a variety of molecular catalysts are known, but few catalysts have been reported that are based on non-precious metals and that work in water rather than organic solvents. In particular, the impact of the solvent for the hydrogenation of CO_2 can be substantial. For bis(diphosphine) complexes of nickel hydrides, even the catalysts with the weakest bond to H^- are incapable of converting CO_2 to HCO_2^- in organic solvents through transfer of H^-. To determine the effect of solvent upon this reaction, $HNi(dmpe)_2^+$ was compared between acetonitrile and water (see Figure 7, with R = Me). In acetonitrile, the transfer of H^- is unfavorable by 8 kcal/mol, whereas in water, the same reaction is favorable by 7 kcal/mol.

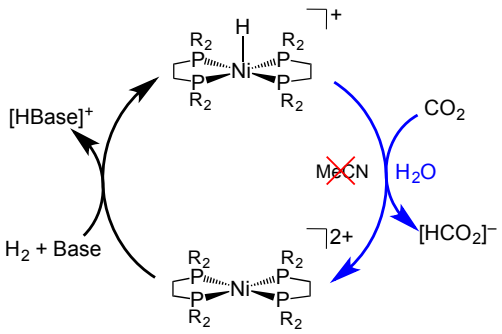

Figure 7. Transfer of H^- from bis(diphosphine) nickel hydride complexes to CO_2 is unfavorable in organic solvents, such as acetonitrile, but favorable in water. Using the free energy for this reaction as a critical parameter, a catalyst system was design and demonstrated.

Using the determined reaction free energies in each solvent and data for related species in acetonitrile, a new, water-soluble nickel complex was designed. The hydride form of this complex was demonstrated to be reactive with CO_2 in aqueous solution, as well as regenerable at a mild pH, thereby leading to an active catalyst system. These results illustrate the critical role that solvent can play in the design of catalysts.

Thermodynamic Linear Scaling Relationships to Optimize Catalytic Reactions in Molecular Complexes. We have used a combination of experimental and computational methods to determine the thermodynamic parameters of the key intermediates leading to the catalytic reduction of CO_2 to formate. Our operating hypothesis is that a balance of the energy landscape minimizes energy sinks in the catalytic cycle leading to optimized rates. This highlight illustrates how concepts successfully utilized in heterogeneous catalysis can be used to test this hypothesis. Given the linear free energy scaling relationships established between H_2 addition, proton abstraction and hydride transfer in previous work we should be able to predict the best homogeneous catalysts. The volcano plot shown in Figure 8 predicts that the cobalt P_2 complex using dmpe as the ligand (green square) should be the best catalyst in the series given the energy balance. The free energy driving force for dihydride formation (orange line), (ii) proton abstraction from the dihydride to form the cobalt hydride (grey line) and (iii) hydride transfer to CO_2 to form formate (blue line) is shown in as a plot of ΔG_{pds} vs. ΔG_{rrs3} confirming the hypothesis that balance thermodynamics play a crucial role in optimizing rates of catalytic reactions.

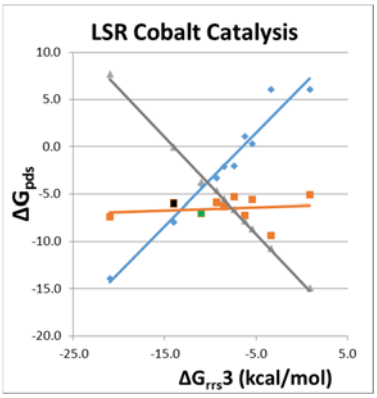

Figure 8. Linear scaling relationships predict that $Co(dmpe)_2$ at the top of the volcano plot should be one of the most efficient catalysts in a series of cobalt P_2 complexes in agreement with experimental rate comparisons.

A dipeptide outer coordination sphere enhances catalytic rates. Amino acids and peptides have been shown to have a significant influence on the H_2 oxidation reactivity of $Ni(P^R{}_2N^{AminoAcid/dipeptide}{}_2)_2$, where $P^R{}_2N^{R'}{}_2$ = 1,5-diaza-3,7-diphosphacyclooctane, and R is cyclohexyl (Cy). Here we investigate the roles of the outer coordination sphere by evaluating amino acids with acidic, basic, and hydrophilic side chains, as well as dipeptides which combine multiple successful features including side chain interactions and –COOH groups. Comparing previous complexes with the six new complexes, the resulting catalytic performance demonstrates that complexes need both interactions between side chain and –COOH groups for fast, efficient catalysis. The fastest of all of the catalysts, Cy(AspPhe), had both of these features, while the dipeptide complexes with an amide replacing the -COOH were both slower; however, the amide group was demonstrated to participate in the proton pathway when side chain interactions are present to position it. Both the hydrophilic and basic side chains, notably lacking in side chain interactions, significantly increased the overpotential, with only modest increases in TOF. Of all of the complexes, only CyAsp was electrocatalytically reversible at room temperature, and only in water, the first of these complexes to demonstrate room temperature aqueous electrocatalyic reversibility for the H_2/H^+ transformation. These results continue to provide and solidify design rules for controlling reactivity and efficiency of $Ni(P_2N_2)_2$ complexes with the outer coordination sphere.

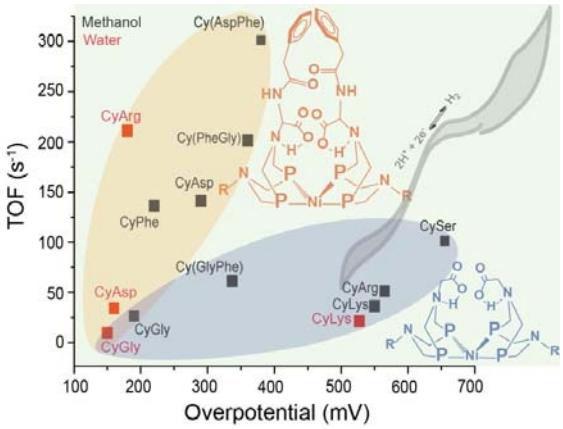

Figure 9. Comparison of the overall performance (TOF and overpotential) of amino acid and dipeptide catalysts for H_2 oxidation, demonstrating that both –COOH groups and side chain interactions are necessary for the best performance.

Publications Acknowledging this Grant in 2014-2017

Publications exclusively funded by this grant

2014

1. Appel, A. M., Carbon-Fuelled Future. *Chemistry & Industry* **2014** *78, 36-39*.
2. Appel, A. M., Electrochemistry: Catalysis at the boundaries. *Nature* **2014**, *508*, 460-461. DOI: 10.1038/nature13226
3. Chen, L.; Li, Z.; Smith, R. S.; Kay, B. D.; Dohnalek, Z., Conversion of 1,2-Propylene Glycol on Rutile TiO_2(110). *J. Phys. Chem. C* **2014**, *118*, 15339-15347. DOI: 10.1021/jp504770f
4. Chen, L.; Li, Z.; Smith, R. S.; Kay, B. D.; Dohnalek, Z., Conversion of 1,3-Propylene Glycol on Rutile TiO_2(110). *J. Phys. Chem. C* **2014**, *118*, 23181-23188. DOI: 10.1021/jp507787m
5. Chen, L.; Li, Z.; Smith, R. S.; Kay, B. D.; Dohnalek, Z., Molecular Hydrogen Formation from Proximal Glycol Pairs on TiO_2(110). *J. Am. Chem. Soc.* **2014**, *136*, 5559-5562. DOI: 10.1021/ja500992b
6. Davidson, S. D.; Sun, J. M.; Hong, Y. C.; Karim, A. M.; Datye, A. K.; Wang, Y., The effect of ZnO addition on Co/C catalyst for vapor and aqueous phase reforming of ethanol. *Catal. Today* **2014**, *233*, 38-45. DOI: 10.1016/j.cattod.2013.12.044
7. Deshlahra, P.; Carr, R. T.; Iglesia, E., Ionic and Covalent Stabilization of Intermediates and Transition States in Catalysis by Solid Acids. *J. Am. Chem. Soc.* **2014**, *136*, 15229-15247. DOI: 10.1021/ja506149c
8. Deshlahra, P.; Iglesia, E., Methanol Oxidative Dehydrogenation on Oxide Catalysts: Molecular and Dissociative Routes and Hydrogen Addition Energies as Descriptors of Reactivity. *J. Phys. Chem. C* **2014**, *118*, 26115-26129. DOI: 10.1021/jp507922u
9. Fang, Z.; Li, Z.; Kelley, M. S.; Kay, B. D.; Li, S.; Hennigan, J. M.; Rousseau, R.; Dohnalek, Z.; Dixon, D. A., Oxidation, Reduction, and Condensation of Alcohols over $(MO_3)_3$ (M = Mo, W) Nanoclusters. *J. Phys. Chem. C* **2014**, *118*, 22620-22634. DOI: 10.1021/jp5072132
10. Kathmann, S. M.; Cho, H.; Chang, T.-M.; Schenter, G. K.; Parab, K.; Autrey, T., Experimental and Theoretical Study of Molecular Response of Amine Bases in Organic Solvents. *J. Phys. Chem. B* **2014**, *118*, 4883-4888. DOI: 10.1021/jp500821u
11. Knaeble, W.; Carr, R. T.; Iglesia, E., Mechanistic interpretation of the effects of acid strength on alkane isomerization turnover rates and selectivity. *J. Catal.* **2014**, *319*, 283-296. DOI: 10.1016/j.jcat.2014.09.005
12. Kovarik, L.; Bowden, M.; Genc, A.; Szanyi, J.; Peden, C. H. F.; Kwak, J. H., Structure of δ-Alumina: Toward the Atomic Level Understanding of Transition Alumina Phases. *J. Phys. Chem. C* **2014**, *118*, 18051-18058. DOI: 10.1021/jp500051j
13. Li, W.-Z.; Kovarik, L.; Mei, D.; Engelhard, M. H.; Gao, F.; Liu, J.; Wang, Y.; Peden, C. H. F., A General Mechanism for Stabilizing the Small Sizes of Precious Metal Nanoparticles on Oxide Supports. *Chem. Mater.* **2014**, *26*, 5475-5481. DOI: 10.1021/cm5013203
14. Li, Y.; Wei, Z.; Gao, F.; Kovarik, L.; Peden, C. H. F.; Wang, Y., Effects of CeO_2 support facets on VO_x/CeO_2 catalysts in oxidative dehydrogenation of methanol. *J. Catal.* **2014**, *315*, 15-24. DOI: 10.1016/j.jcat.2014.04.013

15. Li, Z.; Fang, Z.; Kelley, M. S.; Kay, B. D.; Rousseau, R.; Dohnalek, Z.; Dixon, D. A., Ethanol Conversion on Cyclic $(MO_3)_3$(M = Mo, W) Clusters. *J. Phys. Chem. C* **2014**, *118*, 4869-4877. DOI: 10.1021/jp500255f

16. Liu, C.; Wang, H.; Karim, A. M.; Sun, J.; Wang, Y., Catalytic fast pyrolysis of lignocellulosic biomass. *Chem. Soc. Rev.* **2014**, *43*, 7594-7623. DOI: 10.1039/C3CS60414D

17. Mendez, M.; Francisco, J. S.; Dixon, D. A., Thermodynamic Properties of the Isomers of HNOS , HNO_2S , and $HNOS_2$ and the Role of the Central Sulfur. *Chem.-Eur. J.* **2014**, *20*, 10231-10235. DOI: 10.1002/chem.201404076

18. Mu, R.; Cantu, D. C.; Lin, X.; Glezakou, V.-A.; Wang, Z.; Lyubinetsky, I.; Rousseau, R.; Dohnalek, Z., Dimerization Induced Deprotonation of Water on RuO_2(110). *J. Phys. Chem. Lett.* **2014**, *5*, 3445-3450. DOI: 10.1021/jz501810g

19. Rousseau, R.; Dixon, D. A.; Kay, B. D.; Dohnalek, Z., Dehydration, dehydrogenation, and condensation of alcohols on supported oxide catalysts based on cyclic $(WO_3)_3$ and $(MoO_3)_3$ clusters. *Chem. Soc. Rev.* **2014**, *43*, 7664-7680. DOI: 10.1039/c3cs60445d

20. Sun, J.; Wang, Y., Recent Advances in Catalytic Conversion of Ethanol to Chemicals. *ACS Catal.* **2014**, *4*, 1078-1090. DOI: 10.1021/cs4011343

21. Szanyi, J.; Kwak, J. H., Dissecting the steps of CO_2 reduction: 1. The interaction of CO and CO_2 with γ-Al_2O_3: an in situ FTIR study. *Phys. Chem. Chem. Phys.* **2014**, *16*, 15117-15125. DOI: 10.1039/C4CP00616J

22. Szanyi, J.; Kwak, J. H., Dissecting the steps of CO_2 reduction: 2. The interaction of CO and CO_2 with Pd/γ-Al_2O_3: an in situ FTIR study. *Phys. Chem. Chem. Phys.* **2014**, *16*, 15126-15138. DOI: 10.1039/C4CP00617H

23. Vasiliu, M.; Arduengo, A. J.; Dixon, D. A., Role of Electronegative Substituents on the Bond Energies in the Grubbs Metathesis Catalysts for M = Fe, Ru, Os. *J. Phys. Chem. C* **2014**, *118*, 13563-13577. DOI: 10.1021/jp500472p

24. Vjunov, A.; Hu, M. Y.; Feng, J.; Camaioni, D. M.; Mei, D.; Hu, J. Z.; Zhao, C.; Lercher, J. A., Following Solid-Acid-Catalyzed Reactions by MAS NMR Spectroscopy in Liquid Phase—Zeolite-Catalyzed Conversion of Cyclohexanol in Water. *Angew. Chem., Int. Ed.* **2014**, *53*, 479-482. DOI: 10.1002/anie.201306673

25. Wei, Z.; Karim, A. M.; Li, Y.; King, D. L.; Wang, Y., Elucidation of the roles of Re in steam reforming of glycerol over Pt-Re/C catalysts. *J. Catal.* **2014**. DOI: 10.1016/j.jcat.2014.11.006

26. Wiedner, E. S.; Appel, A. M., Thermochemical Insight into the Reduction of CO to CH_3OH with $[Re(CO)]^+$ and $[Mn(CO)]^+$ Complexes. *J. Am. Chem. Soc.* **2014**, *136*, 8661-8668. DOI: 10.1021/ja502316e

27. Zhang, H.; Sun, J.; Dagle, V. L.; Halevi, B.; Datye, A. K.; Wang, Y., Influence of ZnO Facets on Pd/ZnO Catalysts for Methanol Steam Reforming. *ACS Catal.* **2014**, *4*, 2379-2386. DOI: 10.1021/cs500590t

2015

28. Allayarov, S. R.; Gordon, D. A.; Henderson, P. B.; Fernandez, R. E.; Jackson, V. E.; Dixon, D. A., Photochemistry of long-lived $[(CF_3)_2CF]_2C{\bullet}C_2F_5$ radicals. *J. Fluorine Chem.* **2015**, *180*, 240-247. DOI: 10.1016/j.jfluchem.2015.10.003

29. Dutta, A.; Lense, S.; Roberts, J. A. S.; Helm, M. L.; Shaw, W. J., The Role of Solvent and the Outer Coordination Sphere on H_2 Oxidation Using $[Ni(P^{Cy2}N^{Pyz2})_2]^{2+}$. *Eur. J. Inorg. Chem.* **2015**, *2015*, 5218-5225. DOI: 10.1002/ejic.201500732

30. Hensley, A. J. R.; Schneider, S.; Wang, Y.; McEwen, J.-S., Adsorption of aromatics on the (111) surface of PtM and PtM_3 (M = Fe, Ni) alloys. *RSC Advances* **2015**, *5*, 85705-85719. DOI: 10.1039/C5RA13578H

31. Hensley, A. J. R.; Wang, Y.; McEwen, J.-S., Phenol Deoxygenation Mechanisms on Fe(110) and Pd(111). *ACS Catal.* **2015**, *5*, 523-536. DOI: 10.1021/cs501403w

32. Lee, M.-S.; Peter McGrail, B.; Rousseau, R.; Glezakou, V.-A., Structure, dynamics and stability of water/$scCO_2$/mineral interfaces from ab initio molecular dynamics simulations. *Scientific Reports* **2015**, *5*, 14857. DOI: 10.1038/srep14857

33. Nandasiri, M. I.; Shutthanandan, V.; Manandhar, S.; Schwarz, A. M.; Oxenford, L.; Kennedy, J. V.; Thevuthasan, S.; Henderson, M. A., Instability of Hydrogenated TiO_2. *J. Phys. Chem. Lett.* **2015**, *6*, 4627-4632. DOI: 10.1021/acs.jpclett.5b02219

34. Novotny, Z.; Netzer, F. R.; Dohnalek, Z., Cerium Oxide Nanoclusters on Graphene/Ru (0001): Intercalation of Oxygen via Spillover. *ACS Nano* **2015**, *9*, 8617-8626. DOI: 10.1021/acsnano.5b03987

35. Petrik, N. G.; Henderson, M. A.; Kimmel, G. A., Insights into Acetone Photochemistry on Rutile TiO_2(110). 1. Off-Normal CH_3 Ejection from Acetone Diolate. *J. Phys. Chem. C* **2015**, *119*, 12262-12272. DOI: 10.1021/acs.jpcc.5b02477

36. Petrik, N. G.; Henderson, M. A.; Kimmel, G. A., Insights into Acetone Photochemistry on Rutile TiO_2(110). 2. New Photodesorption Channel with CH_3 Ejection along the Surface Normal. *J. Phys. Chem. C* **2015**, *119*, 12273-12282. DOI: 10.1021/acs.jpcc.5b02478

37. Rodriguez-Maciá, P.; Dutta, A.; Lubitz, W.; Shaw, W. J.; Rüdiger, O., Direct Comparison of the Performance of a Bio-inspired Synthetic Nickel Catalyst and a [NiFe]-Hydrogenase, Both Covalently Attached to Electrodes. *Angew. Chem., Int. Ed.* **2015**, *54*, 12303-12307. DOI: 10.1002/anie.201502364

38. Sun, J.; Zhang, H.; Yu, N.; Davidson, S.; Wang, Y., Effect of Cobalt Particle Size on Acetone Steam Reforming. *ChemCatChem* **2015**, *7*, 2932-2936. DOI: 10.1002/cctc.201500336

39. Szanyi, J.; Kwak, J. H., Photo-catalytic oxidation of acetone on a TiO_2 powder: An in situ FTIR investigation. *J. Mol. Catal. A-Chem.* **2015**, *406*, 213-223. DOI: 10.1016/j.molcata.2015.05.025

40. Thanthiriwatte, K. S.; Vasiliu, M.; Battey, S. R.; Lu, Q.; Peterson, K. A.; Andrews, L.; Dixon, D. A., Gas Phase Properties of MX_2 and MX_4 (X = F, Cl) for M = Group 4, Group 14, Cerium, and Thorium. *J. Phys. Chem. A* **2015**, *119*, 5790-5803. DOI: 10.1021/acs.jpca.5b02544

41. Wang, Y.-G.; Mei, D.; Glezakou, V.-A.; Li, J.; Rousseau, R., Dynamic formation of single-atom catalytic active sites on ceria-supported gold nanoparticles. *Nat. Commun.* **2015**, *6*. DOI: 10.1038/ncomms7511

42. Wang, Z.-T.; Garcia, J. C.; Deskins, N. A.; Lyubinetsky, I., Ability of TiO_2(110) surface to be fully hydroxylated and fully reduced. *Phys. Rev. B* **2015**, *92*, 081402.

43. Wei, Z.; Karim, A.; Li, Y.; Wang, Y., Elucidation of the Roles of Re in Aqueous-Phase Reforming of Glycerol over Pt–Re/C Catalysts. *ACS Catal.* **2015**, *5*, 7312-7320. DOI: 10.1021/acscatal.5b01770

44. Weiss, C. J.; Wiedner, E. S.; Roberts, J. A. S.; Appel, A. M., Nickel phosphine catalysts with pendant amines for electrocatalytic oxidation of alcohols. *Chem. Commun.* **2015**, *51*, 6172-6174. DOI: 10.1039/C5CC01107H

45. Whittemore, S. M.; Edvenson, G.; Camaioni, D. M.; Karkamkar, A.; Neiner, D.; Parab, K.; Autrey, T., Catalytic reduction of polar substrates without metals: A thermodynamic and kinetic study of heterolytic activation of hydrogen by vacancies in frustrated Lewis pairs. *Catal. Today* **2015**, *251*, 28-33. DOI: 10.1016/j.cattod.2014.10.040

46. Yi, C.-W.; Szanyi, J., The thermal behavior of Pd on graphene/Ru(0001). *Surf. Sci.* **2015**, *641*, 154-158. DOI: 10.1016/j.susc.2015.06.005

47. Yoon, Y.; Du, Y.; Garcia, J. C.; Zhu, Z.; Wang, Z.-T.; Petrik, N. G.; Kimmel, G. A.; Dohnalek, Z.; Henderson, M. A.; Rousseau, R.; Deskins, N. A.; Lyubinetsky, I., Anticorrelation between Surface and Subsurface Point Defects and the Impact on the Redox Chemistry of TiO_2(110). *ChemPhysChem* **2015**, *16*, 313-321. DOI: 10.1002/cphc.201402599

48. Zhang, H.; Sun, J.; Liu, C.; Wang, Y., Distinct water activation on polar/non-polar facets of ZnO nanoparticles. *J. Catal.* **2015**, *331*, 57-62. DOI: 10.1016/j.jcat.2015.08.016

49. Zhang, S.; Bullock, R. M., Molybdenum Hydride and Dihydride Complexes Bearing Diphosphine Ligands with a Pendant Amine: Formation of Complexes with Bound Amines. *Inorg. Chem.* **2015**, *54*, 6397-6409. 10.1021/acs.inorgchem.5b00728

2016

50. Asthagiri, A.; Dixon, D. A.; Dohnálek, Z.; Kay, B. D.; Rodriguez, J. A.; Rousseau, R.; Stacchiola, D. J.; Weaver, J. F. *Catalytic Chemistry on Oxide Nanostructures* in *Oxide Materials at the Two-Dimensional Limit*; Netzer, P. F., Fortunelli, A., Eds.; Springer International Publishing: Cham, 2016; pp 251-280.

51. Cai, Q. X.; Wang, J. G.; Wang, Y.; Mei, D. H., First-Principles Thermodynamics Study of Spinel $MgAl_2O_4$ Surface Stability. *J. Phys. Chem. C* **2016**, *120*, 19087-19096. DOI: 10.1021/acs.jpcc.6b02998

52. Comish, A. J.; Ginovska, B.; Thelen, A.; da Silva, J. C. S.; Soares, T. A.; Raugei, S.; Dupuis, M.; Shaw, W. J.; Hegg, E. L., Single-Amino Acid Modifications Reveal Additional Controls on the Proton Pathway of FeFe -Hydrogenase. *Biochemistry* **2016**, *55*, 3165-3173. DOI: 10.1021/acs.biochem.5b01044

53. Davidson, S. D.; Sun, J.; Wang, Y., The effect of ZnO addition on H_2O activation over Co/ZrO_2 catalysts. *Catal. Today* **2016**, *269*, 140-147. DOI: 10.1016/j.cattod.2015.10.016

54. Dutta, A.; Ginovska, B.; Raugei, S.; Roberts, J. A.; Shaw, W. J., Optimizing conditions for utilization of an H_2 oxidation catalyst with outer coordination sphere functionalities. *Dalton Trans* **2016**, *45*, 9786-93. DOI: 10.1039/c6dt00280c

55. Fang, Z.; Thanthiriwatte, K. S.; Dixon, D. A.; Andrews, L.; Wang, X., Properties of Cerium Hydroxides from Matrix Infrared Spectra and Electronic Structure Calculations. *Inorg. Chem.* **2016**, *55*, 1702-1714. DOI: 10.1021/acs.inorgchem.5b02619

56. Fang, Z. T.; Both, J.; Li, S. G.; Yue, S. W.; Apra, E.; Keceli, M.; Wagner, A. F.; Dixon, D. A., Benchmark Calculations of Energetic Properties of Groups 4 and 6 Transition Metal Oxide Nanoclusters Including Comparison to Density Functional Theory. *J. Chem. Theory Comput.* **2016**, *12*, 3689-3710. DOI: 10.1021/acs.jctc.6b00464

57. Fang, Z. T.; Lee, Z.; Peterson, K. A.; Dixon, D. A., Use of Improved Orbitals for CCSD(T) Calculations for Predicting Heats of Formation of Group IV and Group VI Metal Oxide Monomers

and Dimers and UCl_6. *J. Chem. Theory Comput.* **2016**, *12*, 3583-3592. DOI: 10.1021/acs.jctc.6b00327

58. Feller, D.; Peterson, K. A.; Dixon, D. A. *The Impact of Larger Basis Sets and Explicitly Correlated Coupled Cluster Theory on the Feller-Peterson-Dixon Composite Method* in *Annual Reports in Computational Chemistry*; Dixon, D. A., Ed.; Elsevier: Amsterdam, 2016; Vol. 12.

59. Finney, B.; Fang, Z.; Francisco, J. S.; Dixon, D. A., Energetic Properties and Electronic Structure of [Si,N,S] and [Si,P,S] Isomers. *J. Phys. Chem. A* **2016**, *120*, 1691-1697. DOI: 10.1021/acs.jpca.6b00918

60. Ginovska, B.; Raugei, S.; Shaw, W. J. *Molecular Dynamics Studies of Proton Transport in Hydrogenase and Hydrogenase Mimics* in *Computational Approaches for Studying Enzyme Mechanism, Pt B*; Voth, G. A., Ed., 2016; Vol. 578; pp 73-101.

61. Hensley, A. J. R.; Wang, Y.; McEwen, J.-S., Adsorption of guaiacol on Fe (110) and Pd (111) from first principles. *Surf. Sci.* **2016**, *648*, 227-235. DOI: 10.1016/j.susc.2015.10.030

62. Hu, J. Z.; Xu, S.; Kwak, J. H.; Hu, M. Y.; Wan, C.; Zhao, Z.; Szanyi, J.; Bao, X.; Han, X.; Wang, Y.; Peden, C. H. F., High field 27Al MAS NMR and TPD studies of active sites in ethanol dehydration using thermally treated transitional aluminas as catalysts. *J. Catal.* **2016**, *336*, 85-93. DOI: 10.1016/j.jcat.2016.01.006

63. Kwak, J. H.; Lee, J.; Szanyi, J.; Peden, C. H. F., Modification of the acid/base properties of γ-Al_2O_3 by oxide additives: An ethanol TPD investigation. *Catal. Today* **2016**, *265*, 240-244. DOI: 10.1016/j.cattod.2015.07.042

64. Laminack, W.; Gole, J. L.; White, M. G.; Ozdemir, S.; Ogden, A. G.; Martin, H. J.; Fang, Z.; Wang, T.-H.; Dixon, D. A., Synthesis of nanoscale silicon oxide oxidation state distributions: The transformation from hydrophilicity to hydrophobicity. *Chem. Phys. Lett.* **2016**, *653*, 137-143. DOI: 10.1016/j.cplett.2016.04.079

65. Priyadarshani, N.; Dutta, A.; Ginovska, B.; Buchko, G. W.; O'Hagan, M.; Raugei, S.; Shaw, W. J., Achieving Reversible H_2/H^+ Interconversion at Room Temperature with Enzyme-Inspired Molecular Complexes: A Mechanistic Study. *ACS Catal.* **2016**, *6*, 6037-6049. DOI: 10.1021/acscatal.6b01433

66. Reback, M. L.; Ginovska, B.; Buchko, G. W.; Dutta, A.; Priyadarshani, N.; Kier, B. L.; Helm, M. L.; Raugei, S.; Shaw, W. J., Investigating the role of chain and linker length on the catalytic activity of an H_2 production catalyst containing beta-hairpin peptide. *J. Coord. Chem.* **2016**, *69*, 1730-1747. DOI: 10.1080/00958972.2016.1188924

67. Rodriguez-Macia, P.; Priyadarshani, N.; Dutta, A.; Weidenthaler, C.; Lubitz, W.; Shaw, W. J.; Rudiger, O., Covalent Attachment of the Water-insoluble $Ni(P^{Cy2}N^{Phe2})_2$ Electrocatalyst to Electrodes Showing Reversible Catalysis in Aqueous Solution. *Electroanalysis* **2016**, *28*, 2452-2458. DOI: 10.1002/elan.201600306

68. Wang, W. Y.; Wu, K.; Liu, P. L.; Li, L.; Yang, Y. Q.; Wang, Y., Hydrodeoxygenation of p-Cresol over Pt/Al_2O_3 Catalyst Promoted by ZrO_2, CeO_2, and CeO_2-ZrO_2. *Ind. Eng. Chem. Res.* **2016**, *55*, 7598-7603. DOI: 10.1021/acs.iecr.6b00515

69. Wiedner, E. S.; Chambers, M. B.; Pitman, C. L.; Bullock, R. M.; Miller, A. J. M.; Appel, A. M., Thermodynamic Hydricity of Transition Metal Hydrides. *Chem. Rev.* **2016**, *116*, 8655-8692. DOI: 10.1021/acs.chemrev.6b00168

70. Yi, C. W.; Szanyi, J., Pd overlayer on oxygen pre-covered graphene/Ru(0001): Thermal stability. *Surf. Sci.* **2016**, *648*, 271-277. DOI: 10.1016/j.susc.2015.12.018

71. Yu, N.; Zhang, H.; Davidson, S. D.; Sun, J.; Wang, Y., Effect of ZnO facet on ethanol steam reforming over Co/ZnO. *Catal. Commun.* **2016**, *73*, 93-97. DOI: 10.1016/j.catcom.2015.10.018

72. Zhang, S. G.; Li, H. X.; Appel, A. M.; Hall, M. B.; Bullock, R. M., Facile P-C/C-H Bond-Cleavage Reactivity of Nickel Bis(diphosphine) Complexes. *Chem.-Eur. J.* **2016**, *22*, 9493-9497. DOI: 10.1002/chem.201601469

2017

73. Bossola, F.; Pereira-Hernández, X. I.; Evangelisti, C.; Wang, Y.; Dal Santo, V., Investigation of the promoting effect of Mn on a Pt/C catalyst for the steam and aqueous phase reforming of glycerol. *J. Catal.* **2017**, *349*, 75-83. DOI: 10.1016/j.jcat.2017.03.002

74. Burgess, S. A.; Kendall, A. J.; Tyler, D. R.; Linehan, J. C.; Appel, A. M., Hydrogenation of CO_2 in Water Using a Bis(diphosphine) Ni–H Complex. *ACS Catal.* **2017**, *7*, 3089-3096. DOI: 10.1021/acscatal.7b00350

75. Chen, M.; Dixon, D. A., Modeling the formation of TiO_2 ultra-small nanoparticles. *Nanoscale* **2017**, *9*, 7143-7162. DOI: 10.1039/C7NR01749A

76. Christe, K. O.; Haiges, R.; Vasiliu, M.; Dixon, D. A., Formation Mechanism of NF_4^+ Salts and Extraordinary Enhancement of the Oxidizing Power of Fluorine by Strong Lewis Acids. *Angew. Chem., Int. Ed.* **2017**. DOI: 10.1002/anie.201701784

77. Fang, Z. T.; Vasiliu, M.; Peterson, K. A.; Dixon, D. A., Prediction of Bond Dissociation Energies/Heats of Formation for Diatomic Transition Metal Compounds: CCSD(T) Works. *J. Chem. Theory Comput.* **2017**, *13*, 1057-1066. DOI: 10.1021/acs.jctc.6b00971

78. Feng, R. L.; Vasiliu, M.; Peterson, K. A.; Dixon, D. A., Acidity of $M(VI)O_2(OH)_2$ for M = Group 6, 16, and U as Central Atoms. *J. Phys. Chem. A* **2017**, *121*, 1041-1050. DOI: 10.1021/acs.jpca.6b11889

79. Gentil, S.; Lalaoui, N.; Dutta, A.; Nedellec, Y.; Cosnier, S.; Shaw, W. J.; Artero, V.; Le Goff, A., Carbon-Nanotube-Supported Bio-Inspired Nickel Catalyst and Its Integration in Hybrid Hydrogen/Air Fuel Cells. *Angew. Chem., Int. Ed.* **2017**, *56*, 1845-1849. DOI: 10.1002/anie.201611532

80. Hu, J. Z.; Wan, C.; Vjunov, A.; Wang, M.; Zhao, Z.; Hu, M. Y.; Camaioni, D. M.; Lercher, J. A., ^{27}Al MAS NMR Studies of HBEA Zeolite at Low to High Magnetic Fields. *J. Phys. Chem. C* **2017**. DOI: 10.1021/acs.jpcc.7b03517

81. Iglesia, E.; Wang, S.; Agirrezabal-Telleria, I.; Bhan, A.; Simonetti, D.; Takanabe, K., Catalysis for Fuels Introductory Lecture: Catalytic routes to fuels from C1 and oxygenate molecules. *Faraday Discuss.* **2017**. DOI: 10.1039/C7FD00018A

82. Li, W.-Z.; Nie, L.; Cheng, Y.; Kovarik, L.; Liu, J.; Wang, Y., Surface enrichment of Pt in stable Pt-Ir nano-alloy particles on $MgAl_2O_4$ spinel in oxidizing atmosphere. *Catal. Commun.* **2017**, *93*, 57-61. DOI: 10.1016/j.catcom.2017.01.012

83. Li, W. Z.; Kovarik, L.; Cheng, Y. W.; Nie, L.; Bowden, M. E.; Liu, J.; Wang, Y., Stabilization and transformation of Pt nanocrystals supported on $ZnAl_2O_4$ spinel. *Rsc Advances* **2017**, *7*, 3282-3286. DOI: 10.1039/c6ra26159k

84. Liu, Y. S.; Vjunov, A.; Shi, H.; Eckstein, S.; Camaioni, D. M.; Mei, D. H.; Barath, E.; Lercher, J. A., Enhancing the catalytic activity of hydronium ions through constrained environments. *Nat. Commun.* **2017**, *8*. DOI: 10.1038/ncomms14113

85. Vasiliu, M.; Peterson, K. A.; Dixon, D. A., Benchmark-Quality Atomization Energies for BeH and BeH_2. *J. Chem. Theory Comput.* **2017**, *13*, 649-653. DOI: 10.1021/acs.jctc.6b01154

86. Xu, C.-Q.; Lee, M.-S.; Wang, Y.-G.; Cantu, D. C.; Li, J.; Glezakou, V.-A.; Rousseau, R., Structural Rearrangement of Au–Pd Nanoparticles under Reaction Conditions: An ab Initio Molecular Dynamics Study. *ACS Nano* **2017**. DOI: 10.1021/acsnano.6b07409

Publications jointly funded by this grant and other grants with leading intellectual contribution from this grant

2014

87. Bays, J. T.; Priyadarshani, N.; Jeletic, M. S.; Hulley, E. B.; Miller, D. L.; Linehan, J. C.; Shaw, W. J., The Influence of the Second and Outer Coordination Spheres on Rh(diphosphine)$_2$ CO_2 Hydrogenation Catalysts. *ACS Catal.* **2014**, *4*, 3663-3670. DOI: 10.1021/cs5009199

88. Dutta, A.; DuBois, D. L.; Roberts, J. A. S.; Shaw, W. J., Amino acid modified Ni catalyst exhibits reversible H_2 oxidation/production over a broad pH range at elevated temperatures. *Proc. Natl. Acad. Sci. U. S. A.* **2014**, *111*, 16286-16291. DOI: 10.1073/pnas.1416381111

89. Dutta, A.; Roberts, J. A. S.; Shaw, W. J., Arginine-Containing Ligands Enhance H2 Oxidation Catalyst Performance. *Angew. Chem., Int. Ed.* **2014**, *53*, 6487-6491. DOI: 10.1002/anie.201402304

90. Galan, B. R.; Wiedner, E. S.; Helm, M. L.; Linehan, J. C.; Appel, A. M., Effects of Phosphine–Carbene Substitutions on the Electrochemical and Thermodynamic Properties of Nickel Complexes. *Organometallics* **2014**, *33*, 2287-2294. DOI: 10.1021/om500206e

91. Garner, E. B.; Arduengo, A. J.; Streubel, R.; Dixon, D. A., Electronic structure predictions of the properties of non-innocent P-ligands in group 6B transition metal complexes. *Dalton. Trans.* **2014**, *43*, 2069-2078. DOI: 10.1039/c3dt52056k

92. Ginovska-Pangovska, B.; Dutta, A.; Reback, M. L.; Linehan, J. C.; Shaw, W. J., Beyond the Active Site: The Impact of the Outer Coordination Sphere on Electrocatalysts for Hydrogen Production and Oxidation. *Acc. Chem. Res.* **2014**, *47*, 2621-2630. DOI: 10.1021/ar5001742

93. Ginovska-Pangovska, B.; Ho, M.-H.; Linehan, J. C.; Cheng, Y.; Dupuis, M.; Raugei, S.; Shaw, W. J., Molecular dynamics study of the proposed proton transport pathways in [FeFe]-hydrogenase. *Biochimica et Biophysica Acta (BBA) - Bioenergetics* **2014**, *1837*, 131-138. DOI: 10.1016/j.bbabio.2013.08.004

94. He, J.; Lu, L.; Zhao, C.; Mei, D.; Lercher, J. A., Mechanisms of catalytic cleavage of benzyl phenyl ether in aqueous and apolar phases. *J. Catal.* **2014**, *311*, 41-51. DOI: 10.1016/j.jcat.2013.10.024

95. He, J.; Zhao, C.; Lercher, J. A., Impact of solvent for individual steps of phenol hydrodeoxygenation with Pd/C and HZSM-5 as catalysts. *J. Catal.* **2014**, *309*, 362-375. DOI: 10.1016/j.jcat.2013.09.009

96. He, J.; Zhao, C.; Mei, D.; Lercher, J. A., Mechanisms of selective cleavage of C–O bonds in di-aryl ethers in aqueous phase. *J. Catal.* **2014**, *309*, 280-290. DOI: 10.1016/j.jcat.2013.09.012

97. Hensley, A. J. R.; Wang, Y.; McEwen, J.-S., Adsorption of phenol on Fe (110) and Pd (111) from first principles. *Surf. Sci.* **2014**, *630*, 244-253. DOI: 10.1016/j.susc.2014.08.003

98. Jeletic, M. S.; Helm, M. L.; Hulley, E. B.; Mock, M. T.; Appel, A. M.; Linehan, J. C., A Cobalt Hydride Catalyst for the Hydrogenation of CO_2: Pathways for Catalysis and Deactivation. *ACS Catal.* **2014**, *4*, 3755-3762. DOI: 10.1021/cs5009927

99. Jones, A. J.; Carr, R. T.; Zones, S. I.; Iglesia, E., Acid strength and solvation in catalysis by MFI zeolites and effects of the identity, concentration and location of framework heteroatoms. *J. Catal.* **2014**, *312*, 58-68. DOI: 10.1016/j.jcat.2014.01.007

100. Kumar, N.; Camaioni, D. M.; Dupuis, M.; Raugei, S.; Appel, A. M., Mechanistic insights into hydride transfer for catalytic hydrogenation of CO_2 with cobalt complexes. *Dalton. Trans.* **2014**, *43*, 11803-11806. DOI: 10.1039/C4DT01551G

101. Lense, S.; Dutta, A.; Roberts, J. A. S.; Shaw, W. J., A proton channel allows a hydrogen oxidation catalyst to operate at a moderate overpotential with water acting as a base. *Chem. Commun.* **2014**, *50*, 792-795. DOI: 10.1039/C3CC46829A

102. Petrik, N. G.; Kimmel, G. A., Probing the photochemistry of chemisorbed oxygen on TiO_2(110) with Kr and other co-adsorbates. *Phys. Chem. Chem. Phys.* **2014**, *16*, 2338-2346. DOI: 10.1039/C3CP54195A

103. Reback, M. L.; Buchko, G. W.; Kier, B. L.; Ginovska-Pangovska, B.; Xiong, Y.; Lense, S.; Hou, J.; Roberts, J. A. S.; Sorensen, C. M.; Raugei, S.; Squier, T. C.; Shaw, W. J., Enzyme Design from the Bottom Up: An Active Nickel Electrocatalyst with a Structured Peptide Outer Coordination Sphere. *Chem. Eur. J.* **2014**, *20*, 1510-1514. DOI: 10.1002/chem.201303976

104. Thanthiriwatte, K. S.; Spruell, J. M.; Dixon, D. A.; Christe, K. O.; Jenkins, H. D. B., Structures, Vibrational Frequencies, and Stabilities of Halogen Cluster Anions and Cations, $X_n^{+/-}$, n=3, 4, and 5. *Inorg. Chem.* **2014**, *53*, 8136-8146. DOI: 10.1021/ic501211f

105. Vjunov, A.; Fulton, J. L.; Huthwelker, T.; Pin, S.; Mei, D.; Schenter, G. K.; Govind, N.; Camaioni, D. M.; Hu, J. Z.; Lercher, J. A., Quantitatively Probing the Al Distribution in Zeolites. *J. Am. Chem. Soc.* **2014**, *136*, 8296-8306. DOI: 10.1021/ja501361v

106. Weiss, C. J.; Das, P.; Miller, D. L.; Helm, M. L.; Appel, A. M., Catalytic Oxidation of Alcohol via Nickel Phosphine Complexes with Pendant Amines. *ACS Catal.* **2014**, *4*, 2951-2958. DOI: 10.1021/cs500853f

107. Yadav, M.; Linehan, J. C.; Karkamkar, A. J.; van der Eide, E.; Heldebrant, D. J., Homogeneous Hydrogenation of CO_2 to Methyl Formate Utilizing Switchable Ionic Liquids. *Inorg. Chem.* **2014**, *53*, 9849-9854. DOI: 10.1021/ic501378w

108. Yoon, Y.; Rousseau, R.; Weber, R. S.; Mei, D.; Lercher, J. A., First-Principles Study of Phenol Hydrogenation on Pt and Ni Catalysts in Aqueous Phase. *J. Am. Chem. Soc.* **2014**, *136*, 10287-10298. DOI: 10.1021/ja501592y

109. Zhao, Z.; Xu, S.; Hu, M.; Bao, X.; Peden, C. H. F.; Hu, J. Z., Investigation of Aluminum Site Changes of Dehydrated Zeolite H-Beta during a Rehydration Process by High Field Solid State NMR. *J. Phys. Chem. C* **2014**, *119*, 1410-1417. DOI: 10.1021/jp509982r

2015

110. Allayarov, S. R.; Gordon, D. A.; Henderson, P. B.; Fernandez, R. E.; Jackson, V. E.; Dixon, D. A., Photochemistry of long-lived $[(CF_3)_2CF]_2C{\bullet}C_2F_5$ radicals. *J. Fluorine Chem.* **2015**, *180*, 240-247. DOI: 10.1016/j.jfluchem.2015.10.003

111. Dutta, A.; Lense, S.; Roberts, J. A. S.; Helm, M. L.; Shaw, W. J., The Role of Solvent and the Outer Coordination Sphere on H_2 Oxidation Using $[Ni(P^{Cy2}N^{Pyz2})_2]^{2+}$. *Eur. J. Inorg. Chem.* **2015**, *2015*, 5218-5225. DOI: 10.1002/ejic.201500732

112. Foraita, S.; Fulton, J. L.; Chase, Z. A.; Vjunov, A.; Xu, P.; Baráth, E.; Camaioni, D. M.; Zhao, C.; Lercher, J. A., Impact of the Oxygen Defects and the Hydrogen Concentration on the Surface of

Tetragonal and Monoclinic ZrO_2 on the Reduction Rates of Stearic Acid on Ni/ZrO_2. *Chem. Eur. J.* **2015**, *21*, 2423-2434. DOI: 10.1002/chem.201405312

113. Hensley, A. J. R.; Schneider, S.; Wang, Y.; McEwen, J.-S., Adsorption of aromatics on the (111) surface of PtM and PtM_3 (M = Fe, Ni) alloys. *RSC Advances* **2015**, *5*, 85705-85719. DOI: 10.1039/C5RA13578H

114. Hensley, A. J. R.; Wang, Y.; McEwen, J.-S., Phenol Deoxygenation Mechanisms on Fe(110) and Pd(111). *ACS Catal.* **2015**, *5*, 523-536. DOI: 10.1021/cs501403w

115. Hu, J. Z.; Hu, M. Y.; Zhao, Z.; Xu, S.; Vjunov, A.; Shi, H.; Camaioni, D. M.; Peden, C. H. F.; Lercher, J. A., Sealed rotors for in situ high temperature high pressure MAS NMR. *Chem. Commun.* **2015**, *51*, 13458-13461. DOI: 10.1039/C5CC03910J

116. Kasakov, S.; Shi, H.; Camaioni, D.; Zhao, C.; Barath, E.; Jentys, A.; Lercher, J. A., Reductive Deconstruction of Organosolv Lignin Catalysed by Zeolite Supported Nickel Nanoparticles. *Green Chem.* **2015**, *17*, 5079-5090. DOI: 10.1039/C5GC02160J

117. Lee, M.-S.; Peter McGrail, B.; Rousseau, R.; Glezakou, V.-A., Structure, dynamics and stability of water/scCO_2/mineral interfaces from ab initio molecular dynamics simulations. *Scientific Reports* **2015**, *5*, 14857. DOI: 10.1038/srep14857

118. Nandasiri, M. I.; Shutthanandan, V.; Manandhar, S.; Schwarz, A. M.; Oxenford, L.; Kennedy, J. V.; Thevuthasan, S.; Henderson, M. A., Instability of Hydrogenated TiO_2. *J. Phys. Chem. Lett.* **2015**, *6*, 4627-4632. DOI: 10.1021/acs.jpclett.5b02219

119. Novotny, Z.; Netzer, F. R.; Dohnalek, Z., Cerium Oxide Nanoclusters on Graphene/Ru (0001): Intercalation of Oxygen via Spillover. *ACS Nano* **2015**, *9*, 8617-8626. DOI: 10.1021/acsnano.5b03987

120. Petrik, N. G.; Henderson, M. A.; Kimmel, G. A., Insights into Acetone Photochemistry on Rutile TiO_2(110). 1. Off-Normal CH_3 Ejection from Acetone Diolate. *J. Phys. Chem. C* **2015**, *119*, 12262-12272. DOI: 10.1021/acs.jpcc.5b02477

121. Petrik, N. G.; Henderson, M. A.; Kimmel, G. A., Insights into Acetone Photochemistry on Rutile TiO_2(110). 2. New Photodesorption Channel with CH_3 Ejection along the Surface Normal. *J. Phys. Chem. C* **2015**, *119*, 12273-12282. DOI: 10.1021/acs.jpcc.5b02478

122. Rahman, M. M.; Davidson, S. D.; Sun, J.; Wang, Y., Effect of Water on Ethanol Conversion over ZnO. *Top. Catal.* **2015**, *59*, 37-45. DOI: 10.1007/s11244-015-0503-9

123. Rodriguez-Maciá, P.; Dutta, A.; Lubitz, W.; Shaw, W. J.; Rüdiger, O., Direct Comparison of the Performance of a Bio-inspired Synthetic Nickel Catalyst and a [NiFe]-Hydrogenase, Both Covalently Attached to Electrodes. *Angew. Chem., Int. Ed.* **2015**, *54*, 12303-12307. DOI: 10.1002/anie.201502364

124. Shi, H.; Lercher, J. A.; Yu, X.-Y., Sailing Into Uncharted Waters: Recent Advances in the In Situ Monitoring of Catalytic Processes in Aqueous Environments. *Catal. Sci. Technol.* **2015**, *5*, 3035-3060. DOI: 10.1039/C4CY01720J

125. Song, W.; Liu, Y.; Barath, E.; Zhao, C.; Lercher, J. A., Synergistic effects of Ni and acid sites for hydrogenation and C-O bond cleavage of substituted phenols. *Green Chem.* **2015**, *17*, 1204-1218. DOI: 10.1039/C4GC01798F

126. Sun, J.; Zhang, H.; Yu, N.; Davidson, S.; Wang, Y., Effect of Cobalt Particle Size on Acetone Steam Reforming. *ChemCatChem* **2015**, *7*, 2932-2936. DOI: 10.1002/cctc.201500336

127. Szanyi, J.; Kwak, J. H., Photo-catalytic oxidation of acetone on a TiO_2 powder: An in situ FTIR investigation. *J. Mol. Catal. A-Chem.* **2015**, *406*, 213-223. DOI: 10.1016/j.molcata.2015.05.025

128. Thanthiriwatte, K. S.; Vasiliu, M.; Battey, S. R.; Lu, Q.; Peterson, K. A.; Andrews, L.; Dixon, D. A., Gas Phase Properties of MX_2 and MX_4 (X = F, Cl) for M = Group 4, Group 14, Cerium, and Thorium. *J. Phys. Chem. A* **2015**, *119*, 5790-5803. DOI: 10.1021/acs.jpca.5b02544

129. Vjunov, A.; Derewinski, M. A.; Fulton, J. L.; Camaioni, D. M.; Lercher, J. A., Impact of Zeolite Aging in Hot Liquid Water on Activity for Acid-Catalyzed Dehydration of Alcohols. *J. Am. Chem. Soc.* **2015**, *137*, 10374-10382. DOI: 10.1021/jacs.5b06169

130. Wang, Y.-G.; Mei, D.; Glezakou, V.-A.; Li, J.; Rousseau, R., Dynamic formation of single-atom catalytic active sites on ceria-supported gold nanoparticles. *Nat. Commun.* **2015**, *6*. DOI: 10.1038/ncomms7511

131. Wang, Z.-T.; Garcia, J. C.; Deskins, N. A.; Lyubinetsky, I., Ability of TiO_2(110) surface to be fully hydroxylated and fully reduced. *Phys. Rev. B* **2015**, *92*, 081402.

132. Wei, Z.; Karim, A.; Li, Y.; Wang, Y., Elucidation of the Roles of Re in Aqueous-Phase Reforming of Glycerol over Pt–Re/C Catalysts. *ACS Catal.* **2015**, *5*, 7312-7320. DOI: 10.1021/acscatal.5b01770

133. Weiss, C. J.; Wiedner, E. S.; Roberts, J. A. S.; Appel, A. M., Nickel phosphine catalysts with pendant amines for electrocatalytic oxidation of alcohols. *Chem. Commun.* **2015**, *51*, 6172-6174. DOI: 10.1039/C5CC01107H

134. Yoon, Y.; Du, Y.; Garcia, J. C.; Zhu, Z.; Wang, Z.-T.; Petrik, N. G.; Kimmel, G. A.; Dohnalek, Z.; Henderson, M. A.; Rousseau, R.; Deskins, N. A.; Lyubinetsky, I., Anticorrelation between Surface and Subsurface Point Defects and the Impact on the Redox Chemistry of TiO_2(110). *ChemPhysChem* **2015**, *16*, 313-321. DOI: 10.1002/cphc.201402599

135. Zhang, H.; Sun, J.; Liu, C.; Wang, Y., Distinct water activation on polar/non-polar facets of ZnO nanoparticles. *J. Catal.* **2015**, *331*, 57-62. DOI: 10.1016/j.jcat.2015.08.016

2016

136. Alexopoulos, K.; Lee, M.-S.; Liu, Y.; Zhi, Y.; Liu, Y.; Reyniers, M.-F.; Marin, G. B.; Glezakou, V.-A.; Rousseau, R.; Lercher, J. A., Anharmonicity and Confinement in Zeolites: Structure, Spectroscopy, and Adsorption Free Energy of Ethanol in H-ZSM-5. *J. Phys. Chem. C* **2016**, *120*, 7172-7182. DOI: 10.1021/acs.jpcc.6b00923

137. Asthagiri, A.; Dixon, D. A.; Dohnálek, Z.; Kay, B. D.; Rodriguez, J. A.; Rousseau, R.; Stacchiola, D. J.; Weaver, J. F. *Catalytic Chemistry on Oxide Nanostructures* in *Oxide Materials at the Two-Dimensional Limit*; Netzer, P. F., Fortunelli, A., Eds.; Springer International Publishing: Cham, 2016; pp 251-280.

138. Cai, Q. X.; Wang, J. G.; Wang, Y.; Mei, D. H., First-Principles Thermodynamics Study of Spinel $MgAl_2O_4$ Surface Stability. *J. Phys. Chem. C* **2016**, *120*, 19087-19096. DOI: 10.1021/acs.jpcc.6b02998

139. Comish, A. J.; Ginovska, B.; Thelen, A.; da Silva, J. C. S.; Soares, T. A.; Raugei, S.; Dupuis, M.; Shaw, W. J.; Hegg, E. L., Single-Amino Acid Modifications Reveal Additional Controls on the Proton Pathway of FeFe -Hydrogenase. *Biochemistry* **2016**, *55*, 3165-3173. DOI: 10.1021/acs.biochem.5b01044

140. Davidson, S. D.; Sun, J.; Wang, Y., The effect of ZnO addition on H_2O activation over Co/ZrO_2 catalysts. *Catal. Today* **2016**, *269*, 140-147. DOI: 10.1016/j.cattod.2015.10.016

141. Dutta, A.; Ginovska, B.; Raugei, S.; Roberts, J. A.; Shaw, W. J., Optimizing conditions for utilization of an H_2 oxidation catalyst with outer coordination sphere functionalities. *Dalton Trans* **2016**, *45*, 9786-93. DOI: 10.1039/c6dt00280c

142. Fang, Z.; Thanthiriwatte, K. S.; Dixon, D. A.; Andrews, L.; Wang, X., Properties of Cerium Hydroxides from Matrix Infrared Spectra and Electronic Structure Calculations. *Inorg. Chem.* **2016**, *55*, 1702-1714. DOI: 10.1021/acs.inorgchem.5b02619

143. Fang, Z. T.; Both, J.; Li, S. G.; Yue, S. W.; Apra, E.; Keceli, M.; Wagner, A. F.; Dixon, D. A., Benchmark Calculations of Energetic Properties of Groups 4 and 6 Transition Metal Oxide Nanoclusters Including Comparison to Density Functional Theory. *J. Chem. Theory Comput.* **2016**, *12*, 3689-3710. DOI: 10.1021/acs.jctc.6b00464

144. Fang, Z. T.; Lee, Z.; Peterson, K. A.; Dixon, D. A., Use of Improved Orbitals for CCSD(T) Calculations for Predicting Heats of Formation of Group IV and Group VI Metal Oxide Monomers and Dimers and UCl_6. *J. Chem. Theory Comput.* **2016**, *12*, 3583-3592. DOI: 10.1021/acs.jctc.6b00327

145. Feller, D.; Peterson, K. A.; Dixon, D. A. *The Impact of Larger Basis Sets and Explicitly Correlated Coupled Cluster Theory on the Feller-Peterson-Dixon Composite Method* in *Annual Reports in Computational Chemistry*; Dixon, D. A., Ed.; Elsevier: Amsterdam, 2016; Vol. 12.

146. Finney, B.; Fang, Z.; Francisco, J. S.; Dixon, D. A., Energetic Properties and Electronic Structure of [Si,N,S] and [Si,P,S] Isomers. *J. Phys. Chem. A* **2016**, *120*, 1691-1697. DOI: 10.1021/acs.jpca.6b00918

147. Ginovska, B.; Raugei, S.; Shaw, W. J. *Molecular Dynamics Studies of Proton Transport in Hydrogenase and Hydrogenase Mimics* in *Computational Approaches for Studying Enzyme Mechanism, Pt B*; Voth, G. A., Ed., 2016; Vol. 578; pp 73-101.

148. Hensley, A. J. R.; Wang, Y.; McEwen, J.-S., Adsorption of guaiacol on Fe (110) and Pd (111) from first principles. *Surf. Sci.* **2016**, *648*, 227-235. DOI: 10.1016/j.susc.2015.10.030

149. Hu, J. Z.; Xu, S.; Kwak, J. H.; Hu, M. Y.; Wan, C.; Zhao, Z.; Szanyi, J.; Bao, X.; Han, X.; Wang, Y.; Peden, C. H. F., High field 27Al MAS NMR and TPD studies of active sites in ethanol dehydration using thermally treated transitional aluminas as catalysts. *J. Catal.* **2016**, *336*, 85-93. DOI: 10.1016/j.jcat.2016.01.006

150. Kwak, J. H.; Lee, J.; Szanyi, J.; Peden, C. H. F., Modification of the acid/base properties of γ-Al_2O_3 by oxide additives: An ethanol TPD investigation. *Catal. Today* **2016**, *265*, 240-244. DOI: 10.1016/j.cattod.2015.07.042

151. Laminack, W.; Gole, J. L.; White, M. G.; Ozdemir, S.; Ogden, A. G.; Martin, H. J.; Fang, Z.; Wang, T.-H.; Dixon, D. A., Synthesis of nanoscale silicon oxide oxidation state distributions: The transformation from hydrophilicity to hydrophobicity. *Chem. Phys. Lett.* **2016**, *653*, 137-143. DOI: 10.1016/j.cplett.2016.04.079

152. Peroni, M.; Mancino, G.; Baráth, E.; Gutiérrez, O. Y.; Lercher, J. A., Bulk and γAl_2O_3-supported Ni_2P and MoP for hydrodeoxygenation of palmitic acid. *Appl.Catal. B* **2016**, *180*, 301-311. DOI: 10.1016/j.apcatb.2015.06.042

153. Priyadarshani, N.; Dutta, A.; Ginovska, B.; Buchko, G. W.; O'Hagan, M.; Raugei, S.; Shaw, W. J., Achieving Reversible H_2/H^+ Interconversion at Room Temperature with Enzyme-Inspired Molecular Complexes: A Mechanistic Study. *ACS Catal.* **2016**, *6*, 6037-6049. DOI: 10.1021/acscatal.6b01433

154. Reback, M. L.; Ginovska, B.; Buchko, G. W.; Dutta, A.; Priyadarshani, N.; Kier, B. L.; Helm, M. L.; Raugei, S.; Shaw, W. J., Investigating the role of chain and linker length on the catalytic activity of an H_2 production catalyst containing beta-hairpin peptide. *J. Coord. Chem.* **2016**, *69*, 1730-1747. DOI: 10.1080/00958972.2016.1188924

155. Rodriguez-Macia, P.; Priyadarshani, N.; Dutta, A.; Weidenthaler, C.; Lubitz, W.; Shaw, W. J.; Rudiger, O., Covalent Attachment of the Water-insoluble $Ni(P^{Cy2}N^{Phe2})_2$ Electrocatalyst to Electrodes Showing Reversible Catalysis in Aqueous Solution. *Electroanalysis* **2016**, *28*, 2452-2458. DOI: 10.1002/elan.201600306

156. Schreiber, M. W.; Rodriguez-Nino, D.; Gutierrez, O. Y.; Lercher, J. A., Hydrodeoxygenation of fatty acid esters catalyzed by Ni on nano-sized MFI type zeolites. *Catal. Sci. Technol.* **2016**, *6*, 7976-7984. DOI: 10.1039/c6cy01598k

157. Song, W.; Liu, Y.; Baráth, E.; Wang, L. L.; Zhao, C.; Mei, D.; Lercher, J. A., Dehydration of 1-Octadecanol over H-BEA: A Combined Experimental and Computational Study. *ACS Catal.* **2016**, *6*, 878-889. DOI: 10.1021/acscatal.5b01217

158. Wang, W. Y.; Wu, K.; Liu, P. L.; Li, L.; Yang, Y. Q.; Wang, Y., Hydrodeoxygenation of p-Cresol over Pt/Al_2O_3 Catalyst Promoted by ZrO_2, CeO_2, and CeO_2-ZrO_2. *Ind. Eng. Chem. Res.* **2016**, *55*, 7598-7603. DOI: 10.1021/acs.iecr.6b00515

159. Wiedner, E. S.; Chambers, M. B.; Pitman, C. L.; Bullock, R. M.; Miller, A. J. M.; Appel, A. M., Thermodynamic Hydricity of Transition Metal Hydrides. *Chem. Rev.* **2016**, *116*, 8655-8692. DOI: 10.1021/acs.chemrev.6b00168

160. Yu, N.; Zhang, H.; Davidson, S. D.; Sun, J.; Wang, Y., Effect of ZnO facet on ethanol steam reforming over Co/ZnO. *Catal. Commun.* **2016**, *73*, 93-97. DOI: 10.1016/j.catcom.2015.10.018

161. Zhang, S. G.; Li, H. X.; Appel, A. M.; Hall, M. B.; Bullock, R. M., Facile P-C/C-H Bond-Cleavage Reactivity of Nickel Bis(diphosphine) Complexes. *Chem.-Eur. J.* **2016**, *22*, 9493-9497. DOI: 10.1002/chem.201601469

2017

162. Bossola, F.; Pereira-Hernández, X. I.; Evangelisti, C.; Wang, Y.; Dal Santo, V., Investigation of the promoting effect of Mn on a Pt/C catalyst for the steam and aqueous phase reforming of glycerol. *J. Catal.* **2017**, *349*, 75-83. DOI: 10.1016/j.jcat.2017.03.002

163. Burgess, S. A.; Kendall, A. J.; Tyler, D. R.; Linehan, J. C.; Appel, A. M., Hydrogenation of CO_2 in Water Using a Bis(diphosphine) Ni–H Complex. *ACS Catal.* **2017**, *7*, 3089-3096. DOI: 10.1021/acscatal.7b00350

164. Chen, M.; Dixon, D. A., Modeling the formation of TiO_2 ultra-small nanoparticles. *Nanoscale* **2017**, *9*, 7143-7162. DOI: 10.1039/C7NR01749A

165. Christe, K. O.; Haiges, R.; Vasiliu, M.; Dixon, D. A., Formation Mechanism of NF_4^+ Salts and Extraordinary Enhancement of the Oxidizing Power of Fluorine by Strong Lewis Acids. *Angew. Chem., Int. Ed.* **2017**. DOI: 10.1002/anie.201701784

166. Fang, Z. T.; Vasiliu, M.; Peterson, K. A.; Dixon, D. A., Prediction of Bond Dissociation Energies/Heats of Formation for Diatomic Transition Metal Compounds: CCSD(T) Works. *J. Chem. Theory Comput.* **2017**, *13*, 1057-1066. DOI: 10.1021/acs.jctc.6b00971

167. Feng, R. L.; Vasiliu, M.; Peterson, K. A.; Dixon, D. A., Acidity of $M(VI)O_2(OH)_2$ for M = Group 6, 16, and U as Central Atoms. *J. Phys. Chem. A* **2017**, *121*, 1041-1050. DOI: 10.1021/acs.jpca.6b11889

168. Foraita, S.; Liu, Y.; Haller, G. L.; Barath, E.; Zhao, C.; Lercher, J. A., Controlling Hydrodeoxygenation of Stearic Acid to n-Heptadecane and n-Octadecane by Adjusting the Chemical Properties of Ni/SiO_2-ZrO_2 Catalyst. *Chemcatchem* **2017**, *9*, 195-203. DOI: 10.1002/cctc.201601162

169. Gentil, S.; Lalaoui, N.; Dutta, A.; Nedellec, Y.; Cosnier, S.; Shaw, W. J.; Artero, V.; Le Goff, A., Carbon-Nanotube-Supported Bio-Inspired Nickel Catalyst and Its Integration in Hybrid Hydrogen/Air Fuel Cells. *Angew. Chem., Int. Ed.* **2017**, *56*, 1845-1849. DOI: 10.1002/anie.201611532

170. Iglesia, E.; Wang, S.; Agirrezabal-Telleria, I.; Bhan, A.; Simonetti, D.; Takanabe, K., Catalysis for Fuels Introductory Lecture: Catalytic routes to fuels from C1 and oxygenate molecules. *Faraday Discuss.* **2017**. DOI: 10.1039/C7FD00018A

171. Li, W.-Z.; Nie, L.; Cheng, Y.; Kovarik, L.; Liu, J.; Wang, Y., Surface enrichment of Pt in stable Pt-Ir nano-alloy particles on $MgAl_2O_4$ spinel in oxidizing atmosphere. *Catal. Commun.* **2017**, *93*, 57-61. DOI: 10.1016/j.catcom.2017.01.012

172. Li, W. Z.; Kovarik, L.; Cheng, Y. W.; Nie, L.; Bowden, M. E.; Liu, J.; Wang, Y., Stabilization and transformation of Pt nanocrystals supported on $ZnAl_2O_4$ spinel. *Rsc Advances* **2017**, *7*, 3282-3286. DOI: 10.1039/c6ra26159k

173. Vasiliu, M.; Peterson, K. A.; Dixon, D. A., Benchmark-Quality Atomization Energies for BeH and BeH_2. *J. Chem. Theory Comput.* **2017**, *13*, 649-653. DOI: 10.1021/acs.jctc.6b01154

174. Wagenhofer, M. F.; Barath, E.; Gutierrez, O. Y.; Lercher, J. A., Carbon-Carbon Bond Scission Pathways in the Deoxygenation of Fatty Acids on Transition-Metal Sulfides. *ACS Catal.* **2017**, *7*, 1068-1076. DOI: 10.1021/acscatal.6b02753

175. Xu, C.-Q.; Lee, M.-S.; Wang, Y.-G.; Cantu, D. C.; Li, J.; Glezakou, V.-A.; Rousseau, R., Structural Rearrangement of Au–Pd Nanoparticles under Reaction Conditions: An ab Initio Molecular Dynamics Study. *ACS Nano* **2017**. DOI: 10.1021/acsnano.6b07409

Publications jointly funded by this grant and other grants with relatively minor intellectual contribution from this grant

2014

176. DuBois, D. L., Development of Molecular Electrocatalysts for Energy Storage. *Inorg. Chem.* **2014**, *53*, 3935-3960. DOI: 10.1021/ic4026969

177. Hou, J.; Fang, M.; Cardenas, A. J. P.; Shaw, W. J.; Helm, M. L.; Bullock, R. M.; Roberts, J. A. S.; O'Hagan, M., Electrocatalytic H_2 production with a turnover frequency $>10^7$ s^{-1}: The medium provides an increase in rate but not overpotential. *Energy Environ. Sci.* **2014**, *7*, 4013-4017. DOI: 10.1039/C4EE01899K

178. Johnson, M. S.; Kota, R.; Mattern, D. L.; Hill, C. M.; Vasiliu, M.; Dixon, D. A.; Metzger, R. M., A two-faced "Janus-like" unimolecular rectifier exhibits rectification reversal. *J. Mater. Chem. C* **2014**, *2*, 9892-9902. DOI: 10.1039/C4TC01742K

179. Kim, B.; Li, Z.; Kay, B. D.; Dohnalek, Z.; Kim, Y. K., Low-Temperature Desorption of N_2O from NO on Rutile TiO_2(110)-1 x 1. *J. Phys. Chem. C* **2014**, *118*, 9544-9550. DOI: 10.1021/jp501179y

180. Kwak, J. H.; Dagle, R.; Tustin, G. C.; Zoeller, J. R.; Allard, L. F.; Wang, Y., Molecular Active Sites in Heterogeneous Ir–La/C-Catalyzed Carbonylation of Methanol to Acetates. *J. Phys. Chem. Lett.* **2014**, *5*, 566-572. DOI: 10.1021/jz402728e

181. Laws, D. R.; Bullock, R. M.; Lee, R.; Huang, K.-W.; Geiger, W. E., Comparison of the One-Electron Oxidations of CO-Bridged vs Unbridged Bimetallic Complexes: Electron-Transfer Chemistry of $Os_2Cp_2(CO)_4$ and $Os_2Cp^*_2(\mu\text{-}CO)_2(CO)_2$ (Cp = η^5-C_5H_5, Cp* = η^5-C_5Me_5). *Organometallics* **2014**, *33*, 4716-4728. DOI: 10.1021/om401213y

182. Lewandowska-Andralojc, A.; Grills, D. C.; Zhang, J.; Bullock, R. M.; Miyazawa, A.; Kawanishi, Y.; Fujita, E., Kinetic and Mechanistic Studies of Carbon-to-Metal Hydrogen Atom Transfer Involving Os-Centered Radicals: Evidence for Tunneling. *J. Am. Chem. Soc.* **2014**, *136*, 3572-3578. DOI: 10.1021/ja4123076

183. Liu, T.; DuBois, M. R.; DuBois, D. L.; Bullock, R. M., Electrochemical oxidation of H_2 catalyzed by ruthenium hydride complexes bearing P_2N_2 ligands with pendant amines as proton relays. *Energy Environ. Sci.* **2014**, *7*, 3630-3639. DOI: 10.1039/C4EE01262C

184. Norton, J. R.; Spataru, T.; Camaioni, D. M.; Lee, S.-J.; Li, G.; Choi, J.; Franz, J. A., Kinetics and Mechanism of the Hydrogenation of the $CpCr(CO)_3$•/$[CpCr(CO)_3]_2$ Equilibrium to $CpCr(CO)_3H$. *Organometallics* **2014**, *33*, 2496-2502. DOI: 10.1021/om4012399

185. Peterson, E. J.; DeLaRiva, A. T.; Lin, S.; Johnson, R. S.; Guo, H.; Miller, J. T.; Hun Kwak, J.; Peden, C. H. F.; Kiefer, B.; Allard, L. F.; Ribeiro, F. H.; Datye, A. K., Low-temperature carbon monoxide oxidation catalysed by regenerable atomically dispersed palladium on alumina. *Nat. Commun.* **2014**, *5*. DOI: 10.1038/ncomms5885

2015

186. Bayram, E.; Linehan, J. C.; Fulton, J. L.; Szymczak, N. K.; Finke, R. G., Determination of the Dominant Catalyst Derived from the Classic $[RhCp^*Cl_2]_2$ Precatalyst System: Is it Single-Metal Rh_1Cp^*-Based, Subnanometer Rh_4 Cluster-Based, or $Rh(0)_n$ Nanoparticle-Based Cyclohexene Hydrogenation Catalysis at Room Temperature and Mild Pressures? *ACS Catal.* **2015**, *5*, 3876-3886. DOI: 10.1021/acscatal.5b00315

187. Christe, K. O.; Dixon, D. A.; Vasiliu, M.; Wagner, R. I.; Haiges, R.; Boatz, J. A.; Ammon, t. l. H. L., Are DTTO and iso-DTTO Worthwhile Targets for Synthesis? *Propellants, Explosives, Pyrotechnics* **2015**, *40*, 463-468. DOI: 10.1002/prep.201400259

188. Haiges, R.; Skotnitzki, J.; Fang, Z.; Dixon, D. A.; Christe, K. O., The First Molybdenum(VI) and Tungsten(VI) Oxoazides $MO_2(N_3)_2$, $MO_2(N_3)_2 \cdot 2\,CH_3CN$, $(bipy)MO_2(N_3)_2$, and $[MO_2(N_3)_4]^{2-}$ (M=Mo, W). *Angew. Chem., Int. Ed.* **2015**, *54*, 9581-9585. DOI: 10.1002/anie.201504629

189. Haiges, R.; Skotnitzki, J.; Fang, Z.; Dixon, D. A.; Christe, K. O., The Molybdenum(V) and Tungsten(VI) Oxoazides $[MoO(N_3)_3]$, $[MoO(N_3)_3 \cdot 2\,CH_3CN]$, $[(bipy)MoO(N_3)_3]$, $[MoO(N_3)_5]^{2-}$, $[WO(N_3)_4]$, and $[WO(N_3)_4 \cdot CH_3CN]$. *Angew. Chem., Int. Ed.* **2015**, *54*, 15550-15555. DOI: 10.1002/anie.201505418

190. Haiges, R.; Vasiliu, M.; Dixon, D. A.; Christe, K. O., The Vanadium(V) Oxoazides $[VO(N_3)_3]$, $[(bipy)VO(N_3)_3]$, and $[VO(N_3)_5]^{2-}$. *Angew. Chem., Int. Ed.* **2015**, *54*, 9101-9105. DOI: 10.1002/anie.201503985

191. Ho, M.-H.; O'Hagan, M.; Dupuis, M.; DuBois, D. L.; Bullock, R. M.; Shaw, W. J.; Raugei, S., Water-assisted proton delivery and removal in bio-inspired hydrogen production catalysts. *Dalton. Trans.* **2015**, *44*, 10969-10979. DOI: 10.1039/C5DT00782H

192. Kim, B.; Kay, B. D.; Dohnalek, Z.; Kim, Y. K., Ammonia Formation from NO Reaction with Surface Hydroxyls on Rutile $TiO_2(110)$-1 x 1. *J. Phys. Chem. C* **2015**, *119*, 1130-1135. DOI: 10.1021/jp5109619

193. Leclerc, M. C.; Bayne, J. M.; Lee, G. M.; Gorelsky, S. I.; Vasiliu, M.; Korobkov, I.; Harrison, D. J.; Dixon, D. A.; Baker, R. T., Perfluoroalkyl Cobalt(III) Fluoride and Bis(perfluoroalkyl) Complexes: Catalytic Fluorination and Selective Difluorocarbene Formation. *J. Am. Chem. Soc.* **2015**, *137*, 16064-16073. DOI: 10.1021/jacs.5b12003

194. Lee, J.; Jeon, H.; Oh, D. G.; Szanyi, J.; Kwak, J. H., Morphology-dependent phase transformation of γ-Al_2O_3. *Appl.Catal. A* **2015**, *500*, 58-68. DOI: 10.1016/j.apcata.2015.03.040

195. Miranda, B. C.; Chimentão, R. J.; Szanyi, J.; Braga, A. H.; Santos, J. B. O.; Gispert-Guirado, F.; Llorca, J.; Medina, F., Influence of copper on nickel-based catalysts in the conversion of glycerol. *Appl.Catal. B* **2015**, *166–167*, 166-180. DOI: 10.1016/j.apcatb.2014.11.019

196. Schwenzer, B.; Cosimbescu, L.; Glezakou, V.-A.; Karkamkar, A. J.; Wang, Z.; Weber, R. S., Use of Solvatochromism to Assay Preferential Solvation of a Prototypic Catalytic Site. *Top. Catal.* **2015**, *58*, 258-270. DOI: 10.1007/s11244-015-0367-z

197. Sun, J.; Karim, A. M.; Li, X. S.; Rainbolt, J.; Kovarik, L.; Shin, Y.; Wang, Y., Hierarchically structured catalysts for cascade and selective steam reforming/hydrodeoxygenation reactions. *Chem. Commun.* **2015**, *51*, 16617-16620. DOI: 10.1039/C5CC07244A

198. Yang, Y.; Mei, D.; Peden, C. H. F.; Campbell, C. T.; Mims, C. A., Surface-Bound Intermediates in Low-Temperature Methanol Synthesis on Copper: Participants and Spectators. *ACS Catal.* **2015**, *5*, 7328-7337. DOI: 10.1021/acscatal.5b02060

199. Zhang, Z.; Tang, M.; Wang, Z.-T.; Ke, Z.; Xia, Y.; Park, K. T.; Lyubinetsky, I.; Dohnalek, Z.; Ge, Q., Imaging of Formaldehyde Adsorption and Diffusion on TiO_2(110). *Top. Catal.* **2015**, *58*, 103-113. DOI: 10.1007/s11244-014-0349-6

200. Zhu, K.; Xia, Y.; Tang, M.; Wang, Z.-T.; Jan, B.; Lyubinetsky, I.; Ge, Q.; Dohnalek, Z.; Park, K. T.; Zhang, Z., Tracking Site-Specific C-C Coupling of Formaldehyde Molecules on Rutile TiO_2(110). *J. Phys. Chem. C* **2015**, *119*, 14267-14272. DOI: 10.1021/acs.jpcc.5b04781

201. Zhu, K.; Xia, Y.; Tang, M.; Wang, Z.-T.; Lyubinetsky, I.; Ge, Q.; Dohnalek, Z.; Park, K. T.; Zhang, Z., Low-Temperature Reductive Coupling of Formaldehyde on Rutile TiO_2(110). *J. Phys. Chem. C* **2015**, *119*, 18452-18457. DOI: 10.1021/acs.jpcc.5b05639

2016

202. Bligaard, T.; Bullock, R. M.; Campbell, C. T.; Chen, J. G. G.; Gates, B. C.; Gorte, R. J.; Jones, C. W.; Jones, W. D.; Kitchin, J. R.; Scott, S. L., Toward Benchmarking in Catalysis Science: Best Practices, Challenges, and Opportunities. *ACS Catal.* **2016**, *6*, 2590-2602. DOI: 10.1021/acscatal.6b00183

203. Callini, E.; Atakli, Z. O. K.; Hauback, B. C.; Orimo, S.; Jensen, C.; Dornheim, M.; Grant, D.; Cho, Y. W.; Chen, P.; Hjorvarsson, B.; de Jongh, P.; Weidenthaler, C.; Baricco, M.; Paskevicius, M.; Jensen, T. R.; Bowden, M. E.; Autrey, T. S.; Zuttel, A., Complex and liquid hydrides for energy storage. *Appl. Phys. A-Mater. Sci. Process.* **2016**, *122*. DOI: 10.1007/s00339-016-9881-5

204. Deokar, P.; Leitz, D.; Stein, T. H.; Vasiliu, M.; Dixon, D. A.; Christe, K. O.; Haiges, R., Preparation and Characterization of Antimony and Arsenic Tricyanide and Their 2,2'-Bipyridine Adducts. *Chem.-Eur. J.* **2016**, *22*, 13251-13257. DOI: 10.1002/chem.201602436

205. Deokar, P.; Vasiliu, M.; Dixon, D. A.; Christe, K. O.; Haiges, R., The Binary Group 4 Azides $[PPh_4]_2[Zr(N_3)_6]$ and $[PPh_4]_2[Hf(N_3)_6]$. *Angew. Chem., Int. Ed.* **2016**, *55*, 14348-14352. DOI: 10.1002/anie.201609195

206. Du, L.; Shao, Y. Y.; Sun, J. M.; Yin, G. P.; Liu, J.; Wang, Y., Advanced catalyst supports for PEM fuel cell cathodes. *Nano Energy* **2016**, *29*, 314-322. DOI: 10.1016/j.nanoen.2016.03.016

207. Du, Y.; Li, G.; Peterson, E. W.; Zhou, J.; Zhang, X.; Mu, R.; Dohnalek, Z.; Bowden, M.; Lyubinetsky, I.; Chambers, S. A., Iso-oriented monolayer α-MoO_3(010) films epitaxially grown on $SrTiO_3$(001). *Nanoscale* **2016**, *8*, 3119-3124. DOI: 10.1039/C5NR07745A

208. Haiges, R.; Vasiliu, M.; Dixon, D. A.; Christe, K. O., The niobium oxoazides [NbO(N3)3], [NbO(N3)3.2CH3CN], [(bipy)NbO(N3)3], Cs2[NbO(N3)5] and [PPh4]2[NbO(N3)5]. *Dalton Trans* **2016**, *45*, 10523-9. DOI: 10.1039/c6dt01479h

209. Kaneza, N.; Zhang, J.; Liu, H.; Archana, P. S.; Shan, Z.; Vasiliu, M.; Polansky, S. H.; Dixon, D. A.; Adams, R. E.; Schmehl, R. H.; Gupta, A.; Pan, S., Electrochemical and Spectroscopic Properties of Boron Dipyrromethene–Thiophene–Triphenylamine-Based Dyes for Dye-Sensitized Solar Cells. *J. Phys. Chem. C* **2016**, *120*, 9068-9080. DOI: 10.1021/acs.jpcc.6b01611

210. Kelley, S. P.; McCrary, P. D.; Flores, L.; Garner, E. B.; Dixon, D. A.; Rogers, R. D., Structural and Theoretical Study of Salts of the $B_9H_{14}^-$ Ion: Isolation of Multiple Isomers and Implications for Energy Storage. *Chempluschem* **2016**, *81*, 922-925. DOI: 10.1002/cplu.201600270

211. Kim, B.; Dohnálek, Z.; Szanyi, J.; Kay, B. D.; Kim, Y. K., Temperature-programmed desorption study of NO reactions on rutile TiO2(110)-1 × 1. *Surf. Sci.* **2016**, *652*, 148-155. DOI: 10.1016/j.susc.2016.01.032

212. Lao, D. B.; Galan, B. R.; Linehan, J. C.; Heldebrant, D. J., The steps of activating a prospective CO_2 hydrogenation catalyst with combined CO_2 capture and reduction. *Green Chem.* **2016**, *18*, 4871-4874. DOI: 10.1039/c6gc01800a

213. Lee, M. S.; Um, W.; Wang, G.; Kruger, A. A.; Lukens, W. W.; Rousseau, R.; Glezakou, V. A., Impeding (99)Tc(IV) mobility in novel waste forms. *Nat. Commun.* **2016**, *7*, 12067. DOI: 10.1038/ncomms12067

214. Liu, C.; Sun, J.; Brown, H. M.; Marin-Flores, O. G.; Bays, J. T.; Karim, A. M.; Wang, Y., Aqueous phase hydrodeoxygenation of polyols over Pd/WO_3-ZrO_2: Role of Pd-WO_3 interaction and hydrodeoxygenation pathway. *Catal. Today* **2016**, *269*, 103-109. DOI: 10.1016/j.cattod.2015.10.034

215. Liu, X. G.; Zhang, Y. Z.; Li, B.; Zakharov, L. N.; Vasiliu, M.; Dixon, D. A.; Liu, S. Y., A Modular Synthetic Approach to Monocyclic 1,4-Azaborines. *Angew. Chem., Int. Ed.* **2016**, *55*, 8333-8337. DOI: 10.1002/anie.201602840

216. Matthiesen, J. E.; Carraher, J. M.; Vasiliu, M.; Dixon, D. A.; Tessonnier, J. P., Electrochemical Conversion of Muconic Acid to Biobased Diacid Monomers. *ACS Sustain. Chem. Eng.* **2016**, *4*, 3575-3585. DOI: 10.1021/acssuschemeng.6b00679

217. Pruski, M.; Sadow, A. D.; Slowing, I. I.; Marshall, C. L.; Stair, P.; Rodriguez, J.; Harris, A.; Somorjai, G. A.; Biener, J.; Matranga, C.; Wang, C.; Schaidle, J. A.; Beckham, G. T.; Ruddy, D. A.; Deutsch, T.; Alia, S. M.; Narula, C.; Overbury, S.; Toops, T.; Bullock, R. M.; Peden, C. H. F.; Wang, Y.; Allendorf, M. D.; Nørskov, J.; Bligaard, T., Virtual Special Issue on Catalysis at the U.S. Department of Energy's National Laboratories. *ACS Catal.* **2016**, *6*, 3227-3235. DOI: 10.1021/acscatal.6b00823

218. Ramasamy, K. K.; Gray, M.; Job, H.; Santosa, D.; Li, X. S.; Devaraj, A.; Karkamkar, A.; Wang, Y., Role of Calcination Temperature on the Hydrotalcite Derived MgO-Al_2O_3 in Converting Ethanol to Butanol. *Top. Catal.* **2016**, *59*, 46-54. DOI: 10.1007/s11244-015-0504-8

219. Ramasamy, K. K.; Gray, M.; Job, H.; Smith, C.; Wang, Y., Tunable catalytic properties of bi-functional mixed oxides in ethanol conversion to high value compounds. *Catal. Today* **2016**, *269*, 82-87. DOI: 10.1016/j.cattod.2015.11.045

220. Smith, M. F.; Cassidy, S. J.; Adams, I. A.; Vasiliu, M.; Gerlach, D. L.; Dixon, D. A.; Rupar, P. A., Substituent Effects on the Properties of Borafluorenes. *Organometallics* **2016**, *35*, 3182-3191. DOI: 10.1021/acs.organomet.6b00537

221. Sun, J.; Cai, Q. X.; Wan, Y.; Wan, S. L.; Wang, L.; Lin, J. D.; Mei, D. H.; Wang, Y., Promotional Effects of Cesium Promoter on Higher Alcohol Synthesis from Syngas over Cesium-Promoted Cu/ZnO/Al_2O_3 Catalysts. *ACS Catal.* **2016**, *6*, 5771-5785. DOI: 10.1021/acscatal.6b00935

222. Whittemore, S. M.; Bowden, M.; Karkamkar, A.; Parab, K.; Neiner, D.; Autrey, T.; Ishibashi, J. S. A.; Chen, G.; Liu, S. Y.; Dixon, D. A., Blending materials composed of boron, nitrogen and carbon to transform approaches to liquid hydrogen stores. *Dalton. Trans.* **2016**, *45*, 6196-6203. DOI: 10.1039/c5dt04276c

2017

223. Hong, Y.; Zhang, S.; Tao, F.; Wang, Y., Stabilization of Iron-based Catalysts against Oxidation: An in situ Ambient Pressure XPS Study. *ACS Catal.* **2017**. DOI: 10.1021/acscatal.7b00636

224. Lee, J.; Szanyi, J.; Kwak, J. H., Ethanol dehydration on γ-Al_2O_3: Effects of partial pressure and temperature. *Molecular Catalysis* **2017**, *434*, 39-48. DOI: 10.1016/j.mcat.2016.12.013

225. Li, Z.; Yang, X.; Tsumori, N.; Liu, Z.; Himeda, Y.; Autrey, T.; Xu, Q., Tandem Nitrogen Functionalization of Porous Carbon: Toward Immobilizing Highly Active Palladium Nanoclusters for Dehydrogenation of Formic Acid. *ACS Catal.* **2017**, *7*, 2720-2724. DOI: 10.1021/acscatal.7b00053

226. Liu, Z.; Ishibashi, J. S. A.; Darrigan, C.; Dargelos, A.; Chrostowska, A.; Li, B.; Vasiliu, M.; Dixon, D. A.; Liu, S.-Y., The Least Stable Isomer of BN Naphthalene: Toward Predictive Trends for the Optoelectronic Properties of BN Acenes. *J. Am. Chem. Soc.* **2017**, *139*, 6082-6085. DOI: 10.1021/jacs.7b02661

227. Yang, D.; Zhang, S. G.; Xu, P. H.; Browning, N. D.; Dixon, D. A.; Gates, B. C., Single-Site Osmium Catalysts on MgO: Reactivity and Catalysis of CO Oxidation. *Chemistry- A European Journal* **2017**, *23*, 2532-2536. DOI: 10.1002/chem.201605131

Molecular Routes to Interfacing Homogeneous and Heterogeneous Catalysis

Tobin J. Marks, Peter C. Stair, Tracy L. Lohr, Aidan R. Mouat, Titel Jurca, Shengshi Liu, Jeffrey M. Tan, Jiaqi Li, Neil M. Schweitzer, Massimiliano Delferro
Department of Chemistry, Northwestern University, Evanston IL 60208
Laurence D. Marks
Department of Materials Science and Engineering, Northwestern University, Evanston IL 60208

Presentation Abstract

When chemisorbed upon specific metal oxide and carbonaceous surfaces, the reactivity of many types of organometallic molecules is dramatically enhanced. High activities for diverse catalytic olefin and oxygenate transformations are illustrative consequences of such altered reactivity. This presentation focuses on the intricate covalent and non-covalent multi-center interactions that modulate these catalytic processes, focusing on polymerization, hydrogenation, and dehydrogenation processes. Specific topics include: 1) Catalytic chemistry of organo-group 4 catalysts anchored on/activated by oxide surfaces, 2) Definitive structural characterization of these catalysts on "super-acidic" sulfate oxide surfaces, and the scope of their catalytic properties, 3) Organometallic routes to "single-atom" catalysts, 4) Catalytic oxygenate chemistry of group 6 oxo complexes bound to activated carbon. It will be seen that the information obtained leads to design rules for next-generation homogeneous and supported catalysts, and to novel and useful polymerization and hydrogenation/dehydrogenation catalysts, including those for detoxifying gasoline or producing H_2 from bioalcohols.

DE-FG02-03ER15457: Institute for Environmental Catalysis
Postdocs: Tracy L. Lohr, Titel Jurca, Massimiliano Delferro (Now at Argonne Nat. Lab.)
Students: Aidan R. Mouat, Shengshi Liu, Jeffrey M. Tan, Jiaqi Li

RECENT PROGRESS

Organometallic Synthetic Strategies for Isolated Single-Atom Catalysts

The study of isolated, supported late transition metal single-atom heterogeneous catalysts has recently become of intense research interest due to recent promising applications in catalytic CO oxidation, methanol steam reforming, selective alcohol oxidation, ethanol dehydration, olefin and alkyne hydrogenation, the water gas shift reaction, as well as in other transformations. Despite this rapid progress, the synthesis of such catalysts is neither well-controlled nor general. There are a number of strategies for depositing well-defined monatomic late transition metal species onto oxide supports. These include metal evaporation, "soft landing", and the chemisorption of intact metal-organic species. With the goal of producing well-defined, isolated platinum metal sites, T. Marks, L. Marks, and P. Stair explored metal-organic chemisorption due to its ability to deliver

well-defined metal precursors to high surface area supports with uniform nuclearity. Paired with a strategy for mitigating sintering (atomic layer deposition, ALD), a robust synthetic procedure can be envisaged whereby deposited metal-organic complexes remain monatomic even after high temperature thermal treatment and ligand removal.

Our team showed that highly dispersed low-coordinate Pt or Pd sites can be efficiently prepared by surface organometallic chemisorption. Since low-coordination of metal centers can only be fully achieved when atomically dispersed, they envisioned that by combing this methodology with ALD, the synthesis of oxide supported single atom catalysts can be explored in

a rational fashion. We first developed a synthetic approach to stabilizing Pt single-atoms on Al_2O_3 by combining surface organometallic chemisorption with ALD (Scheme 1). First, "pincer" complex (^{Ph}PCP)Pt-OH is chemisorbed on Al_2O_3 from solution. The resulting material is next over-coated with oxide layers by ALD to suppress agglomeration, and then calcined under flowing O_2 at 400 °C to remove the ancillary ligands. The final materials are characterized by aberration-corrected HAADF STEM, CO adsorp-tion/diffuse reflectance IR Fourier transform spectroscopy, and XPS. It was shown that ALD-derived Al_2O_3, TiO_2, and ZnO overlayers effectively suppress Pt sintering and significantly stabilize single Pt atoms. Furthermore, this procedure decreases the Pt nuclearity (~ 1 nm average diameter) versus bare Pt (~3.8 nm average diameter) as assayed by aberration corrected HAADF-STEM. The TiO_2 and ZnO overcoats are significantly more effective at stabilizing single-atom Pt species and decreasing the overall Pt nuclearity than Al_2O_3 overcoats. Vibrational spectroscopy of adsorbed CO also shows that oxidized Pt species commonly thought to be single Pt atoms are inactive for catalytic oxidation of adsorbed CO due to site blockage by the ALD overcoats.

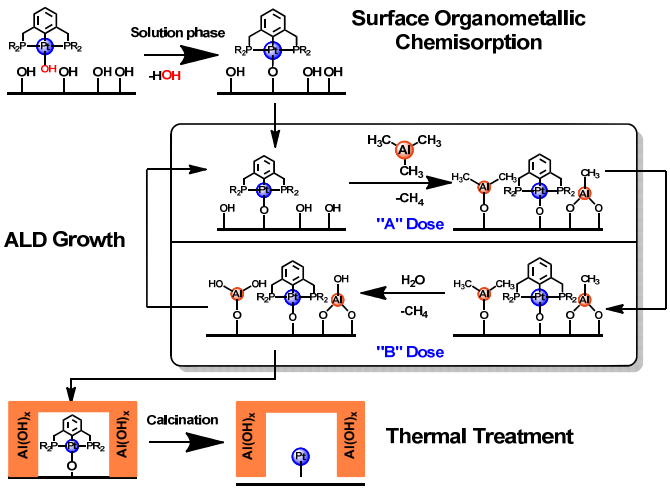

Scheme 1. Overall schematic for proposed single Pt atom synthetic methodology combining surface organometallic chemisorption and ALD

In related work, **Marks**, **Marks**, and **Stair** prepared highly dispersed low-coordinate Pd sites on SiO_2 were created by grafting the PCP-pincer complex (^{tBu}PCP)Pd-OH on SiO_2, followed by calcination with ozone and reduction in H_2 (300 °C). Chemisorption of the adsorbed complex on the oxide support was established by solid state ^{31}P CPMAS NMR, DRIFTS, XPS, and HAADF-STEM. The CO adsorption properties of the Pd centers reveal a surprisingly high fraction of linear CO sites indicative of low-coordinate Pd. Furthermore, the superior catalytic performance of these catalyst centers in aerobic alcohol oxidation versus a conventional catalyst indicates that the low-coordinate sites are the catalytically active sites.

Surface Bound Molecular Catalysts

Single-site, molecule-derived supported catalysts offer molecular level control of catalyst–substrate interactions and permit the rational design of active sites tailored to reactions of interest. Molybdenum oxide ($Mo(O)_x$) based catalysts are known to catalyze numerous reactions, including transesterification, alkane oxidation, ethanolysis, and olefin metathesis. Traditional methods of preparing $Mo(O)_x$ catalysts often involve incipient wetness followed by high temperature

calcination, resulting in poor control over the exact Mo composition. **Marks** and **Stair** showed that a single-site hexavalent molybdenum di-oxo can be prepared by direct grafting of (dme)MoO_2Cl_2 onto activated carbon (Scheme 2). The properties of this **Mo@C** catalyst were fully characterized by N_2 physisorption, ICP-AES/OES, PXRD, STEM, XPS, XAS, TPR-H_2, and TPD-NH_3. The single-site nature of the Mo species is corroborated by the XPS and TPR-H_2 data, which exhibits an extremely low MoO_x T_{max} reduction (218 °C, for 50% of the Mo sites), suggesting a highly reactive Mo center. Mo K-edge XANES indicates Mo^{VI}, and EXAFS fitting shows 2 Mo=O bonds at a distance of 1.68 Å, 1 Mo-O bond at 1.98 Å and 1 Mo-O bond at 2.29 Å indicating that **Mo@C** is closely related to MoO_3, and corroborates the 4-coordinate proposed structure. Reduction with H_2 at 218°C leads to a loss of 0.4 Mo=O bonds and 1 Mo-O, indicating that the species is most likely **Mo^{VI}(=O)(OH)(H)@C**.

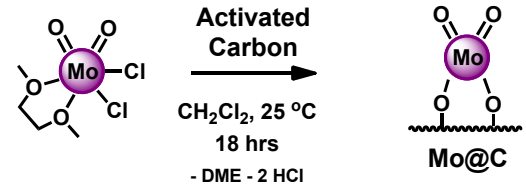

Scheme 2. Adsorption of $Mo(O)_2$ species on activated carbon

Mo@C catalyzes the transesterification of a variety of esters and triglycerides with ethanol (Scheme 3), exhibiting high activity at moderate temperatures (60 – 90 ˚C) and with negligible deactivation. **Mo@C** is resistant to water and can be recycled ≥3x with negligible activity loss. Transesterification is determined to be first-order in [ethanol] and first-order in [Mo]. This highly active carbon-supported single-site dioxo-Mo species is thus an efficient, robust, and low-cost catalyst with significant potential for transesterification processes.

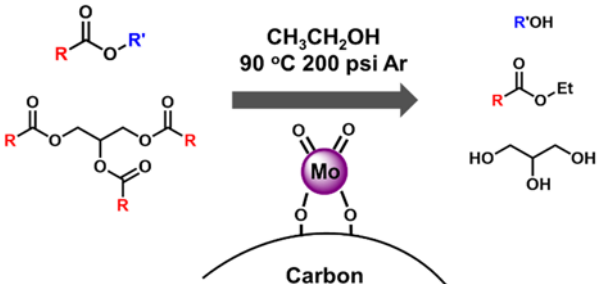

Scheme 3. Mo@C catalyzed transesterifications

In related work, **Marks** and **Stair** find that single-site **Mo@C** also catalyzes the production of H_2 from aqueous MeOH and EtOH with coproduction of the corresponding aldehyde (Scheme 4). H_2 production from renewable biomass is challenging due to sluggish catalytic rates in water (the most common biomass contaminant) and catalyst deactivation. In contrast **Mo@C** rapidly mediates the dehydrogenation of neat, toluene-diluted, or aqueous MeOH and EtOH under inert atmosphere at 90 °C to yield 1.0 equiv. each of H_2 and the corresponding aldehyde, as assayed by NMR, gas-phase mass spectrometry, and chemical titration with 2,4-dinitrophenyl hydrazine. This catalytic system produces significant quantities of H_2 from both MeOH and EtOH at 40 °C. Under the current conditions TOFs reach up to ~24,000 h^{-1} for neat MeOH at 90 °C. This new catalytic system is base- and oxidant-free and not deactivated by water, hence is compatible with biomass-derived alcohol feedstocks. Importantly, there is no detectable co-production of CO_2 or CO, making this system attractive for direct alcohol fuel cells and as a replacement catalyst for formaldehyde production that simultaneously generates a clean energy source.

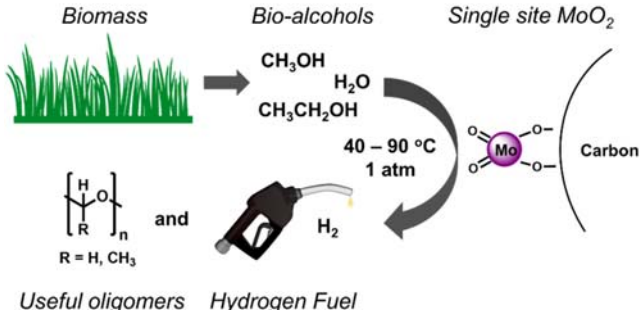

Scheme 4. Mo@C catalyzed alcohol dehydrogenation

Marks and **Stair** also explored the efficacy of **Mo@C** for reducing carbonyl functionalities. Alkyl and aryl ethers are important classes of compounds with wide ranging applications in bioscience and polymers. Despite many advances in in synthetic methodology to produce symmetric ethers, many of these reactions require Pt metals, anhydrous conditions, toxic additives, strongly acidic/-basic conditions, sacrificial ligands, or excess alkali salts. **Mo@C** is found to catalyze the reductive coupling of a diverse array of carbonyl compounds to the corresponding symmetric ethers with dimethylphenylsilane (Scheme 5). Furthermore, this catalyst exhibits both *inter*- and *intra*molecular chemoselectivity for ether synthesis, enabling routes to functionalized ethers with unsaturated and halogenated functional groups. Recycling experiments show that **Mo@C** can be used ≥ 5 times without deactivation.

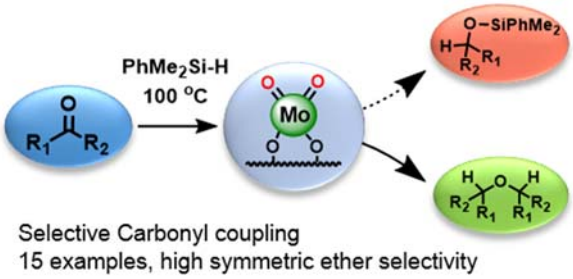

Scheme 5. Mo@C catalyzed carbonyl coupling

Publications Acknowledging this Grant in 2014-2017

(I) Exclusively funded by this grant

1. Tan, J.M.; Liu, S.; Gulec, A.; Crosby, L.A.; Drake, T.L.; Wang, C.; Schweitzer, N.M.; Delferro, M.; Marks, L.D.; Marks, T.J.; Stair, P.C.; Strategy for Stabilizing Single-Atom and Small Domain Platinum via Organometallic Chemisorption and Atomic Layer Deposition, *Organometallics*, **2017**, *36*, 818.
2. Lohr, T. L.; Mouat, A. R.; Schweitzer, N. M.; Stair, P. C.; Delferro, M.; Marks, T. J. Efficient catalytic greenhouse gas-free hydrogen and aldehyde formation from aqueous alcohol solutions *Energy & Environmental Science* **2017**, in press.
3. Mouat, A.R.; Kobayashi, T.; Pruski, M.; Marks, T.J.; Stair, P.C.; Direct Spectroscopic Evidence for Isolated Silanols in SiO_x/Al_2O_3 and Their Formation Mechanism in Atomic Layer Deposition, *J. Phys. Chem. C., **2017**, 121,*6060.
4. Liu, S.; Li, J.; Jurca, T.; Stair, P. C.; Lohr, T. L.; Marks, T. Efficient Carbon-Supported Heterogeneous Molybdenum-Dioxo Catalyst for Chemoselective Reductive Carbonyl Coupling *Catalysis Science & Technology* **2017**, **7**, 2165.
5. Liu, S.; Tan, J.M.; Gulec, A.; Schweitzer, N.M.; Delferro, M.; Marks, L.D.; Stair, P.C.; Marks, T.J.; Direct Access to Low-Coordinate Pd Catalysts Supported on SiO_2 Through Surface Organometallic Chemistry, *ACS Catalysis,* **2016**, 6*,* 8380.
6. Mouat, A. R.; Lohr, T. L.; Wegener, E. C.; Miller, J. T.; Delferro, M.; Stair, P. C.; Marks, T. J. Reactivity of a Carbon-Supported Single-Site Mo Dioxo Catalyst for Biodiesel Synthesis *ACS Catalysis* **2016**, *6*, 6762.
7. Mouat, A.R.; Mane, A.U.; Elam, J.W.; Delferro, M; Marks, T.J.; Stair, P.C.; Volatile Hexavalent Oxo-Amidinate Complexes: Mo and W Precursors for ALD**,** *Chem. Mater.* **2016,** 28, 1907.
8. Liu, S.; Tan, J.M.; Gulec, A.; Schweitzer, N.M.; Delferro, M.; Marks, L.D.; Stair, P.C.; Marks, T.J.; Direct Access to Low-Coordinate Pd Catalysts Supported on SiO_2 Through Surface Organometallic Chemistry*, ACS Catalysis,* **2016***,* 6, 8380.
9. Stalzer, M.M.; Delferro, M.; Marks, T.J.; Supported Single-Site Organometallic Catalysts for the Synthesis of Valuable Polyolefins, *Catalysis Letters*, **2015**, *145*, 3.

10. Liu, S.; Motta, A.; Mouat, A.R.; Delferro, M.; Marks, T.J.; Remarkable Cooperative Effects in Heterobimetallic Titanium-Chromium Catalysts for Ethylene Polymerization/Copolymerization, *J. Amer. Chem. Soc.* **2014**, *136*, 10460.
11. McInnis, J.P.; Delferro, M.; Marks, T.J.; Multinuclear Catalysis: Olefin Polymerization Pathways Modified by Strong Cooperative Effects, *Accts. Chem. Res.*, **2014**, *47*, 2545.
12. Stephenson, C.J.; McInnis, J.P.; Chen, C.; Weberski Jr., M.P.; Motta, A.; Delferro, M.; Marks, T.J. Ni(II) Phenoxyiminato Olefin Polymerization Catalysis: Coordinative Modulation of Hyperbranched Polymer Microstructure and Stability by a Proximate Sulfonyl Group, *ACS Catalysis*, **2014**, *4*, 999.

(II) Jointly funded by this grant and other grants with leading intellectual contribution from this grant

13. Stalzer, M.M.; Nicholas, C.P.; Bhattacharyya, A.; Motta, A.; Delferro, M..; Marks, T.J.; Single-Face/All-*cis* Arene Hydrogenation by a Single-Site d^0 Organozirconium Catalyst Supported on Sulfated Zirconia, *Angew. Chem. Int. Ed.* **2016**, *55*, 5263.
14. Gao, Y.; Mouat, A.R.; Motta, A.; Macchioni, A.; Zuccaccia, C.; Delferro, M.; Marks, T.J.; Bimetallic Pyridyl-Amido Hafnium Polymerization Catalysts for Enhanced α-Olefin Copolymerization, *ACS Catal.* **2015**, *5*, 5272.
15. Gu, W.; Stalzer, M.M.; Nicholas, C.P.; Bhattacharyya, A.; Motta, A.; Gallagher, J.R.; Zhang, G.; Miller, J.T.; Kobayashi, T.; Pruski, M.; Delferro, M.; Marks, T.J.; Benzene Selectivity in Competitive Arene Hydrogenation: Effects of Single-Site Catalyst···Super-Acidic Oxide Surface Binding Geometry, *J. Am. Chem. Soc.* **2015**, *137*, 6770.
16. Klet, R.C.; Tussupbayev, S.; Borycz, J.; Gallagher, J.R.; Stalzer, M.M.; Miller, J.T.; Gagliardi, L.; Hupp, J.T.; Marks, T.J.; Cramer, C.J.; Delferro, M.; Farha, O.; Single-Site Organozirconium Polymerization Catalyst Embedded in a Metal–Organic Framework, *J. Am. Chem. Soc*. **2015,** *137*, 15680.

Shannon S. Stahl

Low-Overpotential Oxygen Reduction with Co-Based Molecular Electrocatalysts

Yu-Heng Larry Wang[1], Colin W. Anson[1], James B. Gerken[1], Zach Goldsmith[2], Patrick Schneider[2], Michael L. Pegis[3], James M. Mayer[3], Sharon Hammes-Schiffer,[2] Shannon S. Stahl[1]

[1]*University of Wisconsin-Madison;*
[2]*University of Illinois at Urbana-Champaign;* [3]*Yale University*

The oxygen reduction reaction (ORR) is a crucial process in fuel cells, and molecular ORR catalyst have been the focus of investigation for more than five decades. We have recently prepared and investigated a series of (pseudo)macrocyclic iron and cobalt complexes and investigated their performance in chemical and electrochemical ORR. The rate of ORR was evaluated for a number of different complexes with different half-wave potentials [$E_{1/2}(M^{III/II}$, M = Fe, Co)]. The data reveal a rather shallow linear free energy correlation between log(TOF) (TOF = turnover frequency) and the $E_{1/2}(Co^{III/II})$ values for pseudomacrocyclic Co complexes relative to a series of Fe-porphyrin complexes. The different slopes of log(TOF) vs $E_{1/2}(M^{III/II})$ correlate with different rate laws for Fe- and Co-catalyzed ORR: rate(Fe) = k[LFe][H^+][O_2] and rate(Co) = k[LCo][H^+]. The data are consistent with pre-equilibrium binding of O_2 followed by rate-limiting protonation of an O_2 adduct in the case of iron, and rate-limiting protonation of a resting-state O_2 adduct in the case of cobalt. Assessment of the standard potentials for ORR in the various organic solvents used in these studies provides the basis for determination of reaction overpotentials. The shallow electronic dependence of the Co-catalyzed ORR provides the basis for very low overpotential reduction of O_2 to hydrogen peroxide.

This research was supported as part of the Center for Molecular Electrocatalysis, an Energy Frontier Research Center funded by the U.S. Department of Energy (DOE), Office of Science, Office of Basic Energy Sciences. Pacific Northwest National Laboratory is operated by Battelle for the DOE.

Discovery of Active Single-atom Heterogeneous Catalysts for Alkene Hydrogenation via the Development of Activity-descriptor Relationships

Cong Liu (congliu@anl.gov),[1] Jeffrey Camacho-Bunquin,[1] Magali Ferrandon,[1] David Kaphan,[1] Hyuntae Sohn,[1] Dali Yang,[1] Ujjal Das,[2] Bing Yang,[2] Adam Hock,[1,3] Peter Stair,[1,4] Larry A. Curtiss,[2] and Massimiliano Delferro[1]
[1]Chemical Sciences and Engineering Division, [2]Material Science Division, Argonne National Laboratory. [3]Department of Chemistry, Illinois Institute of Technology. [4]Department of Chemistry, Northwestern University.

Presentation Abstract

A series of supported single-site first-row transition metal (V^{3+}, Zn^{2+}) and main group element (Ga^{3+}) hydrogenation catalysts have been developed in our program. The generality of the active site design strategy that we demonstrated encouraged us to pursue rational active site design based on molecular-level understanding of catalytic properties and reaction mechanisms. Thus, we have carried out a combined theoretical and experimental study to demonstrate computationally guided active site design strategy, specifically developing descriptors for single-site catalysts for hydrogenation reactions. Density Functional Theory (DFT) calculations are used to investigate the structures and thermodynamic stabilities of active sites of the type M/SiO_2 (M = Ga^{3+}, Zn^{2+}, Mn^{2+} and Ti^{4+}), as well as the periodicity of reaction mechanisms and rate-limiting steps based on representative single-atom catalysts for propylene hydrogenation. A cluster model with six silica rings and up to four hydroxyl groups are used to represent the structure of the M/SiO_2 catalysts. The results show that catalyst activation proceeds through H_2 activation over a M-O bond, resulting in M-H and Si-O-H bond formation. This intermediate can then hydrogenate propylene through two probable metal-dependent mechanisms: Ga^{3+}, $Mn^{2+}$and Ti^{4+} ions go through a concerted hydrogenation step, while Zn^{2+} undergoes a stepwise pathway. The calculations also indicate that the stability of the M-H is critical to the kinetics of hydrogenation. This approach generated a computational activity descriptor that closely correlates with the experimental activity observed during catalysis. The experimental activities show a remarkable trend as a function of the calculated $\Delta G_{M\text{-}H}$. Specifically, an exponential correlation is observed between the calculated $\Delta G_{M\text{-}H}$ and the experimental TOF, enabling the prediction that lower the $\Delta G_{M\text{-}H}$ gives rise to more active single-site catalysts. Among the cationic sites considered, Pd^{2+}, In^{3+} and $Sn^{4+}$are predicted to be more active than the experimentally discovered Ga^{3+} catalyst. The validity of this computationally guided active site design strategy has been confirmed by the higher experimental hydrogenation activity of the In^{3+}/SiO_2 (TOF = 3.4 h^{-1} at 200 °C).

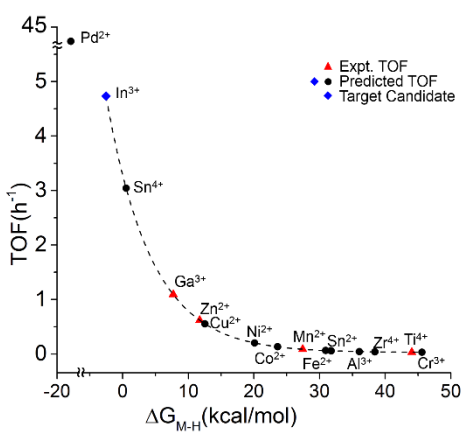

Ping Liu

Tuning Activity and Selectivity toward CO_2 Conversion to Methanol from First Principles

Ping Liu, Shyam Kattel, Yixiong Yang, Michael G. White, Jingguang G. Chen, and Jose A. Rodriguez
Chemistry Division, Brookhaven National Laboratory, Upton, NY 11973

Presentation Abstract

Carbon dioxide (CO_2) recycles as a feedstock for producing chemicals contributes to alleviate global climate changes caused by the increasing CO_2 emissions. Hydrogenation of CO_2 to synthesize carbon monoxide and/or methanol ($CO_2 + 3H_2 \rightarrow CH_3OH + H_2O$) has attracted considerable interests. The leading catalyst that currently used in industry for hydrogenation of CO_2 to methanol is $Cu/ZnO/Al_2O_3$, which suffers from the limited conversion even at elevated pressures. Here, we presented a combined density functional theory (DFT) and Kinetic Monte Carlo (KMC) simulation to study the conversion of CO_2 and H_2 to methanol on Cu,[1] Cu alloys[2] and Cu-oxide systems[3-5]. The results pinpoint the effects of doping on the reaction pathways, the possible intermediates and transition states. The descriptors are identified, which can describe the catalytic activity and therefore are useful for the rational design of better of Cu-based catalysts for CO_2 hydrogenation. The present work provided better understanding of CO_2 conversion on Cu-based catalysts and on the basis developed the descriptor-based method for rational screening of complex catalysts at a theoretical level.

References

[1] Y. Yang, J. Evans, J.A. Rodriguez, M.G. White, P. Liu, Fundamental studies of methanol synthesis from CO_2 hydrogenation on Cu(111), Cu clusters, and Cu/ZnO(0001), Physical Chemistry Chemical Physics, 12 (2010) 9909-9917.
[2] Y. Yang, M. White, P. Liu, Theoretical Study of Methanol Synthesis from CO_2 Hydrogenation on Metal-Doped Cu(111) Surfaces, Journal of Physical Chemistry C, 116 (2012) 248-256.
[3] J. Graciani, K. Mudiyanselage, F. Xu, A.E. Baber, J. Evans, S.D. Senanayake, D.J. Stacchiola, P. Liu, J. Hrbek, J.F. Sanz, J.A. Rodriguez, Highly active copper-ceria and copper-ceria-titania catalysts for methanol synthesis from CO_2, Science, 345 (2014) 546-550.
[4] S. Kattel, P.J. Ramírez, J.G. Chen, J.A. Rodriguez, P. Liu, Active sites for CO_2 hydrogenation to methanol on Cu/ZnO catalysts, Science, 355 (2017) 1296-1299.
[5] S. Kattel, B. Yan, Y. Yang, J.G. Chen, P. Liu, Optimizing Binding Energies of Key Intermediates for CO_2 Hydrogenation to Methanol over Oxide-Supported Copper, Journal of the American Chemical Society, 138 (2016) 12440-12450.

Ethane Aromatization over Zn-Containing Zeolites

Ali Mehdad and Raul F. Lobo
Center for Catalytic Science and Technology

Presentation Abstract

We have investigated the direct transformation of ethane into benzene, toluene and ethylene over Zn-containing zeolite catalysts. The goal is to identify the sites responsible for the various reactions needed to accomplish this transformation: ethane dehydrogenation, oligomerization, cyclization and aromatization. We also want to better understand the role of zinc cations using a combination of reaction kinetic studies and tailored zeolite synthesis. Among several zeolites investigated, the medium-pore ZSM-5 zeolite was found to be the most reactive catalyst followed by the large-pore zeolite beta. Reaction rates increase with the Al content of the zeolite framework and with increasing the Zn content. Over exchange (more Zn cations than Al framework atoms) leads to aggregation of ZnO_n nanoclusters but Bronsted acid sites still remain in the sample after heating as determined by IR spectroscopy. ZSM-5 zeolites containing no aluminum can still carry out the dehydrogenation reaction, but the product is only ethylene without formation of any new C-C bonds. The selectivity to aromatic species decreases over time leading to the formation of butenes as the major reaction product at longer time-on stream. The patterns of reactivity and selectivity suggest that Zn(II) sites, that coordinate to two Al atoms, are primarily responsible for the dehydrogenation/hydrogenation activity, although other sites may contribute to the overall reaction rates. Acid sites carry out many C-C bond-forming reactions such as ethylene dimerization but Zn sites can clearly catalyze the cyclization and aromatization reactions of C6 and C7 intermediates. It is suggested that the cyclization of trienes is catalyzed by Zn cations, as has been suggested by others for Li-cations, via a six-center pericyclic transitionstate.

Award Number DE-SC0014436: Methane Activation on Cu Containing Zeolite Catalysts

Postdoc(s): Ali Mehdad
Student(s): Edward Schreiner

RECENT PROGRESS

Effect of Zeolite Composition and Zn Content on Aromatization Rates

The conversion of ethane on zinc containing zeolites SSZ-13 (CHA), ZSM-5 (MFI) and beta and ethylene on Zn-containing ZSM-5 was investigated using flow micro-reactor at 773 K and atmospheric pressure. Zinc was incorporated in zeolites (Si/Al=11-25) and in silicalite-1 by

ion exchange (Zn< 2.7% w/w, Zn/BAS< 0.8) or by wet impregnation (Zn> 5% w/w and Zn/BAS> 3). It was found that drying of wet-impregnated samples by freeze-drying leads to better dispersion of subnano-sized clusters of ZnO in the zeolite pores, as compared to drying in an oven. Several zinc sites (Zn^{2+}, $[Zn\text{-}O\text{-}Zn]^{2+}$ dimers at ion exchange positions, and $(ZnO)_n$ clusters) can all catalyze the ethane dehydrogenation reaction and that higher zinc content resulted in higher reaction rates. However, Zn in Lewis acid site positions (Zn^{2+} and $[Zn\text{-}O\text{-}Zn]^{2+}$) are much more effective catalysts for aromatization than ZnOH, that catalyzes this reaction only at slow rates.

Small ZnO clusters can only catalyze the dehydrogenation reaction, and on their own do not catalyze aromatization, as 5% Zn/silicalite-1 catalyzed the ethane dehydrogenation to ethylene while it only showed low reaction rates for *ethylene* conversion. Zn-ZSM-5 catalytic properties for ethane/ethylene aromatization depends on the balance between number of metal/Lewis acid sites and BAS (Zn/BAS). For ethane as reactant, Zn/BAS< 0.8 favored ethylene formation while by increasing Zn/BAS both conversion and formation of aromatics increased, implying an essential role of Zn sites for ethane aromatization. For ethylene as reactant, Zn/BAS=3.8 resulted in predominant ethane formation while at Zn/BAS=0.8 aromatics formation was predominant. The difference in product selectivity for ethane/ethylene activation with respect to Zn/BAS could due to the fact that ethylene, unlike ethane, can react quickly on BAS.

Effect of CO_2 and water on Selectivity

When CO_2 is used instead of He, aromatics formation was suppressed. The conversion for all samples was stabilized, and conversion decreased more as compared with the reaction in presence of He. The main changes in selectivity that are observed are a decrease in aromatics, ethylene and methane formation rates, while forming a new product CO which is most likely the result of the RWGS catalyzed by the Zn sites of this system. Figure 1 illustrates the observed changes in selectivety as a function of gas composition and the shift in selectivity (and stability) can be clearly seen after the He purge at ~350 min. We think that this is the result predominantly of water. This molecule seems to bind quickly but reversibly to Zn(II) cations changing the reactivity of the catalytic sites.

Structural Investigations of Active Sites

The small-pore Zn-chabazite (Si/Al=12) offers a unique opportunity to understand the bonding of Zn cations to the zeolite framework as this material has a crystallographically simple structure (one T-atom in the asymmetric unit) and its coordination can be determined with good accuracity. This is not the case in zeolites ZSM-5 and beta. Although this zeolite is nearly inactive in the ethane dehydrogenation reaction, the Zn coordination environment can be extrapolated to other zeolite structures. A neutron diffraction study of this sample

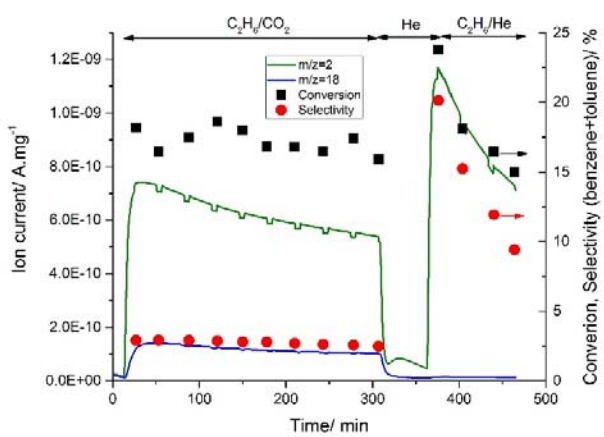

Figure 1: Change in activity of 5% Zn-ZSM-5 (11.5) by changing the feed composition. Rxn. conditions: WHSV= 0.12 g.(g_{cat} .min)$^{-1}$, 500 ºC and 1 atm.

shows that ZnOH is the main exchange species and these are located on the 6-rings of the zeolite with the OH group pointing into the cage.

Publications Acknowledging this Grant in 2014-2017

(I) Exclusively funded by this grant;

1. Mehdad, A., Lobo, R.F., "Ethane and Ethylene Aromatization over Zn-containing Zeolites", *ChemCatChem*, 2017, under review.

Mechanistic Studies of Organometallic Reactions at Paramagnetic Metal Centers

Liviu M. Mirica, Nicholas Ruhs, Andrew Wessel, Wen Zhou, and Kei Fuchigami
Department of Chemistry, Washington University in St. Louis

Presentation Abstract

The long term goal of this project is to develop novel transition metal catalysts by combining successful approaches from organometallic chemistry for the functionalization of unactivated organic molecules with strategies from bioinorganic chemistry for the activation of small molecules. Our approach employs flexible multidentate ligands that can accommodate different metal coordination geometries corresponding to various oxidation states, and thus promote facile redox reactions. Given the importance of Pd systems in catalytic transformations, we have been investigating the electronic properties and organometallic reactivity of uncommon Pd^{III} and Pd^{I} complexes. Of particular interest are aerobic oxidative reactions that lead to formation of new C-C and C-heteroatom bonds. Detailed mechanistic studies of aerobic C-H bond activation reactions will be presented, as well as recent organometallic reactivity studies employing Pd^{III} and/or Pd^{I} species. In addition, recent studies focused on the synthesis and organometallic reactivity of odd-electron Rh and Ir complexes will be described.

Overall, the development of transition metal-catalyzed aerobic oxidative reactions and C-H functionalization reactions should have a significant impact in organometallic catalysis applied to energy-related transformations, in line with the mission of the *Basic Energy Sciences – Catalysis Science Program* of the Department of Energy.

DE-FG02-11ER16254: Novel Redox Catalysts for Greenhouse Gases Utilization

Postdoc(s): Wen Zhou, Hui Duan
Student(s): Nicholas Ruhs, Andrew Wessel, Kei Fuchigami

RECENT PROGRESS

C-H bond activation studies at Pd^{II} and Pd^{III} centers. Recently, Sanford et al. have unambiguously shown that C-H bond activation can occur at Pd^{IV} centers. By comparison, no C-H activation has been observed previously at a Pd^{III} center. In this context, we have employed the $^{Me}N4$ tetradentate ligand (Scheme 1) to show that the isolated $[(^{Me}N4)Pd^{III}(neophyl)Cl]^{+}$ complex reacts with 1 eq AgOAc or TlOAc at RT to yield the C-H activated product $[(^{Me}N4)Pd^{III}(cycloneophyl)]^{+}$, as confirmed by UV-Vis, EPR, and X-ray (Scheme 2, top). Importantly, in this system the C-H bond activation is faster at a Pd^{III} center vs. either a Pd^{II} or Pd^{IV} center, while kinetic isotope effects studies reveal an intermolecular KIE of 1.3 that suggests an acetate-assisted concerted metalation-

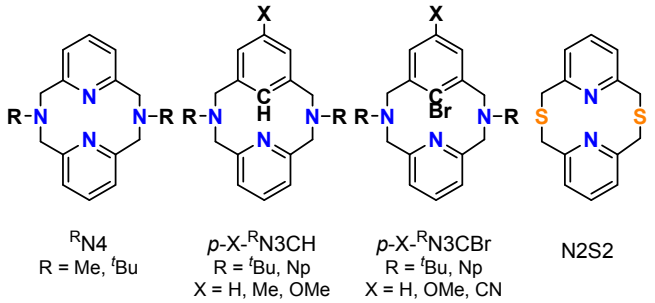

Scheme 1. *Ligands used in the studies described herein.*

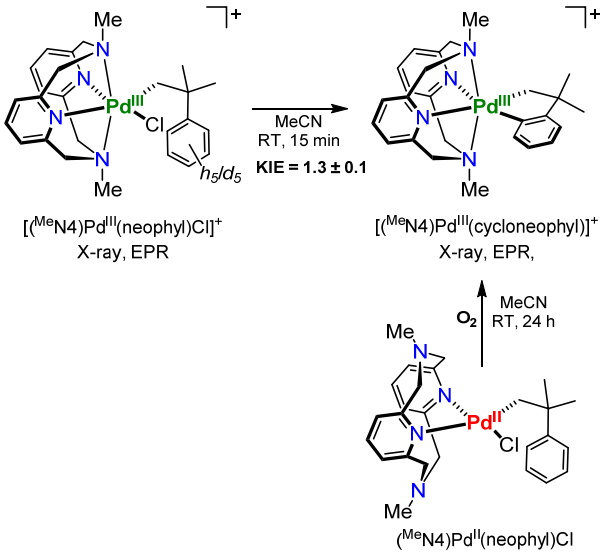

Scheme 2. *C-H activation at a Pd^{III} center and aerobically-induced C-H activation from a Pd^{II} precursor.*

Hammett ρ value of -2.1 for the C-H activation process. Surprisingly, these values are similar to those reported for the classical acetate-assisted C-H activation processes at Pd^{II} centers, although in our case we do not have any acetate of other base present in solution. Kinetic studies performed at various Pd and O_2 concentrations suggest a first order process in both Pd and O_2 for the Pd^{III} species formation. Overall, we are proposing that an unfavorable pre-equilibrium involving the oxidation of deprotonation (CMD) mechanism, similar to the one proposed by Sanford at a Pd^{IV} center. Most exciting is the observation of aerobic oxidatively-induced C-H activation of $(^{Me}N4)Pd^{II}$(neophyl)Cl to generate $[(^{Me}N4)Pd^{III}(cycloneophyl]^+$ (Scheme 2). This provides evidence that mono-alkyl Pd^{II} complexes supported by $^{Me}N4$ can be oxidized aerobically, an important requirement for the targeted aerobic C-H functionalization reactions.

We have also employed pyridinophane-type C-donor ligands in which one of the one pyridine ring is replaced with a phenyl ring containing different *para* substituents (i.e., p-X-^{R}N3CH, Scheme 1). We have found recently that in the presence of $[Pd(MeCN)_4](BF_4)_2$, and in the absence of any other additive, the ^{tBu}N3CH ligand undergoes an unprecedented aerobically-induced C-H activation to generate an isolable organometallic Pd^{III} complex (Scheme 3a). Detailed mechanistic studies using p-X-^{tBu}N3CH/D ligands have been performed to reveal a KIE value of 2.7 for p-Me-^{tBu}N3CH vs p-Me-^{tBu}N3CD, and a

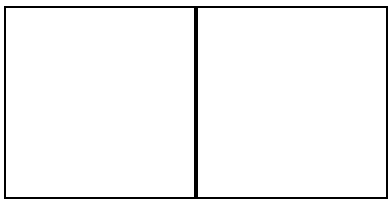

Scheme 3. *a) Mechanistic studies of the aerobically-induced oxidation and C-H bond activation of a dicationic Pd^{II} complex; b) Proposed base-free, dioxygen-assisted C-H bond activation at a Pd^{III} center.*

Pd^{II} by O_2 is occurring (Scheme 3b), and the reduced O_2 species (likely a superoxide moiety) could act as the base to assist the metalation-deprotonation step. Importantly, such a dioxygen-assisted C-H bond activation has not been observed before, and DFT calculations are currently being performed to supplement our mechanistic studies.

Synthesis and reactivity of mononuclear Pd^{I} species. Another goal of our research project is the synthesis and detailed characterization of low-valent Pd complexes that could lead to the development of novel catalysts for reductive transformations. Most Pd^{I} complexes isolated to date are dimeric complexes containing a Pd-Pd bond. Moreover, no isolated mononuclear organometallic Pd^{I} complexes have been reported to date, although they have been proposed as key intermediates in several catalytic transformations. Using the N2S2 ligand (Scheme 1), we have been able to generate EPR-detectable Pd^{I} species upon chemical reduction of Pd^{II} precursors (Scheme 4), while addition of PPh_3 (or tBuNC) leads to formation of more stable Pd^{I} species. These results suggest the use of multidentate ligands and/or exogenous additives with soft atom donors (i.e., S or P) should stabilize the targeted Pd^{I} species and allow for their isolation and detailed characterization. We are particularly interested in these Pd^{I} species in the context of electrocatalytic reduction of CO_2.

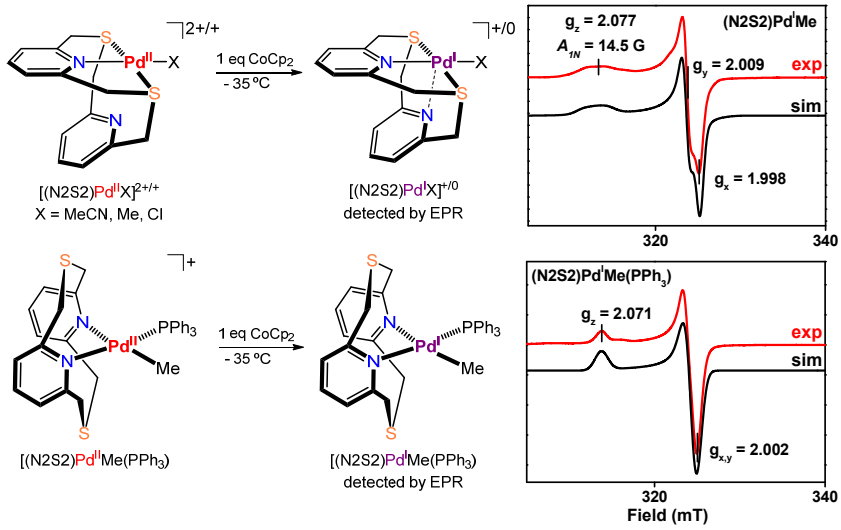

Scheme 4. *Generation of (N2S2)Pd^{I} complexes and their EPR spectra.*

Synthesis and reactivity of mononuclear Pd^{I} species. Another goal of our research project is the synthesis and detailed characterization of low-valent Pd complexes that could lead to the development of novel catalysts for reductive transformations. Most Pd^{I} complexes isolated to date are dimeric complexes containing a Pd-Pd bond. Moreover, no isolated mononuclear organometallic Pd^{I} complexes have been reported to date, although they have been proposed as key intermediates in several catalytic transformations. Using the N2S2 ligand (Scheme 1), we have been able to generate EPR-detectable Pd^{I} species upon chemical reduction of Pd^{II} precursors (Scheme 4), while addition of PPh_3 (or tBuNC) leads to formation of more stable Pd^{I} species. These results suggest the use of multidentate ligands and/or exogenous additives with soft atom donors (i.e., S or P) should stabilize the targeted Pd^{I} species and allow for their isolation and detailed characterization. We are particularly interested in these Pd^{I} species in the context of electrocatalytic reduction of CO_2.

In addition, we have found an unprecedented example of direct generation of monometallic Pd^{III} complexes by the oxidative addition of an aryl-Br bond to a Pd^{I} center (Scheme 5). Compared to the traditional pathway of synthesizing Pd^{III} complexes involving one electron oxidation of Pd^{II} precursors, this two electron process is step-economical. Based on UV-vis and EPR kinetic studies, the generation of Pd^{III} complexes is a first order reaction. In addition, both the sterics of the two

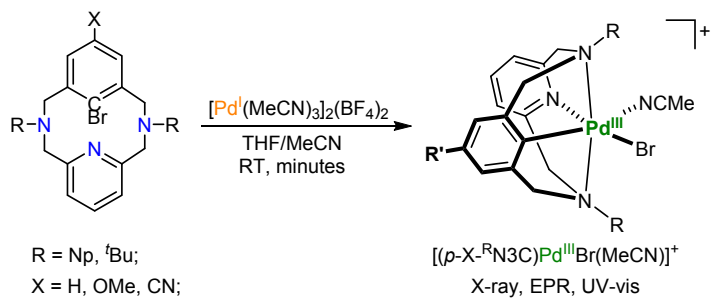

Scheme 5. *Unprecedented synthesis of organometallic Pd^{III} complexes through oxidative addition of an aryl-Br bond to a Pd^{I} precursor.*

amine alkyl arms and the electronics of the *para* substituents of the aromatic ring play a vital role in controlling the reaction rate. Overall, these studies indicate the possibility of designing catalytic transformations employing Pd^{I}/Pd^{III} redox cycles.

<u>*Synthesis and reactivity of odd-electron Rh and Ir complexes.*</u> We have recently reported that the ^{R}N4 ligands (R = Me or tBu, Scheme 1) can be employed to synthesize ^{R}N4Rh^{I}(COD) and ^{R}N4Ir^{I}(COD) complexes (COD = cyclooctadiene). Interestingly, these complexes could be oxidized to generate both Rh^{II} and Ir^{II} species that exhibit characteristic anisotropic EPR spectra suggesting a metal-based radical. However, these complexes exhibit limited reactivity toward exogenous substrates, most likely due to the strong coordination of the COD ligand. Therefore, we also began exploring the chemistry of higher-valent Rh complexes. For example, we have employed ^{R}N4 ligands to generate $[(^{R}N4)Rh^{III}Cl_2]^{+}$ complexes, which are currently being used as precursors in organometallic reactions. For example, we have synthesized a metallacycle Rh^{III} complex that has been obtained through a transmetallation reaction, followed by a subsequent C-H bond activation step (Scheme 6), and we are currently probing the role of various Rh oxidation states in this transformation. In addition, we have synthesized $[(^{R}N4)Rh^{III}H_2]^{+}$ complexes that are optimal precursors for performing photo-induced reductive elimination of H_2 and subsequent alkane C-H activation studies, similar to classical studies such as those of Bergman et al. and Jones et al.

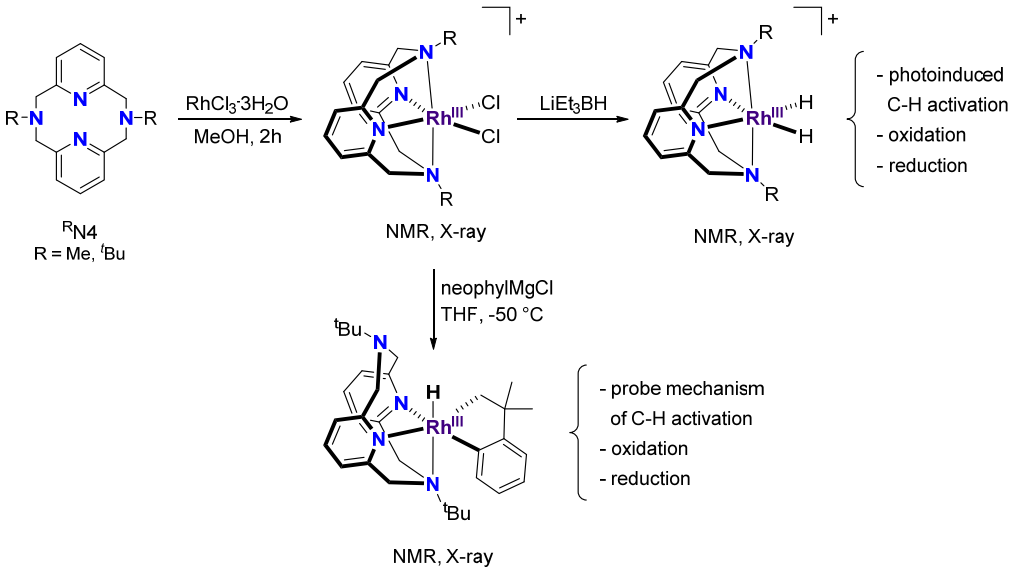

Scheme 6. *Synthesis of various $(^{R}N4)Rh^{III}$ complexes for organometallic reactivity studies.*

Publications Acknowledging this Grant in 2014-2017

(II) Publications exclusively funded by this grant

1. Ruhs, N. Rath, N. P.; Mirica, L. M. "Aerobically-Induced, Base-Free C-H Activation at a Pd Center", *manuscript in preparation*.

2. Zhou, W. Rath, N. P.; Mirica, L. M. "Direct Oxidative Addition of Aryl Halides to Pd(I) to Generate Organometallic Pd(III) Complexes", *manuscript in preparation*.

3. Tang, F.; Park, S.; Rath, N. P.; Mirica, L. M. "C-H Bond Activation at a Pd(III) center", *manuscript in preparation.*

4. Ruhs, N. Khusnutdinova, J. R.; Rath, N. P.; Mirica, L. M. "Mononuclear Organometallic Pd(III) and Pd(IV) Complexes Stabilized by a Pyridinophane Ligand with a C-Donor Group", *submitted*.

5. Tang, F.; Park, S.; Rath, N. P.; Mirica, L. M. "Electronic Versus Steric Effects of Pyridinophane Ligands that Stabilize Pd(III) Complexes", *submitted.*

6. Fuchigami, K.; Rath, N. P.; Mirica, L. M. "Mononuclear Rhodium(II) and Iridium(II) Complexes Supported by Tetradentate Pyridinophane Ligands", *submitted*.

7. Luo, J.; Rath, N. P.; Mirica, L. M. "Synthesis and Spectroscopic Studies of Mononuclear (N2S2)Pd^{I} Complexes", *submitted*.

8. Khusnutdinova, J. R.; Rath, N. P.; Mirica, L. M. "The Conformational Flexibility of the Tetradentate Ligand ^{tBu}N4 is Essential for the Stabilization of (^{tBu}N4)Pd^{III} Complexes", *Inorg. Chem.*, **2014**, *53*, 13112-13129, DOI: 10.1021/ic5023054.

9. Qu, F.; Khusnutdinova, J. R.; Rath, N. P.; Mirica, L. M. "Dioxygen Activation by an Organometallic Pd(II) Precursor: Formation of a Pd(IV)-OH Complex and Its C-O Bond Formation Reactivity", *Chem. Comm.*, **2014**, *50*, 3036-3039; DOI: 10.1039/c3cc49387c.

(III) Jointly funded by this grant and other grants with major intellectual contribution from this grant

10. Wessel, A. J.; Schultz, J. W.; Tang, F.; Khusnutdinova, J. R.; Duan, H.; Mirica, L. M.; "Improved Synthesis of Symmetrically & Asymmetrically N-Substituted Pyridinophane Derivatives", *submitted*.

(IV) Jointly funded by this grant and other grants with relatively minor intellectual contribution from this grant

11. Pedrick, E. A.; Schultz, J. W.; Wu, G.; Mirica, L. M.; Hayton, T. W. "Perturbation of the O–U–O Angle in Uranyl by Coordination to a 12-Membered Macrocycle", *Inorg. Chem.*, **2016**, *55*; DOI: 10.1021/acs.inorgchem.6b00799.

Pathways for Electrochemical Transformation of Small Organic Molecules

William E. Mustain
Department of Chemical & Biomolecular Engineering, University of Connecticut

Presentation Abstract

The overarching goal of this DOE Early Career research program is to discover the nature of the electrochemically active site and to uncover the mechanism for the electrochemical interconversion of small chain organic molecules. To date, this project has primarily focused on the uncovering of new pathways for the creation of methanol. Specific to this presentation, three pathways will be discussed, each starting from its own feedstock: methane, carbon dioxide, and acetic acid.

DE-SC0010531: Room Temperature Electrochemical Upgrading of Methane to Oxygenate Fuels

Postdoc(s): William Rigdon
Student(s): Travis Omasta, Xiong Peng, Neil Spinner

RECENT PROGRESS

In past project presentations, our primary focus was on the conversion of methane to methanol. Here, two other pathways for oxygenate synthesis will be discussed. Some recent advances in these areas are discussed below.

Pathways for the Conversion of Acetic Acid to Methanol

Though acetate electrolysis has been studied for some time, most of the reaction products available in the literature (i.e. ethanol) have been reduction products and pathways for oxidation have been in short supply. This is most likely because there is a minimal supply for naturally-occurring acetic acid and thus limited demand for new reaction pathways allowing for the interchange of acetic acid with other oxygenates. However, as bio-derived energy sources become more available, acetic acid is one of the two most common products. Therefore, there is a projected need to be able to seamlessly exchange organics, and preferably in a sustainable fashion.

To address this projected need, our group has investigated the oxidation of acetic acid to methanol, allowing us to show the potential for a routine electrochemical conversion of biomass into liquid fuels and value-added chemicals. Not only have we shown the possibility for inter-conversion, but also have begun to uncover the related reaction mechanisms. In our experiments, the acetate oxidation was conducted in the IEC with Pt electrodes at both the working and counter

electrode. AgCl/Ag was used as reference electrode. The gas phase products were sent to gas chromatography (GC) and the liquid phase products were characterized by Nuclear magnetic resonance spectroscopy (NMR). Typical gas phase and liquid phase products were shown in Figure 1.

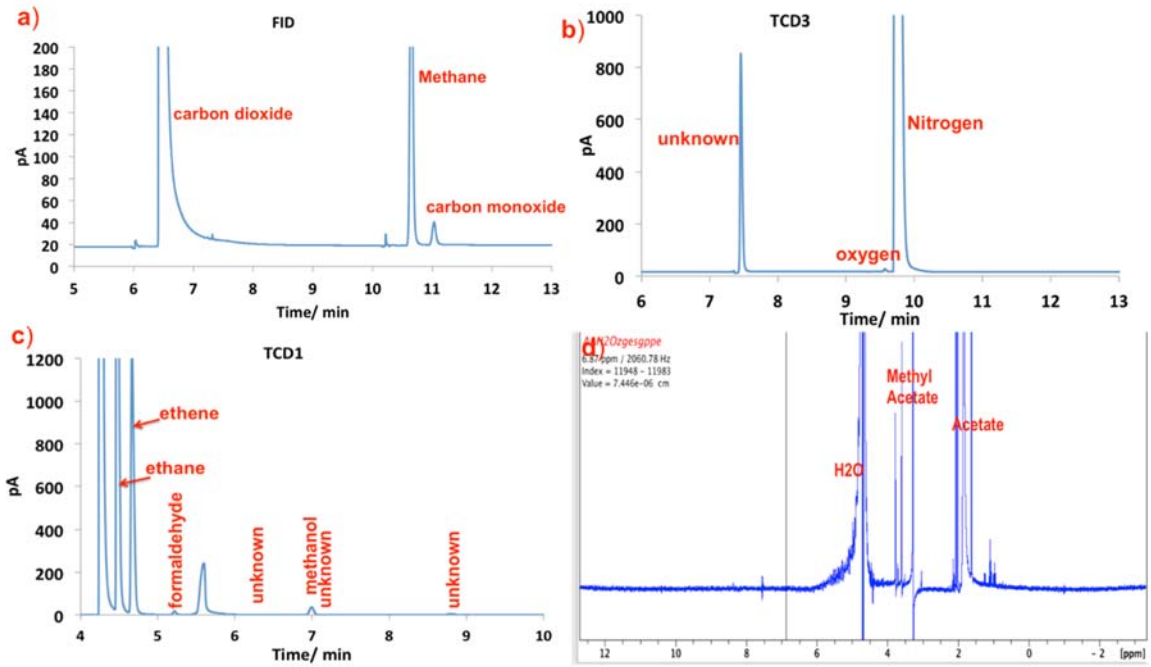

Figure 1. Gas phase product from GC: (a) FID; (b) TCD1; (c) TCD 3; Liquid phase product from NMR

From our study, it is clear that Pt catalyzes the formation of a large number of acetate electrochemical oxidation products, which change as a function of potential. We have observed more products for this reaction than have ever been reported before. Based on the products, we have proposed radical-based and carbenium-based mechanisms, which will be discussed in detail during the presentation. The proposed mechanisms are able to explain all of the products and desorbable intermediates formed during oxidation, including methanol, CO, ethanol, alkanes and alkenes.

Oxide-Derived Ag Particles for Enhanced CO_2 Reduction to CO

An oxidized-derived Ag electrode was prepared by anodization treatment of a Ag foil in CO_2 purged 0.5M $KHCO_3$ electrolyte. The anodization treatment created a layer of Ag_2CO_3 (Figure 2a) on the electrode surface, which was subsequently reduced to Ag nanoparticles (Figure 2b) and then used for CO_2 electrochemical reduction. After reduction, the OD-Ag exhibits a much rougher surface with uniformly distributed particles (Figure 2c,d) and average thickness of 2.5 µm (Figure 2e).

CO_2 electroreduction was performed in an air-tight three-electrode, two compartment, in-operando electrochemical cell (IEC). The gas product was swept from the cell with a N_2 carrier gas and sent to gas chromatograph (GC, Agilent Technologies 7890B series). In the GC, CO_2 and CO are detected and analyzed by a flame ionization detector (FID). Hydrogen, formaldehyde and methanol are detected and analyzed by the thermal conductivity detector (TCD). The GC was well calibrated using standard gas samples. Samples were taken and analyzed in 16 minute intervals.

The CO and H_2 Faradaic Efficiency (FE) are reported below based on the average of all the seven measures.

Figure 3a shows the iR-corrected potential-dependent total reduction current densities, which were measured at steady-state current. The OD-Ag showed a much higher total reduction current density than Ag foil. The CO partial current densities versus iR-corrected potential are shown in Figure 3b. The OD-Ag showed a much higher total reduction current density than Ag foil. The CO partial current densities versus iR-corrected potential are shown in Figure 3b. The OD-Ag electrode and Ag foil showed a Tafel slope of 108 mV/decade and 190 mV/decade, respectively (Figure 3c). The OD-Ag and Ag foil share the same RDS in CO_2 reduction to CO; however, the exchange current density of OD-Ag (7.11×10 mA/cm^2) is about seven times higher than that of Ag foil (1.12×10^{-4} mA/cm^2). Both OD-Ag and Ag foil showed "volcano shape" of CO FE against different operating potentials (Figure 3d). However, the OD-Ag showed enhanced CO selectivity than Ag, even at lower overpotentials. Besides, the maximum CO FE was 87% at operating potential of -0.72 V, which was much higher than that of Ag foil (60%) at also higher operating potential of -0.87 V.

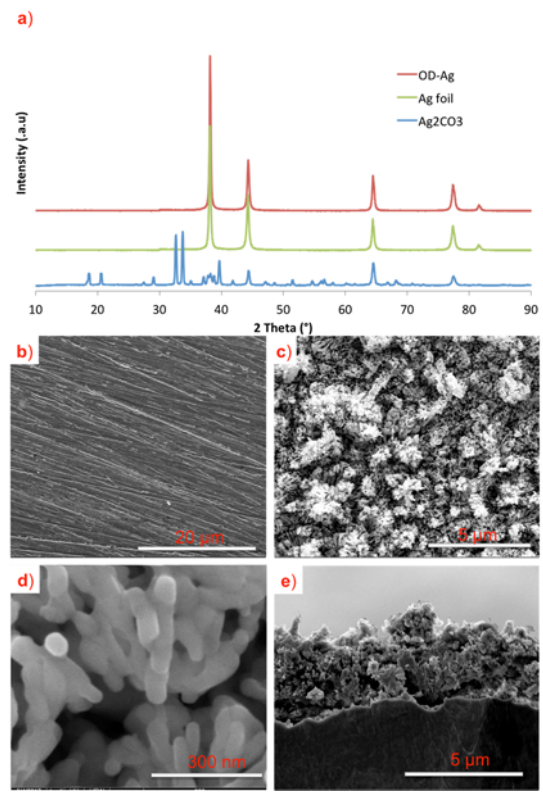

Figure 2. (a) XRD patterns of Ag_2CO_3, OD-Ag and Ag-foil; Representative SEM images of (b) Ag foil surface; (c) (d) (e) OD-Ag surface

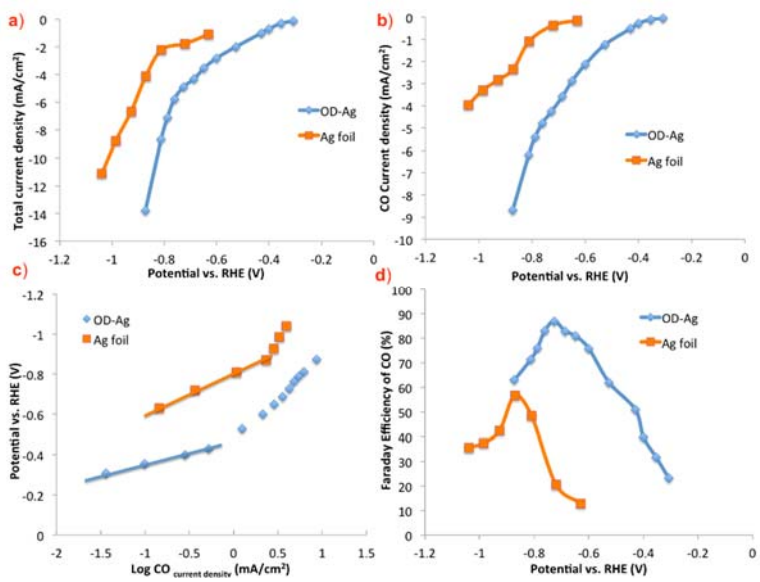

Figure 3. (a) Total reduction current density; (b) CO partial current density as a function of potential for OD-Ag and Ag foil; (c) Tafel plot versus CO partial current density; (d) Faraday efficiency of CO as a function of potential.

Publications Acknowledging this Grant in 2014-2017

Exclusively funded by this grant;

1. Spinner, N.S.; Mustain, W.E. Electrochemical Methane Activation and Conversion to Oxygenates at Room Temperature. *J. Electrochem. Soc.* **2013**, 160, F1275-F1281.
2. Rigdon, W.A.; Omasta, T.J.; Lewis, C.A.; Mustain, W.E. Reaction Dependent Transport of Carbonate and Bicarbonate through Anion Exchange Membranes in Electrolysis and Fuel Cell Operations. *ECS Trans*. **2015,** 69(33), 1-9.
3. Omasta, T.J; Rigdon, W.A.; Lewis, C.A.; Stanis, R.J.; Liu, R.; Fan, C.Q.; Mustain, W.E. Two Pathways for Near Room Temperature Electrochemical Conversion of Methane to Methanol, *ECS Trans.*, **2015**, 66(8), 129-136
4. Peng, X.; Omasta, T.J.; Roller, J.M.; Mustain, W.E. Investigation of Pd-Cu bimetallic catalyst for oxygen reduction in alkaline exchange membrane fuel cells, *Frontiers in Energy*. Accepted, In Press.
5. Spinner, N.S.; Palmieri, A.; Beauregard, N.; Zhang, L.; Campanella, J.; Mustain, W.E. Influence of Conductivity on the Capacity Retention of NiO Anodes in Li-ion Batteries. *J. Power Sources*, **2015**, 276, 46-53.
6. Rigdon, W.A.; Omasta, T.J.; Lewis, C.; Hickner, M.; Varcoe, J.R.; Renner, J.N.; Ayers, K.A.; Mustain, W.E. Carbonate dynamics and opportunities with low temperature, AEM-based electrochemical CO_2 separators. **2017**, 12(2), 020901.
7. Peng, X.; Omasta, T.J.; Rigdon, W.; Mustain, W.E. Fabrication of high performing PEMFC catalyst-coated membranes with a low cost air-assisted cylindrical liquid jets spraying system. *J. Electrochem. Soc.* **2016**, 163, E407-E413.
8. Peng, X.; Zhao, S.; Omasta, T.; Roller, J.M.; Mustain, W.E. Activity and durability of Pt-Ni nanocage electocatalysts in proton exchange membrane fuel cells. *Applied Catalysis B: Environmental*, 203 (2017) 927-935.

Jointly funded by this grant and other grants with leading intellectual contribution from this grant;

9. Omasta, T. J.; Wang, L.; Peng, X.; Lewis, C. A. Lewis; Varcoe, J. R; Mustain, W. E. Importance of Balancing Membrane and Electrode Water in Anion Exchange Membrane Fuel Cells. *J. Power Sources*. **2107**
   DOI: 10.1016/j.jpowsour.2017.05.006.
10. Poynton, S.D.; Slade, R.T.C.; Omasta, T.J.; Mustain, W.E.; Escudero-Cid, R.; Ocon, P. and Varcoe, J.R. Preparation of radiation-grafted powders for use as anion exchange ionomers in alkaline polymer electrolyte fuel cells. *J. Mat. Chem. A*., **2014**, 2, 5124-5130.

Jens K. Nørskov

Some challenges to energy transformation catalysis

Colin Dickens, Charlotte Kirk, Charlie Tsai, Michal Bajdich, Karen Chan, Jens Nørskov
SLAC National Accelerator Laboratory and Stanford University

Presentation Abstract

The rapidly decreasing cost of solar and wind electrical energy provides arguments for a shift towards using electrons to drive chemical transformations, thus enabling sustainable processes for the production of fuels and chemicals. In most cases we do not have suitable catalysts for these electrocatalytic reactions. An analysis of trends in reactivity for the hydrogen evolution reaction, the oxygen evolution reaction, and the oxygen reduction reaction will be presented. The analysis shows why it is so difficult to find good catalysts for the latter two reactions, and it points to new catalyst design strategies.

SUNCAT FWP
SLAC National Accelerator Laboratory

PIs, Co-PIs: *Jens K. Nørskov (Director), Thomas Jaramillo, Thomas Bligaard (Deputy Directors); Frank Abild-Pedersen, Zhenan Bao, Simon Bare, Stacey Bent, Matteo Cargnello, Johannes Voss, Karen Chan, Michal Bajdich, Melis S. Duyar, Drew C. Higgins*

RECENT PROGRESS

Theory of Catalysis and Electrocatalysis *(Jens Nørskov, Karen Chan)*

We seek to establish a systematic theory of heterogeneous catalysis by integrating the work in all four tasks of the SUNCAT FWP. It builds on the existence of scaling relations between energies of different intermediates and transition states. This allows us to define a few descriptors of catalytic activity enabling an understanding of trends in catalytic activity and selectivity from one catalyst to the next, rationalizing decades of experimental observations. The scaling relations also define limitations in our ability to optimize catalysts, and our work recently has highlighted the need to find ways to circumvent scaling relations if we want new catalysts with completely different properties. It has been shown that this is a general conclusion in both heterogeneous and electrochemical catalysis. A number of strategies have been outlined for circumventing scaling relations, that will be pursued theoretically and experimentally in the future, see below.

Specific reactions that have been in focus are i) methane activation, where an understanding of trends in activity among a large class of catalysts have been established; ii) electrochemical

reduction of O_2 to hydrogen peroxide, where properties of defects and dopants in graphitic carbons have been mapped out; iii) 1 and 2 electron electrochemical water oxidation, where an understanding of selectivity patterns to for OH radicals and hydrogen peroxide have been addressed; iv) syngas reactions, where methanol and higher alcohol synthesis have been studied on new catalysts; v) electrochemical hydrogen evolution, where new catalysts formed by making sulphur vacancies in the basal plane of MoS_2 have been developed.

Computational Catalysis *(Frank Abild-Pedersen, Michal Bajdich)*

An understanding of the breaking and making of chemical bonds at a solid surface is the starting point for any fundamental description of reactions at the solid-gas or solid-liquid interface. It is particularly important to understand which properties of the surface determine its chemical activity. The description and understanding of activation energies for elementary surface reactions is a prime focus of this task. In addition to activity of catalysts we also focus our attention on the loss of active surface area through either strong metal-support interactions or sintering. The ability to prevent such side-reactions from happening would greatly enhance catalyst life-times and increase the activity/mass ratio significantly. This task is divided into two very general areas: reactivity of transition metal surfaces and transition metal-oxide surfaces.

We have extended our understanding of sintering processes based on DFT energies. We have found that our kMC model simulations agree nicely with experimental findings and that an overall model based on kMC and mean field treatment of ripening processes can be used to get information of particle size distributions and how they evolve in time.

Our transition state scaling approach have been extended to include more complex reactions and it has proven to be even more accurate and significantly faster than typical linear approaches.

To address the surface reactivity of transition metal-oxides for OER, we have performed extensive calculations for several experimentally relevant OER systems: layered $Ni_xFe_{1-x}OOH$ and Li_xCoO_2, rutile RuO_2 as well as supported CoOx/Au(111). The interaction of OER intermediates (OH*, O*, OOH* and V_O) was accessed for variety of surfaces and surface defects within each system, including the effects of changing stoichiometry. We have identified trends in the reactivity due to the composition as well as the origin of the most active sites in each system. Currently, we are extending the study of OER activity in layered systems to $Ni_xCe_{1-x}OOH$, $Ni_xV_{1-x}OOH$ and $Ni_xAl_{1-x}OOH$. We are mainly focused on explaining the bulk and surface structure, OER trends as function of stoichiometry and the type of the active site to address recent experiments within the Jaramilo and Bao groups.

For the Li_xCoO_2 system, we have computationally discovered that surface reactivity is a very strongly dependent on type of the exposed surface facet. The novel effect of lithium extraction on the other hand can be used to fine-tune the reactivity of a given site. In the near future, we plan employ the delithiation technique to other transition metal-oxides as discussed below.

In the case of rutile RuO_2, we have discovered that experimentally observed high OER activity can be only explained with the existence of highly active surface defects as opposed to activity of a common (110) surface. Our study of large number of defects led to a discovery of an underlying electronic descriptor based on the energy position of the surface's oxygen 2p states. Now, we are in progress of testing the universality of our surface oxygen descriptor to other transition metal-oxide systems.

We have performed additional calculations for ultrathin oxide films supported on metals. Particularly, we have identified edges of CoO/Au(111) nanoparticles to be the active sites for H_2O dissociation, while we have also predicted the edge sites of CoO_2/Au(111) nanoparticles to be highly active towards OER. Additionally, we have also performed calculations for explaining comparative stability and edge structures of the CoOx nanoparticles for Au(111), Pt(111) and Ag(111) supports.

Experimental catalysis *(Thomas Jaramillo, Stacey Bent, Matteo Cargnello, Simon Bare, Melis S. Duyar, Drew C. Higgins)*

The experimental catalysis efforts are focused on synthesis, characterization and testing of catalysts for both thermal heterogeneous catalysis as well as electrocatalysis. This work is closely coupled to the theoretical tasks. Fundamental studies identifying active site motifs and mechanisms and establishing kinetics are core to the program. Novel catalyst synthesis routes are also a key feature, as is the use of i*n situ* synchrotron studies, along with spectroscopy and microscopy techniques for catalyst characterization. A tightly coupled theory-experiment feed-back loop for catalyst discovery is one of the main defining features of the effort.

We have placed great emphasis on catalyst discovery and characterization of the active site for the thermochemical synthesis of methanol, higher alcohols and oxygenates from syngas, as well as the electrochemical reactions for hydrogen evolution, water oxidation and hydrogen peroxide production.

In thermal heterogeneous catalysis, the installation of a new 4-station parallel reactor system has enabled accelerated testing of materials oxygenate synthesis from CO and CO_2 hydrogenation. Bimetallics have been extensively investigated through both theory and experiment, with new synthesis techniques to make optimized CuCo nanoparticles for higher alcohol synthesis developed. We have examined new indium-based bimetallics for improved methanol synthesis selectivity from CO_2, and understood reactivity trends using *operando* XAS spectroscopy at SSRL. Novel molybdenum phosphide catalyst for methanol synthesis have been discovered, and we are currently exploring the effects of sulfur, nitrogen or carbon incorporation. We have achieved a fundamental understanding of metal oxide effects on catalyst reaction activity and selectivity by using ALD to synthesize different catalyst configurations, along with characterizing and observing phase transformations during oxygenate synthesis using XAS. In methane activation, we have established a strong connection between theory and characterization. Experimental work has culminated in the discovery of activity descriptors and catalyst deactivation processes in metallic catalysts. An *in situ* cell was constructed to conduct *operando* x-ray diffraction and spectroscopy to gain structural and electronic property information of catalysts under methane activation or CO/CO_2 hydrogenation reaction conditions. In electrocatalysis, we have established understanding on the influence Au plays on metal-oxide water oxidation catalysts, along with the discovery of new transition metal modified zirconium phosphate catalysts for this reaction. Our understanding of nanostructured carbons catalysts for hydrogen peroxide electrosynthesis has evolved, with experimental and theoretical investigations elucidating effects of pore and carbon defects. Using these design principles, boron and nitrogen co-doped carbon catalysts are under development, with very promising preliminary results.

Data and Computational Infrastructure *(Thomas Bligaard, Johannes Voss, Karen Chan)*

Current catalyst search or design studies have been highly successful in finding new catalyst leads for a number of reactions based on few simulations. It would; however, be strongly desirable if we were able to accurately investigate orders of magnitude more systems in a design study than we currently are. This would for example allow us to investigate reaction networks of a more realistic complexity, and in particular to carry out such an analysis over many (thousands to millions) of facet structures and material compositions in parallel. It would also open for the possibility of utilizing a range of more advanced approaches for calculating free energy contributions to the surface reaction energetics. Such a big-data revolution will soon occur in the computational catalysis field, provided we establish the enabling technologies. This will require a transformation in the way we create and manage simulations, and in the way we featurize the simulations for machine learning purposes. It will transform the way we perform analysis of data and it will deepen the scientific questions that we can address based on simulations. In this Task we aim to lay a foundation for this future - radically more data-rich - computational heterogeneous catalysis and electrocatalysis approach.

We took a step toward establishing a benchmark data set of experimentally-validated computational reaction energy barriers for chemistry at solid surfaces. It turns out that the trouble for exchange-correlation functionals in the GGA formalism in describing reaction energies for gas phase reactions do not necessarily persist for reactions over surfaces. It turns out that GGA functionals, which accurate reproduce gas phase fragmentation energies will tend to yield surprisingly accurate barriers for fragmentation over transition metal surfaces. This helps us understand necessary conditions for exchange-correlation functionals to describe catalytic reactions.

In extending the BEEF-class of exchange-correlation functionals we have analyzed sensitivity of van der Waals kernels in various electronic structure codes and using pseudopotentials and PAW-setups of varying hardness. We have thereby identified transferability problems for density-based van der Waals methods and derived a novel GGA-based functional with the minimally code-sensitive D3-BJ van der Waals force field. This will make the use of error estimation functionals less computationally demanding, especially for small systems, and will drastically reduce the dependence of BEEF-results between different codes and choices of pseudopotential/PAW-setup hardness.

For rapidly screening large and complex reaction networks of catalytic reactions, we have devised a method, which integrates error estimates from the BEEF-class of functionals with machine learning predictions of reaction energies and barriers. This allows us to much faster and more confidently screen complex reaction networks, thus ensuring the robustness of computational catalysis studies while reducing the overall computational workload.

We have further integrated machine learning surrogate models in genetic algorithm searches for atomic-scale ordering of alloy catalyst particles, which has yielded an approximate 200-fold increase in the speed of finding the optimal atomic ordering in Pt-Au alloy particles.

The KMOS kinetic Monte Carlo code has been integrated in CatMAP to allow for kinetic Monte Carlo simulations of the kinetics in trend studies of surface reactivity, and the treatment of electrochemical barriers has been fully implemented in CatMAP. Furthermore, the stability of the steady state mean field microkinetics solver in CatMAP has been significantly improved.

Publications Acknowledging this Grant in 2014-2017

Category I

1. Lu, Z.; Chen, G.; Li, Y.; Wang, H.; Xie, J.; Liao, L.; Liu, C.; Liu, Y.; Wu, T.; Li, Y.; Luntz, A. C.; Bajdich, M.; Cui, Y. Identifying the active surfaces of electrochemically tuned LiCoO2 for oxygen evolution reaction. *JACS* **2017**, *139*, 6270–6276.
2. Tsai, C.; Li, H.; Park, S.; Park, J.; Han, H. S.; Nørskov, J. K.; Zheng, X.; Abild-Pedersen, F. Electrochemical generation of sulfur vacancies in the basal plane of MoS2 for hydrogen evolution. *Nature Communications* **2017**, *8*, 15113.
3. Stegmaier, S.; Voss, J.; Reuter, K.; Luntz, A. C. Li+ Defects in a Solid-State Li Ion Battery: Theoretical Insights with a Li3OCl Electrolyte. *Chem. Mater.* **2017**, *29*, 4330–4340.
4. Ulissi, Z. W.; Medford, A. J.; Bligaard, T.; Nørskov, J. K. To address surface reaction network complexity using scaling relations machine learning and DFT calculations. *Nature Communications* **2017**, *8*, 14621.
5. Doyle, A. D.; Bajdich, M.; Vojvodic, A. Theoretical Insights to Bulk Activity Towards Oxygen Evolution in Oxyhydroxides. *Catal. Lett.* **2017**, *147*.
6. Fields, M.; Tsai, C.; Chen, L. D.; Abild-Pedersen, F.; Nørskov, J. K.; Chan, K. Scaling Relations for Adsorption Energies on Doped Molybdenum Phosphide Surfaces. *ACS Catalysis* **2017**, *7*, 2528–2534.
7. Chen, Z.; Chen, S.; Siahrostami, S.; Chakthranont, P.; Hahn, C.; Nordlund, D.; Dimosthenis, S.; Nørskov, J. K.; Bao, Z.; Jaramillo, T. F. Development of a reactor with carbon catalysts for modular-scale, low-cost electrochemical generation of H 2 O 2. *Reaction Chemistry & Engineering* **2017**,
8. Latimer, A. A.; Aljama, H.; Kakekhani, A.; Yoo, J. S.; Kulkarni, A.; Tsai, C.; Garcia-Melchor, M.; Abild-Pedersen, F.; Nørskov, J. K. Mechanistic insights into heterogeneous methane activation. *Phys. Chem. Chem. Phys.* **2017**, *19*, 3575–3581.
9. Yu, L.; Abild-Pedersen, F. Bond Order Conservation Strategies in Catalysis Applied to the NH3 Decomposition Reaction. *ACS Catalysis* **2017**, *7*, 864–871.
10. Strickler, A.; Jackson, A.; Jaramillo, T. Active and Stable Ir@Pt Core-Shell Catalysts for Electrochemical Oxygen Reduction. *ACS Energy Letters* **2016**, *2*, 224–229.
11. Zhao, W.; Bajdich, M.; Carey, S.; Vojvodic, A.; Nørskov, J. K.; Campbell, C. T. Water Dissociative Adsorption on NiO(111): Energetics and Structure of the Hydroxylated Surface. *ACS Catalysis* **2016**, *6*, 7377–7384.
12. Wang, H.; Xu, S.; Tsai, C.; Li, Y.; Liu, C.; Zhao, J.; Liu, Y.; Yuan, H.; Abild-Pedersen, F.; Prinz, F. B.; Nørskov, J. K.; Cui, Y. Direct and continuous strain control of catalysts with tunable battery electrode materials. *Science* **2016**, *354*, 1031–1036.
13. To, J. W. F. et al. High-performance oxygen reduction and evolution carbon catalysis: From mechanistic studies to device integration. *Nano Research* **2016**, 1–15.
14. Kulkarni, A. R.; Zhao, Z.-J.; Siahrostami, S.; Nørskov, J. K.; Studt, F. Monocopper Active Site for Partial Methane Oxidation in Cu-Exchanged 8MR Zeolites. *ACS Catalysis* **2016**, *6*, 6531–6536.

15. Aljama, H.; Yoo, J. S.; Nørskov, J. K.; Abild-Pedersen, F.; Studt, F. Methanol Partial Oxidation on Ag(111) from First Principles. *ChemCatChem* **2016**, *8*, 1–6.
16. Plessow, P. N.; Abild-Pedersen, F. Sintering of Pt Nanoparticles via Volatile PtO2: Simulation and Comparison with Experiments. *ACS Catalysis* **2016**, *6*, 7098–7108.
17. Garcia-Pintos, D.; Voss, J.; Jensen, A. D.; Studt, F. Hydrodeoxygenation of phenol to benzene and cyclohexane on Rh (111) and Rh (211) surfaces: Insights from density functional theory. *J. Phys. Chem. C* **2016**, *120*, 18529–18537.
18. Lundgaard, K. T.; Wellendorff, J.; Voss, J.; Jacobsen, K. W.; Bligaard, T. mBEEF-vdW: Robust fitting of error estimation density functionals. *Phys. Rev. B* **2016**, *93*, 235162.
19. Zhang, S.; Plessow, P. N.; Willis, J. J.; Dai, S.; Xu, M.; Graham, G. W.; Cargnello, M.; Abild-Pedersen, F.; Pan, X. Dynamical Observation and Detailed Description of Catalysts under Strong Metal-Support Interaction. *Nano Lett.* **2016**, *16*, 4528–4534.
20. Kibsgaard, J.; Jackson, A.; Jaramillo, T. Mesoporous platinum nickel thin films with double gyroid morphology for the oxygen reduction reaction. *Nano Energy* **2016**, *29*, 243–248.
21. Plessow, P. N.; Bajdich, M.; Greene, J.; Vojvodic, A.; Abild-Pedersen, F. Trends in the Thermodynamic Stability of Ultrathin Supported Oxide Films. *J. Phys. Chem. C* **2016**, *120*, 10351–10360.
22. Zhao, Z.-J.; Kulkarni, A.; Vilella, L.; Nørskov, J. K.; Studt, F. Theoretical Insights into the Selective Oxidation of Methane to Methanol in Copper-Exchanged Mordenite. *ACS Catalysis* **2016**, *6*, 3760–3766.
23. Pruski, M. et al. Virtual Special Issue on Catalysis at the U.S. Department of Energy's National Laboratories. *ACS Catalysis* **2016**, *6*, 3227–3235.
24. Jaffe, A.; Lin, Y.; Beavers, C. M.; Voss, J.; Mao, W. L.; Karunadasa, H. I. High-Pressure Single-Crystal Structures of 3D Lead-Halide Hybrid Perovskites and Pressure Effects on their Electronic and Optical Properties. *ACS Central Science* **2016**, *2*, 201–209.
25. Ulissi, Z. W.; Singh, A. R.; Tsai, C.; Nørskov, J. K. Automated Discovery and Construction of Surface Phase Diagrams Using Machine Learning. *J. Phys. Chem. Lett.* **2016**, *7*, 3931.
26. Bertheussen, E.; Verdaguer-Casadevall, A.; Ravasio, D.; Montoya, J. H.; Trimarco, D. B.; Roy, C.; Meier, S.; Wendland, J.; Nørskov, J. K.; Stephens, I. E. L.; Chorkendorff, I. Acetaldehyde as an Intermediate in the Electroreduction of Carbon Monoxide to Ethanol on Oxide-Derived Copper. *Angew. Chem. Int. Ed.* **2016**, *55*, 1450.
27. Zhang, B. et al. Homogeneously-Dispersed Multi-Metal Oxygen- Evolving Catalysts. *Science* **2016**, *352*, 333–337.
28. Chakthranont, P.; Pinaud, B.; Seitz, L.; Forman, A.; Jaramillo, T. Improving the Photoelectrochemical Performance of Hematite by Employing a High Surface Area Scaffold and Engineering Solid-Solid Interfaces. *Advanced Materials Interfaces* **2016**, *3*, 1500626.
29. Reinecke, B. N.; Kuhl, K. P.; Ogasawara, H.; Li, L.; Voss, J.; Abild-Pedersen, F.; Nilsson, A.; Jaramillo, T. F. Elucidating the electronic structure of supported gold nanoparticles and its relevance to catalysis by means of hard X-ray photoelectron spectroscopy. *Surf. Sci.* **2016**, *650*, 24–33.

30. Wolcott, C. A.; Medford, A. J.; Studt, F.; Campbell, C. T. Degree of rate control approach to computational catalyst screening. *J. Catal.* **2015**, *330*, 197–207.
31. Luntz, A.; Voss, J.; Reuter, K. Interfacial Challenges in Solid-State Li Ion Batteries. *J. Phys. Chem. Lett.* **2015**, *6*, 4599–4604.
32. Yoo, J. S.; Zhao, Z.-J.; Nørskov, J. K.; Studt, F. Effect of Boron Modifications of Palladium Catalysts for the Production of Hydrogen from Formic Acid. *ACS Catalysis* **2015**, *5*, 6579–6586.
33. Chen, L. D.; Nørskov, J. K.; Luntz, A. C. Al-Air Batteries: Fundamental Thermodynamic Limitations from First-Principles Theory. *J. Phys. Chem. Lett.* **2015**, *6*, 175–179.
34. Wellendorff, J.; Silbaugh, T. L.; Garcia-Pintos, D.; Nørskov, J. K.; Bligaard, T.; Studt, F.; Campbell, C. T. A benchmark database for adsorption bond energies to transition metal surfaces and comparison to selected DFT functionals. *Surf. Sci.* **2015**, *640*, 36–44.
35. Öberg, H. et al. Optical laser-induced CO desorption from Ru(0001) monitored with a free-electron X-ray laser: DFT prediction and X-ray confirmation of a precursor state. *Surf. Sci.* **2015**, *640*, 80–88.
36. Jauho, T. S.; Olsen, T.; Bligaard, T.; Thygesen, K. S. Improved description of metal oxide stability: Beyond the random phase approximation with renormalized kernels. *Phys. Rev. B* **2015**, *92*, 115140.
37. Li, L.; Abild-Pedersen, F.; Greeley, J.; Nørskov, J. K. Surface Tension Effects on the Reactivity of Metal Nanoparticles. *J. Phys. Chem. Lett.* **2015**, *6*, 3797–3801.
38. Tsai, C.; Latimer, A. A.; Yoo, J. S.; Studt, F.; Abild-Pedersen, F. Predicting Promoter-Induced Bond Activation on Solid Catalysts Using Elementary Bond Orders. *J. Phys. Chem. Lett.* **2015**, *6*, 3670–3674.
39. Chen, L. D.; Nørskov, J. K.; Luntz, A. C. Theoretical Limits to the Anode Potential in Aqueous Mg-Air Batteries. *J. Phys. Chem. C* **2015**, *119*, 19660–19667.
40. Kunkes, E. L.; Studt, F.; Abild-Pedersen, F.; Schlögl, R.; Behrens, M. Hydrogenation of CO2 to methanol and CO on Cu/ZnO/Al2O3: Is there a common intermediate or not? *J. Catal.* **2015**, *328*, 43–48.
41. Santos, E. J. G.; Nørskov, J. K.; Vojvodic, A. Screened Hybrid Exact Exchange Correction Scheme for Adsorption Energies on Perovskite Oxides. *J. Phys. Chem. C* **2015**, *119*, 17662–17666.
42. Singh, V. D.; Cassidy, C.; Abild-Pedersen, F.; Kim, J.-H.; Aranishi, K.; Kumar, S.; Lal, C.; Gspan, C.; Groggerc, W.; Sowwan, M. Engineering high-performance Pd core-MgO porous shell nanocatalysts via heterogeneous gas-phase synthesis. *Nanoscale* **2015**, *7*, 13387–13392.
43. Zhou, M.; Cai, L.; Bajdich, M.; Garcia-Melchor, M.; Li, H.; He, J.; Wilcox, J.; Wu, W.; Vojvodic, A.; Zheng, X. Enhancing Catalytic CO oxidation over Co3O4 Nanowires by Substituting Co2+ with Cu2+. *ACS Catalysis* **2015**, *5*, 4485–4491.
44. Ng, M. L.; Abild-Pedersen, F.; Kaya, S.; Mbuga, F.; Ogasawara, H.; Nilsson, A. Low Barrier Carbon Induced CO Dissociation on Stepped Cu. *Phys. Rev. Lett.* **2015**, *114*, 246101.

45. Montoya, J. H.; Tsai, C.; Vojvodic, A.; Nørskov, J. K. The Challenge of Electrochemical Ammonia Synthesis: A New Perspective on the Role of Nitrogen Scaling Relations. *ChemSusChem* **2015**, *8*, 2180–2186.
46. Medford, A. J.; Vojvodic, A.; Voss, J.; Abild-Pedersen, F.; Studt, F.; Bligaard, T.; Nilsson, A.; Nørskov, J. K. From the Sabatier Principle to a Predictive Theory of Transition Metal Heterogeneous Catalysis. *Journal of Cataysis* **2015**, *328*, 36–42.
47. Koitz, R.; Nørskov, J. K.; Studt, F. A systematic study of metal-supported boron nitride materials for the oxygen reduction reaction. *Phys. Chem. Chem. Phys.* **2015**, *17*, 12722–12727.
48. Plessow, P. N.; Abild-Pedersen, F. Examining the Linearity of Transition State Scaling Relations. *J. Phys. Chem. C* **2015**, *119*, 10448–10453.
49. Pandey, M.; Vojvodic, A.; Thygesen, K. S.; Jacobsen, K. W. Two-Dimensional Metal Dichalcogenides and Oxides for Hydrogen Evolution: A Computational Screening Approach. *J. Phys. Chem. Lett.* **2015**, *6*, 1577–1585.
50. Viswanathan, V.; Hansen, H. A.; Nørskov, J. K. Selective Electrochemical Generation of Hydrogen Peroxide from Water Oxidation. *J. Phys. Chem. Lett.* **2015**, *6*, 4224.
51. Nørskov, J. K.; Niemantsverdriet, H. The Impact Of Haldor Topsoe On Catalysis. *J. Catal.* **2015**, *328*, 1.
52. Bajdich, M.; Nørskov, J. K.; Vojvodic, A. Surface Energetics of Alkaline-Earth Metal Oxides: Trends in Stability and Adsorption of Small Molecules. *Phys. Rev. B* **2015**, *91*, 155401.
53. Wang, C.-M.; Brogaard, R.; Xie, Z.-K.; Studt, F. Transition-state Scaling Relations in Zeolite Catalysis: Influence of Framework Topology and Acid-site Reactivity. *Catalysis Science & Technology* **2015**, *5*, 2814–2820.
54. Studt, F.; Behrens, M.; Kunkes, E. L.; Thomas, N.; Zander, S.; Tarasov, A.; Schumann, J.; Frei, E.; Varley, J. B.; Abild-Pedersen, F.; Nørskov, J. K.; Schlögl, R. The Mechanism of CO and CO2 Hydrogenation to Methanol over Cu-Based Catalysts. *ChemCatChem* **2015**, *7*, 1105–1111.
55. Öström, H. et al. Probing the Transition State Region in Catalytic CO Oxidation on Ru. *Science* **2015**, *347*, 978–982.
56. Vojvodic, A.; Nørskov, J. K. New Design Paradigm for Heterogeneous Catalysts. *National Science Review* **2015**, *2*, 140–149.
57. Walton, A. S.; Fester, J.; Bajdich, M.; Arman, M. A.; Osiecki, J.; Knudsen, J.; Vojvodic, A.; Lauritsen, J. V. Interface Controlled Oxidation States in Layered Cobalt Oxide Nano-Islands on Gold. *ACS Nano* **2015**, *9*, 2445–2453.
58. Medford, A. J.; Shi, C.; Hoffmann, M. J.; Lausche, A. C.; Fitzgibbon, S. R.; Bligaard, T.; Nørskov, J. K. CatMAP: A Software Package for Descriptor-Based Microkinetic Mapping of Catalytic Trends. *Catal. Lett.* **2015**, *145*, 794–807.
59. Luntz, A. C. Beyond Lithium Ion Batteries. *J. Phys. Chem. Lett.* **2015**, *6*, 300–301.
60. Yoo, J. S.; Khan, T. S.; Abild-Pedersen, F.; Nørskov, J. K.; Studt, F. On the role of the surface oxygen species during A-H (A = C, N, O) bond activation: a density functional theory study. *Chem. Commun.* **2015**, *51*, 2621–2624.

61. Hernandez-Fernandez, P.; Masini, F.; McCarthy, D. N.; Strebel, C. E.; Friebel, D.; Deiana, D.; Malacrida, P.; Nierhoff, A.; Bodin, A.; Wise, A. M.; Nielsen, J. H.; Hansen, T. W.; Nilsson, A.; Stephens, I. E. L.; Chorkendorff, I. Mass-selected Nanoparticles of PtxY as Model Catalysts for Oxygen Electroreduction. *Nature Chemistry* **2014**, *6*, 732–738.
62. Kibsgaard, J.; Jaramillo, T. F. Molybdenum Phosphosulfide: An Active, Acid-Stable Earth-Abundant Catalyst for the Hydrogen Evolution Reaction. *Angewandte Chemie International Edition* **2014**, *53*, 14433–14437.
63. Brogaard, R.; Wang, C.; Studt, F. Methanol-Alkene Reactions in Zeotype Acid Catalysts: Insights from a Descriptor-Based Approach and Microkinetic Modeling. *ACS Catalysis* **2014**, *4*, 4504–4509.
64. Lausche, A. C.; Falsig, H.; Jensen, A. D.; Studt, F. Trends in the Hydrodeoxygenation Activity and Selectivity of Transition Metal Surfaces. *Catal. Lett.* **2014**, *144*, 1968–1972.
65. Studt, F.; Behrens, M.; Abild-Pedersen, F. Energetics of the Water-Gas-Shift Reaction on the Active Sites of the Industrially Used Cu/ZnO/Al2O3 Catalyst. *Catal. Lett.* **2014**, *144*, 1973–1977.
66. Casalongue, H. S.; Benck, J. D.; Tsai, C.; Karlsson, R.; Kaya, S.; Ng, M. L.; Pettersson, L.; Abild-Pedersen, F.; Nørskov, J. K.; Ogasawara, H.; Jaramillo, T. F.; Nilsson, A. Operando Characterization of an Amorphous Molybdenum Sulfide Nanoparticle Catalyst during the Hydrogen Evolution Reaction. *J. Phys. Chem. C* **2014**, *118*, 29252–29259.
67. Tang, M. H.; Hahn, C.; Klobuchar, A. J.; Ng, J. W. D.; Wellendorff, J.; Bligaard, T.; Jaramillo, T. F. Nickel-silver alloy electrocatalysts for hydrogen evolution and oxidation in an alkaline electrolyte. *Phys. Chem. Chem. Phys.* **2014**, *16*, 19250–19257.
68. Medford, A. J.; Wellendorff, J.; Vojvodic, A.; Studt, F.; Abild-Pedersen, F.; Jacobsen, K. W.; Bligaard, T.; Nørskov, J. K. Assessing the reliability of calculated catalytic ammonia synthesis rates. *Science* **2014**, *345*, 197–200.
69. Michalsky, R.; Zhang, Y.-J.; Medford, A. J.; Peterson, A. A. Departures from the Adsorption Energy Scaling Relations for Metal Carbide Catalysts. *J. Phys. Chem. C* **2014**, *118*, 13026–13034.
70. Moses, P. G.; Grabow, L. C.; Fernandez, E. M.; Hinnemann, B.; Topsøe, H.; Knudsen, K. G.; Nørskov, J. K. Trends in Hydrodesulfurization Catalysis Based on Realistic Surface Models. *Catal. Lett.* **2014**, *144*, 1425–1432.
71. Brogaarda, R. Y.; Henry, R.; Schuurman, Y.; Medford, A. J.; Moses, P. G.; Beato, P.; Svelle, S.; Nørskov, J. K.; Olsbye, U. Methanol-to-hydrocarbons conversion: The alkene methylation pathway. *J. Catal.* **2014**, *314*, 159–169.
72. Christensen, J. M.; Medford, A. J.; Studt, F.; Jensen, A. D. High Pressure CO Hydrogenation Over Bimetallic Pt-Co Catalysts. *Catal. Lett.* **2014**, *144*, 777–782.
73. Vojvodic, A.; Medford, A. J.; Studt, F.; Abild-Pedersen, F.; Khan, T. S.; Bligaard, T.; Nørskov, J. K. Exploring the limits: A low-pressure, low-temperature Haber-Bosch process. *Chem. Phys. Lett.* **2014**, *598*, 108–112.
74. Wang, C.-M.; Brogaard, R. Y.; Weckhuysen, B. M.; Nørskov, J. K.; Studt, F. Reactivity Descriptor in Solid Acid Catalysis: Predicting Turnover Frequencies for Propene Methylation in Zeotypes. *J. Phys. Chem. Lett.* **2014**, *5*, 1516–1521.

75. Wellendorff, J.; Lundgaard, K. T.; Jacobsen, K. W.; Bligaard, T. mBEEF: An accurate semi-local Bayesian error estimation density functional. *J. Chem. Phys.* **2014**, *140*, 144107.
76. Yoo, J. S.; Abild-Pedersen, F.; Nørskov, J. K.; Studt, F. Theoretical Analysis of Transition-Metal Catalysts for Formic Acid Decomposition. *ACS Catalysis* **2014**, *4*, 1226–1233.
77. McCloskey, B. D.; Garcia, J. M.; Luntz, A. C. Chemical and Electrochemical Differences in Nonaqueous Li-O2 and Na-O2 Batteries. *J. Phys. Chem. Lett.* **2014**, *5*, 1230–1235.
78. Takehiro, N.; Liu, P.; Bergreiter, A.; Nørskov, J. K.; Behm, R. J. Hydrogen adsorption on bimetallic PdAu(111) surface alloys: Minimum adsorption ensemble, ligand and ensemble effects, and ensemble confinement. *Phys. Chem. Chem. Phys.* **2014**, *16*, 23930.
79. Hansen, H. A.; Viswanathan, V.; Nørskov, J. K. Unifying Kinetic and Thermodynamic Analysis of 2e- and 4e- Reduction of Oxygen on Metal Surfaces. *J. Phys. Chem. C* **2014**, *118*, 6706–6718.
80. Xin, H.; Vojvodic, A.; Voss, J.; Nørskov, J. K.; Abild-Pedersen, F. Effects of d-band shape on the surface reactivity of transition-metal alloys. *Phys. Rev. B* **2014**, *89*, 115114.
81. Tsai, C.; Abild-Pedersen, F.; Nørskov, J. K. Tuning the MoS2 Edge-Site Activity for Hydrogen Evolution via Support Interactions. *Nano Lett.* **2014**, *14*, 1381–1387.
82. Studt, F.; Sharafutdinov, I.; Abild-Pedersen, F.; Elkjær, C. F.; Hummelshøj, J. S.; Dahl, S.; Chorkendorff, I.; Nørskov, J. K. Discovery of a Ni-Ga catalyst for carbon dioxide reduction to methanol. *Nature Chemistry* **2014**, *6*, 320–324.
83. Falsig, H.; Shen, J.; Khan, T. S.; Guo, W.; Jones, G.; Dahl, S.; Bligaard, T. On the Structure Sensitivity of Direct NO Decomposition over Low-Index Transition Metal Facets. *Top. Catal.* **2014**, *57*, 80–88.
84. Viswanathan, V.; Hansen, H. A. Unifying Solution and Surface Electrochemistry: Limitations and Opportunities in Surface Electrocatalysis. *Top. Catal.* **2014**, *57*, 215–221.
85. Vojvodic, A.; Nørskov, J. K.; Abild-Pedersen, F. Electronic Structure Effects in Transition Metal Surface Chemistry. *Top. Catal.* **2014**, *57*, 25–32.
86. Jackson, A.; Viswanathan, V.; Forman, A. J.; Larsen, A. H.; Nørskov, J. K.; Jaramillo, T. F. Climbing the Activity Volcano: Core-Shell Ru@Pt Electrocatalysts for Oxygen Reduction. *ChemElectroChem* **2014**, *1*, 67–71.

Category II

87. Siahrostami, S.; Li, G.-L.; Viswanathan, V.; Nørskov, J. K. One- or Two-electron Water Oxidation, Hydroxyl Radical or H2O2 Evolution. *J. Phys. Chem. Lett.* **2017**, *8*, 1157–1160.
88. Li, L.; Plessow, P. N.; Rieger, M.; Sauer, S.; Sanchez, R.; Schaefer, A.; Abild-Pedersen, F. Modeling the Migration of Platinum Nanoparticles on Surfaces Using a Kinetic Monte Carlo Approach. *J. Phys. Chem. C* **2017**, *121*, 4261–4269.
89. Nilsson, A.; LaRue, J.; Öberg, H.; Ogasawara, H.; Dell'Angela, M.; Beye, M.; Öström, H.; Gladh, J.; Nørskov, J. K.; Wurth, W.; Abild-Pedersen, F.; Pettersson, L. G. Catalysis in Real Time using X-ray Lasers. *Chem. Phys. Lett.* **2017**, *675*, 145–173.
90. Fester, J.; Garcia-Melchor, M.; Walton, A.; Bajdich, M.; Li, Z.; Lammich, L.; Vojvodic, A.; Lauritsen, J. V. Edge reactivity and water-assisted dissociation on cobalt oxide nanoislands. *Nature Communications* **2017**,

91. Frydendal, R.; Seitz, L. C.; Sokaras, D.; Weng, T.-C.; Nordlund, D.; Chorkendorff, I.; Stephens, I. E.; Jaramillo, T. F. Operando investigation of Au-MnOx thin films with improved activity for the oxygen evolution reaction. *Electrochim. Acta* **2017**, *230*, 22–28.
92. Seh, Z.; Kibsgaard, J.; Dickens, C. F.; Chorkendorff, I.; Nørskov, J. K.; Jaramillo, T. F. Combining theory and experiment in electrocatalysis: Insights into materials design. *Science* **2017**, *355*.
93. Latimer, A. A.; Kulkarni, A. R.; Aljama, H.; Montoya, J. H.; Yoo, J. S.; Tsai, C.; Abild-Pedersen, F.; Studt, F.; Nørskov, J. K. Understanding trends in C-H bond activation in heterogeneous catalysis. *Nature Materials* **2017**, *16*, 225–229.
94. Montoya, J.; Seitz, L.; Chakthranont, P.; Vojvodic, A.; Jaramillo, T.; Nørskov, J. Materials for solar fuels and chemicals. *Nature Materials* **2017**, *16*, 70–81.
95. Fester, J.; Bajdich, M.; Walton, A. S.; Sun, Z.; Plessow, P. N.; Vojvodic, A.; Lauritsen, J. V. Comparative Analysis of Cobalt Oxide Nanoisland Stability and Edge Structures on Three Related Noble Metal Surfaces: Au(111), Pt(111) and Ag(111). *Top. Catal.* **2016**,
96. Seitz, L.; Dickens, C.; Nishio, K.; Hikita, Y.; Montoya, J.; Doyle, A.; Kirk, C.; Vojvodic, A.; Hwang, H.; Nørskov, J.; Jaramillo, T. A highly active and stable IrOx/SrIrO3 catalyst for the oxygen evolution reaction. *Science* **2016**, *353*, 1011–1014.
97. Beye, M. et al. Chemical Bond Activation Observed with an X-ray Laser. *J. Phys. Chem. Lett.* **2016**, *7*, 3647–3651.
98. Siahrostami, S.; Tsai, C.; Karamad, M.; Koitz, R.; Garcia-Melchor, M.; Bajdich, M.; Vojvodic, A.; Abild-Pedersen, F.; Nørskov, J. K.; Studt, F. Two-Dimensional Materials as Catalysts for Energy Conversion. *Catal. Lett.* **2016**, *46*, 1917–1921.
99. Seh, Z.; Fredrickson, K.; Anasori, B.; Kibsgaard, J.; Strickler, A.; Lukatskaya, M.; Gogotsi, Y.; Jaramillo, T.; Vojvodic, A. Two-Dimensional Molybdenum Carbide (MXene) as an Efficient Electrocatalyst for Hydrogen Evolution. *ACS Energy Letters* **2016**, *1*, 589–594.
100. Plessow, P. N.; Sanchez-Carrera, R. S.; Li, L.; Rieger, M.; Sauer, S.; Schaefer, A.; Abild-Pedersen, F. Modeling the Interface of Platinum and α-Quartz(001): Implications for Sintering. *J. Phys. Chem. C* **2016**, *120*, 10340–10350.
101. Ng, J.; Garcia-Melchor, M.; Bajdich, M.; Chakthranont, P.; Kirk, C.; Vojvodic, A.; Jaramillo, T. Gold-supported cerium-doped NiOx catalysts for water oxidation. *Nature Energy* **2016**, *1*, 16053.
102. Yoo, J. S.; Christensen, R.; Vegge, T.; Nørskov, J. K.; Studt, F. Theoretical Insight into the Trends that Guide the Electrochemical Reduction of Carbon Dioxide to Formic Acid. *ChemSusChem* **2016**, *9*, 358.
103. Seitz, L.; Nordlund, D.; Gallo, A.; Jaramillo, T. Tuning Composition and Activity of Cobalt Titanium Oxide Catalysts for the Oxygen Evolution Reaction. *Electrochim. Acta* **2016**, *193*, 240–245.
104. Varley, J. B.; Wang, Y.; Chan, K.; Studt, F.; Nørskov, J. K. Mechanistic insights into nitrogen fixation by nitrogenase enzymes. *Phys. Chem. Chem. Phys.* **2015**, *17*, 29541–29547.

105. Li, H.-J.; Lausche, A. C.; Peterson, A. A.; Hansen, H. A.; Studt, F.; Bligaard, T. Using microkinetic analysis to search for novel anhydrous formaldehyde production catalysts. *Surf. Sci.* **2015**, *641*, 105–111.

106. Kibsgaard, J.; Tsai, C.; Chan, K.; Benck, J. D.; Nørskov, J. K.; Abild-Pedersen, F.; Jaramillo, T. F. Designing an improved transition metal phosphide catalyst for hydrogen evolution using experimental and theoretical trends. *Energy & Environmental Science* **2015**, *8*, 3022–3029.

107. Tsai, C.; Chan, K.; Nørskov, J. K.; Abild-Pedersen, F. Theoretical Insights into the Hydrogen Evolution Activity of Layered Transition Metal Dichalcogenides. *Surf. Sci.* **2015**, *640*, 133–140.

108. Santos, E. J. G.; Nørskov, J. K.; Harutyunyan, A. R.; Abild-Pedersen, F. Toward Controlled Growth of Helicity-Specific Carbon Nanotubes. *J. Phys. Chem. Lett.* **2015**, *6*, 2232–2237.

109. To, J. W. F.; Chen, Z.; Yao, H.; He, J.; Kim, K.; Chou, H.-H.; Pan, L.; Wilcox, J.; Cui, Y.; Bao, Z. Ultrahigh Surface Area Three-Dimensional Porous Graphitic Carbon from Conjugated Polymeric Molecular Framework. *ACS Central Science* **2015**, *1*, 68–76.

110. Rasmussen, D. B.; Christensen, J. M.; Temel, B.; Studt, F.; Moses, P. G.; Rossmeisl, J.; Riisager, A.; Jensen, A. D. Ketene as a Reaction Intermediate in the Carbonylation of Dimethyl Ether to Methyl Acetate over Mordenite. *Angewandte Chemie International Edition* **2015**, *54*, 7261–7264.

111. Xin, H. et al. Strong Influence of Coadsorbate Interaction on CO Desorption Dynamics Probed by Ultrafast X-ray Spectroscopy and Ab Initio Simulations. *Phys. Rev. Lett.* **2015**, *114*, 156101.

112. Wang, H.; Tsai, C.; Kong, D.; Chan, K.; Abild-Pedersen, F.; Nørskov, J. K.; Cui, Y. Transition Metal Doped Edge Sites in Vertically Aligned MoS2 Catalysts for Enhanced Hydrogen Evolution. *Nano Research* **2015**, *8*, 566–575.

113. Doyle, A. D.; Montoya, J. H.; Vojvodic, A. Improving Oxygen Electrochemistry Through Nanoscopic Confinement. *ChemCatChem* **2015**, *7*, 738–742.

114. Montoya, J. H.; Garcia-Mota, M.; Nørskov, J. K.; Vojvodic, A. Theoretical evaluation of the surface electrochemistry of perovskites with promising photon absorption properties for solar water splitting. *Phys. Chem. Chem. Phys.* **2015**, *17*, 2634–2640.

115. Tsai, C.; Chan, K.; Nørskov, J. K.; Abild-Pedersen, F. Rational design of MoS2 catalysts: tuning the structure and activity via transition metal doping. *Catalysis Science & Technology* **2015**, *5*, 246–253.

116. Siahrostami, S.; Vojvodic, A. Influence of Adsorbed Water on the Oxygen Evolution Reaction on Oxides. *J. Phys. Chem. C* **2015**, *119*, 1032–1037.

117. Tsai, C.; Chan, K.; Nørskov, J. K.; Abild-Pedersen, F. Understanding the Reactivity of Layered Transition-Metal Sulfides: A Single Electronic Descriptor for Structure and Adsorption. *J. Phys. Chem. Lett.* **2014**, *5*, 3884–3889.

118. Rao, R.; Sharma, R.; Abild-Pedersen, F.; Nørskov, J. K.; Harutyunyan, A. R. Insights into carbon nanotube nucleation: Cap formation governed by catalyst interfacial step flow. *Scientific Reports* **2014**, *4*, 6510.

119. Voss, J.; Vojvodic, A.; Chou, S. H.; Howe, R. T.; Abild-Pedersen, F. Inherent Enhancement of Electronic Emission from Hexaboride Heterostructure. *Phys. Rev. Applied* **2014**, *2*, 24004.
120. Chou, S. H.; Voss, J.; Vojvodic, A.; Howe, R. T.; Abild-Pedersen, F. DFT Study of Atomically-Modified Alkali-Earth Metal Oxide Films on Tungsten. *J. Phys. Chem. C* **2014**, *118*, 11303–11309.
121. Tsai, C.; Chan, K.; Abild-Pedersen, F.; Nørskov, J. K. Active edge sites in MoSe2 and WSe2 catalysts for the hydrogen evolution reaction: a density functional study. *Phys. Chem. Chem. Phys.* **2014**, *16*, 13156–13164.
122. Lysgaard, S.; Landis, D. D.; Bligaard, T.; Vegge, T. Genetic Algorithm Procreation Operators for Alloy Nanoparticle Catalysts. *Top. Catal.* **2014**, *57*, 33–39.
123. Medford, A. J.; Sehested, J.; Rossmeisl, J.; Chorkendorff, I.; Studt, F.; Nørskov, J. K.; Moses, P. G. Thermochemistry and micro-kinetic analysis of methanol synthesis on ZnO (0001). *J. Catal.* **2014**, *309*, 397–407.

Category III

124. Singh, A. R.; Rohr, B. A.; Schwalbe, J. A.; Cargnello, M.; Chan, K.; Jaramillo, T. F.; Chorkendorff, I.; Nørskov, J. K. Electrochemical Ammonia Synthesis - The Selectivity Challenge. *ACS Catalysis* **2017**, *7*, 706–709.
125. Chen, L. D.; Urushihara, M.; Chan, K.; Nørskov, J. K. Electric Field Effects in Electrochemical CO2 Reduction. *ACS Catalysis* **2016**, *6*, 7133–7139.
126. Hoffmann, M. J.; Medford, A.; Bligaard, T. Framework for Scalable Adsorbate-Adsorbate Interaction Models. *J. Phys. Chem. C* **2016**, *120*, 13087–13094.

Kinetic and Spectroscopic Studies of Catalytic Mechanisms: Hydrodeoxygenation of Biomass Feedstocks on Transition Metal Phosphides

S. Ted Oyama
Virginia Tech, Department of Chemical Engineering
Blacksburg, VA 24061

Presentation Abstract

The study of mechanisms of reaction is an active area of chemical kinetics, even though it is generally held that mechanisms cannot be proven on the basis of kinetics alone. This work shows that reactivity, spectroscopic, and transient data can be combined to give a unified picture of a reaction mechanism. The reaction studied is the hydrodeoxygenation of a pyrolysis liquid model compound, gamma-valerolactone (GVL). Use is made of in situ Fourier transform infrared spectroscopy and in situ x-ray absorption near-edge spectroscopy to probe adsorbed species and the nature of the catalyst surface at reaction studies.

The application of the work is in the conversion of pyrolysis liquids derived from biomass, whose high oxygen content (~40 wt.%) results in low heating value (about half that of petroleum liquids), high acid content (leading to corrosion problems), and low stability (resulting in increasing viscosity with storage). The catalyst studied is a member of a new family of catalysts, the transition metal phosphides, which have outstanding activity for removal of heteroatoms such as sulfur, nitrogen, and oxygen, from hydrocarbon feedstreams.

A contact time study allowed the determination of a reaction sequence for GVL HDO on Ni_2P/SiO_2 and it was found that C-O bond cleavage of the lactone ring to generate n-pentanoic acid was the rate-determining step. This was followed by hydrogen transfer steps to produce oxygen free compounds, *n*-pentane or *n*-butane. Fitting of the results using a rake mechanism that considers adsorbed intermediates indicates that the surface species from the pentanoic acid are majority species. In situ infrared and in situ x-ray absorption near-edge spectroscopy measurements support this reaction mechanism.

Grant or FWP Number: DEFG0296ER14669
Grant Title: Kinetics and Mechanism of Hydrodeoxygenation on Metal Phosphides

Postdoc(s): Phuong Bui, Gwang-Nam Yun, Xiaoru Zhu
Affiliations(s): Virginia Tech

RECENT PROGRESS

Mechanism studies

The hydrodeoxygenation (HDO) mechanism of the cyclic five-membered ester γ-valerolactone (GVL-$C_5H_8O_2$) as a model compound for pyrolysis oil derived from biomass was studied on a Ni_2P/MCM-41 catalyst. Reaction tests for the HDO of GVL were conducted in a fixed-bed continuous flow reactor at 300 °C and 0.5 MPa. A contact time analysis determined the reaction pathway, and it was found that ring-opening of GVL to produce pentanoic acid was the rate-determining step. This was followed by formation of pentanal and decarbonylation to generate n-butane or hydrogenation to form n-pentane.

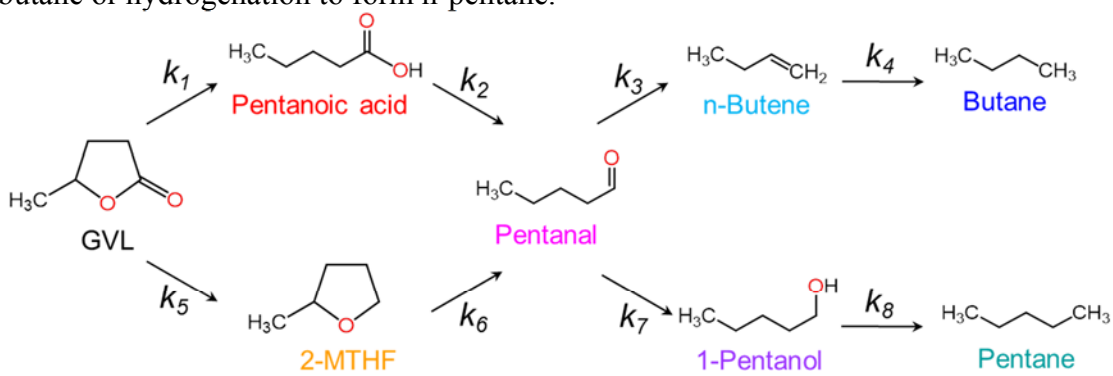

Rate constants (s^{-1})

k_1	k_2	k_3	k_4	k_5	k_6	k_7	k_8	R^2
0.18	0.6	120	8	0.0035	0.25	4.0	1.5	0.97

A partial pressure analysis of H_2 and GVL was consistent with a rate equation derived from a Langmuir-Hinshelwood (L-H) mechanism. The kinetic analysis allowed calculation of coverages.

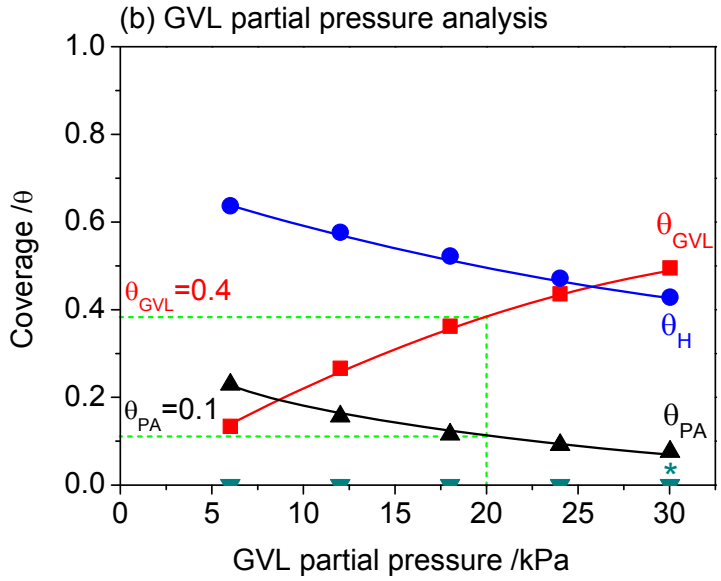

In situ infrared measurements under reactive H_2 and inert N_2 confirmed a reaction mechanism with ring-opening to form pentanoic acid, in which the number of CH_2 groups in adsorbed species increased under H_2 flow. Furthermore, in situ quick X-ray absorption fine structure measurements showed the participation of $Ni^{\delta+}$ species in the reaction as would be expected for the adsorption of electron withdrawing oxygenated species like carboxylic acids. The results allowed the establishment of a complete picture of the reaction mechanism.

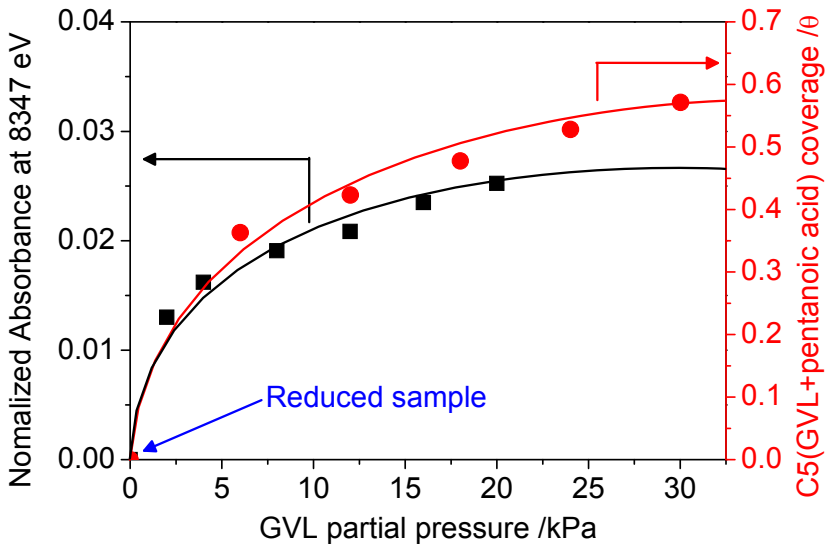

Publications Acknowledging this Grant in 2016-2017

(I) *Exclusively funded by this grant;*

(1) Bui, P. P.; Takagaki, A.; Kikuchi, R.; Oyama, S. T. Kinetic and Infrared Spectroscopy Study of Hydrodeoxygenation of 2-Methyltetrahydrofuran on a Nickel Phosphide Catalyst at Atmospheric Pressure, *ACS Catal.* **2016**, 6, 7701−7709.

(2) Bui, P.P.; Oyama, S.T., Takagaki, A.; Carrow, B.P.; Nozaki, K., Reactions of 2-Methyltetrahydropyran on Silica-Supported Nickel Phosphide in Comparison with 2-Methyltetrahydrofuran, *ACS Catal.* **2016**, 6, 4549−4558.

Towards the rational design of MoS_2-based nanocatalyst

Talat S. Rahman[1], Ludwig Bartels[2], and Peter A. Dowben[3]
[1]University of Central Florida, [2]Univeristy of California, Riverside, [3]University of Nebraska, Lincoln

Presentation Abstract

The objective of our joint theoretical and experimental project is to enable the design of MoS_2-based catalysts for (higher) alcohol formation from syngas ($CO + H_2$) through a microscopic understanding of the factors that determine site activity and selectivity. These efforts have focused on extracting the role of vacancy structures, interface with a metal substrate or with adsorbed metallic nanoparticles, and dopants (hydrogen, Na, Co, F) on the electronic structure and chemical properties of single – layer and bulk MoS_2. Density functional theory (DFT) based calculations of reaction pathways and kinetic Monte Carlo (KMC) simulations of reaction rates find the local atomic environment on several such MoS_2 based composites facile for methanol and ethanol formation. We trace this to the charge transfer and charge redistribution in the system and eventually to the proximity of the local frontier orbitals (which thus identify the active sites) to the Fermi level. Preliminary experimental data on the activation energy barriers for methoxy adsorption on MoS_2 are encouraging and in good agreement with our calculated values. To establish trends and broaden our choice of catalyst material, we have obtained results for single and multilayered WS_2 and WSe_2, doped and undoped, synthesized via chemical vapor deposition (CVD) and characterized via angle resolved photo emission (ARPES) and DFT. Complementary investigation of the reactivity and selectivity of defect-laden hexagonal boron niride, with and without an interface with Au nanostructures, provides another promising avenue for achieving cost-effective catalysts for hydrogenation reactions.

DE-FG02-07ER15842: Controlling Structural, Electronic, and Energy Flow Dynamics of Catalytic Processes through Tailored Nanostructures

PIs: Talat S. Rahman (UCF), Ludwig Bartels (UCR), Peter Dowben (UNL)
Postdocs: Duy Le (UCF), Volodymyr Turkowski (UCF), Hae-Kyung Jeong (UNL)
Students: UCF: T. B. Rawal, T. Jiang, Z. Hooshmand, N. Uddin, S. R. Acharya ; UNL: I. Tanabe, P. Evans ; UCR : K. Yamaguchi, M. Isarraraz, M. Gomez, C. Merida, A. Nguyen, J. Martinez, S. Naghibi, A. Berges, K. Almeida, D. Barroso, A. Martinez.

RECENT PROGRESS

Below are highlights of some projects that we have completed in the reporting period. References 1-18 provide details of the projects so far completed in the period 2014 to present.

Single-layer MoS_2 and metal nanoparticle composite for oxidation & hydrogenation reactions

Employing dispersion-corrected DFT, we have investigated the propensity for adsorption, desorption, dissociation, diffusion and reaction barriers for a large number of molecules of interest on a composite consisting of single-layer MoS_2 supported, small (13-29 atoms) Cu, Ag and Au nanoparticles.[13,18] Both pristine and defect-laden (S vacancies) MoS_2 are found to transform the electronic and geometric structure of the nanoparticles, the effect being stronger for the latter. The d-band center and frontier orbitals of specific nanoparticle atoms shift towards the Fermi level. Interestingly, this effect is most noticeable for Au_{29} apex atoms which we show to facilitate oxidation reactions. The strong binding energy of the nanoparticles (between 4 – 7 eV) is facilitated by notable charge transfer and mid-gap states introduced by S vacancies. The MoS_2 support also increases the number of adsorption sites for molecules and hinders reverse reactions. For the Au_{13}/MoS_2 system in particular we find a remarkable selectivity for methanol synthesis via the CO hydrogenation route (Fig. 1), in stark contrast to the catalytic activity of Au_{13}/TiO_2 which promotes methanol decomposition. Calculations of reactions rates are underway as are experimental verification of our findings.

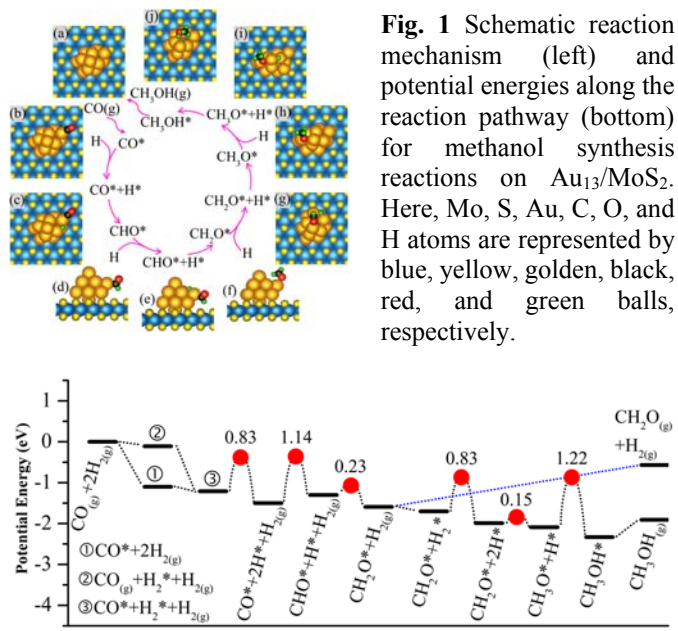

Fig. 1 Schematic reaction mechanism (left) and potential energies along the reaction pathway (bottom) for methanol synthesis reactions on Au_{13}/MoS_2. Here, Mo, S, Au, C, O, and H atoms are represented by blue, yellow, golden, black, red, and green balls, respectively.

MoS_2 vacancies and edges for detection of free radicals

Motivated by our earlier predictions of vacancy-induced reactivity of MoS_2,[1] we have collaborated with the group of S. Seal (UCF) to examine the adsorption and dissociation characteristics of hydrogen peroxide on few nm sized MoS_2 nanoparticles.[14] We trace the ultra low sensing properties of these nano-particles to the higher Mo edge density arising from sulfur deficiency, as verified by accompanying x-ray photoelectron spectroscopy study. DFT-based electronic structure calculations of MoS_2 nanoparticles of several size reveal that the sharp, occupied d-state peak near the Fermi level (E_F) tends to smoothen and shift away from E_F with increasing nanoparticle size, indicating that larger particles are less catalytically active than the

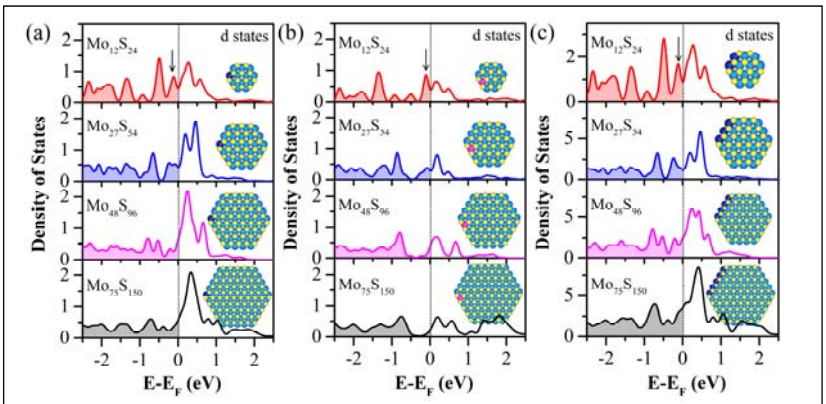

Fig. 2 (a) Electronic density of states of (a) Mo atom (dark blue) at $(10\bar{1}0)$ edge; (b) Mo atom (pink) at $(\bar{1}010)$ edge; (c) all Mo atoms (dark blue) at $(10\bar{1}0)$ edge.

smaller ones. Our DFT calculations further reveal that the spontaneous dissociative adsorption of H_2O_2 occurs at the $(10\bar{1}0)$ edge, and that the adsorption energy of OH and H_2O at the $(10\bar{1}0)$ (Mo) edge are higher than those at $(\bar{1}010)$ (S) edge, suggesting Mo edges to be catalytically more active than the S-edges. In short, both S-deficiency and a high density of Mo-edges in small MoS_2 particles contribute to the pico-/nano molar level detection of various chemical species that are relevant to biological processes.

Higher alcohol formation on Cu(111)-supported single-layer MoS_2

Despite being the preferred structure in single layer MoS_2, we found that the sulfur vacancy row is not very facile for alcohol synthesis from syngas as its narrow structure limits adsorption, diffusion, and formation of possible intermediates. On the other hand, we find that MoS_2 grown on Cu(111) displays strong interactions with the substrate which reduces any corrugation caused by the sulfur vacancy rows, resulting in a greater exposure to of active sites to adsorbates. Our dispersion-corrected DFT calculations show that: (1) there is significant charge transfer from Cu(111) to MoS_2 enhancing its catalytic properties, (2) the binding energies of CO and dissociated H_2 increase by 0.3 eV in comparison to that on unsupported MoS_2, indicating stronger interactions, and (3) the barriers for forming intermediate species in the alcohol synthesis process reduce significantly in comparison to that on unsupported MoS_2. On the basis of these energetic (Fig. 3), one may conclude that the Cu(111) substrate promotes methanol synthesis from syngas on single-layer MoS_2 with a vacancy row. This conclusion is placed on stronger grounds by accompanying Kinetic Monte Carlo simulations consisting of a complex and sophisticated reaction pathway involving more than 60 elementary reactions resulting in competing products, CH_4, H_2O, CH_3OH, and C_2H_5OH. We establish CO and H_2 partial pressures that lead to high selectivity towards alcohol formation Preliminary results from external collaborator Blair already confirms our prediction. Further controlled experiments are being implemented. Some headway has already been made in such experimental studies. In the catalytic syngas production of methanol ($CO_2 + 2H_2 \rightarrow CH_3OH$), the last of the reaction step is the conversion of a surface methoxy species and hydrogen to methanol ($CH_3O^* + H^* \rightarrow CH_3OH$). While this final intermediate reaction would be difficult to observe under standard methods, the reverse reaction of exposure of MoS_2 substrate to methanol to produce the more stable intermediate methoxy species while also producing the predicted surface sulfur vacancies should be immediately apparent under STM. Within this study, catalysis of methanol on MoS_2 was explored in part for substantiation of the theory in addition to understanding the energetics of the process. With an estimated 1.4 eV barrier between the methoxy and methanol stages, observation of such energy barrier would further support the proposed syngas reaction. As

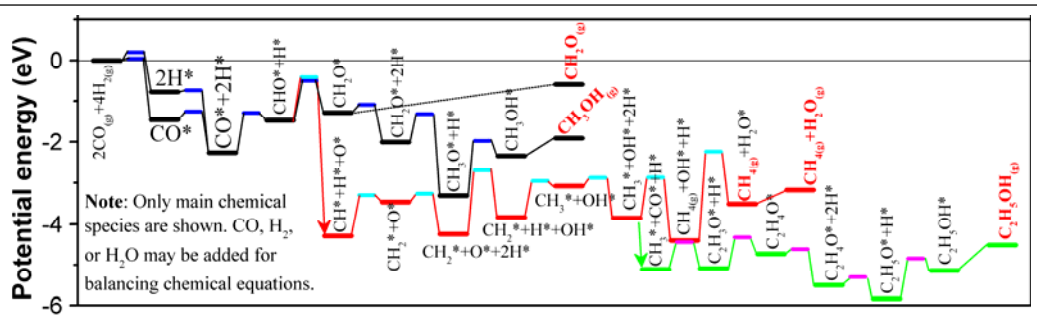

Fig. 3 Potential energies along the reaction pathway of alcohol synthesis from syngas on defect-laden MoS_2 supported by Cu(111). The horizontal black, red, and green bars represent the intermediates states involved in the reaction while small blue, cyan, and magenta bars represent the transition states.

depicted in Fig. 4 and 5, the effects of the methanol to methoxy reaction are directly observed in our STM and photoluminescence investigations. This methoxy formation leads to the creation of point defects, as shown in Fig. 4(b). Continued reaction of methanol, to create methoxy, leads to line vacancies and larger multipoint defects on MoS_2, as shown in Fig. 4(c) and the inset, consistent with the sulfur-vacancy row formation predicted by theory. Fig. 5 also demonstrates that defect creation is caused by the methoxy formation, from methanol on MoS_2. The resonant luminescence of MoS_2 significantly decreased (Fig. 5(b)) after the deposition of methanol compared to that (Fig. 5(a)) of clean MoS_2, indicating serious deformation of the MoS_2 structure, consistent with the scanning tunneling microscopy and X-ray photoemission results. As previously described by the theory and XPS results, the conversion of the adsorbed methanol to methoxy consumes sulfur atoms of MoS_2, leaving the sulfur vacancies in the lattice, which is consistent with the defect formation on MoS_2.

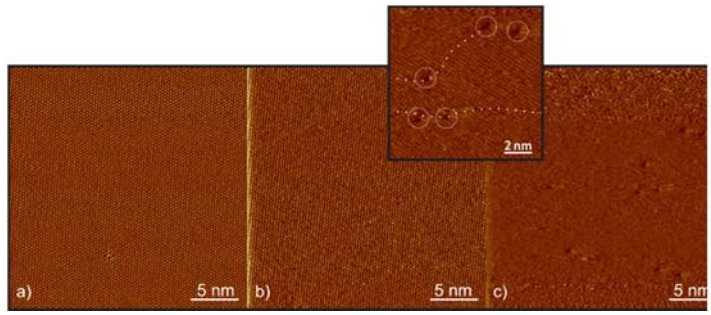

Fig. 4 Imaging noting the creation of point defects and larger defects on MoS_2 with a) clean MoS_2 (0.900 V gap voltage, 800 pA constant current) b) areas of point defects and c) larger 1 nm divots on sample after two rounds of methanol deposition on 350 K sample followed by deposition of methanol on 110 K sample with final annealing at 350 K (2.00 V gap voltage, 400 pA constant current). The insert gives a larger view of defects within c) with dotted lines tracing line defects and circled multipoint defects.

Investigation of Catalytic Promoters

We have investigated the influence of metal adsorbates (sodium, gold, and cobalt) on the occupied and unoccupied electronic structure of MoS_2(0001) and WSe_2(0001), through a combination of photoemission and inverse photoemission (Fig. 6). The electronic structure is rigidly shifted in both the WSe_2 and MoS_2 systems, with either Na or Co adsorption, generally as predicted by accompanying density functional theory based calculations. Na adsorption is found to behave as an electron donor (n-type) in MoS_2, while Co adsorption acts as an electron acceptor (p-type) in WSe_2. The binding energy shifts have some correlation with the work function differences between the metallic adlayer and the transition metal dichalcogenide substrate. The impact of these electronic structural changes on the catalytic properties of the composites is under investigation.

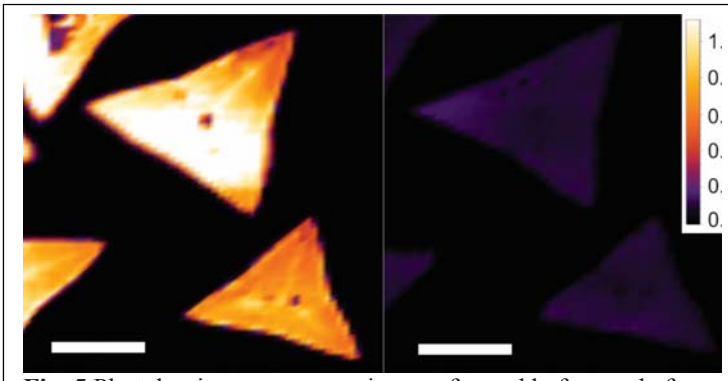

Fig. 5 Photoluminescence mapping, performed before and after the exposure of CVD grown molybdenum disulfide (MoS_2) islands to methanol (CH_3OH) at 338 K, over a period of 4 hours. Decrease in photoluminescence indicates deformation and/or inhomogeneity to structure. The scale bar is 10 μm.

We have also investigated the utility of chemical vapor deposition coating of an inert irreducible oxide (SiO_2) by MoS_2 for activation of gold nanoparticles on it. In particular we

investigated the size-dependent electronic structure of Au nanoparticles prepared on MoS_2 on SiO_2/Si using synchrotron-based photoelectron spectroscopy. We find that even a single-layer of MoS_2 is capable of locking Au nanoparticles into a shape that offers active undercoordinated Au edge atoms that are capable of binding small-molecule species such as CO even at room temperature (Fig. 7). In contrast to other 2D materials such as graphene, a single-layer of MoS_2 prevents aggregation of Au nanoparticles and causes high dispersion. Further investigation of the catalytic property of this synthesized Au-MoS_2 system is underway. Our theory-led, joint experimental and computational efforts have thus brought us closer to understanding the factors that control the local atomic environment that eventually enables catalytic activity in MoS_2. Projects currently underway should help place the above findings on firmer grounds.

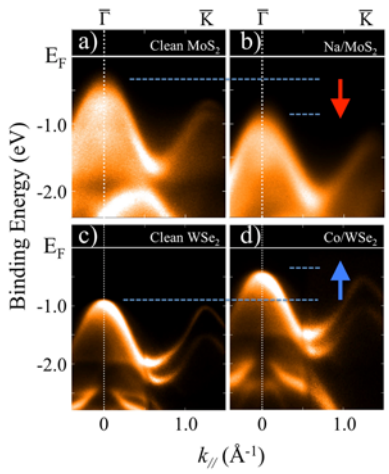

Fig. 6 The shift in the valence band structure for 2H-MoS_2(0001) single crystal before (a) and after (b) Na adsorption and a 2H-WSe_2(0001) single crystal before (c) and after (d) Co adsorption, derived from

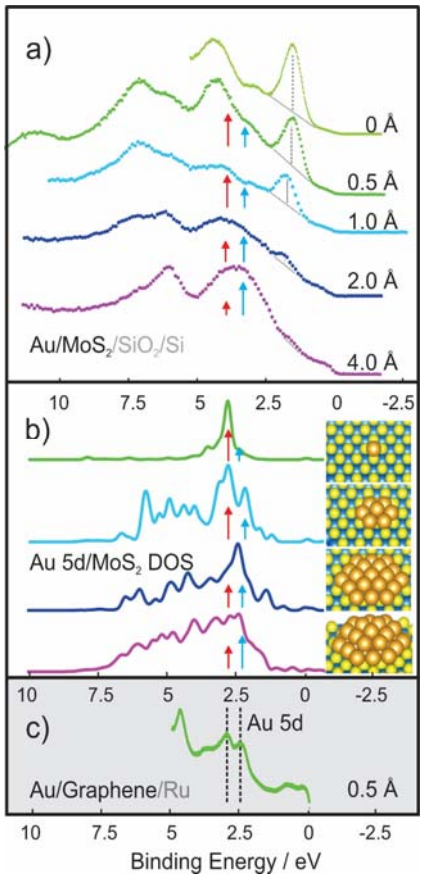

Fig. 7 a) Experimental valence band spectra of Au on the same spot of an island of single-layer MoS_2/SiO_2/Si. With increasing gold coverage, the Au-derived signal dominates the spectrum and shifts from higher (red arrow) to lower (blue arrow) binding energy while the MoS_2 valence band intensity (dashed line) is reduced and broadened by Au-MoS_2 interactions; b) computational Au 5d density of state of the four clusters indicated. As the cluster size increases, lower binding energy gold DOS (blue arrow) augments and ultimately overshadowed the higher binding energy DOS (red arrow) found for a single Au atom. As these calculations do

Publications Acknowledging DOE Grant DE-FG02-07ER15842 in the period 2014-2017

1. D. Le, T.B. Rawal, and T.S. Rahman, "Single-Layer MoS_2 with Sulfur Vacancies: Structure and Catalytic Application," The Journal of Physical Chemistry C 118, 5346-5351 (2014). DOI: 10.1021/jp411256g
2. S.I. Shah, S. Hong, and T.S. Rahman, "Combined Density Functional Theory and Kinetic Monte Carlo Study of Selective Oxidation of NH3 on Rutile RuO_2(110) at Ambient Pressures," The Journal of Physical Chemistry C 118, 5226-5238 (2014). DOI: 10.1021/jp407865e
3. J. Mann, Q. Ma, P.M. Odenthal, M. Isarraraz, D. Le, E. Preciado, D. Barroso, K. Yamaguchi, G. von Son Palacio, A. Nguyen, T. Tran, M. Wurch, A. Nguyen, V. Klee, S. Bobek, D. Sun, T.F. Heinz, T.S. Rahman, R. Kawakami, and L. Bartels, "2-Dimensional Transition Metal Dichalcogenides with Tunable Direct Band Gaps: $MoS_{2(1-x)}Se_{2x}$ Monolayers," Advanced Materials 26, 1399-404 (2014). DOI: 10.1002/adma.201304389
4. Q. Ma, M. Isarraraz, C.S. Wang, E. Preciado, V. Klee, S. Bobek, K. Yamaguchi, E. Li, P.M. Odenthal, A. Nguyen, D. Barroso, D. Sun, G. von Son Palacio, M. Gomez, A. Nguyen, D. Le, G. Pawin, J. Mann, T.F. Heinz, T.S. Rahman, and L. Bartels, "Post-Growth Tuning of the Bandgap of Single-Layer Molybdenum Disulfide Films by Sulfur/Selenium Exchange," ACS Nano 8, 4672-7 (2014). DOI: 10.1021/nn5004327
5. E.A. Lewis, D. Le, A.D. Jewell, C.J. Murphy, T.S. Rahman, and E.C.H. Sykes, "Segregation of Fischer-Tropsch reactants on cobalt nanoparticle surfaces," Chemical Communications 50, 6537-9 (2014). DOI: 10.1039/C4CC01680G
6. T. Komesu, D. Le, Q. Ma, E.F. Schwier, Y. Kojima, M. Zheng, H. Iwasawa, K. Shimada, M. Taniguchi, L. Bartels, T.S. Rahman, and P.A. Dowben, "Symmetry Resolved Surface-Derived Electronic Structure of MoS2(0001)," Journal of Physics: Condensed Matter 26, 455501 (2014). DOI: 10.1088/0953-8984/26/45/455501
7. T. Komesu, D. Le, X. Zhang, Q. Ma, E.F. Schwier, Y. Kojima, M. Zheng, H. Iwasawa, K. Shimada, M. Taniguchi, L. Bartels, T.S. Rahman, and P.A. Dowben, "Occupied and unoccupied electronic structure of Na doped MoS_2(0001)," Applied Physics Letters 105, 241602 (2014). DOI: 10.1063/1.4903824
8. D. Le, A. Barinov, E. Preciado, M. Isarraraz, I. Tanabe, T. Komesu, C. Troha, L. Bartels, T.S. Rahman, and P.A. Dowben, "Spin-Orbit Coupling in the Band Structure of Monolayer WSe_2," Journal of Physics: Condensed Matter 27, 182201 (2015). DOI: 10.1088/0953-8984/27/18/182201
9. D.J. Nash, D.T. Restrepo, N.S. Parra, K.E. Giesler, R.A. Penabade, M. Aminpour, D. Le, Z. Li, O.K. Farha, J.K. Harper, T.S. Rahman, and R.G. Blair, "Heterogeneous Metal-Free Hydrogenation over Defect-Laden Hexagonal Boron Nitride," ACS Omega 1, 1343-1354 (2016). DOI: 10.1021/acsomega.6b00315
10. P. Patoka, G. Ulrich, A.E. Nguyen, L. Bartels, P.A. Dowben, V. Turkowski, T.S. Rahman, P. Hermann, B. Kastner, A. Hoehl, G. Ulm, and E. Ruhl, "Nanoscale plasmonic phenomena in CVD-grown MoS_2 monolayer revealed by ultra-broadband synchrotron

radiation based nano-FTIR spectroscopy and near-field microscopy," Optics Express 24, 1154-1164 (2016). DOI: 10.1364/Oe.24.001154

11. I. Tanabe, T. Komesu, D. Le, T.B. Rawal, E.F. Schwier, M. Zheng, Y. Kojima, H. Iwasawa, K. Shimada, T.S. Rahman, and P.A. Dowben, "The symmetry-resolved electronic structure of 2H-WSe_2(0001)," Journal of Physics: Condensed Matter 28, 345503 (2016). DOI: 10.1088/0953-8984/28/34/345503
12. I. Tanabe, M. Gomez, W.C. Coley, D. Le, E.M. Echeverria, G. Stecklein, V. Kandyba, S.K. Balijepalli, V. Klee, A.E. Nguyen, E. Preciado, I.H. Lu, S. Bobek, D. Barroso, D. Martinez-Ta, A. Barinov, T.S. Rahman, P.A. Dowben, P.A. Crowell, and L. Bartels, "Band structure characterization of WS_2 grown by chemical vapor deposition," Applied Physics Letters 108, 252103 (2016). DOI: 10.1063/1.4954278
13. T.B. Rawal, D. Le, and T.S. Rahman, "Effect of Single-Layer MoS_2 on the Geometry, Electronic Structure, and Reactivity of Transition Metal Nanoparticles," The Journal of Physical Chemistry C 121, 7282-7293 (2017). DOI: 10.1021/acs.jpcc.7b00036
14. A. Gupta, T.B. Rawal, C.J. Neal, S. Das, T.S. Rahman, and S. Seal, "Molybdenum disulfide for ultra-low detection of free radicals: electrochemical response and molecular modeling," 2D Materials 4, 025077 (2017). DOI: 10.1088/2053-1583/aa636b
15. (Category II; PAD) L.G. Abdul Halim, Z. Hooshmand, M.R. Parida, S.M. Aly, D. Le, X. Zhang, T.S. Rahman, M. Pelton, Y. Losovyj, P.A. Dowben, O.M. Bakr, O.F. Mohammed, and K. Katsiev, "pH-Induced Surface Modification of Atomically Precise Silver Nanoclusters: An Approach for Tunable Optical and Electronic Properties," Inorganic Chemistry 55, 11522-11528 (2016). DOI: 10.1021/acs.inorgchem.6b02067
16. H.K. Jeong, E. Echeverria, P. Chakraborti, H.T. Le, and P.A. Dowben, "Electronic structure of cyclodextrin-carbon nanotube composite films," RSC Advances 7, 10968-10972 (2017). DOI: 10.1039/c6ra26900a
17. T. Komesu, I. Tanabe, D. Le, E. Schwier, Y. Kojima, M. Zheng, K. Taguchi, M. Koji, T. Okuda, H. Iwasawa, K. Shimada, T.S. Rahman, and P. Dowben, "Adsorbate doping of MoS_2 and WSe_2: the Influence of Na and Co," Journal of Physics: Condensed Matter 29, 285501 (2017). DOI: 10.1088/1361-648X/aa7482
18. T.B. Rawal, D. Le, and T.S. Rahman, "MoS_2-Supported Gold Nanoparticle for CO Hydrogenation," submitted to Journal of Physics: Condensed Matter.
19. G. Shafai, S. Hong, and T. S. Rahman, “Effects of γ-Al_2O_3 support on the morphology and electronic structure of Pt nanoparticles,” submitted to J. Phys. Chem. C.

Catalytic Reactions at Extended Solid-Liquid Interfaces: Calorimetric evaluation of solvent effects and their influence on reaction mechanisms

Robert M. Rioux
Department of Chemical Engineering and Chemistry, The Pennsylvania State University, University Park, PA 16801

Presentation Abstract

Heterogeneous catalytic reactions of non-volatile reactants require processing in the condensed phase where the reaction at the solid-liquid interface is influenced by the presence of solvent. These solvent effects impact both activity and selectivity of heterogeneously-catalyzed reactions, but are poorly characterized and quantified. Our research quantifies solvent effects in supported metal- and acid-catalyzed reactions, which are used to rigorously describe the kinetics and mechanism of substrate conversion utilizing calorimetric measurements of substrate-catalyst interactions in various solvents, the thermodynamic behavior of solute-solvent (i.e., non-ideal thermodynamic properties) and evaluation of the relevant reaction kinetics. This study aims to provide absolute measurements rather than relative solvent dependent trends of the influence of solvent on competitive adsorption with substrate, the influence of catalyst structure/composition on solvent-catalyst interactions, and the impact of these solvent effects on the measured reaction kinetics and the condensed-phase reaction mechanism. The predominant focus of this work focuses on biomass-relevant conversion catalysts (i.e., aqueous-based solutions); the approach and methods developed in this work are amenable to the study of other catalytic reactions occurring at buried solid-liquid interfaces. We further demonstrate the utility of solution calorimetry to quantify catalyst synthesis and the impact of conditions at the solid-liquid interface influence on final catalyst properties, including the isolation of single atoms. Solvent effects have profound impacts on observed kinetics, reaction mechanism, optimal catalyst formulation and the final properties of supported catalysts through direct interfacial interactions and through solution via non-ideal thermodynamic effects.

Grant or FWP Number: DE-SC0016192

PI: Robert M Rioux
Postdoc(s): Choumini Balasanthiran
Student(s): William Elliott, Ahana Mukhopadhyay
Affiliations(s): Pennsylvania State University

RECENT PROGRESS

Assessing Solvent Effects via Inner- and Outer-Sphere Catalyst Modification

The ability to develop active sites that possess local (outer and inner-sphere) modifications relative to the remainder of the catalyst matrix allows potential tuning of solvent effects. This has traditional been done by introducing hydrophobicity (or hydrophilicity) to the active site or its vicinity. While this approach has typically utilized modification via grafting of hydrophobic alkyl groups to silica, the control and quantification of the impact of the hydrophobic modification is primarily inconclusive; rate enhancements as well as decrements have been observed. We hypothesize this inconsistency exists because of the various reaction conditions these prior results have been conducted in with no apparent consideration for the impact of the bulk solution conditions (i.e., their non-ideal thermodynamics). We have recently demonstrated the impact of solution composition and solvent affinity for a heterogeneous catalyst during the base-catalyzed isomerization of glucose to fructose.

Solution Composition Effects on Acid-catalyzed Reactions

In collaboration with Professor Jim Dumesic, we are developing calorimetric and conductivity measurements to quantify the impact of aqueous solvent composition on the pKa of various inorganic and organic acids. The accurate assessment of pKa allows rigorous evaluation of activity for single catalyst type in different solvent composition or different catalysts in identical solvent compositions. For example, we have measured the pKa with conductivity measurements (and independently confirmed with calorimetry) for various acids in three different aqueous (10 wt. %) solutions (Table 1). It is apparent the pKa changes substantial for all four acids as the solvent is changed. These changes in pKa (log scale in $[H^+]$) will have profound consequences on the observed activity.

Table 1. Conductivity measurements for the calculation of pKa at 298 K in 10 wt. % water/organic solvent solutions.

	pKa (at 298 K)		
	MeCN	GVL	DMSO
Trifluoroacetic acid	3.00	2.98	2.28
HCl	2.42	1.80	1.03
MeSA	2.31	1.81	0.91
Triflic acid	0.97	0.22[a]	$K_D \rightarrow \infty$

Measured pKa in various aqueous solutions are used to compare measured rates (turnover frequencies) for fructose dehydration. After assessing the strength and reactivity of a wide range of homogeneous acids, we intend to develop an 'acid strength scale' for solid acid catalysts in the liquid phase. Ultimately, this combined conductivity (to calculate [H+]), calorimetry and acid-catalyzed reactivity will aid in the development of general rules for rational solvent selection for acid-catalyzed reactions.

In a related study, we are examining the impact of solution ($DMSO/H_2O$) composition on the reactivity for dehydration of fructose. We have chosen DMSO since fructose is soluble across the entire $DMSO/H_2O$ composition space. The impact of solvent composition on rigorously determined turnover frequencies for fructose dehydration to HMF (at low conversions) will be demonstrated. Figure 1 demonstrates different acid strengths which when appropriately accounted for may rectify differences in reported turnover frequency values.

Inner- and Outer-sphere Effects on the Hydrophobic Properties of Acid Catalysts

A standard approach to induce hydrophobicity to the active site is via inner (functionality to which active site is attached) or outer (local through space) modification of the active site. A survey of survey of the literature clearly demonstrates a lack of consequence on the influence of these effects. Utilizing esterification of acetic acid by methanol (and other alkanols) as our model reaction, we demonstrate that inner-sphere modification has little effect on reactivity under wet conditions. On the other hand, outer-sphere effects have a dramatic influence on the measured reactivity; inclusion of hydrophobic 'residues' decreases the turnover frequency rather than increases it. This is a natural consequence of the hydrophilic nature of the reactants themselves and the fact they are solvated by water. Figure 2 demonstrates the impact of outer-sphere modification of a supported propyl-SO_3H/SiO_2 catalyst with trimethyl, propyl or octyl groups. The heat of wetting decreases slightly with modification demonstrating the dominance of acid dissociation in all catalyst types (-43 J/g for unmodified propyl-SO_3H/SiO_2 versus -38 J/g for propyl-modified propyl-SO_3H/SiO_2). A comparison of the heat of wetting between nude silica and trimethyl and propyl modified silica demonstrates a substantial reduction in heat of wetting. The comparable heat of wetting is suggestive of similar proton availability, yet Figure 2 demonstrates a decrease in the turnover frequency for the hydrophobic silica. The impact of hydrophobic modification is high dependent on the choice of solvent. For the same, reaction, utilizing a neat acetic acid-methanol solution, the turnover frequency changes very little in the presence of 1M water compared with a predominant dioxane solution on propyl–SO_3H/SBA-15 and octyl-modified propyl–SO_3H/SBA-15. It is apparent solvent choice has an apparent impact on the influence of hydrophobic modification. We will demonstrate that the impact of hydrophobic modification can be correlated with the heat of wetting of the modified silica and its water-octanol partition coefficient.

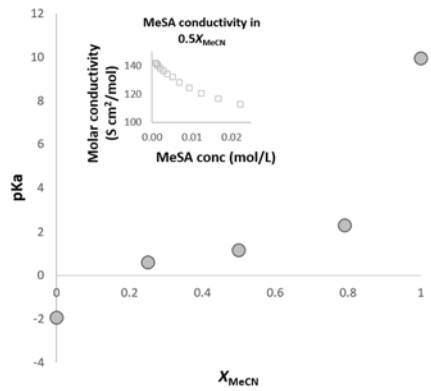

Figure 1. pKa value for methanesulfonic acid (MeSA) in $MeCN/H_2O$ solutions at 298 K. Inset is a conductivity plot for MeSA in 50 mol. % $MeCN/H_2O$ solution at 298 K.

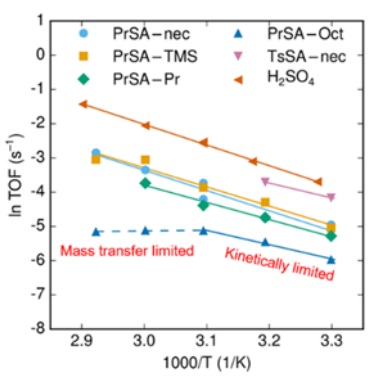

Figure 2. Turnover frequency for esterification over unmodified and modified (TMS, Pr, Oct) propyl-SO_3H/SiO_2. H_2SO_4 is included for comparison. Reaction conditions are 30-70°C, 3 M acetic acid, 6 M methanol and 0 M water ('dry' conditions).

Catalyst Synthesis – A Poorly Characterized Solid-Liquid Interface

We reported the use of solution-based isothermal titration calorimetry (ITC) to

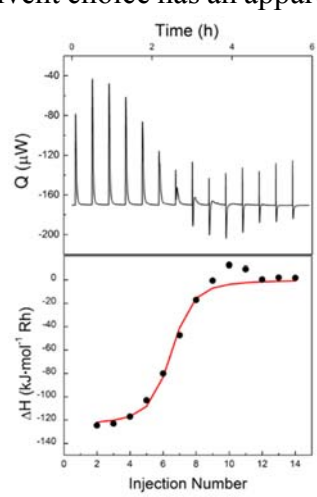

Figure 3. A) Real-time ITC thermogram for the addition of $RhCl_3$ aqueous solution to perovskite sheets in excess TBA^+OH^- solution and B) the integrated heat data with an independent model fit. Extracted heats of adsorption were negative on all perovskites (-35 kJ/mol) and endothermic on SiO_2 (25 kJ/mol) and Al_2O_3 (55 kJ/mol).

quantify the heat of interaction between rhodium hydroxide nanoparticles and several early transition metal oxide and main group oxide supports [6,9] (Figure 3). These heats were also found to be strongly dependent on the oxide support composition. Stronger interfacial bonding was found to inhibit nanoparticle sintering in vacuum and under reducing atmospheres at elevated temperatures. Rhodium hydroxide nanoparticles bond exothermically to early transition metal (niobium, tantalum, and tungsten) oxide supports, which inhibit nanoparticle sintering. Conversely, the interfacial bonding to main group oxide supports, such as silica and alumina, is endothermic and particle growth on these oxides occurs at a much lower temperature.

Publications Acknowledging this Grant in 2014-2017

1. Y. Yang, R. M. Rioux. Highly stereoselective anti-Markovnikov hydrothiolation of alkynes and electron-deficient alkenes by a supported Cu-NHC complex. *Green Chem*. **2014**, 16, 3916-3925. (I)
2. D. J. Childers, N. M. Schweitzer, S. M. K. Shahri, R. M. Rioux, J. T. Miller, R. J. Meyer. Evidence for geometric effects in neopentane conversion on PdAu catalysts. *Catal. Sci. Technol*. **2014**, 4, 4366-4377. (II)
3. C. S. Spanjers, T. P. Senftle, A. C. T. van Duin, M. J. Janik, A. I. Frenkel, R. M. Rioux. Illuminating surface atoms in nanoclusters by differential X-ray absorption spectroscopy. *Phys. Chem. Chem. Phys*. 2014, **48**, 26528-26538. (III)
4. M. A. Smith, A. Zoelle, Y. Yang, R. M. Rioux, N. G. Hamilton, K. Arnakawa, P. K. Nielsen, A. Trunschke. Surface roughness effects in the catalytic behavior of vanadia supported on SBA-15. *J. Catal.* **2014**, 312, 170-178. (III)
5. M. E. Strayer, J. M. Binz, M. Tanase, S. M. K. Shahri, R. Sharma, R. M. Rioux, T. E. Mallouk. Interfacial Bonding Stabilizes Rhodium and Rhodium Oxide Nanoparticles on Layered Nb Oxide and Ta Oxide Supports. *J. Am. Chem. Soc*. **2014**, 136, 5687-5696 (I)
6. D. J. Childers, N. M. Schweitzer, S. M. K. Shahari, R. M. Rioux, J. T. Miller, R. J. Meyer. Modifying structure-sensitive reactions by addition of Zn to Pd. *J. Catal.* **2014**, 318, 75-84. (II)
7. B. Panthi, A. Mukhopadhyay, L. Tibbits, J. Saavedra, C. J. Pursell, R. M. Rioux, B. D. Chandler. Using Thiol Adsorption on Supported Au Nanoparticle Catalysts to Evaluate Au Dispersion and the Number of Active Sites for Benzyl Alcohol Oxidation. *ACS Catal*. **2015**, 5 2232-2241. (III)
8. M. E. Strayer, T. P. Senftle, J. P. Winterstein, N. M. Vargas-Barbosa, R. Sharma, R. M. Rioux, M. J. Janik, T. E. Mallouk. Charge Transfer Stabilization of Late Transition Metal Oxide Nanoparticles on a Layered Niobate Support. *J. Am. Chem. Soc*. **2015**, 137, 16216-16224. (I)
9. J. Saavedra, T. Whittaker, Z. F. Chen, C. J. Pursell, R. M. Rioux, B. D. Chandler. Controlling activity and selectivity using water in the Au-catalysed preferential oxidation of CO in H_2. *Nature Chemistry* **2016**, 8, 585-590. (II)
10. C. S. Spanjers, P. Guillo, T. D. Tilley, M. J. Janik, R. M. Rioux. Identification of Second Shell Coordination in Transition Metal Species Using Theoretical XANES: Example of Ti-O-(C, Si, Ge) Complexes. *J. Phys. Chem. A* **2017**, 121, 162-167. (I)
11. S. Varapragasam, C. Balasanthiran, A. Gurung, Q. Qiao, R.M. Rioux, J.D. Hoefelmeyer. Kirkendall Growth of Hollow Mn_3O_4 Nanoparticles Upon Galvanic Reaction of MnO with Cu^{2+} and Evaluation as Anode for Lithium-Ion Batteries. *J. Phys. Chem. C* **2017**, 121, 11089-11099. (III)
12. G. Kumar, L. Tibbits, J. Newell, B. Panthi, A. Mukhopadhyay, R. M. Rioux, C. J. Pursell, M. J. Janik, B. D. Chandler. Evaluating Electronic Changes at Catalytic Active Sites on Au using Hammett and DFT Studies. *Nature Chem*. Submitted May 2017. (III)
13. A. Mukhopdhyay, J. M. Binz, R. M. Rioux. Quantifying Adsorption of Platinum Precursors on SiO_2 and Al_2O_3 Supports during Heterogeneous Catalyst Synthesis. Submitted to *J. Am. Chem. Soc*. (2017) (I)

Fundamental Studies on the Conversion of C-O bonds

José A. Rodriguez, Ping Liu, Sanjaya Senanayake, Dario Stacchiola and Michael G. White
Brookhaven National Laboratory, Chemistry Department

Presentation Abstract

The forward and reverse water-gas shift reaction (WGS: $CO + H_2O \leftrightarrow H_2 + CO_2$) and the hydrogenation of CO_2 to methanol ($CO_2 + 3H_2 \rightarrow CH_3OH + H_2O$) involve the formation or cleavage of C-O bonds. The design and optimization of catalysts for these processes depends on a better understanding of catalyst structure and how a particular configuration of surface sites can make or destroy a C-O bond. Fundamental studies have been performed to investigate the chemistry associated with the WGS reaction and CO_2 hydrogenation on a series of model and powder metal/oxide and metal/carbide catalysts. Several *in-situ* techniques {X-ray diffraction (XRD), pair-distribution function analysis (PDF), X-ray absorption spectroscopy (XAS), environmental scanning tunneling spectroscopy (ESTM), infrared spectroscopy (IR) and ambient-pressure X-ray photoelectron spectroscopy (AP-XPS)} and theoretical calculations {Density Functional Theory and kinetic Monte Carlo} were used to characterize the properties of the active phase in the catalysts and the reaction mechanism. These data indicate that metal/oxide and metal/carbide catalysts useful for the WGS and CO_2 hydrogenation are dynamic entities that change with reaction conditions. The metal-oxide (metal-carbide) interface can enhance the catalytic properties of the metal and oxide (carbide) components through electronic interactions, and it provides various types of adsorption sites which can cooperate in the catalytic process for making or destroying C-O bonds. Our work indicates that highly active WGS and CO_2 hydrogenation catalysts are bifunctional with the metal and oxide (or carbide) catalyzing different parts of the reaction.

FWP-BNL-CO040: Catalysis for Advanced Fuel Synthesis and Energy

Co-PIs: Ping Liu, Sanjaya Senanayake, Dario Stacchiola, and Michael G. White
Postdoc(s): Zongyuan Liu, Robert Palomino, David Grinter
Student(s): Si Luo, Zongyuan Liu, Fang Xu, Dimitriy Vovchok, Zhijun Zuo.
Affiliations(s): all students are from SUNY Stony Brook, Department of Chemistry

RECENT PROGRESS

C1 chemistry involves the conversion of molecules that contain one carbon atom into valuable products. C1 chemistry is expected to become a major area of interest for the transportation fuel and chemical industries in the relatively near future. In general, the feedstocks for C1 chemistry include natural gas (mostly methane), carbon monoxide, carbon dioxide, methanol and synthesis gas (a mixture of carbon monoxide and hydrogen). Thus, a fundamental understanding of the conversion of C-O bonds is essential

for controlling C1 chemistry. The Catalysis Group at BNL has been quiet active in this area. In the period 2014-2016, nineteen papers have been published in peer-reviewed journals (Science, Angewandte Chemie, Journal of the American Chemical Society).[1-19] Experimental and theoretical studies have been performed exploring correlations between the structure and reactivity of typical metal catalysts or catalysts that contain oxides and carbides. Work was done with high-surface area powders and model catalysts. In the last three years, major research achievements within this program have been:

- Discovery of the important role played by metal-support interactions in active catalysts for the water-gas shift and CO_2 hydrogenation.[1,2,5,7]
- Identification of $Cu/CeO_x/TiO_2$, $Au/CeO_x/TiO_2$ and Cu/MoC as highly active and stable catalysts for the hydrogenation of CO_2 to methanol. [1,5,8]
- Discovery of the important role played by the metal-oxide, metal-carbide, and metal-sulfide interfaces in active catalysts for the water-gas shift and CO_2 hydrogenation.[2,7]
- Identification of HOCO as a key intermediate for the water-gas shift reaction by *In-situ* and theoretical studies.[10,16]
- Detailed proof through *operando* studies that metal/oxide catalysts are dynamic entities during the water-gas shift changing in chemical state as a function of reaction conditions.[7,11], [12,19]
- Discovery of the high surface mobility of K as a promoter of the activity of catalysts used for the water-gas shift and CO_2 hydrogenation.

A. Studies on the water-gas shift reaction

A.1 *In-situ studies of WGS catalysts with XRD, PDF, XAFS and TEM : Evolution of metal/oxide catalysts*

The active phase of a series of metal/oxide powder catalysts (Cu/CeO_2-spheres, Cu/CeO_2-rods, Cu/CeO_2-cubes, $Pt/CeOx/TiO_2$, $Au/CeO_x/TiO_2$, $Ce_{1-x}Ni_xO_{2-y}$, CeO_x/CuO) was investigated using a combination of *in-situ* time-resolved X-ray diffraction (XRD), Pair-distribution function (PDF) analysis, X-ray absorption fine structure (XAFS) and environmental TEM.[2,12,17,19] Under reaction conditions most of these WGS catalysts underwent chemical transformations that drastically modified their chemical composition with respect to that obtained during the synthesis process. The active phase of catalysts which combine Cu or Au and ceria consisted of metal nano-particles on partially reduced ceria.[2,12,17,19]

Pulse experiments showed that the oxide was not a simple spectator.[12] Significant differences in chemical and catalytic activity were found when the morphology of the ceria was changed from spheres, to rods, and to cubes.[12,19] The order of catalytic activity increased following the sequence: Cu/CeO_2-cubes < Cu/CeO_2-rods < Cu/CeO_2-spheres, Figure 1. This order matched well trends in the degree of dispersion of copper. Small Cu particles and a strong metal-support interaction were found for the Cu/CeO_2-spheres system. On the opposite end was the Cu/CeO_2-cubes system which

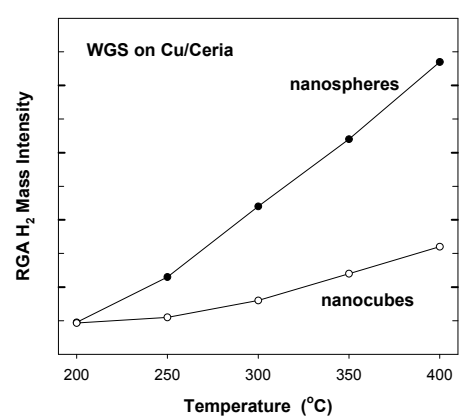

Figure 1. Catalytic activity for the WGS on $Cu-CeO_2$-spheres and $Cu-CO_2$-cubes

exhibited big copper particles and a weak metal-support interaction.[12,19]

A.2 *Importance of metal-oxide interface for the water-gas shift*

Inverse oxide/metal catalysts have been quite useful in the study of the conversion of C-O bonds. The CeO_x/Cu(111) system has shown the important role played by the metal-oxide interface during the WGS reaction.[10,14] Cu(111) has problems dissociating the molecule and is a poor catalysts for the WGS. On this surface, the WGS follows a redox mechanism. The addition of CeO_x to Cu(111) opens a new route for the WGS and increases the rate of reaction by 2-3 orders of magnitude.[2,10,14] Experiments of ambient-pressure XPS and infrared spectroscopy revealed that the metal-oxide interface is very active for the dissociation of water and the formation of a HOCO intermediate that eventually decomposes to CO_2 and H. Thus, the reaction follows an associative mechanism.[10] Results of DFT calculations indicate that all the important steps of the reaction occur at the metal-oxide interface with the reactants and intermediates bound to metal and O centers. Furthermore, the calculations show a huge reduction in the key energy barriers for the reaction that leads to a very large increase in the rate for the production of hydrogen and CO_2.[10]

A.3 *Metal-carbide low-temperature water-gas shift catalysts*

Transition metal nanoparticles dispersed on oxides supports are among the most frequently used catalysts for the WGS in the chemical industry.[2] However, in recent years, it has become clear that metal carbides can be excellent supports for the dispersion of metal catalysts.[14] The metal carbides have interesting catalytic properties on their own, and they also can modify the reactivity of a supported metal through chemical bonding.[1,14] The metal carbides on their own are able to catalyze the WGS reaction.[14] A carbon/metal ratio of 1-to-1 usually gives good stability.[1,14]

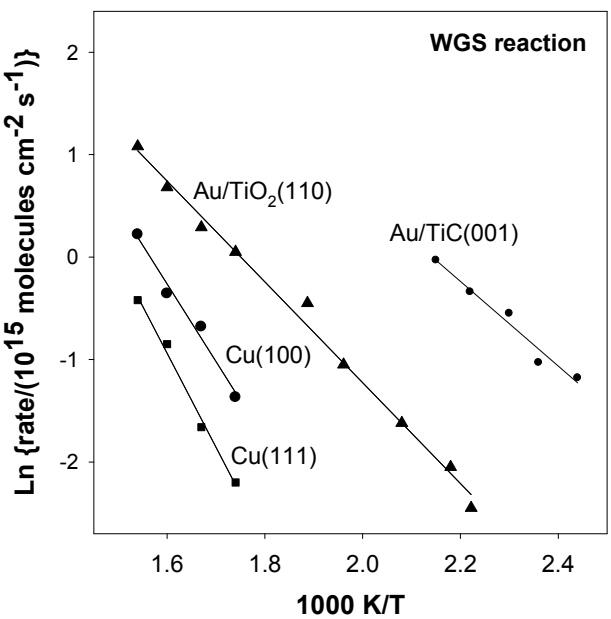

Figure 2. Arrhenius plots for the WGS on Cu(111), Cu(100), Au/TiO_2(110) and Au/TiC(001) catalysts (20 Torr of CO and 10 Torr of H_2O). Surfaces of metallic Au are not active for the WGS reaction. The coverages of Au on TiO_2(110) and TiC(001) were 0.4 and 0.15 ML, respectively.

In Figure 2, we compare the WGS activity of Au/TiC(001) and Au/TiO_2(110) surfaces.[14] The coverages of Au on TiO_2(110) and TiC(001) were 0.4 and 0.15 ML, respectively. For comparison, we include the results for two benchmarks: Cu(111) and Cu(100). At temperatures of 550-625 K, Au/TiO_2 is known to be a very good catalyst for the WGS with an activity that is higher than that of Cu/ZnO which is used as an industrial WGS catalyst.[14] The results in Figure 9 indicate that Au/TiC(001) is a much better low-temperature WGS catalysts than Au/TiO_2(110).[14] The apparent activation energy for the WGS process decreases from 18 ± 2 kcal/mol on Cu(111) to 10 ± 3 kcal/mol on Au/TiO_2(110) and 8 ± 2 kcal/mol on Au/TiC(001). The apparent activation energy on Au/TiO_2(110) is close to that found on Au/TiO_2 powders, 11 kcal/mol. At

relatively low temperatures (< 470 K), Au/TiC(001) exhibits a WGS activity that is observed on copper surfaces and on Cu/oxide or Au/oxide (oxide= TiO_2, ZnO, CeO_2, MgO) catalysts only at elevated temperatures (> 500 K).[14]

Preliminary experiments indicate that Au/MoC exhibits a catalytic behavior not very different from that of Au/TiC, but quite different from that of Au/Mo_2C. It seems that the carbon/metal ratio in the carbide has indeed a strong influence on the WGS catalytic properties. In future work we plan to study this point in detail. Furthermore, in a set of experiments we plan to examine how the nature of the metal (Au, Cu, Pt, Ni) supported on TiC or MoC affects the activity and selectivity for the WGS.

B. Studies on CO_2 hydrogenation

B.1 *Activation and conversion of CO_2 on metal-oxide interfaces*

Reducible oxides have a strong tendency to react with CO_2. Since CeO_x/Cu(111) has a high catalytic activity for the WGS reaction,[10] we investigated its performance in a $CO_2 \rightarrow CH_3OH$ conversion.[16] The rate of methanol production on CeO_x/Cu(111) is ~ 200 times faster than on Cu(111) and ~ 14 times faster than on Cu/ZnO(000$\bar{1}$) (Figure 3). Furthermore, the apparent activation energy for methanol synthesis decreases sequentially on going from Cu(111) to Cu/ZnO(000$\bar{1}$) and CeO_x/Cu(111). According to the DFT calculations on CeO_x/Cu(111), Ce^{3+} centers facilitate CO_2 adsorption in the form

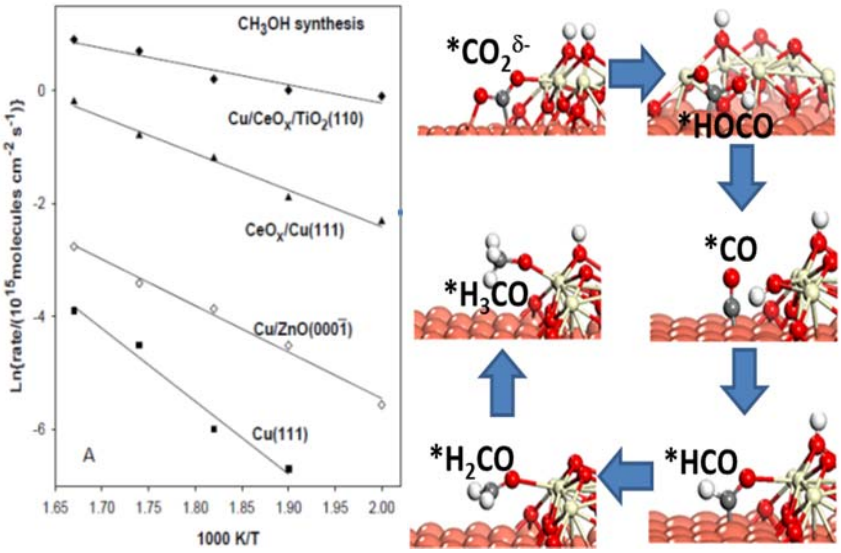

Figure 3 Left: Arrhenius plot for methanol synthesis on Cu(111), 0.2 ML of Cu on ZnO(000$\bar{1}$), a Cu(111) surface covered 20% by ceria, and 0.1 ML of Cu on a TiO_2(110) surface pre-covered 15% with ceria. In a batch reactor the catalysts were exposed to 0.5 atm of CO_2 and 4.5 atm of H_2. The reported values are steady-state rates measured at 600, 575, 550, 525 and 500 K; Right: DFT- optimized structures for the main intermediates for CO_2 hydrogenation on the CeO_x/Cu(111).[16]

of a carboxylate $*CO_2^{\delta-}$ at the ceria-copper interface (Figure 3), consistent with the from AP-IR and AP-XPS under reaction conditions.[5,16] The rest of the reactions follows the RWGS + CO-hydrogenation pathway via *HOCO, *CO, *HCO, $*H_2CO$, and H_3CO intermediates, while the observed *HCOO via the formate pathway acts only as a spectator. The theoretical results indicate that the thermochemistry of the reaction steps associated with the formation of methanol on a ceria-

copper interface is predominantly downhill with an overall exothermic process, which is not the case for the thermochemistry of the reaction on pure copper or copper alloys.[5,16] The ceria-copper interface provides sites of different nature which work in a cooperative way to facilitate the $CO_2 \rightarrow CH_3OH$ transformation.

B.2 *Activation and conversion of CO_2 on metal-carbide interfaces*

For small Cu and Au clusters supported on TiC(001), strong admetal ↔ $C_{surface}$ interactions induce charge polarization over the surface.[1,14] As a result, there is a significant enhancement in the catalytic activity when going from metal bulk surfaces to the carbide-supported small clusters toward the activation of SO_2, C_4H_4S and H_2O. Is such charge polarization capable of transforming CO_2 into methanol?

Experimentally, a promotion in activity and selectivity of CO_2 hydrogenation is observed by depositing small particles of Au, Cu or Ni on TiC(001).[1,9] Although the major product is CO, in the cases of Au/TiC(001) and Cu/TiC(001), a substantial amount of methanol is also produced and no methane is detected. On the other hand, Ni/TiC(001) produces a mixture of CO, methanol, and methane. For all three systems, the highest catalytic activity is found for small 2D particles or clusters of the admetals in close contact with TiC(001) In addition, Cu/TiC is more active for the synthesis of methanol than Au,Ni/TiC and a model for a Cu/ZnO industrial catalysts. DFT calculations show that the charge polarization induced by the Cu-C interaction enhances the CO_2 adoption via a η^3-C,O,O bonding configuration on Cu/TiC(001), and therefore the production of methanol probably involves the hydrogenation of a HCOO intermediate or of the CO generated by the RWGS.

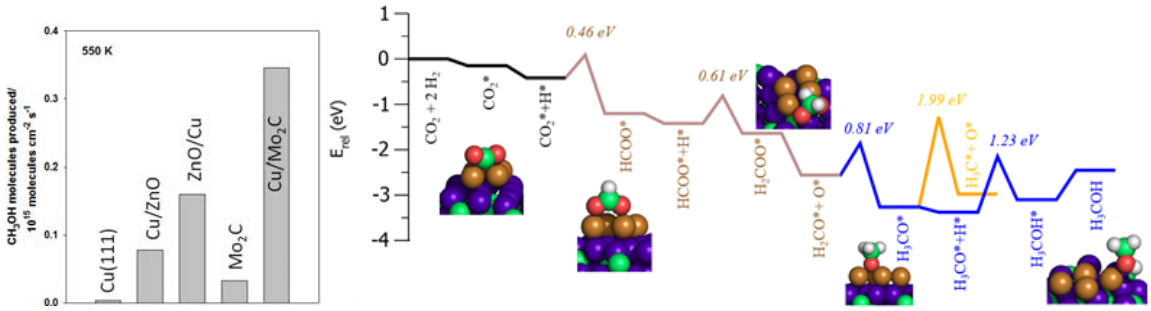

Figure 4 Left: Rates for the production of methanol on Cu(111), Cu/ZnO(000$\bar{1}$), ZnO/Cu(111)**Error! Bookmark not defined.** bare β-Mo_2C(001) and Cu/Mo_2C(001). In a batch reactor, the catalysts were exposed to 0.049 MPa (0.5 atm) of CO_2 and 0.441 MPa (4.5 atm) of H_2 at a temperature of 550 K; Right: DFT-calculated energy profile of methanol on a Cu_4/β-Mo_2C(001) surface model.[4]

Depositing Cu clusters on β-Mo_2C(001) increases the methanol production to a level above that seen for a model of a technical catalyst (Figure 4); besides, it lowers the selectivity to methane according to our experimental observations.[1,4] DFT calculations on surfaces with C- and Mo-terminations corroborate the experimental observations.

Publications Acknowledging this Grant in 2014-2016

Jointly funded by this grant and other grants with leading intellectual contribution from this grant;

2016

1. Posada-Pérez, S.; Ramírez, P. J.; Evans, J.; Viñes, F.; Liu, P.; Illas, F.; Rodriguez, J. A., Highly Active Au/δ-MoC and Cu/δ-MoC Catalysts for the Conversion of CO_2: The Metal/C Ratio as a Key Factor Defining Activity, Selectivity, and Stability. *Journal of the American Chemical Society* **2016,** *138* , 8269-8278.
2. Plata, J. J.; Graciani, J.; Evans, J.; Rodriguez, J. A.; Fernandez Sanz, J., Cu Deposited on CeOx-Modified TiO_2(110): Synergistic Effects at the Metal−Oxide Interface and the Mechanism of the WGS Reaction. *ACS Catalysis* **2016,** *6*, 4608-4615.
3. Grinter, D. C.; Park, J. B.; Agnoli, S.; Evans, J.; Hrbek, J.; Stacchiola, D. J.; Senanayake, S. D.; Rodriguez, J. A., Water-gas shift reaction over gold nanoparticles dispersed on nanostructured CeO_x-TiO_2(110) surfaces: Effects of high ceria coverage. *Surface Science* **2016,** *650*, 34-39.
4. Posada-Perez, S.; Ramirez, P. J.; Gutierrez, R. A.; Stacchiola, D. J.; Vines, F.; Liu, P.; Illas, F.; Rodriguez, J. A., The conversion of CO_2 to methanol on orthorhombic ß-Mo_2C and Cu/ß-Mo_2C catalysts: mechanism for admetal induced change in the selectivity and activity. *Catalysis Science & Technology* **2016**, *6,* 6766-6777.
5. Senanayake, S. D.; Ramirez, P. J.; Waluyo, I.; Kundu, S.; Mudiyanselage, K.; Liu, Z.; Liu, Z.; Axnanda, S.; Stacchiola, D. J.; Evans, J.; Rodriguez, J. A., Hydrogenation of CO_2 to Methanol on CeO_x/Cu(111) and ZnO/Cu(111) Catalysts: Role of the Metal-Oxide Interface and Importance of Ce^{3+} Sites. *Journal of Physical Chemistry C* **2016,** *120*, 1778-1784.

2015

6. Asara, G.; Ricart, J. M.; Rodriguez, J. A.; Illas, F., Exploring the Activity of a Novel Au/TiC(001) Model Catalyst Towards CO and CO_2 Hydrogenation. *Surface Science* **2015,** *640*, 141-149.
7. Rodriguez, J. A.; Liu, P.; Stacchiola, D.; Senanayake, S. D.; White, M. G.; Chen, J. G., Hydrogenation of CO_2 to Methanol: Importance of Metal-Oxide and Metal-Carbide Interfaces in the Activation of CO_2. *ACS Catalysis* **2015,** *5*, 6696-6706. (Subtask 2)
8. Yang, X.; Kattel, S.; Senanayake, S. D.; Boscoboinik, J. A.; Nie, X.; Graciani, J.; Rodriguez, J. A.; Liu, P.; Stacchiola, D. J.; Chen, J. G., Low pressure CO_2 hydrogenation to methanol over gold nanoparticles activated on a CeO_x/TiO_2 interface. *Journal of the American Chemical Society* **2015,** *137*, 10104-10107.
9. Xu, W.; Ramirez, P. J.; Stacchiola, D.; Brito, J. L.; Rodriguez, J. A., Carburization of Trasition Metal Molybdates and the Generation of Highly Active Metal/Carbide Catalysts for CO_2 Hydrogenation. *Catalysis Letters* **2015,** *145*, 1365-1373.
10. Mudiyanselage, K.; Senanayake, S. D.; Ramirez, P. J.; Kundu, S.; Baber, A.; Yang, F.; Agnoli, S.; Axnanda, S.; Liu, Z.; Hrbek, J.; Evans, J.; Rodriguez, J. A.; Stacchiola, D., Intermediates Arising from the Water-Gas Shift Reaction over Cu Surfaces: From UHV to Near Atmospheric Pressures. *Topics in Catalysis* **2015,** *58*, 271-280.

11. Carrasco, J.; Lopez-Duran, D.; Liu, Z.; Duchon, T.; Evans, J.; Senanayake, S. D.; Crumlin, E. J.; Matolin, V.; Rodriguez, J. A.; Veronica Ganduglia-Pirovano, M., In Situ and Theoretical Studies for the Dissociation of Water on an Active Ni/CeO_2 Catalyst: Importance of Strong Metal-Support Interactions for the Cleavage of O-H Bonds. *Angewandte Chemie-International Edition* **2015,** *54*, 3917-3921.
12. Zhao, F.; Liu, Z.; Xu, W.; Yao, S.; Si, R.; Johnston-Peck, A.; Martínez-Arias, A.; Hanson, J.; Senanayake, S.; Rodriguez, J., Pulse Studies to Decipher the Role of Surface Morphology in CuO/CeO_2 Nanocatalysts for the Water Gas Shift Reaction. *Catalysis Letters* **2015,** *145*, 808-815.
13. Posada-Perez, S.; Vines, F.; Rodriguez, J. A.; Illas, F., Fundamentals of Methanol Synthesis on Metal Carbide Based Catalysts: Activation of CO_2 and H_2. *Topics in Catalysis* **2015,** *58*, 159-173. **(Invited)**

<u>2014</u>

14. Rodriguez, J. A.; Ramírez, P. J.; Asara, G. G.; Viñes, F.; Evans, J.; Liu, P.; Ricart, J. M.; Illas, F., Charge Polarization at a Au–TiC Interface and the Generation of Highly Active and Selective Catalysts for the Low-Temperature Water–Gas Shift Reaction. *Angewandte Chemie International Edition* **2014,** *53* , 11270-11274.
15. Xu, W.; Ramirez, P. J.; Stacchiola, D.; Rodriguez, J. A., Synthesis of α-MoCx and ß-MoCy Catalysts for CO_2 Hydrogenation by Thermal Carburization of Mo-oxide in Hydrocarbon and Hydrogen Mixtures. *Catalysis Letters* **2014,** *144,* 1418-1424.
16. Graciani, J.; Mudiyanselage, K.; Xu, F.; Baber, A. E.; Evans, J.; Senanayake, S. D.; Stacchiola, D. J.; Liu, P.; Hrbek, J.; Sanz, J. F.; Rodriguez, J. A., Highly active copper-ceria and copper-ceria-titania catalysts for methanol synthesis from CO_2. *Science* **2014,** *345*, 546-550.
17. Zhao, F.; Liu, Z.; Xu, W.; Yao, S.; Kubacka, A.; Johnston-Peck, A. C.; Senanayake, S. D.; Zhang, A.-Q.; Stach, E. A.; Fernandez-Garcia, M.; Rodriguez, J. A., Water Gas Shift Reaction on Ni -W-Ce Catalysts: Catalytic Activity and Structural Characterization. *The Journal of Physical Chemistry C* **2014,** *118*, 2528-2538.
18. Posada-Perez, S.; Vines, F.; Ramirez, P. J.; Vidal, A. B.; Rodriguez, J. A.; Illas, F., The Bending Machine: CO_2 Activation and Hydrogenation on δ-MoC(001) and ß-Mo2C(001) Surfaces. *Physical Chemistry Chemical Physics* **2014,** *16*, 14912-14921.
19. Yao, S. Y.; Xu, W.; Johnston-Peck, A.; Zhao, F.; Liu, Z.; Luo, S.; Heckler, I.; Senanayake, S. D.; Martinez, A.; Liu, W.; Rodriguez, J., Morphological effects of nanostructured ceria supports on the activity and stability of CuO/ CeO_2 catalysts for the water-gas shift reaction. *Physical Chemistry Chemical Physics* **2014,** *16* (32), 17183-17195.

Structural Reconstruction of a Au-Pd Binary Nanoalloy under Reduced and Oxidized Conditions: An Ab Initio Molecular Dynamics Study

Cong-Qiao Xu[1,2], Mal-Soon Lee[2], Yang-Gang Wang[2], Jun Li[1,3], Vassiliki-Alexandra Glezakou[2] and Roger Rousseau[2*]

[1]*Department of Chemistry, Tsinghua University, Beijing 100084, China*

[2]*Institute for Interfacial Catalysis, Pacific Northwest National Laboratory, Richland, Washington 99352, United States*

[3]*William R. Wiley Environmental Molecular Sciences Laboratory, Pacific Northwest National Laboratory, Richland, Washington 99352, United States*

E-Mails: roger.rousseau@pnnl.gov

Presentation Abstract

Nanoparticles of mono and bi metallic species have been widely studied in the past decades because of their remarkable electronic and optical properties, and are particularly active in various catalytic reactions. Among the binary nanoalloys, gold-palladium (Au-Pd) nanoparticles have attracted considerable attentions because of their superior performance in various catalytic reactions, such as synthesis of H_2O_2, oxidation of CO, vinyl acetate synthesis etc. Structure, composition, and distribution of nanoalloys under operating conditions are significant in determining catalytic activity. In the present work, *ab initio* molecular dynamics simulations are performed to understand the structural behavior of Au-Pd nanoalloy supported on TiO_2 under different redox conditions. We find that the AuPd alloy structure is strongly dependent on the redox properties of the support, originating from the so-called strong metal-support interaction (SMSI). Under reducing conditions, Pd atoms are inclined to move towards the interface evidenced by the significant increase of Pd-Ti bonds. This could be attributed to the charge localization at the interface that leads to a Coulomb attraction to the positively charged Pd. In contrast, Pd atoms would rather stay inside or the alloy surface under oxidizing conditions. Pd atoms on Au-Pd alloy can be stabilized by hydrogen adsorption, forming Pd-H bonds, which are stronger than Au-H bonds. Our work provides an important insight into the structure design of Pd-Au nanoalloy catalyst and may lead to potential applications in dioxygen activation processes where Pd atoms are generally considered to be the active sites.

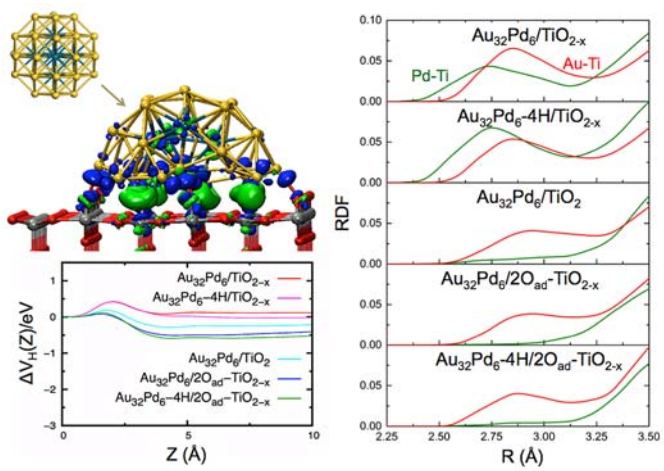

Figure 2. Redox effects on the structure and morphology of supported AuPd nanoalloys.

Kinetic Analyses for Bridging the Pressure Gap: Alcohol Oxidation in Liquid and Gas Phases

Aditya (Ashi) Savara, Yafen Zhang, Michelle Kidder, David R. Mullins
Chemical Sciences Division, Oak Ridge National Laboratory

Presentation Abstract

One of the objectives of our research is to connect the kinetics and mechanisms of surface chemistry under vacuum pressures (VP) on ~1 cm^2 flat crystals, to that which occurs under ambient pressure (AP) conditions on nanoparticles and powders. Here, we present one of our success stories (liquid phase benzylic alcohol oxidation on precious metal nanoparticles), and an ongoing study (gas phase small alcohol oxidation over complex metal oxides). The two examples are geared towards elucidating cooperativity between different elements/sites, where the activity or selectivity is enabled or promoted in a synergistic manner by having the two elements/sites together.

In the first example, kinetic simulation + fitting of experimental data was used to close the pressure gap in aerobic benzylic alcohol oxidation over precious metal nanoparticles (Pd and AuPd). Prior to this three-paper study, the mechanism and kinetics of aerobic benzylic alcohol oxidation over the precious metal nanoparticles was not known, despite the potential for sustainable industrial aldehyde production. A mechanism was constructed based on knowledge from VP single crystal studies, and refined using transient kinetics data. It was determined that the mechanism split into two pathways to reach the six products observed: A) an alkoxy pathway leading to toluene, benzaldehyde, and benzyl ether, and B) a carbonyl-oxyl pathway ("neutral carboxylate") leading to benzoic acid, benzene, and benzyl benzoate. With this mechanism, the first micro-kinetic modeling of benzylic alcohol oxidation over the precious metal nanoparticles was conducted; this may be the first study over any catalyst to show consistency with a realistic sticking coefficient for micro-kinetic modeling in a liquid-solid heterogeneous catalysis reaction. Finally, micro-kinetic modeling showed that that the role of Au was to weaken the oxygen-surface interaction, leading to a lower oxygen surface coverage, which explained the changes in product selectivity. In this example, VP surface science techniques provided the elementary chemical reaction steps that ultimately enabled quantitative kinetic modeling of the reaction under potentially industrially relevant conditions.

In a second and ongoing example, the oxidation of small alcohols (methanol, ethanol, and isopropanol) over complex metal oxides is being studied. $LaMnO_3$ and $La_xSr_{1-x}MnO_3$ show suitable activity to study the alcohol oxidation selectivity with single crystal samples under VP conditions, and also with packed bed powders under AP conditions. We are gaining kinetic parameters under both sets of conditions by conducting temperature programmed reactions as well as steady state experiments, where we vary the flux/pressure and temperature. The VP steady state experiments are conducted using an effusive molecular beam. Additionally, AP and VP x-ray photon spectroscopy measurements are being utilized to characterize the surface intermediates in both pressure ranges. The intent is to connect both the mechanisms and the kinetics between the pressure ranges in a global mechanistic and kinetic model, and to understand the cooperativity by varying the cationic La/Sr ratio.

This research is part of FWP ERKCC96: Fundamentals of Catalysis and Chemical Transformations. For a full description of recent progress see Extended Abstract for ERKCC96.

New Approaches to Modeling Non-Ideal Metal Surface Adsorption and Reactions

William F. Schneider
University of Notre Dame, Dept. of Chemical and Biomolecular Engineering

Presentation Abstract

Computation modeling of surface reactions relies on our ability to efficiently model the free energies of adsorption. These free energies depend on the surface and adsorbate (reactant, intermediate, or product) of interest, system temperature and adsorbate coverage. The free energy represents a balance between the energetic driving force for creating bonds between an adsorbate and a surface and the entropic cost of moving an adsorbate from a fluid phase to a surface. Standard density functional theory (DFT) approaches generally begin by optimizing the location of an adsorbate on a surface, computing a binding energy, and approximating the internal, translational, and configurational contributions to the free energy. In this contribution, we explored both the aspects of free energy, the contribution from creation of bonds leading to adsorption and the estimation of entropic contribution to the free energy.

DFT based approaches are useful in accurately calculating the adsorption energies but limit us to small reaction systems as the computational cost increases exponentially as the system size increases. In order to study properties of realistic systems with thousands of molecules, we need simplified models that can provide a quick estimation of the energies. We developed cluster expansion and simplified mean-field coverage models for NO-O co-adsorption on Pt(111) to perform kinetic studies on the system. The entropic contributions to the free energy are usually obtained using the standard harmonic approximations. We explore the accuracy of the harmonic oscillator models by comparing the results with a more detailed free energy estimates based on DFT-quantified potential energy surfaces and enumeration of surface densities of states.

DE-FG02-06ER15839: Towards Realistic Models of Heterogeneous Catalysis: Simulations of Oxidation Catalysis from First Principles

Post-docs: Dr. Hanyu Ma
Students: Anshumaan Bajpai, Gray Laughlin

RECENT PROGRESS

Reliable Adsorbate-Adsorbate Interactions for Kinetics

In the conventional density functional theory (DFT) approach, adsorption energies at a metal surface are computed at a fixed coverage, say in a 2 × 2 or 3 × 3 supercell representation of a particular metal facet of interest. Such an approach is useful for comparing energies across facets, between metals, or even between adsorbates. At realistic reaction conditions, however, adsorbate

coverages can differ significantly from idealized models and, because of pervasive adsorbate-adsorbate interactions, adsorption energies can deviate significantly from the ideal, coverage-independent limit.

In past work, we have explored the use of lattice-based cluster expansions (CEs) to model surface energies as a function of the coverage and arrangement of adsorbates. We focused specifically on oxygen (O) adsorbates on the late transition metal surfaces, chosen because these are the most abundant surface species present during catalytic NO oxidation to NO_2 and because they exhibit strong adsorbate-adsorbate interactions important to the underlying catalysis. We compared predicted NO oxidation rates computed in the ideal (no interactions) limit with those computed from the fully interacting CE combined with Monte Carlo simulations and DFT-parameterized O_2 dissociation barriers. We found that computed rates in the fully interacting model deviate substantial from the ideal case, that rates are sensitive both to the coverage and the degree of "ordering" of the adsorbates, and that the inclusion of interactions changes the optimal metal catalyst (Figure 1).

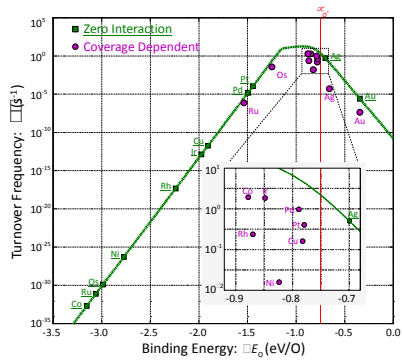

Figure 1: Computed NO oxidation rates on (111) facets vs. low coverage O binding energy neglecting (green) and explicitly including (purple) adsorbate interactions.

A CE can in principle be applied to any number of co-adsorbates. We chose the O-NO-vacancy combination on Pt(111) to demonstrate the CE fitting procedure and to explore co-adsorption effects on computed NO oxidation kinetics. Figure 2 shows the DFT-computed formation energies of many NO and O co-adsorbate configurations. We found that a 5-fold cross-validation provided a superior balance of accuracy and reliability than more conventional parameterization approaches. While the fitted ternary CE faithfully reproduces the DFT energies, the DFT dataset is large and the fitting demanding. An alternative is to write the formation energy as a sum over O-O, NO-NO, and NO-O contributions, each of which can be captured in CE's fit to the three legs of the ternary diagram. We found that this "three-binary-single-ternary" (TBST) approach performs quite well in reproducing the full ternary diagram, especially in the moderate coverage region expected to be most catalytically relevant. Reaction rates are more sensitive to the details of the energy model than are adsorbate coverages. Figure 3 compares the coverages and turn-over rates predicted by

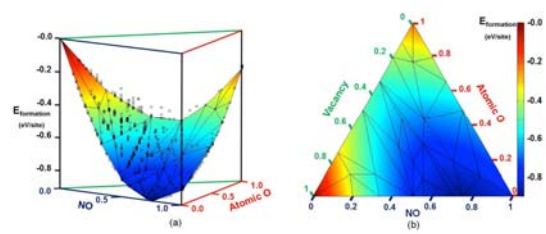

Figure 2: "Ternary" diagram for the NO/O/vacancy system on Pt(111). Left plot illustrates full DFT database and minimum energy hull with respect to NO and ½ O_2. Right shows top view, color-coded by formation energy.

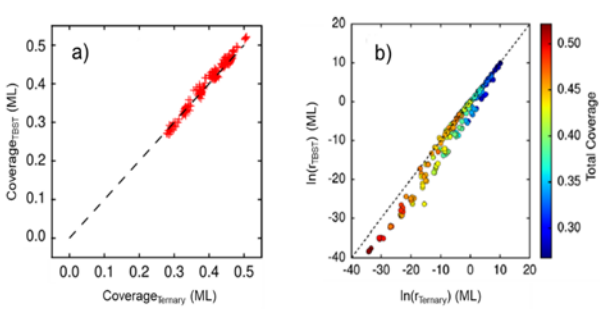

Figure 3: (a) Parity plot of TBST vs full ternary total coverage across relevant NO oxidation condition. (b) Parity plot of TBST vs full ternary ln *r* across same conditions.

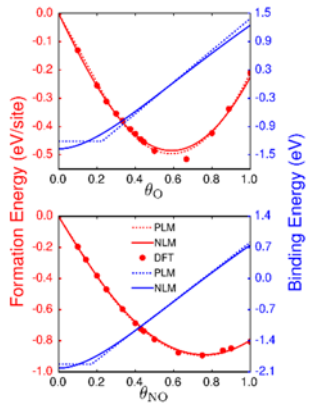

Figure 4: Comparison of piece-wise (PLM) and non-linear (NLM) fits to coverage-dependent O (top) and NO (bottom) per site (red) and per adsorbate (blue) adsorption energies.

the two models across 225 different NO oxidation reaction conditions using the same underlying kinetic model. Total surface coverages lie very close to the parity line while the TORs diverge at high coverage. Nonetheless, the TBST model provides a semi-quantitative reproduction of the full CE kinetic results.

Lattice-based kinetic models capture both the energetic and ensemble effects of coverage on rates. A simpler approach, appropriate to a mean-field microkinetic model, is to write binding energies as an explicit function of coverage. Figure 4 compares a previously proposed piecewise linear model (PLM) with a non-linear (NLM) form inspired by the Wilson equation for the formation energy of mixtures. The NLM captures the gradual change in adsorbate binding energy at low coverages and converges to the PLM at higher coverages. Further, as shown in Figure 5, when inserted into a microkinetic model for NO oxidation, the NLM predicts variations in surface coverage with temperature that are more consistent with the full CE model than does the PLM. The NLM naturally includes terms for self- and cross-adsorbate interactions that we intend to parameterize.

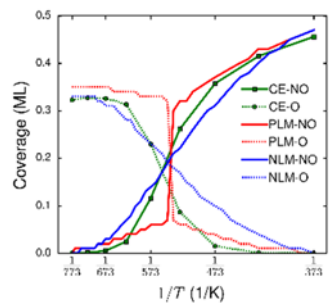

Figure 5: Comparison of temperature-dependent surface coverages from full CE and two coverage-dependent binding energy parameterizations. T = 773 K, P_{NO} = 100 ppm, $\ln(P_{NO2}/P_{NO}) = -2$.

Ternary Interactions Across Adsorbates and Metals

The NO-O results on Pt(111) motivate a broader survey of mixed adsorption on metals. We have computed coverage-dependent adsorption energies of pairwise combinations of N/H/O on the (111) facets of Ag, Au, Cu, Ir, Ni, Pd, Pd, Rh. Figure 6 shows representative results for N/O pairs, plotted as formation energies relative to N_2 and O_2. We have fit all combinations to CEs. We intend to explore correlations between the terms that contribute to the overall interactions as well as to apply the NLM model to extract interaction terms that can be applied more generally.

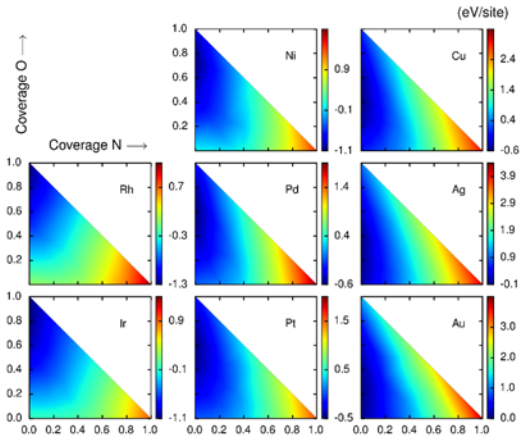

Figure 6: Formation energy contour plots depicting DFT calculated convex hull for N-O adsorbate pair on 111 surface of fcc transition metals.

Adsorbate Free Energies

Appropriate models for the finite-temperature free energies of adsorbates is an area of active research. Analytical expressions are known for simple limiting cases, including a free translator and a harmonic oscillator, and intermediate hindered translator approaches have been proposed. The translational contributions to free energy can in principle be determined exactly by sampling the adsorbate potential energy surface, solving the

Schrödinger equation for the adsorbate, and computing the partition function and free energy by summation.

Figure 7 shows as an example the DFT-computed lateral potential energy surface (PES) for a C adsorbate on Pt(100), obtained by rastering the adsorbate laterally and allowing to relax vertically. Preferred hollow sites and high energy atop sites are evident. We solved the single particle Schrödinger equation numerically to obtain the translational wavefunctions and energy spectrum, from which we compute partition functions and free energies. Free energy results for this and other adsorbates on Pt(100) and Au(100) are shown in Figure 8. For comparison, we fit the PES to harmonic models and computed harmonic oscillator free energies, also shown in Figure 8. For these cases the full PES results are generally quite close to a harmonic model, especially at low temperature. Adsorbed H on both metals, N on Pt(100), and O on Au(100) show the largest deviations.

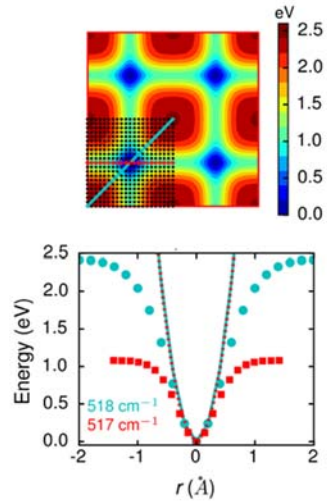

Figure 7: DFT-calculated PES for C on Pt(100) (top) and harmonic fits along the two normal modes (bottom).

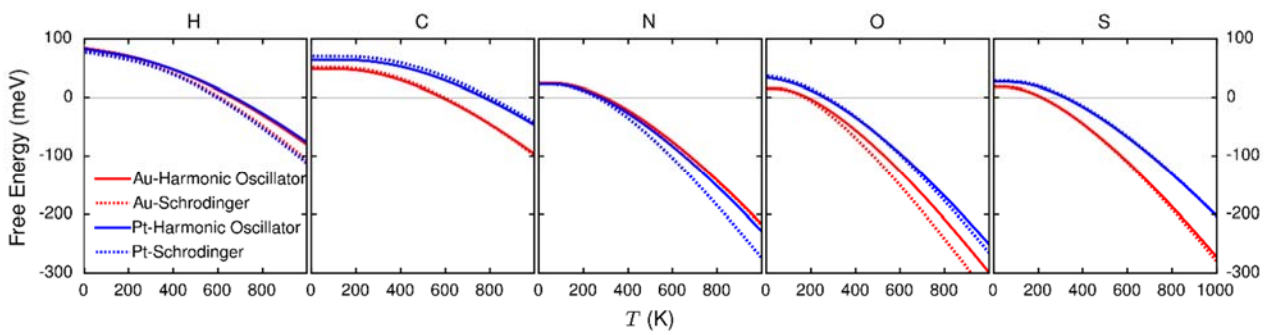

Figure 8: Free energy as a function of temperature for H, C, N, O and S adsorption on Au(100) and Pt(100) surfaces

These results illustrate the potential for exact evaluations of free energies, but obtaining the full PES for all intermediates involved in a given reaction using DFT is computationally too demanding. To accelerate the calculation of the PES, we are exploring the use of DFT-trained artificial neural network (ANN) potentials. We find that these machine learned potentials are able to reproduce the full PES with accuracy comparable to DFT, when trained with as few as 60-100 single point DFT calculations. The combination of DFT + ANN is thus an attractive approach to evaluate the non-electronic contributions to the adsorption free energies at moderate computational cost.

Publications Acknowledging this Grant in 2014-2017

Exclusively funded by this grant;

J. M. Bray and W. F. Schneider, "Coverage-dependent adsorption at a low symmetry surface: DFT and statistical analysis of oxygen chemistry on kinked Pt(321)," *Top. Catal.,* **2014**, *57*, 89-105.

J. M. Bray, I. Skavdahl, J.-S. McEwen, and W. F. Schneider, "First-principles Reaction Site Model for Coverage-Sensitive Surface Reactions: Pt(111)-O Temperature-Programmed Desorption," *Surf. Sci. Lett.*, **2014**, *622*, L1-L6.

J. M. Bray and W. F. Schneider, "First-Principles Analysis of Structure Sensitivity in NO Oxidation on Pt," *ACS Catal.*, **2015**, *5*, 1087-1099.

L. M. Herder, J. M. Bray, and W. F. Schneider, "Comparison of Cluster Expansion Fitting Algorithms for Interactions at Surfaces," *Surf. Sci.,* **2015**, 640, 104-111.

A. Bajpai, K. Frey, and W. F. Schneider, "Binary Approach to Ternary Cluster Expansions: NO–O–Vacancy System on Pt(111)," *J. Phys. Chem. C,* **2017**, 121, 7344-7354.

Jointly funded by this grant and other grants with leading intellectual contribution from this grant

K. Frey, D. J. Schmidt, C. Wolverton and W. F. Schneider, "Implications of coverage-dependent O adsorption for catalytic NO oxidation on the late transition metals," *Catal. Sci. Tech.*, **2014**, *4*, 4356-4365.

Activation of Metal Oxide Catalysts by Olefins

Susannah L. Scott,[a,b] Baron Peters,[a,b] and Albert E. Stiegman[c]
[a] Department of Chemical Engineering, University of California, Santa Barbara CA
[b] Department of Chemistry & Biochemistry, University of California, Santa Barbara CA
[c] Department of Chemistry & Biochemistry, Florida State University, Tallahassee FL

Presentation Abstract

The reactions of fully inorganic dispersed group 6 and 7 metal oxides with olefins leads to industrially relevant activity in olefin metathesis and polymerization via the formation of organometallic active sites. The nature of these reactions remains obscure because the active sites (metal alkylidenes and alkyls) are rare and have not been directly observed. Using a combination of spectroscopic probes, kinetics, identification of organic products, and studies with model organometallic compounds, we have made significant progress in identifying some of the key reactions involved in these transformations, while ruling out others on the basis of the absence of essential spectroscopic or mechanistic signatures. For example, Cr^{II}/SiO_2 is oxidized by ethylene to $Cr^{III}(-CH{=}CH_2)$ sites with liberation of ethyl radicals that subsequently dimerize to give *n*-butane. In silica-supported catalysts prepared with pre-installed, bulky Cr^{III}-R bonds, direct ethylene insertion competes with reactions like α-H elimination and alkylidene coupling.

DE-FG-02-03ER15467: Hierarchical Design of Supported Organometallic Catalysts for Hydrocarbon Transformations

Lead PI: Susannah L. Scott
CoPIs: Baron Peters, Albert E. Stiegman
Postdoc: Fan Zhang
Students: Fangwen Cheng, Colin Gardner, Hitomi Hayashibara, Salman Khan, Spencer Klepper, Hyunjin Moon, Nathan Peek, Youhong Wang

RECENT PROGRESS

Spectroscopic studies of Cr(VI)/SiO₂. A detailed UV-vis spectroscopic study was carried out on Cr(VI)/SiO_2. The goal of this study was to assign the electronic transitions and assess excited state properties of the monomeric Cr(VI) site. UV-vis absorption, emission and emission excitation spectra were recorded at room temperature and at ca. 10 K. State assignments were made by analysis of the spectra in combination with time-dependent density functional theory (TD-DFT) calculations. These state determinations are designed to assist in our analysis of the resonance Raman spectra.

Raman and resonance Raman spectra of Cr(VI)/SiO_2 materials were recorded to investigate the local structures of the Cr sites. In general, prior work from our team and others demonstrated that its vibrational spectra are consistent with a pseudo-tetrahedral, C_{2v}-symmetry site with two short terminal Cr=O bonds and two chromasiloxane bridges. Recently, resonance Raman spectra, collected by exciting into the lowest energy excited state (458 nm, $^1B_1$), have been claimed to support a five-coordinate site with one terminal Cr=O bond and four chromasiloxane bridges. We collected a series of resonance Raman spectra by exciting into all of the observed absorption bands. We determined that excitation at 458 nm into the first excited state results in photo-decomposition, yielding bands associated not with the primary Cr(VI) structure, but with the decomposition product. One of these bands is erroneously assigned to the putative monoxo species, whose energy is computed to be much higher than the dioxo site.

Mechanistic studies on reduction of Cr(VI)/SiO_2. We undertook studies of reduction processes of silica-dispersed Cr(VI) ions to lower oxidation states. We showed that reduction by CO proceeds via two 2-electron reductions from Cr(VI) to Cr(IV) to Cr(II) as a function of temperature. We have also studied H_2 reduction. A recent temperature programmed reduction (TPR) under H_2 reported two distinct reduction steps at ca. 425 and 485 °C, which were assigned to reduction of a Cr mono and dioxo species, respectively. Monitoring changes in the UV-vis spectrum that accompany reduction at the temperatures observed in the TPR as well as characterization by electron spin resonance and X-ray absorption spectroscopy indicate that these are sequential reductions of a single Cr species. There is no support for the claim that these processes involve different chromium structures.

Mechanism of ethylene activation in the Phillips catalyst. Using DFT, we investigated H atom transfer within $(SiO)_2Cr^{II}(C_2H_4)_2$ site to yield a $(SiO)_2Cr^{IV}$(ethyl)(ethenyl) site. Our calculations showed that coordination of neighboring siloxane groups facilitates Cr-C bond homolysis of $(SiO)_2Cr^{IV}$(ethyl)(ethenyl) to give ethyl radicals and creates the active $(SiO)_2Cr^{III}$-ethenyl initiating sites. This finding explains our experimental observation of alkyl radicals by EPR, and n-butane (from dimerization of ethyl radicals) by GC. However, we have not yet identified geometric arrangements of siloxane ligands that would simultaneously facilitate both the homolysis and H-transfer steps.

We also showed that $(SiO)_2Cr^{II}$ sites can adsorb ethylene to give a chromacyclopentane, after spin-crossing. The latter site can undergo direct homolysis of one Cr-C bonds resulting in a tethered *n*-butyl radical with an overall effective free energy of 124 kJ/mol. If the dangling butyl radical is sufficiently close to another Cr(II) or mono(ethylene)Cr(II) site, the dangling radical can react to give a pair of Cr(III) sites connected by an alkyl bridge, and both of the resulting alkylCr(III) sites will be active for polymerization. Even at very low loadings, a small fraction of Cr sites may exist in close proximity to each other. We used Poisson statistics to estimate the time scale and fraction of sites that could be activated in this way. However, the per-site activity of the Phillips catalyst *increases* as Cr loading decreases. This seems like a contradiction, but we note that additional processes might amplify the initial activation events. As the first sites begin to polymerize, stresses due to polymer generation within pores cause the support to fracture, exposing dangling bonds that abstract H from ethylene or from polyethylene. The resulting alkyl and vinyl radicals could then react with dormant Cr(II) sites to create active alkyl-Cr(III) sites. According to DFT, the tethered homolysis mechanism is the first energetically viable route from Cr(II) sites to alkyl-Cr(III) polymerization sites.

Support-induced activation of Re-based metathesis catalysts. Oxide-supported Re catalysts spontaneously initiate olefin metathesis near room temperature, but suffer from low active site fractions and rapid deactivation. CH_3ReO_3 deposited on the same supports is much more active and allows us to study the more abundant active sites with greater sensitivity. Previously, we identified Lewis acid sites on silica-alumina and alumina as key in anchoring and activating the Re sites, and speculated that Bronsted acid sites were responsible for deactivation. In the past year, we manipulated the Lewis/Bronsted ratios to increase activity and stability. Extensive chlorination of alumina results in the formation of highly Lewis acidic surface domains depleted in surface hydroxyl groups. Adsorption of CH_3ReO_3 onto these chlorinated domains serves to activate it as a low temperature, heterogeneous olefin metathesis catalyst and confers both high activity *and* high stability. Characterization of the catalyst reveals that the immobilized CH_3ReO_3 undergoes partial ligand exchange with the surface, whereby some Re sites acquire a chloride ligand from the modified alumina while donating an oxo ligand to the support. More specifically, Re L_{III}-edge EXAFS and DFT calculations support facile ligand exchange to generate $[CH_3ReO_2Cl^+]$ fragments that interact with a bridging oxygen of the support via a Lewis acid–base interaction. The chloride-promoted metathesis catalyst easily achieved a TON of 100 000 for propene metathesis in a flow reactor at 10 °C (compared to TON < 5000 for the non-chlorinated catalyst). Increased activity is a consequence of both a larger fraction of active sites and a higher intrinsic activity for the new sites. Increased stability is attributed to a stronger interaction between MTO and chlorinated surface regions, as well as extensive depletion of the Brønsted acidic surface hydroxyl population.

Machine learning in the sampling of rare active sites. In a distribution of sites with different activation energies, the kinetic properties are dominated by sites with the lowest kinetic energies. Therefore, an efficient estimator for any kinetic property will require thorough sampling of sites in the low energy tail of the activation energy distribution. We have re-purposed advanced sampling methods from rare events to achieve this goal. Biased sampling can accelerate convergence of estimates for all relevant kinetic properties: the site-averaged activation energy, the site-averaged rate constant, and the fraction of sites (Z) that are responsible for a fraction X of the overall activity. The biased sampling algorithms converge about 10 times faster than standard sampling procedures. These calculations also illustrate that (even with the most efficient estimators) hundreds of sites must be sampled to converge an estimate of the activation energy or the rate. This represents a step change improvement over the few efforts in the literature to compute site-averaged properties for these catalysts, which have used inefficient estimators and ca. 10 sites in constructing their estimates.

Publications Acknowledging this Grant in 2014-2017

(I) Exclusively funded by this grant

Brown, C.; Krzystek, J.; Achey, R.; Lita, A.; Fu, R., Meulenberg, R.; Polinski, M.; Peek, N.; Wang, Y.; can de Burgt, L. J.; Profeta, S.; Stiegman, A. E.; Scott, S. L. Mechanism of Initiation in the Phillips Ethylene Polymerization Catalyst: Redox Processes Leading to the Active Sites, *ACS Catal.* **2015**, *5*, 5574-5583.

Peters, B; Scott, S.L.; Fong, A.; Wang, Y.; Stiegman, A. E., Reexamining the Evidence for Proton Transfers in Ethylene Polymerization, *Proc. Natl. Acad. Sci. USA* **2015**, *112*, E4160-4161.

Peters, B.; Scott, S. L. Single atom catalysts on amorphous supports: A quenched disorder perspective, *J. Chem. Phys.*, **2015**, *142*, 104708.

Fong, A.; Yuan, Y.; Ivry, S. L.; Scott, S. L.; Peters, B. Computational Kinetic Discrimination of Ethylene Polymerization Mechanisms for the Phillips (Cr/SiO_2) Catalyst, *ACS Catal*. **2015**, *5*, 3360-3374.

Goldsmith, B. R.; Hwang, T.; Seritan, S.; Peters, B.; Scott, S. L., Rate-Enhancing Roles of Water Molecules in Methyltrioxorhenium-Catalyzed Olefin Epoxidation by Hydrogen Peroxide, *J. Am. Chem. Soc.* **2015**, *137*, 9604-9616.

Coller, D. H.; Vicente, B. C.; Scott, S. L., Rapid Extraction of Quantitative Kinetic Information from Variable-temperature Reaction Profiles, *Chem. Eng. J.* **2016**, *303*, 182-193.

Fong, A.; Peters, B.; Scott, S. L. One-Electron Redox Activation of the Reduced Phillips Polymerization Catalyst via Alkylchromium(IV) Homolysis: A Computational Assessment, *ACS Catal.* **2016**, *6*, 6073-6085.

Brown, C.; Lita, A.; Tao, Y.; Peek, N.; Crosswhite, M.; Mileham, M.; Krzystek, J.; Achey, R.; Fu, R.; Kaur, J.; Polinski, M.; Wang, Y.; van de Burgt, L. J.; Jeffcoat, D.; Profeta, Jr., S.; Stiegman, A. E.; Scott, S. L. Mechanism of Initiation in the Phillips Ethylene Polymerization Catalyst: Ethylene Activation by Cr(II) and the Structure of the Resulting Active Site, in review.

(II) Jointly funded by this grant and other grants with leading intellectual contribution from this grant

Szeto, K. C.; Gallo, A.; Hernandez-Morejudo, S.; Olsbye, U.; De Mallmann, A.; Lefebvre, F.; Gauvin, R. M.; Delevoye, L.; Scott, S. L.; Taoufik, M., Selective grafting of $Ga(i\text{-}Bu)_3$ on the silanols of mesoporous H-ZSM-5 by surface organometallic chemistry, *J. Phys. Chem. C*, **2015**, *119*, 26611-16619.

Nguyen, T.D.; Jones, Z.R.; Leto, D.F.; Wu, G.; Scott, S.L.; Hayton, T.W. Ligand-Exchange-Induced Growth of an Atomically Precise Cu_{29} Nanocluster from a Smaller Cluster, *Chem. Mater.* **2016**, *28*, 8385-8390.

Gallo, A.; Fong, A.; Szeto, K.C.; Rieb, J.; Delevoye, L.; Gauvin, R.M.; Taoufik, M.; Peters, B.; Scott, S. L. Ligand exchange-mediated activation and stabilization of a Re-based olefin metathesis catalyst by chlorinated alumina, *J. Am. Chem. Soc.* **2016**, *138*, 12935-12947.

Bligaard, T.; Bullock, R. M.; Campbell, C. T.; Chen, J. G.; Gates, B. C.; Gorte, R. J.; Jones, C. W.; Jones, W. D.; Kitchin, J. R.; Scott, S. L., Towards Benchmarking in Catalysis Science: Best Practices, Challenges, and Opportunities, *ACS Catal.* **2016**, *6*, 2590-2602.

Goldsmith, B. R.; Johnson, J. K.; Gates, B. C.; Scott, S. L. Beyond ordered materials: Understanding catalytic sites on amorphous solids, in review.

Annabella Selloni

Formation and structure of black TiO_2: insights from first principles simulations

Xunhua Zhao, Sencer Selcuk and Annabella Selloni
Department of Chemistry, Princeton University, Princeton, N.J. 08544

Presentation Abstract

Recently a great deal of attention has been focused on "black TiO_2", a modified TiO_2 material that can absorb visible light much more efficiently than pristine TiO_2. Black TiO_2 consists of nanoparticles (NPs) with a crystalline TiO_2 core covered by a highly reduced outer shell, whose chemical composition and atomic structure are not known in detail. To obtain insight into the stability and properties of these NPs, we have carried out first principles calculations on model structures consisting of reduced overlayers on the majority (101) surface of anatase, the TiO_2 phase typically found in nanomaterials. The overlayers are formed by aggregation of extended defects known as crystallographic shear planes (CSPs), which are relatively frequent in TiO_2 and other reducible oxides.

Our results show that formation of a reduced overlayer ("shell") on the anatase surface is thermodynamically favorable under a wide range of experimental conditions. This shell has Ti_2O_3 stoichiometry and its structure is not the well-known corundum-like Ti_2O_3 phase (the mineral "tistarite"), but a novel phase that has not yet been reported. DFT calculations with various exchange-correlation functionals predict that this new phase − denoted csp-Ti_2O_3, to distinguish it from standard corundum Ti_2O_3 − is very close in stability to corundum Ti_2O_3 and has a band gap of 1.2-1.8 eV, which is consistent with the absorption of black TiO_2. These findings suggest a possible important role of csp-Ti_2O_3 in the properties black TiO_2 nanomaterials. In a broader context, analogous structures could be relevant for describing the reduced surface region of nanomaterials of other metal oxides as well.

DE-SC0007347 : Understanding Surfaces and Interfaces of Photocatalytic Oxide Materials with First Principles Theory and Simulations

Postdocs: Xunhua Zhao, Sencer Selcuk
Students: Xiao Shi, Marcos Calegari Andrade

RECENT PROGRESS

Reduction of Oxygen on Anatase TiO_2 (101) – We have investigated the reactions of O_2 and H_2O coadsorbed on the (101) surface of reduced TiO_2 anatase using a combined theoretical and experimental approach (experiments carried out by the group of Ulrike Diebold at TU Wien). While water adsorbs molecularly on the anatase (101) surface, the reaction with O_2 leads to water dissociation and formation of terminal OH groups. We find that these terminal OHs are the final and stable reaction product on reduced anatase. We identify OOH as a metastable intermediate in the reaction. The water dissociation reaction runs as long as the surface can transfer enough electrons to the adsorbed species. The energy balance and activation barriers for the individual reaction steps also depend on the number of electrons available, and our results indicate that the presence of donor dopants can significantly reduce activation barriers for oxygen reduction on anatase.

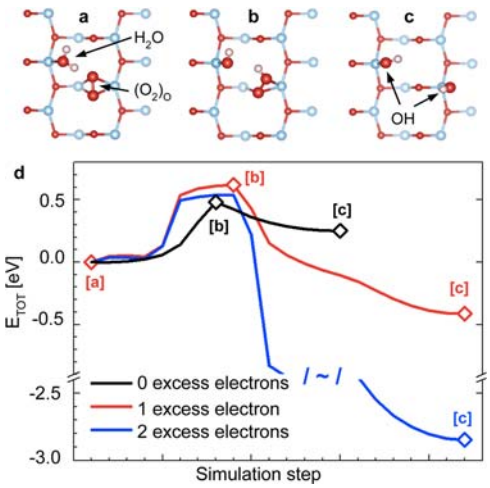

Figure 1. Calculated NEB pathway for the reaction of H_2O with an interstitial peroxo species, $(O_2)_O$, on the anatase (101) surface. (a) H_2O adsorbs near the $(O_2)_O$, forming a hydrogen bond. (b) One hydrogen is transferred to the $(O_2)_O$. (c) Relaxation into a pair of terminal OH groups. (d) Energy profile of the reaction for 0, 1, and 2 excess electrons in the slab. Positions corresponding to snapshots a–c are marked in the energy profile. The black line in panel d is shorter because a smaller number of images was used in the corresponding NEB calculation.

Bulk and surface properties of spinel $NiCo_2O_4$. In a series of papers, we have extended our previous work on spinel Co_3O_4 to investigate the structure, electronic properties and reactivity of $NiCo_2O_4$, a promising catalyst for CO and methane oxidation. All studies were carried out using Density Functional Theory (DFT) calculations with on-site Hubbard U corrections.

i. <u>*Formation, electronic structure and defects*</u>. Analysis of the electronic structure of $Ni_xCo_{3-x}O_4$ as a function of x= 0 - 1 shows that Ni acts as a p-type dopant in Co_3O_4, gradually transforming the minority spin channel from insulating to conducting. As a result, the inverse spinel $NiCo_2O_4$ (NCO) has a ferrimagnetic half-metallic ground state with fractional valence on Ni and Co cations at tetrahedral sites (Td), in agreement with experimental observations. Projected Densities of States confirm that the states around the Fermi energy originate from Ni and Co(Td) 3d states hybridized with oxygen 2p orbitals. Two common defects, Ni↔Co(Td) exchanges and oxygen vacancies, have been also investigated. Our results are consistent with the experimental observation that intermediate structures between inverse spinel and normal spinel occur frequently in NCO. Oxygen vacancies are predicted to occur more frequently at sites coordinated to a larger number of Ni ions and found to have only minor effects on the conductivity and magnetic structure.

ii. *Oxygen deficiency and reactivity of $NiCo_2O_4$ (001) surfaces.* We examined surfaces with different Co/Ni compositions and found that the formation of surface oxygen vacancies (V_{OS}) on NCO(001) is strongly affected by the neighboring cation in the 3rd layer: the computed formation energy is largest (≈1.2 eV) for O-vacancies coordinated to 3rd layer Co and smallest (≈0.5 eV) for V_{OS} coordinated to a Ni neighboring another Ni ion. As a result, V_O formation is generally much easier on NCO (001) than on Co_3O_4 (001) surfaces, suggesting that NCO may be a better catalyst than Co_3O_4 for oxidation reactions based on the Mars Van Krevelen mechanism. Surface oxygen vacancies on reduced NCO surfaces can be healed through dissociative water adsorption at room temperature. In contrast, adsorption of molecular oxygen at V_{OS} is energetically unfavorable under ambient conditions, suggesting that O_2 adsorption is the thermodynamic limiting step for oxidation reactions on NCO(001) surfaces.

Publications Acknowledging this Grant in 2014-2017

(I) Exclusively funded by this grant;

1. Sencer Selçuk and Annabella Selloni, Excess Electrons at TiO_2 Anatase Surfaces and Interfaces: insights from first principles simulations, *Journal of Physics D: Applied Physics,* **2017**, *50*, 273002.
2. Sencer Selçuk and Annabella Selloni, Facet-dependent trapping and dynamics of excess electrons at anatase TiO_2 surfaces and aqueous interfaces, *Nature Materials*, **2016**, *15*, 1107-1112.
3. Ye-Fei Li and Annabella Selloni, Pathway of Photocatalytic Oxygen Evolution on Aqueous TiO_2 Anatase and Insights into the Different Activities of Anatase and Rutile, *ACS Catalysis*, **2016**, *6*, 4769-4774.
4. U. Aschauer, A. Selloni, Adsorption of biomedical coating molecules, amino acids, and short peptides on magnetite (110), *J. Chem. Phys.*, **2015**, *143*, 044705
5. S. Selcuk, A. Selloni, DFT+U Study of the Surface Structure and Stability of Co_3O_4(110): Dependence on U, *J. Phys. Chem. C*, **2015**, *119*, 9973-9979.
6. U. Aschauer, A. Tilocca, A. Selloni, Ab initio simulations of the structure of thin water layers on defective anatase TiO_2(101) surfaces, *Int. J. Quantum Chemistry* **2015**, *115*, DOI: 10.1002/qua.24918
7. Jun Hee Lee and A. Selloni, TiO_2/Ferroelectric Heterostructures as Dynamic Polarization-Promoted Catalysts for Photochemical and Electrochemical Oxidation of Water, *Phys. Rev. Letters* **2014**, *112*, 196102.
8. Ye-Fei Li, Ulrich Aschauer, Jia Chen, and Annabella Selloni, Adsorption and Reactions of O_2 with Anatase TiO_2, *Acc. Chem. Res.* **2014**, *47*, 3361-3368.
9. Y. F. Li and A. Selloni, Mechanism and Activity of Water Oxidation on Selected Surfaces of Pure and Fe-doped NiO_x, *ACS Catal.* **2014**, *4*, 1148-1153
10. S. Selçuk, A. Selloni, "Influence of External Electric Fields on Oxygen Vacancies at the Anatase (101) Surface", *J. Chem. Phys.* **2014**, *141*, 084705.
11. Ye-Fei Li and Annabella Selloni, Mosaic Texture and Double c-axis Periodicity of β-NiOOH: Insights from First Principles and Genetic Algorithm Calculations, *J. Phys. Chem. Lett.* **2014**, *5*, 3981-3985.

(II) Jointly funded by this grant and other grants with leading intellectual contribution from this grant;

12. Honghong Wang, Taicheng An, Annabella Selloni, Effect of reducible oxide-metal cluster charge transfer on the structure and reactivity of adsorbed Au and Pt atoms and clusters on anatase TiO_2, *J. Chem. Phys.* **2017**, *146*, 184703.
13. Martin Setvin, Jan Hulva, Honghong Wang, Thomas Simschitz, Michael Schmid, Gareth S Parkinson, Cristiana Di Valentin, Annabella Selloni, Ulrike Diebold, Formaldehyde adsorption on the anatase TiO_2(101) surface: Experimental and Theoretical Investigation, *J. Phys. Chem. C,* **2017**, *121*, 8914-8922.
14. Xiao Shi, Steven L. Bernasek, and Annabella Selloni, Oxygen Deficiency and Reactivity of Spinel $NiCo_2O_4$ (001) Surfaces, *J. Phys. Chem. C,* **2017**, *121*, 3929-3937.
15. Francesca Nunzi, Filippo De Angelis, and Annabella Selloni, Ab Initio Simulation of the Absorption Spectra of Photoexcited Carriers in TiO_2 Nanoparticles, *J. Phys. Chem. Lett.*, **2016**, *7*, 3597-3602
16. Martin Setvin, Ulrich Aschauer, Jan Hulva, Thomas Simschitz, Benjamin Daniel, Michael Schmid, Annabella Selloni, and Ulrike Diebold, Following the Reduction of Oxygen on TiO_2 Anatase (101) Step by Step, *J. Am. Chem. Soc.* **2016**, *138*, 9565-9571.
17. Xiao Shi, Steven L. Bernasek, and Annabella Selloni, Formation, Electronic Structure, and Defects of Ni Substituted Spinel Cobalt Oxide: a DFT+U Study, *J. Phys. Chem. C*, **2016**, *120,* 14892-14898
18. He Lin, Guido Fratesi, Sencer Selçuk, Gian Paolo Brivio, and Annabella Selloni, Effects of Thermal Fluctuations on the Structure, Level Alignment, and Absorption Spectrum of Dye-Sensitized TiO_2: A Comparative Study of Catechol and Isonicotinic Acid on the Anatase (101) and Rutile (110) Surfaces*, J. Phys. Chem. C*, **2016**, *120*, 3899–3905.
19. Martin Setvin, Maria Buchholz, Weiyi Hou,Cui Zhang, Bernhard Stöger, Jan Hulva, Thomas Simschitz, Xiao Shi, Jiri Pavelec, Gareth S. Parkinson, Mingchun Xu, Yuemin Wang, Michael Schmid, Christof Wöll, Annabella Selloni, Ulrike Diebold, A Multi-Technique Study of CO Adsorption on the TiO_2 Anatase (101) Surface, *J. Phys. Chem. C*, **2015,** *119*, 21044-21052.
20. Zhiqiang Wang, Bo Wen, Qunqing Hao, Li-Min Liu, Chuanyao Zhou, Xinchun Mao, Xiufeng Lang, Wen-Jin Yin, Dongxu Dai, Annabella Selloni, and Xueming Yang, Localized Excitation of Ti^{3+} Ions in the Photoabsorption and Photocatalytic Activity of Reduced Rutile TiO_2, *J. Am. Chem. Soc*., **2015**, *137*, 9146–9152.
21. Xiao Shi, Ye-Fei Li, S. L. Bernasek, A. Selloni, Structure of the $NiFe_2O_4$(001) surface in contact with gaseous O_2 and water vapor, *Surf. Sci.* **2015**, *640*, 73-79.
22. F. Nunzi, S. Agrawal, A. Selloni, F. De Angelis, Structural and Electronic Properties of Photoexcited TiO_2 Nanoparticles from First Principles, *J. Chem. Theory Comput.* **2015**, *11*, 635-645.
23. Martin Setvin, Benjamin Daniel, Ulrich Aschauer, Weiyi Hou, Ye-Fei Li, Michael Schmid, Annabella Selloni, Ulrike Diebold, "Identification of Adsorbed Molecules Via STM Tip Manipulation: CO, H_2O, and O_2 on TiO_2 Anatase (101)", *Phys. Chem. Chem. Phys*. **2014**, *16*, 21524.

24. F. De Angelis, C. Di Valentin, S. Fantacci, A. Vittadini, A. Selloni, Theoretical Studies on Anatase and Less Common TiO_2 Phases: Bulk, Surfaces and Nanomaterials, *Chem. Rev*. **2014**, 9708-9753.
25. Mariachiara Pastore, Annabella Selloni, Simona Fantacci, and Filippo De Angelis, Electronic and Optical Properties of Dye-Sensitized TiO_2 interfaces, *Top Curr Chem* **2014**, *347*, 1-46.

(III) Jointly funded by this grant and other grants with relatively minor intellectual contribution from this grant;

26. Wentao Yuan, Yong Wang, Hengbo Li, Hanglong Wu, Ze Zhang, Annabella Selloni, and Chenghua Sun, Real time observation of reconstruction dynamics on TiO_2 (001) surface under oxygen via an environmental TEM, *Nanolett.*, **2016**, *16*, 132-137.
27. Xiong Xiao, Fumitaka Hayashi, Hiromasa Shiiba, Sencer Selçuk, Kazuhiro Ishihara, Kenta Namiki, Lei Shao, Hiromasa Nishikiori, Annabella Selloni, and Katsuya Teshima, Platy KTiNbO5 as a Selective Sr Ion Adsorbent: Crystal Growth, Adsorption Experiments, and DFT Calculations, *J. Phys. Chem. C*, **2016**, *120*, 11984-11992.

Conversion of C-H bonds: Production of Hydrogen and Chemicals from Methane

Sanjaya D. Senanayake, Feng Zhang, Zongyuan Liu, Robert Palomino,
David C. Grinter, Ping Liu, Jose A. Rodriguez
Chemistry Department, Brookhaven National Laboratory
Upton, NY 11973 (USA)

Our recent studies indicate that, in spite of the high stability of methane, systems such as Ni-CeO_2 and Cu-CeO_2 can break C-H bonds even at room temperature, through careful manipulation of metal-support interactions and using C1 oxidants (CO_2, O_2/H_2O), opening the door for new chemical transformations. Our approach is to rely on *in-situ* studies, using AP measurements with XRD, XAFS, XPS, infrared spectroscopy and TEM/STM coupled with DFT/KMC to study powder and model systems consisting of earth abundant metals (Ni, Co, Cu) combined with reducible oxide supports like ceria.

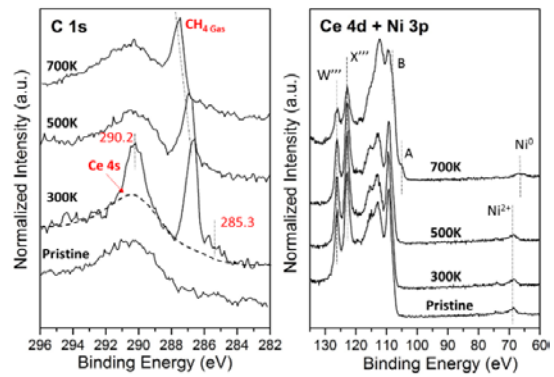

Figure 1. C 1s and Ce 4d + Ni 3p spectra of the Ni/CeO_2(111) ($\Theta_{Ni} \approx 0.1$ ML) surface under 100 mTorr of CH_4 at 300, 500 and 700 K.

We have studied Dry Reforming of Methane (DRM: $CH_4+CO_2 \rightarrow 2CO+2H_2$) over Ni-$CeO_x$ powder and model catalysts to elucidate the active species and reaction mechanism. We have identified interactions between small Ni nanoparticles ($Ni^0/Ni^{\delta+}$) and reduced CeO_x surfaces (Ce^{4+}/Ce^{3+}). While the small supported Ni nanoparticles are present as Ni^0/Ni_xC essential for the C-H conversion processes, the Ni2+ facilitates the low temperature C-H pathway. The catalyst has a multifunctional, synergistic role in which Ni, CeO_x and the interface provide an ensemble effect in the active chemistry that to H_2.

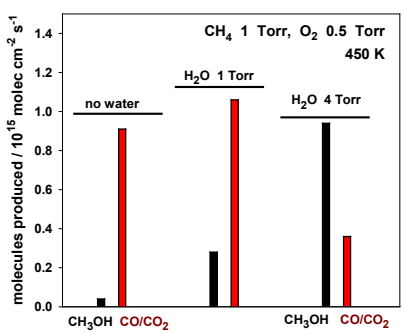

Figure 2. Production of methanol and CO/CO_2 as a function of water pressure on a CeO_2/Cu_2O/Cu(111) catalyst in which ~ 40% of the Cu_2O was covered by ceria. The samples were exposed to 1 Torr of CH_4, 0.5 Torr of O_2 and 0, 1 or 4 Torr of H_2O at 450 K.

We have also started to develop a method for the direct conversion of methane to methanol. We have found that a CeO_2/Cu_2O/Cu(111) inverse system is able to activate methane at room temperature and then, with the help of water, performs a catalytic cycle, which is highly selective to the production of methanol (Figure 2). The pressure of water has a strong effect on the selectivity towards the production of methanol. These possibilities will be explored in detail using a combination of theory with AP-XPS and IR spectroscopy.

1. Liu et al. Angewandte Chemie (2016) 128 (26), 7581-7585.
2. Lustemberg et al. ACS Catalysis (2016) 6 (12), 8184-8191.
3. Zuo et al. JACS (2016) 138 (42), 13810-13813.

Production of Higher Alcohols from Methane over $NiO/Ce_xZr_{1-x}O_2$ Catalysts

Carsten Sievers, Chukwuemeka Okolie, Yimeng Lyu
Georgia Institute of Technology – School of Chemical & Biomolecular Engineering

Presentation Abstract

The enormous scale of conventional and non-conventional methane reserves has motivated significant research activities regarding its conversion to fuels and chemicals. Since large amounts of natural gas are located in remote areas and transporting gases in pipelines is difficult, processes for converting methane into denser, preferably liquid, value-added products are highly desirable. Significant efforts have been undertaken to activate and upgrade methane, but in many cases, different temperatures are required for different parts of the catalytic cycle, or expensive oxidants (e.g., H_2O_2 or organic perioxides) are consumed in the process.

To address these challenge, we developed a multi-functional NiO/ceria-zirconia (NiO/CZ) catalyst that is capable of converting methane to alcohols at steady state in a single reactor. The process occurs at moderate temperatures using O_2 as an oxidant. The activity of this catalyst depends on the Lewis acidity of well-dispersed NiO clusters and the redox activity of the CZ support. Specifically, methane is activated on Lewis acid sites to form surface alkyl/alkoxy groups. When steam is provided in the feed, these surface species appear to be hydrolyzed to form alcohols. The redox active support activates O_2, which converts some of the surface species to CO_2 or H_2O, providing a thermodynamic driving force for the reaction. Besides alcohols, CO_2 and H_2 are formed as the main by-products. Importantly, formation of alcohols occurs at 450 °C under steady state conditions with a turnover frequency of at least 50 h^{-1}. This is a clear improvement from previously reported catalysts, which required a high-temperature calcination step for every turnover. The nature and synergy of active sites and potential reactions mechanisms will be discussed.

Grant or FWP Number: DE-SC0016486 (Production of Higher Alcohols from Methane over $NiO/Ce_xZr_{1-x}O_2$ Catalysts)

Student(s): Chukwuemeka Okolie, Yimeng Lyu

RECENT PROGRESS

In this reporting period, our efforts were focused on advanced characterization of NiO/CZ catalysts to provide more insight into the nature and role of the active sites. Based on this novel insight, we started to explore alternative preparation techniques to improve the performance of NiO/CZ.

Identification of Active Sites

Two reference materials were synthesized to probe the effect of the size of NiO clusters and the nature of the support on the unique reaction path towards alcohol production. First, we prepared 2 wt.% NiO on SiO_2 ($2NiO/SiO_2$). Complete deactivation of $2NiO/SiO_2$ occurred within a few hours of reaction, and no alcohols were formed. We also prepared another reference material, which consisted of the same CZ support but contained 5 wt.% Ni (5NiO/CZ) instead of 2 wt.%. 5NiO/CZ showed a more rapid decline in methane conversion as well as reduced selectivity to alcohols compared to 2NiO/CZ. EDX maps revealed the size distribution of NiO particles on these catalysts and confirmed our hypothesis that the small cluster size of NiO on CZ has an important effect on the alcohol selectivity over NiO/CZ (Figure 1). Specifically, the EDX maps of NiO/CZ with 2 wt.% Ni showed the presence of well-dispersed Ni on the entire surface of the CZ support (Figure 1a). It can be concluded that they should be present as NiO clusters below ~2-3 nm in size. In addition to the well dispersed NiO, some larger particles (up to 10 nm) were also observed. In contrast, the EDX map of NiO/SiO_2 only revealed Ni in the form of larger particles of 10 – 25 nm (Figure 1b). An increase of the Ni loading on CZ to 5 wt.% also resulted in the formation of larger NiO clusters (Figure 1c).

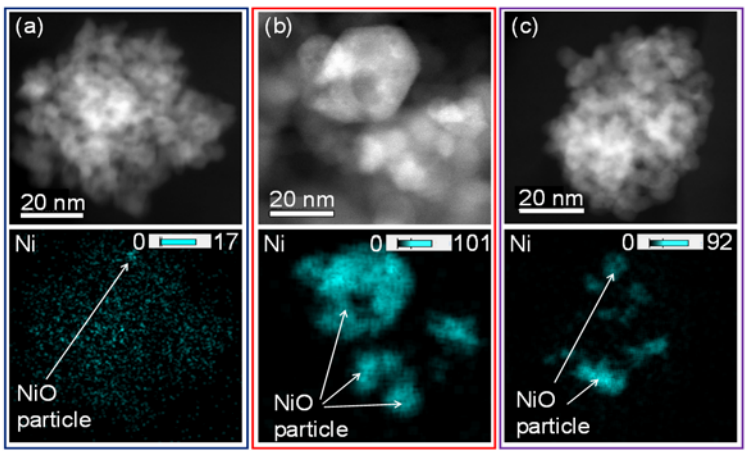

Figure 1. HAADF images and corresponding EDX maps of Ni for (a) 2 wt.% NiO/CZ (b) 2 wt.% NiO/SiO_2 (c) 5 wt.% NiO/CZ.

Prior to this reporting period, in-situ XANES measurements revealed that easily reducible surface ceria could act as an oxygen reservoir, which supplies oxygen to nickel during exposure to methane. XPS was used to independently confirm these results. Figure 2 shows XPS results for ceria and nickel after activation in nitrogen, after exposure to methane for an hour and after exposure to methane for 4 hours. After activation in nitrogen, only Ce $3d_{5/2}$ $4f^2$ and $4f^1$ features at 882 and 889 eV were observed, which are indicative of surface Ce^{4+} species (1). This means that ceria is fully oxidized at this point. The appearance of Ce $3d_{5/2}$ $4f^2$ and $4f^1$ features at 880 and 885 eV, respectively, after exposure to methane for 1 h represent conversion of some surface Ce^{4+} species into Ce^{3+} species (1). The features from Ce^{3+} intensified after exposure to methane for 4 h. The spectra were deconvoluted to estimate the degree of surface reduction. It was found that about 50% of the Ce^{4+} species within 3 nm from the surface were reduced to Ce^{3+} after 4 h of exposure to methane at 450 ^oC. In Figure 2b, the nickel 2p XP spectra for NiO surface before and after treatment with methane are shown. Before exposure to methane, the Ni $2p_{3/2}$ feature and its satellite at ~855.6 eV and ~862 eV and the Ni $2p_{1/2}$ feature at ~872.5 eV were seen, which can be

attributed to Ni^{2+} (2). After 1 h of exposure to methane, the same features were seen on the Ni 2p spectrum indicating that no reduction of nickel oxide had occurred. After exposure to methane for 4 h, there was a shift of the Ni $2p_{3/2}$ and the Ni $2p_{1/2}$ features to ~852.5 eV and ~869.8 eV, which indicates a reduction to metallic Ni^0. This observation is in exact agreement with our XANES results showing that ceria can supply oxygen to NiO clusters until the reactive oxygen species at or near the surface are depleted.

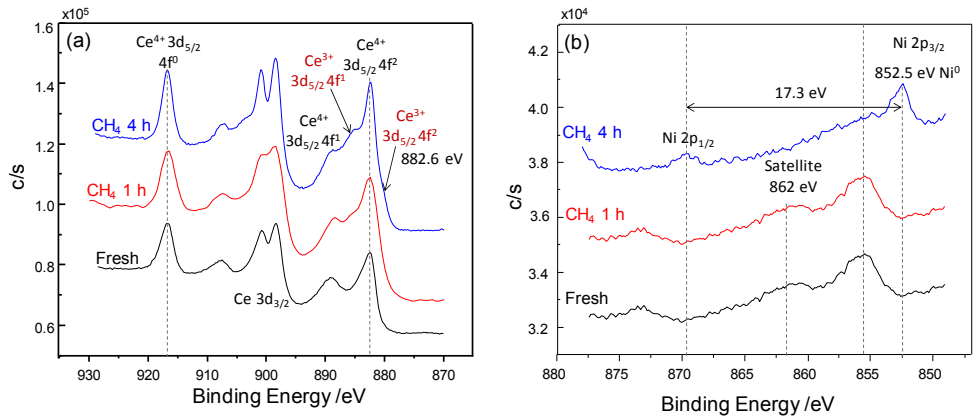

Figure 2. XPS after in-situ treatment of NiO/CZ with methane at 450 °C (a) Ce 3d spectra (c) Ni 2p.

Synthesis of NiO/CZ Catalysts with Increased Performance

The reactivity of NiO/CZ as well as its detailed characterization led us to believe that small NiO clusters on CZ play a significant role in alcohol formation. Consequently, we hypothesized that increasing the dispersion of NiO on CZ will improve its selectivity towards alcohol formation. Thus, we used different synthesis techniques to prepare NiO/CZ aiming to increase the dispersion of NiO (Figure 3). For strong electrostatic adsorption (SEA), a net surface charge was introduced on the support, which allowed for adsorption of nickel precursors with the opposite charge. In this technique, the working hypothesis is that strong adsorption of the metal complex on the surface reduces agglomeration during calcination. Co-precipitation (CP) was also used to prepare NiO/CZ. Since CP is a bulk technique and only a fraction of nickel atoms ends up on the surface, several catalysts with different loadings of Ni were prepared to find the optimum loading.

All catalysts were characterized by XRD and pyridine adsorption followed by IR spectroscopy, and their reactivity was tested. The XRD traces for samples with 2 wt.% Ni showed no NiO diffractions regardless of the synthesis technique used. This indicates that the NiO clusters were below the detection limit. For CP catalysts, NiO diffractions were observed for NiO/CZ with 6 and 10 wt.% showing the presence of bigger NiO particles.

The concentration of accessible Lewis acidic sites (LAS) on different catalysts with 2 wt.% Ni loading was measured by pyridine adsorption followed by IR spectroscopy. The highest LAS concentration was observed for NiO/CZ_SEA, indicating the SEA method gave the best NiO dispersion of 31%. The lower LAS concentration for the catalyst prepared by CP is not surprising because only a fraction of the Ni is expected to be accessible on the surface. Due to the size of the pyridine molecule, it might not be possible to adsorb two molecules on adjacent sites, but these results clearly show that NiO is highly dispersed.

Among the catalysts with 2 wt.% Ni, the one prepared by SEA gave the best performance in terms of methane conversion and alcohol selectivity (Figures 3 c and d), which is consistent with

the highest dispersion of NiO. The conversion of methane over 2NiO/CZ_CP was lower compared to the other catalysts, this samples had the same high alcohol selectivity as the sample prepared by SEA. This indicates that the fraction of surface NiO that is exposed is very well dispersed. Varying the Ni loading of catalysts prepared by CP showed that the catalyst prepared with 6 wt.% Ni loading had the optimal composition, as it provided the best alcohol yield.

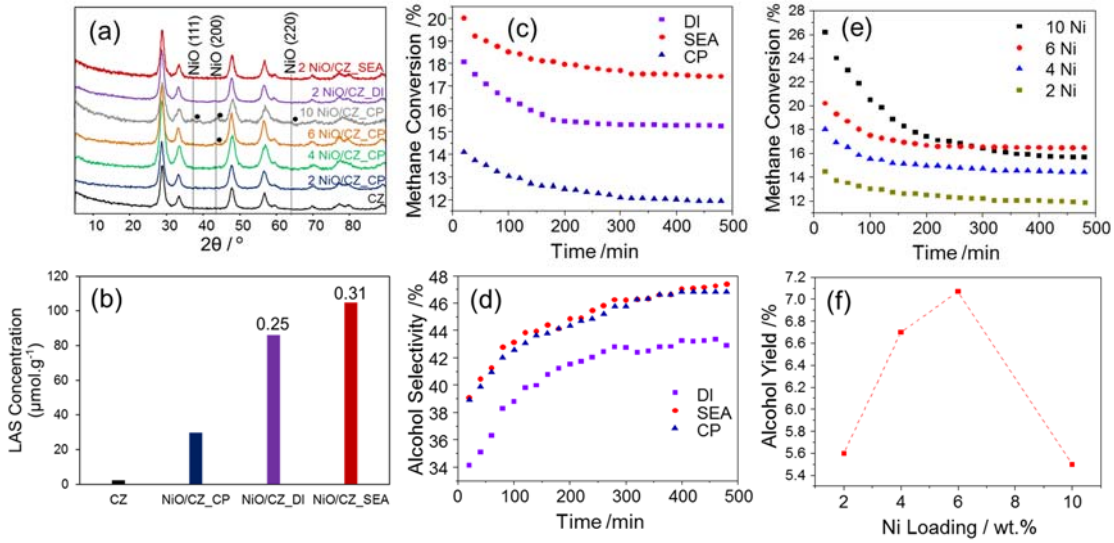

Figure 3. (a) XRD patterns for different NiO/CZ catalysts (b) Lewis acid site concentration for different catalysts with 2 wt.% Ni loading and the support (c) methane conversion over 2 NiO/CZ prepared from different techniques (d) alcohol selectivities over 2 NiO/CZ prepared by different techniques (e) methane conversion over NiO/CZ_CP with different Ni loadings (f) alcohol yields over CP catalysts as a function of Ni loading.

References

1. Henderson, M. A.; Perkins, C. L.; Engelhard, M. H.; Thevuthasan, S.; Peden, C. H. F., Redox properties of water on the oxidized and reduced surfaces of CeO_2(111). *Surf Sci* **2003,** *526* (1-2), 1-18.
2. Uhlenbrock, S.; Scharfschwerdt, C.; Neumann, M.; Illing, G.; Freund, H. J., The Influence of Defects on the Ni-2p and O-1s XPS of NiO. *J Phys-Condens Mat* **1992,** *4* (40), 7973-7978.

Publication Acknowledging this Grant in 2014-2017

Jointly funded by this grant and other grants with leading intellectual contribution from this grant:

1. Okolie, C.; Belhseine, Y. F.; Stavitski, E.; Kovarik, L.; Sievers, C., Conversion of Methane to Methanol and Ethanol over Nickel Oxide on Ceria-Zirconia Catalysts in a Single Reactor. *Angew. Chem. Int. Ed.* **submitted**.

Interfacial catalysts for reactions of oxygenates: design, characterization, catalytic activity and reaction mechanisms

Aaron D. Sadow, Takeshi Kobayashi, Marek Pruski, Igor I. Slowing
Ames Laboratory, U.S. DOE, Iowa State University, Ames, IA 50011-3111

PRESENTATION ABSTRACT

The overreaching goal of this collaborative research is to understand catalytic phenomena at liquid-solid interfaces and thereby enable the rational design of catalysts for selective and efficient heterogeneous conversions, particularly for redox transformations of oxygenated compounds. This project confronts these challenges by combining expertise in mesoporous catalyst synthesis, transition metal chemistry, mechanisms of catalytic reactions, and solid-state (SS)NMR, particularly with the uniquely sensitive dynamic nuclear polarization (DNP) methodology. Herein, we highlight the development of methods to control and quantify the effects of local polarity on the activity of interfacial catalytic sites and the design of novel multifunctional rare earth-based supported catalysts for synergistic hydrogenolysis reactions. In addition, we present the synthesis, structural and spectroscopic properties, and catalytic behavior of rare earth silazido compounds and surface-grafted analogues that provide a comparison between homogeneous and interfacial chemistry. The synthesis of a series of homoleptic organolanthanides stabilized by benzyl- and dimethylsilyl-containing ligands as suitable precatalysts for related studies. Finally, we report the investigation of the structure and distribution of molecular species on amorphous surfaces with unprecedented detail via DNP enhanced SSNMR spectroscopy. These ultrasensitive characterizations include the study of spatial distribution of surface groups on mesoporous silica and ceria, the binding of molecular species at interfacial sites between Pd and γ-Al_2O_3 support, and the measurement of O–H bond lengths in metal oxides with sub-picometer resolution via natural abundance ^{17}O DNP NMR.

AL-03-380-011: Homogeneous and Interfacial Catalysis in 3D Controlled Environments
Student(s): Walikadage Boteju, Abhranil Biswas, Zachary Weinstein, Zhuoran Wang, Naresh Eedugurala, Bosky Parikh, Dilini Singappuli, Pranjali Naik, Younghun Park, Andrew Kendell, Juan Manzano

RECENT PROGRESS

(1) Quantitative control of local polarity regulates catalytic activity at liquid-solid interfaces. The capacity of surface organic moieties to affect local environments and induce solvent-like effects on interfacial catalytic sites was investigated.[1] A series of organic groups including phenyl-, cyano-, mercapto-, and methoxy- substituted alkylsilanes were produced on the pore surfaces of

mesoporous silica nanoparticles (MSN). Adsorption of the solvatochromic dye Prodan onto the functionalized MSN followed by fluorescence spectroscopy analysis of their aqueous suspensions indicated differences in the local solvation environments of the dye, which correlated with the DFT-calculated dipole moments of the organic groups. Linear correlations between the Stokes shifts of the free dye in different solvents and their relative polarities were used to assign polarity values to the functionalized pores. The dependence of local polarity on the type and surface density of the organic groups was further confirmed by similar measurements of Nile Red fluorescence intensities and of vibronic band structure of pyrene adsorbed at the interface. The changes in Stokes shifts, fluorescence intensities and band structures as a function of surface functionality indicated that the dielectric properties at the interfaces are distinct from that of the bulk solvent. The precise control of interfacial polarity provided means to systematically control the catalytic activity of TEMPO for the aerobic oxidation of furfuryl alcohol in water, enabling rational optimization of catalytic conditions. An inverse relationship was found between interfacial mesopore polarity and catalytic activity of adsorbed TEMPO, demonstrating that the local polarity around a confined active site influences its catalytic behavior. Remarkably, the catalytic activity of TEMPO adsorbed inside hydrophobic mesopores of water-suspended MSN is much higher than its performance as a homogeneous catalyst in water or in heptane. These quantitative relationships between surface functionalization and interfacial polarity should provide new insights into previous and future studies of chemical processes at interfaces.

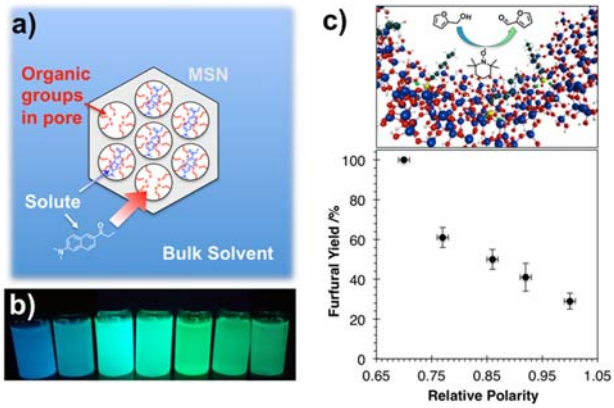

Figure 1. a) Local polarity at the interface of organofunctionalized mesoporous silica nanoparticles with bulk water probed by fluorescence spectroscopy of the solvatochromic dye Prodan. b) Surface groups with different dipole moments give rise to different fluorescent response indicating variations in the effective dielectric properties at the interface, and c) control the catalytic activity of TEMPO for the oxidation of furfuryl alcohol inside of the pores.

(2) Ceria-based multifunctional catalyst for synergistic hydrolysis/hydrogenation of lignin models. Reaction of ceria surface with sub-monolayer equivalents of trimethylphosphate followed by thermal treatment led to formation of surface orthophosphates without loss of ceria fluorite structure as indicated by ^{31}P SS-NMR, XRD and XPS.[2] Introduction of phosphates on the ceria surface generated Brønsted acidic sites at the expense of the Lewis sites as determined by NH_3 TPD, pyridine adsorption DRIFTS, and zeta titration.

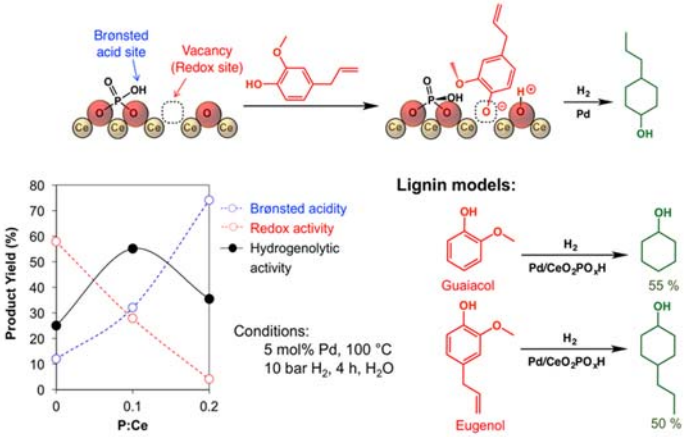

Figure 2. Multifunctional phosphate-modified ceria as a support for Pd catalyst. Controlling the phosphate density on the material allows regulating and enhancing hydrogenolysis of lignin models.

Hydrolytic and redox activities of materials modified with different amounts of surface phosphate were measured by the catalytic hydrolysis of propylene oxide and the photocatalytic degradation of indigo carmine, respectively. These studies allowed establishing structure-activity relationships between surface density of phosphate groups and catalytic performance. Following deposition of Pd catalyst, the multifunctional material demonstrated enhanced activity for the hydrogenolysis of eugenol and guaiacol compared to Pd on phosphate-free support. This enhancement was attributed to cooperativity between Lewis sites that activate eugenol for dearomatization, and redox and Brønsted sites that catalyze hydrogenolysis. Tuning the ratio of phosphate to surface ceria atoms allowed controlling product distribution for the overall conversion. Further studies exploring derivatized organophosphates and phosphonates will likely uncover new possibilities for introducing additional functionalities to the surface of ceria, and therefore produce more advanced hierarchical multicatalytic materials.

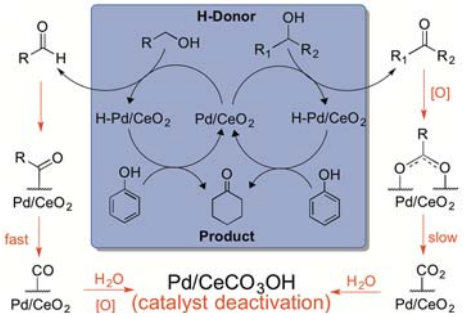

Scheme 1. Possible pathways of Pd/CeO_2 deactivation upon reaction with alcohols.

(3) Mechanistic studies of Pd/CeO_2 catalyst deactivation by reaction with alcohols. The behavior of palladium supported on ceria (Pd/CeO_2) was studied during liquid flow transfer hydrogenation using primary and secondary alcohols as hydrogen donors.[3] Use of primary alcohols led to catalyst deactivation and was concurrent with reduction of the support to cerium hydroxy carbonate. In contrast, no cerium hydroxy carbonate was observed during the same time period using secondary alcohols as hydrogen donors, and the catalyst was stable upon prolonged reaction. Catalyst regeneration through oxidation/reduction sequences succeeded in removing the hydroxy carbonate phase but did not restore initial activity levels, likely due to irreversible catalyst restructuring. A deactivation mechanism involving C-C scission of acyl and carboxylate intermediates was proposed.

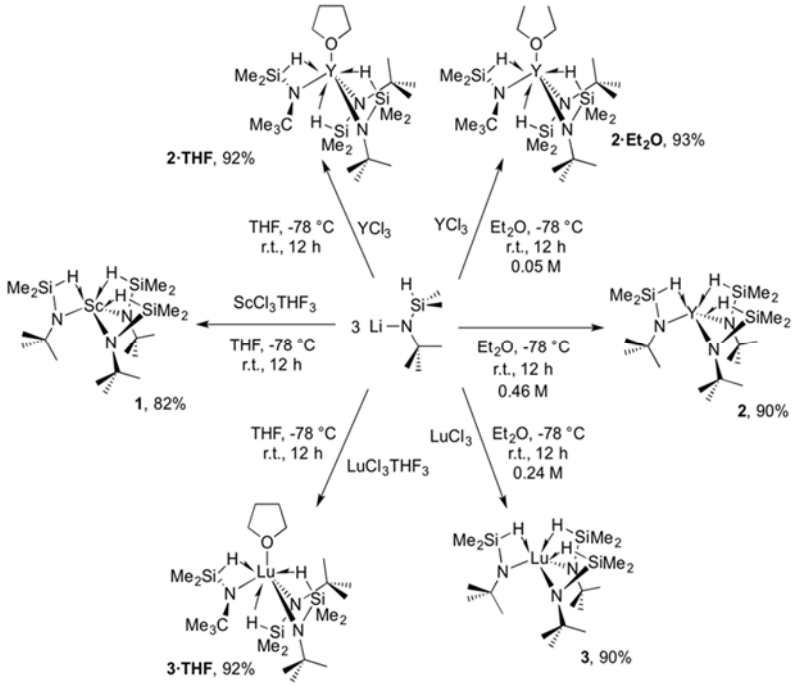

Scheme 2. Synthesis of $Ln\{N(SiHMe_2)tBu\}_3$ (Ln = Sc, Y, Lu) and solvent adducts.

(4) Rare earth silazido compounds for interfacial catalysis. A series of homoleptic rare earth silazido compounds of the type $Ln\{N(SiHMe_2)tBu\}_3$ and their mesoporous silica-grafted derivatives were prepared to compare spectroscopic characteristics of soluble and grafted species, as well as to compare catalytic features of a desymmetrization and hydroamination reaction under homogeneous and interfacial conditions. Previously, we had observed that the diastereoselectivity in a

zirconium-catalyzed desymmetrization of aminodialkenes was sensitive to the concentration of the aminodialkene substrate, as well as the reaction temperature and the substrate's isotopic substitution (NH vs ND).[4] We sought to determine if similar effects might be observed in rare-earth catalyzed hydroamination/desymmetrizations because rare earth systems are often much more active than zirconium-based catalysts, and then to use comparison between related homogeneous and heterogeneous catalyst to study changes at the catalytic interface.

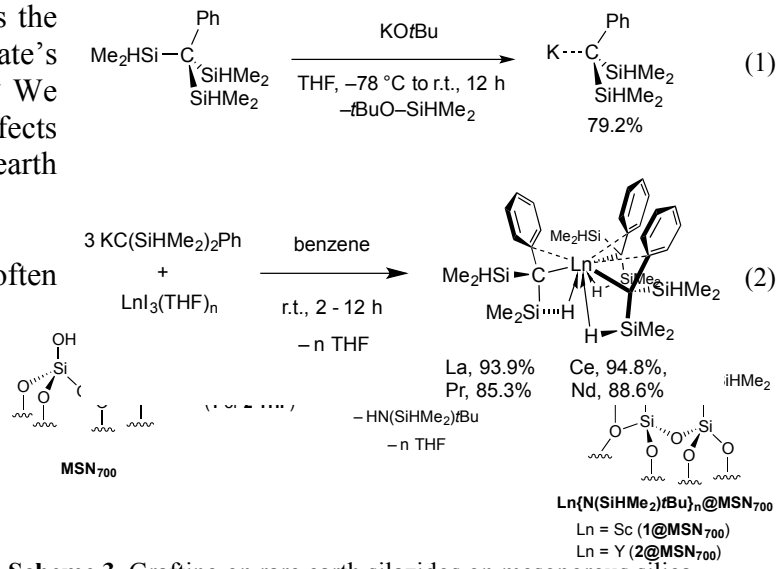

Scheme 3. Grafting on rare earth silazidos on mesoporous silica.

Trivalent tris(silazido) compounds Ln{N(SiHMe$_2$)*t*Bu}$_3$ (Ln = Sc (**1**), Y (**2**), Lu (**3**)) are prepared in high yield by salt metathesis reactions.[5] Solution-phase and solid-state characterization of **1-3** by NMR and IR spectroscopy and X-ray diffraction reveals secondary Ln⋯H–Si interactions. These features are retained in solvent coordinated **2·Et$_2$O**, **2·THF**, and **3·THF**. The change in spectroscopic features characterizing the secondary interactions (ν_{SiH}, $^1J_{SiH}$) from the unactivated SiH in the silazane HN(SiHMe$_2$)*t*Bu follows the trend **3** > **2** > **1** ~ **2·Et$_2$O** > **2·THF** ~ **3·THF**. Ligand lability follows the same pattern, with Et$_2$O readily dissociating from **2·Et$_2$O** while THF being displaced only during surface grafting reactions. **1** and **2·THF** graft onto mesoporous silica nanoparticles (MSN) to give Ln{N(SiHMe$_2$)*t*Bu}$_n$@MSN (Ln = Sc (**1@MSN**), Y (**2@MSN**)) along with THF and protonated silazido as HN(SiHMe$_2$)*t*Bu and H$_2$N*t*Bu. The surface species are characterized by multinuclear, multidimensional solid-state (SS)NMR spectroscopic techniques, as well as diffuse reflectance FTIR, elemental analysis, and reaction stoichiometry. A key $^1J_{SiH}$ SSNMR measurement reveals that the grafted sites most closely resemble Ln·THF adducts, suggesting that siloxane coordination occurs in grafted compounds and that its donor ability is comparable to THF. These species catalyze the hydroamination/bicyclization of aminodialkenes, and both solution-phase and interfacial conditions provide the bicyclized product with equivalent cis:trans ratios. Similar diastereoselectivity mediated by catalytic sites under the two conditions suggests similar effective environments for the catalytic sites.

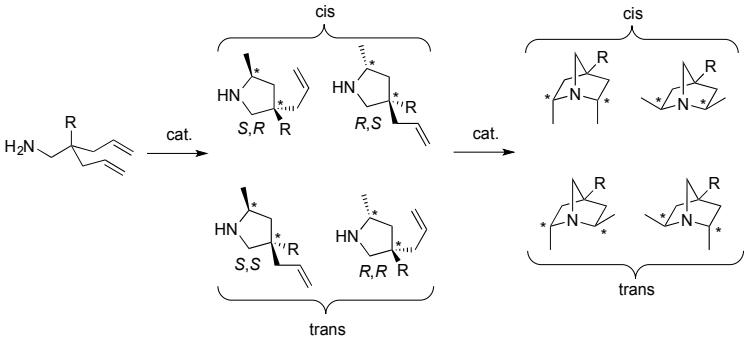

Scheme 4. Hydroamination/desymmetrization of aminodialkenes.

(5) Synthesis of homoleptic organolanthanides supported by a combined dimethylsilyl and benzyl ligand. Homoleptic rare earth organometallic compounds (containing only one type of

ligand) are precursors to heteroleptic catalysts or are precatalysts in their own right. However, synthesis of homoleptic organolanthanides is challenging, particular of the larger early lanthanides (La, Ce, Pr, Nd) for which relatively few compounds are readily accessible and none are reliably employed as catalytic precursors. The typical alkyl ligands are either benzylic type species, or a trimethylsilylmethyl derivative, and both functionalities are observed to provide stabilization of complexes through secondary interactions. We sought to combine these functionalities into a single alkyl ligand – $C(SiHMe_2)_2Ph$ and synthesize homoleptic early lanthanide compounds containing that ligand. The $KC(SiHMe_2)_2Ph$ synthon is readily synthesized by reaction of $PhC(SiHMe_2)_3$ and KO*t*Bu, and $Ln\{C(SiHMe_2)_2Ph\}_3$ (Ln = La, Ce, Pr, Nd) are easily prepared in high yield.[6]

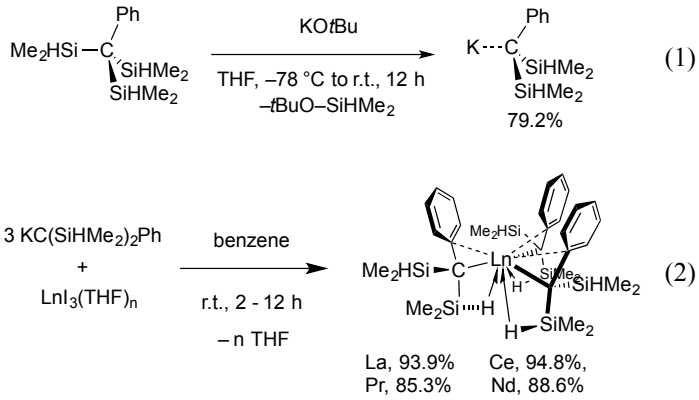

(6) Characterization of Catalytic Materials by DNP-Enhanced Solid-State NMR. Dynamic nuclear polarization (DNP) is uniquely suited for the studies of catalytic systems, because it can efficiently or even selectively sensitize surfaces and interfaces, enabling measurements that are off-limits to conventional solid-state (SS)NMR. Indeed, since its introduction to surface science a few years ago, DNP has revolutionized SSNMR spectroscopy of catalytic systems by offering signal enhancements of 2 orders of magnitude and savings in experimental time of up to *4-5 orders of magnitude*. We reported several discoveries enabled by the recently installed 400 MHz DNP NMR spectrometer funded by DOE Basic Energy Sciences.

Spatial distribution of organic functional groups. SSNMR spectroscopy, both conventional and DNP-enhanced, was used to elucidate, for the first time, the distributions of functional groups attached to the surfaces of MCM-41-type mesoporous silica materials by post-synthesis grafting and by co-condensation. The most revealing information was provided by DNP-enhanced 2D ^{29}Si-^{29}Si correlation measurements (Figure 3), which unambiguously showed that (1) grafting yielded more homogeneous distributions of propyl and mercaptopropyl functionalities on the external and internal surfaces, regardless of the loading or the method used to remove the surfactant, (2) co-condensation produced a significant fraction of clustered organic moieties, partly embedded into the silica walls, and (3) the most efficient, homogeneous grafting was achieved when the surfactant partly occupied the pores.[7] These insights are attributable to the 80-fold signal enhancement by DNP, which enabled ^{29}Si-^{29}Si correlation measurements at natural abundance. Further advances in

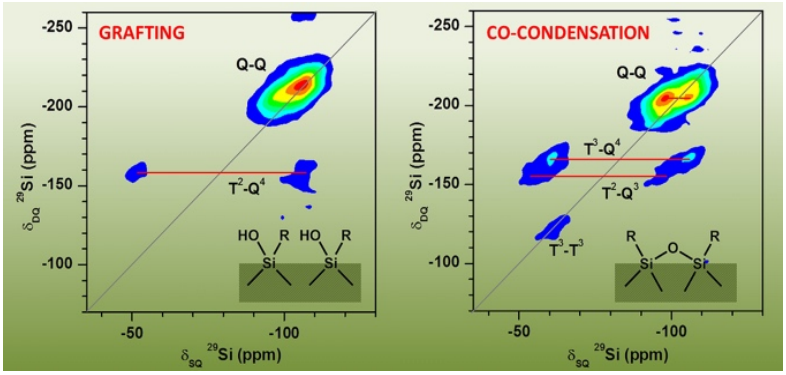

Figure 3. DNP ^{29}Si-^{29}Si correlation spectra reveal the spatial distribution of functional groups deployed on silica.

DNP will allow a more precise analysis of the T sites distribution and clustering. Such methods can be applied to optimize the reaction conditions for synthesis of other silica-based materials and refine the strategies for controlling their chemical topology. These studies will include the co-condensation conditions (e.g., the role of simultaneous vs sequential addition of TEOS and organosilanes), grafting conditions (e.g., kinetics as a function of temperature or concentration), silylative passivation of selective surfaces, functionalization with cooperative catalysts and creation of functional domains.

Structural origins of surface acidity. Heterogeneous Brønsted acid catalysts are important in industry, particularly in catalytic cracking processes. We demonstrated that these Brønsted acid sites can be directly observed at natural abundance by DNP-enhanced ^{17}O SSNMR spectroscopy.[8, 23] In addition, the O-H distances can be measured with a sub-picometer precision by natural abundance ^{17}O DNP NMR to enable a direct structural gauge of the lability of protons in a given material, which is correlated with the material's pH of zero point of charge. The length of the O–H bond correlated directly with the surface acidity, thus confirming a long-standing belief in catalysis. Experiments performed on materials impregnated with pyridine also allowed for the direct detection of intermolecular hydrogen bonding interactions through the lengthening of O−H bonds.

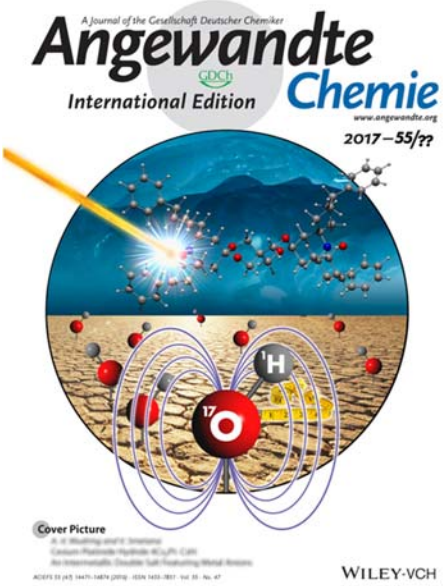

Studies of interfacial sites on the surface of γ-Al_2O_3. We have shown that elusive interfacial sites at the surface of γ-Al_2O_3 can be scrutinized by DNP-enhanced $^{13}C\{^{27}Al\}$ RESPDOR experiments.[24] Specifically, we determined the intermolecular interactions between a protective PVA coating with natural ^{13}C abundance and the surface of a Pd/γ-Al_2O_3 catalyst. Furthermore, we discovered that methionine, a commonly encountered inhibitor of reduced metal catalysts, binds to interfacial Pd sites and is stabilized by coordinating to Al_2O_3 through its carbonyl group, as determined by DNP-enhanced 2D ^{13}C-^{13}C spectra.[25] This important new methodology can be broadly applied to measure coordination geometries and conformations of dilute organic species at alumina surfaces, and to establish structure-activity relationships in other industrially-relevant heterogeneous catalyst systems.

SSNMR studies of other catalytic systems. Conventional and DNP SSNMR enabled studies of several challenging catalytic systems and reactions. (1) We used $^{1}H\{^{13}C\}$ and $^{1}H\{^{29}Si\}$ idHETCOR, 2D *J*-resolved ^{29}Si SSNMR, as well as DNP-enhanced ^{15}N and ^{89}Y spectra to determine the structures of surface-bound tris(silazido) rare earth compounds, such as $Y\{N(SiHMe_2)tBu\}_3$.[5] (2) 2D ^{31}P-^{31}P DQMAS and $^{31}P\{^{1}H\}$ HETCOR spectra were used to identify the surface species on phosphate modified ceria.[2] (4) DNP-enhanced 2D ^{29}Si-^{29}Si correlation spectra were used to provide direct evidence of the formation mechanism of isolated SiO_x surface species in SiO_x/Al_2O_3. In contrast to previous reports, we showed that with the use of appropriate post-treatment conditions both CLD and ALD grafting methods can generate isolated Brønsted-acidic silanols.[26] (5) We demonstrated that DNP enables acquisition of 2D ^{13}C-^{13}C measurements on natural abundance samples of lignocellulosic biomass. The technique was applied to achieve

atomic-scale understanding of the industrially important catalytic depolymerization of lignin.[27] (6) DNP-enhanced wideline spectra were measured for the first time, and used to determine the coordination of atomic Pt species within the pores of metal organic frameworks (MOFs).[28] We developed a method for detection of 'infinite-speed' MAS SSNMR spectra of heavy spin-1/2 nuclides, and applied it to measure the first isotropic spectra of ^{195}Pt in MOFs and other solids.[29]

Publications Acknowledging this Grant in 2014-2017

Source of support for the work published:

(I) *Exclusively funded by this grant*

1. Singappuli-Arachchige, D.; Manzano, J. S.; Sherman, L. M.; Slowing, I. I., Polarity Control at Interfaces: Quantifying Pseudo-solvent Effects in Nano-confined Systems. *ChemPhysChem* **2016,** *17*, 2982-2986. http://dx.doi.org/10.1002/cphc.201600740
2. Nelson, N. C.; Wang, Z.; Naik, P.; Manzano, J. S.; Pruski, M.; Slowing, I. I., Phosphate modified ceria as a Bronsted acidic/redox multifunctional catalyst. *J. Mater. Chem. A* **2017,** *5*, 4455-4466. http://dx.doi.org/10.1039/C6TA08703E
3. Nelson, N. C.; Manzano, J. S.; Slowing, I. I., Deactivation of Ceria Supported Palladium through C–C Scission during Transfer Hydrogenation of Phenol with Alcohols. *J. Phys. Chem. C* **2016,** *120*, 28067-28073. http://dx.doi.org/10.1021/acs.jpcc.6b09828
4. Manna, K.; Eedugurala, N.; Sadow, A. D., Zirconium-Catalyzed Desymmetrization of Aminodialkenes and Aminodialkynes through Enantioselective Hydroamination. *J. Am. Chem. Soc.* **2015,** *137*, 425-435. http://dx.doi.org/10.1021/ja511250m
5. Eedugurala, N.; Wang, Z.; Yan, K.; Boteju, K. C.; Chaudhary, U.; Kobayashi, T.; Ellern, A.; Slowing, I. I.; Pruski, M.; Sadow, A. D., β-SiH-Containing Tris(silazido) Rare-Earth Complexes as Homogeneous and Grafted Single-Site Catalyst Precursors for Hydroamination. *Organometallics* **2017,** *36*, 1142-1153. http://dx.doi.org/10.1021/acs.organomet.6b00956
6. Boteju, K. C.; Ellern, A.; Sadow, A. D., Homoleptic organolanthanide compounds supported by the bis(dimethylsilyl)benzyl ligand. *Chem. Commun.* **2017,** *53*, 716-719. http://dx.doi.org/10.1039/C6CC09304C
7. Kobayashi, T.; Singappuli-Arachchige, D.; Wang, Z.; Slowing, I. I.; Pruski, M., Spatial distribution of organic functional groups supported on mesoporous silica nanoparticles: a study by conventional and DNP-enhanced ^{29}Si solid-state NMR. *Phys. Chem. Chem. Phys.* **2017,** *19*, 1781-1789. http://dx.doi.org/10.1039/C6CP07642D
8. Perras, F. A.; Wang, Z.; Naik, P.; Slowing, I. I.; Pruski, M., Natural Abundance 17O DNP NMR Provides Precise O−H Distances and Insights into the Brønsted Acidity of Heterogeneous Catalysts. *Angew. Chem. Int. Ed.* **2017**, *In Press*. http://dx.doi.org/10.1002/anie.201704032
9. Eedugurala, N.; Hovey, M.; Ho, H.-A.; Jana, B.; Lampland, N. L.; Ellern, A.; Sadow, A. D., Cyclopentadienyl-bis(oxazoline) Magnesium and Zirconium Complexes in Aminoalkene Hydroaminations. *Organometallics* **2015,** *34*, 5566-5575. http://dx.doi.org/10.1021/acs.organomet.5b00771

10. Althaus, S. M.; Mao, K. M.; Stringer, J. A.; Kobayashi, T.; Pruski, M., Indirectly detected heteronuclear correlation solid-state NMR spectroscopy of naturally abundant N-15 nuclei. *Solid State Nucl. Magn. Reson.* **2014,** *57-58*, 17-21. http://dx.doi.org/10.1016/j.ssnmr.2013.11.001

11. Bataineh, H.; Pestovsky, O.; Bakac, A., Iron(II) Catalysis in Oxidation of Hydrocarbons with Ozone in Acetonitrile. *ACS Catal.* **2015,** *5*, 1629-1637. http://dx.doi.org/10.1021/cs501962m

12. Eedugurala, N.; Wang, Z.; Chaudhary, U.; Nelson, N.; Kandel, K.; Kobayashi, T.; Slowing, I. I.; Pruski, M.; Sadow, A. D., Mesoporous Silica-Supported Amidozirconium-Catalyzed Carbonyl Hydroboration. *ACS Catal.* **2015,** *5*, 7399-7414. http://dx.doi.org/10.1021/acscatal.5b01671

13. Kandel, K.; Chaudhary, U.; Nelson, N. C.; Slowing, I. I., Synergistic Interaction between Oxides of Copper and Iron for Production of Fatty Alcohols from Fatty Acids. *ACS Catal.* **2015,** *5*, 6719-6723. http://dx.doi.org/10.1021/acscatal.5b01664

14. Nelson, N.; Chaudhary, U.; Kandel, K.; Slowing, I., Heterogeneous Multicatalytic System for Single-Pot Oxidation and C–C Coupling Reaction Sequences. *Top. Catal.* **2014,** *57*, 1000-1006. http://dx.doi.org/10.1007/s11244-014-0263-y

15. Carraher, J. M.; Bakac, A., Generation of free oxygen atoms O(P-3) in solution by photolysis of 4-benzoylpyridine N-oxide. *Phys. Chem. Chem. Phys.* **2014,** *16*, 19429-19436. http://dx.doi.org/10.1039/c4cp02751e

16. Kandel, K.; Anderegg, J. W.; Nelson, N. C.; Chaudhary, U.; Slowing, I. I., Supported iron nanoparticles for the hydrodeoxygenation of microalgal oil to green diesel. *J. Catal.* **2014,** *314*, 142-148. http://dx.doi.org/10.1016/j.jcat.2014.04.009

17. Carraher, J. M.; Ellern, A.; Bakac, A., Preparation and reactivity of macrocyclic rhodium(III) alkyl complexes. *Inorg. Chim. Acta* **2014,** *409*, 254-258. http://dx.doi.org/10.1016/j.ica.2013.09.022

18. Xu, S. C.; Manna, K.; Ellern, A.; Sadow, A. D., Mixed N-Heterocyclic Carbene-Bis(oxazolinyl)borato Rhodium and Iridium Complexes in Photochemical and Thermal Oxidative Addition Reactions. *Organometallics* **2014,** *33*, 6840-6860. http://dx.doi.org/10.1021/om500891h

19. Xu, S.; Magoon, Y.; Reinig, R. R.; Schmidt, B. M.; Ellern, A.; Sadow, A. D., Organometallic Complexes of Bulky, Optically Active, C_3-Symmetric Tris(4S-isopropyl-5,5-dimethyl-2-oxazolinyl)phenylborate (To^{P}*). *Organometallics* **2015,** *34*, 3508-3519. http://dx.doi.org/10.1021/acs.organomet.5b00225

20. Nishiyama, Y.; Kobayashi, T.; Malon, M.; Singappuli-Arachchige, D.; Slowing, I. I.; Pruski, M., Studies of minute quantities of natural abundance molecules using 2D heteronuclear correlation spectroscopy under 100 kHz MAS. *Solid State Nucl. Magn. Reson.* **2015,** *66-67*, 56-61. http://dx.doi.org/10.1016/j.ssnmr.2015.02.001

21. Wang, C. J.; Ackerman, D. M.; Slowing, I. I.; Evans, J. W., Langevin and Fokker-Planck Analyses of Inhibited Molecular Passing Processes Controlling Transport and Reactivity in Nanoporous Materials. *Phys. Rev. Lett.* **2014,** *113*, 038301. http://dx.doi.org/10.1103/PhysRevLett.113.038301

22. Wang, J.; Garcia, A.; Ackerman, D. M.; Gordon, M. S.; Slowing, I. I.; Kobayashi, T.; Pruski, M.; Evans, J. W., Multi-functionalization of nanoporous catalytic materials to enhance reaction yield: Statistical mechanical modeling for conversion reactions with restricted diffusive transport. *MRS Proceedings* **2014,** *1641*. http://dx.doi.org/10.1557/opl.2014.321

(II) *Jointly funded by this grant and other grants leading intellectual contribution from this grant*

23. Perras, F. A.; Chaudhary, U.; Slowing, I. I.; Pruski, M., Probing Surface Hydrogen Bonding and Dynamics by Natural Abundance, Multidimensional, ^{17}O DNP-NMR Spectroscopy. *J. Phys. Chem. C* **2016,** *120* (21), 11535-11544. http://dx.doi.org/10.1021/acs.jpcc.6b02579

24. Johnson, R. L.; Perras, F. A.; Kobayashi, T.; Schwartz, T. J.; Dumesic, J. A.; Shanks, B. H.; Pruski, M., Identifying low-coverage surface species on supported noble metal nanoparticle catalysts by DNP-NMR. *Chem. Commun.* **2016,** *52*, 1859-1862. http://dx.doi.org/10.1039/C5CC06788J

25. Perras, F. A.; Padmos, J. D.; Johnson, R. L.; Wang, L.-L.; Schwartz, T. J.; Kobayashi, T.; Horton, J. H.; Dumesic, J. A.; Shanks, B. H.; Johnson, D. D.; Pruski, M., Characterizing Substrate–Surface Interactions on Alumina-Supported Metal Catalysts by Dynamic Nuclear Polarization-Enhanced Double-Resonance NMR Spectroscopy. *J. Am. Chem. Soc.* **2017,** *139*, 2702-2709. http://dx.doi.org/10.1021/jacs.6b11408

26. Mouat, A. R.; Kobayashi, T.; Pruski, M.; Marks, T. J.; Stair, P. C., Direct Spectroscopic Evidence for Isolated Silanols in SiO_x/Al_2O_3 and Their Formation Mechanism. *J. Phys. Chem. C* **2017,** *121*, 6060-6064. http://dx.doi.org/10.1021/acs.jpcc.6b11196

27. Perras, F. A.; Luo, H.; Zhang, X.; Mosier, N. S.; Pruski, M.; Abu-Omar, M. M., Atomic-Level Structure Characterization of Biomass Pre- and Post-Lignin Treatment by Dynamic Nuclear Polarization-Enhanced Solid-State NMR. *J. Phys. Chem. A* **2017,** *121*, 623-630. http://dx.doi.org/10.1021/acs.jpca.6b11121

28. Kobayashi, T.; Perras, F. A.; Goh, T. W.; Metz, T. L.; Huang, W.; Pruski, M., DNP-Enhanced Ultrawideline Solid-State NMR Spectroscopy: Studies of Platinum in Metal–Organic Frameworks. *J. Phys. Chem. Lett.* **2016,** *7*, 2322-2327. http://dx.doi.org/10.1021/acs.jpclett.6b00860

29. Perras, F. A.; Venkatesh, A.; Hanrahan, M. P.; Goh, T. W.; Huang, W.; Rossini, A. J.; Pruski, M., Indirect detection of infinite-speed MAS solid-state NMR spectra. *J. Magn. Reson.* **2017,** *276*, 95-102. http://dx.doi.org/ 10.1016/j.jmr.2017.01.010

30. Webb, J. D.; Seki, T.; Goldston, J. F.; Pruski, M.; Crudden, C. M., Selective functionalization of the mesopores of SBA-15. *Microporous Mesoporous Mater.* **2015,** *203*, 123-131. http://dx.doi.org/10.1016/j.micromeso.2014.10.032

31. Perras, F. A.; Kobayashi, T.; Pruski, M., Magnetic resonance imaging of DNP enhancements in a rotor spinning at the magic angle. *J. Magn. Reson.* **2016,** *264*, 125-130. http://dx.doi.org/10.1016/j.jmr.2016.01.004

32. Perras, F. A.; Kobayashi, T.; Pruski, M., Natural Abundance ^{17}O DNP Two-Dimensional and Surface-Enhanced NMR Spectroscopy. *J. Am. Chem. Soc.* **2015,** *137*, 8336-8339. http://dx.doi.org/10.1021/jacs.5b03905

33. Perras, F. A.; Kobayashi, T.; Pruski, M., PRESTO polarization transfer to quadrupolar nuclei: implications for dynamic nuclear polarization. *Phys. Chem. Chem. Phys.* **2015,** *17*, 22616-22622. http://dx.doi.org/10.1039/C5CP04145G

34. Kobayashi, T.; Perras, F. A.; Slowing, I. I.; Sadow, A. D.; Pruski, M., Dynamic Nuclear Polarization Solid-State NMR in Heterogeneous Catalysis Research. *ACS Catal.* **2015,** *5*, 7055-7062. http://dx.doi.org/10.1021/acscatal.5b02039

35. Hull, E. A.; West, A. C.; Pestovsky, O.; Kristian, K. E.; Ellern, A.; Dunne, J. F.; Carraher, J. M.; Bakac, A.; Windus, T. L., UV-visible spectroscopy of macrocyclic alkyl, nitrosyl and halide complexes of cobalt and rhodium. Experiment and calculation. *Dalton Trans.* **2015,** *44*, 3811-3816. http://dx.doi.org/10.1039/C4DT03143A

36. Xu, S.; Boschen, J. S.; Biswas, A.; Kobayashi, T.; Pruski, M.; Windus, T. L.; Sadow, A. D., Mild partial deoxygenation of esters catalyzed by an oxazolinylborate-coordinated rhodium silylene. *Dalton Trans.* **2015,** *44*, 15897-15904. http://dx.doi.org/10.1039/C5DT02844B

37. Reichert, M. D.; Lin, C. C.; Vela, J., How Robust are Semiconductor Nanorods? Investigating the Stability and Chemical Decomposition Pathways of Photoactive Nanocrystals. *Chem. Mater.* **2014,** *26*, 3900-3908. http://dx.doi.org/10.1021/cm500896n

38. Alvarado, S. R.; Guo, Y. J.; Ruberu, T. P. A.; Tavasoli, E.; Vela, J., Inorganic chemistry solutions to semiconductor nanocrystal problems. *Coord. Chem. Rev.* **2014,** *263*, 182-196. http://dx.doi.org/10.1016/j.ccr.2013.09.001

39. Xu, S.; Everett, W. C.; Ellern, A.; Windus, T. L.; Sadow, A. D., Oxygen insertion reactions of mixed N-heterocyclic carbene-oxazolinylborato zinc alkyl complexes. *Dalton Trans.* **2014,** *43*, 14368-14376. http://dx.doi.org/10.1039/C4DT01011F

40. Reinig, R. R.; Mukherjee, D.; Weinstein, Z. B.; Xie, W.; Albright, T.; Baird, B.; Gray, T. S.; Ellern, A.; Miller, G. J.; Winter, A. H.; Bud'ko, S. L.; Sadow, A. D., Synthesis and Oxidation Catalysis of [Tris(oxazolinyl)borato]cobalt(II) Scorpionates. *Eur. J. Inorg. Chem.* **2016**, 2486-2494. http://dx.doi.org/10.1002/ejic.201600237

41. Perras, F. A.; Reinig, R. R.; Slowing, I. I.; Sadow, A. D.; Pruski, M., Effects of biradical deuteration on the performance of DNP: towards better performing polarizing agents. *Phys. Chem. Chem. Phys.* **2016,** *18*, 65-69. http://dx.doi.org/10.1039/C5CP06505D

42. Kobayashi, T.; Nishiyama, Y.; Pruski, M., Heteronuclear Correlation SSNMR Spectroscopy with Indirect Detection under Fast Magic Angle Spinning. In *Modern Methods in Solid-State NMR*, RSC Press: 2017.

43. Nelson, N. C.; Boote, B. W.; Naik, P.; Rossini, A. J.; Smith, E. A.; Slowing, I. I., Transfer hydrogenation over sodium-modified ceria: Enrichment of redox sites active for alcohol dehydrogenation. *J. Catal.* **2017,** *346*, 180-187. http://dx.doi.org/ 10.1016/j.jcat.2016.12.018

44. Guo, Z. Y.; Kobayashi, T.; Wang, L. L.; Goh, T. W.; Xiao, C. X.; Caporini, M. A.; Rosay, M.; Johnson, D. D.; Pruski, M.; Huang, W. Y., Selective Host-Guest Interaction between Metal Ions and Metal-Organic Frameworks Using Dynamic Nuclear Polarization Enhanced Solid-State NMR Spectroscopy. *Chem. Eur. J.* **2014,** *20*, 16308-16313. http://dx.doi.org/10.1002/chem.201403884

(III) *Jointly funded by this grant and other grants with relatively minor intellectual contribution from this grant*

45. de Lima Batista, A. P.; Zahariev, F.; Slowing, I. I.; Braga, A. A. C.; Ornellas, F. R.; Gordon, M. S., Silanol-Assisted Carbinolamine Formation in an Amine-Functionalized Mesoporous Silica Surface: Theoretical Investigation by Fragmentation Methods. *J. Phys. Chem. B* **2016,** *120*, 1660-1669. http://dx.doi.org/10.1021/acs.jpcb.5b08446

46. Gu, W.; Stalzer, M. M.; Nicholas, C. P.; Bhattacharyya, A.; Motta, A.; Gallagher, J. R.; Zhang, G.; Miller, J. T.; Kobayashi, T.; Pruski, M.; Delferro, M.; Marks, T. J., Benzene Selectivity in Competitive Arene Hydrogenation: Effects of Single-Site Catalyst···Acidic Oxide Surface Binding Geometry. *J. Am. Chem. Soc.* **2015,** *137*, 6770-6780. http://dx.doi.org/10.1021/jacs.5b03254

47. Mouat, A. R.; George, C.; Kobayashi, T.; Pruski, M.; van Duyne, R. P.; Marks, T. J.; Stair, P. C., Highly Dispersed SiOx/Al2O3 Catalysts Illuminate the Reactivity of Isolated Silanol Sites. *Angew. Chem. Int. Ed.* **2015,** *54*, 13346-13351. http://dx.doi.org/10.1002/anie.201505452

48. Opembe, N. N.; Guild, C.; King'ondu, C.; Nelson, N. C.; Slowing, I. I.; Suib, S. L., Vapor-Phase Oxidation of Benzyl Alcohol Using Manganese Oxide Octahedral Molecular Sieves (OMS-2). *Ind. Eng. Chem. Res.* **2014,** *53*, 19044-19051. http://dx.doi.org/10.1021/ie5024639

49. Mudring, A. V.; Alammar, T.; Slowing, I.; Anderegg, J., Ionic Liquid-Assisted Microwave Synthesis of Solid Solutions of Perovskite Sr1-xBaxSnO3 for Photocatalytic Applications. *ChemSusChem*, **2017**, *In Press*. http://dx.doi.org/10.1002/cssc.201700615

50. Dairo, T. O.; Nelson, N. C.; Slowing, I. I.; Angelici, R. J.; Woo, L. K., Aerobic Oxidation of Cyclic Amines to Lactams Catalyzed by Ceria-Supported Nanogold. *Catal. Lett.* **2016,** *146*, 2278-2291. http://dx.doi.org/ 10.1007/s10562-016-1834-2

51. Egner, T.K.; Naik, P.; Nelson, N. C.; Slowing, I. I.; Venditti, V., Mechanistic Insights into Nanoparticle Surface Adsorption by Solution NMR Spectroscopy in an Aqueous Gel. *Angew. Chem. Int. Ed.,* **2017,** *Accepted.*

Cooperativity between Copper(II) and Redox-Active Organic Cocatalysts for Aerobic Alcohol Oxidation: Mechanistic Comparison of Cu/Nitroxyl- and Cu/Azodicarboxylate Catalysts

Shannon S. Stahl
Department of Chemistry, University of Wisconsin - Madison

Cooperative catalysis between Cu^{II} and redox-active organic cocatalysts is a key feature of important chemical and enzymatic aerobic oxidation reactions, such as alcohol oxidation mediated by Cu/TEMPO (TEMPO = 2,2,6,6-tetramethylpiperidine-*N*-oxyl) and galactose oxidase. Nearly twenty years ago, Markó and coworkers reported that azodicarboxylates, such as di-*tert*-butyl azodicarboxylate (DBAD), are effective redox-active cocatalysts in Cu-catalyzed aerobic alcohol oxidation reactions, but the nature of the cooperativity between Cu and azodicarboxylates was not well defined. Both Cu/nitroxyl- and Cu/DBAD-catalyzed aerobic alcohol oxidation have been proposed to involve C–H bond cleavage through hydride transfer from a Cu–alkoxide to the coordinated organic cocatalyst via a six-membered-ring transition state. Mechanistic studies of these two catalyst systems, however, reveal key differences in the degree of redox cooperativity between Cu and the different cocatalysts. Most notably, the Cu/DBAD catalyst exhibits a breakdown in cooperativity arising from the two-electron reactivity of the DBAD cocatalyst. This feature limits scope and synthetic utility of Cu/DBAD relative to the corresponding Cu/nitroxyl catalyst systems.

DE-FG02-05ER15690
Copper-Catalyzed Aerobic Oxidation of O–H and N–H Bonds

Postdocs: Damian P. Hruszkewycz, Susan L. Zultanski
Student(s): Scott D. McCann, Aristidis Vasilopoulos, Kelsey C. Miles

RECENT PROGRESS

Our DOE-sponsored research has primarily focused on the development and mechanistic characterization of Cu-catalyzed aerobic oxidation reactions. A central question that has guided much of our work is, "How does a one-electron redox-active catalyst (Cu) mediate two-electron oxidations with a four-electron oxidant (O_2)?",(ref. 4) and we have observed at least three different mechanistic pathways that address this question (Fig. 1). The first is initiated by single-electron transfer (SET) from electron-rich substrates to Cu^{II}, as observed in the oxyhalogenation of arenes and heterocycles (Fig. 1A). This pathway is perhaps the one most widely associated with Cu^{II}-catalyzed and Cu^{II}-mediated

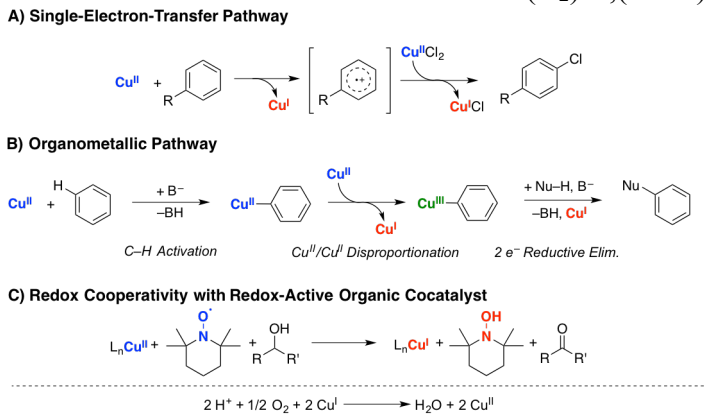

Fig. 1. Pathways for copper-catalyzed oxidation of organic substrates.

oxidation of organic molecules. A second pathway involves an organometallic mechanism. A Cu^{II}–aryl or related organometallic Cu^{II} intermediate, formed via transmetalation (e.g., from a boronic acid) or C–H activation, is oxidized by a second Cu^{II} species to generate an organocopper(III) species that can form a C–heteroatom bond via a classical two-electron reductive elimination step (Fig. 1B). The third pathway has been the focus of much of our recent work and involves redox cooperativity between Cu^{II} and a redox-active nitroxyl cocatalyst (Fig. 1C). This pathway provides the basis for highly versatile and efficient alcohol and amine oxidation reactions.(ref. 1) Collectively, these pathways show how Cu-based oxidation mechanisms can resemble, but also deviate significantly from, mechanisms typically associated with noble metals, such as Pd. For example, the organometallic C–H activation and reductive elimination steps closely resemble steps involved in Pd chemistry, whereas the one-electron steps, such as single-electron transfer and cooperativity with redox-active organic fragments, are not typically observed with Pd.

Mechanism of Cu/DBAD-Catalyzed Aerobic Alcohol Oxidation (ref. 6). In recent years, we have spent considerable time investigating the mechanism of Cu/nitroxyl catalyst systems for aerobic alcohol oxidation. In the course of this work, we became intrigued by a catalyst system developed by Istvan Markó that uses a (phen)Cu catalyst in combination with di-*tert*-butylazodicarboxylate (DBAD) as a redox-active organic cocatalyst (Fig. 2; *Science* **1996**, *274*, 2044). We were interested in understanding the similarities and/or differences between nitroxyl vs. azodicarboxylate cocatalysts in these otherwise very similar catalyst systems. In situ IR spectroscopic studies allowed us to monitor the oxidation of 1-phenylethanol, while simultaneously monitoring the cocatalyst speciation (Fig. 3). The data revealed an initial burst of product formation that quantitatively correlated with the consumption of DBAD, followed by steady-state aerobic catalytic turnover in which the hydrazine, $DBADH_2$, was present as the resting-state of the cocatalyst. Kinetic and spectroscopic studies (in situ IR, EPR) were used to analyze both the burst and steady-state phases of the reaction to determine the Cu and cocatalyst resting states and the rate law in each case. Another key observation was that (phen)Cu/DBAD-catalyzed alcohol oxidation exhibited a steady-state turnover rate two-fold faster than the rate of alcohol oxidation with (phen)Cu alone (i.e., in the absence of DBAD). These data and a series of kinetic-isotope-effect studies (incl. independent-rate measurements and competition studies) revealed that the (phen)Cu and DBAD cocatalysts do not exhibit cooperative behavior. The reaction instead proceeds via a bicyclic catalytic mechanism, shown in Fig. 4. The top cycle corresponds to a Cu-only alcohol oxidation pathway, and this cycle limits the overall turnover rate of the reaction. The bottom cycle consists of a fast Cu/DBAD pathway in which DBAD is activated by a Lewis acidic Cu species and mediates very rapid two-electron alcohol oxidation. The latter cycle accounts for the kinetic burst but is kinetically invisible during normal catalytic turnover because of its rapid rate relative to the Cu-only cycle. The two-fold rate

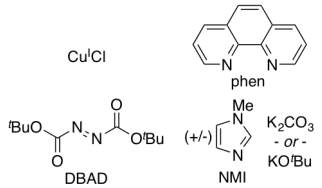

Fig. 2. Cu/DBAD catalyst system.

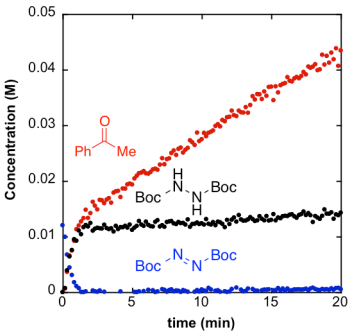

Fig. 3. Time-course data for Cu/DBAD-catalyzed aerobic 1-phenylethanol oxidation.

enhancement of Cu/DBAD- relative to Cu-only-catalyzed alcohol oxidation reflects the rapid DBAD cycle, which combines with the top Cu-only cycle to achieve oxidation of two equivalents of alcohol each time the top cycle turns over. The two cycles are connected by the aerobic reoxidation of 2 Cu^I and $DBADH_2$ (cf. the black arrows at the interface between the two cycles). The fast Cu/DBAD cycle can only take place after Cu^I activates O_2 and mediates the oxidation of $DBADH_2$ to DBAD. This result implies that an activated oxygen species is involved in the oxidation of $DBADH_2$ (e.g., a mono- or binuclear peroxo-/oxo-Cu species). These insights have important implications for the development and understanding of cooperative catalyst systems for aerobic oxidation reactions, and they raise important questions about N–H bond activation (i.e., in the oxidation of $DBADH_2$ to DBAD).

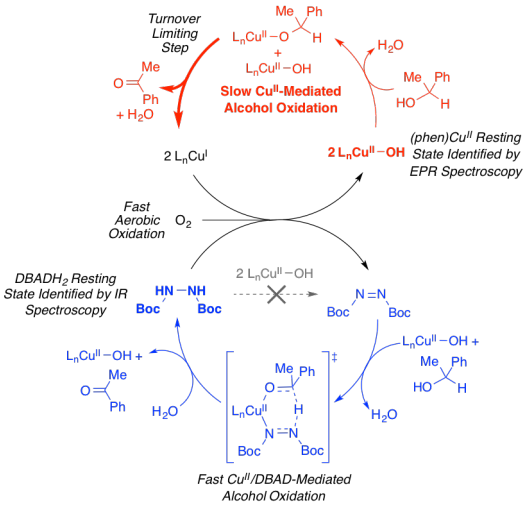

Fig. 4. Mechanism of Cu/DBAD catalyzed alcohol oxidation.

Cu- and Co-Catalyzed Oxidation of Benzylic C–H Bonds Mediated by Imidoxyl, Alkoxyl, and Sulfonimidyl Radicals (refs. 7-9) Toluene, xylenes, and ethylbenzene are some of the the largest volume platform chemicals in the commodity chemical industry, and the low cost of these molecules underlies their use as industrial solvents and components of gasoline. Moreover, liquid-phase radical-chain autoxidation reactions are amongst the largest-scale industrial oxidation reactions. Prominent examples include the Co/Mn/Br-catalyzed oxidation of *p*-xylene to terephthalic acid in variations of the Mid-Century process, autoxidation of cumene en route to phenol and acetone in the Hock process, and radical-chain autoxidation of cyclohexane to a mixture of cyclohexanone and cyclohexanol ("KA oil"). In connection with our interest in studying transition-metal/organic-radical cocatalyst systems for aerobic oxidation, we have began investigating Cu- and Co-catalyzed C–H oxidation reaction that employ co-catalytic imidoxyls (e.g., phthalimide-*N*-oxyl, PINO) or peroxide-type oxidants. This effort seeks to expand the scope of useful chemical transformations that leverage insights from the commodity-scale processes.

In one recent effort, we implemented a simple cobalt(II)-*N*-hydroxyphthalimide (NHPI) catalyst system to achieve selective conversion of benzylic methylene groups in pharmaceutically relevant (hetero)arenes to the corresponding (hetero)aryl ketones (Fig. 5). The radical reaction pathway tolerates electronically diverse benzylic C–H bonds, contrasting recent oxygenation reactions that are initiated by deprotonation of a benzylic C–H bond. The reactions proceed under practical reaction conditions (1 M substrate in BuOAc or EtOAc solvent, 12 hr, 90-100 °C), and they tolerate common heterocycles, such as pyridines and imidazoles. A cobalt-free, electrochemical, NHPI-catalyzed oxygenation method overcomes challenges encountered with chelating substrates that

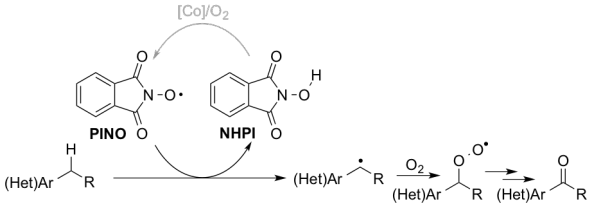

Fig. 5. Simplified mechanism depicting C–H abstraction by phthalimido-*N*-oxyl (PINO) and radical oxygenation by O_2.

inhibit the chemical reaction.

In parallel studies we have been exploring Cu-catalyzed C–H oxidation reactions inspired by the Kharasch-Sosnovsky reaction, a reaction first reported in 1958 (*J. Am. Chem. Soc.* **1958**, *80*, 756) that uses a Cu catalyst in combination with a peroxide-based oxidant (originally *t*BuOOBz) to achieve allylic oxygenation (Fig. 6A). These reactions are proposed to be initiated by abstraction of an allylic C–H bond by an alkoxy radical, followed by reaction of the carbon-centered radical with a Cu^{II}–OR species to form the C–O bond (Fig. 6C, left cycle). We speculated that benzylic arylation could be achieved via transmetalation from an arylboronic acid to the Cu^{II}–OR species within the catalytic cycle en route to an aryl(benzyl)copper species that undergoes C–C coupling (Fig. 6B and 6C, right cycle). This hypothesis has been validated, and a recent pubication (ref. 9) shows that a wide range of readily available methyl- and alkylarenes undergo arylation with diverse arylboronic esters, including heterocyclic derivatives, to afford valuable benzhydryl derivatives. While this work was in progress, Prof. Guosheng Lui (SIOC) approached us in 2015 to collaborate on a complementary C–H oxidation method that employs an N–F-based oxidant, rather than a peroxide. The reaction involves reductive activation of *N*-fluorobenzenesulfonimide (NFSI) by Cu^{I}, which generates a nitrogen-centered radical that performs radical C–H abstraction. The resulting radical reacts with a bis(oxazoline)-ligated Cu^{II}–CN complex, ultimately resulting in C–CN bond formation (Fig. 7A). The reaction proceeds under mild conditions (Fig. 7B), exhibits exceptionally broad substrate scope encompassing diverse alkylarenes and heteroatom-containing substrates, and achieves excellent enantioselectivity. Mechanistic studies support the involvement of a diffusible organic radical (e.g., via competition with radical traps: $BrCCl_3$, O_2). DFT calculations suggest the radical reacts with Cu^{II} to afford an alkyl-Cu^{III} intermediate and that the reaction of the radical with Cu^{II} is reversible, with reductive elimination as the enantioselectivity-determining step. This "radical relay" method for sp^3 C–H oxidation employs the hydrocarbon substrate as the limiting reagent, which will significantly enhance the utility of this method relative to previous methods, which require a large excess of substrate relative to the oxidant.

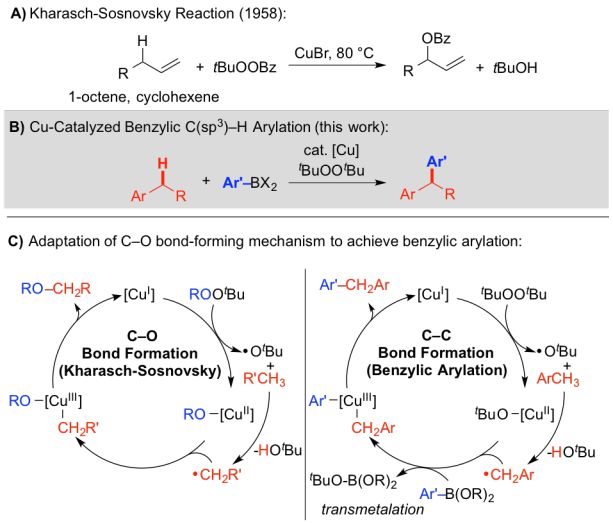

Fig. 6. Cu-catalyzed benzylic C–H arylation method and its relationship to the Kharasch-Sosnovsky reaction.

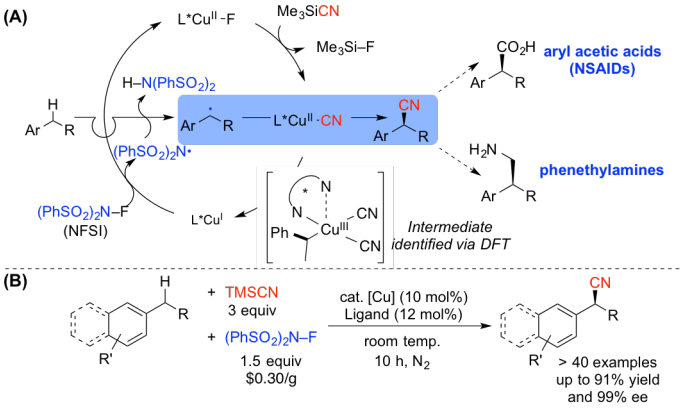

Fig. 7. Radical-relay cyanation of benzylic C–H bonds: (A) mechanistic hypothesis and (B) reaction conditions.

Publications Acknowledging this Grant, 2014-2017

Jointly funded by this grant and other grants with leading intellectual contribution from this grant:

1. Ryland, B. L.; Stahl, S. S. Practical Aerobic Oxidations of Alcohols and Amines with Homogeneous Cu/TEMPO and Related Catalyst Systems. *Angew. Chem. Int. Ed.* **2014**, *53*, 8824-8838.
2. Ryland, B. L.; McCann, S. D.; Brunold, T. C.; Stahl, S. S. Mechanism of Alcohol Oxidation Mediated by Copper(II) and Nitroxyl Radicals. *J. Am. Chem. Soc.* **2014**, *136*, 12166-12173.
3. Xie, X.; Stahl, S. S. Efficient and Selective Cu/Nitroxyl-Catalyzed Methods for Aerobic Oxidative Lactonization of Diols. *J. Am. Chem. Soc.* **2015**, *137*, 3767-3770.
4. McCann, S. D.; Stahl, S. S. Copper-Catalyzed Aerobic Oxidations of Organic Molecules: Pathways for Two-Electron Oxidation with a Four-Electron Oxidant and a One-Electron Redox-Active Catalyst. *Acc. Chem. Res.* **2015**, *48*, 1756-1766.
5. Steves, J. E.; Stahl, S. S. Stable TEMPO and ABNO Catalyst Solutions for User-Friendly (bpy)Cu/Nitroxyl-Catalyzed Aerobic Alcohol Oxidation. *J. Org. Chem.* **2015**, *80*, 11184-11188.
6. McCann, S. D.; Stahl, S. S. Mechanism of Copper/Azodicarboxylate-Catalyzed Aerobic Alcohol Oxidation: Evidence for Uncooperative Catalysis. *J. Am. Chem. Soc.* **2016**, *138*, 199-206.
7. Zhang, W.; Wang, F.; McCann, S. D; Wang, D.; Chen, P.; Stahl, S. S.; Liu, G. Enantioselective Cyanation of Benzylic C–H Bonds via Copper-Catalyzed Radical Relay. *Science,* **2016***, 353,* 1014-1018.
8. Hruszkewycz, D. P.; Miles, K. C.; Thiel, O. R.; Stahl, S. S. Co/NHPI-mediated aerobic oxygenation of benzylic C–H bonds in pharmaceutically relevant molecules. *Chem. Sci.* **2017**, *8*, 1282-1287.
9. Vasilopoulos, A.; Zultanski, S. L.; Stahl, S. S. Feedstocks to Pharmacophores: Cu-Catalyzed Oxidative Arylation of Inexpensive Alkylarenes Enabling Direct Access to Diarylalkanes. *J. Am. Chem. Soc.* **2017**, 139, 7705-7708.

Jointly funded by this grant and other grants with relatively minor intellectual contribution from this grant;

10. Tsybizova, A.; Ryland, B. L.; Tsierkezos, N.; Stahl, S. S.; Roithová, J.; Schröder. D. Speciation Behaviour of Copper(II) Acetate in Simple Organic Solvents Revealing the Effect of Trace Water. *Eur. J. Inorg. Chem.* **2014**, *2014*, 1407-1412.
11. Osterberg, P. M.; Niemeier, J. K.; Welch, C. J.; Hawkins, J. M.; Martinelli, J. R.; Johnson, T. E.; Root, T. W.; Stahl, S. S. Experimental Limiting Oxygen Concentrations for Nine Organic Solvents at Temperatures and Pressures Relevant to Aerobic Oxidations in the Pharmaceutical Industry. *Org. Process Res. Dev.* **2015**, *19*, 1537-1543.
12. Miles, K. C.; Stahl S. S. Practical Aerobic Alcohol Oxidation with Cu/Nitroxyl and Nitroxyl/NO_x Catalyst Systems. *Aldrichimica Acta* **2015**, *48*, 8-10.
13. Kim, J.; Stahl, S. S. Cu-Catalyzed Aerobic Oxidative Three-Component Coupling Route to *N*−Sulfonyl Amidines via an Ynamine Intermediate. *J. Org. Chem.* **2015**, *80*, 2448-2454.

Catalytic Selective Oxidations with Porous Transition Metal Oxides

Steven L. Suib
Departments of Chemistry, Chemical and Biomolecular Engineering, and Institute of Materials Science, University of Connecticut, Storrs, CT 06269-3060

Presentation Abstract

The goals of this project are as follows:

(a) To Investigate in Detail Selective Gas and Liquid-Phase Oxidations of Hydrocarbons.
(b) To Study Types of Oxygen Species Active During Selective Oxidation.
(c) To Control Such Species Via Oxide Composition, Nanostructure, Porosity, and Oxidation State Manipulations.
(d) To Determine Detailed Mechanisms and Kinetics with Various Organic Functionalities.
(e) To Elucidate the Bonding, Insertion, or Bond Breaking Steps as Influenced by Nanostructures and Steric Constraints.
(f) To Determine How Various Parts of the Inorganic Catalyst Structure Activate the Different Functionalities of Multifunctional Organic Species in a Concerted or Un-Concerted Manner.

Porous transition metal oxides and their role in selective catalytic oxidations are the focus of our research. Micropores (< 2 nm), mesopores (2-50 nm), macropores (> 50 nm), and sometimes combinations of these are important in control of mass transport and selectivity. The control of particle size in the nanometer regime can lead to enhanced activity in some reactions. Such nano-size materials can have markedly different properties than similar bulk materials (m and above). Control of morphologies of porous transition metal oxides such as hollow spheres, rods, helices, spirals, and many other shapes is also a factor in the control of catalytic activity, selectivity, and stability. Numerous other variables in the design of selective oxidation catalysts besides the above-mentioned properties may be significant such as mixed valency, surface area, thermal stability, chemical stability, electronic effects, active sites, and others.

Grant or FWP Number: DE-FG02-86ER13622: CATALYTIC SELECTIVE OXIDATIONS WITH POROUS TRANSITION METAL OXIDES

PI: Steven L. Suib
Postdoc(s): Ben Liu, Sanjubala Sahoo
Student(s): Curt Guild, Biswanath Dutta, Dave Kriz, Sourav Biswas, Tahereh Jafari, Chung Hao Kuo, Yongtao Meng, Wenqiao Song, Madhavi Pahalagedara, Lakshitha Pahalagedara, Saiful

Seraji, Weina Li, Altug Poyraz, Sheng-Yu Chen, Homer Genuino, Zhu Luo, Aparna Iyer, Wei Zhong, Abdel El Sawy, Ting Jiang, Jing Jin, Aimee Morey, Eric Njagi, Chunhu Chen, Ran Miao, Becca Gottlieb, Dinithi Rathnatake, M. D. Shakil, Niluka Wasalathanthri, Shanka Dissanayake.

RECENT PROGRESS

Recent Accomplishments

In the area of selective oxidations, we have studied the mechanisms of redox catalytic cycles in the oxidation of alcohols, CO, carbon hydrogen bonds such as with 9H-fluorene, toluene, phenol, ethane, propane, olefins, dyes, and others. A key factor in these reactions is the limitation due to mass transfer with small molecules or in the interconnectivity of different types of pores. We focused on mixed valent amorphous manganese oxide materials since we have considerable experience with these materials and they are excellent catalysts for selective oxidations and degradation of toxic chemicals as well as simulants of chemical warfare agents. However, when large substrates are used, reactivity is markedly diminished. We proposed a Mars Van Krevelen mechanism for selective oxidations of hydrocarbons over microporous manganese oxides (OMS-2) many years ago. This research concerns development of an expanded mechanism of such selective catalytic oxidations.

Our initial significant thrust in the area of mesoporous materials was an early paper showing how mesoporous octahedral molecular sieve MOMS-1 and MOMS-2 materials could be made. This was the first report of semiconducting transition metal oxide mesoporous materials with crystalline walls. Excellent adsorption and catalytic (selective oxidations) properties were observed. It took decades to totally understand the MOMS systems. In the past 3 years we have developed related crystalline walled mesoporous systems of numerous compositions and structures that are thermally stable, have controllable and monomodal pore sizes, high surface areas, and unique chemical and physical properties. More than 65 families of materials have been developed of these University of Connecticut (UCT) systems.

Some preliminary data of multiple esterifications from single long chain alcohols have been studied. There are no literature examples of this type of reaction. Some results are shown in the following Table 1;

Table 1, Solvent Free Oxidative Esterification of 1-octanol.[a]

Entry	Catalyst	Conversion[b] (%)	TOF[c] (h^{-1})	Selectivity[b] (%)		
				I	II	III
1	UCT-18-Cs	99	0.75 (2222)	16	63	21
2	UCT-1	72	0.52	26	67	7
3[d]	K-OMS-2	2	0.50	nd	50	25
4	AMO	42	1.25	28	28	14
5	Comm Mn_2O_3	0	0	Nd	Nd	Nd
6	No	0	-	Nd	Nd	Nd

[a] Reaction Conditions: 1-Octanol (5 mL), catalyst (100 mg), 130°C, air flow, 72 h. [b] Determined by GC-MS. [C] TOF (h^{-1}) = TON / time (h). TON = no of moles of substrate converted per mole of catalyst. In parenthesis: TOF was calculated based on Cs^+ as the limiting active sites. [d] The other major product was 1-octanal. Nd= not detected in GC-MS.

These multi-step reactions are believed to follow a decarboxylation catalyzed by manganese oxide along with an oxygen rebound step for this process. Though the reaction time is much longer (2-3 days) under air, the UCT-18-Cs (mesoporous Cs doped Mn_2O_3) performed best among all the manganese oxide catalysts tested under identical conditions. The reaction times can be improved by use of molecular oxygen instead of air. The bifunctional nature of UCT-18-Cs plays an important role in the higher activity, where the Mn and O are active sites for the oxidation of alcohol and Cs^+ ions increase the basic character to promote the esterification. This reaction allows study of one of our goals of Determining How Various Parts of an Inorganic Catalyst Structure Activate the Different Functionalities of Multifunctional Organic Species in a Concerted Manner**,** Goal (f). An oxygen rebound mechanism is supported by temperature programmed desorption (TPD) data and radical inhibitor studies. These bifunctional and potentially concerted reactions involve activity that largely depends on basicity and the oxidative power of the catalyst.

Publications Acknowledging this Grant in 2014-2017

(I) Exclusively funded by this grant;

1. Ren, Z.; Botu, V.; Wang, S.; Meng, Y.; Song, W.; Guo, Y.; Ramprasad, R.; Suib, S. L.; Gao, P. X., Monolithically Integrated Spinel MxCo3-xO4 (M=Co, Ni and Zn) Nano-Array Catalysts: Scalable Synthesis and Cations Manipulation for Tunable Low Temperature CH_4 and CO Oxidation, *Angew. Chem*., 2014, **53**, 7223-7227.

2. Pahalagedara, M.; Pahalagedara, L.; Kuo, C. H. ; Dharmarathna, S.; Suib, S. L., Ordered mesoporous mixed metal oxides: Remarkable effect of pore size on the catalytic activity, *Langmuir*, 2014, **30**, 8228-8237.

3. Kuo, C. H.; Li, W.; ; Song, W.; Luo, Z.; Poyraz, A.; Guo, Y.; Ma, A.; Suib, S.; He, Jie, Facile synthesis of Co3O4@CNT with high catalytic activity for CO oxidation under moisture-rich conditions, *ACS Appl. Mat. & Interf*., 2014, **16**, 785-791.

4. Poyraz, A.; Song, W.; Kriz, D.; Kuo, C. H.; Seraji, M.; Suib, S., Crystalline Mesoporous K2-xMn8O16 and ε-MnO2 by Mild Transformations of Amorphous Mesoporous Manganese Oxides and Their Enhanced Redox Properties, *ACS Appl. Mat. & Interf*., 2014, **6,** 10986-10991.

5. Meng, Y.; Song, W.; Huang, H.; Ren, Z.; Chen, S. Y.; Suib, S., Structure-Property Relationship of Bifunctional MnO_2 Nanostructures: Highly Efficient, Ultra-Stable Electrochemical Water Oxidation and Oxygen Reduction Reaction Catalysts Identified in Alkaline Media, *J. Am. Chem. Soc*., 2014, **136**, 11452-11464.

6. Genuino, H.; Seraji, M. S.; Meng, Y.; Valencia, D.; Suib, S. L., Combined Experimental and Computational Study of CO Oxidation Promoted by Nb in Manganese Oxide Octahedral Molecular Sieves *Appl. Catal. B: Environmental*, 2015, **163**, 361-369.

7. Kuo, C. .H; Mosa, I.; Poyraz, A. S; Biswas, S.; El-Sawy, A.; Song, W.; Luo, Z.; Chen, S. Y.; Rusling, J.; He, J. ; Suib, S., Robust Mesoporous Manganese Oxide Catalysts for Water Oxidation, *ACS Catalysis*, 2015, **5**, 1693-1699.

8. Kuo, C. H.; Li, W.; Pahalagedara, L.; El-Sawy, A. M.; Kriz, D.; Genz, N.; Guild, C.; Ressler, T.; Suib, S. L.; He, J., Understanding the Role of Gold Nanoparticles in Enhancing the Catalytic Activity of Manganese Oxides in Water Oxidation Reactions, *Ang. Chem. Int. Ed*., 2015, **54**, 2345 –2350.

9. Biswas, S.; Poyraz, A. S.; Meng, Y.; Kuo, C. H.; Guild, C.; Tripp, H.; Suib, S. L. Ion induced promotion of activity enhancement of mesoporous manganese oxides for aerobic oxidation reactions, *Appl. Catal., B: Env*., 2015, 165, 731-741.

10. Jiang, T.; Poyraz, A.; Iyer, A.; Zhang, Y.; Luo, Z.; Zhong, W.; Miao, R.; El-Sawy, A.; Guild, C.; Sun, Y.; Kriz, D.; Suib, S., L., Synthesis of Mesoporous Iron Oxides by an Inverse Micelle Method and Their Application in the Degradation of Orange II under Visible Light at Neutral pH, *J. Phys. Chem*., 2015, **19**, 10454-10468.

11. Kuo, C. H.; Mosa, I. M.; Thanneeru, S.; Sharma, V.; Zhang, L.; Biswas, S.; Aindow, M.; Alpay, S. P.; Rusling, J. F.; Suib, S. L.; He, J., Facet-dependent catalytic activity of MnO electrocatalysts for oxygen reduction and oxygen evolution reactions, *J. C. S. Chem. Comm*., 2015, **51**, 5951-5954.

12. Jiang, T.; Du, S.; Jafari, T.; Zhong, W.; Sun, Y.; Song, W.; Luo, Z.; Hines, W. A.; Suib, S., Synthesis of mesoporous gamma-Fe_2O_3 supported palladium nanoparticles and investigation of their roles as magnetically recyclable catalysts for nitrobenzene hydrogenation, *Appl. Catal. A: Gen*., 2015, **502**, 105-113.

13. Jin, J.; Hines, W. A.; Kuo, C. H.; Perry, D. M.; Poyraz, A. S.; Xia, Y.; Zaidi, T.; Nieh, M. P.; Suib, S. L.,Magnetic Studies of Mesoporous Nanostructured Iron Oxide Materials Synthesized by One-Step Soft-Templating, *Dalton Trans.*, 2015, **44**, 11943-11953.

14. Biswas, S.; Dutta, B.; Mullick, K.; Kuo, C. H.; Poyraz, A.; Suib, S. L., Efficient Aerobic Oxidation of Amines to Imines by Cesium Promoted Mesoporous Manganese Oxide, *ACS Catal*., 2015, **5**, 4394-4403.

15. Liu, B.; Kuo, C. H.; Chen, J.; Luo, J.; Thanneeru, S.; Li, W.; Song, W.; Biswas, S.; Suib, S. L.; He, J., Ligand-Assisted Co-Assembly Approach toward Mesoporous Hybrid Catalysts of Transition-Metal Oxides and Noble Metals: Photochemical Water Splitting, *Ang. Chem., Int. Ed*., 2015, **54**, 9061-9065.

16. Liu, B.; Luo, Z.; Federico, A.; Song, W.; Suib, S.; He, J., Colloidal amphiphile-templated growth of highly crystalline mesoporous non-siliceous oxides, *Chem. Mat*., 2015, **27**, 6173-6176.

17. Chen, C. H.; Njagi, E.; Chen, S. Y.; Horvath, D.; Xu, L.; Morey, A.; Mackin, C.; Joesten, R.; Suib, S. L., Structural Distortion of Molybdenum-doped Manganese Oxide Octahedral Molecular Sieves for Enhanced Catalytic Performance, *Inorg. Chem*., 2015, **54**, 10163-71.

18. Dutta, B.; Biswas, S.; Sharma, V.; Savage, N. O.; Alpay, S. P.; Suib, S. L., Mesoporous Manganese Oxide Catalyzed Aerobic Oxidative Coupling of Anilines to Aromatic Azo Compounds, *Ang. Chem. Int. Ed*., 2016, **55**, 2171-2175.

19. El-Sawy, A.; Suib, S. L., Controlling the Active Sites of Sulfur Doped Carbon Nanotube-Graphene Nanolobes for Highly Efficient Oxygen Evolution and Reduction Catalysis, *Adv. Energy Mat*., 2016, **6**.

20. Poyraz, A.; Meng, Y.; Biswas, S.; Suib, S. L., Mesoporous TM Oxide Materials by Surfactant-Assisted Soft templating, in Perovskites and Mixed Metal Oxides, Granger, P., Parvulescu, V. I.; Kaliaguine, S. I.; Prellier, W., Eds., Wiley VCH, NY, 701-714.

21. Mosa, I. M.; Biswas, S.; El-Sawy, A. M.; Botu, V.; Guild, C.; Song, W.; Ramprasad, R.; Rusling, J. F.; Suib, S. L., Tunable mesoporous manganese oxide for high performance oxygen reduction and evolution reactions, *J. Mat. Chem. A*, 2016, **4**, 620-631.

22. Miao, R.; Luo, Z.; Zhong, W.; Chen, S. Y.; Jiang, T.; Suib, S. L., Mesoporous TiO_2 Modified with Carbon Quantum Dots as a High-Performance Visible Light Photocatalyst, *Appl. Catal. B, Env*., 2016, **189**, 26-38.

23. Pahalegedara, M.; Pahalegedara, L.; He, J,; Miao, R.; Gottlieb, B.; Rathnayake, D.; Suib, S. L., Room Temperature Selective Reduction of Nitrobenzene to Azoxybenzene over Magnetically Separable Urchin-like Ni /Graphene Nanocomposites, *J. Catal*., 2016, **336**, 41-48.

24. He, J.; Liu, Y.; Meng, Y.; Sun, X.; Biswas, S.; Shen, M.; Luo, Z.; Miao, R.; Zhang, L.; Mustain, W. E.; Suib, S. L., High-rate long-life of Li-ion batteries using reduced graphene oxide/Co_3O_4 as anode materials, *RSC Adv*., 2016, **6**, 24320 - 24330.

25. Luo, Z.; Cetegen, S. A.; Miao, R.; Jiang, T.; Chen, S. Y.; Jafari, T.; Zhang, Y.; Suib, S. L., Structure-Property Relationships of Copper Modified Mesoporous TiO2 Materials on Alkyne Homocoupling Reactions*, J. Catal*., 2016, **338**, 94-103.

26. Liu, B.; Yao, H.; Song, W.; Jin, L.; Mosa, I. M.; Rusling, J. F.; Suib, S. L.; He, J., Ligand-Free Noble Metal Nanocluster Catalysts on Carbon Supports 2 via "Soft" Nitriding, *J. Am. Chem. Soc*., 2016, **138**, 4718-4721.

27. Liu, B.; Mosa,I. M.; Song, W.; Zheng, H.; Kuo, C. H.; Rusling, J. F.; Suib, S. L.; He, J., Unconventional structural and morphological transitions of nanosheets, nanoflakes and nanorods of AuNP@MnO_2, *J. Mat. Chem. A*, 2016, 4, 6447-6455.

28. Liu, B.; Yao, H.; Daniels, R. A.; Song, W.; Zheng, H.; Jin, L.; Suib, S. L.; He, J., A facile synthesis of Fe_3C@mesoporous carbon nitride nanospheres with superior electrocatalytic activity, *Nanoscale*, 2016, **8**, 5441-5445.

29. Liu, Y.; Palmieri, A.; He, J.; Meng, Y.; Beauregard, N.; Suib, S. L.; Mustain, W., Highly Conductive In-SnO_2/RGO Nano-Heterostructures with Improved Lithium-Ion Battery Performance, *Sci. Rep*., 2016, **6**, 25860.

30. Luo, Z.; Huan, T. D.; Mosa, I. M.; Poyraz, A. S.; Miao, R.; Zhong, W.; Cloud, J.; Kriz, D.; Thanneeru, S.; Ramprasad, R.; Suib, S. L., Mesoporous, Blue MoO_{3-x} Material as Efficient Electrocatalyst for Hydrogen Evolution Reaction, *Adv. Energy Mat*., 2016, **6,** 16.

31. Biswas, S.; Mullick, K.; Chen,S. Y.; Kriz, D. A.; Shakil, M. D.; Kuo, C. H.; Angeles-Boza, A. M.; Rossi, A. R.; Suib, S. L., Mesoporous Copper/Manganese Oxide Catalyzed Coupling of Alkynes: Evidence for Synergistic Cooperative Catalysis, *ACS Catal*., 2016, **6**, 5069-5080.

32.Song, W.; Ren, Z.; Chen, S. Y.; Meng, Y.; Biswas, S.; Nandi, P.; Elsen, H.; Gao, P. X.; Suib, S. L., Ni and Mn-Promoted Mesoporous Co_3O_4: a Stable Bifunctional Catalyst with Surface Structure Dependent Activity for Oxygen Reduction Reaction and Oxygen Evolution Reaction, *ACS Applied Materials & Interfaces*, 2016, **8**, 20802-20813.

33. Wasalathanthri, N.; SantaMaria, T. M.; Kriz, D. A.; Dissanayake, S. L.; Kuo, C. H.; Biswas, S.; Suib, S. L., Mesoporous Manganese Oxides for NO_2 Assisted Catalytic Soot Oxidation, *Appl. Catal. B*, 2016, **201**, 543-551.

34. Pahalagedara, L.; Kriz, D.; Wasalathanthri, N.; Weerakkodi, C.; Meng, Y.; Dissanayake, S.; Pahalagedara, M.; Luo, Z.; Suib, S. L.; Nandi, P.; Benchmarking of Manganese Oxide Materials with CO Oxidation as Catalysts for Low Temperature Selective Oxidation, *Appl. Catal. B*, 2017, 204, 411-420.

35. Miao, R.; He, J.; Sahoo, S.; Luo, Z.; Zhong, W.; Chen, S. Y.; Guild, C.; Jafari, T.; Dutta, B.; Cetegen, S.; Wang, M.; Alpay, S. P.; Suib, S., Reduced Graphene Oxide Supported Nickel-Manganese-Cobalt Spinel Ternary Oxide Nanocomposites and Their Chemical-Converted Sulfide Nanocomposites as Efficient Electrocatalysts for Alkaline Water Splitting, *ACS Catalysis*, 2016, **7**, 819–832.

36. Mullick, K.; Biswas, S.; Angeles-Boza, A. M.; Suib, S. L., Heterogeneous Mesoporous Manganese Oxide Catalyst for Aerobic and Additive-Free Oxidative Aromatization of N-Heterocycles, *Chem. Comm*., 2017, **53**, 2256-2259.

37. Liu, L.; Luo, Y.; Tan, W.; Liu, F.; Suib, S. L., Zhang, Y.; Qiu, G., Zinc removal from aqueous solution using deionization pseudocapacitor with high-performance nanostructured birnessite electrode, *Env. Sci. : Nano*, 2017, **4**, 811-823.

38. Iyer, A.; Kuo, C. H.; Dharmarathna,S.; Luo, Z.; Rathnayake, D.; He, J.; Suib, S. L., An ultrasonic atomization assisted synthesis of self-assembled manganese oxide octahedral molecular sieve nanostructures and their application in catalysis and water treatment, *Nanoscale*, 2017, **9**, 5009.

39. Guild, C.; Vovchok, D.; Kriz, D. A.; Bruix, A.; Hammer, B.; Llorca, J.; Xu, W.; El-Sawy, A.; Biswas, S.; Rodriguez, J. A.; Senanayake, S. D.; Suib, S. L.; Water Gas Shift over Metal-Free Nanocrystalline Ceria: An Experimental and Theoretical Study, *ChemCatChem*, 2017, **9**, 1373-1377.

40. Liu, B.; Jiang, T.; Zheng, H.; Dissanayake, S.; Song, W.; Federico, A.; Suib, S. L.; He, J., Nanoengineering of Aggregation-Free and Thermally-Stable Gold Nanoparticles in Mesoporous Frameworks, *Nanoscale*, 2017, in press.

41. Liu, B.; Wang, P.; Lopes, A.; Jin, L.; Zhong, W.; Pei, Y.; Suib, S., L.; He, J, Au-carbon electronic interaction mediated selective oxidation of styrene, *ACS Catal*., 2017, **7**, 3483-3488.

42. Wang, W.; Wang, Z.; Liu, J.; Luo, Z.; Suib, S. L.; He, P.; Ding, G.; Zhang, Z.; Sun, L., Single-step One-pot Synthesis of TiO2 Nanosheets Doped with Sulfur on Reduced Graphene Oxide with Enhanced Photocatalytic Activity, *Sci. Reports*, 2017, **7**, 46610.

43. Liu, G.; Liu, J.; Li, W.; Liu, C.; Wang, F.; He, J.; Guild, C.; Jin, J.; Kriz, D.; Suib, S. L., Aerobic oxidation of alcohols over Ru-Mn-Ce and Ru-Co-Ce catalysts: The effect of calcination temperature, *Appl. Catal., A: Gen*., 2017, **535**, 77-84.

44. Palmieri, A.; Liu, Y.; He, J.; Meng, Y.; Suib, S. L**.**; Mustain, W. E., Metal Oxide/Reduced Graphene Oxide Anodes or Lithium batteries, *ECS Transactions*, 2015, **66**, (9, Lithium-Ion Batteries and Beyond), 47-55.

45. Biswas, S.; Mullick, K.; Chen, S. Y.; Gudz, A.; Carr, D. M.; Mendoza, C.; Angeles-Boza, A.M.; Suib, S. L., Facile Access to Versatile Functional Groups from Alcohols by Single Multifunctional Reusable Catalysts, *Appl. Catal., B: Env*., 2017, **203**, 607-614.

46. Zhong, W.; Jiang, T.; Jafari, T.; Poyraz, A. S.; Wu, W.; Kriz, D. A.; Du, S.; Biswas, S.; Pettes, M. T.; Suib, Steven L., Modified Inverse Micelle Synthesis for Mesoporous Alumina with a High D4 Siloxane adsorption Capacity, *Micropor. Mesopor. Mat.,* 2017, **239**, 328-335.

47. Xing, Y.; Liu, Z.; Wu, D.; Guo, X.; Qu, X.; Fang, S.; Suib, S. L.; Self-assembly synthesis of Mn_3O_4 hierarchical micro/nano architectures as supercapacitor electrodes, *J. Mat. Sci*., 2017, in press.

Distinguishing Volmer-Heyrovsky from Volmer-Tafel Pathway for Hydrogen Evolution Reaction on Pt in Acidic Electrolyte

YuYe J. Tong and De-Jun Chen
Georgetown University, Department of Chemistry

Presentation Abstract

Although it seems to be deceptively simple, the two-electron hydrogen evolution reaction (HER) is of both fundamental and practical importance for the so-called "hydrogen economy". However, despite being studied rather intensively and persistently for almost six decades that goes back to Parson's early "speculative" work in 1958, the exact reaction mechanism is still under lengthy debate as to whether the HER follows the Volmer-Heyrovsky ($H^+ + e^- \rightarrow H_{ad}$ and $H_{ad} + H^+ + e^- \rightarrow H_2$) or the Volmer-Tafel ($2H^+ + 2e^- \rightarrow 2H_{ad}$ and $2H_{ad} \rightarrow H_2$) pathway. In this presentation, we will report the first clear evidence that shows that HER on Pt in acidic electrolyte, $2H^+ + 2e^- \rightarrow H_2$, follows the Volmer-Heyrovsky pathway. Specifically, we observed that although the adsorbed CO can block completely hydrogen adsorption/desorption, it does not impede at all the HER from proton: $2H^+ + 2e^- \rightarrow H_2$. This observation is consistent more with the Volmer-Heyrovsky pathway than with the Volmer-Tafel pathway. *In situ* total attenuated reflection surface enhanced IR absorption spectroscopic (ATR-SEIRAS) investigation confirmed the full stability of adsorbed CO. It showed further that for a Pt surface fully pre-covered by adsorbed CO, the influx of protons and out-flux of generated hydrogen gas beyond the onset of HER broke the dipole-dipole coupling between adsorbed CO molecules and pushed part of initially linear bound CO to bridge-bound CO in a fully reversible fashion. A reaction model consistent with the experimental observations will be presented and discussed.

DE-FG02-07ER15895: Exploring Electrocatalysis of Methane on Transition Metal Surfaces
PI: YuYe J. Tong
Postdoc(s): Eric G. Sort, De-Jun Chen, Hamed Etaee-Esfahani
Student(s): A. M. Levendorf, L. Huang, M. Zhan, Yanyan Wang, Safia Jilani

RECENT PROGRESS

Synthesizing carbon-coated nanoscale zeolite-mordenite (ZMOR)-encaged tri-copper oxygen cluster for partial electrochemical oxidation of methane

This work was inspired by the observation that ZMOR-encaged tri-copper oxygen cluster or ligand-stabilized tri-copper cluster can catalyze efficient CH_4 oxidation to methanol (MeOH) heterogeneously at 200 °C (the former) and homogeneously at 25 °C (the latter). We have

proposed to explore an electrochemical version of such a system, that is, the carbon-coated nanoscale ZMOR-encaged tri-copper oxygen cluster for partial oxidation of CH_4 to MeOH. We first synthesized ZMOR particles using a literature-reported hydrothermal method whose wide-angle XRD pattern (Fig. 1a(II)) was in excellent agreement with that of the commercial ZMOR (Fig. 1a(I)). Cu-containing ZMOR (Cu-ZMOR) was then prepared by sequential ion-exchanges, first with NH_4^+ whose thermal decomposition led to H-ZMOR, then with Cu^{2+} that produced Cu-ZMOR. Carbon coating was achieved by calcination of citric acid impregnated Cu-ZMOR under Ar. The XRD pattern (Fig. 1a(III)) of the latter indicates that the ZMOR structure was intact. The electrochemical feasibility of the carbon-coated nanoscale Cu-ZMOR was demonstrated by the cyclic voltammogram presented in Fig. 1b. The next step is to text its activity toward the partial electrooxidation of CH_4.

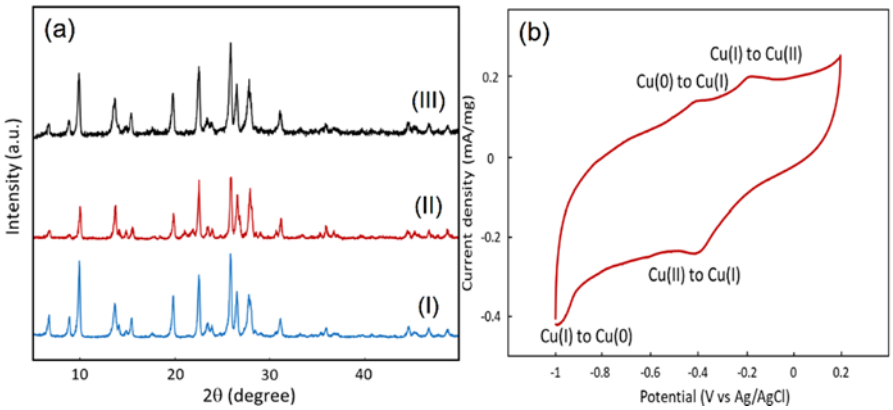

Figure 1. (a) Wide-angle XRD patterns of (I) commercial mordenite as a reference, (II) the as synthesized MOR, and (III) Cu-ZMOR. (b) CV of Cu-ZMOR in Ar-saturated 0.1 M NaOH.

Electrooxidation of methane on Pd vs Pt

Fig. 2a shows the 1st (black) and 2nd (red) cycles of the CV at 40 °C of Pd black in CH_4-saturated 0.5 M H_2SO_4 electrolyte after the adsorption of CH_4 with a scan rate of 50 mV/s. The 1st cycle reveals clear evidence of dissociative CH_4 adsorption that blocked partially the hydrogen adsorption/desorption and the subsequent oxidation with an onset potential at ~0.1 V (vs Ag/AgCl). However, that the 2nd cycle barely observed any activity suggests a slow dissociative CH_4. Similar results were also observed on a commercial carbon-supported Pt electrocatalyst but with an onset potential that was ~ 0.1 V more positive than that on Pd. The latter suggests that the CH_4 electrooxidation activity is higher on Pd than on Pt. Interestingly, despite that increasing temperature would decrease the solubility of CH_4 in electrolyte, it actually led to an increase in the CH_4 electrooxidation activity (Fig. 2c). The latter indicates that dissociative adsorption of CH_4 has a rather high energy barrier.

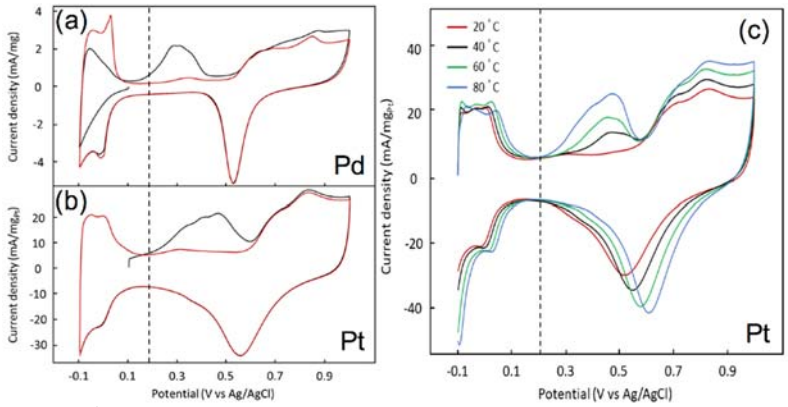

Figure 2. 1st (black) and 2nd (red) CVs at 40 °C of (a) Pd black and (b) Pt/C (40% Pt loading) electrocatalyst in CH_4-saturated 0.5 M H_2SO_4. (c) CVs of the Pt/C electrocatalyst at different temperatures in CH_4 -saturated 0.5 M H_2SO_4.

Unraveling the mechanistic reasons for unusually higher activity in electrooxidation of solution CO on Au electrode

*C*O electro*o*xidation *r*eaction (COR) of CO dissolved in solution (CO_{sol}) on Au electrode is remarkably more active than on Pt electrode and the activity is general higher in alkaline than in acid media. By combining in situ ATR-SEIRAS with DFT calculations, we identified that in acidic media the weakly-bound CO was formed on-top of strongly-bound CO via dipole-dipole interaction and served as the active reaction intermediate for facile COR of CO_{sol}, as illustrated in Fig. 3.

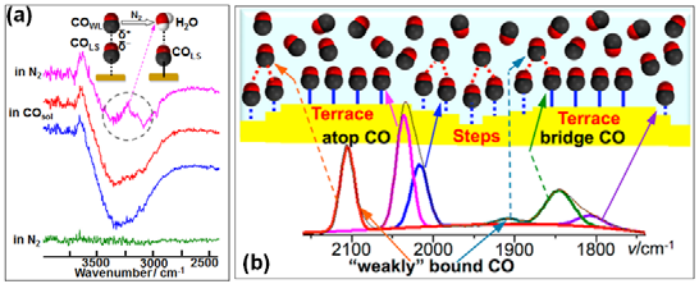

Figure 3. (a) A schematic illustration of the interaction between the strongly bound CO_{LS} (LS=linear on steps) and hydrogen-bound water after the desorption of the CO_{WL} (WL=weakly bound linear). (b) The illustration of formation of weakly-bound CO_w on Au, the active reaction intermediate for CO oxidation reaction (COR) in the CO-saturated acidic supporting electrolyte.

Weakly-bound CO was also spectroscopically identified in alkaline media for the first time. In addition to confirm experimentally that the strong adsorbed CO enhanced the OH adsorption, reaction mechanism similar to that in acidic media was proposed.

Operando investigation of Li-ion battery chemistry

Following the successful prove-of-concept application of a dual-electrode in situ IR spectroscopic cell to conducting operando investigation of a methanol fuel cell (Publication 4 below), we extended the method to explore operando investigation of battery chemistry. Figure 1 shows in-situ electrochemical ATR-SEIRAS spectra for the charge and discharge processes on the graphite/electrolyte interface of a lithium battery anode. Using the reference spectrum at

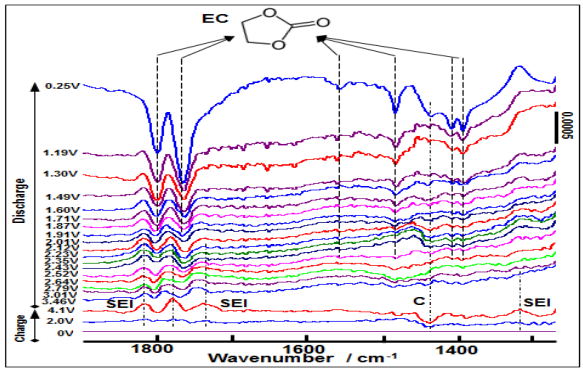

Figure 4. In-situ electrochemical ATR-SEIRAS spectra for the charge and discharge processes on graphite/electrolyte interface of lithium-ion battery anode. Electrolyte is $LiPF_6$/EC/DEC(1:1:1, 1M).

initial cell potential of 0V, four bands at 1820, 1780, 1736 and 1316 cm^{-1} were observed at 4.1 V (cell potential) during charging and are associated with the formation of SEI (solid-electrolyte interphase). The first 3 bands are assigned to carbonyl group (ν(C=O) of different composition inside the SEI and the last one is from the ν(C-O) single bond vibration. The decreasing of the band at 1435 cm^{-1} is corresponding to the ν(C-H) from the graphite due to the lithium intercalation from its edge.[2] When the LIB discharged from 4.1 V to 2.52 V (Figure 1), the bands of ν(C=O) at 1736 cm^{-1} gradually disappeared. A further discharge from 2.52 V to 0.25 V (Figure 1) evidences the significant loss of ethylene carbonate (EC) on the anode surface. The irreversibility of this process could impede lithium intercalation since lithium ion in electrolyte mainly coordinates with the most polar EC molecules. Our results demonstrate that the *in-situ* ATR-SEIRAS is a powerful technique to unravel the chemical information of SEI and therefore will benefit the LIB community for advancing the battery development.

Publications Acknowledging this Grant in 2014-2017

(I) Exclusively funded by this grant

1. Chen, D.-J.; Sun, S.-G.; Tong, Y. Y. J. On the chemistry of activation of a commercial carbon-supported PtRu electrocatalyst for the methanol oxidation reaction. *Chem. Comm.* **2014**, *50*, 12963-12965.
2. Chen, D.-J.; Tong, Y. Y. J. In situ Raman spectroscopic measurement of near-surface proton concentration changes during electrochemical reactions. *Chem. Comm.* **2015**, *51*, 5683-5686.
3. Huang, L. ; Sorte, E. G. ; Sun, S.-G. ; Tong, Y. Y. J. A Straightforward Implementation of *in situ* Solution Electrochemical ^{13}C NMR Spectroscopy for Studying Reactions on Commercial Electrocatalysts: Ethanol Oxidation. *Chem. Comm.* **2015**, *51*, 8086-8088.
4. Sorte, E. G. ; Chen, D.-J.; Tong, Y. Y. J. Dual-Electrode *in situ* Infrared Spectroscopy for Fuel Cells. *J. Electrochem. Soc*. **2016**, *163*, H3038-H3042.
5. Chen, D.-J.; Allison, T. C. ; Tong, Y. Y. J. Mechanistic Insights into Electro-Oxidation of Solution CO on the Polycrystalline Gold Surface as Seen by in Situ IR Spectroscopy. *J. Phys. Chem. C.* **2016**, *120*, 16132−16139.
6. Sorte, E. G. ; Tong, Y. Y. J. Interdigitated metal electrodes for high-resolution in situ electrochemical NMR. *J. Electroanal. Chem*. **2016**, *769*, 1-4.
7. Wang, Y.-Y.; Chen, D.-J.; Tong, Y. Y. J. Mechanistic Insight into Sulfide-Enhanced Oxygen Reduction Reaction Activity and Stability of Commercial Pt Black: an *in situ* Raman Spectroscopic Study. *ACS Catal.* **2016**, *6*, 5000−5004.
8. Sorte, E. G. ; Jilani, S. ; Tong, Y. Y. J. Methanol and Ethanol Electrooxidation on PtRu and PtNiCu as Studied by High- Resolution In Situ Electrochemical NMR Spectroscopy with Interdigitated Electrodes. *Electrocatal.* **2017**, *9*, 95–102

9. Chen, D.-J.; Tong, Y. Y. J. An in-situ electrochemical IR investigation of solution CO electro-oxidation on a polycrystalline Au surface in an alkaline electrolyte: Identification of active reaction intermediates. *J. Electroanal. Chem*. **2017**, 10.1016/j.jelechem.2017.04.045.

(II) Jointly funded with leading intellectual contribution from this grant

10. Levendorf, A. M.; Sun, S.-G.; Tong, Y. Y. J. In situ FT-IR Investigation of Methanol and CO Electro-oxidation on Cubic and Octahedral/ Tetrahedral Pt Nanoparticles Having Residual PVP. *Electrocatal*. **2014**, *5*, 248-255.
11. Levendorf, A. M.; Chen, D.-J.; Rom, C. L.; Liu, Y.-W.; Tong, Y. Y. J. Electrochemical and in situ ATR-SEIRAS Investigation of Methanol and CO Electrooxidation on PVP-Free Cubic and Octahedral/Tetrahedral Pt Nanoparticles. *RSC Adv.* **2014**, *4*, 21284-21293.
12. Huang, L.; Sun, J.-Y.; Cao, S.-H.; Zhan, M.; Nie, Z.-R.; Sun, H.-J.; Chen, Z.; Zhou, Z.-Y.; Sorte, E. G.; Tong, Y. Y. J.; Sun, S.-G. Combined EC-NMR and In Situ FTIR Spectroscopic Studies of Glycerol Electrooxidation on Pt/C, PtRu/C, and PtRh/C. *ACS Catal.* **2016**, *6*, 7686-7695.
13. Tong, Y. Y. J. Electrochemical Energy Generation and Storage as Seen by in-situ NMR. *Springer Handbook of Electrochemical Energy*, **2016**, *Chapter 12*, 331-363.

(III) Jointly funded with relatively minor intellectual contribution from this grant

14. Gao, Y.; Liu, Y.-W.; Li, Y.; Zaluzhna, O.; Tong, Y. Y. J. Mechanistic Insights into the Brust–Schiffrin Synthesis of Organochalcogenolate-Stabilized Metal Nanoparticles. *RSC Smart Materials Series*, **2014**, *Chapter 1*, 1-24.

Molecular-Level Design of Heterogeneous Chiral Catalysts

Wilfred T. Tysoe, Andrew Gellman, Charles Sykes and Francisco Zaera
Department of Chemistry and Biochemistry, University of Wisconsin-Milwaukee
Department of Chemical Engineering, Carnegie Mellon University
Department of Chemistry, Tufts University
Department of Chemistry, University of California-Riverside

Presentation Abstract

The fact that two enantiomers of a chiral compound can have completely different physiological effects means that chiral pharmaceuticals must be synthesized in their enantiomerically pure forms creating the enormous market for chiral compounds. Currently, pharmaceuticals are synthesized by *homogeneous*–phase catalysts, many of which are achiral and produce racemic products requiring separation of the catalyst and enantioseparation of the product, issues that are addressed by the use of *heterogeneous*-phase chiral catalysts which can be synthesized by using a chiral modifier. While there are few examples of heterogeneous chiral catalysts, one is the enantioselective hydrogenation of methyl pyruvate to methyl lactate on modified transition metals. This enantioselective chemistry is explored on a R-1-(1-naphthyl)ethylamine (NEA)-modified Pd(111) model catalyst where temperature-programmed desorption experiments reveal that NEA accelerates the rates of both MP hydrogenation and H/D exchange. NEA+MP docking complexes are identified using scanning tunneling microscopy supplemented by density functional theory calculations to allow the most stable docking complexes to be identified. The results show that diastereomeric interactions between NEA and MP occur predominantly by binding of the C=C of the enol tautomer of MP to the surface, while simultaneously optimizing C=O$\cdots$$H_2N$ hydrogen-bonding interactions. The combination of chiral-NEA driven diastereomeric docking with a tautomeric preference enhances the hydrogenation activity since C=C bonds hydrogenate more easily than C=O bonds thus providing a rationale for the catalytic observations. The catalytic hydrogenation of MP on NEA-modified Pd(111) is also studied at high pressures to correlate the results obtained in ultrahigh vacuum with the catalytic kinetics under more realistic conditions.

Grant Number: DE-SC008703:
Molecular-Level Design of Heterogeneous Chiral Catalysts

Postdoc(s): Mausumi Mahapatra, Amanda Larson, Stavros Karakalos.
Student(s): Jerry Praeger, Mathew Michels, Hannah Kraffczyk, Burcu Karagoz, Soham Dutta, Andrew Therrien, Matthew Uhlman, Gardenia Rodriguez, Yufei Ni, Florisa Tanicala.

RECENT PROGRESS

Naturally Chiral Surfaces

Work has focused on understanding the enantioselectivity of naturally chiral metal surface by investigating the autocatalytic explosion mechanism of aspartic acid (Asp) decomposition on Cu surfaces that results in extremely highly enantiospecific kinetics. This is facilitated by the availability of **L*-Asp in multiple isotopomeric forms to allow the decomposition pathways to be studied with unprecedented detail. In addition, since **L*-Asp can be obtained in enantiomerically pure, isotopically labelled form, experiments can be performed using mixtures of *D*- and **L*-Asp and mass spectrometry is used to identify and quantify the enantiospecific yield of reaction products. These capabilities have enabled unprecedented insights into several enantiospecific surface phenomena occurring on both chiral and achiral surfaces.

In the same way as TA on naturally chiral Cu(*hkl*)$^{R\&S}$, Asp decomposition on Cu(*hkl*)$^{R\&S}$ occurs *via* an autocatalytic, vacancy-mediated explosion that leads to highly enantiospecific decomposition kinetics on Cu(643)$^{R\&S}$. Extensive kinetic data on Cu(110) and Cu(100) surfaces have revealed the characteristics of the autocatalytic, vacancy mediated explosion mechanism where rate laws can be developed for the decomposition kinetics that include a nucleation step, k_n, that creates vacancies in the Asp overlayer, and an explosive step, k_e, that is vacancy mediated. The form of the rate law is:

$$r = k_n \theta_{Asp}^{l} + k_e \theta_{Asp}^{m} \left(1 - \theta_{Asp}\right)^n$$

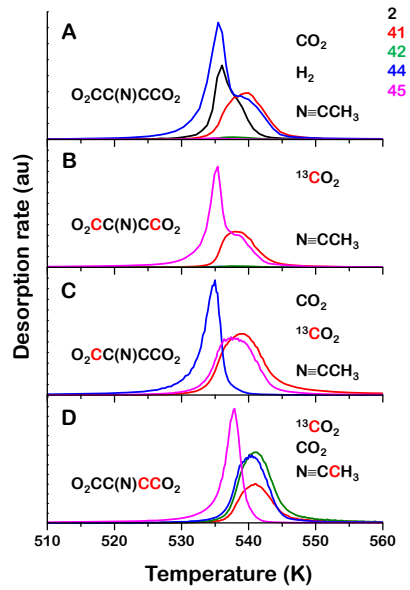

Figure 1. TPR spectra of *L*-Asp, 1,4-^{13}C-*L*-Asp, 1-^{13}C-*L*-Asp, and 3,4-^{13}C-*L*-Asp decomposition on Cu(110). Signals were collected at *m/z* = 2 for H_2, *m/z* = 41 and 42 for $N{\equiv}CCH_3$, and *m/z* = 44, 45 for CO_2. Heating rate was 1 K/s. The signals have been normalized to be proportional to the expected product distribution (other than the *m/z* = 41 signal for 3,4-^{13}C-*L*-Asp which is proportional to is contribution to the $N{\equiv}C^{13}CH_3$ fragmentation pattern.)

with the reaction orders and rate constants being determined from the experimental data. A variety of isotopomers have been used to elucidate the mechanism at the level of its various elementary steps. Asp adsorbs in its doubly deprotonated state at 400 K. The decomposition products are CO_2 from the two carboxylic acid groups, acetonitrile ($N{\equiv}CCH_3$) from the central two carbons, and H_2. TPD experiments (Figure 1) using *L*-Asp ($HO_2CCH(NH_2)CH_2CO_2H$), 1,4-$^{13}C_2$-*L*-Asp ($HO_2{}^{13}CCH(NH_2)CH_2{}^{13}CO_2H$), 1-^{13}C-*L*-Asp ($HO_2{}^{13}CCH(NH_2)CH_2CO_2H$) and 3,4-$^{13}C_2$-*L*-Asp ($HO_2CCH(NH_2){}^{13}CH_2{}^{13}CO_2H$) allowed the elementary reaction steps to be identified.

In addition, methods have been developing methods for comprehensively studying structure-sensitive surface chemistry with the aim of understanding the influence of surface structure on enantioselective surface reactions by using S^{4}Cs, curved single crystal surfaces that expose

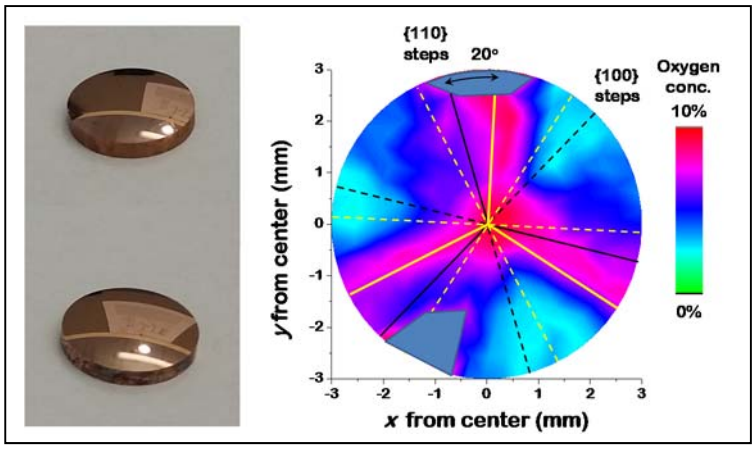

Figure 2. Left) Cu(100) and Cu(110) S^4Cs. Right) O 1s XPS map of the oxygen concentration across a Cu(111)-S^4C after annealing adsorbed *L*-Asp at 470 K. The regions of least decomposition are colored in red and those of greatest conversion in cyan. *L*-Asp is most stable along directions (solid yellow) rotated 20° clockwise from the {110} step edges (solid black).

continuous distributions of surface orientations (Figure 2). The kinetics of Asp decomposition has been mapped on a Cu(111)-S^4C by first adsorbing a monolayer of Asp and then heating the surface to 470 K to decompose ~70% of the adsorbed layer. The O 1*s* XPS map of the surface reveals those regions in which Asp is still adsorbed and intact (Figure 2, right). The map shows the three-fold symmetry of the surface. More importantly it reveals clear enantiospecificity of the decomposition kinetics because the regions of lowest and highest reactivity fall into the regions between the high-symmetry (achiral) directions across the crystal face. These data are used to map the rate constants for decomposition across continuous regions of surface orientation space and thereby identify those surface orientations with the greatest enantioselectivity.

Chirally Templated Surfaces

Chiral templates are those in which several adsorbates act in concert to provide a chiral adsorption site. It has been found that hexagonal structures form during the autocatalytic decomposition, of *R*,*R*-TA, just before the decomposition of the molecular film. This is illustrated by STM experiments to image nanoscale surface structures as the system is heated. Figure 3 displays the changes in surface structure of a monolayer of *R*,*R*-tartaric acid after being heated for different times at 455 K. Fig 3A shows a large-scale STM image of the surface after heating to

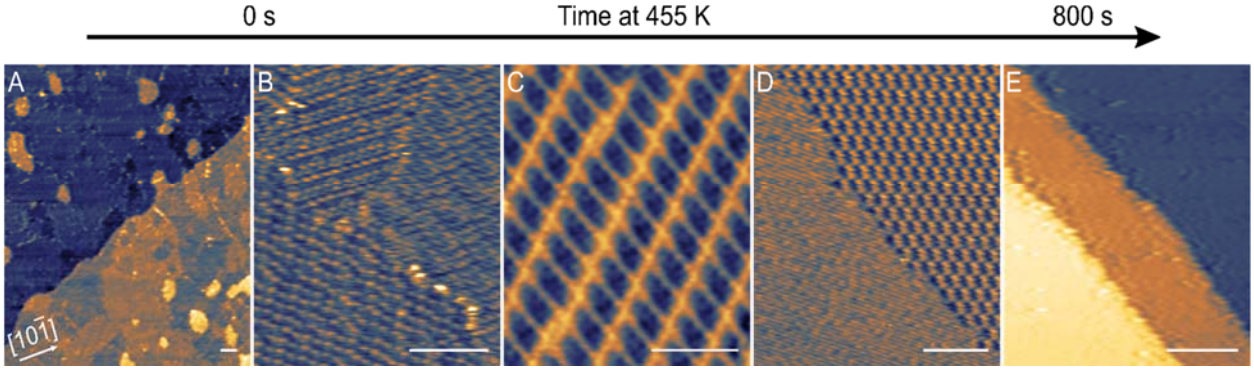

Figure 3. STM images of the various R,R-tartaric acid molecular overlayers on Cu(111). (A) Large scale image of the surface after a 405 K anneal, islands one Cu step in height can be seen. (B) STM image of the same surface at higher resolution to resolve the molecular structure. (C) STM image after 50 s anneal at 455 K, a new rectangular unit cell emerges. (D) STM image after 700 s anneal at 455 K revealing molecular rows and the hexagonal structure. (E) STM image after 800 s at 455 K, revealing the absence of a tartaric acid overlayer. Imaging conditions: -0.2 V, 50-500 pA, all scale bars are 10 nm.

405 K to desorb multilayers, which reveals islands with a height of one monotonic Cu step with an absolute coverage of approximately 0.1 ML. Fig. 3B shows a smaller-scale image of the same surface, displaying a chiral (5,5; -11,3) unit cell. After just 50 s at 455 K the entire molecular overlayer rearranges to form a larger chiral (14,10; -11,14) lattice, shown in Fig. 3C. After 100 s of isothermal treatment at 455 K a new molecular-row structure emerges and the previous structures are no longer present. The molecular rows are shown on the left side of Fig. 3D, and run in a chiral direction 24° (counterclockwise) from the Cu(111) high-symmetry $[10\bar{1}]$ direction (shown in the bottom corner of Fig. 4A). Finally, after 800 s at 455 K the tartaric acid has decomposed, with the absence of an overlayer as seen in Fig. 3E.

We hypothesize that the porous hexagonal structure derives from two types of hydrogen-bonding, with the upright carboxylic acid groups holding together the three monotartrates and the outward dangling alcohols hydrogen-bonding the trimer units together. In comparison to the surface explosion of TA on Cu(110), no such porous structure formed.

It has been shown that Asp adsorbed on Pd(111) also forms extended, two-dimensional hydrogen-bonded networks on the surface at low temperatures, but dehydrogenates at higher temperature to form polysuccinimides.

Monte Carlo algorithms have been developed to explain previous experimental results associated with the kinetics of the uptake of chiral molecules on solid surfaces. The specific system simulated in this study is the adsorption of propylene oxide (PO) on Pt(111). The surface was represented by a square lattice, and the time evolution of the adsorption, starting from a clean surface, was simulated *via* a number of sequential events chosen using a stochastic approach based on the so-called Master equation. Two main assumptions were required to explain the experimental results: (1) that adsorption is assisted by previously adsorbed molecules; and (2) that the geometry adopted by the new adsorbate is defined, but different for homochiral *versus* heterochiral pairs. The model was able to quantitatively reproduce the experimental data and to explain a number of observations associated with the fact that the adsorbates are chiral: (1) the final PO saturation depends on the enantiocomposition of the gas phase, yielding a layer approximately 20% less dense with a racemic mixture than with enantiopure *S*-PO or *R*-PO; (2) the same changes in saturation coverages are seen if PO of different chirality are dosed sequentially; (3) the sticking probability is also higher with enantiopure adsorbates, at least in the initial stages of the uptake; (4) the sticking probability initially increases with increasing exposure, until reaching a maximum at about 20% of saturation; and (5) the adsorbed layers do not show any long-range ordering but display small linear clusters. It was also possible to reproduce the experimental observation that the addition of a prochiral molecule such as propylene (Py) to a surface dosed with a small amount of a chiral "seed" (PO) leads to an amplification of the initial enantioselectivity of that surface.

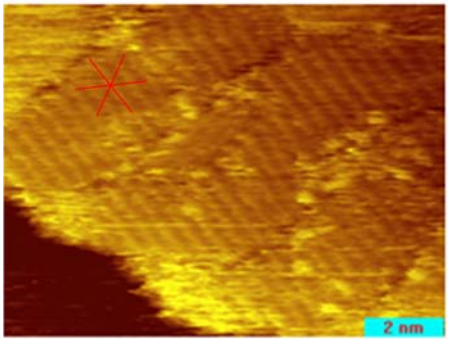

Figure 4. STM images for a high coverage of propylene oxide adsorbed and imaged on a Pd(111) surface at 120 K. Showing the presence of close-packed rows of propylene oxide which order on the surface in lamellae (V_b = - 0.16 V, I_t = 80 pA). The orientation of the close packed $<11\bar{0}>$ direction of the underlying lattice is shown.

In order to further understand the enrichment in enantiocomposition of PO on Pt(111) described above, experiments were carried out on chemically similar Pd(111). Surprisingly, this revealed no coverage differences between racemic and enantiopure PO, in contrast to the ~20%

difference found on Pt(111). STM image of both PO (Figure 4) and glycidol were collected on Pd(111) to provide insights into this difference. In contrast to Pt(111), where little order was seen for adsorbed PO, several linear structures were found on Pd(111).

One-to-One Modifiers

One-to-one modifiers are those that are proposed to act *via* direct diastereomeric interaction between the chiral modifier and the prochiral reactant. The adsorption structures of one-to-one modifiers was studied by combining infrared absorption spectroscopy, performed in situ at the solid-liquid interface, on a set of related compounds with targeted substitutions. The adsorption of 1-(1-naphthyl)-ethylamine (NEA), used as a chiral modifier in hydrogenation catalysis on the surface of platinum supported catalysts, was determined to occur *via* the amine group, not the aromatic ring as widely believed. It was established that neither naphthalene-based molecules without amine groups nor ones with tertiary amine moieties are capable of adsorbing on the metal surface to any significant extent from solution. However, a direct correlation was found between the extent of adsorption of the amines and their performance as chiral modifiers, imparting enantioselectivity during the hydrogenation of α-keto esters such as ethyl pyruvate.

This appears to contrast with work on NEA in UHV using STM, surface infrared spectroscopy and TPD in which the naphthyl ring is found to lie parallel to the surface. The interaction between NEA and methyl pyruvate (MP) was explored group using STM and TPD in UHV. TPD experiments revealed that co-adsorbed NEA significantly accelerates the rates of both MP hydrogenation and H/D exchange. NEA+MP docking complexes were imaged using STM and supplemented by DFT calculations to allow the most stable docking complexes to be identified. The results show that diastereomeric interactions between NEA and MP occur predominantly by binding of the C=C of the enol tautomer of MP to the surface, while simultaneously optimizing C=O$\cdots$$H_2N$ hydrogen-bonding interactions. The combination of chiral-NEA driven diastereomeric docking with a tautomeric preference enhances the hydrogenation activity since C=C bonds hydrogenate more easily than C=O bonds thus providing a rationale for the catalytic observations. Similar results have been found by others for other prochiral adsorbates interacting with NEA on Pt(111). It may therefore be that the geometry of the chiral modifier is different under reaction conditions and in UHV. Indeed, DFT calculations have shown that the NEA adsorption site is controlled by the ligation of the amine group to the surface, which moves the naphthyl group from its most favorable site. In order explore this, and to investigate whether the results obtained in UHV are relevant to enantioselective reactions carried out at higher pressures, the gas-phase hydrogenation of MP on a Pd(111) model catalyst is investigated in a high-pressure catalytic reactor incorporated into a UHV chamber and so uses the same model catalyst as that used for the surface science experiments. This operates as a recirculating batch reactor. The results show that MP does not hydrogenate on clean Pd(111). However, dosing the surface with NEA gave measurable activity at 313 and 323 K with a MP: H_2 ratio of 1:1. This indicates that the model system shows a similar rate enhancement under catalytic conditions as found with TPD under UHV conditions.

Publications Acknowledging this Grant in 2014-2017

(I) Exclusively funded by this grant

1. Mahapatra, M.; Burkholder, L.; Bai, Y.; Garvey, M.; Boscoboinik, J.A.; Hirschmugl, C.; Tysoe, W.T. Formation of Chiral Self-Assembled Structures of Amino Acids on Transition-Metal Surfaces: Alanine on Pd(111). *J. Phys. Chem. C*, **2014**, *118,* 6856–6865.
2. Structure and Decomposition Pathways of D-(-)-Tartaric Acid on Pd(111). Mausumi Mahapatra and Wilfred T. Tysoe, *Surf. Sci.* **2014,** *629,* 132-138.
3. Shukla, N.; Ondeck, N.; Gellman, A.J. Quantitation of Enantiospecific Adsorption on Chiral Nanoparticles from Optical Rotation. *Surf. Sci.* **2014,** *629,* 15–19.
4. Gordon, A.D.; Karakalos, S.; Zaera, F. Dependence of the Adsorption of Chiral Compounds on their Enantiomeric Composition. *Surf. Sci.,* **2014,** *629,* 3–10
5. Mahapatra, M.; Tysoe, W.T. Adsorption and Reaction Pathways of a Chiral Probe Molecule, S-glycidol on a Pd(111) Surface. *Catal. Sci. Technol.* **2015,** *5*, 738-742.
6. Mahapatra, M.; Tysoe, W.T. Chemisorptive Enantioselectivity of Chiral Epoxides on Tartaric-Acid Modified Pd(111): Three-Point Bonding. *Phys. Chem. Chem. Phys.* **2015,** *17,* 5450-5458.
7. Gellman, A.J.; Tysoe, W.T.; Zaera, F. Surface Chemistry for Enantioselective Catalysis. *Catal. Lett.* **2015,** *145*, 220-232.
8. Yun Y., Gellman A.J., Auto-amplification of Enantiomeric Excess on an Achiral Surface. *Nature Chem.* **2015**, *7*, 520 – 525
9. Shukla N., Ondeck N., Khosla N., Klara S., Petti A., Gellman A.J., Polarimetric detection of Enantioselective Adsorption by Chiral Au Nanoparticles: Effects of Temperature, Wavelength and Size. *Nanomater. Nanotechno.* **2015**, *5*, 1-8
10. Yun Y., Gellman A.J., Enantiospecificity of Amino Acids on Naturally Chiral Cu{3,1,17}$^{R\&S}$ Surfaces: Alanine, Aspartic Acid, Lysine, Phenylalanine, Serine. *Langmuir* **2015**, *31*, 6055–6063
11. Burkholder, L.; Mahapatra, M.; Devarajan, S.; Boscoboinik J.A.; Garvey, M.; Bai, Y.; Tysoe, W.T. Formation of Induced Fit Chiral Templates by Amino Acid Functionalized Pd(111) Surfaces. *J. Phys. Chem. C*, **2015,** *119,* 3556-3563.
12. Karakalos, S.; Zaera, F. Amplification of Enantioselectivity on Solid Surfaces using Non-Chiral Adsorbates. *J. Phys. Chem. C*, **2015**, *119(24)*, 13785-13790.
13. Mahapatra, M.; Tysoe, W.T. Local and Extended Structures of D-(-)-Tartaric Acid on Pd(111). *J. Phys. Chem. C.,* **2016,** *120,* 2309-2319
14. Hong, J.; Karakalos, S.; Zaera, F. Changes in the Enantiomeric Composition of Chiral Mixtures Upon Adsorption on a Non-Chiral Surface. *Angew. Chem., Int. Ed.*, **2016**, *55,* 6225-6228.
15. Shukla N., Yang D., Gellman A.J., Enantiomeric Separations of Chiral Pharmaceuticals using Chirally Modified Tetrahexahedral Au Nanoparticles. *Surf. Sci.* **2016**, *648*, 29-34
16. Liriano M. L., Carrasco J., Lewis E. A., Murphy C. J., Lawton T. J., Marcinkowski M. D., Therrien A. J. Michaelides A., and Sykes E. C. H., The Interplay of Covalency, Hydrogen Bonding and Dispersion Leads to a Long Range Chiral Network: The Example of 2-Butanol. *J. Chem. Phys.* **2016**, *114*, 094703
17. Reinicker, A.D., Therrien, A.J., Lawton, T.J., Ali, R., Sykes E.C.H., and Gellman, A. J., Influence of Step Faceting on the Enantiospecific Decomposition of Aspartic Acid on Chiral Cu Surfaces Vicinal to Cu{111}. *Chem. Commun.* **2016,** *52,* 11263 – 11266
18. Mhatre, B.S, Dutta, S., Reinicker, A., Karagoz, B, and Gellman, A.J., Explosive Enantiospecific Decomposition of Aspartic Acid on Cu Surfaces. *Chem. Commun*. **2016,** *52,* 14125 - 14128
20. Yun, Y., and Gellman, A.J., Competing Forces in Chiral Surface Chemistry: Enantiospecificity versus Enantiomer Aggregation. *J. Phys. Chem. C* **2016,** *120,* 27285–27295

21. Therrien, A.J., Lawton, T.J., Mernoff, B., Lucci, F.R., Pushkarev, V.V., Gellman A.J., and Sykes, E.C.H. Chiral Nnanoscale Pores Created During the Surface Explosion of Tartaric Aacid on Cu(111). *Chem. Commun.* **2016,** *52,* 14282-14285
22. Liriano, M. L., Carrasco, J., Lewis, E. A., Murphy, C. J., Lawton, T. J., Marcinkowski, A. J., Therrien, M. D., Michaelides, A. and Sykes, E. C. H., The Interplay of Covalency, Hydrogen Bonding and Dispersion Leads to a Long Range Chiral Network: The Example of 2-Butanol. *J. Chem. Phys.* **2016,** *114,* 094703
23. Karakalos, S,. Hong, J., and Zaera, F., Changes in the Enantiomeric Composition of Chiral Mixtures Upon Adsorption on a Non-Chiral Surface, *Angew. Chem., Int. Ed.*, **2016,** *55,* 6225–6228.
24. Mahapatra, M., and Tysoe, W.T., Local and Extended Structures of D-(-)-Tartaric Acid on Pd(111), *J. Phys. Chem. C.,* **2016***, 120,* 2309-2319
25. Gellman, A.J., Huang, Y., Koritnik, A., and Horvath, J.D., Structure-sensitive Enantiospecific Adsorption on Naturally Chiral Cu(hkl)R&S Surfaces" *J. Phys.-Condensed Matter* **2017,** *29,* 034001
26. Ni, Y., Gordon, A.D., Tanicala, F., and Zaera, F., Correlation Between Chiral Modifier Adsorption and Enantioselectivity in Hydrogenation Catalysis. *Angew. Chem., Int. Ed.*, **2017**, *56*, 7963-7966
27. Mahapatra, M., Burkholder, L., Garvey, M., Bai, Y., Saldin, D., and Tysoe, W.T., Enhanced Hydrogenation Activity and Diastereomeric Interactions of Methyl Pyruvate Co-adsorbed with R-1-(1-Naphthylethylamine) on Pd(111). *Nat. Commun.* **2017**, *7,* 12380
27. Tysoe, W.T., Surface Chemistry: Giving Catalysts a Hand, *Nat. Chem.* **2017**, *9*, 503-504
28. Adsorption, Assembly and Oligomerization of Aspartic Acid on Pd(111), Mausumi Mahapatra, Jerry Praeger and Wilfred T. Tysoe, *J. Phys. Chem. C*, **2017,** *121*, 13293-13248

(II) Jointly funded by this grant and other grants with leading intellectual contribution from this grant;

1. Zaera, F. New Advances in Infrared Absorption Spectroscopy for the Characterization of Heterogeneous Catalytic Reactions. *Chem. Soc. Rev.*, **2014**, *43*, 7624-7663.
2. Yun, Y., Wei, D., Sholl, D.S., Gellman, A.J., Equilibrium adsorption of D- and L-alanine mixtures on naturally chiral Cu{3,1,17}$^{R\&S}$ surfaces, *J. Phys. Chem. C* **2014** *118*, 14957-14966
3. Hong, J., Lee, I., and Zaera, F., Correlated Bifunctionality in Heterogeneous Catalysts: Selective Tethering of Cinchonidine Next to Supported Pt Nanoparticles. *Catal. Sci. Technol.*, **2015**, *5*, 680-689.
4. Gellman A.J., Baker L.D., and Holsclaw B.S., Xe Adsorption Site Distributions on Pt(111), Pt(221) and Pt(531) *Surf. Sci.* **2016**, *646*, 83-89
5. Zaera, F., Use of Molecular Beams for Kinetic Measurements of Chemical Reactions on Solid Surfaces. *Surf. Sci. Rep.*, **2017,** *72*, 59-104

Exchange-correlation Functionals and Benchmark Data For Computational Heterogeneous Catalysis

Johannes Voss, Thomas Bligaard, and Jens K. Nørskov
SUNCAT Center for Interface Science and Catalysis, Photon Science Directorate,
SLAC National Accelerator Laboratory

Presentation Abstract

The importance of different types of chemical interactions in heterogeneous catalysis poses a big challenge for the atomistic level computational design of new catalysts. At the density functional level of theory, the exchange-correlation functional must capture both catalyst structure and interactions with and between adsorbates and gas phases with reasonable accuracy.
Using a functional optimization method we have developed (1), we will construct complex functionals targeting an accurate description of all relevant energetics from metallic bonding to gas phase reaction barriers. Rather than augmenting common exchange-correlation functionals with e.g. screened exact-exchange interactions, we will fit the shape of the underlying semi-local part of hybrid functionals to benchmark data aiming at optimal predictive performance. Reliable benchmark data is crucial for this approach, and we thus are establishing benchmarks for surface reaction energetics.

(1) Lundgaard, K. T.; Wellendorff, J.; Voss, J.; Jacobsen, K. W.; Bligaard, T. mBEEF-vdW: Robust fitting of error estimation density functionals. *Phys. Rev. B* **2016**, 93, 235162.

FWP Number: 10049 SLAC National Laboratory
SUNCAT Center for Interface Science and Catalysis
FWP section in extended abstract by Jens K. Nørskov

Molecular Level Foundation for Olefin Metathesis by Heterogeneous Supported Molybdena Catalysts

Israel E. Wachs
Lehigh University, Department of Chemical and Biomolecular Engineering

Presentation Abstract

Despite being discovered 50 years ago and its industrial importance, there is very little literature concerning the fundamental details of the supported MoO_x/Al_2O_3 catalyst for olefin metathesis and the few reported details are sometimes even contradictory. This lack of clarity derives from the absence of spectroscopic methods that are capable of *directly* probing the catalyst surface during the catalytic reaction. It is, thus, crucial to determine the fundamental molecular level details of these catalysts so they may be rationally designed to further help meet the rising propylene demand.

To address the molecular details of olefin metathesis by supported MoO_x/Al_2O_3 catalysts, modern *in situ* molecular spectroscopic techniques were applied before and during reaction conditions. The initial oxidized supported MoO_x/Al_2O_3 catalysts were found to contain a combination of isolated and polymeric sites, dependent on molybdena concentration; at low loadings of molybdena (<9%, 2.1 Mo atoms/nm^2), only isolated dioxo ($(O=)_2MoO_4$) sites are present, but as molybdena loading is increased, isolated ($O=MoO_4$) and polymeric (Mo-O-Mo) mono-oxo sites co-exist with the isolated dioxo site. The use of *in situ* DRIFTS of the hydroxyl region also revealed that the MoO_x preferentially anchor to the basic HO-μ_1-Al sites. *In situ* Raman spectroscopy during olefin metathesis revealed that the isolated dioxo surface sites may still be present at high molybdena coverage since they are present after the bands due to the mono-oxo sites reduce. The C_3H_6-TPSR experiments corroborated these results since the activity of propylene metathesis to 2-butene was observed to increase with oligomerization of the surface MoO_x sites. The TPSR results also suggested that acetone is a necessary intermediate for propylene metathesis. It has been determined that the MoO_x anchored to the neutral and acidic hydroxyls are the active sites for olefin metathesis, while MoO_x anchored to the basic sites are only spectators. These studies are beginning to establish the molecular structure-activity relationships for olefin metathesis by supported MoO_x/Al_2O_3 catalysts.

Grant FG02-93ER14350: Molecular Level Foundation for Olefin Metathesis by Heterogeneous Supported Molybdena Catalysts

Student(s): Anisha Chakrabarti

RECENT PROGRESS

In situ Raman Spectroscopy

In situ Raman spectroscopy was performed to characterize the supported MoO_x/Al_2O_3 catalysts. It was determined from the Raman spectroscopy of the dehydrated catalysts, that at low loadings of 3-6%MoO_x/Al_2O_3 (0.7-1.4 Mo atoms/nm^2) that there are only isolated dioxo sites. At intermediate loadings of 9-18%MoO_x/Al_2O_3 (2.1-4.1 Mo atoms/nm^2) isolated dioxo, mono-oxo, and polymeric mono-oxo sites co-exist. At the highest loadings of 20-25%MoO_x/Al_2O_3 (>4.6 Mo atoms/nm^2), nanoparticles are observed (see Figure 1). Figure 2 presents the Raman spectra taken during propylene metathesis. It was observed that at low loadings of 3%MoO_x/Al_2O_3 (0.7 Mo atoms/nm^2), the isolated surface MoO_x sites are only minimally perturbed during propylene metathesis. However, at intermediate loadings of 9%MoO_x/Al_2O_3 (2.1 Mo atoms/nm^2), only the oligomeric surface MoO_x sites are activated by propylene, while the isolated surface MoO_x sites remain stable and do not react.

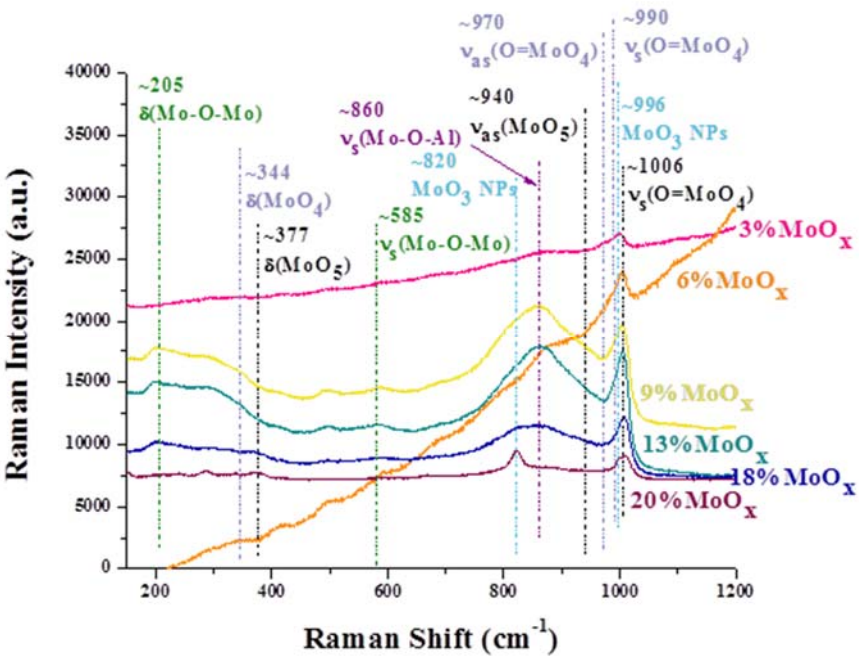

Figure 1. *In situ* Raman spectroscopy of dehydrated supported MoO_x/Al_2O_3 catalysts (percent represents MoO_x weight loading). Catalysts were dehydrated at 500°C under 10%O_2/Ar for 1 h. Spectra were obtained at 30°C under UHP Ar with the 442nm laser.

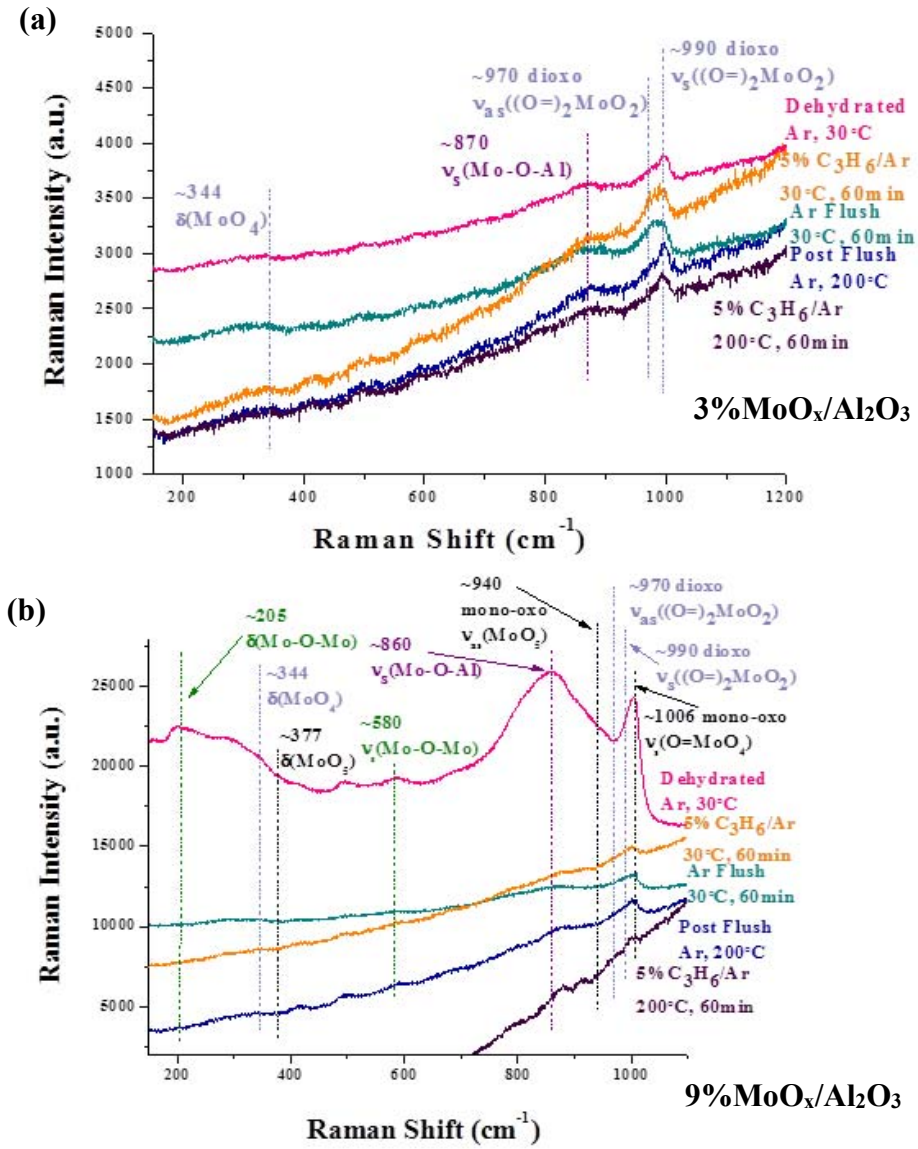

Figure 2. *In situ* Raman spectroscopy of supported MoO_x/Al_2O_3 catalysts (percent represents MoO_x weight loading) (a) $3\%MoO_x/Al_2O_3$ and (b) $9\%MoO_x/Al_2O_3$ during propylene metathesis. The experimental procedure consisted of dehydrating at 500°C for 1 h under 10% O_2/Ar, cooling to 30°C in UHP Ar, adsorbing $5\%C_3H_6$/Ar for 60 min at 35°C, flushing with UHP Ar for 60 min to remove gaseous and physisorbed propylene, heating to 200°C under UHP Ar, and finally flowing $5\%C_3H_6$/Ar for 60 min at 200°C. The catalyst was monitored with Raman spectroscopy throughout the procedure, employing a 442nm laser with a D0.6 laser filter.

C_3H_6-TPSR Spectroscopy

TPSR spectroscopy experiments were performed to determine the relative activations of the series of catalysts. The main products (2-butene (m/z=56), ethylene (m/z=27), and propylene

(m/z=42)) and oxygenated products (H_2O (m/z=18), HCHO (m/z=30), CO_2 (m/z=44), CO (m/z=28), and O_2 (m/z=32)) were monitored by an online MS. It was determined that first peak temperature (T_p) *decreases* with *increasing* MoO_x loading. This indicates that the activity of the catalysts for propylene metathesis to 2-butene increases with the oligomerization of the surface MoO_x sites (the presence of increasing amounts of oligomer sites is confirmed by Raman spectroscopy). Additionally, more than one T_p was detected in most cases, indicating the presence of multiple active sites. The presence of only one T_p at a very high temperature of 544°C for the 3%MoO_x/Al_2O_3 catalyst supports evidence from the Raman spectroscopy suggesting that the isolated dioxo site present at low loadings is inactive for propylene metathesis. During TPSR, small amounts of O_2, acetaldehyde (CH_3CHO (m/z=43)), and acetone (CH_3COCH_3 (m/z=58)), were also observed to form during the reaction. In the case of the 3%MoO_x/Al_2O_3 catalyst containing only isolated dioxo sites, no ethylene or 2-butene is formed until very high temperatures of above 400°C. There is also no formation of acetone in this case, suggesting that acetone is a necessary intermediate for propylene metathesis to ethylene and 2-butene. Samples containing above monolayer MoO_x that exhibited nanoparticles exhibited decreased olefin metathesis activity. This was evidenced by the much lower amount of 2-butene produced by the 20 and 25%MoO_x/Al_2O_3 catalyst samples.

Table 1. Summary of TPSR Results

wt% Mo	Type of Sites	T_p (°C)		
3	Isolated			544
9	Isolated + oligomeric	70	204	535
13	Isolated + oligomeric	112		500
18	Isolated + oligomeric	83		450
20	Isolated + oligomeric + NPs	74		450
25	Isolated + oligomeric + NPs	74		450

The consumption of propylene is minor below 400°C as the metathesis reaction proceeds. Above 400°C, however, the propylene is extensively combusted with oxygen from the surface MoO_x sites, producing large amounts of H_2O and CO_2, revealing that high temperatures open up a new undesirable reaction pathway. Thus, temperatures less than 400°C represent the best metathesis performance with supported MoO_x/Al_2O_3 catalysts.

In situ DRIFTS

In situ DRIFTS was performed to determine the nature of the hydroxyl surface sites and the surface intermediates. The dehydrated spectra of the hydroxyl region of the catalysts is shown in Figure 3. At low MoO_x loading, the HO-μ_1-Al_{IV} hydroxyl site (3787 cm^{-1}) is completely consumed, while some of the HO-μ_1-Al_{VI} (3768 cm^{-1}), HO-μ_1-Al_V (3743 cm^{-1} and 3728 cm^{-1}), and HO-μ_3-Al_{VI} (3670 cm^{-1}) surface hydroxyls are consumed. As the MoO_x loading increases to

9wt%, the HO-μ_1 and HO-μ_3 surface hydroxyls are mostly consumed. As the loading is further increased to 13wt%, the rest of the HO-μ_1-Al_{VI} (3768 cm^{-1}) band is consumed, and some of the HO-μ_2-Al_V (3694 cm^{-1}) surface hydroxyl is consumed. By 18wt%, the remainder of the HO-μ_2 surface hydroxyl is also consumed. Thus, it was determined that the MoO_x preferentially anchor to the surface hydroxyl sites in the order HO-μ_1 > HO-μ_3 > HO-μ_2.

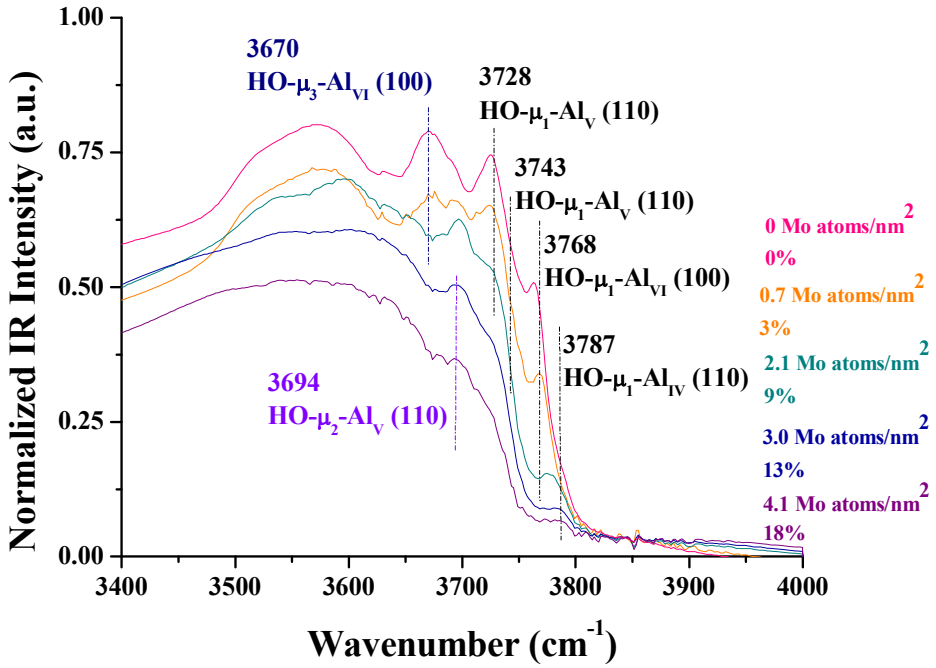

Figure 3. *In situ* DRIFTS of dehydrated supported MoO_x/Al_2O_3 catalysts. Catalysts were dehydrated at 500°C for 1 h under 10%O_2/Ar, then cooled under UHP Ar. Spectra shown here were taken at 200°C under flowing UHP Ar.

The *in situ* DRIFTS during the temperature programmed portion after propylene adsorption at 120°C. At low loading of MoO_x (3%MoO_x/Al_2O_3), a band was observed at 1400 cm^{-1} for the $\delta_s(CH_2)$ for the -CH=CH_2 vinyl intermediate. Bands were also observed for ν(C=C) (1630 cm^{-1}), $\delta_s(CH_2)$ (1377 cm^{-1} and 1466 cm^{-1}), $\nu_s(CH_2)$ (2877 cm^{-1}), $\nu_{as}(CH_2)$ (2941 cm^{-1}), and $\nu_{as}(CH_3)$ (2985 cm^{-1}) for the adsorbed propylene π-complex. At high loadings of MoO_x (18%MoO_x/Al_2O_3), the observed bands were similar. The band for the $\delta_s(CH_2)$ for the -CH=CH_2 vinyl intermediate was observed at 1416 cm^{-1}. Bands for the adsorbed propylene π-complex were also observed (ν(C=C) (1653 cm^{-1}), $\delta_s(CH_2)$ (1379 cm^{-1}), $\nu_s(CH_2)$ (2877 cm^{-1}), $\nu_{as}(CH_2)$ (2929 cm^{-1}), and $\nu_{as}(CH_3)$ (2974-2985 cm^{-1}). The presence of the MoO_x polymer sites in the 18%MoO_x/Al_2O_3 catalyst (see Figures 1 and 2) thus increases the number of intermediates present on the surface of the catalyst, increasing the reactivity. In a separate set of experiments, propylene was adsorbed at 30°C, and similar bands were observed as compared to adsorption at 120°C. It was determined that the higher propylene adsorption temperature increases the amount of adsorption.

Michael G. White

Applications of Model Nanocatalysts Prepared by Size-Selected Cluster Deposition

M. Xue,[2] K. Goodman,[2] P. Liu[1] and M. G. White[1,2]
[1]Chemistry Department, Brookhaven National Laboratory, Upton NY 11973
[2]Department of Chemistry, Stony Brook University, Stony Brook, NY 11794

Presentation Abstract

Small clusters exhibit electronic and chemical properties that can differ significantly from that of the bulk and offer a unique opportunity for preparing novel catalysts whose reactivity can be modified at the atomic level. Here, we use mass-selected cluster deposition to prepare model "inverse" catalysts comprised of small metal oxide (M_xO_y: M = Ti, Nb, Mo, Ce, W) and sulfide (M_xS_y: M = Mo, W) clusters deposited on Cu and Au surfaces, respectively, for reactivity studies related to the water-gas-shift reaction (WGSR) and CO/CO_2 activation. A key advantage of cluster deposition is that it allows control over cluster stoichiometry which provides a means of introducing oxygen/sulfur "vacancies" and varying the average cation oxidation state. Measurements show that the Ti_xO_y and Nb_xO_y clusters on Cu(111) promote water dissociation, with the 'reduced' Ti_xO_y clusters being more active, while both stoichiometric and reduced Nb_xO_y clusters are active. The differences reflect the active sites for water dissociation which are correlated with the "O-vacancies" in Ti_xO_y and the presence of Nb=O oxo groups in the Nb_xO_y clusters. Recent ambient pressure XPS measurements at NSLS-II show that small Ti_nO_{2n} (n = 3, 4, 5) clusters on Cu(111) are active for catalyzing the WGSR reaction through the observation of reaction-induced O-vacancy formation and the appearance of formate intermediates. These observations are consistent with a bi-functional mechanism where "reduced" clusters act as active sites for water dissociation.

FWP: Number: CO-040
Title: Catalysis for Advanced Fuel Synthesis and Energy
Subtask 3: Nanostructured Materials for Catalysis
PIs: Ping Liu, Jose Rodriguez, Sanjaya Senanayake, Michael White
Postdocs: David Grinter
Graduate Students: Rebecca Hamlyn, Shizhong Liu, Meng Xue, Pamela Carrillo

RECENT PROGRESS

A common theme of the activities within this subtask is the use of reducible metal oxides at interfaces with metals or other oxides to enhance chemical reactivity for specific steps in a reaction mechanism. The latter include metal oxide clusters (MO_x: M = Mo, W, Ti, Nb), nanostructures (CeO_x, FeO_x) and thin films ($CuTiO_x$, CuO_x) on metal supports (e.g., Cu(111), Ru(0001), Au(111)) all of which exhibit unique structure and reactivity as a result of strong electronic interactions at their interface. Electronic interactions at the interface can stabilize highly reduced CeO_x nanostructures supported on metals and oxides, whereas the $CuTiO_x$ mixed oxide thin film supported of Cu(111) stabilizes the highly reactive Cu^+ cations. This subtask also includes new efforts on the synthesis and characterization of novel powder systems that explore control over morphology, doping and other multicomponent architectures. Investigations in this subtask exploit BNL capabilities in high resolution electron microscopy (HR-TEM, STEM, EELS) at the Center for

Functional Nanomaterials as well as new in-house and facility-based (NSLS-II) ambient pressure characterization tools (AP-STM, AP-XPS, APS-LEEM). The experimental work is complemented by advances in theoretical methods that take account of reaction environment on surface restructuring and chemical modification. Specific highlights are given below.

Metal oxide/Cu(111) inverse catalysts by size-selected deposition

We are using size-selected cluster deposition to prepare model inverse catalysts of metal oxides on Cu surfaces that have proved to be highly active for the WGSR and CO/CO_2 hydrogenation. Specifically, inverse catalysts composed of metal oxide clusters (MO_x; M = Mo, W, Ti, Nb) clusters on Cu(111) and Cu_2O/Cu(111) surfaces were studied for their ability to promote water dissociation, a key step in the WGSR. Size-selected cluster deposition is unique in its ability to control cluster stoichiometry which provides a means of introducing oxygen "vacancies" and varying the average cation oxidation state. The Mo_3O_9 and W_3O_9 clusters on Cu(111) were found to be inactive for water dissociation, whereas 'reduced' Ti_xO_y clusters (x/y = 3/5, 4/7) were found to be more active than their stoichiometric counterparts (x/y = 3/6, 4/8). The Nb_xO_y clusters behave differently, with both stoichiometric (x/y = 3/7, 4/10) and reduced clusters (x/y = 3/5, 4/8) able to dissociate water on Cu(111). From a combination of XPS and DFT calculations it was determined that the likely active sites for water dissociation on the Nb_xO_y clusters are Nb=O oxo groups (Nb^{5+}). On Cu_2O, the Nb=O group is lost to binding to lattice oxygen resulting in a loss of observable activity. These results show that cluster stoichiometry, cation coordination and cluster-support interactions strongly influence surface chemical reactivity. More recently, we have demonstrated that Ti_nO_{2n} (n = 3, 4, 5) clusters deposited on Cu(111) are active for catalyzing the WGSR under ambient pressure (AP) conditions ($CO:H_2O$, 1:1, 28 mTorr) using the AP-XPS end station at NSLS-II. Under these conditions, we observe reaction-induced O-vacancy formation via the appearance of Ti^{3+} (Ti 2p spectra) as well as the formation of formate intermediates (C 1s spectra) (see Fig.1). These results show that under elevated pressures, the very small stoichiometric oxide clusters can be reduced and thereby act as active site for water dissociation. Currently, we are developing a laser ablation cluster source to allow extension of these studies to the deposition of ceria (Ce_xO_y) clusters on Cu(111) which are expected to be highly active for both WGSR and CO_2/CO hydrogenation to methanol.

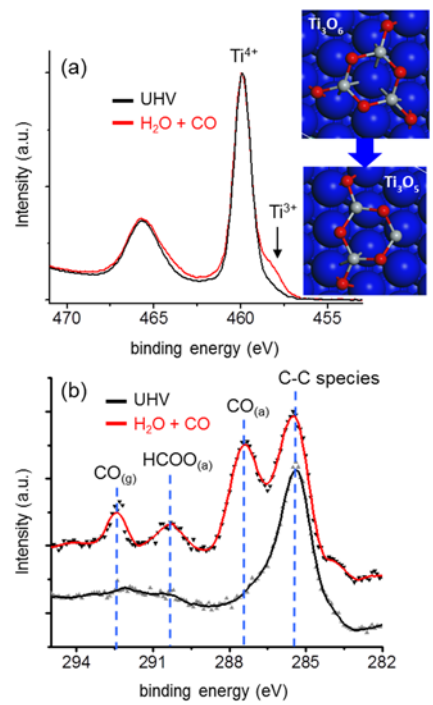

Fig. 1: AP-XPS core level spectra for (a) Ti 2p and (b) C 1s for Ti_3O_6 deposited on Cu(111) under ambient pressures of $CO+H_2O$ (28 mTorr) at 300 K. The lowest energy structures for Ti_3O_6 and "reduced" Ti_3O_5 on Cu(111) from DFT calculations are shown in (a).

Thin film oxides as model catalysts and supports

Cu_2O/Cu(111): Copper oxides are widely used in catalytic processes for C-O, C-H and O-H bond conversions such as CO oxidation, the epoxidation of hydrocarbons, partial oxidation of methanol to formaldehyde; however, Cu oxides are readily reduced at high temperatures and the loss of the most reactive Cu^+ cations can lead to deactivation of the catalyst. To gain a better understanding of bond conversion reactions on Cu oxides, we studied the CO titration over model Cu_xO thin films supported on Cu(111) using a combination of AP-STM, AP-XPS and DFT. Reduction of the oxide film was followed by observing the non-stoichiometric "44" and "5-7" structures, both of which are evident during $Cu_2O \leftrightarrow Cu$ reduction-oxidation processes (Fig. 2, top). Such atomically-resolved images under elevated CO pressure (10 mTorr) are the

first to be recorded for an oxide surface undergoing a chemical reaction by STM. The transformation between the various oxide and metal phases during CO exposure is shown in the bottom plot in Fig. 2. The DFT results suggest that at the initial stage of the CO titration the strong electronic interactions between the Cu_xO film and the Cu(111) substrate are able to stabilize the monolayer Cu_xO film and hinder the CO_2 formation by removal of O-atoms from the lattice. However, with the formation of more oxygen vacancies, the binding between the Cu_xO film and Cu(111) support is weakened along with significant structural distortion in the Cu_xO film. The 5-7 structure is a key intermediate state during this process and can also be advantageous in terms of exploring its activity toward C-H and C-O bond conversion reactions.

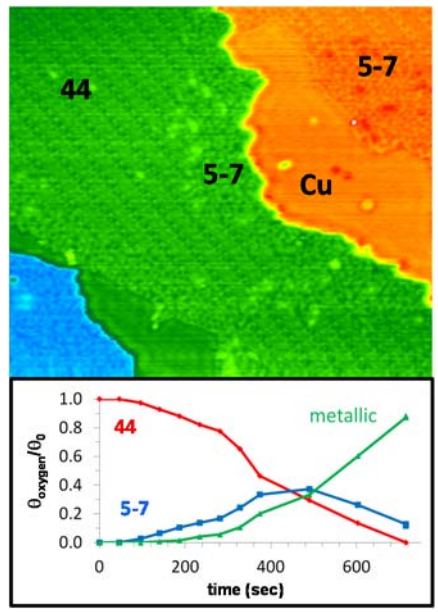

Fig. 2 : In situ AP-STM images during the CO (10 mTorr) reduction of a Cu_xO/Cu(111) surface at 300 K (top) together with the corresponding change in oxide coverage as a function of time (bottom).

Phase transition of FeO_x/Au(111) under reaction conditions: Gold nanoparticles supported on FeOx have been found as one of the most active catalysts for several reactions including C-O bond activations. We constructed the inverse catalysts for Au/FeO_x, FeO_x nanostructures deposited on Au(111), and carried out a combined STM, XPS and DFT study to gain better understanding of the reaction mechanism and active phase. Our results show that the FeO thin film undergoes a significant phase transition during CO oxidation depending on the pressures of CO and O_2. In agreement with XPS measurements at elevated pressures, DFT calculations identify Fe_3C, Fe_2O_3 and Fe_3O_4/Au(111) as the three stable phases under typical CO oxidation conditions, while the interface of Fe_3O_4/Au(111) is determined as the only active phase to catalyze CO oxidation. Strong FeO_x-Au interactions stabilize Fe_3O_4 nanostructures under reaction conditions and tune the catalytic properties of the Fe_3O_4/Au(111) interface with both FeO_x and Au participating in the reaction directly. This mechanistic study using the inverse model allows us to pinpoint the important role that the practical chemical environment can play in enhancing the catalytic performance of the oxide component in metal-oxide catalysts.

<u>Mixed metal oxide surfaces</u>

$CuTiO_x$/Cu(111): We have recently demonstrated that the activity of Cu_2O/Cu(111) surfaces can be promoted via the controlled addition of titanium. This mixed oxide system demonstrates a novel and promising way to stabilize catalytically active Cu^+ ions, avoiding the tendency for such centers to fully reduce to Cu^0 or oxidize to Cu^{2+} in contact with reactive gases. The presence of stabilized Cu^+ improves the already high catalytic activity of Cu_2O catalysts for CO oxidation. DFT calculations predict that the mixed oxide film corresponds to a single Cu_2TiO_3 trilayer structure. Two mophologies are adopted, which are consistent with the observations using STM (see Fig. 3). In both cases, each Cu^+ cation is separated in the TiO_x matrix, preventing further oxidation to Cu^{+2}. All the Ti atoms in the mixed oxide film remain in the subsurface region of the film, in agreement with the results from NEXAFS and IRRAS. DFT calculations show that conversion of CO to CO_2 occurs at step edges, where Cu^+ ions, the TiO_x matrix and the Cu(111) support all contribute. By contrast, isolated Cu^+ sites are found to tune the selectivity for epoxidation reactions, which are challenging because of the strong tendency for complete combustion. In this case, the DFT calculations show that the highly dispersed and stabilized Cu^+ cations in $CuTiO_x$ are the active sites for anchoring the key surface oxametallacycle intermediate, which is responsible for higher selectivity for propylene epoxidation.

CeOx-TiO$_2$(110): Mixed Ce-Ti oxide surfaces were prepared using sequential loading of two oxides using vapor deposition and wet chemical methods, in planar model and powder catalysts, respectively. The resulting mixed oxide surfaces yield rich structural and chemical properties not obtainable in their single component counterparts. Specifically, deposition of an overlayer of ceria on a TiO_2(110) substrate results in two types of domains. About half of the surface is covered by an ordered ceria film with a near-c(6 × 2) relationship to the underlying TiO_2(110)-(1 × 1) support. The other half is comprised of CeO_x nanoparticles and reconstructed TiO_x structures. Deposition of a small amount of gold resulted in the formation of isolated gold atoms and small clusters on the ordered ceria film and TiO_2(110)-(1 × 1) areas. The Au/CeO_x/TiO_2(110) model system proved to be a good catalyst for the water-gas-shift (WGS) reaction, exhibiting much higher turnover frequencies (TOFs) than Cu(111) and Pt(111) benchmarks, or the individual Au/TiO_2(110) and Au/CeO_2(111) systems. We have also tested the metal–oxide interface of Au nanoparticles anchored and stabilized on a CeO_x/TiO_2 substrate to generate active centers for CO_2 adsorption and its low pressure hydrogenation, leading to a higher selectivity toward methanol.

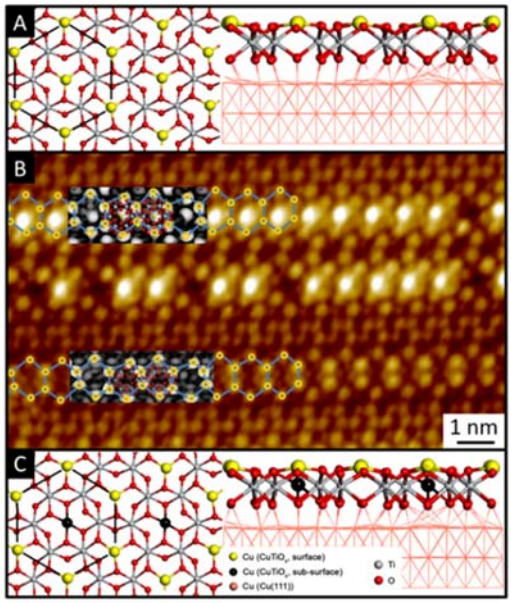

Fig. 3: Comparison of DFT predicted structures with an STM image from $CuTiO_x$ terraces. (A) all Cu atoms at the surface layer; (B) DFT structures and simulated images superimposed to an STM image (-0.50 V, 0.27 nA); (C) central Cu atoms (black) in the subsurface of the film.

CuO$_x$-TiO$_2$ powder catalysts: Stimulated by the high activity of Cu-TiO_x/Cu(111) planar model surfaces for promoting oxidation reactions, we have prepared and characterized the analogous CuO_x-TiO_2 powder (5wt% Cu loading). Both CuO_x-TiO_2 and pure CuO_x powders were investigated in order to identify the effects of Cu-TiO_2 interactions structure, electronic properties and activity. Electron microscopy (STEM) was employed to examine the local catalyst morphology (Fig. 4), while *in situ* XRD, EXAFS and IR-DRIFTS measurements were used to follow the atomic structure, cation oxidation states, and surface intermediates of the oxides under CO oxidation reaction conditions, respectively. Similar to the Cu-TiOx/Cu(111) planar surfaces, the results suggest that the increased activity of Cu_2O/TiO_2 compared to unsupported Cu_2O is a result of stabilized Cu^+ species at the CuO_x–TiO_2 interface.

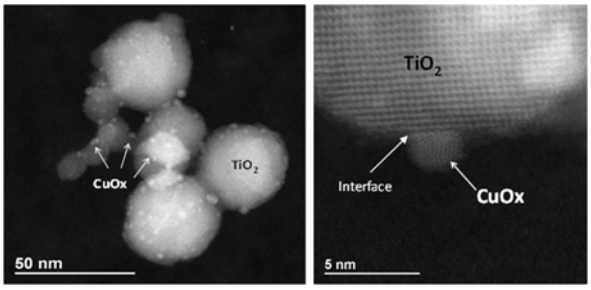

Fig. 4: STEM images of CuO_x-TiO_2 catalyst showing small CuO_x nanoparticles supported on TiO_2 with interface region between the two oxides.

Publications Acknowledging this Grant in 2014-2017

Exclusively funded by this grant

1. An, W.; Liu, P. Complex behavior of Pd_7 cluster supported on TiO_2(110) during CO oxidation: adsorbate-driven promoting effect, *Phys, Chem. Chem. Phys.: Comm.* **2016**, *18*, 30881-3134.

2. Magee, J. W.; Palomino, R. M.; White, M. G. Infrared Spectroscopy Investigation of Fe-Promoted Rh Catalysts Supported on Titania and Ceria for CO Hydrogenation, *Catal. Lett.* **2016**, *146*, 1771-1779.
3. Hoffmann, F. M.; Hrbek, J.; Ma, S.; Park, J. B.; Rodriguez, J.A.; Stacchiola, D. J.; Senanayake, S. D. Enhancing the Reactivity of Gold: Nanostructured Au(111) adsorbs CO Surface Science, *Surf. Sci.* **2016**, *650*, 17–23.
4. Liu, S.; White, M. G.; Liu, P. Mechanism of oxygen reduction reaction on Pt(111) in alkaline solution: importance of chemisorbed water on surface, *J. Phys. Chem. C* 2016, *120*, 15288-15298.
5. Stacchiola D. Tuning the Properties of Copper-Based Catalysts Based on Molecular in Situ Studies of Model Systems, *Acc. Chem. Res.* **2015**, *48*, 2151–2158.
6. An, W.; Liu, P. Rationalization of Au concentration and distribution in AuNi@Pt core-shell nanoparticles for oxygen reduction reaction, *ACS Catal.* **2015**, *5*, 6328-6336.
7. An, W.; Xu, F.; Stacchiola, D.; Liu, P. Potassium-induced effect on structure and chemical activity of Cu_xO/Cu(111) ($x \leq 2$) surface: a combined STM and DFT study, *ChemCatChem* **2015**, *7*, 3865-3872.
8. Magee, J. W.; Zhou, W.-P.; White, M. G. Promotion of Pt Surfaces for Ethanol Electro-Oxidation by the Addition of Small SnO_2 Nanoparticles: Activity and Mechanism, *Appl. Catal. B: Environ*. **2014**, *152–153*, 397–402.

Jointly funded by this grant and other grants with leading intellectual contribution from this grant;

9. Zhang, T.; Lei, W.; Liu, P.; Rodriguez, J. A.; Yu, J.; Qi, Y.; Liu, G.; Liu, M. Organic pollutant photodecomposition by Ag/$KNbO_3$ nanocomposites: A combined experimental and theoretical study, *J. Phys. Chem. C* **2016**, *120*, 2777-2786.
10. Lei, W.; Zhang, T.; Liu, P.; Rodriguez, J. A.; Liu, G.; Liu, M. Bandgap and local field-dependent photoactivity of Ag-black phosphorus nanohybrids, *ACS Catalysis* **2016**, *6*, 8009-8020.
11. Li, H.; Pan, C.; Zhao, S.; Liu, P.; Zhu, Y.; Rafailovich, M. H. Enhancing performance of PEM fuel cells: Using the Au nanoplatelet/Nafion interface to enable CO oxidation under ambient conditions, *J. Catal.* **2016**, *339*, 31-37.
12. Rodriguez, J. A.; Liu, P.; Graciani, J.; Senanayake, S. D.; Grinter, D. C.; Stacchiola, D.; Hrbek, J.; Fernández-Sanz, J. Inverse Oxide/Metal catalysts in fundamental studies and practical applications: a perspective of recent developments, *J. Phys. Chem. Lett.* **2016***,* 7, 2627-2639.
13. Grinter, D. C.; Senanayake, S. D.; Flege, J. I. In situ growth, structure, and real-time chemical reactivity of well-defined CeOx-Ru(0001) model surfaces, *Appl. Catal. B* **2016**, *197*, 286-298.
14. Höcker, J.; Duchoň, T.; Veltruská, K.; Matolín, V.; Falta, J.; Senanayake, S. D.; Flege, J. I. Controlling Heteroepitaxy by Oxygen Chemical Potential: Exclusive Growth of (100) Oriented Ceria Nanostructures on Cu(111)", *J. Phys. Chem. C* **2016**, *120*, 4895-4901.
15. Flege, I.; Höcker, J.; Kaemena, B.; Mentes, T. O.; Sala, A.; Locatelli, A.; Gangopadhyay, S.; Sadowski, J. T.; Senanayake, S. D.; Falta, J. Growth and Characterization of Epitaxially Stabilized Ceria(001) Nanostructures on Ru(0001), *Nanoscale*, **2016**, *8*, 10849-10856.
16. Nguyen-Phan, T. D.; Luo, S.; Vovchok, D.; Llorca, J.; Sallis, S.; Kattel, S.; Xu, W.; Piper, L. F. J.; Polyansky, D. E.; Senanayake, S. D.; Stacchiola, D. J.; Rodriguez, J. A. "Three-Dimensional Ruthenium-Doped TiO_2 Sea Urchins for Enhanced Visible-Light-Responsive H_2 Production," *Phys. Chem. Chem. Phys.* 18, 15972-15979 (2016).
17. Eren, B.; Liu, Z.; Stacchiola, D.; Somorjai, G. A.; Salmeron, M. Structural Changes of Cu(110) and Cu(110)-(2 × 1)-O Surfaces under Carbon Monoxide in the Torr Pressure Range Studied with Scanning Tunneling Microscopy and Infrared Reflection Absorption Spectroscopy, *J. Phys. Chem. C* **2016,** *120*, 8227−8231.

18. Mudiyanselage, K.; Luo, S. Kim, H. Yang , X.; Baber, A. E.; Hoffmann, F. M.; Rodriguez, J. A.; Chen, J.G.; Liu, P.; Stacchiola, D. J. How to stabilize highly active Cu^+ Cations in a mixed-oxide catalyst? *Catal. Today* **2016,** *263*, 4-10.
19. Nguyen-Phan, T.D.; Liu, Z.; Luo, S.; Gamalski, A. D.; Vovchok, D.; Xu, W.; Stach, E. A.; Polyansky, D. E.; Fujita, E.; Rodriguez J. A.; Senanayake, S. D. Unraveling the Hydrogenation of TiO_2 and Graphene Oxide/TiO_2 Composites in Real Time by In Situ Synchrotron X-ray Powder Diffraction and Pair Distribution Function Analysis, *J. Phys. Chem. C* **2016***, 120*, 3472–3482.
20. Zhang, T.; Lei, W.; Liu, P.; Rodriguez, J. A.; Yu, J.; Qi, Y.; Liu, G.; Liu, M. Insights into Structure-Photoreactivity Relationships in Well-Defined Perovskite Ferroelectric $KNbO_3$ Nanowires, *Chem. Sci.* **2015**, *6,* 4118-4123.
21. Liu, H.; An, W.; Li, Y.; Frenkel, A. I.; Sasaki, K.; Koenigsmann, C.; Su, D.; Anderson, R. M.; Crooks, R. M.; Adzic, R. R.; Liu, P.; Wong, S. S. In situ probing of the active site geometry of ultrathin nanowires for the oxygen reduction reaction, *J. Am. Chem. Soc.* **2015**, *137*, 12597-12609.
22. Palomino, R.; Magee, J. W.; Llorca, J.; Senanayake, S. D.; White, M. G. The Effects of Fe-Rh Alloying on CO Hydrogenation to C_{2+} Oxygenates, *J. Catal*. **2015,** *329,* 87–94.
23. Graciani, J.; Yang, F.; Evans, J.; Vidal, A.B.; Stacchiola, D.; Rodriguez, J.A.; Sanz, J.F. "When ruthenia met titania: Achieving extraordinary catalytic activity at low temperature by nanostructuring oxides," *Phys. Chem. Chem. Phys.* 2015, **17**, 26813-26818.
24. Corchado-García, J.; Betancourt, L. E.; Vélez, C. A.; Senanayake, S. D.; Stacchiola, D.; Sasaki, K.; Guinel, M. J.-F.; Zhou, Y., Cheung, C. L., Cabrera, C. R. Cerium Oxide as a Promoter for the Electro-Oxidation Reaction of Ethanol: In-situ XAFS Characterization of the Pt Nanoparticles Supported on CeO_2 Nanoparticles and Nanorods, *Phys. Chem. Chem. Phys.* 2015, *17*, 32251-32256.
25. Mudiyanselage, K.; Xu, F.; Hoffmann, F. H.; Hrbek, J.; Waluyo, I.; Boscoboinik, J. A.; Stacchiola, D. Adsorbate-Driven Morphological Changes on Cu(111) Nano-Pits, *Phys. Chem. Chem. Phys.* **2015,** *17*, 3032-3038.
26. Yu, L.; Liu, Y.; Yang, F.; Evans, J.; Rodriguez, J. A.; Liu, P. CO oxidation on gold-supported Iron oxides: new insights into strong Oxide-Metal interactions, *J. Phys. Chem. C* **2015**, *119*, 16614-16622.
27. Vajda, S.; White, M. G. "Catalysis Applications of Size-selected Cluster Deposition," *ACS Catalysis,* **2015**, *5*, 7152–7176.
28. Nakayama, M.; Xue, M.; An, W.; Liu, P.; White, M. G. "Influence of Cluster-Support Interactions on Reactivity of Size-Selected NbxOy Clusters," J. Phys. Chem. C 2015, 119, 14756-14768.
29. Höcker, J.; Menteş, T. O.; Sala, A.; Locatelli, A.; Schmidt, T.; Falta, J.; Senanayake, S. D.; Flege, J. I. Hydrogen: Unraveling the Dynamic Nanoscale Reducibility ($Ce^{4+} \rightarrow Ce^{3+}$) of CeOx–Ru in Hydrogen Activation, *Adv. Mat. Interfaces* **2015,** *2*, 1500314-1500320.
30. Luo, S.; Nguyen-Phan, T.D.; Johnston-Peck, A. C.; Barrio, L.; Sallis, S.; Arena, D. A.; Kundu, S.; Xu, W.; Piper, L. F. J.; Stach, E. A.; Polyanskiy, D.; Fujita, E.; Rodriguez, J. A.; Senanayake, S. D. Hierarchical Heterogeneity at the CeOx-TiO2 Interface: Electronic and Geometric Structural Influence on the Photocatalytic Activity of Oxide on Oxide Nanostructures, *J. Phys. Chem.* C **2015,** *119*, 2669-2679.
31. Nguyen-Phan, T.-D.; Luo, S.; Liu, Z.; Gamalski, A. D.; Tao, J.; Xu, W.; Stach, E. A.; Polyansky, D. E.; Senanayake, S. D.; Fujita, E.; Rodriguez, J. A. Striving Towards Noble-Metal-Free Photocatalytic Water Splitting: The Hydrogenated-Graphene-TiO+ Prototype, *Chem. Mat*. **2015**, *27*, 6282–6296.
32. Nguyen-Phan, T.-D.; Luo, S.; Vovchok, D.; Llorca, J.; Graciani, J.; Sanz, J. F.; Sallis, S.; Xu, W.; Bai, J.; Piper, L. F. J.; Polyansky, D. E.; Fujita, E.; Senanayake, S. D.; Stacchiola, D. J.; Rodriguez, J. A. Visible Light-Driven H_2 Production over Highly Dispersed Ruthenia on Rutile TiO_2 Nanorods, *ACS Catal.* **2015**, *6*, 407–417.

33. An, W.; Baber, A. E.; Xu, F.; Soldemo, M.; Weissenrieder, J.; Stacchiola, D.; Liu, P. Mechanistic study of CO titration on Cu_xO/Cu(111) ($x \leq 2$) surfaces, *ChemCatChem*, **2014**, *6*, 2364-2372.
34. Xu, F.; Mudiyanselage, K.; Baber; A. E.; Soldemo, M.; Weissenrieder, J.; White, M. G.; Stacchiola, D. J. Redox-Mediated Reconstruction of Copper during Carbon Monoxide Oxidation, *J. Phys. Chem. C* **2014**, *118*, 15902–15909.
35. Weissenrieder, J.; Gustafson, J.; Stacchiola, D. Reactivity and mass transfer of low dimensional catalysts, *Chem. Rec.* **2014**, *14*, 857–868.
36. Guzmán-Blas, R.; Suazo-Dávila, D.; Velez, C. A.; Daza, C. E.; Stacchiola, D. J. ; Sasaki, K.; Senanayake, S. D.; Johnston-Peck, A. C.; Molina, R. ; Cabrera, C. R. EDTA-Ce(III) Modified Pt Vulcan XC-72 Catalyst Synthesis for Methanol Oxidation in Acid Solution, *Electrocatalysis* **2014**, *5*, 50-61.
37. Baber, A. E.; Yang, X.; Kim, H. Y.; Mudiyanselage, K.; Soldemo, M.; Weissenrieder, J.; Senanayake, S. D.; Al-Mahboob, A.; Sadowski, J. T.; Evans, J.; Rodriguez, J. A.; Liu, P.; Hoffmann, F. M.; Chen, J. G.; Stacchiola, D. J. Stabilization of catalytically active Cu+ surface sites on Titanium–Copper mixed-oxide films, *Angew. Chem. Int. Ed.* **2014**, *53*, 5336-5340.

FWP ERKCC96: Fundamentals of Catalysis and Chemical Transformations

PIs: Zili Wu, Sheng Dai, De-en Jiang (UC-Riverside), Michelle K. Kidder, Daniel A. Lutterman, David R. Mullins, Aditya (Ashi) Savara, Huiyuan Zhu
Postdocs: Chengcheng Tian, Guo Shiou Foo, Felipe Polo Garzon, Yafen Zhang, Ruihong Huang (UC-Riverside)
Students: Michelle Lukosi, Victor Fung (UC-Riverside)
Affiliation: Oak Ridge National Laboratory

RECENT PROGRESS

The overarching goal of this project is to understand how to control reaction selectivity through tuning cooperativity in multi-functional catalysts. The vision of our research is that by fundamentally understanding the composition and structure of catalytic sites and the mechanistic pathways, we will be enabled to precisely assemble different sites/entities into a cooperative catalyst to achieve the desired level of selectivity and activity. Specifically, we elucidate the cooperativity among site geometry, surface and bulk composition, acid-base and redox sites, and metal-support interactions in controlling reactivity and selectivity in reactions catalyzed by oxides surfaces and supported metal particles**.** We summarize here our recent progress along these lines. To understand the catalytic consequence of composition and structure of oxides, we choose perovskites as the initial model binary oxides because of the wide tunability of the A and B cations in ABO_3 perovskites that can result in tunable catalytic chemistry. One of the foci of our research is to bridge the so-called "pressure and material gaps" by investigating both model single crystal, thin film surfaces and nanoparticles with defined shapes. From these studies, we learned about the importance of the synergy of different surface sites in catalyzing acid-base and redox reactions. We have also investigated how to tune the cooperativity at the interface between metal and support to stabilize metal particles and enhance the catalytic reactivity. These include utilizing perovskite as a support to stabilize Au nanoparticles, sacrificial carbon layers to enhance metal-support interactions and thus stabilize Au nanoparticles, utilizing interfacial charge flow from novel BN support to Pt nanoparticles for enhanced oxidation reaction, and construction of hierarchical bimetallic catalysts with enhanced activity.

Composition and structure effect in oxide catalysis

Adsorption and reaction of oxygenates and hydrocarbons can be controlled not only by the surface structure of oxides such as oxide particles with different facets, but also by the surface and bulk composition of oxides such as binary oxides including perovskites and mixed oxides. We have used the comparison of oriented film vs shaped nanocrystals to probe structure-function relationships in oxide catalysis. We probed the surface species over thin film surfaces with ambient pressure x-ray photoelectron spectroscopy (AP-XPS), sum frequency generation (SFG) spectroscopy and the desorption products in TPD. For nanoshaped particles, similar reactions were studied via reaction kinetic measurements, DRIFTS, microcalorimetry, and inelastic neutron scattering (INS). Comparison of these results with adsorbed states and transition state barriers

computed by DFT has enhanced our understanding of the reaction mechanism and the surface structure and composition. Together these studies have led to a detailed description of reaction pathways of these model oxygenates and understanding of the cooperativity of various surface sites.

Acid-base catalysis over perovskite particles. Although perovskite catalysts are well-known for their excellent redox property, their *acid-base reactivity remains largely unknown*. To explore the potential of perovskites in acid-base catalysis, we made a comprehensive investigation on the acid-base properties and reactivity of a series of selected perovskites, $SrTiO_3$, $BaTiO_3$, $SrZrO_3$, and $BaZrO_3$, via a combination of various approaches including adsorption microcalorimetry, in situ FTIR spectroscopy, steady state kinetic measurements and density functional theory (DFT) modeling.[29] The perovskite surfaces are shown to be dominated with intermediate and strong basic sites with the presence of some weak Lewis acid sites, due to the preferred exposure of SrO/BaO on the perovskite surfaces as evidenced by low energy ion scattering (LEIS) measurements. Using the conversion of 2-propanol as a probe reaction, we found that the reaction is more selective to dehydrogenation over dehydration due to the dominant surface basicity of the perovskites. Furthermore, the adsorption energy of 2-propanol ($\Delta H_{ads,2-propanol}$) is found to be related to both a bulk property (tolerance factor) and the synergy between surface acid and base sites. The results obtained in this work pave a path for further exploration and understanding of acid-base catalysis over perovskite catalysts.

Since the above work over the four perovskites manifests the importance of understanding not only the bulk structure but also the surface structure and composition for catalysis over complex oxides such as perovskites, we focused on one perovskite, $SrTiO_3$ (STO) and studied its surface reconstruction and the catalytic consequence on acid-base catalysis. We show, using the conversion of 2-propanol as a probe reaction, that surface reconstruction of $SrTiO_3$ allows tuning its acid/base properties, providing selectivities inaccessible using single metal oxides, SrO and TiO_2. Controlled enrichment of Sr or Ti at the surface of $SrTiO_3$, attained via thermal and chemical treatments was revealed via LEIS and high-angle annular dark-field (HAADF) scanning transmission electron microscopy (STEM) as shown in **Figure 1**. Methanol adsorption followed by FTIR spectroscopy along with adsorption microcalorimetry measurements revealed the synergistic nature of the surface Sr and Ti sites for 2-propanol conversion. DFT calculations were in good agreement with experimental data and showed that both the dehydrogenation and dehydration pathways proceed via the 2-propoxy intermediate. Furthermore, the work expanded to $BaZrO_3$ suggests that the potential of utilizing the surface reconstruction of perovskites for controlling catalytic selectivity is general. The finding of this work has significant implication for catalysis by mixed oxides where the surface and bulk compositions can be different depending on treatment and reaction conditions. It underscores the importance and necessity of surface sensitive characterization of bulk mixed oxides (prior to and post reaction, ideally under reaction conditions) for unambiguous structure – catalysis correlations.

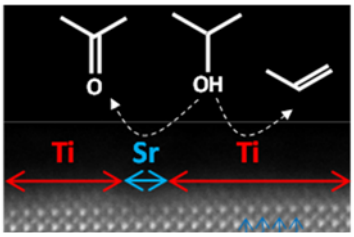

Figure 1. HAADF-STEM image of STO (100) surface exposing both Ti and Sr cations for the conversion of IPA to acetone and propene.

Bridging pressure and materials gaps via alcohol oxidation reactions on perovskite via AP-XPS. Pressure gap: For alcohol reaction over several perovskite surfaces, our TPD experiments under UHV conditions indicated only a weak interaction between the alcohols and the surface with the

alcohols desorbing by room temperature while catalytic studies on powder samples indicated that the alcohols could be oxidized to various products at temperatures between 250°C and 350°C. The difference in reactivity between UHV conditions and under reaction conditions at elevated pressure suggests that there is a "pressure gap" in the alcohol oxidation reaction, i.e. the catalysis differs at low pressure and at elevated pressure. To investigate the so-called "pressure gap" AP-XPS experiments were conducted at nominally 10^{-5} torr and at 0.1 torr between 250 and 350° C as shown in **Figure 2** using ethanol reaction on $La_{0.7}Sr_{0.3}$-MnO_3(100) thin film as an example. Ethanol forms ethoxy when adsorbed on the perovskite surface at 300° C. Ethoxy was the only C-containing surface species observed at 10^{-5} torr (top figure). When the pressure was raised to 0.1 torr (bottom figure) a significant amount of the ethoxy was oxidized to acetate. At the higher pressure the Mn 2p spectra indicated that the alcohol partially reduced Mn^{3+} to Mn^{2+} and there was also an indication in the O 1s spectra that O was removed from the surface. These observations indicated that methanol was being oxidized through reaction with the surface. When O_2 was exposed along with the ethanol, ethoxy was again the only C-containing species at 10^{-5} torr. When the pressures of ethanol and O_2 were increased to nominally 0.1 torr, acetate was the only C-containing species evident on the surface. Gas phase CO_2 and H_2O products were also detected in the C 1s and O 1s spectra. Similar observations were made for methanol reaction on this thin film surface. It is obvious that both surface coverage and surface speciation are pressure dependent, which cautions us when correlating UHV result with ambient pressure ones.

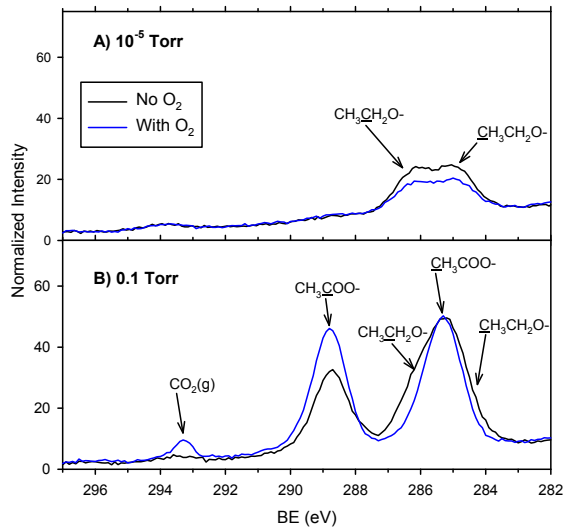

Figure 2. C 1s spectra from $La_{0.7}Sr_{0.3}$-MnO_3(100) exposed to ethanol at 300°C.

Material gap: We compared methanol oxidation at ambient pressure over $SrTiO_3$(001) single crystal and nanocube surfaces in order to understand material gap. APXPS was employed to follow surface species during methanol adsorption and oxidation over the single crystal surface while FTIR was used for the nanocubes. Surprisingly, acetate species was observed on the single crystal surface at pressure of 0.1 Torr methanol at 250° C regardless of the presence of O_2 with simple oxidation products such as CO, CO_2 and H_2O detected. In contrast, IR spectra from methanol adsorption and oxidation at ambient pressure and 250° C over the nanocubes showed the dominance of formate species. There is an obvious material gap here. Further electron microscopy characterization showed that the surface termination is different for the single crystal and nanocube of $SrTiO_3$: the single crystal surface is terminated with TiOx layer while the nanocubes are enriched with SrOx. DFT modelling of methanol over the AOx and BOx terminated $SrTiO_3$ indicate quite different reaction pathways: coupling of methoxy species to a very stable acetate-like species on the TiOx surface while the coupling is very difficult (activation energy > 2.5 eV) on the SrOx surface. This agrees well with the surface termination of the two types of $SrTiO_3$ surfaces and explains the observed material gap. Yet it remains intriguing why there is such material gap. We hypothesize that other facets or defects on the $SrTiO_3$ nanocubes are resulting in different surface reconstruction behaviour than the ideal single crystal surface and thus leading to the material gap. This will be further tested using different faceted $SrTiO_3$ nanocrystals.

Neutron and sum frequency generation spectroscopy of surface chemistry on oxide catalysts In the conversion of hydrocarbon and oxygenates over oxide surfaces, hydrogen transfer is commonly involved in the dehydration, dehydrogenation and oxidation reactions. To understand how an oxide manages surface hydrogen, we started with a single component oxide, CeO_2 to investigate the nature of surface H species upon interaction with H_2. Plus, ceria has recently shown intriguing hydrogenation reactivity in catalyzing alkyne selectively to alkenes. However, the mechanism of the hydrogenation reaction, especially the activation of H_2, remains elusive. Utilizing in situ inelastic neutron scattering (INS) spectroscopy (**Figure 3**), we showed the first direct spectroscopy evidence for the presence of both surface and bulk Ce-H species upon H_2 dissociation over ceria via. Combined with *in situ* AP-XPS, IR and Raman spectroscopic studies, the results together point to a heterolytic dissociation mechanism of H_2 over ceria, leading to either homolytic products (surface OHs) on close-to-stoichiometric ceria surface or heterolytic products (Ce-H and OH) with the presence of induced oxygen vacancies in ceria. The finding of this work has significant implications for understanding catalysis by oxides in reactions where hydrogen is involved. We also have strong interest in DFT prediction of how hydrogen interacts with both oxide and metal surfaces[32] and found various surface H species (H^0, H^-) depending on the nature of the surfaces. The insights from these work will help to undstand some of the key reaction steps involved in oxygenates and hydrocarbon conversion over both oxides and metal nanoparticles.

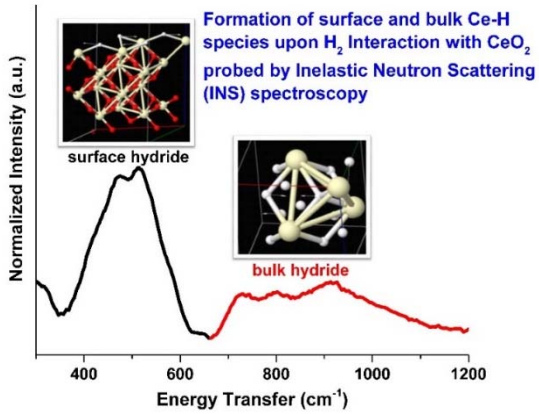

Figure 3. INS spectrum from H_2 adsorption on ceria rods at 673 K, showing the formation of both surface and bulk Ce-H species.

Recently we also explored non-linear optical spectroscopy such as sum frequency generation (SFG) to understand surface chemistry of oxygenate reactions over oxide surface. Isopropanol adsorption was investigated on the (100) surface of two model catalysts, CeO_2 and $SrTiO_3$ thin films.[47] The structure and absolute molecular orientation of isopropanol were revealed via SFG in conjunction with DFT calculations. The results unambiguously show that the speciation and molecular orientation of isopropanol on the two model surfaces are quite different, possible reason for the subsequent surface reactivity. This work presents a new paradigm for studies of chemical selectivity at catalyst interfaces that takes advantage of precision materials synthesis, surface specific optical experiments, and first principles theory.

Descriptors of catalytic activity of perovskites for methane activation:(Fung, Polo-Garzon et al. 2017) Diversity of perovskites offers many opportunities for catalysis, but an overall trend has been elusive. Using density functional theory, we studied a large set of perovskite compositions in the ABO_3 formula via descriptors of oxygen reactivity such as vacancy formation energy, hydrogen adsorption energy, and C-H activation energy (**Figure 4**). It was found that changing the identity of B within a period increases oxygen reactivity from the early to late transition metals, while changing A within a group has a much smaller effect on oxygen reactivity. Within the same group, B in the 4d period has the most reactive lattice oxygen than in the 3d or 5d period. For certain perovskite compositions, different terminations have large differences in reactivity. Using

methane oxidative coupling (OCM) as an example, we found a volcano relationship between 1st C-H activation and C-C coupling barriers. Perovskites with large A cations and non-transition metal B cations were predicted to be promising in facilitating OCM by preventing complete oxidation. These insights provide a valuable contribution to rational design of perovskite catalysts for methane activation.

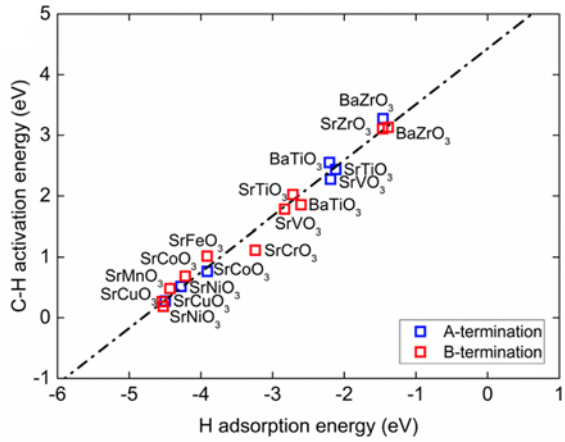

Figure 4. Correlation between first C-H activation energy of methane with hydrogen adsorption energy on the A- and B-terminations of the (100) surfaces of the ABO_3 perovskite family.

Tune metal-support interface for enhanced catalysis

It is widely accepted that the interface between metal nanoparticles and the support plays an essential role in stabilization of metal NPs and enhancement of the catalysis. We have explored various ways to tailor the interfacial structure and electronic property to achieve highly stable metal nps and enhanced catalytic reactivity.

Ultra-stable and active Au nps on perovskite support: Perovskites are known to stabilize noble metal nps, yet not demonstrated for Au. We utilized a heterostructured $LaFeO_3$ perovskite support to stabilize An nps up to 800 °C.[34] Strikingly, small Au nanoparticles (4−6 nm) are obtained after calcination in air at 800 °C and under reaction conditions. The designed Au catalyst not only possessed extreme sintering resistance but also showed high catalytic activity and stability because of the strong interfacial interaction between Au and the heterostructured perovskite support as shown in **Figure 5**. Furthermore, we have recently found that it is possible stabilize even single atom Au over the heterostructured $LaFeO_3$ surface up to 700 °C and the single atom Au showed high activity in CO oxidation. We are in the process of understanding this unusual stabilization mechanism by the perovskite surface of single atoms.

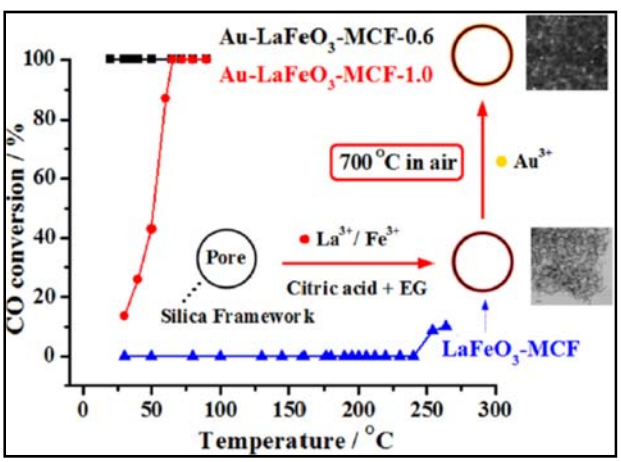

Figure 5. Ultra-stable Au nps on $LaFeO_3$ for low temperature CO oxidation.

Stabilization of Au Colloids through enhanced metal-support interactions: In addition to the stabilization of Au nps over perovskite support, we also discovered a general synthetic strategy to protect Au NPs from sintering in high-temperature oxidation processes over other oxide surfaces.[45,50] Specifically, sacrificial carbon layers are constructed on the surface after coating dopamine on Au. Upon annealing at high temperature under an inert atmosphere, the interactions between support and NPs are dramatically enhanced, while the sacrificial carbon layers can be subsequently removed through oxidative calcination in air. Owing to the improved metal−support contact and

strengthened electronic interactions, the resulting Au catalysts are resistant to sintering and exhibit excellent durability for catalytic combustion of propylene at elevated temperatures. Based on the similar methodology, we further took the advantage of long-chain surface-capping ligands on Au to construct such protective carbon shell through a simple yet efficient thermal approach. After being annealed in N_2 flow, the surface-bound surfactants are carbonized in situ as sacrificial architectures that form a conformal coating on NPs and assist in creating an enhanced metal-support interaction between NPs and substrate, thus slowing down the Ostwald ripening process during post-oxidative calcination to remove surface covers.

Control charge-flow at metal-2D support interface to enhance reactivity: Taming interfacial electronic effects on metal nps modulated has emerged as an intriguing approach to optimize the catalytic performance of the metal nps. Recently we report an interfacial electronic effect on Pt induced by *h*-BNNS with N-vacancies (N_V) and B-vacancies (B_V) for a superior CO oxidation catalysis (see **Figure 6**).[52] Based on our Bader Charge analysis, we found that when Pt sits on B_V, the *h*-BNNS serves as a Lewis acid to accept electrons from Pt; while when Pt sits on N_V, the *h*-BNNS acts as a Lewis base for donating electrons to Pt. The strong interaction between Pt NPs and N_V/B_V was confirmed by electron energy loss spectroscopy (EELS) and density functional theory. According to *in-situ* IR study, we identified an electron-rich feature of Pt after assembling on *h*-BNNS. Such an interfacial electronic effect makes Pt NPs favors the adsorption of O_2, alleviating the CO poisoning and promoting the catalysis. Consequently, the Pt NPs supported on h-BNNS readily catalyzes CO oxidation with a full conversion temperature (T_{100}) at 67°C. This study gives novel understandings of the interfacial electronic effects between Pt and a non-redox active support and provides a new strategy to tailor the Pt electronic structure for enhanced catalysis.

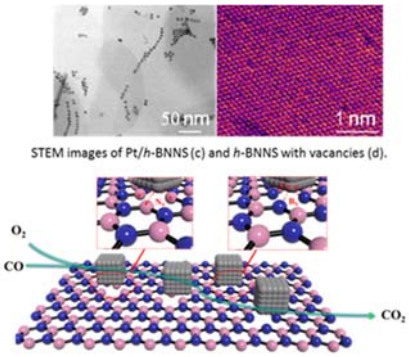

Figure 6. Schematic of charge transfer from BN to Pt for enhanced CO oxidation.

Construction of hierarchical metal-oxide interface: Exemplified by AuCu alloy NPs with face centered cubic (*fcc*) and face centered tetragonal (*fct*) structure, we have discovered a remarkable difference in phase segregation and catalytic performance depending on the crystal structure. During the thermal treatment in air, the Cu component in *fcc*-AuCu alloy NPs segregates more easily onto the alloy surface compared with that in fct-AuCu alloy NPs. As a result, after annealing at 250 °C in air for 1h, the fcc- and fct-AuCu alloy NPs are phase transferred into Au/CuO and AuCu/CuO core/shell structures, respectively (**Figure 7**).[51] More importantly, this variation in heterostructures introduces a significant difference in CO adsorption on two catalysts, leading to a largely enhanced catalytic activity of AuCu/CuO catalyst for CO oxidation. The same concept can be extended to other alloy NPs, making it possible to fine-

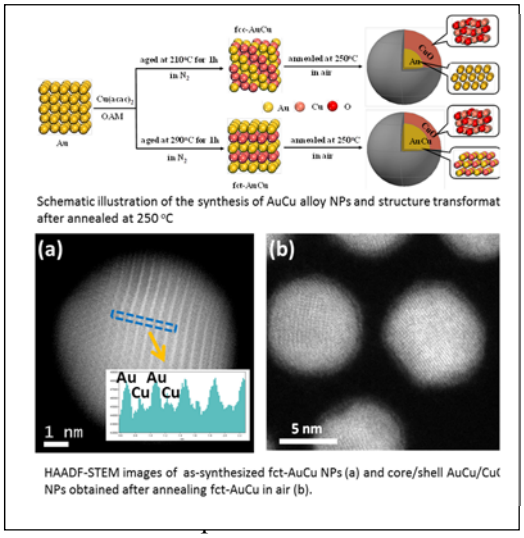

tune NP catalysis for many different chemical reactions. We further report to tune the structure and chemistry of FePt-FeO_x core-shell NPs at atomic level by varying post-synthesis conditions. The evolution of NPs' morphology, elemental segregation and phase transition for individual NPs as a function of temperature, gaseous environment and time, have been systematically investigated by high-angle annular dark-field scanning transmission electron microscopy (HAADF-STEM) imaging on FePt-FeO_x, combined with *in-situ* IR spectroscopy. A hierarchical yolk-shell like FePt-FeO_x interface was found to be highly effective for CO oxidation.

Kinetic simulation of bimetallic catalysis: One of our goals is to use kinetic modeling to connect fundamental surface science studies with liquid or gas phase reactor studies. One of such examples is the kinetic simulation + fitting of aerobic benzylic alcohol oxidation over Pd and AuPd nanoparticles to elucidate cooperativity effect in the bimetallic system. Prior to this set of studies, the mechanism and kinetics of aerobic benzylic alcohol oxidation over the precious metal nanoparticles was not known, despite the potential for industrial use. In our studies,[23,33] a mechanism was constructed based on knowledge from ultrahigh vacuum single crystal studies Pd and AuPd, and the first study of Pd surface determined that there are two reaction paths to the six products observed: A) an alkoxy pathway leading to toluene, benzaldehyde, and benzyl ether, and B) a carbonyloxyl pathway ("neutral carboxylate") leading to benzoic acid, benzene, and benzyl benzoate. The second study reported the first micro-kinetic modeling of liquid-solid catalytic benzylic alcohol oxidation over the Pd nanoparticles, and this may be the first study (over any catalyst) to show consistency with a realistic sticking coefficient for microkinetic modeling in a liquid-solid heterogeneous catalysis reaction. In the third study, the microkinetic modeling was extended to AuPd bimetallic nanoparticles to understand the cooperative role of the gold atoms in changing the selectivity. It was found that the role of gold was to weaken the strength of the interaction of oxygen with the surface (**Figure 8**), leading to a lower oxygen surface coverage and that this difference explained all of the changes in product selectivity. These studies show that our approach of starting with reduced complexity and moving to greater complexity has been successful, and that we have been able to translate mechanistic knowledge from ultrahigh vacuum studies to ambient pressure catalytic systems.

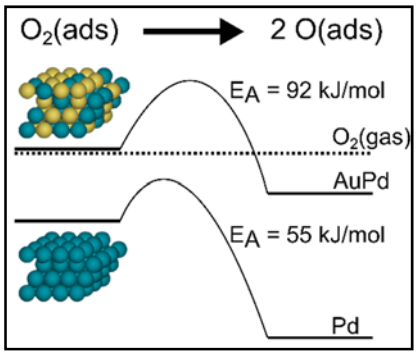

Figure 8. Au changes the selectivity of Pd solely by reducing the oxygen adsorption at the surface.

Publications Acknowledging this Grant in the past three years (August 2014 – June 2017)

(I) Exclusively funded by this grant:

1. Li, L.; Chai, S.-H.; Binder, A.; Brown, S.; Veith, G. M.; Dai, S., Catalytic CO Oxidation Over Gold Nanoparticles: Support Modification by Monolayer- and Submonolayer-Dispersed Sb_2O_3. . *Catalysis Letters* **2014**, *144*, 912.

2. Tian, C. C.; Zhu, X.; Chai, S. H.; Wu, Z. L.; Binder, A.; Brown, S.; Li, L.; Luo, H. M.; Guo, Y. L.; Dai, S., Three-Phase Catalytic System of H_2O, Ionic Liquid, and $VOPO_4$-SiO_2 Solid Acid for Conversion of Fructose to 5-Hydroxymethylfurfural. . *Chemsuschem* **2014**, *7*, 1703-1709.

3. Wu, Z. L.; Overbury, S. H., Infrared Spectroscopic insights into the role of supports in heterogeneous Au catalysis. In *Heterogeneous Gold Catalysts and Catalysis*, Ma, Z.; S., D., Eds. The Royal Society of Chemistry: RSC 2014; pp 512-532.
4. Beste, A.; Overbury, S. H., Pathways for Ethanol Dehydrogenation and Dehydration Catalyzed by Ceria (111) and (100) Surfaces. *J. Phys. Chem C* **2015**, *119*, 2447−2455.
5. Calaza, F. C.; Chen, T.-L.; Mullins, D. R.; Xu, Y.; Overbury, S. H., Reactivity and reaction intermediates for acetic acid adsorbed on CeO_2(111). *Catalysis Today* **2015**, *253*, 65-76.
6. Mann, A. K. P.; Wu, Z. L.; Overbury, S. H., The Characterization and Structure-dependent Catalysis of Ceria with Well-defined Facets In *Catalysis by Materials with Well-Defined Structures (edition 1)*, Wu, Z.; Overbury, S. H., Eds. Elsevier: 2015.
7. Mullins, D. R., The Surface Chemistry of Cerium Oxide. *Surface Science Reports* **2015**, *70*, 42.
8. Wu, Z.; Mann, A. K. P.; Li, M.; Overbury, S. H., Spectroscopic Investigation of Surface-Dependent Acid–Base Property of Ceria Nanoshapes. *J Phys Chem C* **2015**, *119*, 7340-7350.
9. Wu, Z. L.; Overbury, S. H., Catalysis by Materials with Well-defined Structures. **2015**.
10. Zhang, P.; Lu, H.; Zhou, Y.; Zhang, L.; Wu, Z.; Yang, S.; Shi, H.; Zhu, Q.; Chen, Y.; Dai, S., Mesoporous MnCeOx solid solutions for low temperature and selective oxidation of hydrocarbons. *Nature Communications* **2015**, *6*, 8446.
11. Zhang, P.; Qiao, Z.-A.; Jiang, X.; Veith, G. M.; Dai, S., Nanoporous ionic organic networks: stabilizing and supporting gold nanoparticles for catalysis. *Nano Letters* **2015**, *15*, 823-8.
12. Zhu, H.; Wu, Z.; Su, D.; Veith, G. M.; Lu, H.; Zhang, P.; Chai, S.-H.; Dai, S., Constructing Hierarchical Interfaces: TiO2-Supported PtFe–FeOx Nanowires for Room Temperature CO Oxidation. *Journal of the American Chemical Society* **2015**, *137*, 10156-10159.
13. Zhu, H.; Zhang, P.; Dai, S., Recent Advances of Lanthanum-Based Perovskite Oxides for Catalysis. *ACS Catalysis* **2015**, *5*, 6370−6385.
14. Beste, A.; Overbury, S. H., Dehydrogenation of methanol to formaldehyde catalyzed by pristine and defective ceria surfaces. *Physical Chemistry Chemical Physics* **2016**, *18*, 9990-9998.
15. Lukosi, M.; Zhu, H. Y.; Dai, S., Recent advances in gold-metal oxide core-shell nanoparticles: Synthesis, characterization, and their application for heterogeneous catalysis. *Frontiers of Chemical Science and Engineering* **2016**, *10*, 39-56.
16. Mullins, D. R., The interaction of carbon monoxide with rhodium on potassium-modified CeO2(111). *Surface Science* **2016**, *652*, 238-246.
17. Mullins, D. R., SO2 Adsorption on CeO2(100) and CeO2(111). *Topics in Catalysis* **2016**, 1-9.
18. Poutsma, M. L., Comment on “Radicalicity: A scale to compare reactivities of radicals” (Chem. Phys. Lett. 618 (2015) 99–101). *Chemical Physics Letters* **2016**, *654*, 139-140.
19. Poutsma, M. L., Extension of Structure–Reactivity Correlations for the Hydrogen Abstraction Reaction by Bromine Atom and Comparison to Chlorine Atom and Hydroxyl Radical. *The Journal of Physical Chemistry A* **2016**, *120*, 183-190.
20. Poutsma, M. L., Extension of Structure–Reactivity Correlations for the Hydrogen Abstraction Reaction to the Methyl Radical and Comparison to the Chlorine Atom, Bromine Atom, and Hydroxyl Radical. *The Journal of Physical Chemistry A* **2016**, *120*, 4447-4454.
21. Savara, A., Comment on "Equilibrium Constants and Rate Constants for Adsorbates: Two-Dimensional (2D) Ideal Gas, 2D Ideal Lattice Gas, and Ideal Hindered Translator Models". *J Phys Chem C* **2016**, *120*, 20478-20480.
22. Savara, A., Simulation and fitting of complex reaction network TPR: The key is the objective function. *Surface Science* **2016**, *653*, 169-180.
23. Savara, A.; Rossetti, I.; Chan-Thaw, C. E.; Prati, L.; Villa, A., Microkinetic Modeling of Benzyl Alcohol Oxidation on Carbon-Supported Palladium Nanoparticles. *Chemcatchem* **2016**, *8*, 2482-2491.
24. Tian, C. C.; Zhu, X.; Abney, C. W.; Tian, Z. Q.; Jiang, D. E.; Han, K. S.; Mahurin, S. M.; Washton, N. M.; Dai, S., Use of steric encumbrance to develop conjugated nanoporous polymers for metal-free catalytic hydrogenation. *Chemical Communications* **2016**, *52*, 11919-11922.

25. Wu, Z.; Hu, G.; Jiang, D.-e.; Mullins, D. R.; Zhang, Q.-F.; Allard, L. F.; Wang, L.-S.; Overbury, S. H., Diphosphine-Protected Au22 Nanoclusters on Oxide Supports Are Active for Gas-Phase Catalysis without Ligand Removal. *Nano Letters* **2016**, *16*, 6560-6567.
26. Yue, Y.; Li, Y.; Bridges, C. A.; Rother, G.; Zhang, J.; Chen, J.; Hensley, D. K.; Kidder, M. K.; Richardson, B. C.; Parans Paranthaman, M., et al., Hierarchically Superstructured Metal Sulfides: Facile Perturbation-Assisted Nanofusion Synthesis and Visible Light Photocatalytic Characterizations. *ChemNanoMat* **2016**, *2*, 1104-1110.
27. Yue, Y. F.; Zhang, L.; Chen, J. H.; Hensley, D. K.; Dai, S.; Overbury, S. H., Mesoporous xEr(2)O(3)center dot CoTiO3 composite oxide catalysts for low temperature dehydrogenation of ethylbenzene to styrene using CO2 as a soft oxidant. *RSC Adv.* **2016**, *6*, 32989-32993.
28. Beste, A., Methanol Adsorption and Dissociation on LaMnO3 and Sr Doped LaMnO3 (001) Surfaces. *Surface Science* **2017**, *Accepted*.
29. Foo, G. S.; Polo-Garzon, F.; Fung, V.; Jiang, D.-e.; Overbury, S. H.; Wu, Z., Acid–Base Reactivity of Perovskite Catalysts Probed via Conversion of 2-Propanol over Titanates and Zirconates. *ACS Catalysis* **2017**, 4423-4434.
30. Fung, V.; Jiang, D.-e., Exploring Structural Diversity and Fluxionality of Ptn (n = 10–13) Clusters from First-Principles. *The Journal of Physical Chemistry C* **2017**, *121*, 10796-10802.
31. Gill, L.; Beste, A.; Chen, B.; Li, M.; Mann, A. K. P.; Overbury, S. H.; Hagaman, E. W., Fast MAS 1H NMR Study of Water Adsorption and Dissociation on the (100) Surface of Ceria Nanocubes: A Fully Hydroxylated, Hydrophobic Ceria Surface. *The Journal of Physical Chemistry C* **2017**, *121*, 7450-7465.
32. Hu, G.; Tang, Q.; Lee, D.; Wu, Z.; Jiang, D.-e., Metallic Hydrogen in Atomically Precise Gold Nanoclusters. *Chemistry of Materials* **2017**, *DOI: 10.1021/acs.chemmater.7b00776*.
33. Savara, A.; Chan-Thaw, C. E.; Sutton, J. E.; Wang, D.; Prati, L.; Villa, A., Molecular Origin of the Selectivity Differences between Palladium and Gold–Palladium in Benzyl Alcohol Oxidation: Different Oxygen Adsorption Properties. *ChemCatChem* **2017**, *9*, 253-257.
34. Tian, C.; Zhu, X.; Abney, C. W.; Liu, X.; Foo, G. S.; Wu, Z.; Li, M.; Meyer, H. M.; Brown, S.; Mahurin, S. M., et al., Toward the Design of a Hierarchical Perovskite Support: Ultra-Sintering-Resistant Gold Nanocatalysts for CO Oxidation. *ACS Catalysis* **2017**, *7*, 3388-3393.

(II) Jointly funded by this grant and other grants with leading intellectual contribution from this grant:

35. Liu, Z.; Wu, Z.; Peng, X.; Binder, A.; Chai, S.; Dai, S., The Origin of Active Oxygen in a Ternary CuOx/Co3O4-CeO2 Catalyst for CO Oxidation. *J Phys.Chem C* **2014**, *118*, 27870-27877.
36. Ren, Y.; Ma, Z.; Dai, S., Nanosize Control on Porous beta-MnO_2 and Their Catalytic Activity in CO Oxidation and N_2O Decomposition. . *Materials* **2014**, *7*, 3547.
37. Wu, Z. L., Multi-wavelength Raman spectroscopy study of supported vanadia catalysts: Structure identification and quantification. *Chinese Journal of Catalysis* **2014**, *35*, 1591-1608.
38. Binder, A. J.; Toops, T. J.; Unocic, R. R.; Parks, J. E.; Dai, S., Low-Temperature CO Oxidation over a Ternary Oxide Catalyst with High Resistance to Hydrocarbon Inhibition. *Angewandte Chemie International Edition* **2015**, *54*, 13263-13267.
39. Lin, Y.; Wu, Z.; Wen, J.; Ding, K.; Yang, X.; Poeppelmeier, K. R.; Marks, L. D., Adhesion and Atomic Structures of Gold on Ceria Nanostructures:The Role of Surface Structure and Oxidation State of Ceria Supports. *Nano Letters* **2015**, *15*.
40. Lu, H.; Zhang, P.; Qiao, Z.-A.; Zhang, J.; Zhu, H.; Chen, J.; Chen, Y.; Dai, S., Ionic liquid-mediated synthesis of meso-scale porous lanthanum-transition-metal perovskites with high CO oxidation performance. *Chem. Communications* **2015**, *51*, 5910--5913.
41. Zhang, P.; Li, H.; Veith, G. M.; Dai, S., Soluble Porous Coordination Polymers by Mechanochemistry: From Metal-Containing Films/Membranes to Active Catalysts for Aerobic Oxidation. *Advanced Materials* **2015**, *27*, 234-239.

42. D'Angelo, A. M.; Wu, Z.; Overbury, S. H.; Chaffee, A. L., Cu-Enhanced Surface Defects and Lattice Mobility of Pr-CeO2 Mixed Oxides. *The Journal of Physical Chemistry C* **2016**, *120*, 27996-28008.
43. Li, H. Y.; Meng, B.; Chai, S. H.; Liu, H. L.; Dai, S., Hyper-crosslinked beta-cyclodextrin porous polymer: an adsorption-facilitated molecular catalyst support for transformation of water-soluble aromatic molecules. *Chemical Science* **2016**, *7*, 905-909.
44. Wu, P. W.; Zhu, W. S.; Chao, Y. H.; Zhang, J. S.; Zhang, P. F.; Zhu, H. Y.; Li, C. F.; Chen, Z. G.; Li, H. M.; Dai, S., A template-free solvent-mediated synthesis of high surface area boron nitride nanosheets for aerobic oxidative desulfurization. *Chemical Communications* **2016**, *52*, 144-147.
45. Zhan, W. C.; He, Q.; Liu, X. F.; Guo, Y. L.; Wang, Y. Q.; Wang, L.; Guo, Y.; Borisevich, A. Y.; Zhang, J. S.; Lu, G. Z., et al., A Sacrificial Coating Strategy Toward Enhancement of Metal-Support Interaction for Ultrastable Au Nanocatalysts. *JACS* **2016**, *138*, 16130-16139.
46. Zhu, W.; Gao, X.; Li, Q.; Li, H.; Chao, Y.; Li, M.; Mahurin, S. M.; Li, H.; Zhu, H.; Dai, S., Controlled Gas Exfoliation of Boron Nitride into Few-Layered Nanosheets. *Angewandte Chemie International Edition* **2016**, *55*, 10766-10770.
47. Doughty, B.; Goverapet Srinivasan, S.; Bryantsev, V. S.; Lee, D.; Lee, H. N.; Ma, Y.-Z.; Lutterman, D. A., Absolute Molecular Orientation of Isopropanol at Ceria (100) Surfaces: Insight into Catalytic Selectivity from Interfacial Structure. *JPCC* **2017**, *DOI: 10.1021/acs.jpcc.7b03272*.
48. Kwak, K.; Choi, W.; Tang, Q.; Kim, M.; Lee, Y.; Jiang, D.-e.; Lee, D., A molecule-like PtAu24(SC6H13)18 nanocluster as an electrocatalyst for hydrogen production. *Nature Communications* **2017**, *8*, 14723.
49. Wang, T.; Zhang, P.; Sun, Y.; Liu, B.; Liu, Y.; Qiao, Z.-A.; Huo, Q.; Dai, S., New Polymer Colloidal and Carbon Nanospheres: Stabilizing Ultrasmall Metal Nanoparticles for Solvent-Free Catalysis. *Chemistry of Materials* **2017**, *29*, 4044-4051.
50. Zhan, W.; Shu, Y.; Sheng, Y.; Zhu, H.; Guo, Y.; Wang, L.; Guo, Y.; Zhang, J.; Lu, G.; Dai, S., Surfactant-Assisted Stabilization of Au Colloids on Solids for Heterogeneous Catalysis. *Angewandte Chemie International Edition* **2017**, *56*, 4494-4498.
51. Zhan, W.; Wang, J.; Wang, H.; Zhang, J.; Liu, X.; Zhang, P.; Chi, M.; Guo, Y.; Guo, Y.; Lu, G., et al., Crystal Structural Effect of AuCu Alloy Nanoparticles on Catalytic CO Oxidation. *Journal of the American Chemical Society* **2017**, *DOI: 10.1021/jacs.7b01784*.
52. Zhu, W.; Wu, Z.; Foo, G. S.; Gao, X.; Zhou, M.; Liu, B.; Veith, G. M.; Wu, P.; Browning, K. L.; Lee, H. N., et al., Taming interfacial electronic properties of platinum nanoparticles on vacancy-abundant boron nitride nanosheets for enhanced catalysis. *Nature Communications* **2017**, *8*, 15291.

(III) Jointly funded by this grant and other grants with relatively minor intellectual contribution from this grant:

53. Pistner, A. J.; Lutterman, D. A.; Ghidiu, M. J.; Walker, E.; Yap, G. P. A.; Rosenthal, J., Factors Controlling the Spectroscopic Properties and Supramolecular Chemistry of an Electron Deficient 5,5-Dimethylphlorin Architecture. . *J. Phys. Chem. C* **2014**, *118*, 14124-14132.
54. Pistner, A. J.; Pupillo, R. C.; Yap, G. P. A.; Lutterman, D. A.; Ma, Y. Z.; Rosenthal , J., Electrochemical, Spectroscopic, and O-1(2) Sensitization Characteristics of 10,10-Dimethylbiladiene Complexes of Zinc and Copper, . *J. PHYS. CHEM. A* **2014**, *118,*, 10639-10648.
55. Dong, Y.; Brooks, J. D.; Chen, T.-L.; Mullins, D. R.; Cox, D. F., Methylene migration and coupling on a non-reducible metal oxide: The reaction of dichloromethane on stoichiometric α-Cr2O3(0001). *Surface Science* **2015**, *632*, 28-38.
56. Dong, Y.; Brooks, J. D.; Chen, T.-L.; Mullins, D. R.; Cox, D. F., Reactions of Methyl Groups on a Non-reducible Metal Oxide: The Reaction of Iodomethane on Stoichiometric α-Cr2O3(0001). *Surface Science,* **2015**, *641*, 148.
57. Jang, G. G.; Jacobs, C. B.; Ivanov, I. N.; Joshi, P. C.; III, H. M. M.; Kidder, M.; Armstrong, B. L.; Datskos, P. G.; Graham, D. E.; Moon, J.-W., In situ capping for size control of monochalcogenide (ZnS,

CdS and SnS) nanocrystals produced by anaerobic metal reducing bacteria. *Nanotechnology* **2015**, *26*, 325602.
58. Liu, F. J.; Liu, C.; Kong, W. P.; Qi, C. Z.; Zheng, A. M.; Dai, S., Design and synthesis of micro-meso-macroporous polymers with versatile active sites and excellent activities in the production of biofuels and fine chemicals. *Green Chemistry* **2016**, *18*, 6536-6544.
59. Liu, F. J.; Wu, Q.; Liu, C.; Qi, C. Z.; Huang, K.; Zheng, A. M.; Dai, S., Ordered Mesoporous Polymers for Biomass Conversions and Cross-Coupling Reactions. *Chemsuschem* **2016**, *9*, 2496-2504.
60. Mathis, J.; Kidder, M.; Li, Y.; Zhang, J.; Paranthaman, M., Controlled synthesis of mesoporous codoped titania nanoparticles and their photocatalytic activity. *Advances in Nano Research* **2016**, *4*, 157.
61. Mathis, J. E.; Lieffers, J. J.; Mitra, C.; Reboredo, F. A.; Bi, Z.; Bridges, C. A.; Kidder, M. K.; Paranthaman, M. P., Increased photocatalytic activity of TiO2 mesoporous microspheres from codoping with transition metals and nitrogen. *Ceramics International* **2016**, *42*, 3556-3562.
62. Moon, J.-W.; Phelps, T. J.; Fitzgerald Jr, C. L.; Lind, R. F.; Elkins, J. G.; Jang, G. G.; Joshi, P. C.; Kidder, M.; Armstrong, B. L.; Watkins, T. R., et al., Manufacturing demonstration of microbially mediated zinc sulfide nanoparticles in pilot-plant scale reactors. *Applied Microbiology and Biotechnology* **2016**, *100*, 7921-7931.
63. Pruski, M.; Sadow, A. D.; Slowing, I. I.; Marshall, C. L.; Stair, P.; Rodriguez, J.; Harris, A.; Somorjai, G. A.; Biener, J.; Matranga, C., et al., Virtual Special Issue on Catalysis at the U.S. Department of Energy's National Laboratories. *ACS Catalysis* **2016**, *6*, 3227-3235.
64. Wen, J.; Lin, Y.; Sheng, H.; Wang, L.; Miller, D. J.; Wu, Z.; Poeppelmeier, K. R.; Marks, L. D., Atomic Surface Structures of Oxide Nanoparticles with Well-defined Shapes. *Microscopy and Microanalysis* **2016**, *22*, 360-361.
65. Zhang, Y.; Kidder, M.; Ruther, R. E.; Nanda, J.; Foo, G. S.; Wu, Z.; Narula, C. K., Promotional Effects of In on Non-Oxidative Methane Transformation Over Mo-ZSM-5. *Catal. Lett.* **2016**, *146*, 1903.
66. Abney, C. W.; Patterson, J.; Gilhula, J. C.; Wang, L.; Hensley, D. K.; Chen, J.; Foo, G. S.; Wu, Z.; Dai, S., Controlling Interfacial Properties in Supported Metal Oxide Catalysts through Metal-Organic Framework Templating. *Journal of Materials Chemistry A* **2017**, *DOI: 10.1039/c7ta03894a*.
67. Ding, S.; Tian, C.; Zhu, X.; Abney, C. W.; Tian, Z.; Chen, B.; Li, M.; Jiang, D.-e.; Zhang, N.; Dai, S., Pd-Metalated Conjugated Nanoporous Polycarbazoles for Additive-Free Cyanation of Aryl Halides: Boosting Catalytic Efficiency through Spatial Modulation. *Chemsuschem* **2017**, *10*, 2348-2351.
68. Lepore, A. W.; Li, Z.; Davison, B. H.; Foo, G. S.; Wu, Z.; Narula, C. K., Catalytic Dehydration of Biomass Derived 1-Propanol to Propene over M-ZSM-5 (M = H, V, Cu, or Zn). *Industrial & Engineering Chemistry Research* **2017**, *56*, 4302-4308.
69. Li, Z.; Lepore, A. W.; Salazar, M.; Foo, G. S.; Davison, B. H.; Wu, Z.; Narula, C., Selective Conversion of Bio-Derived Ethanol to Renewable BTX over Ga-ZSM-5. *Green Chemistry* **2017**, *DOI: 10.1039/C7GC01188A*.
70. Liu, J.; Olds, D.; Peng, R.; Yu, L.; Foo, G. S.; Qian, S.; Keum, J.; Guiton, B. S.; Wu, Z.; Page, K., Quantitative analysis of the morphology of {101} and {001} faceted anatase TiO2 nanocrystals and its implication on photocatalytic activity. *Chemistry of Materials* **2017**, *10.1021/acs.chemmater.7b01172*.
71. Seipp, C. A.; Williams, N. J.; Kidder, M. K.; Custelcean, R., CO2 Capture from Ambient Air by Crystallization with a Guanidine Sorbent. *Angewandte Chemie International Edition* **2017**, *56*, 1042.
72. Wang, B.; Di, J.; Zhang, P.; Xia, J.; Dai, S.; Li, H., Ionic liquid-induced strategy for porous perovskite-like PbBiO2Br photocatalysts with enhanced photocatalytic activity and mechanism insight. *Applied Catalysis B: Environmental* **2017**, *206*, 127-135.
73. Zhang, P.; Wang, L.; Yang, S.; Schott, J. A.; Liu, X.; Mahurin, S. M.; Huang, C.; Zhang, Y.; Fulvio, P. F.; Chisholm, M. F., et al., Solid-state synthesis of ordered mesoporous carbon catalysts via a mechanochemical assembly through coordination cross-linking. *Nature Communications* **2017**, *8*, 15020.
74. Zhang, P.; Zhang, J.; Dai, S., Mesoporous Carbon Materials with Functional Compositions. *Chemistry – A European Journal* **2017**, *23*, 1986-1998.

Electrochemical and Photochemical Reduction of Carbon Dioxide

Peidong Yang
Chemical Sciences Division, Lawrence Berkeley National Laboratory

Presentation Abstract

With catalytic conversion of atmospheric CO_2 considered imperative to realize a carbon-neutral society, our group`s research is focused on developing efficient electro- and photocatalytic materials and novel combinatory approaches. Three fundamental scales (atomic, nano, and ensemble) dictating electrocatalytic properties of inorganic nanomaterials have been studied. Precise control of atomic configurations in gold-copper bimetallic systems has led to identifying active site motifs for a variety of syngas compositions. Furthermore, reducing CO_2 to complex products, such as hydrocarbons and oxygenates, with multiple electron transfers, has been achieved by controlling the morphological features of a nanoscale catalyst and utilizing an ensemble of nanoparticles as a catalytic platform. Our efforts in coupling solid-state semiconductors with whole-cell microorganisms target to combine their merits, which is the high light-harvesting efficiency and selective catalytic performance, respectively. Photosynthetic reduction of CO_2 to acetic acid is realized by the reducing equivalents, produced from inorganic photocatalysts, that drive the carbon fixation cycles of bacteria.

Precise control of elemental configurations within multimetallic nanoparticles could enable access to functional nanomaterials with significant performance benefits. This can be achieved down to the atomic level by the disorder-to-order transformation of individual nanoparticles. By systematically controlling the ordering degree, we show that the atomic ordering transformation applied to AuCu nanoparticles activates them to perform as selective electrocatalysts for CO_2 reduction. In contrast to the disordered alloy nanoparticle, which is catalytically active for hydrogen evolution, ordered AuCu nanoparticles selectively converted CO_2-to-CO at faradaic efficiency reaching ~80%. CO formation could be achieved with a reduction in overpotential of ~200mV and catalytic turnover was enhanced by 3.2-fold. Structural investigations at the atomic level were conducted for the first time in this system, revealing around three atomic gold layers over the intermetallic core to be the origin of enhanced catalytic behavior, which is further supported by DFT analysis.

Recently, we found that a wide range of syngas compositions can be produced by the controlled Cu-enrichment of Au surfaces. This flexibility is desirable for the use of electrosynthesized syngas as a precursor to more complex products, which can be converted downstream by fermentation or thermochemistry. *In-situ* SERS combined with DFT calculations elucidated how the surface electronic structure is tuned by the degree of Cu-enrichment. Furthermore, the influence of the surface electronic structure to intermediate binding was studied to predict the competition between CO and H_2 formation. Insights gained from the model systems were translated to nanostructured

electrocatalysts whereby controlled Cu enrichment enables tunable syngas production at current densities greater than 20 mA/cm^2.

Grant no: DE-AC02-05CH11231, FWP no. CH030201
Title: Catalysis Research Program

Postdoc(s): Christopher Kley, Mike Ross, Hao Liu, Fan Cui, Yude Su
Student(s): Dohyung Kim, Chenlu Xie, Yifan Li, Hao Zhang, Sunmoon Yu, Sheena Louisia, Stefano Cestellos-Blanco

Publications Acknowledging this Grant in 2014-2017

(I) Exclusively funded by this grant

1. Li, Y.; Cui, F.; Ross, M. B.; Kim, D.; Sun, Y.; Yang, P. Structure-Sensitive CO_2 Electroreduction to Hydrocarbons on Ultrathin 5-Fold Twinned Copper Nanowires. *Nano Lett.* **2017**, *17* (2), 1312–1317.
2. Kim, D.; Becknell, N.; Yu, Y.; Yang, P. Room-Temperature Dynamics of Vanishing Copper Nanoparticles Supported on Silica. *Nano Lett.* **2017**, *17* (4), 2732–2737.
3. Sakimoto, K. K.; Kornienko, N.; Yang, P. Cyborgian Material Design for Solar Fuel Production: The Emerging Photosynthetic Biohybrid Systems. *Acc. Chem. Res.* **2017**, *50* (3), 476–481.
4. M. Ross; C. T. Dinh; Y. Li; D. Kim; P. De Luna; E. Sargent; P. Yang, Tunable Cu-Enrichment Enables Designer Syngas Electrosynthesis from CO_2, *J. Am. Chem. Soc*. **2017** In Press

(II) Jointly funded by this grant and other grants with leading intellectual contribution from this grant

1. Choi, K. M.; Kim, D.; Rungtaweevoranit, B.; Trickett, C. A.; Barmanbek, J. T. D.; Alshammari, A. S.; Yang, P.; Yaghi, O. M. Plasmon-Enhanced Photocatalytic CO_2 Conversion within Metal–Organic Frameworks under Visible Light. *J. Am. Chem. Soc.* **2017**, *139* (1), 356–362.
2. Kim, D.; Xie, C.; Becknell, N.; Yu, Y.; Karamad, M.; Chan, K.; Crumlin, E. J.; Norskov, J. K.; Yang, P. Electrochemical Activation of CO_2 through Atomic Ordering Transformations of AuCu Nanoparticles. *J. Am. Chem. Soc.* **2017**, Article ASAP.

Catalysis Research P.I. Meeting
July 25-28, 2017

Participant List

Aaron Appel
Pacific Northwest National Laboratory
Aaron.Appel@pnnl.gov

Simon Bare
SLAC National Accelerator Laboratory
simon.bare@slac.stanford.edu

Alexis Bell
Lawrence Berkeley National Laboratory
alexbell@berkeley.edu

John Berry
University of Wisconsin, Madison
berry@chem.wisc.edu

Guy Bertrand
University of California, San Diego
guybertrand@ucsd.edu

Thomas Bligaard
SLAC National Accelerator Laboratory
Bligaard@stanford.edu

Suzanne Blum
University of California, Irvine
blums@uci.edu

Chris Bradley
U.S. Department of Energy/BES
chris.bradley@science.doe.gov

Phillip Britt
Oak Ridge National Laboratory
brittpf@ornl.gov

R. Morris Bullock
Pacific Northwest National Laboratory
morris.bullock@pnnl.gov

Matteo Cargnello
Stanford University
mcargnello@stanford.edu

Peng Chen
Cornell University
pc252@cornell.edu

Jingguang Chen
Columbia University
jgchen@columbia.edu

Paul Chirik
Princeton University
pchirik@princeton.edu

David Cox
Virginia Technical Institute
dfcox@vt.edu

Richard Crooks
University of Texas
crooks@cm.utexas.edu

Thomas Cundari
University of North Texas
tomc@unt.edu

Sheng Dai
Oak Ridge Naltional Laboratory
dais@ornl.gov

Paul Dauenhauer
University of Minnesota
hauer@umn.edu

Massimiliano Delferro
Argonne National Laboratory
delferro@anl.gov

Zdenek Dohnalek
Pacific Northwest National Laboratory
zdenek.dohnalek@pnnl.gov

Peter Dowben
University of Nebraska
pdowben1@unl.edu

Catalysis Research P.I. Meeting
July 25-28, 2017

Participant List

Chris Fecko
U.S. Department of Energy/BES
Christopher.Fecko@science.doe.gov

Gregory Fiechtner
U.S. Department of Energy/BES/CPIMS
gregory.fiechtner@science.doe.gov

Richard Finke
Colorado State University
rfinke@lamar.colostate.edu

Alison Fout
University of Illinois at Urbana-Champaign
fout@illinois.edu

Cynthia Friend
Harvard University
friend@fas.harvard.edu

Laura Gagliardi
University of Minnesota
gagliard@umn.edu

Bruce Garrett
U.S Department of Energy/BES
bruce.garrett@science.doe.gov

Bruce Gates
University of California Davis
bcgates@ucdavis.edu

Raymond Gorte
University of Pennsylvania
gorte@seas.upenn.edu

Lauren Greenlee
University of Arkansas
greenlee@uark.edu

Thomas Gunnoe
University of Virginia
tbg7h@virginia.edu

Oliver Yair Gutierrez Tinoco
Pacific Northwest National Laboratory
oliver.gutierrez@pnnl.gov

Alexander Harris
Brookhaven National Laboratory
alexh@bnl.gov

John Hartwig
University of California, Berkeley
jhartwig@berkeley.edu

David Heldebrant
Pacific Northwest National Laboratory
david.heldebrant@pnnl.gov

Graeme Henkelman
University of Texas, Austin
henkelman@utexas.edu

Jason Hicks
University of Notre Dame
jhicks3@nd.edu

Joseph Hupp
Northwestern University
j-hupp@northwestern.edu

Timothy Jackson
University of Kansas
taj@ku.edu

Seung Soon Jang
Georgia Institute of Technology
seungsoon.jang@mse.gatech.edu

Cynthia Jenks
Argonne National Laboratory
cjenks@anl.gov

Johannes Lercher
Pacific Northwest National Laboratory
Johannes.Lercher@pnnl.gov

Catalysis Research P.I. Meeting
July 25-28, 2017

Participant List

Cong Liu
Argonne National Laboratory
congliu@anl.gov

Ping Liu
Brookhaven National Laboratory
pingliu3@bnl.gov

Raul Lobo
University of Delaware
lobo@udel.edu

George Maracas
U.S. Department of Energy/BES
george.maracas@science.doe.gov

Diane Marceau
U.S. Department of Energy/BES
diane.marceau@science.doe.gov

Tobin Marks
Northwestern University
t-marks@northwestern.edu

Robert McCabe
National Science Foundation
rmccabe@nsf.gov

Maureen McCann
Purdue University
mmccann@purdue.edu

Raul Miranda
U.S. Department of Energy/BES
raul.miranda@science.doe.gov

Liviu Mirica
Washington University, St. Louis
mirica@wustl.edu

Karl Mueller
Pacific Northwest National Laboratory
karl.mueller@pnnl.gov

William Mustain
University of Connecticut
mustain@engr.uconn.edu

Jens Nørskov
SLAC / Stanford University
norskov@stanford.edu

Eranda Nikolla
Wayne State University
erandan@wayne.edu

Justin Notestein
Northwestern University
j-notestein@northwestern.edu

Colin Nuckolls
Columbia University
cn37@columbia.edu

Ted Oyama
Virginia Technical Institute
oyama@vt.edu

Charles Peden
U.S. Department of Energy/BES
charles.peden@science.doe.gov

Peter Pfromm
Kansas State University
pfromm@ksu.edu

Talat Rahman
University of Central Florida
talat.rahman@ucf.edu

Robert Rioux
Pennsylvania State University
rioux@engr.psu.edu

Jose Rodriguez
Brookhaven National Laboratory
rodrigez@bnl.gov

Catalysis Research P.I. Meeting
July 25-28, 2017

Participant List

Yuriy Roman
Massachusetts Institute of Technology
yroman@mit.edu

Roger Rousseau
Pacific Northwest National Laboratory
Roger.Rousseau@pnnl.gov

Aaron Sadow
Ames Laboratory
sadow@iastate.edu

Aditya Savara
Oak Ridge National Laboratory
savaraa@ornl.gov

William Schneider
University of Notre Dame
wschneider@nd.edu

Viviane Schwartz
U.S. Department of Energy/BES/Catalysis
viviane.schwartz@science.doe.gov

Susannah Scott
University of California, Santa Barbara
sscott@engineering.ucsb.edu

Annabella Selloni
Princeton University
aselloni@princeton.edu

Sanjaya Senanayake
Brookhaven National Laboratory
ssenanay@bnl.gov

Carsten Sievers
Georgia Institute of Technology
carsten.sievers@chbe.gatech.edu

Sara Skrabalak
Indiana University
sskrabal@indiana.edu

Igor Slowing
Ames Laboratory
islowing@iastate.edu

Milton Smith
Michigan State University
smithmil@msu.edu

Robert Stack
U.S. Department of Energy
Robert.Stack@science.doe.gov

Shannon Stahl
University of Wisconsin, Madison
stahl@chem.wisc.edu

Steve Suib
University of Connecticut
Steven.Suib@uconn.edu

Christine Thomas
Brandeis University
thomasc@brandeis.edu

YuYe Tong
Georgetown University
yyt@georgetown.edu

F. Dean Toste
University of California, Berkeley/LBNL
fdtoste@berkeley.edu

Wilfred Tysoe
University of Wisconsin, Milwaukee
wtt@uwm.edu

Dionisios Vlachos
University of Delaware
vlachos@udel.edu

Johannes Voss
SLAC National Accelerator Laboratory
vossj@slac.stanford.edu

Catalysis Research P.I. Meeting
July 25-28, 2017

Participant List

Israel Wachs
Lehigh University
iew0@lehigh.edu

Marcus Weck
New York University
mw125@nyu.edu

Kevin Wilson
Lawrence Berkeley National Laboratory
krwilson@lbl.gov

Michael White
BNL/Stony Brook University
mgwhite@bnl.gov

Zili Wu
Oak Ridge National Laboratory
wuz1@ornl.gov

Peidong Yang
University of California, Berkeley
p_yang@berkeley.edu

Cover images courtesy of: Brent Gunnoe/Tom Cundari (Virginia/UNT), Ken Raymond (LBNL), Don Tilley (LBNL), Max Delferro (ANL), Paul Chirik (Princeton), Zdenek Dohnálek/Roger Rousseau (PNNL), Talat Rahman (USF), Jens Nørskov (SLAC), Younan Xia (Georgia Tech), Peng Chen (Cornell), and Jose Rodriguez (BNL)

U.S. DEPARTMENT OF ENERGY | Office of Science

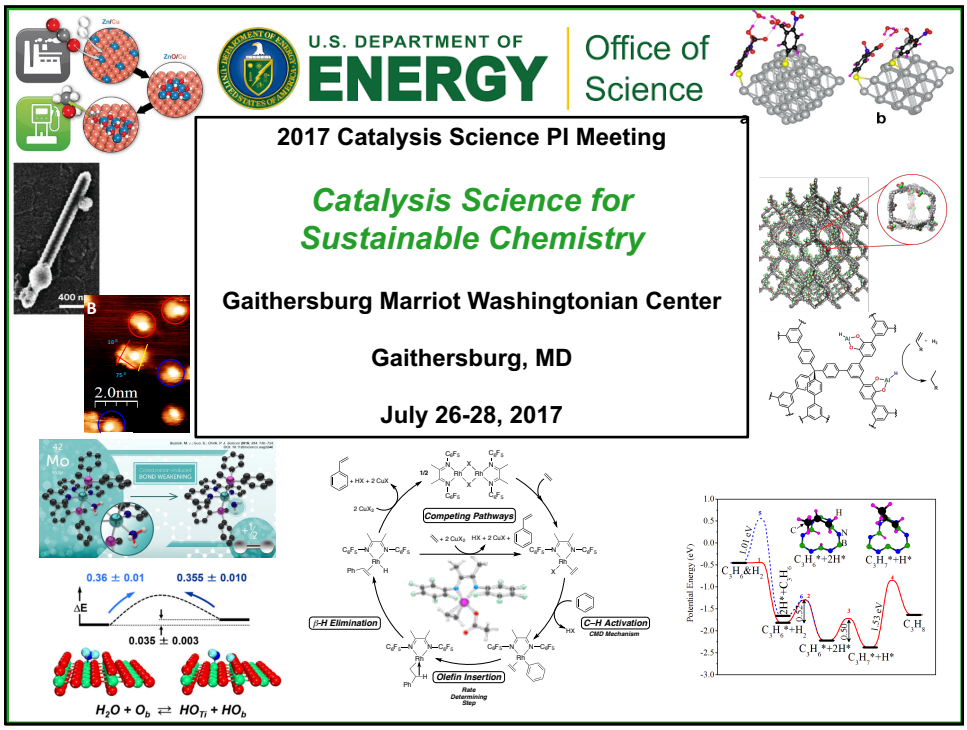

Catalysis Science Program Goals

- **Catalysis Science Program Goals**
- Discover **fundamental principles** and **novel approaches** to predict structure-reactivity behavior.
- **Understand** and **control** the chemical conversion of natural and artificial feedstocks.
- Impact the **efficiency of conversion** of natural resources into fuels, chemicals, materials, or other forms of energy, while **minimizing environmental impact**.

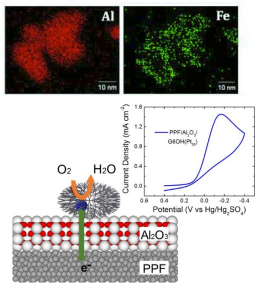

Integrated advances in…

- Chemical and materials synthesis
- *In situ/operando* characterization techniques
- Chemical dynamics and reaction kinetics
- Computational methods and approaches

…drive control of chemical reactivity.

Catalysis Program News

Basic Research Needs (BRN) Workshop

Basic Research Needs for Catalysis Science to Transform Energy Technologies

May 8-10, 2017 Washingtonian Center, Gaithersburg, MD

Workshop Goals:

a) Refresh 2007 Catalysis BRN

b) Inform on Current Catalysis Science Program Strategic Directions

Workshop Chair

Carl Koval
U. Of Colorado

Associate Workshop Chairs

Johannes Lercher
PNNL/TUM

Susannah Scott
UC Santa Barbara

~80 Participants from Universities, National Laboratories, and Industry

Four panels: 1) Energy Feedstocks & Carriers, 2) Energy Transformations, 3) Advanced Chemical Conversion, and 4) Cross-cutting Capabilities

U.S. DEPARTMENT OF ENERGY | Office of Science

5

Catalysis Program News

Basic Research Needs (BRN) Workshop

Four panels helped shape 5 Priority Research Directions (PRDs) which will form the foundation of the final written report (Winter 2017/Spring 2018).

2007 PRDs

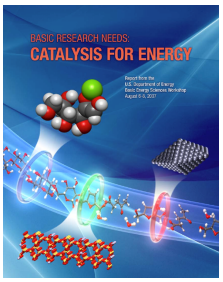

Selective Fossil Feedstock Conversions
Deconstruction of Lignocellulosic Biomass
Photo- and Electro-conversion of CO_2 and H_2O

2017 PRDs

Thursday
11:30 am BRN Overview
(Scott/Lercher)
1:15 pm BRN Panel Discussion
(Appel, Dai, Dauenhauer, Gunnoe)

U.S. DEPARTMENT OF ENERGY | Office of Science

6

Catalysis Program News

Deadlines for FY 18 Proposals:

- All renewals/new proposals will be reviewed simultaneously
- Target date for ALL Proposals: **December 4, 2017**
- For New proposals: white paper by **mid-September**
- Award start dates: **August or September 2018**

Occasionally, other FOAs are released. For more information, see:
https://science.energy.gov/bes/funding-opportunities/

Information on Renewal Proposals

- **Please, include a complete list of publications during the last funding period when reporting your progress to help the reviewers and program manager gauge the impact of the work.**
- **Classify publications into 3 categories according to the source of support:**
  - Exclusively funded by the grant
  - Jointly funded by the DOE award and other grants with leading intellectual contribution from the DOE grant
  - Jointly funded by the DOE award and other grants with relatively minor intellectual contribution from the DOE grant

Update on Strategic Planning in CSGB: Assessments of Catalysis Science Core Research Areas (CRAs)

- **Inventory assessment: what is in the program and why?**
  - What is the overarching goal? Why is it important? What areas are addressed? Why are they the right research areas?
- **Opportunity assessment: what new opportunities have emerged?**
  - What are the most pressing scientific needs and key scientific challenges? What are the highest priorities for focusing the program on areas with high potential impact?
- **Capability assessment: what is needed to succeed?**
  - What current research areas and capabilities can help move the program into new directions? What is missing, i.e., what new research areas and capabilities are required?

U.S. DEPARTMENT OF ENERGY | Office of Science

9

Informing Current Catalysis Program Strategic Directions

An essential role for PI meetings

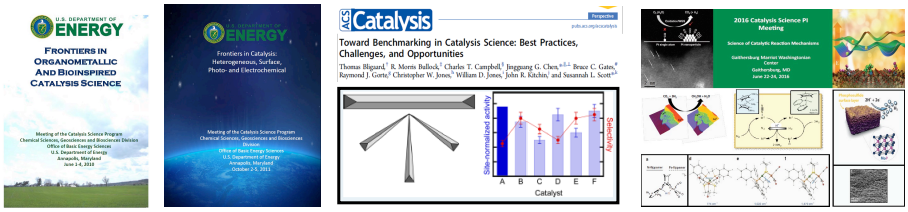

U.S. DEPARTMENT OF ENERGY | Office of Science

10

Catalysis Science Program: Programmatic Direction

Decreasing efforts in:	Increasing emphasis in:
Stoichiometric organometallic reactions	Complex network mechanistic studies (tandem/cascade reactions, cooperative effects, instrumentation for monitoring complex reactions)
Studies primarily focused on catalyst synthesis (without a strong relation to reaction mechanism)	Hybrid materials with emphasis on catalytic multifunctionality (bio-inspired materials, earth abundant metals, stimuli responsiveness, real-time imaging)
Traditional surface science studies (focused solely on individual elementary steps or surface structure and composition)	Novel routes for shale gas conversion
Catalysis for refining heavy fossil fuels and chiral/stereoselective fine chemical synthesis	Catalysts for low-temperature conversion and modular processes
	Design of catalysts for non-thermal processes (catalytic descriptors for electrified surfaces)
	Data science applied to catalysis (machine learning, data mining, data sharing)

Progress Report – Format and Submission Guidelines

- **Progress Report submission done entirely through PAMs!**
- **Progress reports are due 3 months in advance of the current funding period**
- **PAMs will send an automatic email 1 month before the due date**
  - **Program managers *will not* send reminders regarding progress reports.**
- ***Please answer all the required fields!***
  - Full Participant List, Impact on Human Resources/Society, **Estimated Carryover**
  - It is acceptable to attach a document including a more detailed information on the project progress including figures and tables
- ***Timely submission of progress reports is critical to avoid delayed release of funds.***

Proper Acknowledgement of DOE-BES Support

- **Acknowledging sole DOE BES program support:**

  Grant: "This work was supported by the U.S. Department of Energy, Office of Science, Basic Energy Sciences, Catalysis Science Program, under Award # XXX."

  FWP: "This work was supported by the U.S. Department of Energy, Office of Science, Basic Energy Sciences, Chemical Sciences, Geosciences, and Biosciences Division."

  http://science.energy.gov/funding-opportunities/acknowledgements/

- **Acknowledging multiple funding sources *with Clear Delineation*:**

  An example that is not acceptable:

  This work was funded by grants from the U.S. Department of Energy and from the National Science Foundation.

Why is it important to acknowledge BES support properly?

- BES is properly credited with support of the research in the public record making the research activity funded by the agency relevant;
- Avoid questions of whether two or more federal agencies are duplicating effort and funding the same work.
- Critical in the case of multiple BES funding streams:

  Clearly delineate between EFRC, JCAP, and the Catalysis Science Program!!

U.S. DEPARTMENT OF ENERGY | Office of Science

13

Acknowledgement of Partial DOE-BES Support

- **Suggestions to indicate the extent of delineation:**

  *'This work was primarily supported by [**name of the agency**]….'*

- **Delineation can be accomplished by:**
  - Acknowledging who was supported by which sponsor (e.g. '**Investigator name/initials**' was supported by…)
  - Indicating what aspects of the research was supported by each sponsor (e.g. 'structural characterization of catalysts was supported by…)
  - Designating which techniques were supported by which sponsor (e.g. 'TEM or X-ray absorption studies' were funded by…)

U.S. DEPARTMENT OF ENERGY | Office of Science

14

HIGHLIGHTS Submissions

- **Highlights are vital to the program, and are used in a variety of venues *validating the continuing support of our program*!**
- **Standard Format Templates Available**

General Publication/Patent Highlight Format

Title
Scientific Achievement
Significance/Impact
Research Details
Citation
Figures

Mechanistic Studies of Rh(I)-Catalyzed Single-Step Styrene Production

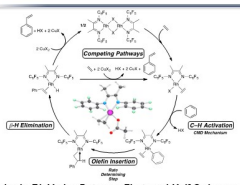

Order in Rh Varies Between First- and Half-Order as a Function of Temperature and Ethylene Concentration

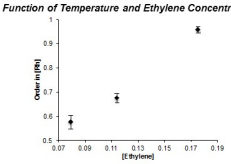

Scientific Achievement:
Styrene is produced annually on a ~20 million ton scale and is used to make a variety of plastics and elastomers. The current route to styrene is multi-step and energy intensive. Chemists at the Universities of Virginia and North Texas have developed a rhodium catalyst that converts benzene and ethylene to styrene in a single-step with high yield and selectivity using an air-recyclable copper(II) oxidant.

Significance and Impact:
Understanding the mechanistic details that result in the high selectivity and yield for styrene production using this catalyst give insight into how to make a more industrially viable catalyst.

Research Details:
- Detailed mechanistic studies revealed a complex mechanism that involves two competing catalytic cycles
- Olefin insertion into rhodium-phenyl bonds is rate-limiting, which could lead to ability to control linear/branched selectivity when using α-olefins
- Order in Rh varies between first- and half-order with temperature and $[C_2H_4]$, which supports competing dimeric and monomeric pathways

Supported by the Office of Basic Energy Sciences' Catalysis Science program through grants DE-SC0000776 and DE-FG02-03ER15387.

Vaughan, B.A.; Khani, S.K.; Gary, J.B.; Kammert, J.D.; Webster-Gardiner, M.S.; McKeown, B.A.; Davis, R.J.; Cundari, T.R.; Gunnoe, T.B. *J. Am. Chem. Soc.* **2017**, *139*, 1485. DOI: 10.1021/jacs.6b10658

UNIVERSITY of VIRGINIA

CASCaM

3 Panel Basic Science to Technology Highlights

Solvent Effects on Conversion of Biomass Derived Feedstocks

BES Basic Science | **Applied R&D** | **Development & Commercialization**

Use of γ-valerolactone (GVL) as a solvent increases rates and selectivities for acid-catalyzed biomass conversion processes compared to water by decreasing the solvation of protons.

Angew. Chem. **126,** 12066 (2014)

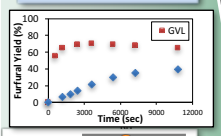

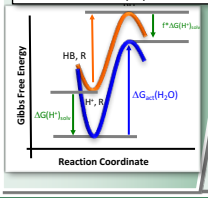

Lignocellulosic biomass is fractionated into concentrated solutions of C_6 sugars, C_5 sugars and solid lignin in GVL solvent.

Science **343,** 277 (2014)

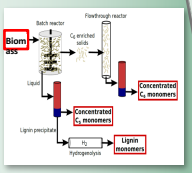

The process separates ligno-cellulosic biomass into its three main components, cellulose, hemicellulose, and lignin. All three fractions can then be upgraded separately into high value products without diminishing the value of any of the fractions.

The *TriVersa Process™*

Releasing Possibilities

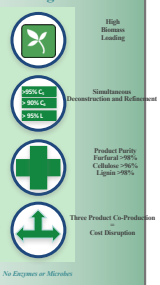

Glucan Biorenewables, LLC is scaling up the technology to produce furfural from C_5 sugars, high purity cellulose and glucose from C_6 sugars, and lignin monomers from lignin using GVL as solvent

2017 PI Meeting Overview: Catalysis Science for Sustainable Chemistry

MISSION of the CATALYSIS SCIENCE PROGRAM

Impact the **efficiency of conversion** of natural resources into fuels, chemicals, materials, or other forms of energy, while **minimizing environmental impact**.

Wednesday

Sustainability and Catalysis

Metal Oxides/Extended Structures

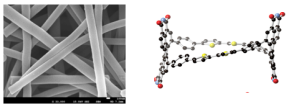

Catalysis Science Impact in DOE/BES EFRCs

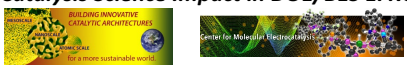

IMASC

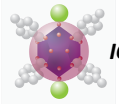

CME

ICDC

CCEI

Unique Catalytic Environments

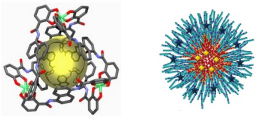

U.S. DEPARTMENT OF ENERGY | Office of Science

17

2017 PI Meeting Overview: Catalysis Science for Sustainable Chemistry

MISSION of the CATALYSIS SCIENCE PROGRAM

Impact the **efficiency of conversion** of natural resources into fuels, chemicals, materials, or other forms of energy, while **minimizing environmental impact**.

Thursday

Sustainability and Catalysis

Sustainable NH_3 Synthesis/Use

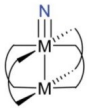

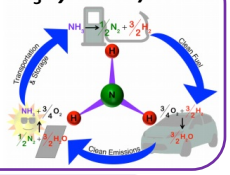

Nanoscale Catalysis I/II

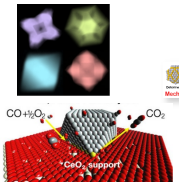

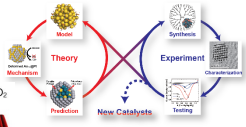

BRN Overview/Panel Discussion

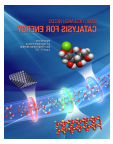

U.S. DEPARTMENT OF ENERGY | Office of Science

18

2017 PI Meeting Overview: Catalysis Science for Sustainable Chemistry

MISSION of the CATALYSIS SCIENCE PROGRAM

Impact the **efficiency of conversion** of natural resources into fuels, chemicals, materials, or other forms of energy, while **minimizing environmental impact**.

Friday

Sustainability and Catalysis

Hydrocarbon Catalysis

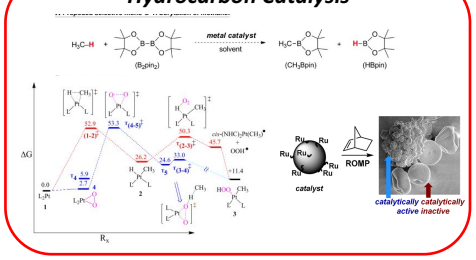

Biomass Conversion

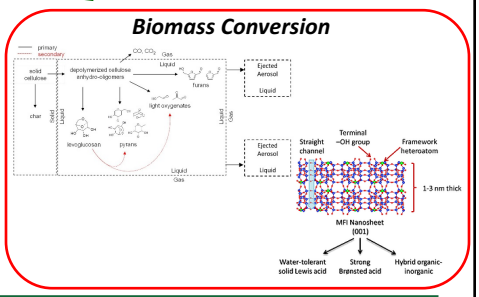

U.S. DEPARTMENT OF ENERGY | Office of Science

11
9

Acknowledgements

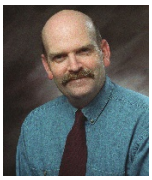

MANY THANKS to:

Program Chairs: Paul Chirik and Ray Gorte

Program Manager: Chuck Peden
(transitioning from Catalysis in August 2017)

Invited Speakers and Guests
EFRC Speakers and BRN Chairs/Panelists
Session Moderators
PIs
Diane Marceau
Connie Lansdon, ORISE Staff

U.S. DEPARTMENT OF ENERGY | Office of Science

20